DOTTORATO DI RICERCA IN CHIMICA

Convenzione tra
UNIVERSITÀ DEGLI STUDI DI TRIESTE
e
UNIVERSITÀ CA' FOSCARI DI VENEZIA

CICLO XXX

PREPARATION OF NEW WATER-SOLUBLE Ru(II) COMPOUNDS FOR THE SYNTHESIS OF METAL CONJUGATES

Settore scientifico-disciplinare: CHIM/03

DOTTORANDA
FEDERICA BATTISTIN

COORDINATORE
PROF. MAURO STENER

SUPERVISORE DI TESI
PROF. ENZO ALESSIO

ANNO ACCADEMICO 2016/2017

Table of Contents

Riassunto

L'Introduzione (Capitolo 1) riporta una descrizione generale dei coniugati metallici, in particolar modo quelli contenenti porfirine e delle loro applicazioni. Sono descritte le caratteristiche di un ideale precursore di Ru(II) per la formazione di coniugati. Inoltre viene presentato il legante utilizzato in questo lavoro di tesi per impartire solubilità in acqua, l'1,3,5-triaza-7-fosfoadamantano (PTA).

I Capitoli dal 2 al 5 descrivono il progetto principale seguito durante la Tesi, ovvero la sintesi e caratterizzazione di diversi complessi di Ru(II) con PTA, quali precursori per la formazione di coniugati metallici. In particolar modo, il Capitolo 2 riprende quanto è noto in letteratura sui complessi neutri Ru(II)-PTA, ovvero *trans*- e *cis*-$RuCl_2(PTA)_4$. Viene descritta la stabilità di questi complessi e la loro reattività nei confronti di leganti azotati bidentati, quali bpy, usata come modello per i *linker* di-imminici chelanti, cppH e bpyAc. Inoltre viene descritto lo studio della reattività di noti precursori di Ru(II)-dmso, *trans*- e *cis*-$RuCl_2(dmso)_4$ nei confronti del PTA.

Il Capitolo 3 indaga la reattività dei precursori neutri carbonilici di Ru(II) dalla formula generale $RuCl_2(CO)_x(dmso)_{4-x}$ (x = 1-3) nei confronti del PTA, visto che in letteratura non sono noti esempi di complessi carbonilici con PTA. Viene descritta la sintesi di sette nuovi composti, tra cui due dimeri. Tutti i complessi sono stati completamente caratterizzati sia spettroscopicamente che attraverso la struttura ai raggi X dei cristalli (eccezion fatta per i dimeri). Inoltre viene descritta anche la reattività dei complessi *trans*- e *cis*-$RuCl_2(PTA)_4$ nei confronti del CO.

Nel Capitolo 4 è riportata la reattività dei composti descritti nel Capitolo 3 nei confronti del legante azotato bpy. Sono descritti e caratterizzati quattro nuovi derivati carbonilici di Rutenio-PTA con bpy. Inoltre viene anche indagato il comportamento

di questi complessi nei confronti della luce, indagine che ha portato all'isolamento di altri due isomeri dei complessi precedentemente descritti.

Dal momento che in letteratura gli unici esempi di complessi Ru(II)-PTA con applicazione antitumorale sono composti organometallici contenenti areni, il Capitolo 5 descrive un'indagine preliminare dell'attività antitumorale dei complessi *trans*- e *cis*-$RuX_2(PTA)_4$ (con X = Cl o Br) e del complesso di Ru(III) tipo NAMI-A *trans*-$RuCl_4(PTA)_2$ (già descritti nel Capitolo 1).

I Capitoli dal 6 all'8 sono invece focalizzati su tre diversi *side projects* seguiti durante il lavoro di Tesi.

Il Capitolo 6 descrive la sintesi degli isomeri di legame di Ru(II) col *linker* cppH, *trans*,*cis*-$RuCl_2(CO)_2$(cppH-κN^p) e *trans*,*cis*-$RuCl_2(CO)_2$(cppH-κN^o). In particolar modo vengono utilizzati gli esperimenti ^{1}H-^{15}N HMBC per determinare il modo di coordinazione del cppH. Il metodo è stato validato usando due complessi isomeri di legame già noti in letteratura, [Ru([9]aneS_3)(cppH-κN^p)(PTA)]$(Cl)_2$ e [Ru([9]aneS_3)(cppH-κN^o)(PTA)]$(Cl)_2$. Inoltre viene studiata la reattività dei noti precursori neutri di Ru(II)-dmso *trans*- e *cis*-$RuCl_2(PTA)_4$ nei confronti del legante mpp. Anche in questo caso, il modo di coordinazione del legante è stato determinato, oltre che attraverso la struttura ai raggi X dei cristalli, registrando degli esperimenti ^{1}H-^{15}N HMBC.

Successivamente, i due complessi *trans*,*cis*-$RuCl_2(CO)_2$(cppH-κN^p) e *trans*,*cis*-$RuCl_2(CO)_2$(cppH-κN^o) vengono utilizzati per la sintesi di bioconiugati col peptide neurotensina, nell'ambito di una mobilità Erasmus di sei mesi presso il gruppo del prof. Nils Metzler-Nolte a Bochum. La preparazione dei bioconiugati viene riportata nel Capitolo 7, insieme alla loro caratterizzazione NMR per determinare il modo di coordinazione del cppH e lo studio delle loro proprietà biologiche.

Infine, il Capitolo 8 riporta la sintesi di cinque complessi del tipo [Ru([9]aneS_3)(chel)(py)]$(Cl)_2$, dove chel è una di-immina chelante. È stata studiata la fotodissociazione della piridina di questi composti, nell'ambito di una

collaborazione col gruppo della dr. Anna Renfrew dell'Università di Sidney. Infatti, la nostra idea è di verificare se, in futuro, alcuni complessi di questa serie aventi delle molecole farmacologicamente attive al posto della piridina possano essere usati nella chemioterapia fotoattivata, un approccio terapeutico in cui un profarmaco viene attivato irreversibilmente attraverso irraggiamento con luce visibile che può indurre la rottura di un gruppo protettivo fotolabile o isomerizzazione.

List of abbreviations

[9]aneS_3	1,4,7-trithiacyclononane
1D	Mono-dimensional
2D	Bi-dimensional
4,7-Ph_2phen	4,7-diphenil-1,10-phenanthroline
4′MPyP	5-(4′-pyridyl)-10,15,20-(phenyl)-porphyrin
4′PyPs	4′-*meso*-pyridylphenylporphyrins
Arg	Arginine
bpy	2,2′-bipyridine
bpyAc	4′-methyl-2,2′-bipyridine-4-carboxylic acid
bq	2,2′-biquinoline
chel	Chelating diimine
CIS	Coordination Induced Shift
COD	1,5-cyclooctadiene
COSY	Correlation Spectroscopy
cppH	2-(2′-pyridyl)pyrimidine-4-carboxylic acid
cyt C	Cytochrome C
DCM	Dichloromethane
DFT	Density Functional Theory
DIPEA	*N*,*N*-Diisopropylethylamine
dmbpy	6,6′-dimethyl-2,2′-bipyridine
DMF	Dimethylformamide
DMSO	Dimethyl sulfoxide as solvent
dmso	Dimethyl sulfoxide as ligand
DOS	Density of States
dppz	dipyrido-[3,2-*a*:2′,3′-*c*]phenazine
DSS	4,4-dimethyl-4-silapentane-1-sulfonic acid
ESI-MS	Electron Spray Ionization Mass Spectroscopy
Et	Ethyl
FLG 29.1	Human osteoclasts and preosteoclast cells

FMOC	Fluorenylmethyloxycarbonyl
HCT-116	Human colon cancer cells
HMBC	Heteronuclear Multiple Bond Correlation
HOBT	Hydroxybenzotriazole
HOMO	Highest Occupied Molecular Orbital
HPLC	High Performance Liquid Chromatography
HSQC	Heteronuclear Single Quantum COSY
HT-29	Colon Adenocarcinoma Cells
Ile	Isoleucine
im	Imidazole
ind	Indazole
IR	infrared
Leu	Leucine
LUMO	Lowest Unoccupied Molecular Orbital
MCF-7	Breast Cancer Cells
MDA-MB-231	Human Mammary Carcinoma Cell Lines
Me	Methyl
MLCT	Metal Ligand Charge Transfer
mpp	4-methyl-2-(2′-pyridyl)pyrimidine
MTT	3-(4,5-dimethylthiazol-2-yl)-2,5-diphenyltetrazolium bromide
NMR	Nuclear Magnetic Resonance
NOESY	Nuclear Overhauser Spectroscopy
NT	Neurotensin
PACT	Photoactivated Chemotherapy
PDT	Photodynamic Therapy
phen	1,10-phenanthroline
Pro	Proline
PS	Photosensitizer
PT-45	Pancreatic Cancer Cells
PTA	1,3,5-triaza-7-phosphoadamantane
$PTAH^+$	Protonated PTA
PTAO	PTA oxide
py	Pyridine
PyBOP	benzotriazol-1-yl-oxytripyrrolidinophosphonium hexafluorophosphate
RAPTA	Ruthenium-Arene-PTA

RNase A	Ribonuclease A
ROS	Reacting Oxygen Species
SPPS	Solid Phase Peptide Synthesis
TBTU	O-(Benzotriazol-1-yl)-N,N,N',N'-tetramethyluronium tetrafluoroborate
TFA	Trifluoracetic Acid
TON	Turnover Number
tpy	2,6-bis(2-pyridyl)pyridine
Tyr	Tyrosine

CHAPTER 1

Introduction

1.1 Metal Conjugates

Recent years have witnessed a growing interest in the use of metal conjugates in several fields. In general, a metal conjugate (Figure 1.1) is a complex molecule in which an organometallic or coordination compound is attached through a linker to an organic macromolecule, usually with a high molecular weight.

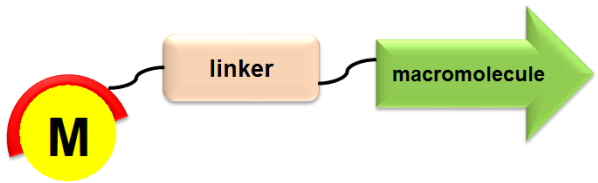

Figure 1.1. Schematic structure of a metal conjugate.

In the preparation of metal conjugates, the linker is a molecule that connects the metal compound to the organic macromolecule; in particular, the linker is often a bifunctional chelating agent, that is a molecule with two functional groups – which typically point in opposite directions – that binds both the organic molecule through an organic bond and coordinates the metal fragment (Figure 1.1). Since the metal coordination has to be stable in both kinetic and thermodynamic terms, chelating fragments are often used for this purpose.[1,2] Between the linker and the functional groups appropriate spacers can be introduced. Typically, the coordination of the metal to the chelating part of the linker represents the last step in the sequence of reactions that lead to the construction of the conjugate.

A typical example of linker is 4′-methyl-2,2′-bipyridine-4-carboxylic acid (bpyAc), a diimine chelating ligand that allows for the formation of a covalent bond through the carboxylic group in position 4, i.e. in the opposite direction compared to the metal coordination (Figure 1.2).

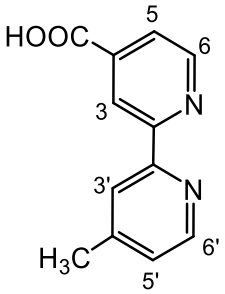

bpyAc

Figure 1.2. Structure of 4′-methyl-2,2′-bipyridine-4-carboxylic acid.

In particular, in the group where I did my Ph D Thesis, there is a deep interest towards developing conjugates between porphyrins and metal complexes with potential applications in several fields: medicinal inorganic chemistry, supramolecular chemistry, and photo-catalysis. In general, porphyrins have several appealing features: a rigid and planar geometry; a large, flat and aromatic surface; inherent symmetry; intense electronic absorption bands in the visible region; a relatively long fluorescence decay time, and facile tunability of their optical and redox properties by metallation/functionalization.[3] In particular, 4′-*meso*-pyridylphenylporphyrins (4′PyPs) are extensively used in the group as building blocks for the preparation of metal-conjugates. These macromolecules provide geometrically well-defined connections to as many as four metal centers by coordination of the pyridyl groups. Considering the number and relative geometry of the peripheral N(py) groups in the *meso* positions, 4'PyPs can be classified as *terminal*, *90° angular*, *linear*, *T-shaped* and *cruciform* donor building blocks (Figure 1.3).

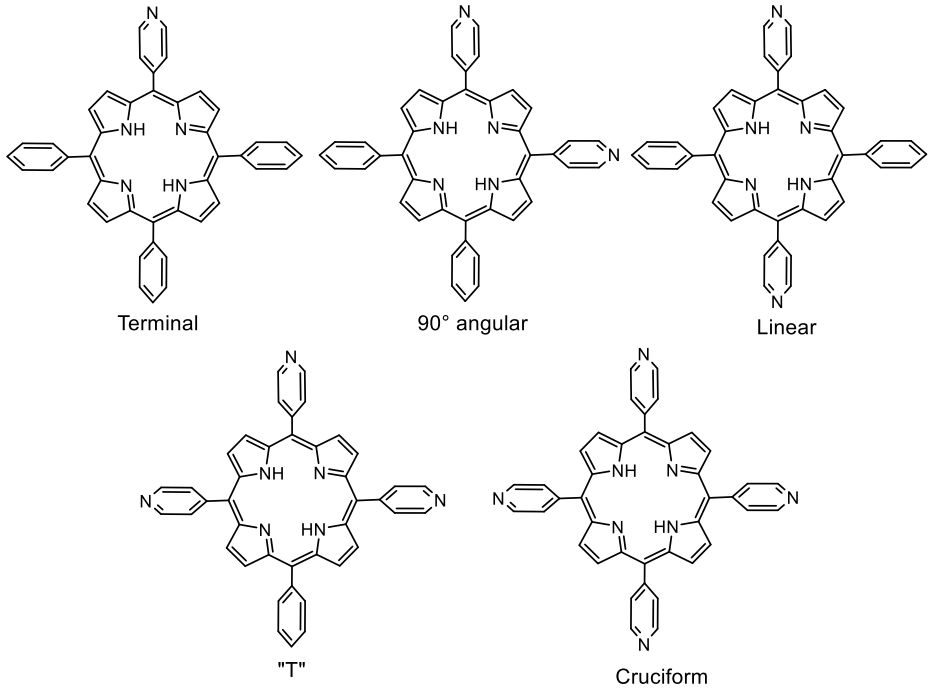

Figure 1.3. The 4′-*meso*-pyridylphenylporphyrins with their schematic building block labels.

In medicinal inorganic chemistry porphyrins, both natural and synthetic, have been widely investigated – and used – as photosensitizers (PS) in photodynamic therapy (PTD),[4,5,6] a clinically approved treatment for some skin diseases, age-related macular degeneration and some cancers. PDT uses a photosensitizer at non-toxic concentrations that, upon excitation with visible light, catalytically generates cytotoxic singlet oxygen ($^1O_2$).[7] In addition, porphyrins are studied as potential targeting molecules because, due to their preferential uptake and retention in tumor tissues, they might be capable of transporting cytotoxic metal fragments into cancer cells for synergistic affects. Functionalized porphyrins bearing from one to four peripheral bpyAc chelating moieties have been already synthesized in the group and used to prepare different metal-conjugates (an example is shown in Figure 1.4).[8,9,10] Also in the field of photo-catalysis metal conjugates with light-absorbing units are investigated for building molecular dyads and triads capable of accomplishing photo-induced charge separation (i.e. for the photocatalytic conversion of water into H_2 and

O_2 or for the photo-reduction of CO_2). There are many examples in which synthetic porphyrins are used as chromophores and the metal center is typically a Ru(II) or Re(I) complex. An example of a photo-catalyst for the reduction of CO_2 prepared in the group is shown in Figure 1.4.[11,12]

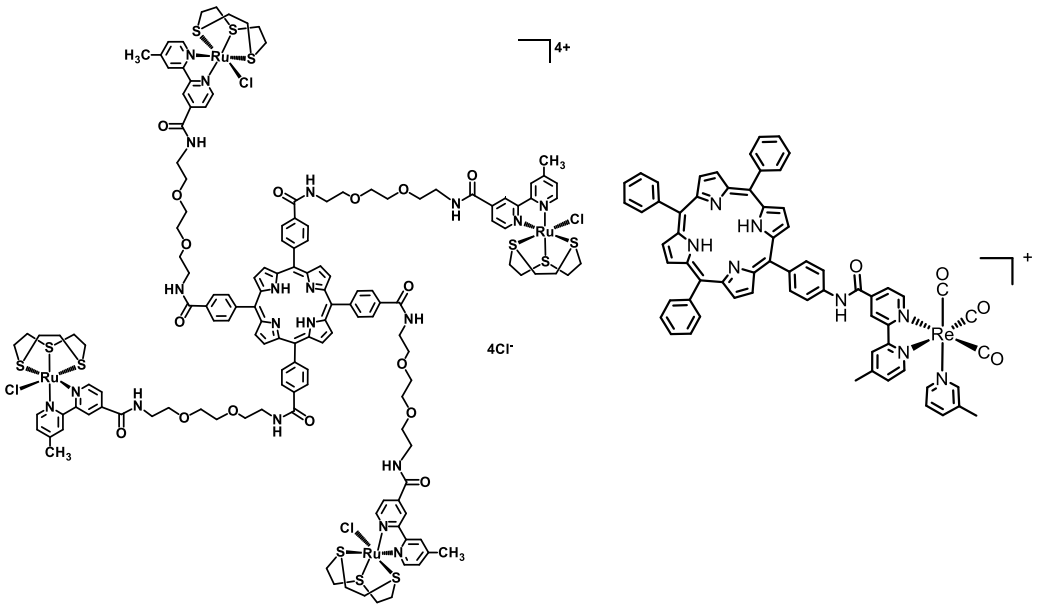

Figure 1.4. Example of a phototoxic Ru(II)-porphyrin conjugate (left) and of a Re(I)-porphyrin conjugate studied as photo-catalyst for CO_2 reduction (right).

Finally, in the field of supramolecular chemistry the group pursues the synthesis of metal-mediated multi-porphyrin assemblies. These synthetic multi-chromophore systems have the potential to behave as artificial light harvesting devices for the photoinduced energy transfer in artificial photosynthesis. In addition, cage structures are investigated for molecular recognition and supramolecular (photo)catalysis.[13]

The metal-mediated self-assembly approach, which exploits the formation of coordination bonds between peripheral basic site(s) on the porphyrins and the metal centers, has recently allowed the design and preparation in reasonable yields of increasingly sophisticated supramolecular architectures.[14,15] Depending on whether the metal centers of the acceptor building blocks belong to other porphyrins or to

coordination compounds, very different discrete ordered architectures can be constructed (Scheme 1.1).

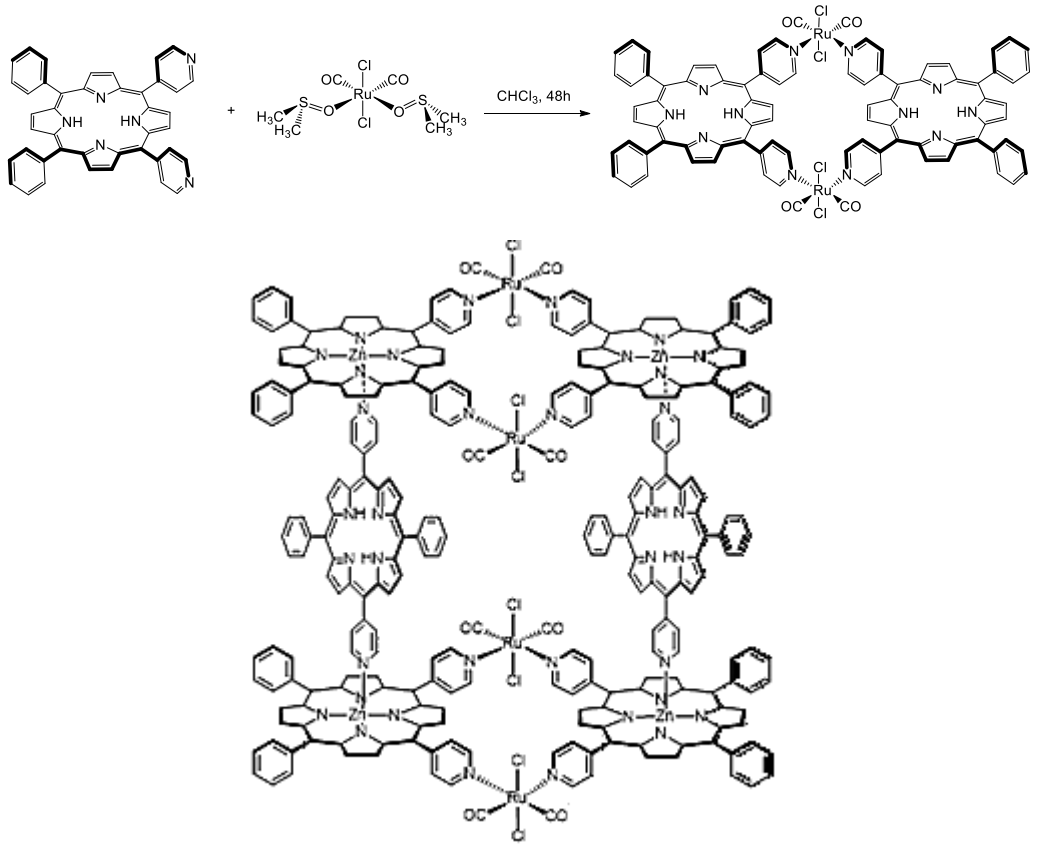

Scheme 1.1. Examples of a 2+2 molecular square of porphyrins (top) prepared from the reaction between *trans,cis,cis*-$RuCl_2(CO)_2(dmso\text{-}O)_2$ and 4′-*cis*-dipyridilporphyrin, and a 2:2 sandwich structure (bottom) formed by two zincated molecular squares and two connecting 4′-*trans*-dipyridilporphyrin.[16]

In all the above mentioned applications, water solubility is of paramount importance. However, since synthetic porphyrins have essentially a hydrophobic nature, suitable strategies must be developed for attaining some solubility in water (or at least in compatible solvents such as DMSO or alcohols). A commonly adopted approach involves the functionalization of the porphyrins with water-solubilizing moieties, either neutral or charged. Since we are dealing with porphyrin-metal conjugates or metal-mediated supramolecular assemblies of porphyrins, we thought that it might

be possible to introduce water solubility by an appropriate choice of the supporting (or ancillary) ligands in the metal fragments. For this reason, we are particularly interested to the design and synthesis of suitable Ru(II) precursors for the preparation of water-soluble ruthenium-porphyrin conjugates. In this context, the leaving ligands in the ideal metal precursor need to match either the number and geometry of 4'PyPs used for the construction of the supramolecular assembly or the binding preferences of the bifunctional linker used for connecting the porphyrin(s) (Scheme 1.2).

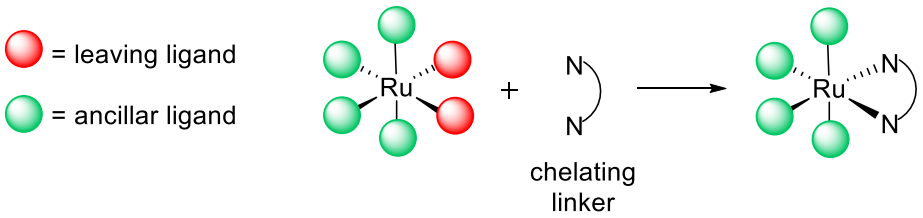

Scheme 1.2. Schematic representation of a Ru(II) precursor with leaving ligands in *cis* geometry that allows the coordination of a chelating linker.

Our approach is that of using the residual coordination sites of the ruthenium precursors (those not used by the linker or by the 4'PyPs) for attaching inert ancillary ligands that give high water solubility to the complex and – as a consequence – also of the conjugates.

Moreover it is highly desirable that the metal precursors generate highly symmetrical fragments in order to minimize the formation of stereoisomers when bound to the linker.

In the past, my group has largely exploited Ru(II)-dmso, Ru(II)-dmso-CO,[17,18,19] and Ru(II)-[9]aneS$_3$ ([9]aneS$_3$ = 1,4,7-trithiacyclononane) complexes as precursors for the preparation of ruthenium-porphyrin conjugates and supramolecular assemblies.[8,10,20,21] Nevertheless, most of them – even though well behaved in terms of reactivity – did not provide sufficient solubility in water.

To improve water solubility we decided to prepare new Ru(II) precursors introducing in the coordination sphere one or more highly water-soluble 1,3,5-triaza-7-phosphoadamantane (PTA) supporting ligands.[19,22]

1.2 1,3,5-triaza-7-phosphaadamantane (PTA)

The cage-like phosphine 1,3,5-triaza-7-phosphaadamantane (PTA, Figure 1.5), first reported in 1974 by Daigle and co-workers,[23] is an amphiphilic, air-stable, neutral monodentate ligand that – besides dissolving in several organic solvents – is characterized by a high solubility in water (ca. 235 g/L) by virtue of H-bonding to the tertiary amine nitrogens.

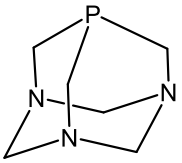

Figure 1.5. Schematic structure of PTA.

The coordination chemistry of PTA has been thoroughly reviewed by Peruzzini and co-workers.[24] It typically binds strongly to metal ions through the P atom in a monodentate fashion. It has moderate steric demand (cone angle 103°), good σ- and π-bonding abilities (comparable to those of $P(OMe)_3$) and, above all, it typically imparts excellent water solubility to its complexes.

This ligand is commercially available at moderate cost but it can be synthesized in two different ways: by the condensation of trishydroxymethylphosphine with formaldehyde and hexamethylenetetramine in ice-water (Scheme 1.3, route a) or by using a solution of ammonia and formaldehyde in place of hexamethylenetetraamine (Scheme 1.3, route b).[23a]

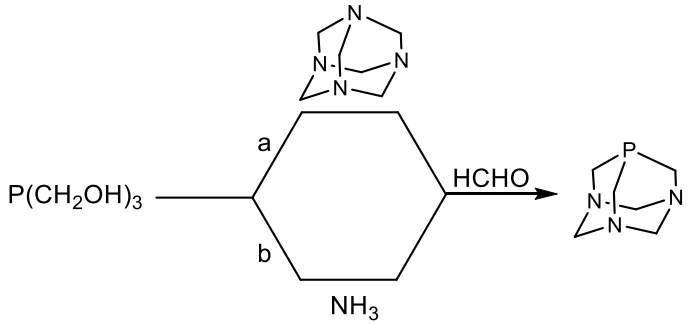

Scheme 1.3. Synthesis of PTA.

Using $H_2N(CH_2)nNH_2$ (n = 0, 2 and 6) instead of ammonia, various PTA-related compounds, bearing differently sized spacers between the nitrogen groups, have been prepared by Majoral and co-workers (Figure 1.6).[25,26]

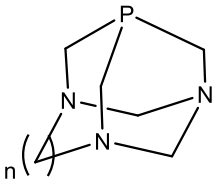

Figure 1.6. PTA-related compounds prepared using $H_2N(CH_2)nNH_2$ (n = 0, 2 and 6) instead of formaldehyde.

PTA can be *N*-alkylated rather easily at one nitrogen atom using MeI,[27] EtI,[28] $PhCH_2Cl$,[29,30] or $I(CH_2)_4I$[31] in refluxing acetone or methanol (Figure 1.7). The resulting alkyl salts $PTA(R)^+X^-$ (R = alkyl, X = Cl, I) are air and water stable. However, consistent with their ionic character, they are less soluble in organic solvents than PTA.[23b,27] Nevertheless, high solubility in water is maintained except when the anion is PF_6^-. The *N*-alkylated PTA salts, similarly to PTA, bind to transition metal through the phosphorus donor atom.

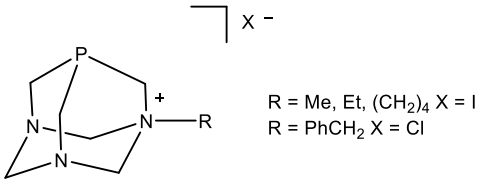

Figure 1.7. *N*-alkylated PTA.

At moderately acidic pH (pK_a = 5.89)[32] the regioselective protonation of one N atom – to generate $PTAH^+$ – occurs. Experimental data and *ab initio* calculations show that a further protonation of $PTAH^+$ is thermodynamically less favorite. The pK_a decreases after the coordination of the ligand to a metal center (in Ru(II) complexes pK_a has a value of ca 3).[33,34] Also the oxidation of the phosphorus atom decreases the basicity of nitrogen atoms: the pK_a of PTA oxide, PTAO, is 2.52.[24a]

The ^{1}H NMR spectrum of free PTA shows two resonances of 6H each. Usually, NCH_2P protons have a chemical shift between 3.9 and 4.1 ppm, while NCH_2N

protons are downfield shifted at 4.5 – 4.6 ppm. The chemical shift and multiplicity of signals are solvent-dependent: Figure 1.8 shows that in $CDCl_3$ the resonance at higher frequency appears as a broad singlet at 4.61 ppm, whereas in D_2O the same NCH_2N protons give a well resolved quartet (typical of an AB spin system) centered at 4.52 ppm ($\Delta\delta_{AB} = 0.04$, $J_{AB} = 12.7$ Hz). In both solvents the resonance of NCH_2P protons appears as a doublet attributed to an AB spin system with a small J_{AB}.

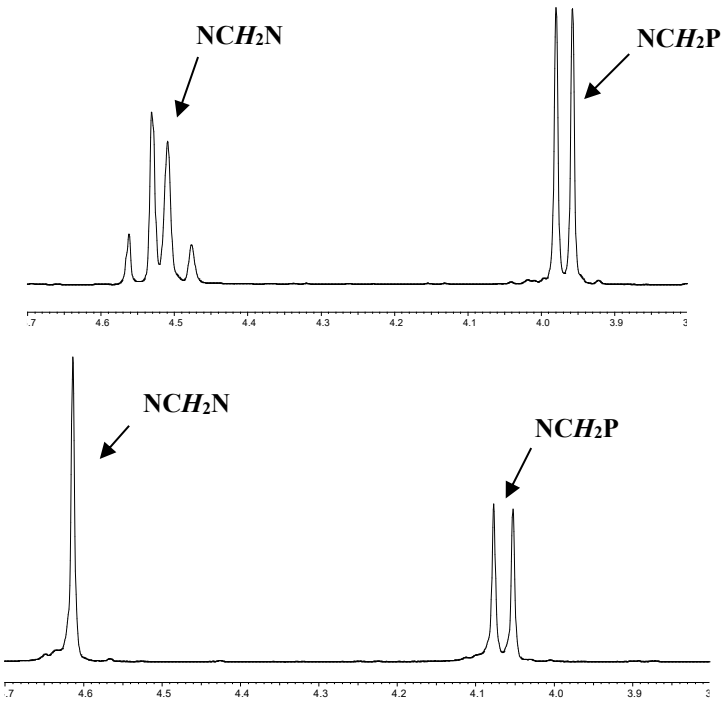

Figure 1.8. ^{1}H NMR spectra of PTA in D_2O (top) e in $CDCl_3$ (bottom).

The ^{13}C NMR spectrum of PTA in D_2O shows two different resonances: a doublet centered at 47.7 ppm ($^{1}J_{CP} = 20.1$ Hz) that belongs to PCH_2N carbons and a doublet at 70.8 ($^{3}J_{CP} = 1.3$ Hz) ppm for NCH_2N carbons.[a] The carbon resonances are not particularly affected by the nature of the solvent. Finally, the ^{31}P NMR spectrum shows a singlet at ca. –100 ppm. Also in this case the chemical shift is solvent depending: in CD_3OD the resonance is at –97.4 ppm, in D_2O at –98.2 ppm, in $CDCl_3$

[a] In all the Thesis it will use the abbreviation ^{13}C NMR and ^{31}P NMR instead of $^{13}C\{^{1}H\}$ and $^{31}P\{^{1}H\}$ i.e. the ^{13}C and ^{31}P NMR experiments with decoupled proton signals.

at –102.3 ppm, in DMSO-d_6 a –103.7 ppm.[24a] The coordination of PTA to diamagnetic metal centers affects strongly the ^{31}P resonance, and much less the ^{1}H and ^{13}C resonances. Usually the resonances of the NCH_2N and NCH_2P methylene protons are well resolved also for metal-bound PTA.[24]

By virtue of their solubility properties Ru-PTA complexes have been investigated as homogeneous catalysts, either directly in aqueous solution or in biphasic aqueous-organic conditions (see Chapter 1).[34,24,35,36,37]

Moreover, the solubility properties PTA-metal complexes were considered to be potentially very useful for the development of new metal anticancer drugs. In fact, metal complexes containing PTA as co-ligand are anticipated to have good solubility in water for ease of *in vitro* investigation and *in vivo* administration, whereas maintaining sufficient lipophilicity to cross cell membranes and hence enter cancer cells. Finally, PTA appears to be a quite safe molecule in terms of toxicity. Indeed, several Ru compounds containing PTA as supporting ligand have been investigated as potential anticancer drugs.[33,38,39,40,41,42,43] Among them, the most well-known are the organometallic RAPTA-type compounds $RuCl_2(\eta^6$-arene)(PTA) (RAPTA = Ruthenium-Arene-PTA) developed by the group of Dyson (Figure 1.9),[39] but other Ru(II) compounds containing PTA have been also investigated for their anticancer[33,40,41,44] or DNA-binding[45] properties.

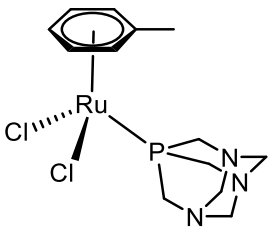

Figure 1.9. A representative example of the RAPTA compounds (RAPTA-T).

When this work started, only few Ru(II) complexes with PTA as main ligand were known, i.e. *trans*- and *cis*-$RuCl_2(PTA)_4$ (respectively **1** and **2**).[35,46] Thus, we decided to perform a systematic investigation of the reactivity of this ligand with well-known

neutral Ru(II) complexes, such as Ru-dmso and Ru-dmso-CO compounds, with the aim of preparing novel water-soluble Ru(II) complexes that might behave as suitable precursors for the synthesis of metal conjugates (Figure 1.10).[19,22,47] Chapters 2 and 3 describe in detail the results of this study.

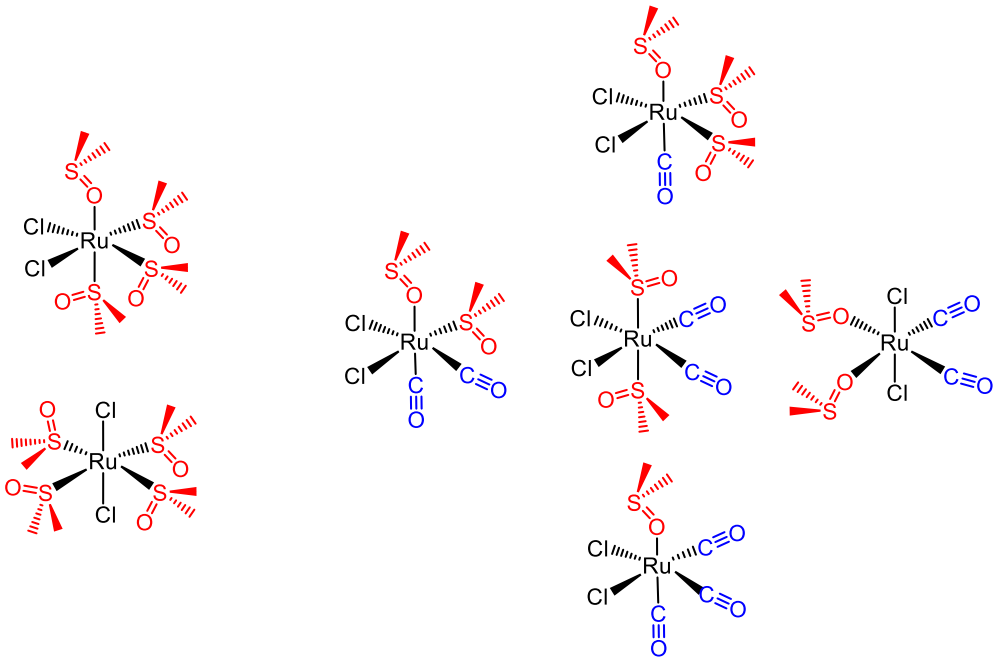

Figure 1.10. Examples of Ru(II) complexes whose reactivity with PTA was investigated: Ru-dmso (left, Chapter 2) and Ru-dmso-CO (right, Chapter 3) complexes.

Moreover, all the new compounds prepared were reacted with 2,2′-bipirydine, used as model for diimmine linkers. In some cases the reactivity with pyridine, used as model for 4'PyPs, was also investigated. These aspects are extensively described in Chapters 2 and 4 of this Thesis.

Finally, since mainly organometallic Ru(II)-PTA complexes have been tested as potential anticancer agents, an explorative investigation of the *in vitro* anticancer properties, as well as protein and DNA binding ability of *trans*- and *cis*-$RuX_2(PTA)_4$ (X = Cl, Br) and of the Ru(III)-PTA complex, *trans*-$[RuCl_4(PTAH)_2]Cl$, was performed. The results of this investigation are described in Chapter 5.

1.3 Side-Projects

In addition to the above-described main project, during the three years of Ph D I was involved in other side-projects in the field of bioinorganic chemistry, whose results are included in this Thesis. The topics of these side-projects are briefly introduced here, whereas a more exhaustive introduction will be found in the corresponding Chapters.

In particular, during a six-month stage in the group of Prof. Nils Metzler-Nolte at the University of Bochum (Germany), new Ru(II)-peptide bioconjugates with potential antitumor activity were prepared and characterized.[18]

The group of Prof. Metzler-Nolte has a consolidate experience in the preparation, characterisation and utilisation of novel metal-bioconjugates with peptides or other biomolecules. Particularly interesting is the use of receptor-binding peptides, such as neurotensin and ocreotide, an analogue of somatostatin.[48] Such peptides have a high affinity for receptors that are overexpressed in several tumors so they can be used positively to target cancer cells.[49] We decided to prepare novel bioconjugates using Ru(II) precursors prepared in Trieste and the neurotensin synthesized in Bochum. In particular, we were interested to assess the individual properties of two stereoisomeric conjugates, obtained – in principle – by linking neurotensin to the two Ru(II) complexes of the cppH linker (cppH = 2-(2′-pyridyl)pyrimidine-4-carboxylic acid) that are linkage isomers: *trans*,*cis*-$RuCl_2(CO)_2$(cppH-κN^p) and *trans*,*cis*-$RuCl_2(CO)_2$(cppH-κN^o) (Figure 1.11). Details of this project are reported in Chapter 6 and 7.

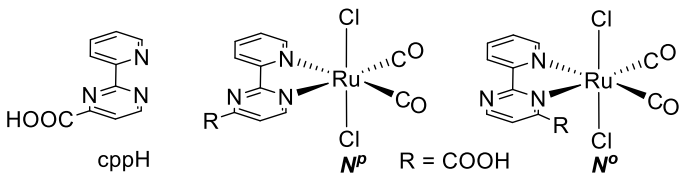

Figure 1.11. Schematic structure of cppH, and of *trans*,*cis*-$RuCl_2(CO)_2$(cppH-κN^p) (left) and *trans*,*cis*-$RuCl_2(CO)_2$(cppH-κN^o) (right).

As part of a collaborative project with the group of Dr. Anna Renfrew from the University of Sidney (Australia), we prepared a series of complexes of the type $[Ru([9]aneS_3)(chel)(py)](Cl)_2$, where chel is a chelating diimine (Figure 1.12).

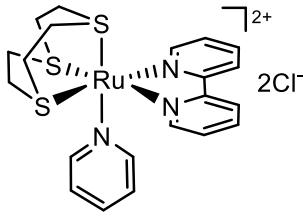

Figure 1.12. Schematic representation of complexes $[Ru([9]aneS_3)(chel)(py)](Cl)_2$ in the case of chel = bpy.

These model compounds are inert in the dark but rapidly and quantitatively release the pyridine ligand in aqueous solution when illuminated with blue light (λ = 420 nm).[21b] Since the photo-generated aqua species $[Ru([9]aneS_3)(bpy)(OH_2)]^{2+}$ showed a substantial lack of cytotoxicity (against the MDA-MB-231 human mammary carcinoma cell line) we suggested that Ru(II) compounds of this type might be suitable agents for the light-triggered release of coordinated drugs (*photo-uncaging*).[21c] This strategy belongs to the so-called *Photoactivated Chemotherapy* (PACT), a phototherapy approach in which a kinetically inert and biologically non-active prodrug is irreversibly activated by irradiation with visible light that – for example – induces the cleavage of a photolabile protecting group or an isomerization.[50]

Our aim was that of establishing if, in the future, complexes of this series, bearing a pharmacologically active molecule in the place of pyridine, can be realistically used within this strategy. Renfrew's group, in fact, is studying the photo-triggered release of CHS-828 (Figure 1.13). This cyanoguanidine, which has shown interesting properties as a potential anticancer agent, behaves also as a ligand and binds to a metal center through the pyridine moiety.[51] Chapter 8 describes the results of this project.

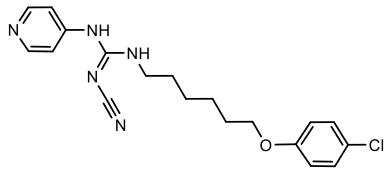

Figure 1.13. Schematic structure of CHS-828.

1.4 Bibliography

[1] M. D. Bartholoma, *Inorg. Chim. Acta*, **2012,** *389,* 36 - 51.

[2] R. Alberto, in *Bioinorganic Medicinal Chemistry* (Ed. E. Alessio), Wiley-VCH, Weinheim, Germany, **2011**, 253 - 282.

[3] a) F. Scandola, C. Chiorboli, A. Prodi, E. Iengo, E. Alessio, *Coord. Chem. Rev.*, **2006**, *250*, 1471 - 1496; b) I. Beletskaya, V.S. Tyurin, A.Y. Tsivadze, R. Guilard, C. Stern, *Chem. Rev.*, **2009**, *109*, 1659 - 1713.

[4] J. F. Norman, T. W. Hambley in *Bioinorganic Medicinal Chemistry*, (Ed: E. Alessio), Wiley-VCH, Weinheim, **2011**, 49 - 78.

[5] C. S. Cutler, H. M. Hennkens, N. Sisay, S. Huclier-Markai, S. S. Jurisson, *Chem. Rev.*, **2013**, *113*, 858 - 883.

[6] C. Spagnul, R. Alberto, G. Gasser, S. Ferrari, V. Pierroz, A. Bergamo, T. Gianferrara, E. Alessio, *J. Inorg. Biochem.*, **2013**, *122*, 57 - 65.

[7] a) T. J. Dougherty, C. J. Gomer, B. W. Henderson, G. Jori, D. Kessel, M. Korbelik, J. Moan, Q. Peng, *J. Natl. Cancer Inst.*, **1998**, *90*, 889 - 905; b) I. J. Mcdonald, T. J. Dougherty, *J. Porph. Phthalocyan.*, **2001**, *5*, 105 - 129; c) D. E. J. G. J. Dolmans, D. Fukumura, R. K. Jain, *Nat. Rev. Cancer*, **2003**, *3*, 380 - 387; d) A. Juzeniene, Q. Peng, J. Moan, *Photochem. Photobiol. Sci.*, **2007**, *6*, 1234 - 1245; e) T. Debele, S. Peng, H.-C. Tsai, *Int. J. Mol. Sci*., **2015**, *16*, 22094 - 22136.

[8] T. Gianferrara, A. Bergamo, I. Bratsos, B. Milani, C. Spagnul, G. Sava, E. Alessio, *J. Med. Chem.*, **2010**, *53*, 4678 - 4690.

[9] A. Gabrielsson, F. Hartl, H. Zhang, J. R. L. Smith, M. Towrie, J. Vicek, R. N. Perutz, *J. Am. Chem. Soc.*, **2006**, *128,* 4253 - 4266.

[10] a) T. Gianferrara, I. Bratsos, E. Iengo, B. Milani, A. Oštrić, C. Spagnul, E. Zangrando, E. Alessio, *Dalton Trans.*, **2009**, 10742 - 10756.

[11] D. Gust, T. A. Moore, A. L. Moore, *Acc. Chem. Res.*, **2009**, *42*, 1890 - 1898.

[12] a) C. D. Windle, M. V. Càmpian, A.-K. Duhme-Klair, E. A. Gibson, R. N. Perutz, J. Schneider, *Chem. Commun.*, **2012**, *48*, 8189 - 8191; b) J. Schneider, K. Q. Vuong, J. A. Calladine, X.-Z. Sun, A. C. Whitwood, M. W. George, R. N. Perutz, *Inorg. Chem.*, **2011**, *50*, 11877 - 11889.

[13] a) Y. Kobuke, *Eur. J. Inorg. Chem.*, **2006**, 2333 - 2351; b) M.-S. Choi, T. Yamazaki, I. Yamazaki and T. Aida, *Angew. Chem. Int. Ed.*, **2004**, *43*, 150 - 158; c) N. Aratani, A. Osuka, H. S. Cho and D. Kim, *J. Photochem. Photobiol.*, C, **2002**, *3*, 25 - 52.

[14] M. D. Ward, *Chem. Soc. Rev.*, **1997**, *26*, 365 - 375.

[15] For comprehensive reviews see: a) J.-C. Chambron, V. Heitz, J.-P. Sauvage, in *The Porphyrin Handbook*, (Ed. K. M. Kadish, K. M. Smith, R. Guillard, R., Academic Press, **2000**, *6*, 1 - 42. b) J. Wojaczynski, L. Latos Grazynsky, *Coord. Chem. Rev.*, **2000**, *204*, 113 - 171; c) T. Imamura, K. Fukushima, *Coord. Chem. Rev.*, **2000**, *198*, 133 - 156.

[16] E. Iengo, E. Zangrando, M. Bellini, E. Alessio, A. Prodi, C. Chiorboli, F. Scandola, *Inorg. Chem.*, **2005**, *44*, 9752 - 9762.

[17] a) E. Iengo, B. Milani, E. Zangrando, S. Geremia, E. Alessio, *Angew. Chem. Int. Ed.*, **2000**, *39*, 1096 - 1099; b) E. Iengo, E. Zangrando, R. Minatel, E. Alessio, *J. Am. Chem. Soc.*, **2002**, *124*, 1003 - 1013; c) E. Iengo, E. Zangrando, E. Alessio, *Acc. Chem. Res.*, **2006**, *39*, 841 - 851; d) E. Iengo, T. Gatti, E. Zangrando, M. T. Indelli, F. Scandola, E. Alessio, *Chem. Commun.*, **2011**, *47*, 1616 - 1618; e) E. Alessio, M. Casanova, E. Zangrando, E. Iengo, *Chem. Commun.*, **2012**, *48*, 5012 - 5015; f) E. Iengo, P. Cavigli, D. Milano, P. Tecilla, *Inorg. Chim. Acta*, **2014**, *417*, 59 - 78.

[18] F. Battistin, G. Balducci, N. Demitri, E. Iengo, B. Milani, E. Alessio, *Dalton Trans.*, **2015**, *44*, 15671 - 15682.

[19] E. Alessio, *Chem. Rev.*, **2004**, *104*, 4203 - 4242.

[20] E. Iengo, N. Demitri, G. Balducci, E. Alessio, *Dalton Trans.*, **2014**, *43*, 12160 - 12163.

[21] a) I. Bratsos, S. Jedner, A. Bergamo, G. Sava, T. Gianferrara, E. Zangrando, E. Alessio *J. Inorg. Biochem.*, **2008**, *102*, 1120 - 1133; b) G. Ragazzon, I. Bratsos, E. Alessio, L. Salassa, A. Habtemariam, R. McQuitty, G. J. Clarkson, P. J. Sadler,

Inorg. Chim. Acta, **2012**, *393*, 230 - 238; c) I. Finazzi, I. Bratsos, T. Gianferrara, A. Bergamo, N. Demitri, G. Balducci, E. Alessio, *Eur. J. Inorg. Chem.*, **2013**, 4743 - 4753.

[22] a) E. Alessio, B. Milani, M. Bolle, G. Mestroni, P. Faleschini, F. Todone, S. Geremia, M. Calligaris, *Inorg. Chem.*, **1995**, *34*, 4722 - 4734; b) E. Alessio, E. Iengo, S. Geremia, M. Calligaris, *Inorg. Chim. Acta*, **2003**, *344*, 183 - 189. c) I. Bratsos, S. Calmo, E. Zangrando, G. Balducci, E. Alessio, *Inorg. Chem.*, **2013**, *52*, 12120 - 12130.

[23] a) D. J. Daigle, A. B. Pepperman Jr., S. L. Vail, *J. Heterocycl. Chem.*, **1974**, *11*, 407 - 408; b) D. J. Daigle, *Inorg. Synth.*, **1998**, *32*, 40 - 45.

[24] a) A. D. Phillips, L. Gonsalvi, A. Romerosa, F. Vizza, M. Peruzzini, *Coord. Chem. Rev.*, **2004**, *248*, 955 - 993; b) J. Bravo, S. Bolaño, L. Gonsalvi, M. Peruzzini, *Coord. Chem. Rev.*, **2010**, *254*, 555 - 607. A. Guerriero, M. Peruzzini, L. Gonsalvi, *Coord. Chem. Rev.*, **2017**, DOI: doi.org/10.1016/j.ccr.2017.09.024

[25] J. Navech, R. Kraemer, J.-P. Majoral, *Tetrahedron Lett.*, **1980**, *21*, 1449 - 1452.

[26] M. Benhammou, R. Kraemer, H. Germa, J.-P. Majoral, J. Navech, *Phosphorus Sulfur*, **1982**, *14*, 105 - 119.

[27] D.J. Daigle, A.B. Pepperman Jr., *J. Heterocycl. Chem.*, **1975**, *12*, 579 - 580.

[28] J.M. Forward, R.J. Staples, C.W. Liu, J.P. Fackler, *Acta Cryst. C*, **1997**, *53*, 195 - 197.

[29] K.J. Fisher, E.C. Alyea, N. Shahnazarian, *Phosphorus Sulfur*, **1990**, *48*, 37 - 40.

[30] E. Fluck, J.E. Förster, J. Weidlein, E. Hädicke, *Z. Naturforsch.*, **1977**, *32*, 499 - 506.

[31] J.M. Forward, R.J. Staples, J.P. Fackler Jr., *Z. Kristallogr.*, **1996**, *211*, 129 - 130.

[32] J. Kovács, F. Joó, A. Bényei, G. Laurenzy, *Dalton Trans.*, **2004**, 2336 - 2340.

[33] B. Serli, E. Zangrando, T. Gianferrara, C. Scolaro, P. J. Dyson, A. Bergamo, E. Alessio, *Eur. J. Inorg. Chem.*, **2005**, 3423 - 3434.

[34] A. Udvardy, A. C. Bényei, Á. Kathó, *J. Organomet. Chem.*, **2012**, *717*, 116 - 122.

[35] a) D. J. Darensbourg, F. Joó, M. Kannisto,A. Katho, J. H. Reibenspies, *Organometallics*, **1992**, *11*, 1990 - 1993; b) D. J. Darensbourg, F. Joó, M. Kannisto, A. Kathó, J. H. Reibenspies, D. J. Daigle, *Inorg. Chem.*, **1994**, *13*, 200 - 208.

[36] a) G. Laurenczy, F. Joó, L. Nádasdi, J. Elek, *Chem. Commun.*, **1999**, 971 - 972; b) G. Laurenczy, F. Joó, L. Nádasdi, *Inorg. Chem.*, **2000**, *39*, 5083 - 5088; c) G. Laurenczy, F. Joó, L. Nádasdi, *High Pressure Res.*, **2000**, *18*, 251 - 255; d) G. Kovács, L. Nádasdi, G. Laurenczy, F. Joó, *Green Chem.*, **2003**, *5*, 213 - 217.

[37] W.-C. Lee, B. J. Frost, *Green Chem.*, **2012**, *14*, 62 - 66.

[38] D. N. Akbayeva, L. Gonsalvi, W. Oberhauser, M. Peruzzini, F. Vizza, P. Brueggeller, A. Romerosa, G. Sava, A. Bergamo, *Chem. Commun.*, **2003**, 264 - 265.

[39] a) C. S. Allardyce, P. J. Dyson, D. J. Ellis, S. L. Heath, *Chem. Commun.*, **2001**, 1396 - 1397; b) C. Scolaro, A. Bergamo, L. Brescacin, R. Delfino, M. Cocchietto, G. Laurenczy, T. J. Geldbach, G. Sava, P. J. Dyson, *J. Med. Chem.*, **2005**, *48*, 4161 - 4171; b) P. J. Dyson, G. Sava, *Dalton Trans.*, **2006**, 1929 - 1933; c) P. J. Dyson, *Chimia*, **2007**, *61*, 698 - 703; d) A. Bergamo, A. Masi, P. J. Dyson, G. Sava, *Int. J. Oncol.*, **2008**, *33*, 1281 - 1289; e) W. H. Ang, A. Casini, G. Sava, P. J. Dyson, *J. Organomet. Chem.*, **2011**, *696*, 989 - 998; f) C. M. Clavel, E. Paunescu, P. Nowak-Sliwinska, A. W. Griffioen, R. Scopelliti, P. J. Dyson, *J. Med. Chem.*, **2015**, *58*, 3356 - 3365; g) M. V. Babak, S. M. Meier, K. V. M. Huber, J. Reynisson, A. A. Legin, M. A. Jakupec, A. Roller, A. Stukalov, M. Gridling, K. L. Bennett, J. Colinge, W. Berger, P. J. Dyson, G. Superti-Furga, B. K. Keppler, C. G. Hartinger, *Chem. Sci.*, **2015**, *6*, 2449 - 2456; h) A. Weiss, X. Ding, J. R. van Beijnum, I. Wong, T. J. Wong, R. H. Berndsen, O. Dormond, M. Dallinga, L. Shen, R. O. Schlingemann, R. Pili, C.-M. Ho, P. J. Dyson, H. van den Bergh, A. W. Griffioen, P. Nowak-Sliwinska, *Angiogenesis*, **2015**, *18*, 233 - 244; i) B. S. Murray, M. V. Babak, C. G. Hartinger, P. J. Dyson, *Coord. Chem. Rev.*, **2016**, *306*, 86 - 114.

[40] S. Grguric-Sipka, C. R. Kowol, S.-M. Valiahdi, R. Eichinger, M. A. Jakupec, A. Roller, S. Shova, V. B. Arion, B. K. Keppler, *Eur. J. Inorg. Chem.*, **2007**, 2870 - 2878.

[41] a) A. García-Fernández, J. Díez, Á. Manteca, J. Sánchez, R. García-Navas, B. G. Sierra, F. Mollinedo, M. Pilar Gamasa, E. Lastra, *Dalton Trans.*, **2010**, *39*, 10186 - 10196; b) E. Menéndez-Pedregal, J. Díez, Á. Manteca, J. Sánchez, A. C. Bento, R.

García-Navas, F. Mollinedo, M. Pilar Gamasa, E. Lastra, *Dalton Trans.*, **2013**, *42*, 13955 - 13967.

[42] R. Pettinari, F. Marchetti, F. Condello, C. Pettinari, G. Lupidi, R. Scopelliti, S. Mukhopadhyay, T. Riedel, P. J. Dyson, *Organometallics*, **2014**, *33*, 3709 - 3715.

[43] A. Wołoszyn, C. Pettinari, R. Pettinari, G. V Badillo Patzmay, A. Kwiecień, G. Lupidi, M. Nabissi, G. Santoni, P. Smoleński, *Dalton Trans.*, **2017**, *46*, 10073 - 10081.

[44] S. Seršen, J. Kljun, K. Kryeziu, R. Panchuk, B. Alte, W. Körner, P. Heffeter, W. Berger, I. Turel, *J. Med. Chem.*, **2015**, *58*, 3984 - 3996.

[45] a) A. Romerosa, T. Campos-Malpartida, C. Lidrissi, M. Saoud, M. Serrano-Ruiz, M. Peruzzini, J. A. Garrido-Cárdenas, F. García-Maroto, *Inorg. Chem.*, **2006**, *45,* 1289 - 1298; b) A. Romerosa, M. Saoud, T. Campos-Malpartida, C. Lidrissi, M. Serrano-Ruiz, M. Peruzzini, J. A. Garrido, F. García-Maroto, *Eur. J. Inorg. Chem.*, **2007**, 2803 - 2812; c) A. García-Fernández, J. Díez, Á. Manteca, J. Sánchez, M. Pilar Gamasa, E. Lastra, *Polyhedron*, **2008**, *27,* 1214 - 1228.

[46] a) C. A. Mebi, B. J. Frost, *Inorg. Chem.*, **2007**, *46*, 7115 - 7120; b) R. Girotti, A. Romerosa, S. Mañas, M. Serrano-Rui, R. N. Perutz, *Inorg. Chem.*, **2009**, *48*, 3692 - 3698.

[47] I. P. Evans, A. Spencer, G. J. Wilkinson, *J. Chem. Soc., Dalton Trans.*, **1973**, 204 - 209.

[48] a) M. Maschke, J. Grohmann, C. Nierhaus, M. Lieb, N. Metzler-Nolte, *ChemBioChem*, **2015**, *16*, 1333 - 1342; b) A. Gross, D. Habig, N. Metzler-Nolte, *ChemBioChem*, **2013**, *14*, 2472 - 2479.

[49] M. De Jong, W.A Breeman,W. H. Bakker, P. P. Kooij, B. F. Bernard, L. J. Hofland, T. J. Visser, A. Srinivasan, M. A.Schmidt, J. L. Erion, J. E. Bugaj, H. R. Mäcke, E. P. Krenning, *Cancer Res.*, **1998**, *58*, 437 - 441.

[50] G. Mayer, A. Heckel, *Angew. Chem. Int. Ed.*, **2006**, *45*, 4900 - 4921.

[51] a) C. Schou, E. R. Ottosen, F. Bjorkling, S. Latini, P. V. Hjarnaa, E. Bramm, L. Binderup, *Bioorg. Med. Chem. Lett.*, **1997**, *7*, 3095 - 3100; b) P. J. Hjarnaa, E. Jonsson, S. Latini, S. Dhar, R. Larsson, E. Bramm, T. Skov, L. Binderup, *Cancer*

Res., **1999**, *59*, 5751 - 5757; c) E. Jonsson, L. E. Friberg, M. O. Karlsson, S. B. Hassan, P. Nygren, J. Kristensen, B. Tholander, L. Binderup, R. Larsson, *Cancer Lett.*, **2001**, *162*, 193 - 200; d) A. Aleskog, S. Bashir-Hassan, P. Hovstadius, J. Kristensen, M. Hoglund, B. Tholander, L. Binderup, R. Larsson, E. Jonsson, *Anticancer Drugs*, **2001**, *12*, 821 - 827.

CHAPTER 2

Part of this Chapter was published in: F. Battistin, G. Balducci, E. Iengo, N. Demitri, E. Alessio, *Eur. J. Inorg. Chem,* **2016**, 2850–2860

Neutral Ru(II) complexes with PTA

2.1 State of the art

When we started this work, in the literature there were only few examples of Ru(II) complexes in which PTA is the main ligand and not simply a co-ligand. Darensbourg's group was the first to report in 1992 the synthesis of the complex $RuCl_2(PTA)_4$, that precipitated in high yield when hydrate $RuCl_3$ was treated with an excess of PTA in refluxing ethanol (Scheme 2.1).[1] The complex, based on the X-ray structure of crystals obtained by recrystallization of the raw product from water, had a *cis* geometry. However, in that paper there was an incongruence between the single-crystal X-ray structure of the complex and the NMR data in solution. In fact, the ^{31}P NMR spectrum showed only a singlet, whereas for a *cis* compound an A_2X_2 system, composed by two triplets of same intensity, is expected. The information if the ^{31}P NMR spectrum had been recorded on the raw material or on the crystals was missing also in a subsequent 1994 publication from the same group. Afterwards (2007) Mebi and Frost reported that the synthesis proposed by Darensbourg's group actually led to the formation of the *trans* isomer, *trans*-$RuCl_2(PTA)_4$ (**1**), in agreement with the spectroscopic data reported in both papers.[2] The geometry of the complex was also confirmed by an X-ray structure performed on single crystals obtained by recrystallization of the raw product from a dichloromethane solution. The conflicting results of Darensbourg's group were caused by the instability of **1** in water, that slowly isomerizes to the *cis* isomer, *cis*-$RuCl_2(PTA)_4$ (**2**) at room temperature. In conclusion, whereas **2** is the thermodynamically stable isomer, **1** is the kinetic product of the reduction of hydrate $RuCl_3$ in the presence of PTA.

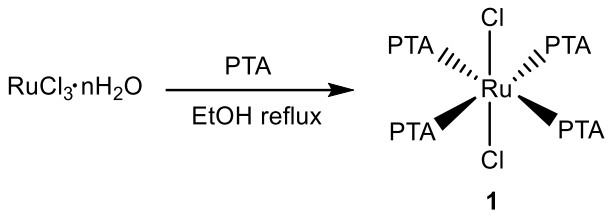

1

Scheme 2.1. Preparation of *trans*-$RuCl_2(PTA)_4$ (**1**).

The X-ray structures of the two isomers show that the Ru–Cl bond lengths in **1** are equal (2.437(2) Å) and shorter than those in **2** (2.488(2) Å e 2.503(2) Å). The Ru–P bond distances in **1** are between 2.317(2) and 2.353(2) Å, i.e. shorter than that of the mutually *trans* PTAs in **2** (2.370(2) Å) and longer than that of PTA *trans* to Cl (2.260(2) Å).

Finally, Darensbourg's group reported also the single-crystal X-ray structure of the Ru(III) complex *trans*-$[RuCl_4(PTAH)_2]Cl$ (**3**) (PTAH = protonated PTA), obtained in small amount upon recrystallization of **1** from 0.1M HCl (Figure 2.1).[1b] The structure shows that the two mutually *trans* PTAs have a protonated nitrogen: the protonation causes an elongation of the corresponding N–C distances. In fact, the average NH^+–C bond length (1.520(8) Å) is slightly longer than that of the other six N–C bonds (1.462(8) Å). According to the Authors, compound **3** could derive from two processes: adventitious air oxidation of **1** during prolonged crystal growing experiments and incomplete reduction of Ru(III) in the initial preparation.

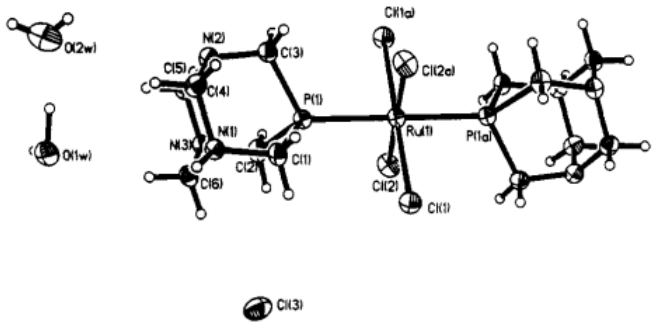

Figure 2.1. X-ray molecular structure of *trans*-$[RuCl_4(PTAH)_2]Cl$ (**3**).[1b]

According to Mebi and Frost, the partial isomerization from *trans*- to *cis*-$RuCl_2(PTA)_4$ occurs (slowly) also in $CDCl_3$ at room temperature and was followed by ^{31}P NMR spectroscopy: in a few days the singlet of **1** decreased in intensity in favor of the two new triplets of **2**. Equilibrium between the two isomers was reached in a week (*cis*/*trans* ratio ≈ 1.84). Afterwards, Romerosa and coworkers found that **1** is stable in $CDCl_3$ if protected from light: its ^{31}P NMR spectrum remained unchanged for 25 days.[3] The same group studied the effect of visible light on the interconversion of the two isomers.[2] According to their findings, **1** (yellow) isomerizes rapidly and completely to **2** (pale yellow) by irradiation of a chloroform solution with visible light ($\lambda > 416$ nm), whereas the reverse isomerization occurs by irradiation of a chloroform solution of **2** with light at $\lambda = 367$ nm (Scheme 2.2).

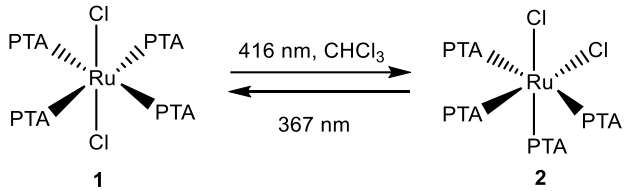

Scheme 2.2. Light-induced interconversion of *trans*-$RuCl_2(PTA)_4$ (**1**) and *cis*-$RuCl_2(PTA)_4$ (**2**).

Conversely, the light-induced isomerization of **1** in water was found to be irreversible, no back-isomerization occurred when an aqueous solution of **2** was irradiated at $\lambda = 367$ nm.

By virtue of their very good solubility in water, *trans*- and *cis*-$RuCl_2(PTA)_4$ have been used as catalyst precursors in several reactions in aqueous solution or in biphasic systems (very often without specifying which isomer was being employed).[4,5,6,7] Compound **1** was used for hydrogenation of various aldehydes and substituted benzaldehydes into alcohols in aqueous-organic biphasic systems with conversions from 95% (for benzaldehyde) to 23.6% (for 2-methoxybenzaldehyde).[1b,4,8,9] Recently, this compound was also used for nitrile hydration to amides in water with high conversion (99% for different substrates).[7]

Laurency and coworkers found that **1** shows moderate activity in the reduction of CO_2 and HCO_3^- to formic acid in water. More recently the same group found that **1** catalyzes the direct hydrogenation of CO_2 to HCOOH in DMSO without any additive, with a TON = 159 at 60°C (TON = Turnover Number).[10]

Very recently the group of Romerosa reported the synthesis of other Ru(II) derivatives with PTA. The complex *trans,mer*-$RuCl_2(OH_2)(PTA)_3$ (**4**) was obtained by the reaction between $RuCl_2(PPh_3)_3$ and 3 eq of PTA.[11] The ^{31}P NMR spectrum in D_2O of **4** consists in an AX_2 system with a triplet centered at –5.1 ppm for the PTA *trans* to OH_2 and a doublet at –46.8 ppm ($^2J_{P\text{-}P}$ = 34.6 Hz) for the two mutually *trans* PTAs.

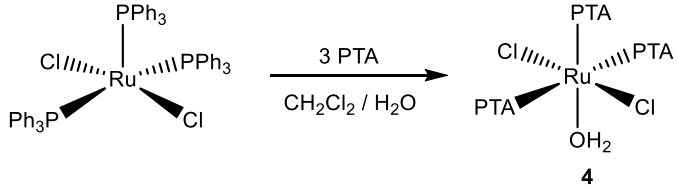

4

Scheme 2.3. Preparation of *trans,mer*-$RuCl_2(OH_2)(PTA)_3$ (**4**).[11]

When **4** is treated in aqueous solution with 1 eq of PTA the weakly bound water molecule is replaced yielding *trans*-$RuCl_2(PTA)_4$ (**1**), whereas when the solution is heated at reflux or irradiated with an halogen lamp the dinuclear species [{$Ru(PTA)_3$}$_2$($\mu Cl)_3$]Cl (**5**) is obtained (Scheme 2.4). The ^{31}P NMR spectrum of this complex in D_2O shows a singlet at –14.6 ppm. The structure is confirmed by X-ray quality crystals obtained by layering 2-propanol on an aqueous solution of the complex.

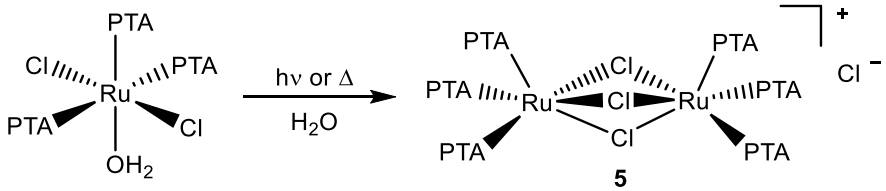

5

Scheme 2.4. Preparation of the dimer [{$Ru(PTA)_3$}$_2$($\mu Cl)_3$]Cl (**5**).

Dissolution of *trans,mer*-$RuCl_2(OH_2)(PTA)_3$ (**4**) in a 1M HCl solution results in protonation of all PTA ligands yielding *mer*-$[RuCl_3(PTAH)_3](Cl)_2$ (**6**). The ^{31}P NMR in D_2O shows the signals of *mer*-$[RuCl_3(PTAH)_3]^{2+}$ in equilibrium with those of the aqua species *trans,mer*-$[RuCl_2(OH_2)(PTAH)_3]^{3+}$ (**6aq**). In fact, the spectrum presents two AX_2 systems in ca. 2/1 ratio. The main set (a triplet centrered at –4.6 ppm for the PTAH *trans* to Cl, and a doublet at –40.6 ppm ($^2J_{P\text{-}P}$ = 33.3 Hz) for the two mutually *trans* PTAHs) was attributed to *mer*-$[RuCl_3(PTAH)_3]^{2+}$, while the minor set (a triplet centered at –2.3 ppm for the PTAH *trans* to OH_2, and a doublet at –36.3 ppm ($^2J_{P\text{-}P}$ = 35.6 Hz) for the mutually *trans* PTAHs) was attributed to the aqua species *trans,mer*-$[RuCl_2(OH_2)(PTAH)_3]^{3+}$. X-ray quality crystals, obtained by diffusion of 2-propanol to a 1M HCl solution of **6**, confirmed the proposed structure, i. e. *mer*-$[RuCl_3(PTAH)_3](Cl)_2$ (**6**).

Romerosa's group reported also that when irradiated with visible light in aqueous solution **6** isomerizes to *fac*-$[RuCl_3(PTAH)_3](Cl)_2$ (**7**) that precipitates as X-ray quality crystals (Scheme 1.4).

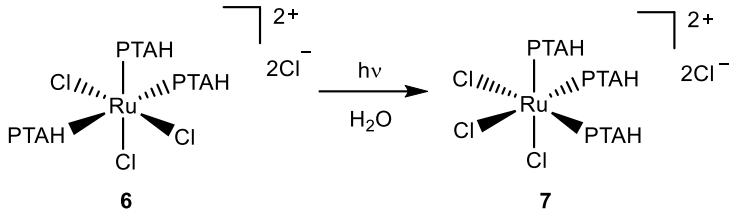

6 **7**

Scheme 2.5. Light-induced interconversion of *mer*-$[RuCl_3(PTAH)_3](Cl)_2$ (**6**) to *fac*-$[RuCl_3(PTAH)_3](Cl)_2$ (**7**).

Also the *fac*- isomer in D_2O is in equilibrium with the aqua species; in fact the ^{31}P NMR spectrum presents a singlet at –12.8 ppm for the three equivalent PTAHs *trans* to Cl of **7** and an AX_2 system consisting of a triplet at –4.6 ppm and a doublet at –12.5 ppm ($^2J_{P\text{-}P}$ = 36.5 Hz) for the aqua species, **7aq**.

2.2 Aim of the Chapter

The reactivity of **1** and **2** was largely unexplored. For this reason, we decided to investigate if they might be exploited as precursors for the preparation of water-soluble conjugates.

This Chapter reports a thorough investigation of the chemical behavior of the isomers **1** and **2** in water and other coordinating solvents, as well as of their reactivity towards 2,2'-bipyridine (bpy), used as a model for chelating diimine linkers (i.e. cppH and bpyAc – Figure 2.2).

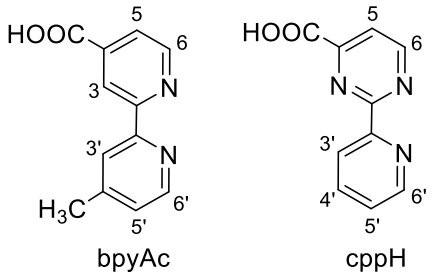

Figure 2.2. Diimine linkers bpyAc (left) and cppH (right) with proton numbering scheme.

Such linkers might allow us to connect a $\{RuCl_x(PTA)_y\}$ fragment (x = 0-2, y = 2-4, x+y = 4) to an appropriately functionalized vector (e.g. a porphyrin) through the formation of an amidic or esteric bond.[12,13]

In addition, the reactivity of the well-known Ru(II)-Cl-dmso isomers *cis*-$RuCl_2(dmso)_4$ (**8**) and *trans*-$RuCl_2(dmso\text{-}S)_4$ (**9**) (Figure 2.3) towards PTA was also investigated. In fact, an ideal precursor for the preparation of conjugates might have one or more PTAs as co-ligands for solubility and one or more dmso ligands (with appropriate geometry) for facile replacement by the linker.

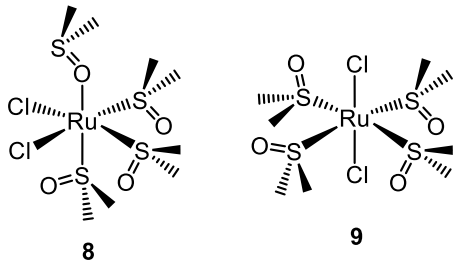

Figure 2.3. Schematic structures of *cis*-$RuCl_2(dmso)_4$ (**8**) and *trans*-$RuCl_2(dmso\text{-}S)_4$ (**9**).

Complex **8** is an extremely versatile compound since, depending on the reaction conditions, it can replace the relatively labile dmso ligands or chlorides, or both – completely or partially – with neutral or anionic ligands. In addition, it is easily prepared with high yield and purity and has a good solubility in many solvents, from water to chloroform. For these reasons, it is widely used as precursor for the synthesis of Ru(II) complexes.[14] The *trans* isomer **9** is similarly well-behaved, but has been much less explored.

Usually, neutral nitrogen ligands (*N*) replace from one to four dmso's of **8** depending on their nature and reaction conditions. The O-bonded dmso is the most labile ligand and can be selectively replaced by strong σ-donor ligands (i.e. NH_3 or pyridine) in mild conditions, yielding mono-substituted complexes *cis,fac*-$RuCl_2$(dmso-S)$_3$(*N*). By increasing the reaction temperature and the stoichiometric ratio it is possible to obtain di-substituted derivatives, whose geometry can be either *trans,cis,cis*-$RuCl_2$(dmso-S)$_2$(*N*)$_2$ or *cis,cis,cis*-$RuCl_2$(dmso-S)$_2$(*N*)$_2$, depending on the conditions. On the other hand, **9** selectively reacts with monodentate nitrogen ligands (*N*, i.e. NH_3, pyridine, imidazole) in mild conditions (at room temperature) leading to di-substituted *trans,cis,cis*-$RuCl_2$(dmso-S)$_2$(*N*)$_2$ derivatives exclusively.

In the literature there are not many examples of the reactivity of **8** and **9** with monodentate phosphines and usually they are quite dated.[14] As better detailed below, only recently Kathó and coworkers studied the reactivity of **8** with 2 eq of PTA in chloroform affording *cis,cis,trans*-$RuCl_2$(dmso-S)$_2$(PTA)$_2$ (**10**).[15]

We confirmed and expanded these results,[15] and investigated the yet unexplored reactivity of **10** towards imine ligands and 4′-*meso*-pyridylphenylporphyrins since this complex, by virtue of the presence of two potentially labile ligands (the dmso's), seems to be a promising precursor for the synthesis of water-soluble conjugates.

2.3 *trans*-$RuCl_2(PTA)_4$ (1) and *cis*-$RuCl_2(PTA)_4$ (2)

The complex *trans*-$RuCl_2(PTA)_4$ (**1**) was prepared as described in the literature (Scheme 2.6).[1]

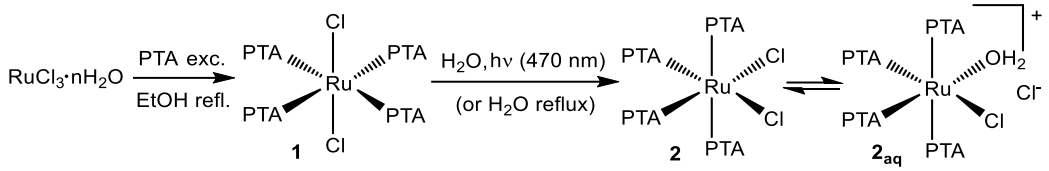

Scheme 2.6. Preparation of isomers **1** and **2**.

In our hands, the best synthetic procedure for the preparation of **2** was irradiation of an aqueous solution of **1** with blue light (λ = 470 nm) for 1 h.[3] Evaporation of the solvent afforded pure **2** quantitatively (according to NMR analysis). The isomerization of **1** could be performed also thermally, by heating to reflux the aqueous solution (1h). However, according to the ^{31}P NMR spectrum, the thermal reaction was not as clean as the photochemical one, leading to the formation of by-products, including PTA oxide (PTAO),[16] characterized by a sharp singlet at δ = –2.1 ppm in the ^{31}P NMR spectrum.

A complete, and yet missing, NMR characterization of **1** and **2** is reported in Table 2.1 (in D_2O) and Table 2.2 (in $CHCl_3$). The ^1H and ^{31}P NMR spectra of **1** in $CDCl_3$ are quite straightforward, due to the high symmetry of the complex. The ^{31}P NMR spectrum of **2**, consistent with the A_2X_2 spin system, presents two equally intense triplets at δ = –24.1 and –59.4 ppm ($^2J_{P\text{-}P}$ = 28.6 Hz). Based on the spectrum of **1** (Table 2.2) and literature data,[4] the most shielded triplet was assigned to the pair of mutually *trans* PTA ligands. The ^1H NMR spectrum of **2** in $CDCl_3$ (that, contrary to what reported, is considerably less soluble than **1** in this solvent),[3] never described before, is more complex and consists of two relatively broad singlets (12H each) at δ = 4.04 and 4.47 ppm, and of a multiplet (24H) centered at δ = 4.48 ppm (Appendix, A2.1). The singlets (or better, unresolved multiplets) belong to the NC*H*$_2$P groups of the two pairs of equivalent PTA ligands: in fact, in the ^1H-^1H COSY spectrum they

are both coupled to the multiplet (generated by the NCH_2N groups), whereas in the ^{1}H-^{13}C HSQC spectrum (Appendix, A2.2) they have distinct crosspeaks with carbon atoms that resonate in the NCH_2P region (Table 2.2). Thus, both the ^{1}H and ^{13}C resonances of the NCH_2P groups are sensitive to the PTA position in the complex. An ^{1}H-^{31}P HMBC spectrum (Figure 2.4) allowed us to assign unambiguously the two NCH_2P singlets in the ^{1}H NMR spectrum, that are pairwise related to the two triplets in the ^{31}P dimension. The shielded singlet – that has a crosspeak with the ^{31}P triplet at δ = –24.1 ppm – was assigned to the PTAs *trans* to Cl, and the other to the mutually *trans* PTA ligands.

Using hydrate $RuBr_3$ as precursor and the same synthetic procedures described above, the corresponding – and unprecedented – bromo complexes *trans*-$RuBr_2(PTA)_4$ (**11**) and *cis*-$RuBr_2(PTA)_4$ (**12**) were isolated in good yields and fully characterized. The ^{1}H and ^{31}P NMR features of **11** and **12** and their chemical behavior in aqueous solution are similar to those of the corresponding chloro compounds (Table 2 and 2 – D_2O and $CHCl_3$ respectively, see also Appendix, A2.7-A2.10).[1,2,3]

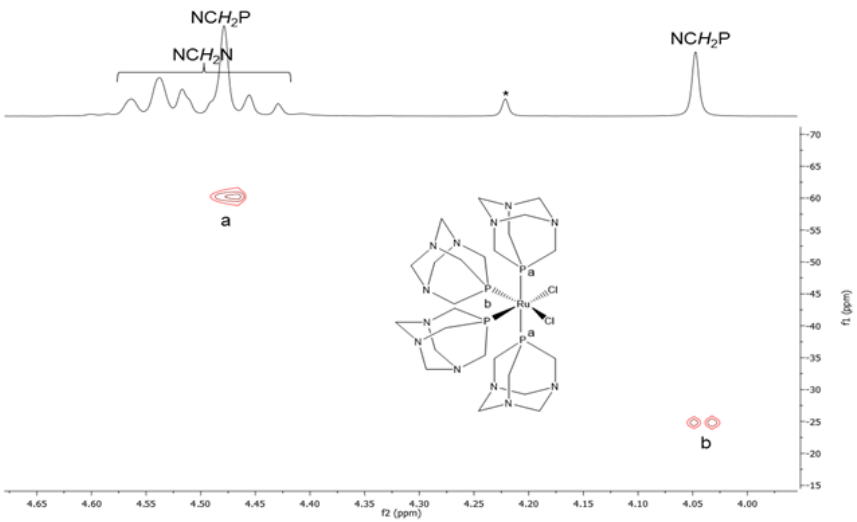

Figure 2.4. ^{1}H-^{31}P HMBC NMR spectrum in $CDCl_3$ of *cis*-$RuCl_2(PTA)_4$ (**2**) with ^{2}J = 5Hz. The peak marked with an asterisk belongs to a minor unidentified impurity.

Table 2.1. ^{1}H, ^{13}C, ^{31}P NMR characterization (δ, ppm; *J*, Hz) of *trans*-$RuCl_2(PTA)_4$ (**1**), *cis*-$RuCl_2(PTA)_4$ (**2**), *cis*-$[RuCl(OH_2)(PTA)_4]^+$ (**2aq**), *trans*-$RuBr_2(PTA)_4$ (**11**), *cis*-$RuBr_2(PTA)_4$ (**12**) and *cis*-$[RuBr(OH_2)(PTA)_4]^+$ (**12aq**), in D_2O.

	^{1}H (*J*)	**$^{13}C\{^{1}H\}$**	**$^{31}P\{^{1}H\}$ (*J*)**	**Solvent**
trans-$RuCl_2(PTA)_4$ (**1**)	4.63, br s, 24H, NC*H*$_2$N	70.8 N*C*H$_2$N	–49.6, s, mutually *trans* PTAs	D_2O
	4.35, br s, 24H, NC*H*$_2$P	50.8 N*C*H$_2$P		
cis-$RuCl_2(PTA)_4$ (**2**)	4.65, m, 24H, NC*H*$_2$N	n.d.	–21.6, t, (28.5) PTAs *trans* to Cl	D_2O*
	4.47, br s, 12H, NC*H*$_2$P, mutually *trans* PTAs		–57.6, t, (28.5) mutually *trans* PTAs	
	4.14 br s, 12H NC*H*$_2$P, PTA *trans* to Cl			
trans-$RuBr_2(PTA)_4$ (**11**)	4.61, br s, 24H, NC*H*$_2$N	70.5 N*C*H$_2$N	–54.5, s, mutually *trans* PTAs	D_2O
	4.40, br s, 24H, NC*H*$_2$P	51.9 N*C*H$_2$P		
cis-$RuBr_2(PTA)_4$ (**12**)	4.70, m, 24H, NC*H*$_2$N	n.d.	–24.1, t, (28.2), PTA *trans* to Br	D_2O**
	4.56 br s, 12H, NC*H*$_2$P		–64.7 t, (28.2), mutually *trans* PTAs	
	4.23 br s, 12H, NC*H*$_2$P			

	^{1}H (J)	^{13}C{^{1}H}	^{31}P{^{1}H} (J)	Solvent
cis-[RuCl(OH_2)(PTA)$_4$]$^+$ (**2$_{aq}$**)	4.59, m, 24H, NCH_2N	70.3 NCH_2N	–12.7, dt, (30.3,34.8) PTA *trans* to OH_2	D_2O
	4.26, d, 12H, NCH_2P	49.8 NCH_2P	–22.7, dt, (26.1,34.8) PTA *trans* to Cl	
	4.11, s, 6H, NCH_2P	54.9 NCH_2P	–52.6, dd, (26.1, 30.3) mutually *trans* PTAs	
	3.97, s 6H NCH_2P	54.6 NCH_2P		
cis-[RuBr(OH_2)(PTA)$_4$]$^+$ (**12$_{aq}$**)			–13.01, dt, (30.5, 33.9), PTA *trans* to OH_2 –23.24, dt, (33.9, 25.7), PTA *trans* to Br –55.88, dd, (30.5, 25.7), mutually *trans* PTAs	D_2O

* Recorded in the presence of ca. 1M NaCl, ** Recorded in the presence of ca. 1M NaBr.

Table 2.2. ^{1}H, ^{13}C, ^{31}P NMR characterization (δ, ppm; *J*, Hz) of *trans*-$RuCl_2(PTA)_4$ (**1**), *cis*-$RuCl_2(PTA)_4$ (**2**), *trans*-$RuBr_2(PTA)_4$ (**11**) and *cis*-$RuBr_2(PTA)_4$ (**12**) in $CDCl_3$.

	^{1}H (*J*)	$^{13}C\{^{1}H\}$	$^{31}P\{^{1}H\}$ (*J*)	Solvent
trans-$RuCl_2(PTA)_4$ (**1**)	4.61, 4.57 ABq, 24H, NCH_2N (13.7)	73.3 NCH_2N	–50.6, s mutually *trans* PTAs	$CDCl_3$
	4.40, br s, 24H, NCH_2P	53.1 NCH_2P		
cis-$RuCl_2(PTA)_4$ (**2**)	4.48, m, 24H, NCH_2N	73.1 NCH_2N		$CDCl_3$
	4.47, br s, 12H, NCH_2P, mutually *trans* PTAs	54.0 NCH_2P	–59.4, t, (28.6) mutually *trans* PTAs	
	4.04, br s, 12H, NCH_2P, PTA *trans* to Cl	58.7 NCH_2P	–24.1, t, (28.6) PTAs *trans* to Cl	
trans-$RuBr_2(PTA)_4$ (**11**)	4.60, 4.55 ABq 24H, NCH_2N, (13.2)	73.5 NCH_2N	–56.5, s, mutually *trans* PTAs	$CDCl_3$
	4.46, br s, 24H, NCH_2P	54.0 NCH_2P		
cis-$RuBr_2(PTA)_4$ (**12**)	4.54, br s,12H, NCH_2P	73.9 NCH_2N	–27.0 t, (27.4), PTA *trans* to Br	$CDCl_3$
	4.50, m, 24 H, NCH_2N	59.6 NCH_2P	–67.3 t, (27.4) mutually *trans*	
	4.10, br s, 12H, NCH_2P	55.4 NCH_2P	PTAs	

The single-crystal X-ray structures of **11** and **12** (Figure 2.5) are closely comparable with those of the corresponding dichloro derivatives.[1,2] To begin with, they show distortions from the perfect octahedral geometry around Ru(II) very similar to those found in **1** and **2**. In complex **11** the two pairs of *trans* PTA ligands are vertically displaced in opposite directions from the average equatorial plane (163.46(2) and

164.05(2)°). In complex **12** the two *trans* PTA ligands make a P–Ru–P angle of 164.639(18)° (164.8(1)° in **2**) and are bent towards the Br atoms. A similar bending is found for the two *cis* PTAs (97.067(19)° vs 96.5(1)° in **2**). Thus, in both isomers the PTA moieties move towards the less sterically encumbered region occupied by the two Br ligands. The two *trans* Ru–Br distances in **11** are nearly equal (2.5695(4) and 2.5582(4) Å) and slightly shorter than those found in the *cis* isomer **12** (2.6142(14) and 2.6289(4) Å), consistent with the stronger *trans* influence of PTA. Similarly, the Ru–P distances in the *trans* isomer range between 2.3253(7) and 2.3484(7) Å (cfr 2.316(2) – 2.353(2) Å in **1**), whereas in **12** the two Ru–P distances *trans* to Br are considerably shorter (2.2805(13) and 2.2655(5) Å; cfr 2.260(2) Å *trans* to Cl in **2**) than those of the two *trans* PTAs (2.4001(5) and 2.3562(5) Å; cfr 2.370(2) Å in **2**), which – in turn – are close to (but slightly longer than) those in the *trans* isomer.

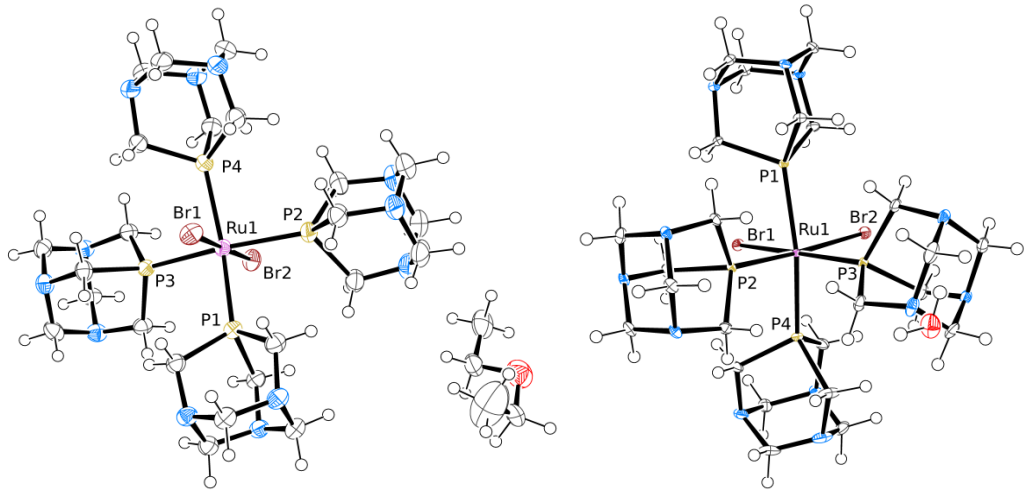

Figure 2.5. X-ray molecular structures (50% probability ellipsoids) of *trans*-[$RuBr_2(PTA)_4$]·0.682($C_4H_{10}O$) (**11**, left) and *cis*-[$RuBr_2(PTA)_4$]·0.37(H_2O) (**12**, right). The crystallization water molecule with minor occupancy factor in the structure of **12** has been omitted for clarity. Coordination distances (Å): **11**: Ru1–Br1 = 2.5695(4), Ru1–Br2 = 2.5582(4), Ru1–P1 = 2.3461(7), Ru1–P2 = 2.3253(7), Ru1–P3 = 2.3484(7), Ru1–P4 = 2.3378(7). **12**: Ru1–Br1 = 2.6142(14), Ru1–Br2 = 2.6289(4), Ru1–P1 = 2.4001(5), Ru1–P2 = 2.2655(5), Ru1–P3 = 2.2805(13), Ru1–P4 = 2.3562(5).

The behavior of the two chloro isomers in aqueous solution was also reinvestigated. In agreement with published data,[3] **2** rapidly equilibrates with the mono-aqua species *cis*-$[RuCl(OH_2)(PTA)_4]^+$ (**2aq**), that was isolated as PF_6^- salt following another synthetic route (see below). The ^{31}P resonances of the mixture of **2** and **2aq** were readily distinguished with a ^{31}P-^{31}P COSY spectrum (Appendix, A2.6). Integration of such resonances afforded an equilibrium constant K = 1.39×10^{-2} M. The ^{31}P NMR spectrum of **2aq** presents an AM_2X spin system (Table 2.1), with multiplets centered at δ = –12.7 (PTA *trans* to OH_2), –22.7 (PTA *trans* to Cl), and –52.6 ppm (mutually *trans* PTAs). The assignments are consistent with the multiplicity and intensity of each signal, as well as with the spectrum of **2** and literature data.[3] The ^1H NMR spectrum of the mixture **2** + **2aq** is quite complex. Pure **2** – according to the ^{31}P NMR spectrum – was obtained upon addition of an excess of NaCl (ca. 1M) to the D_2O solution. The yet unreported ^1H NMR spectrum of **2** in D_2O (Table 2) is quite similar to that recorded in $CDCl_3$. Release of the second chloride from **2aq** and formation of the di-aqua species *cis*-$[Ru(OH_2)_2(PTA)_4]^{2+}$, characterized by two equally intense triplets in the ^{31}P NMR spectrum at δ = –16.0 ($^2J_{P\text{-}P}$ = 27.1 Hz, PTA *trans* to OH_2) and –45.9 ppm (mutually *trans* PTAs), became apparent for concentrations of **2** < 5 mM. This species had been previously obtained upon addition of an excess of PTA to a solution of $[Ru(OH_2)_6]^{2+}$.[17] Treatment of an aqueous solution of **2** with one eq of $AgCF_3SO_3$ for 48 h at room temperature afforded the triflate salt of **2aq**, *cis*-$[RuCl(OH_2)(PTA)_4](CF_3SO_3)$, in moderate yield.[3] The chloride abstraction was accompanied by the formation of Ag and/or Ag_2O (the AgCl precipitate was dark grey). Attempts to remove also the second chloride from **2** by increasing the Ag^+/Ru ratio, and to isolate the corresponding dicationic salt *cis*-$[Ru(OH_2)_2(PTA)_4](CF_3SO_3)_2$ were unsuccessful. Consistent with literature data on Ru(II)-halide complexes, the bromide ligands proved to be more easily released than the chlorides.[18] An equilibrium constant of 2.42×10^{-2} M was measured between **12** and its mono-aqua derivative *cis*-$[RuBr(OH_2)(PTA)_4]^+$ (**12aq**).

Contrary to what reported in the literature,[3] we found that a light-protected D_2O solution of **1** is perfectly stable at room temperature: the NMR spectra remained unchanged for days (Appendix, A2.3). On the contrary, exposure of the NMR tube to diffused indoor light induced the slow isomerization (days) of **1** to a mixture of **2** and $\mathbf{2_{aq}}$, as witnessed by the appearance of the corresponding resonances in the ^{31}P NMR spectrum.

The thermal stability of **1** in the coordinating solvents DMSO and CH_3CN was also investigated. When a concentrated solution of **1** in DMSO (where the complex is only partially soluble) was heated to 150 °C for 4 h, complete thermal isomerization to the *cis* isomer **2** (that partially precipitates from the warm solution) was observed. When the reaction was performed at lower temperatures, a pale yellow solid was isolated upon addition of acetone. According to the ^{31}P NMR spectrum, this precipitate is a mixture of **2** and of an intermediate characterized by an AX_2 spin system: a triplet at δ = –25.6 ppm attributable to a PTA *trans* to Cl, and doublet at δ = –61.0 ppm ($^2J_{P\text{-}P}$ = 27.9 Hz) in the region of mutually *trans* PTAs (Appendix, A2.11). The proton spectrum, besides several PTA peaks, shows a singlet at δ = 3.20 ppm attributable to dmso-S in a symmetrical environment (equivalent methyl groups). Based on this spectral evidence, the intermediate species was identified as *cis,mer*-$RuCl_2$(dmso-S)$(PTA)_3$ (**13**, Figure 2.6). The intermediate **13** could not be isolated in pure form: the highest **13**/**2** ratio (40:60, without residual **1**) was obtained by running the reaction at 70 °C for 1h.

A similar behavior was observed when **1** was heated in acetonitrile. In this case the complex dissolves completely under reflux conditions and a pale yellow solid precipitates spontaneously from the solution. According to the ^{31}P NMR spectrum (Appendix, A2.12-A2.13) it is a mixture of **2** (whose amount increases with the reflux time) and of two intermediates, **14** (major) and **15** (minor), both characterized by AX_2 spin systems (Figure 2.6). According to the chemical shifts of the multiplets, the major intermediate **14** (triplet at δ = –16.1 ppm, doublet at δ = –53.3 ppm, $^2J_{P\text{-}P}$

= 28.5 Hz) was identified as *trans,mer*-$RuCl_2(CH_3CN)(PTA)_3$ whereas the minor one (triplet at δ = –24.0 ppm, doublet at δ = –54.3 ppm, $^2J_{P\text{-}P}$ = 37.2 Hz) as *cis,mer*-$RuCl_2(CH_3CN)(PTA)_3$ (i.e. **15** is the counterpart of **13** isolated in DMSO). Consistently, the corresponding ^{1}H NMR spectrum shows, besides the overlapped PTA resonances, two singlets at δ = 2.30 and 2.46 ppm, in the same ratio as the resonances of **14** and **15** in the ^{31}P NMR spectrum, attributed to coordinated CH_3CN.

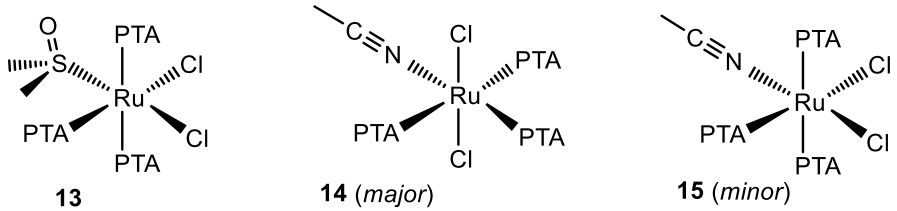

Figure 2.6. Intermediates isolated (not in pure form) when the thermal isomerization of **1** to **2** was performed in DMSO (**13**), or in acetonitrile (**14** and **15**).

In an unsuccessful attempt to prepare the presumed Ru(III) and Ru(II) intermediates *trans*-$[RuCl_4(PTAH)_2]Cl$ (**3**) and *trans*-$RuCl_4(PTAH)_2$ (**16**), respectively, that had been occasionally isolated in the recrystallization of **1**,[1,19] we found that the reaction between hydrate $RuCl_3$ and PTA in ethanol occurs also at room temperature, even though it is very slow (days) and affords low yields of **1**. The Ru(III) compound **3** was instead selectively prepared in high yield by a different route, i.e. by treatment of the Ru(III)-dmso precursor $[(dmso)_2H]$*trans*-$[RuCl_4(dmso\text{-}S)_2]$ with PTA in MeOH/HCl mixtures (Scheme 2.7). Due to the acidic conditions used in the preparation, both PTA ligands undergo protonation and the complex precipitates spontaneously in almost quantitative yield in its cationic form.

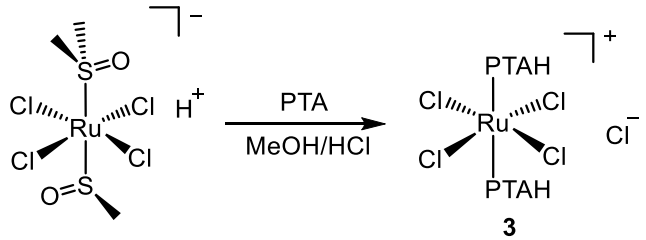

Scheme 2.7. Selective preparation of *trans*-$[RuCl_4(PTAH)_2]Cl$ (**3**) from the Ru(III)-dmso precursor $[(dmso)_2H]$*trans*-$[RuCl_4(dmso\text{-}S)_2]$.

Dark crystals of *trans*-[$RuCl_4(PTAH)_2$]Cl·H_2O (**3**·H_2O) suitable for X-ray structure determination were obtained upon recrystallization of the raw product from water (Figure 2.7).

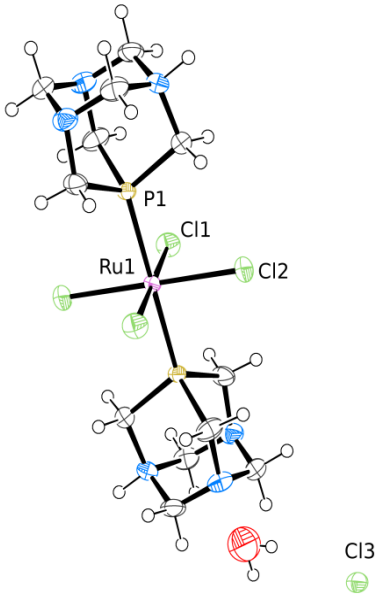

Figure 2.7. Molecular structure of *trans*-[$RuCl_4(PTAH)_2$]Cl·H_2O (**3**·H_2O). Only the chloride in the position of maximum occupancy is shown. Coordination distances (Å): Ru1–P1 = 2.3427(5), Ru1–Cl1 = 2.3565(12), Ru1–Cl2 = 2.3649(16).

The molecular structure of complex **3** is in close agreement with that already published for this species.[1b] One N atom in each PTA ligand is fully protonated, as confirmed by lengthening of the corresponding C–N bonds from 1.456(4) Å to 1.516(4) Å in the protonated form.[4,15] The positive charge of the complex is balanced by an external chloride ion that is disordered over three different positions.

The ^{1}H NMR spectrum of **3** in D_2O consists of two relatively broad peaks for bound PTA (one for the PCH_2N and the other for the NCH_2N protons) shifted upfield with respect to the typical PTA region (δ = 0.37 and –1.17 ppm, no assignment could be made, Appendix, A2.14). Consistent with the fact that P of PTA is directly bound to the paramagnetic Ru(III) nucleus, we were unable to observe any resonance in the ^{31}P NMR spectrum (most likely the expected singlet is too broad to be detected).

2.3.1 Reactivity of 1 and 2 towards diimine ligands

The above reported results suggest that, even though PTA binds strongly to Ru(II), replacement of at least one chloride and one PTA from isomers **1** and **2** seems to be possible, depending on the solvent and reaction conditions. Thus, we investigated the reactivity of **1** and **2** towards 2,2'-bipyridine (bpy) as model for the diimine linkers 4′-methyl-2,2′-bipyridine-4-carboxylic acid (bpyAc, Figure 2.2) and 2-(2′-pyridyl)pyrimidine-4-carboxylic acid (cppH, Figure 2.2).

Both **1** and **2** were found to react with bpy in refluxing water (in light protected conditions), as evidenced by a progressive color change of the solution from pale to deep yellow. More specifically, treatment of **1** with 1 eq of bpy in refluxing water (1 h), followed by evaporation of the solvent, afforded almost quantitatively the complex *mer*-[Ru(bpy)Cl(PTA)$_3$]Cl (**17**, Scheme 2.8).

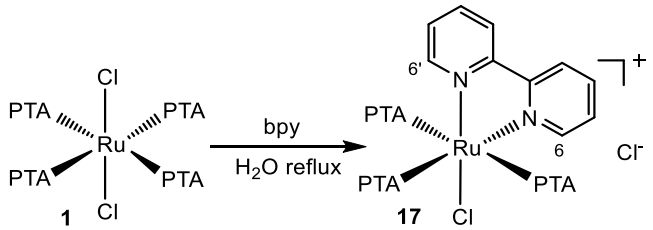

Scheme 2.8. Preparation of *mer*-[Ru(bpy)Cl(PTA)$_3$]Cl (**17**) upon treatment of **1** with bpy in water at reflux.

Compound **17** was fully characterized by NMR and mass spectrometry (as PF_6 salt, see the experimental section) and its single-crystal X-ray structure was also determined (Figure 2.8). The ^{1}H NMR spectrum (Appendix, A2.15) shows eight aromatic resonances, typical of bpy in an unsymmetrical environment. In agreement with previous findings,[20,21] the most deshielded doublet was assigned to H6, i.e. the proton with a partial positive charge that points towards the adjacent chloride (Scheme 2.8). The PTA region of the spectrum consists of two similar and partially overlapping sets of equally intense signals, an AB quartet and a broad singlet, in a 1:2 ratio. The most intense and upfield shifted set was attributed to the two equivalent *trans* PTA ligands, whose protons fall in the shielding cone of the adjacent bpy. The

^{1}H-^{13}C HSQC spectrum established that, in each set, the deshielded quartet belongs to the N*CH*$_2$N protons and the singlet to the N*CH*$_2$P protons. The ^{31}P NMR spectrum (Appendix, A2.19) consists of an AX_2 spin system: a triplet at δ = –30.2 ppm attributable to a PTA *trans* to N, and doublet at δ = –47.6 ppm ($^{2}J_{P\text{-}P}$ = 32.8 Hz) for the mutually *trans* PTAs. The spectra did not change upon addition of NaCl, suggesting that they can be safely attributed to the intact *mer*-[Ru(bpy)Cl(PTA)$_3$]$^{+}$ cation (see below). Interestingly, the crystals of **17** obtained upon recrystallization of the raw product from water/ethanol contain a network of water molecules distributed in parallel rows along the [001] direction, which arguably contribute to the cohesive energy of the crystal by means of hydrogen bonding to the N atoms of the PTA moieties. The coordination distances are in general agreement with the known *trans* influence of the ligands: thus, the Ru–P bond lengths of the two *trans* PTA ligands (2.3427(5) and 2.3275(5) Å) are slightly longer than the Ru–P distance *trans* to N (2.3018(5) Å) and the Ru–N bond length *trans* to P (2.1154(14) Å) is longer that *trans* to Cl (2.0770(13) Å).

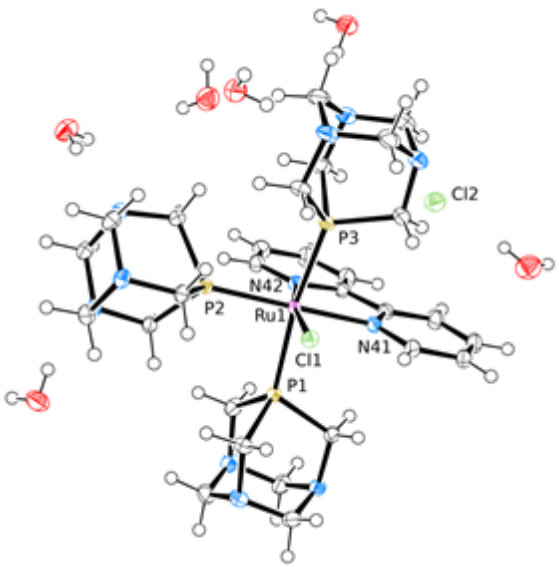

Figure 2.8. X-ray molecular structure (50% probability ellipsoids) of *mer*-[Ru(bpy)Cl(PTA)$_3$]Cl·6H$_2$O (**17**). Coordination distances (Å): Ru1–Cl1 = 2.4354(4), Ru1–N41 = 2.1154(14), Ru1–N42 = 2.0770(13), Ru1–P1 = 2.3427(5), Ru1–P2 = 2.3018(5), Ru1–P3 = 2.3275(5).

The reaction between **2** and bpy is slower and less selective: when a slight excess of bpy was used (bpy/Ru = 1.5), full conversion required ca. 10 h of reflux. According to the NMR spectra, the final mixture contained – besides some unidentified minor species and PTAO – compound **17** as main product and another species identified as *fac*-[Ru(bpy)Cl(PTA)$_3$]Cl (**18**) (**17**/**18** = ca. 10). We found that an increase of the bpy/Ru ratio from 1.5 to 5, together with the addition of 1 eq of $AgNO_3$, led to full conversion of **2** after 1h of reflux. In addition, in this case the main product was the *fac* isomer **18** (**18**/**17** = ca. 7, Scheme 2.9), that was obtained in pure form for unambiguous characterization as PF_6 salt (**18PF$_6$**, see experimental section). An increase of the reaction time involved a progressive decrease of the **18**/**17** ratio, suggesting that **18** is the kinetic product of the reaction between **2** and bpy, whereas **17** is thermodynamically more stable.

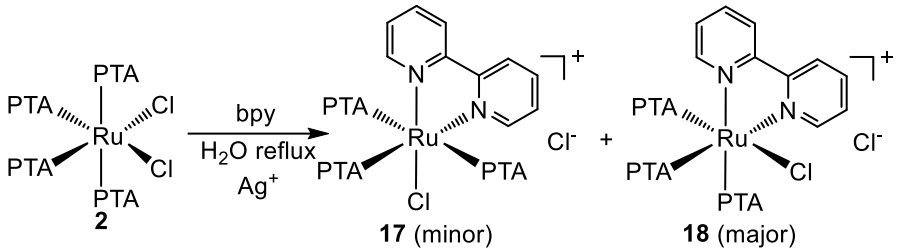

Scheme 2.9. Preparation of a mixture of the cationic isomers *mer*-[Ru(bpy)Cl(PTA)$_3$]Cl (**17**) and *fac*-[Ru(bpy)Cl(PTA)$_3$]Cl (**18**) upon reaction of **2** with bpy in water at reflux.

Immediately after dissolution in D_2O, the ^{1}H NMR spectrum of **18** has only four aromatic resonances, in agreement with a symmetrical coordination for bpy. However, a second set of four bpy resonances, each one slightly downfield shifted with respect to the parent one and attributed to the aqua species *fac*-[Ru(bpy)(OH_2)(PTA)$_3$]$^{2+}$ (**18$_{aq}$**) grows slowly with time at the expenses of the original one (Figure 2.9).

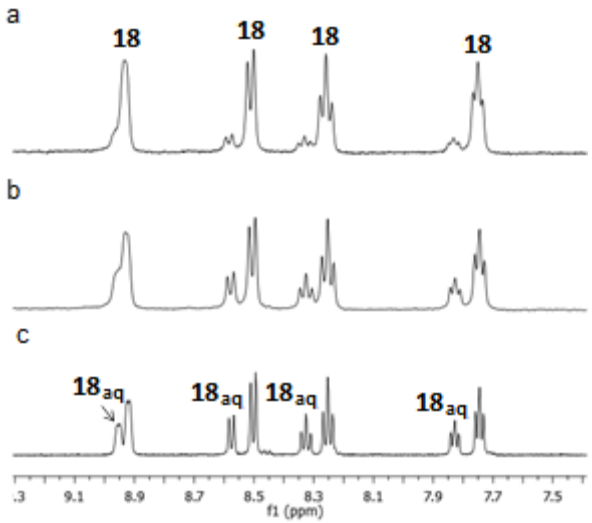

Figure 2.9. ^{1}H NMR spectra of *fac*-[Ru(bpy)Cl(PTA)$_3$](PF$_6$) (**18PF$_6$**) in D$_2$O registered immediately after dissolution (a); after 1 hour in the dark (b); after 24 hours in the dark (c).

Equilibrium (**18**/**18$_{aq}$** = ca. 1.5) was reached within 24h at room temperature. Consistently, the ^{31}P NMR spectrum shows two AX$_2$ spin systems, attributed (based on their relative intensities and time evolution) to **18** (triplet at δ = –24.3 ppm, PTA *trans* to Cl) and to **18$_{aq}$** (triplet at δ = –17.7 ppm, PTA *trans* to OH$_2$) (Figure 2.10). The two doublets overlap almost completely at δ = –44.2 ppm, i.e. in the typical region of PTA *trans* to N ($^{2}J_{P\text{-}P}$ = 29.2 Hz).

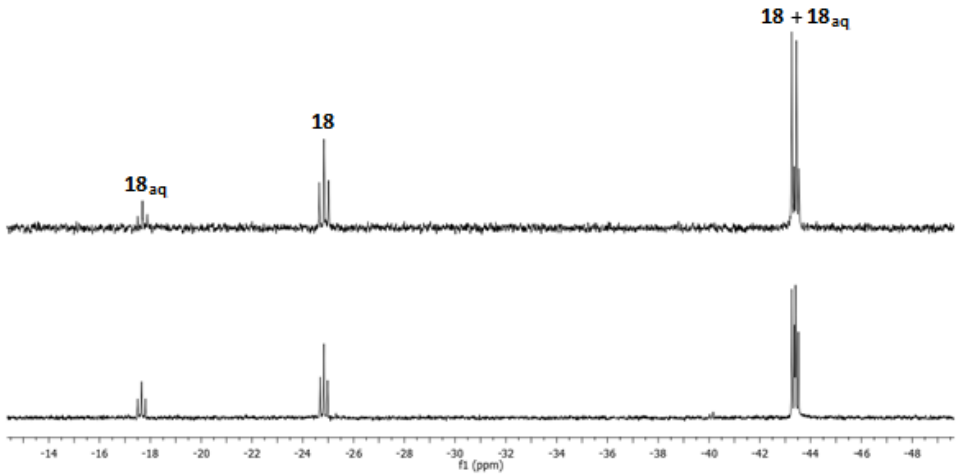

Figure 2.10. ^{31}P NMR spectra of *fac*-[Ru(bpy)Cl(PTA)$_3$](PF$_6$) (**18PF$_6$**) in D$_2$O registered immediately after dissolution (top) and after 24 hours in the dark (bottom).

The PTA region of the ^{1}H NMR spectrum is quite complicated due to the overlapping resonances of **18** and **18$_{aq}$**. It simplifies upon addition of an excess of NaCl (ca. 1M) that reverts completely the equilibrium towards **18**. Under these conditions the spectrum is similar to that of **17**, but in this case is the less intense set of signals, attributed to the PTA *trans* to Cl, to be shielded by bpy. Taken together, the NMR features are totally consistent with the proposed geometry. X-ray diffraction performed on single crystals of the protonated derivative *fac*-[Ru(bpy)Cl(PTAH)$_{2.5}$(PTA)$_{0.5}$](ClO$_4$)$_{3.5}$·2.5H$_2$O, obtained upon addition of HClO$_4$ to an aqueous solution of **18**, allowed us to confirm the geometry of the complex (Appendix, A2.48).

In conclusion, we found that the coordination of bpy to **1** and **2** in aqueous solution involves the replacement of one chloride and one PTA ligand, and affords – depending on the conditions – the two isomers **17** and **18**. To be noted that formation of compound **18** was not observed in the reaction between **1** and bpy, indicating that the mechanisms of the two substitution reactions are different.

Consistent with these findings, the reactivity of both isomers **1** and **2** with bpy in organic solvents in which chloride release is unfavorable (e.g. CH$_3$CN, CHCl$_3$) is much less pronounced, when not altogether negligible. For example, in refluxing chloroform no reaction was observed between **2** and bpy, whereas **1** reacted to a minor extent affording (after 5h) a complex mixture of products that – based on the ^{31}P NMR spectrum – contained **2**, **18**, PTAO and other minor uncharacterized species.

Since *trans*-RuCl$_2$(PTA)$_4$ (**1**) reacts selectively with bpy forming only one of the possible stereoisomers, the reaction with the linker cppH was also investigated. This diimine ligand can originate linkage isomers; in fact, its pyrimidine ring can bind to the metal ion either through the nitrogen atom *ortho* (N^o) or *para* (N^p) to the carboxylate linked to C4. Most of the cppH-Ru(II) conjugates reported so far were

prepared following a synthetic route that led selectively to the N^p coordination mode (see also Chapter 6).[22,23,24,25,26]

The reaction between **1** and cppH (actually obtained as cppH·HNO_3) in refluxing water led to a main geometrical and linkage isomer, formulated as *mer*-[RuCl(cppH-N^p)$(PTA)_3$]Cl (**19**), in a mixture with minor uncharacterized species (Scheme 2.10). In fact, the ^{1}H NMR spectrum of the raw product in D_2O presents one main set of aromatic resonances for coordinated cppH, whereas the PTA region of the spectrum present several multiplets, including those of free PTA (Appendix, A2.23). The ^{31}P NMR spectrum of **19** consists of an AX_2 system composed by a triplet centered at –39.9 ppm and a doublet centered at ppm –51.9 ($^2J_{P\text{-}P}$ = 35.5 Hz). Since the chemical shifts for the three bound PTA ligands are similar to the those of **17**, also in this case the *mer* geometry was assigned to **19**. Comparison of the chemical shifts of H6 and H6′ with those of other known Ru(II)-cppH complexes suggests that the cppH in **19** is bonded N^p (see Chapter 5).[21] However, we are unable to establish whether the pyridine or the pyrimidine ring of cppH is *trans* to PTA. Attempts to obtain **19** in pure form were unsuccessful.

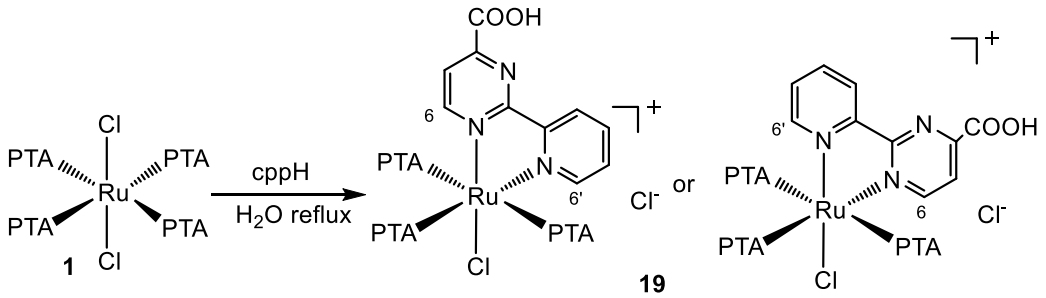

Scheme 2.10. Reactivity of *trans*-$RuCl_2(PTA)_4$ (**1**) towards cppH.

2.4 Reactions of Ru(II)-dmso complexes with PTA

As mentioned above, the reactivity of the well-known Ru(II) precursors, *cis*- and *trans*-$RuCl_2(dmso)_4$ (**8** and **9**, respectively) towards PTA was investigated, with the aim to prepare new water-soluble precursors.

After starting our work, we became aware that the reactivity of **8** towards PTA had been recently investigated by Kathó and coworkers.[15] In good agreement with their results, we found that the treatment of **8** with PTA at room temperature leads selectively to the formation of *cis,cis,trans*-$RuCl_2(dmso\text{-}S)_2(PTA)_2$ (**10**) regardless of the nature of the solvent (e.g. in MeOH) and of the PTA/Ru ratio (Scheme 2.11). Even when less than two eq of PTA were used, compound **10** was obtained together with unreacted precursor. Replacement of all dmso-S ligands (with formation of a mixture of **1**, **2** and **10**) was observed when the reaction (PTA:Ru = 4) was performed in refluxing MeOH. Conversely, we found that treatment of *trans*-$RuCl_2(dmso\text{-}S)_4$ (**9**, not investigated before) with PTA at room temperature leads exclusively to **1** (Scheme 2.11). Also in this case the nature of the product does not depend on the PTA/Ru ratio employed. For example, when PTA/Ru = 2, a ca. 1:1 mixture of **1** and unreacted precursor was recovered at the end. In neither case any intermediate could be detected, suggesting that the replacement of two *trans* dmso ligands by two PTA ligands occurs rapidly and quantitatively. As already mentioned (see above), the same behavior, i.e. facile substitution of two *trans* dmso-S ligands, was observed also with the Ru(III)-dmso precursor $[(dmso)_2H]$*trans*-$[RuCl_4(dmso\text{-}S)_2]$ that afforded **3**.

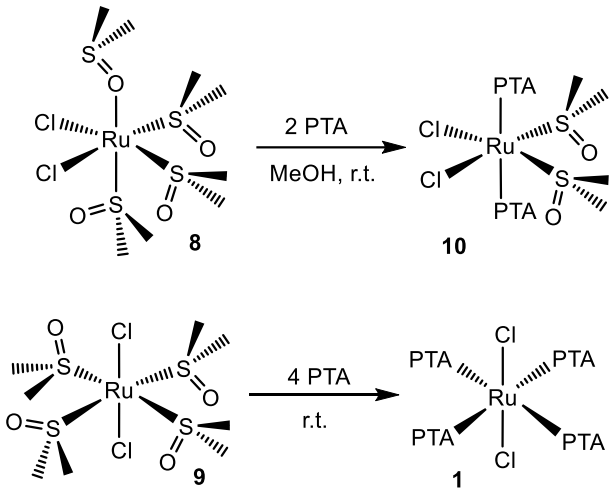

Scheme 2.11. Reactivity of *cis*-$RuCl_2(dmso)_4$ (**8**, top) and *trans*-$RuCl_2(dmso\text{-}S)_4$ (**9**, bottom) towards PTA at room temperature.

The spectroscopic characterization of compound **10** (Appendix, A2.24) as well as its single-crystal X-ray structure (Figure 2.11) are in good agreement with what reported in the literature.[15,27]

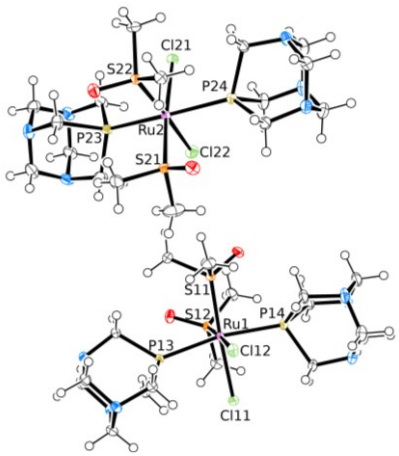

Figure 2.11. Molecular structure (50% probability ellipsoids) of the two crystallographically independent units of *cis,cis,trans*-$RuCl_2(dmso\text{-}S)_2(PTA)_2$ (**10**). Disordered and under-occupied methanol and water crystallization molecules have been omitted for clarity. Coordination distances (Å): Ru1–Cl11 = 2.4482(7), Ru1–Cl12 = 2.4483(6), Ru1–S11 = 2.2488(6), Ru1–S12 = 2.2522(6), Ru1–P13 = 2.3764(7), Ru1–P14 = 2.3755(8). Ru2–Cl21 = 2.4583(6), Ru2–Cl22 = 2.4606(6), Ru2–S21 = 2.2358(6), Ru2–S22 = 2.2578(6), Ru2–P23 = 2.3780(8), Ru2–P24 = 2.3304(8).

Compound **10** is well soluble in water, DMSO, $CHCl_3$, CH_2Cl_2 and, upon warming, also in MeOH and EtOH. We observed that the ^1H NMR spectrum of a light-

protected D_2O solution of **6** changes very slowly (days) at room temperature (Appendix, A2.25). Since no signals for free DMSO or PTA were detected, the spectral changes were attributed to the progressive release of a chloride with formation of the mono-aqua species *cis,cis,trans*-$[RuCl(OH_2)(dmso\text{-}S)_2(PTA)_2]^+$ (**10$_{aq}$**). Consistent with this hypothesis, in the ^{31}P NMR spectrum a new singlet at δ = –53.0 ppm grows slowly at the expenses of the original one at δ = –57.9 ppm (Appendix, A2.26). In the ^1H spectrum, besides new signals in the PTA region, two new singlets for dmso-S grow at δ = 3.37 and 3.41 ppm (i.e. very close to the original singlet at δ = 3.38 ppm). In fact, in **10$_{aq}$**, whereas the two *trans* PTAs are still equivalent, the two sulfoxides are not.

We also investigated the possibility of obtaining complexes with either five or six bound PTA moieties, using the cationic Ru(II)-dmso precursors *cis,fac*-$[RuCl(dmso\text{-}O)_2(dmso\text{-}S)_3](PF_6)$ (**20**) and *fac*-$[Ru(dmso\text{-}O)_3(dmso\text{-}S)_3](CF_3SO_3)_2$ (**21**), respectively. We found that treatment of **20** with 5 eq of PTA in methanol at room temperature afforded *cis*-$[RuCl(OH_2)(PTA)_4](PF_6)$ (**2$_{aq}$**) in moderate yield. The ^1H NMR spectrum of the complex in D_2O corresponds to that of **2$_{aq}$** observed in equilibrium with **2** (see above) with, in addition, a singlet for free MeOH (crystallization molecule). The nature of the compound was also confirmed by a low quality X-ray structural determination (Appendix, A2.49). Repeated attempts to obtain better crystals were unsuccessful. When the same reaction was performed at reflux temperature, precipitation of **2** occurred, whereas the resonances of **2$_{aq}$**, *cis*-$[Ru(OH_2)_2(PTA)_4]^{2+}$ and PTAO were found in the ^{31}P NMR spectrum of the mother liquor (D_2O). Since there is no external source of chloride, this finding suggests that the disproportionation of **2$_{aq}$** into di-chloro (**2**) and di-aqua {$Ru(PTA)_4$} species occurs in these conditions.

Conversely, treatment of **21** with 6 eq of PTA in methanol or acetone at room temperature afforded no product, but PTA was completely converted to PTAO within a few hours. When the reaction was performed in refluxing chloroform (no

reaction occurred at room temperature), precipitation of **2** was observed in moderate yield, implying chloride abstraction from the solvent. This finding suggests that cationic Ru(II)-PTA species have a very high affinity for chloride.

Compound **10** was studied by Katho's group as catalyst for the isomerization of allylic alcohol to the corresponding ketone; no further investigations about its reactivity were done.[15] Only very recently Romerosa's group studied the behavior of this compound with light. They reported that overnight irradiation of an aqueous solution of **10** with white light in presence of 3 eq of PTA affords the dimer $[\{Ru(PTA)_3\}_2(\mu\text{-}Cl)_3]Cl\cdot 9H_2O$ (**5**) (described above) (Scheme 2.12). Conversely, when the irradiation was done in the presence 4 eq of PTA, to *trans*-$RuCl_2(PTA)_4$ (**1**) was obtained.[11]

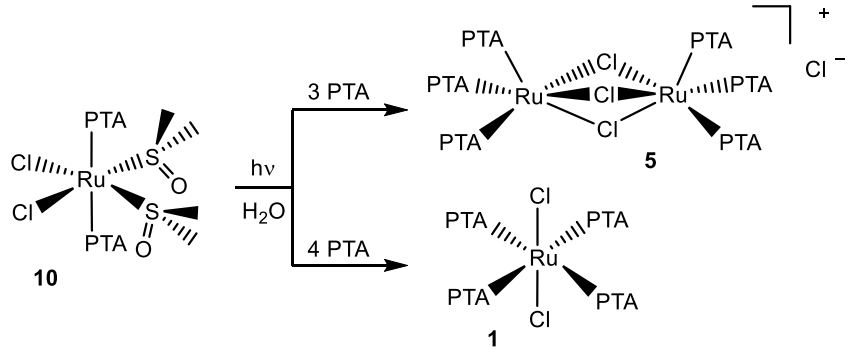

Scheme 2.12. Reactivity of *cis,cis,trans*-$RuCl_2(dmso\text{-}S)_2(PTA)_2$ (**10**) with PTA under irradiation with white light in water.

The complexes *cis,cis,trans*-$RuCl_2(dmso\text{-}S)_2(PTA)_2$ (**10**), however, has the characteristics for being a good precursor for the preparation of Ru(II)-PTA derivatives, since it has the two dmso-S ligands that might be replaced with relative ease by a chelating ligand (e.g. a diimine) and – in principle – also by two monodentate ligands (e.g. pyridine). Indeed, we found that when **10** is treated with a slight excess of bpy in refluxing ethanol, the original pale-yellow solution becomes progressively ruby-red. A product of the same color, identified as *cis,cis*-$Ru(bpy)Cl_2(PTA)_2$ (**22**), was isolated in moderate-to-good yield (Scheme 2.13).

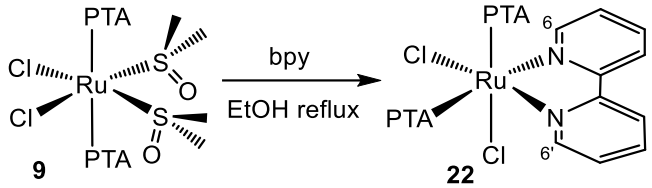

Scheme 2.13. Preparation of *cis,cis*-Ru(bpy)$Cl_2(PTA)_2$ (**22**) upon treatment of *cis,cis,trans*-$RuCl_2$(dmso-S)$_2(PTA)_2$ (**6**) with bpy in refluxing ethanol.

Thus, the selective replacement of the two sulfoxides by bpy is accompanied by the concomitant isomerization, yielding the less symmetrical all-*cis* product. Compound **22**, which is well soluble in water, in chloroform and DMSO, and moderately soluble in MeOH and EtOH, was fully characterized by NMR and mass spectrometry and its single-crystal X-ray structure was determined (Figure 2.12).

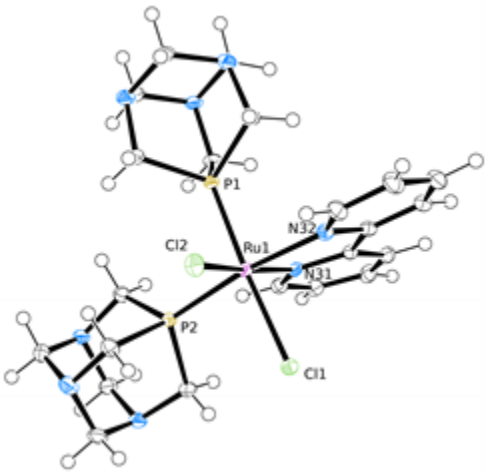

Figure 2.12. Molecular structure (50% probability ellipsoids) of *cis,cis*-Ru(bpy)$Cl_2(PTA)_2$ (**22**). The three MeOH molecules of crystallization have been omitted for clarity. Coordination distances (Å): Ru1–Cl1 = 2.4789(4), Ru1–Cl2 = 2.4421(4), Ru1–N31 = 2.0540(14), Ru1–N32 = 2.1167(15), Ru1–P1 = 2.2318(4), Ru1–P2 = 2.2849(4).

In the ^{1}H NMR spectrum of **22** in $CDCl_3$, bpy presents eight well resolved resonances (1H each, Appendix, A2.27). As above, the most deshielded doublet was assigned to H6 (Scheme 2.12). The two inequivalent PTAs give four resolved resonances (6H each, Figure 2.13), pairwise coupled in the ^{1}H-^{1}H COSY spectrum (Appendix, A2.28). The two most upfield multiplets are attributed to the PTA *trans* to Cl that

falls into the shielding cone of the adjacent bpy. The assignments are confirmed by an ^{1}H-^{31}P HMBC spectrum.

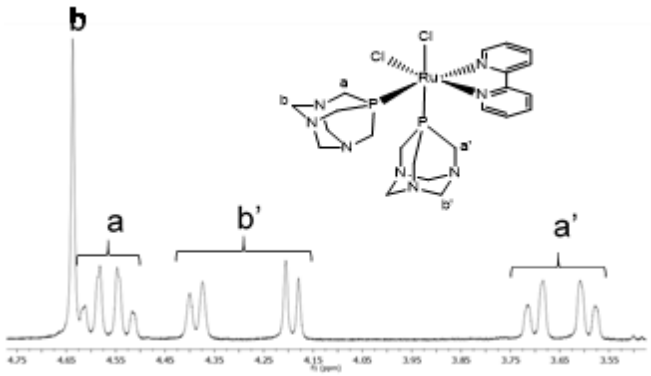

Figure 2.13. ^{1}H NMR spectrum (PTA region) in $CDCl_3$ of *cis,cis*-Ru(bpy)Cl_2(PTA)$_2$ (**22**). See the inset drawing for the peak labels.

The ^{31}P NMR spectrum of **22** in D_2O (two doublets at δ = –7.0 and –31.9 ppm, $^{2}J_{P\text{-}P}$ = 37.7 Hz) is similar to that in $CDCl_3$ (Appendix, A2.31). However, whereas the shielded resonance is compatible with a P *trans* to N, the other doublet falls in the region of PTA *trans* to O (see for example the spectra of $\mathbf{2}_{aq}$ and $\mathbf{18}_{aq}$) rather than *trans* to Cl (expected at about –15 ppm). Thus, we hypothesized that, upon dissolution in water, complex **22** undergoes rapid, quantitative and selective release of the Cl *trans* to PTA affording *cis,cis*-$[Ru(bpy)Cl(OH_2)(PTA)_2]^{+}$ ($\mathbf{22}_{aq}$, Scheme 24). This hypothesis is consistent with: *i*) what observed above with other complexes (e.g. **2** and **18**) having Cl *trans* to PTA; *ii*) the larger *trans*-influence of PTA compared to bpy, which is reflected by the solid state data, according to which the Ru–Cl bond *trans* to PTA (2.4789(4) Å) is longer than that *trans* to bpy (2.4422(4) Å); *iii*) the downfield shifted resonance of H6 implies that the adjacent Cl remains bound to ruthenium.

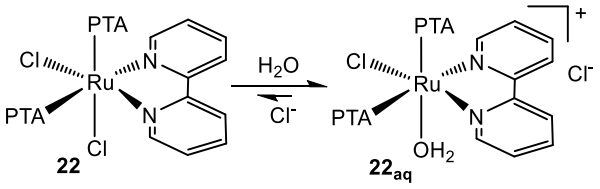

Scheme 2.14. Selective aquation of complex **22**.

Indeed, we found that addition of aliquots of NaCl to the D_2O solution leads to the progressive growth of a new set of resonances in the NMR spectra – attributed to intact **22** – at the expenses of the original ones thus unambiguously attributed to **22_{aq}**. Figure 2.14 shows an intermediate situation in the ^{31}P NMR spectrum (see also Appendix, A2.32, for the ^{1}H NMR spectrum). As expected, the chemical shift of the new deshielded doublet in the ^{31}P NMR spectrum ($\delta = -12.7$) is now in the region compatible with P *trans* to Cl. The complete transformation of **22_{aq}** to **22** upon addition of excess NaCl (ca. 1M) induces also a minor shift in the absorption maximum of the UV-vis absorption spectrum from 413 (**22_{aq}**) to 418 nm (**22**) (Appendix, A2.45).

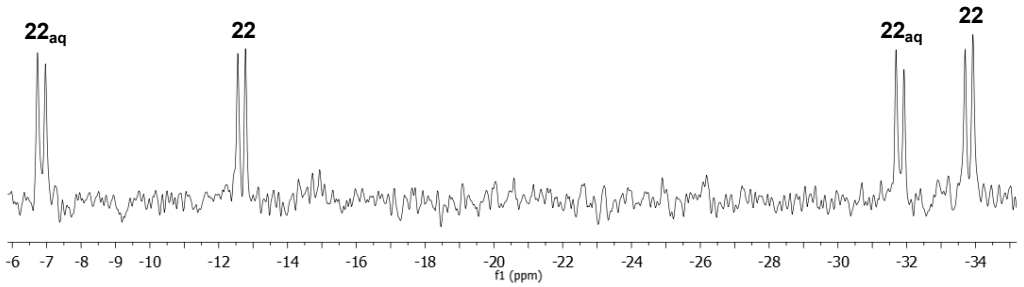

Figure 2.14. ^{31}P NMR spectrum in D_2O of *cis,cis*-$[Ru(bpy)Cl(OH_2)(PTA)_2]^+$ (**22_{aq}**) after addition of an aliquot of NaCl (ca. 0.2M), affording a mixture of **22** and **22_{aq}**.

Similarly, treatment of **10** with bpyAc in refluxing ethanol afforded *cis,cis*-$Ru(bpyAc)Cl_2(PTA)_2$ (**23**) as a nearly 1:1 mixture of the two stereoisomers **23a** (4-carboxylic acid *trans* to PTA) and **23b** (4-carboxylic acid *trans* to Cl) (Scheme 2.15).

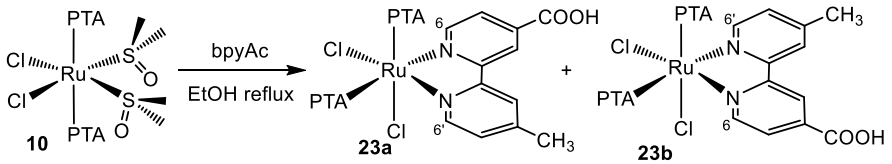

Scheme 2.15. Preparation of *cis,cis*-$Ru(bpyAc)Cl_2(PTA)_2$ (**23**) as a 50/50 mixture of the two stereoisomers **23a** and **23b**.

The spectroscopic features of **23a** and **23b** (Appendix, A2.33) are quite similar, except for the bpyAc resonances in the ^{1}H NMR spectrum, where twelve well-resolved signals (1H each, six for each stereoisomer) were found in the aromatic

region, plus two methyl singlets (3H each). The most deshielded doublet (δ = 9.58 ppm) was assigned to the H6 proton in **23a** for the following reasons: *i*) in free bpyAc H6 gives the most deshielded resonance (8.87 ppm vs 8.57 ppm for H6′); *ii*) in the complex this proton is further deshielded – besides by coordination – by the adjacent chloride (see above). The second most downfield doublet was assigned to H6′ in **23b**, where it points towards the adjacent Cl. All other bpyAc resonances were then unambiguously assigned by means of 2D ^{1}H-^{1}H COSY and NOESY spectra. Particularly relevant were the cross peaks between the CH_3 (in position 4′) and the H3′ singlets in the COSY spectrum, and those between the singlets of H3 and H3′ in the NOESY spectrum. As in the case of **22**, when dissolved in water also **23** releases the chloride *trans* to PTA, affording a mixture of **23a$_{aq}$** and **23b$_{aq}$**, even though at a slower rate.

The reactivity of **10** towards pyridine (py), used as a model for the 4′-*meso*-pyridylphenylporphyrins, was also investigated. Treatment of **10** with an excess of py in refluxing ethanol led to an orange product that precipitates spontaneously upon concentration of the solution. The compound was identified as *trans,cis,cis*-$RuCl_2(PTA)_2(py)_2$ (**24**), and was isolated in moderate-to-good yield (Scheme 2.16).

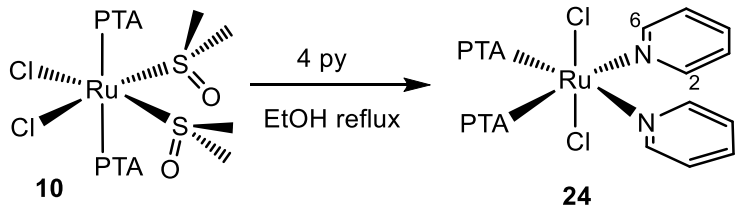

Scheme 2.16. Preparation of *trans,cis,cis*-$RuCl_2(PTA)_2(py)_2$ (**24**) upon treatment of *cis,cis,trans*-$RuCl_2(dmso\text{-}S)_2(PTA)_2$ (**10**) with py in refluxing ethanol.

Compound **24**, which is soluble in water, chloroform and DMSO, and moderately soluble in MeOH and EtOH, was fully characterized by NMR spectroscopy and mass spectrometry and its single-crystal X-ray structure was also determined (Figure 2.15).

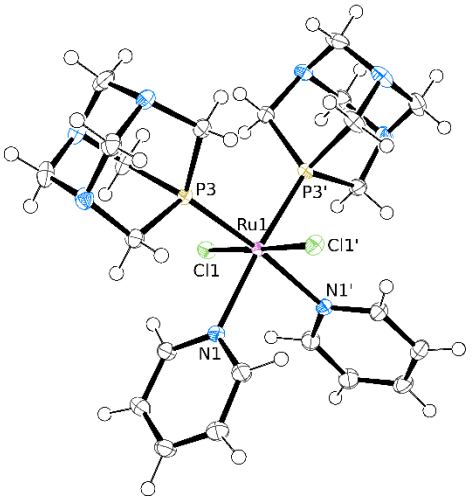

Figure 2.15. Molecular structure (50% probability ellipsoids) of *trans,cis,cis*-$RuCl_2(PTA)_2(py)_2$ (**24**). Coordination distances (Å): Ru1–Cl1 = 2.4291(4), Ru1–N1 = 2.1933(8), Ru1–P3 = 2.2543(3).

In the ^1H NMR spectrum in $CDCl_3$, the two equivalent py ligands show three well resolved resonances in the aromatic region. The two equivalent PTAs give two resolved resonances, a singlet and a multiplet (12H each, Figure 2.16), pairwise coupled in the ^1H-^1H COSY spectrum. As above, the singlet centered at 4.02 ppm belongs to the NCH_2P protons while the multiplet at 4.25 ppm to the NCH_2N protons. Integration of PTA and py signals is consistent with a 1:1 ratio. The ^{31}P NMR spectrum consists of a singlet at –20.4 ppm for the two equivalent PTAs *trans* to pyridine.

Thus, as with the diimine ligands, the selective replacement of the two sulfoxides by pyridine is accompanied by the isomerization of two PTAs from *trans* to *cis*. However, in this case, also the geometry of the two chlorides changes from *cis* to *trans*.

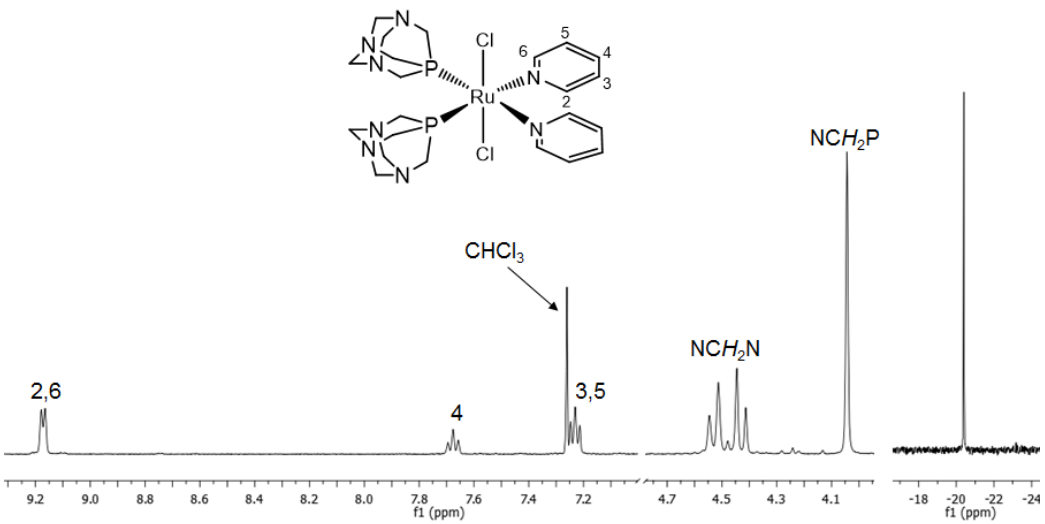

Figure 2.16. ^{1}H (left) and ^{31}P (right) NMR spectra in $CDCl_3$ of *trans,cis,cis*-$RuCl_2(PTA)_2(py)_2$ (**24**).

The same reaction was also performed at reflux temperature in $CHCl_3$. In this case a different – and unexpected – product, identified as *trans,mer*-$RuCl_2(py)(PTA)_3$ (**25**), precipitated in pure form as a yellow powder in moderate yield after the addition of diethyl ether to the solution (Scheme 2.17). In fact, the ^{31}P NMR spectrum in $CDCl_3$ of the precipitate presents only an AX_2 system with a doublet centered at –54.2 ppm, attributed to two mutually *trans* PTAs, and a triplet centered at –22.5 ppm ($^{2}J_{P\text{-}P}$ = 34.5 Hz) for a PTA *trans* to py (Appendix, A2.40). In the ^{1}H NMR spectrum py presents three well resolved resonances; the PTA region shows two pairs of signals in 1 : 2 ratio: each pair is composed by an AB system (the most downfield shifted signal) and a broad singlet, pairwise coupled in the ^{1}H-^{1}H COSY spectrum (Appendix, A.38). The most intense pair of signal, respectively centered at 4.42 and 3.92 ppm (12H each) were attributed to the two equivalent *trans* PTA ligands, while the other two signals, respectively centered at 4.59 ppm (partially overlapped with the water signal) and 4.27 ppm to the PTA *trans* to py. The ^{1}H-^{13}C HSQC spectrum established that, in each set, the deshielded quartet belongs to the N*CH*$_2$N protons and the upfield singlet to the N*CH*$_2$P protons. (Appendix, A2.39). Integration is consistent with a py/PTA ratio = 3. Since there is no external source of PTA, the formation of **25** implies a disproportionation.

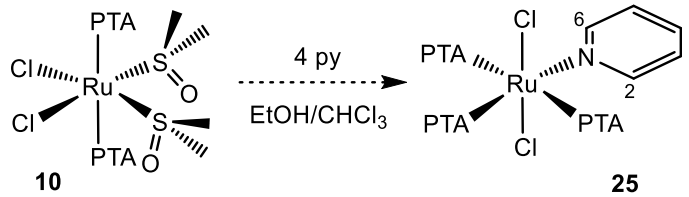

Scheme 2.17. Preparation of *trans,mer*-$RuCl_2(py)(PTA)_3$ (**25**) upon treatment of *cis,cis,trans*-$RuCl_2(dmso\text{-}S)_2(PTA)_2$ (**10**) with py in a refluxing mixture of $EtOH/CHCl_3$ (5/4 ratio).

X-ray qualities crystals were obtained upon addition of diethyl ether to a chloroform solution of **25**; the structure is in agreement with the NMR findings (Figure 2.17). The coordination distances are in general agreement with the known *trans* influence of the ligands: thus, the Ru–P bond lengths of the two *trans* PTA ligands (2.3439(5) and 2.3391(6) Å) are slightly longer than the Ru–P distance *trans* to N (2.251(1) Å).

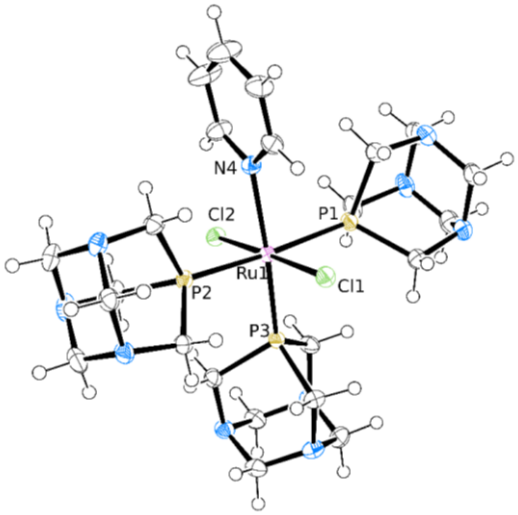

Figure 2.17. Molecular structure (50% probability ellipsoids) of *trans,mer*-$RuCl_2(py)(PTA)_3$ (**25**). Coordination distances (Å): Ru1–Cl1 = 2.4451(6), Ru1–Cl2 = 2.4546(6), Ru1–N4 = 2.224(2), Ru1–P1 = 2.3439(5), Ru1–P2 = 2.3391(6), Ru1–P3 = 2.251(1).

Compound **25** was isolated also when the reaction between **10** and pyridine was done in a 5/4 $EtOH/CHCl_3$ mixture. This mixture of solvents was chosen because it allows the solubilization of pyridylporphyrins.

Indeed, some test reactions between **10** and two eq of 5-(4′-pyridyl)-10,15,20-(phenyl)-porphyrin (4′MPyP) were performed, at reflux temperature, either in a 5/4

EtOH/DCM[b] mixture or in $CHCl_3$. The reactions were monitored by TLC (silica gel, $CHCl_3$/EtOH 98/2); in addition, samples were periodically withdrawn and, after evaporation of the solvent, analyzed by ^1H and ^{31}P NMR spectroscopy in $CDCl_3$.
The ^{31}P NMR spectrum in $CDCl_3$ of the crude reaction product after 8h showed only a low broad singlet centered at –20.0 ppm and no resonances for unreacted **10**. On the contrary, in the ^1H NMR spectrum the most intense signals corresponded to unreacted 4′MPyP (Appendix, A2.41), and very small signals for coordinated 4′MPyP, belonging to different unidentified adducts, were observed in the aromatic region. Therefore, according to NMR spectroscopy, **10** underwent transformation/decomposition, but its reactivity towards 4′MPyP was only minimal. The crude reaction product was thus redissolved in a 5/4 EtOH/DCM mixture and, after addition of one equivalent of **10**, it was heated to reflux for additional 8h. The final NMR spectra were very similar to the previous ones, again consistent with the decomposition of the complex. Attempts to increase the conversion by performing the reaction in a microwave reactor in $CHCl_3$ at 75°C for 2.5 h were unsuccessful.
Similarly unsuccessful were the attempts to purify the crude reaction product by column chromatography, using either silica gel or alumina as stationary phase. The ^1H NMR spectra performed on all the collected fractions suggested that the product(s) with coordinated 4′MPyP either decomposed during the elution or were retained on the stationary phase, since only the peaks of free 4′MPyP were observed.

[b] DCM was initially preferred to $CHCl_3$ to avoid HCl traces that could be present in chloroform. The acid environment may cause the protonation of porphyrins, that could affect the reactivity. However, no difference in reactivity was observed when the reaction was performed in the refluxing EtOH/DCM mixture or in pure chloroform.

2.5 Conclusions

In summary, this Chapter reports a thorough investigation of the neutral Ru(II)-chloride-PTA isomers *trans*- and *cis*-$RuCl_2(PTA)_4$ (respectively **1** and **2**), including their comprehensive NMR characterization (^1H, ^{13}C, and ^{31}P) both in D_2O and in $CDCl_3$ (Table 2.1 and 1.2 respectively). The corresponding and unprecedented bromide derivatives, *trans*- and *cis*-$RuBr_2(PTA)_4$ (respectively **11** and **12**), were also prepared and fully characterized. Next, the almost unexplored reactivity of **1** and **2** was addressed: when warmed in a coordinating solvent, such as DMSO and acetonitrile, the kinetic complex **1** isomerizes to the thermodynamically stable *cis* isomer **2**, as in water. The neutral intermediates *cis,mer*-$RuCl_2$(dmso-S)$(PTA)_3$ (**13**), *trans,mer*-$RuCl_2(CH_3CN)(PTA)_3$ (**14**), and *cis,mer*-$RuCl_2(CH_3CN)(PTA)_3$ (**15**) were isolated, even though not in pure form. Most interestingly, by virtue of these results, we found that both **1** and **2** can be used as precursors of the $\{RuCl(PTA)_3\}^+$ fragment. In fact, they react in refluxing water with chelating diimines such as bpy replacing selectively one chloride and one PTA ligand, and affording – depending on the conditions – two unprecedented isomeric derivatives: the thermodynamic product *mer*-[Ru(bpy)Cl$(PTA)_3$]Cl (**17**) and the kinetic product *fac*-[Ru(bpy)Cl$(PTA)_3$]Cl (**18**).

The reactivity of the Ru(II)-dmso complexes *cis*-$RuCl_2(dmso)_4$ (**8**), *trans*-$RuCl_2$(dmso-S)$_4$ (**9**), *cis,fac*-[RuCl(dmso-O)$_2$(dmso-S)$_3$](PF_6) (**20**), and *fac*-[Ru(dmso-O)$_3$(dmso-S)$_3$]$(CF_3SO_3)_2$ (**21**) towards PTA was also investigated. Expanding the results reported by Kathó and coworkers,[15] we found that PTA reacts rapidly and under mild conditions with the neutral Ru-dmso precursors replacing with high selectivity pairs of mutually *trans* dmso ligands. Replacement of both dmso's occurs also when PTA is in stoichiometric defect. Thus, **8** affords selectively *cis,cis,trans*-$RuCl_2$(dmso-S)$_2(PTA)_2$ (**10**), whereas **9** gives **1**. In both cases no

intermediates could be isolated or even detected. Conversely, no new cationic Ru(II)-PTA complex was obtained from **20** and **21**.

In addition, we found that *cis,cis,trans*-$RuCl_2(dmso\text{-}S)_2(PTA)_2$ (**10**) easily replaces the two molecules of dmso when treated with imine or diimine ligands in refluxing solvents (Scheme 2.18). The substitution of the dmso's is accompanied by the isomerization of the geometry of the other ligands. In fact, the reaction with chelating diimines afforded the less symmetrical all-*cis* products *cis,cis*-$Ru(bpy)Cl_2(PTA)_2$ (**22**) and *cis,cis*-$Ru(bpyAc)Cl_2(PTA)_2$ (**23**, as a 50/50 mixture of the two stereoisomers **23a** and **23b**), and that with pyridine yielded *trans,cis,cis*-$RuCl_2(PTA)_2(py)_2$ (**24**).

Interestingly, when the reaction with pyridine was performed in a refluxing $CHCl_3$ and EtOH/$CHCl_3$ mixture, an unusual disproportion was observed with formation of *trans,mer*-$RuCl_2(PTA)_3(py)$ (**25**), in which one dmso is replaced by pyridine and the other by a PTA (coming from **10**).

In general, we observed that the *trans*-{$Ru(PTA)_2$} and *mer*-{$Ru(PTA)_3$} fragments are particularly stable (see also Chapter 3); only three among the new complexes do not have two mutually *trans* PTAs: *cis,cis*-$Ru(chel)Cl_2(PTA)_2$ (chel = bpy (**22**) or bpyAc (**23**)) and *trans,cis,cis*-$RuCl_2(PTA)_2(py)_2$ (**24**).

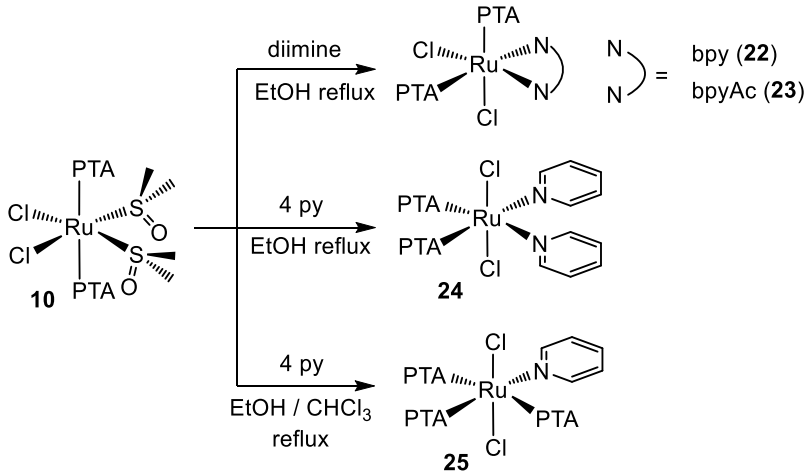

Scheme 2.18. Reactivity of *cis,cis,trans*-$RuCl_2(dmso\text{-}S)_2(PTA)_2$ (**10**) towards mono and diimine ligands.

As anticipated, all the neutral Ru-PTA complexes acquire the amphiphilic nature of PTA and are typically quite soluble both in organic solvents (e.g. chloroform) and in water. Perhaps counterintuitively, the solubility in water decreases upon protonation of coordinated PTA, to such an extent that addition of a strong mineral acid to an aqueous solution of a neutral Ru-PTA complex is often a convenient approach for obtaining crystals of the corresponding charged PTAH derivative. The single-crystal X-ray structure of the following complexes was also determined: *trans*-$[RuCl_4(PTAH)_2]Cl\cdot H_2O$ (**3**·H_2O), *trans*-$[RuBr_2(PTA)_4]\cdot 0.682(C_4H_{10}O)$ (**11**), *cis*-$[RuBr_2(PTA)_4]\cdot 0.37(H_2O)$ (**12**), *mer*-$[Ru(bpy)Cl(PTA)_3]Cl\cdot 6H_2O$ (**17**), *cis,cis*-$Ru(bpy)Cl_2(PTA)_2$ (**22**), *trans,cis,cis*-$RuCl_2(PTA)_2(py)_2$ (**24**) and *trans,mer*-$RuCl_2(py)(PTA)_3$ (**25**).

In aqueous solution all the above-reported complexes share common hydrolytic features, consistent with the rather high *trans*-influence of PTA: in both neutral and cationic species the selective dissociation of a chloride *trans* to PTA occurs (to different extents and with different rates, depending on the species), whereas mutually *trans* chlorides are stable and their dissociation is negligible.

Furthermore, the color of the complex is affected by the chloride geometry: complexes with the {*trans*-$RuCl_2$} fragment typically are yellow, whereas those with the {*cis*-$RuCl_2$} fragment are colorless (or very pale yellow).

Regarding the NMR characterization of octahedral Ru–PTA compounds, in general the ^{1}H NMR spectra are not particularly informative about the ligand geometry. Coordinated PTA typically gives two resolved resonances (broad singlets or AB quartets) between 3.5 and 4.9 ppm. The one at higher frequency belongs to the NCH_2N protons and the other to the NCH_2P protons. In addition, they are coupled to well separated carbon resonances in the HSQC spectra: ca. 70-75 ppm for NCH_2N carbons whereas 50-59 ppm for NCH_2P. The ^{31}P NMR spectra are instead very informative about the number of coordinated PTAs and their geometry in the complex. In fact, the phosphorous chemical shift is strongly influenced by the nature

of the ligand in *trans* position and it can thus be used as a diagnostic tool to establish the PTA geometry in octahedral Ru–PTA complexes.[28] The typical chemical-shift regions as well as the corresponding interval for the Ru(II)–P bond lengths are reported in Table 2.3. With the exception of the bis(hydride) complex *cis*-$RuH_2(PTA)_4$,[2,22] there is a rough correlation between the two parameters: as the Ru–P bond length increases, the ^{31}P NMR resonance shifts progressively to lower frequencies. Moreover, we observed that when PTA is *trans* to an imine nitrogen (i.e. py, bpy), the ^{31}P NMR chemical shift is affected by the nature of the ligand: when *trans* to py it falls in the range –20 ÷ –23 ppm, whereas when *trans* to bpy or bpyAc it falls in the range –34 ÷ –50 ppm. We argue that this behavior might be due to the different orientation of the aromatic rings containing the imine nitrogen: chelating diimine ligands (i.e. bpy, bpyAc) are in the plane containing PTA, whereas pyridine is typically almost orthogonal to such plane. The different orientation, and consequently different involvement of the π orbitals of these ligands, could explain the different ^{31}P chemical shift intervals for PTA *trans* to pyridine and *trans* to diimine ligands.

Table 2.3. Typical ^{31}P chemical shift intervals (Δ) and Ru–P distances for PTA bound to octahedral Ru(II) complexes as a function of the nature of the *trans* ligand.

Ligand *trans* to PTA	Δ ^{31}P (ppm)[a]	Δ Ru–P distance (Å)	Ref.
OH_2/OH	–5 ÷ –16	-	this Chapter, 17, 11
N[b]	–20 ÷ –23	2.1933 ÷ 2.224	this Chapter
Cl	–14 ÷ –26	2.232 ÷ 2.283	this Chapter, 1b, 11
Br	–24 ÷ –27	2.266 ÷ 2.281	this Chapter
S[c]	–30 ÷ –45	2.280 ÷ 2.318	20, 29
N[d]	–34 ÷ –50	2.260 ÷ 2.344	this Chapter, 30, 31, 32, 33, 34, 35, 36, 37
H	–26.6[e]	2.299 ÷ 2.300	2
P[f]	–45 ÷ –60	2.290 ÷ 2.400	this Chapter, 1b, 2, 11, 15, 17, 19, 37, 38
C[g]	–68.4[e]	2.395(1)	39

[a] For comparison, the singlet of free PTA falls at δ = –98.2 ppm in D_2O and at –102.3 ppm in $CDCl_3$. [b] From pyridine. [c] From [9]aneS3 = 1,4,7-trithiacyclononane. [d] From imine or azole. [e] Single hit. [f] From PTA. [g] From cyclometallated 2-phenylpyridine.

2.6 Bibliography

[1] a) D. J. Darensbourg, F. Joó, M. Kannisto, A. Katho, J. H. Reibenspies, *Organometallics,* **1992**, *11*, 1990 - 1993; b) D. J. Darensbourg, F. Joó, M. Kannisto, A. Kathó, J. H. Reibenspies, D. J. Daigle, *Inorg. Chem.*, **1994**, *13*, 200 - 208.

[2] C. A. Mebi, B. J. Frost, *Inorg. Chem.*, **2007**, *46*, 7115 - 7120.

[3] R. Girotti, A. Romerosa, S. Mañas, M. Serrano-Rui, R. N. Perutz, *Inorg. Chem.*, **2009**, *48*, 3692 - 3698.

[4] a) A. D. Phillips, L. Gonsalvi, A. Romerosa, F. Vizza, M. Peruzzini, *Coord. Chem. Rev.*, **2004**, *248*, 955 - 993; b) J. Bravo, S. Bolaño, L. Gonsalvi, M. Peruzzini, *Coord. Chem. Rev.*, **2010**, *254*, 555 - 607.

[5] For a recent review see: P. Crochet, V. Cadierno, *Dalton Trans.*, **2014**, *43*, 12447 - 12462.

[6] a) G. Laurenczy, F. Joó, L. Nádasdi, J. Elek, *Chem. Commun.*, **1999**, 971 - 972; b) G. Laurenczy, F. Joó, L. Nádasdi, *Inorg. Chem.*, **2000**, *39*, 5083 - 5088; c) G. Laurenczy, F. Joó, L. Nádasdi, *High Pressure Res.*, **2000**, *18*, 251 - 255; d) G. Kovács, L. Nádasdi, G. Laurenczy, F. Joó, *Green Chem.*, **2003**, *5*, 213 - 217.

[7] W.-C. Lee, B. J. Frost, *Green Chem.*, **2012**, *14*, 62 - 66.

[8] A. Guerriero, M. Peruzzini, L. Gonsalvi, *Coord. Chem. Rev.*, **2017**, (doi.org/10.1016/j.ccr.2017.09.024).

[9] D.J. Darensbourg, T.J. Decuir, J.H. Reibenspies, in: *Aqueous Organometallic Chemistry and Catalysis*, (Ed: I.T. Horváth, F. Joó), Kluwer Academic Publishers, Dordrecht, **1995**, 61 - 80.

[10] S. Moret, P. J. Dyson, G. Laurenczy, *Nature Commun.*, **2014**, *5*, 1 - 7.

[11] A. Udvardy, M. Serrano-Ruiz, V. Passarelli, E. Bolyog-Nagy, F. Joó, Á. Kathó, A. Romerosa, *Inorg. Chim. Acta*, **2017**. (doi.org/10.1016/j.ica.2017.04.054).

[12] a) T. Gianferrara, I. Bratsos, E. Iengo, B. Milani, A. Oštrić, C. Spagnul, E. Zangrando, E. Alessio, *Dalton Trans.*, **2009**, *48*, 10742 - 10756; b) T. Gianferrara,

A. Bergamo, I. Bratsos, B. Milani, C. Spagnul, G. Sava, E. Alessio, *J. Med. Chem.*, **2010**, *53*, 4678 - 4690.

[13] a) C. Spagnul, R. Alberto, G. Gasser, S. Ferrari, V. Pierroz, A. Bergamo, T. Gianferrara, E. Alessio, *J. Inorg. Biochem.*, **2013**, *122*, 57 - 65; b) T. Gianferrara, C. Spagnul, R. Alberto, G. Gasser, S. Ferrari, V. Pierroz, A. Bergamo, E. Alessio, *ChemMedChem*, **2014**, *9*, 1231 - 1237.

[14] E. Alessio, *Chem. Rev.*, **2004**, *104*, 4203 - 4242.

[15] A. Udvardy, A. C. Bényei, Á. Kathó, *J. Organomet. Chem.*, **2012**, *717*, 116 - 122.

[16] a) D. J. Daigle, A. B. Pepperman Jr., S. L. Vail, *J. Heterocycl. Chem.*, **1974**, *11*, 407 - 408; b) D. J. Daigle, *Inorg. Synth.*, **1998**, *32*, 40 - 45.

[17] J. Kovács, F. Joó, A. Bényei, G. Laurenzy, *Dalton Trans.*, **2004**, 2336 - 2340.

[18] C. M. Duff, G. A. Heath, *J. Chem. Soc. Dalton Trans.*, **1991**, 2401 - 2411.

[19] D. N. Akbayeva, S. Moneti, M. Peruzzini, L. Gonsalvi, A. Ienco, F. Vizza, *C. R. Chimie*, **2005**, *8*, 1491 - 1496.

[20] E. Iengo, N. Demitri, G. Balducci, E. Alessio, *Dalton Trans.*, **2014**, *43*, 12160 - 12163.

[21] F. Battistin, G. Balducci, N. Demitri, E. Iengo, B. Milani, E. Alessio, *Dalton Trans.*, **2015**, *44*, 15671 - 15682.

[22] N. Nickita, G. Gasser, P. Pearson, M. J. Belousoff, L. Y. Goh, A. M. Bond, G. B. Deacon, L. Spiccia, *Inorg. Chem.*, **2009**, *48*, 68 - 81.

[23] (*a*) T. Joshi, G. J. Barbante, P. S. Francis, C. F. Hogan, A. M. Bond, G. Gasser, L. Spiccia, *Inorg. Chem.*, **2012**, *51*, 3302 - 3315; (*b*) T. Joshi, G. Gasser, L. L. Martin, L. Spiccia, *RSC Adv.*, **2012**, *2*, 4703 - 4712; (*c*) T. Joshi, M. Patra, L. Spiccia, G. Gasser, *Artificial DNA: PNA & XNA*, **2013**, *4*, 11 - 18; (*d*) C. Bischof, T. Joshi, A. Dimri, L. Spiccia, U. Schatzschneider, *Inorg. Chem.*, **2013**, *52*, 9297 - 9308.

[24] T. Joshi, V. Pierroz, S. Ferrari, G. Gasser, *ChemMedChem*, **2014**, *9*, 1231 - 1237.

[25] V. Pierroz, T. Joshi, A. Leonidova, C. Mari, J. Schur, I. Ott, L. Spiccia, S. Ferrari, G. Gasser, *J. Am. Chem. Soc.*, **2012**, *134*, 20376 - 20387.

[26] T. Joshi, V. Pierroz, C. Mari, L. Gemperle, S. Ferrari, G. Gasser, *Angew. Chem. Int. Ed.*, **2014**, *53*, 2960 - 2963.

[27] In the ^{1}H NMR spectrum of **13** in $CDCl_3$ the most downfield signal, assigned to the NC*H*$_2$N protons of the equivalent PTAs, is a well resolved AB quartet centered at $\delta = 4.50$, rather than a singlet as reported in ref. 15.

[28] However, the ^{31}P chemical shift of coordinated PTA in D_2O depends on the pH and typically shifts to higher frequencies as the pH decreases. The largest shifts are encountered at pH values of ca. 3, which corresponds to the average pKa of PTA coordinated to a Ru(II) center. As an example, the titration of **10** is reported in the Appendix (Figure A2.47); see also ref. 15.

[29] B. Serli, E. Zangrando, T. Gianferrara, C. Scolaro, P. J. Dyson, A. Bergamo, E. Alessio, *Eur. J. Inorg. Chem.*, **2005**, 3423 - 3434.

[30] S. Bolaño, J. Bravo, J. Castro, M. M. Rodriguez-Rocha, M. F. C. G. da Silva, A. J. L. Pombeiro, L. Gonsalvi, M. Peruzzini, *Eur. J. Inorg. Chem.*, **2007**, 5523 - 5532.

[31] A. García-Fernández, J. Díez, A. Manteca, J. Sánchez, M. P. Gamasa, E. Lastra, *Polyhedron,* **2008**, *27*, 1214 - 1228.

[32] S. Bolaño, M. M. Rodriguez-Rocha, J. Bravo, J. Castro, E. Onate, M. Peruzzini, *Organometallics,* **2009**, *28*, 6020 - 6030.

[33] S. Miguel, J. Diez, M. P. Gamasa, M. E. Lastra, *Eur. J. Inorg. Chem.*, **2011**, *951*, 4745 - 4755.

[34] E. Menéndez-Pedregal, J. Díez, Á. Manteca, J. Sánchez, A. C. Bento, R. García-Navas, F. Mollinedo, M. Pilar Gamasa, E. Lastra, *Dalton Trans.*, **2013**, *42*, 13955 - 13967.

[35] A. Garcia-Fernandez, J. Diez, M. Pilar Gamasa, E. Lastra, *Eur. J. Inorg. Chem.*, **2014**, *5*, 917 - 924.

[36] F. Scalambra, M. Serrano-Ruiz, S. Nahim-Granados, A. Romerosa, *Eur. J. Inorg. Chem.*, **2016**, *10*, 1528 - 1540.

[37] A. Wołoszyn, C. Pettinari, R. Pettinari, G. V Badillo Patzmay, A. Kwiecień, G. Lupidi, M. Nabissi, G. Santoni, P. Smoleński, *Dalton Trans.*, **2017**, *46*, 10073 - 10081.

[38] S. Grguric-Sipka, C. R. Kowol, S.-M. Valiahdi, R. Eichinger, M. A. Jakupec, A. Roller, S. Shova, V. B. Arion, B. K. Keppler, *Eur. J. Inorg. Chem.*, **2007**, 2870 - 2878.

[39] L. Leyva, C. Sirlin, L. Rubio, C. Franco, R. Le Lagadec, J. Spencer, P. Bischoff, C. Gaiddon, J.-P. Loeffler, M. Pfeffer, *Eur. J. Inorg. Chem.*, **2007**, 3055 - 3066.

CHAPTER 3

Ru(II)-PTA carbonyls

3.1 State of the art

In literature there are no clear examples of Ru(II) carbonyl complexes with 1,3,5-triaza-7-phosphoadamantane (PTA). It was only reported that the reaction of *trans*-$RuCl_2(PTA)_4$ (**1**) with CO (1 atm) leads to a complex of undefined geometry formulated as $RuCl_2(CO)(PTA)_3$, characterized only by elemental analysis and by the presence of an IR band for bound CO at 1987 cm^{-1}.[1]

In general, the literature about Ru(II)-CO phosphine compounds is quite dated, most of the studies were performed in the late 60's – early 70's of last century, and often important details are missing. Both mono- and dicarbonyl neutral complexes with phosphines, of general formula $RuCl_2(CO)(L)_3$ and $RuCl_2(CO)_2(L)_2$, respectively, are known. Typically, the monocarbonyl compounds present the three phosphines (e.g. L = PPh_3, PMe_2Ph, PEt_2Ph) in a *mer* geometry (i.e. *trans,mer*-$RuCl_2(CO)(L)_3$ and *cis,mer*-$RuCl_2(CO)(L)_3$,), whereas the three stereoisomers *cis,cis,trans*-, all-*trans*-, and all-*cis*-$RuCl_2(CO)_2(L)_2$, have been identified for the dicarbonyl compounds.[2]

Such Ru(II) compounds were mainly prepared by the addition of the phosphine to a carbonyl precursor: typically, hydrate $RuCl_3$ was boiled in an organic solvent (i.e. ethanol or 2-methoxhyethanol) with bubbling CO, generating a poorly characterized "red carbonyl solution", that most likely contains a mixture of the dinuclear species $[RuCl_2(CO)_3]_2$ and of the less well characterized polymeric species $[RuCl_2(CO)_2]_n$.[3] Addition of two or three equivalents of the desired phosphine to this solution afforded the di- or monocarbonyl compounds, respectively.[2,4] The monocarbonyl $RuCl_2(CO)(L)_3$ complexes were typically obtained with the *cis*,*mer* geometry, whereas the two *cis,cis,trans*- and all-*trans*- stereoisomers, either pure or in mixture,

were obtained for the dicarbonyl $RuCl_2(CO)_2L_2$ compounds, depending on the reaction conditions after the addition of the phosphine. Column chromatography of the mixture afforded the pure isomers.[5]

In another synthetic strategy, a mixture of the all-*trans* and *cis*,*cis*,*trans*-$RuCl_2(CO)_2(PPh_3)_2$ isomers was obtained by bubbling CO in a warm acetone solution of $RuCl_2(PPh_3)_4$. The pure isomers were obtained by recrystallization.[2b]

The group of Mawby investigated the thermal- and light-induced interconversion of the dicarbonyl complexes.[6] They reported that the *cis,cis,trans*-$RuCl_2(CO)_2(L)_2$ isomer can be converted by irradiation with a mercury lamp (125 W) to the all-*trans* isomer, that appears to be a kinetic product: by heating at 40°C it converts into the all-*cis* isomer, whereas at higher temperature it converts to the more stable *cis,cis,trans* isomer. Consistently, the all-*cis* isomer was fully converted to the *cis,cis,trans*-$RuCl_2(CO)_2(L)_2$ compound upon heating (Scheme 3.1).

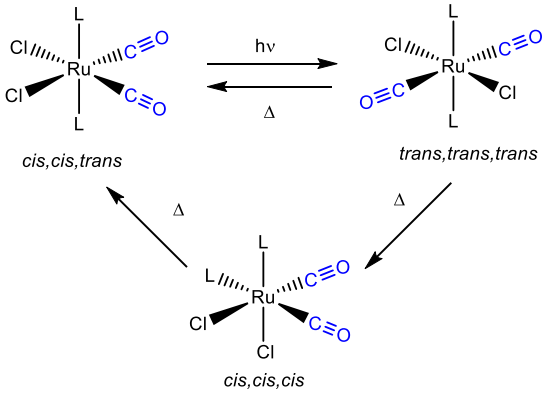

Scheme 3.1. Thermal- and light-induced interconversion of the dicarbonyl Ru(II)-phosphine compounds (L = phospine).

3.2 Aim of the Chapter

As stated in the Introduction, our aim is that of preparing new water-soluble complexes for the construction of supramolecular assemblies or metal-conjugates that maintain solubility in water.[7] In this respect, Ru(II)-PTA carbonyls, in particular if possessing residual dmso ligands, might have suitable requisites. In addition, water-soluble Ru-PTA-CO complexes might be of interest also as catalysts in aqueous medium or in biphasic systems, in particular for reactions involving CO and/or CO_2, where carbonyl species are likely intermediates.

Finally, they might also be investigated as potential CO-releasing molecules (*CORMs*).[8] This is an emerging field of medicinal chemistry in which several compounds, including metal carbonyls, are investigated for the release of CO in tissues or cells. In fact, controlled amounts of carbon monoxide show a positive role in cardiovascular and inflammatory impairment, in promoting wound healing, and have bactericidal action.[9] Ideally, controlled CO-release should be triggered by an endogenous chemical or biochemical stimulus or by applying an external stimulus such as visible light (photo CO-releasing molecules or photo-*CORMs*). Up to date the most promising Ru(II) *CORM* is the water-soluble compound $Ru(CO)_3Cl$(glycinate) (CORM-3) which has been extensively studied in the biological environment to understand the influence of CO inside the cells.[10]

Here we reinvestigated the reactions of both *trans*- and *cis*-$RuCl_2(PTA)_4$ isomers with CO. Moreover, the investigation was extended to the complex *cis,cis,trans*-$RuCl_2$(dmso-S)$_2(PTA)_2$ (**6**).

As the above compounds showed a rather poor reactivity towards CO, we decided to explore a different approach: instead of adding CO to Ru(II)-PTA complexes, the yet unexplored reactivity of a series of well-known neutral Ru(II)-CO-dmso compounds with PTA was investigated. These compounds, whose general formula is $[RuCl_2(CO)_x(dmso)_{4-x}]$ (x = 1-3, Figure 3.1), have from one to three carbonyls.

Besides the two chlorides – that can be either in *cis* or *trans* geometry – the coordination sphere is completed by dmso ligands.[3,11] In such complexes when a dmso is coordinated *trans* to CO it is always bonded through oxygen (dmso-O), is rather labile and easily replaced by monodentate N-donor ligands (e.g. py or NH_3). However, also the more strongly bonded dmso-S ligands (if present) can be rather easily replaced by neutral ligands, e.g. by chelating diimines.

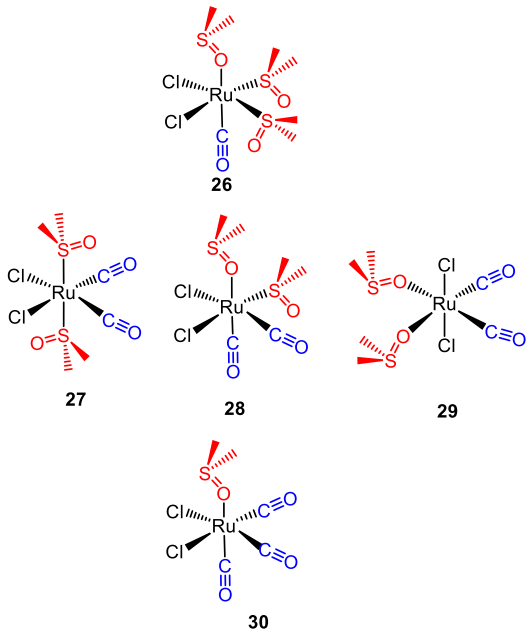

Figure 3.1. Schematic structures of the Ru(II)-CO-dmso compounds used in this Chapter: the monocarbonyl *fac*-$RuCl_2(CO)(dmso)_3$ (**26**); the three dicarbonyl isomers *cis*,*cis*,*trans*-$RuCl_2(CO)_2(dmso\text{-}S)_2$ (**27**), *cis*,*cis*,*cis*-$RuCl_2(CO)_2(dmso)_2$ (**28**), and *trans*,*cis*,*cis*-$RuCl_2(CO)_2(dmso\text{-}O)_2$ (**29**); the tricarbonyl *fac*-$RuCl_2(CO)_3(dmso\text{-}O)$ (**30**).

For the sake of clarity the reactivity of the neutral Ru(II)-CO-dmso compounds towards PTA will be reported first, followed by the reinvestigation of the behavior of neutral Ru(II)-PTA complexes with CO.

3.3 Reactions of neutral Ru(II)-CO-dmso compounds with 1,3,5-triaza-7-phosphoadamantane

Even though two meridional stereoisomers of the monocarbonyl compound *fac*-$RuCl_2(CO)(dmso)_3$ (**26**) are also known,[10] only **26** has been investigated here.

We found that treatment of **26** with two equivalents of PTA in methanol at room temperature afforded a pale yellow precipitate identified as *cis*,*cis*,*trans*-$RuCl_2(CO)(dmso\text{-}S)(PTA)_2$ (**31**) (Scheme 3.2). This complex is well soluble in water, chloroform and DMSO. The ^{31}P NMR spectrum in $CDCl_3$ shows a singlet at –55.2 ppm, the typical region of mutually *trans* PTAs.[12] The ^{1}H NMR spectrum of **31** in $CDCl_3$ shows three different resonances: a broad singlet at 4.53 ppm (12H), an AB system centered at 4.41 ppm (12H), and a sharp singlet at 3.26 ppm (6H) (Appendix, A3.2). The two downfield signals, that are coupled to one another in the ^{1}H-^{1}H COSY spectrum, belong respectively to the NC*H*$_2$N and to the NC*H*$_2$P groups of the two equivalent PTA ligands (Appendix, A3.2) The upfield singlet belongs to the equivalent methyl groups of dmso-S (thus indicating that it has to be in a symmetrical environment and *trans* to a Cl rather than to CO).

The NMR spectra in D_2O are similar to those in chloroform, but the complex slowly (days) partially releases a chloride (presumably that *trans* to CO). In fact, immediately after dissolution in D_2O the ^{31}P NMR spectrum of **31**, presents exclusively a singlet at –52.8 ppm, but after three days in the dark a new singlet at –47.7 ppm appears. This latter was found to disappear upon the addition of an excess of NaCl. (Appendix, A3.5). The corresponding ^{1}H NMR spectrum in D_2O after three days shows three new resonances downfield shifted compared those of **31**. No signal for free DMSO was observed.

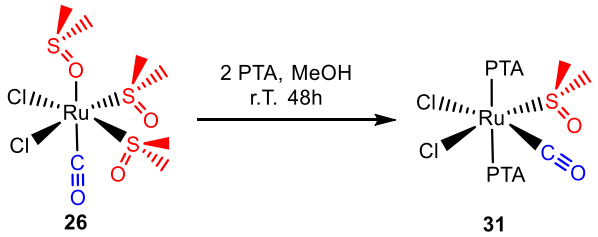

Scheme 3.2. Preparation of *cis*,*cis*,*trans*-$RuCl_2(CO)(dmso\text{-}S)(PTA)_2$ (**31**) upon treatment of *fac*-$RuCl_2(CO)(dmso)_3$ **(26)** with PTA in methanol.

The presence of coordinated CO was supported by the solid state IR spectrum, that presents a carbonyl stretching band at 1950 cm^{-1} (Table 3.1). The geometry of the complex was confirmed by single-crystal X-ray diffraction (Figure 3.2).

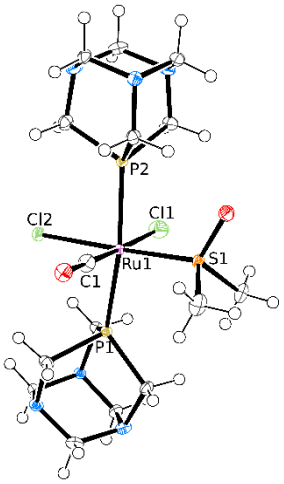

Figure 3.2. X-ray molecular structure (50% probability ellipsoids) of *cis*,*cis*,*trans*-$RuCl_2(CO)(dmso\text{-}S)(PTA)_2$ (**31**). Crystals obtained by recrystallization of the raw product from chloroform/diethyl ether. Coordination distances in ångström (Å): Ru1–Cl1 = 2.432(2), Ru1–Cl2 = 2.40(1), Ru1–S1 = 2.72(1), Ru1–C1 = 1.80(1), Ru1–P1 = 2.385(1), Ru1–P2 = 2.357(1).

When the reaction was repeated using only one equivalent of PTA, a mixture of **31** and unreacted **26** was obtained. Similar results were obtained performing the reaction at 4°C. Under all the conditions examined, **26** reacts with PTA forming always a complex with two mutually *trans* PTAs, even when a defect of the ligand is used. Moreover, the coordination of PTA causes the isomerization of CO from being *trans* to dmso to being *trans* to Cl.

The reaction of **26** with two equivalents of PTA in refluxing solvents led to a mixture of **31** and of a new complex in which three PTAs replaced all the dmso ligands. In fact the ^{31}P NMR spectrum of the raw product shows, in addition to the singlet of **26**, an AX_2 system consisting of a doublet centered at –55.9 ($^2J_{P\text{-}P}$ = 40.4 Hz) ppm and a triplet centered at –63.6 ppm. The chemical shift of the doublet is consistent with two mutually *trans* PTAs, while that of the triplet falls in an unusual region: since PTA *trans* Cl usually is between –21 and –26 ppm (see Chapter 2, Table 2.3), it was supposed that the triplet belongs to a PTA *trans* to CO, so the new species was formulated as *trans*,*mer*-$RuCl_2(CO)(PTA)_3$ (**32**). We found that this new complex can be isolated in pure form in two different ways (Scheme 3.3): *i*) by refluxing an ethanol solution of **26** and 4 eq of PTA for 15h or *ii*) by treating the same mixture in a microwave reactor at 140°C for 30 min. Both procedures afforded **32** as a yellow precipitate in good yield. Compound **32** is well soluble in water and DMSO and sufficiently soluble in $CHCl_3$ (e.g. for NMR purposes). The ^{1}H NMR spectrum of **32** in $CDCl_3$ (Appendix, A3.6) shows resonances only in the region of coordinated PTA: two relatively broad singlets at δ = 4.32 (6H) and 4.37 ppm (12H), and a multiplet (18H) centered at δ = 4.57 ppm. The singlets belong to the NC*H*$_2$P groups of the two types of PTA ligands: in fact, in the ^{1}H-^{1}H COSY spectrum they are both coupled to the multiplet (generated by the NC*H*$_2$N groups), whereas in the ^{1}H-^{13}C HSQC spectrum they have distinct cross-peaks with carbon atoms that resonate in the N*C*H$_2$P region. The NMR spectra in D_2O – in which **32** is more soluble – are similar to those in $CDCl_3$ and showed no change after one week in the dark. This finding is consistent with the *trans* geometry of the two chlorides, that is typically quite stable. Solid state IR spectrum confirmed the presence of coordinated CO with a band at 1986 cm^{-1} (Table 3.1). To be noted that a different isomerization process occurs in this case (compared to **31**): the two originally *cis* chlorides, have a *trans* geometry in the product, whereas CO is *trans* to a PTA.

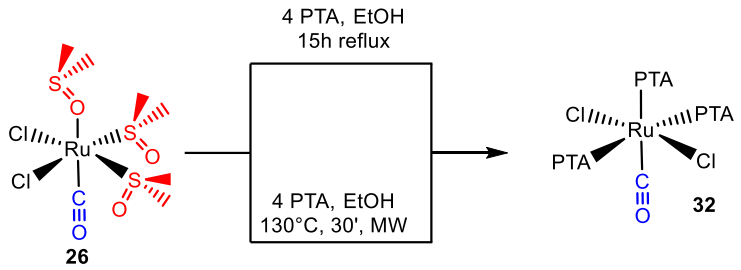

Scheme 3.3. Preparation of *trans,mer*-$RuCl_2(CO)(PTA)_3$ (**32**) upon treatment of *fac*-$RuCl_2(CO)(dmso)_3$ (**26**) with PTA in ethanol.

The geometry of the complex was confirmed by single-crystal X-ray diffraction (Figure 3.3). The Ru–PTA distance *trans* to CO (2.3821(7) Å) is slightly longer than those of the mutually *trans* PTAs (2.33458(6) and 2.3399(7) Å), suggesting that CO has a stronger *trans*-influence than PTA (Table 3.2). This is the first reported structure of a Ru(II) complex in which PTA is *trans* to CO.

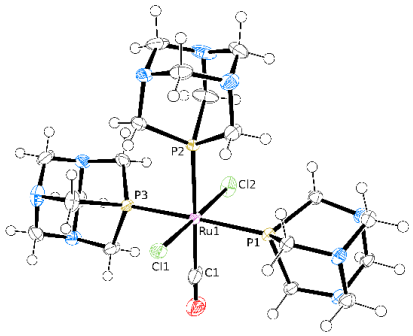

Figure 3.3. X-ray molecular structure (50% probability ellipsoids) of *trans*,*mer*-$RuCl_2(CO)(PTA)_3$ (**32**). Crystals obtained by recrystallization of the raw product from chloroform/diethyl ether. Coordination distances in ångström (Å): Ru1–Cl1 = 2.4049(8), Ru1–Cl2 = 2.4253(7), Ru1–C1 = 1.928(3), Ru1–P1 = 2.3399(7), Ru1–P2 = 2.3821(7), Ru1–P3 = 2.3458(5).

When the reaction of **26** with three equivalents of PTA was performed in refluxing water, rather than in ethanol, the pale yellow *cis* isomer of **32**, i.e. *cis*,*mer*-$RuCl_2(CO)(PTA)_3$ (**33**), in which CO is *trans* to a Cl rather than to a PTA, was isolated upon evaporation of the solvent. (Scheme 3.4).

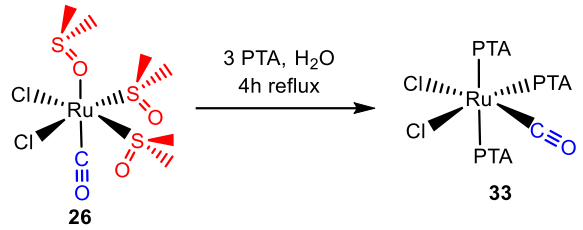

Scheme 3.4. Preparation of *cis,mer*-$RuCl_2(CO)(PTA)_3$ (**33**) upon treatment of *fac*-$RuCl_2(CO)(dmso)_3$ (**26**) with PTA in water.

The presence of the coordinated CO was confirmed by the solid state IR spectrum that presents a CO stretching band at 1942 cm^{-1} (Table 3.1). Single-crystal X-ray analysis confirmed the geometry of the complex (Figure 3.4). The Ru–PTA bond length *trans* to Cl (2.2865(6) Å) is very short, whereas the Ru–P distances of the mutually *trans* PTAs (2.3811(5) and 2.3488(5) Å) are even longer than those found in **32**.

This complex is well soluble in water and DMSO, but – contrary to **32** – sparingly soluble in chloroform. Immediately after the dissolution in D_2O, the ^{31}P NMR spectrum of **33** shows two AX_2 systems in ca. 1/4 ratio, consisting of two triplets centered respectively at –16.4 ($^2J_{P\text{-}P}$ = 26.8 Hz) and –20.9 ppm ($^2J_{P\text{-}P}$ = 25.5 Hz) and two doublets centered respectively at –48.2 and –51.9 ppm. By addition of an excess of NaCl the downfield (and minor) AX_2 system disappeared, in agreement with the presence of an equilibrium between **33** and the aqua species $\mathbf{33_{aq}}$ (Appendix, A3.10-A3.12) (Scheme 3.5).

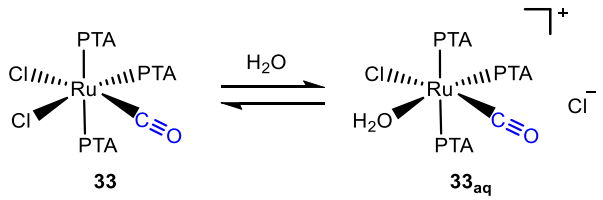

Scheme 3.5. Chloride hydrolysis equilibrium of the complex *cis,mer*-$RuCl_2(CO)(PTA)_3$ (**33**) in aqueous solution.

According to the chemical shifts, in **33** the triplet belongs to a PTA *trans* to Cl and the doublet to the mutually *trans* PTAs, whereas in the aqua species $\mathbf{33_{aq}}$ the triplet

belongs to a PTA *trans* to H_2O. Therefore the selective dissociation of the chloride *trans* to PTA occurs. This hypothesis is supported also by the X-ray data (Table 3.2) in which the Ru–Cl bond length *trans* to PTA (2.4694(6) Å) is longer than that *trans* to CO (2.4419(7) Å). This behavior is also consistent with what observed in other Ru-PTA complexes featuring Cl *trans* to PTA (e.g. compound **17PF$_6$** and **22** in Chapter 2). However, this finding is apparently in contradiction with the lower *trans*-influence of PTA compared to CO found in **32**, and suggests that not only the length of the Ru–PTA bond but also its *trans*-influence depend on the nature of the *trans* ligand: PTA prefers to be bound *trans* to σ-donors such as Cl (short Ru–P bond length) that, however, are remarkably destabilized (long Ru–Cl bond). The ^{1}H NMR spectrum of **33** in D_2O (registered with an excess of NaCl) shows three different resonances: two broad singlets and a multiplet centered respectively at 4.12, 4.33 and 4.49 ppm. The upfield singlet (6H) belongs to the NC*H*$_2$P groups of the PTA *trans* to Cl, while the other singlet (12H) belongs to the NC*H*$_2$P group of the mutually *trans* PTAs. Both singlets are coupled in the ^{1}H-^{1}H COSY spectrum with the multiplet (generated by the NC*H*$_2$N groups) (Appendix, A3.10-A3.12).

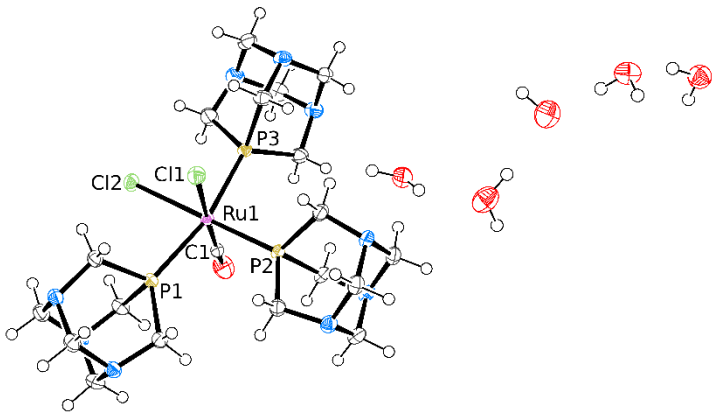

Figure 3.4. Molecular structure (50% probability ellipsoids) of *cis*,*mer*-$RuCl_2(CO)(PTA)_3$ (**33**). Crystals formed spontaneously from a DMSO solution. Coordination distances in ångström (Å): Ru1–Cl1 = 2.4419(7), Ru1–Cl2 = 2.4694(6), Ru1–C1 = 1.926(3), Ru1–P1 = 2.3811(5), Ru1–P2 = 2.2865(6), Ru1–P3 = 2.3488(5).

We found that, when heated in refluxing water, **32** isomerizes completely to **33** in 5 h (Scheme 3.6), thus indicating that **33** is the thermodynamic isomer.

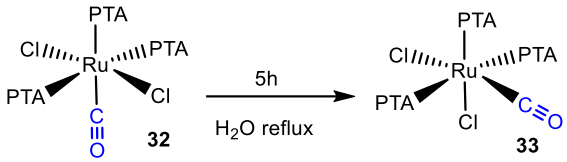

Scheme 3.6. Isomerization of *trans*,*mer*-$RuCl_2(CO)(PTA)_3$ (**32**) to *cis*,*mer*-$RuCl_2(CO)(PTA)_3$ (**33**) in refluxing water.

Moreover, since other Ru(II)-PTA complexes undergo light-induced isomerization (see Chapter 2),[13] and **32** has an absorption band at 431 nm, we monitored by NMR spectroscopy the behavior of a water solution of **32** irradiated with blue light (λ = 470 nm, 40 mW) (Scheme 3.7). After 1h of irradiation the ^{31}P NMR spectrum shows the presence of a new main AX_2 system (in 2.5 : 1 ratio with **32**) formed by a doublet centered at –27.9 ppm and a triplet centered at –64.3 ppm ($^2J_{P\text{-}P}$ = 32.1 Hz) (Figure 3.5). According to the position of the signals, this spectrum belongs to a new monocarbonyl complex that has two equivalent PTAs *trans* to Cl and a PTA *trans* to CO, i.e. to *fac*-$RuCl_2(CO)(PTA)_3$ (**34**), a stereoisomer of **32** and **33**. For longer irradiation times, **32** disappeared completely and the resonances of **33** and $\mathbf{33_{aq}}$ appeared besides those of **34** (Figure 3.5). Unfortunately it was not possible to isolate **34** in pure form and register the IR spectrum.

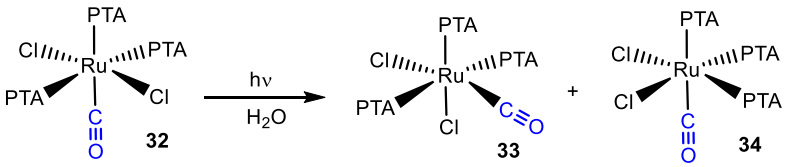

Scheme 3.7. Light-induced isomerization (λ = 470 nm) of *trans*,*mer*-$RuCl_2(CO)(PTA)_3$ (**32**) to *cis*,*mer*-$RuCl_2(CO)(PTA)_3$ (**33**) and *fac*-$RuCl_2(CO)(PTA)_3$ (**34**).

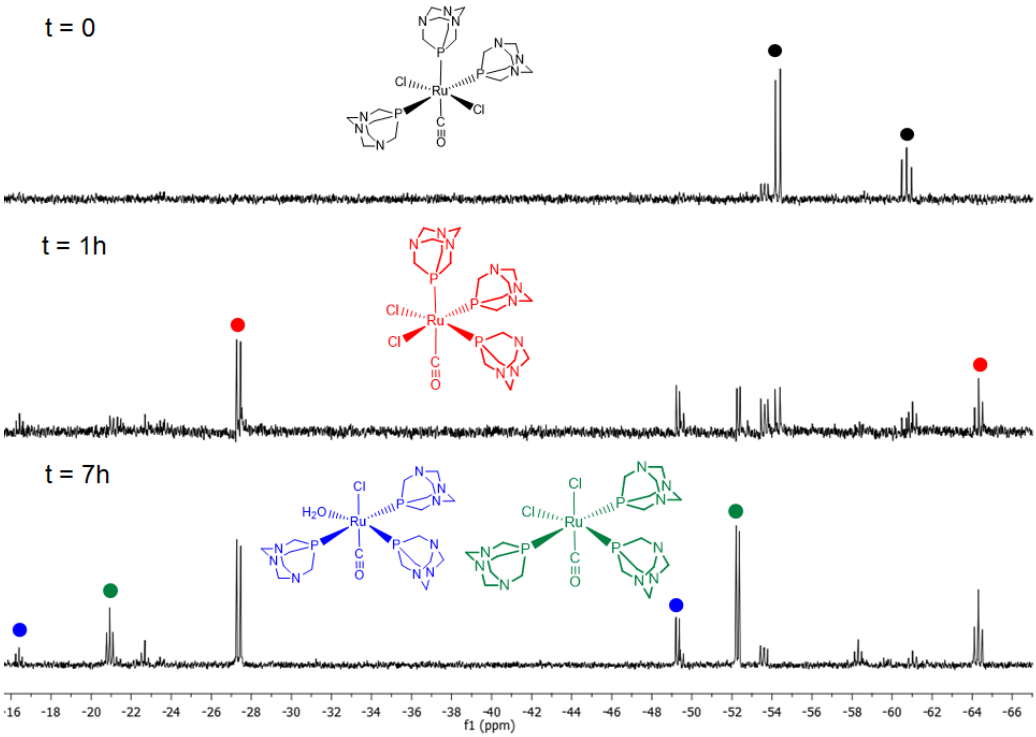

Figure 3.5. ^{31}P NMR spectra of *trans*,*mer*-$RuCl_2(CO)(PTA)_3$ (**32**, black dots) registered immediately after dissolution in D_2O (top), after 1 hour of irradiation with blue light (middle) and after 7 hours of irradiation (bottom). The signals of *fac*-$RuCl_2(CO)(PTA)_3$ (**34**) are labeled with red dots, while those of *cis*,*mer*-$RuCl_2(CO)(PTA)_3$ (**33**) and *cis*,*mer*-$RuCl(OH_2)(CO)(PTA)_3$ (**33$_{aq}$**) with green and blue dots, respectively.

The reactivity of *fac*-$RuCl_2(CO)(dmso)_3$ (**26**) towards PTA is summarized in Scheme 3.8. From this precursor we were unable to prepare monocarbonyl Ru(II) complexes with a single PTA ligand. Even sub-stoichiometric amounts of PTA replaced at least two dmso ligands in **26**; in addition, we notice that all the three isolated isomers **31** – **33** have two mutually *trans* PTAs, suggesting that this geometry is particularly stable.

Even though the Ru–CO bond lengths in the isomers **32** and **33** are similar (1.928(3), 1.926(3) Å respectively), i.e. are not significantly affected by the nature of the ligand in *trans* position, we notice that the CO stretching frequency in **32** (1986 cm^{-1}, CO *trans* to PTA) is significantly higher than in **33** (1942 cm^{-1}, CO *trans* to Cl). This finding is consistent with the presence of a π back-bonding component in the Ru–

PTA bond, that in **32** is in competition with the *trans* CO ligand. Conversely, Cl is a good π-donor and therefore reinforces the π-back donation onto the *trans* carbonyl. Indeed, as seen above, **33** is more thermodynamically stable than **32**. The CO stretching frequency in **31**, that corresponds to **33** with a dmso-S in the place of the PTA *trans* to Cl, is indeed similar to that of **33** (1950 vs 1942 cm^{-1}. This finding is consistent with the fact that dmso-S is a moderately good π-acceptor and suggests that the CO stretching frequency is mainly affected by the nature of the *trans* ligand rather than by those in the other coordination positions.

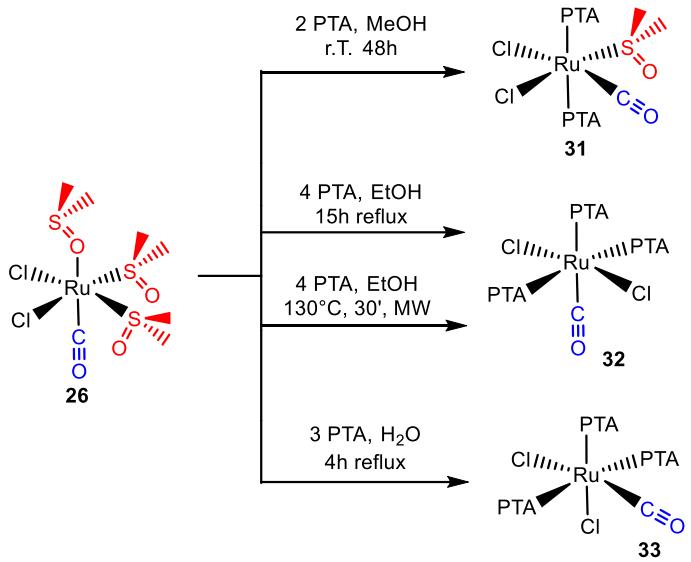

Scheme 3.8. Reactivity of *fac*-$RuCl_2(CO)(dmso)_3$ (**26**) with PTA.

We found that both di-carbonyl isomers *cis*,*cis*,*trans*-$RuCl_2(CO)_2(dmso\text{-}S)_2$ (**27**) and *cis*,*cis*,*cis*-$RuCl_2(CO)_2(dmso)_2$ (**28**), as well as a mixture of them, when treated with 2 equivalents of PTA in methanol at room temperature afforded the mono-carbonyl compound **31** in good yield (Scheme 3.9). The observed reactivity is consistent with the established preference of the two PTA ligands for being mutually *trans*. Nevertheless, it is quite remarkable that in both cases the phosphine easily replaces a molecule of CO rather than the second dmso ligand. In the case of **27**, the coordination is also accompanied by isomerization.

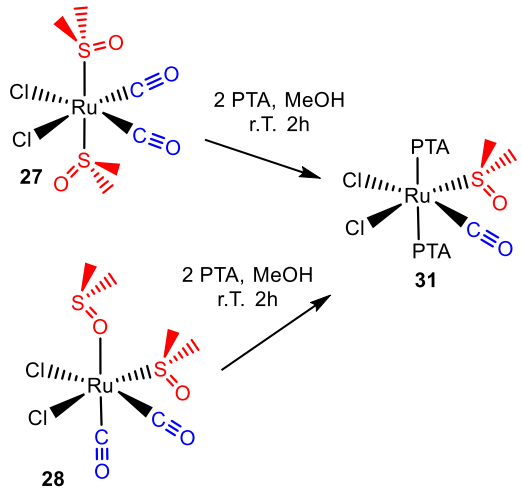

Scheme 3.9. Preparation of *cis*,*cis*,*trans*-$RuCl_2(CO)(dmso\text{-}S)(PTA)_2$ (**31**) upon treatment of either *cis*,*cis*,*trans*-$RuCl_2(CO)_2(dmso\text{-}S)_2$ (**27**) or *cis*,*cis*,*cis*-$RuCl_2(CO)_2(dmso)_2$ (**28**) with PTA in methanol.

A different reactivity was found when the isomer *trans*,*cis*,*cis*-$RuCl_2(CO)_2(dmso\text{-}O)_2$ (**29**) was treated with two equivalents of PTA in methanol at room temperature (Scheme 3.10). The reaction afforded a precipitate that, according to the ^{31}P NMR spectrum, is a mixture of **32** and a new species (**35**) characterized by a singlet at –47.6 ppm, consistent with two mutually *trans* PTAs. Complex **35** was isolated in pure form and good yield, upon evaporation of the solvent, when the reaction was performed in water rather than in methanol. The ^{1}H NMR spectrum of **35** in D_2O consists of a multiplet and a broad singlet centered respectively at 4.57 and 4.27 ppm (12H each) (Appendix, A3.13); no signal for coordinated dmso is present. The upfield resonance belongs to NCH_2N groups while the other to NCH_2P groups, in fact in the ^{1}H-^{13}C HSQC spectrum the multiplet has a crosspeak with a carbon resonance at 70.7 ppm while the singlet with a carbon resonance at 47.3 ppm. Solid state IR shows a band at 1941 cm^{-1}, attributed to a coordinated CO. The yellow color of the complex is consistent with the presence of *trans* chlorides. The ESI-MS spectrum (positive mode) shows a main peak at 479.1 m/z, compatible with the fragment $[RuCl(CO)(PTA)_2]^+$. Overall, the experimental data suggest that complex **35** has two mutually *trans* PTAs, two *trans* chlorides, one CO and one "vacant

position". Thus, as in the case of **27** and **28**, also with the third isomer **29** PTA easily replaces a molecule of CO. The elemental analysis is consistent either with a monomeric species formulated as *trans,trans,trans*-$RuCl_2(CO)(OH_2)(PTA)_2 \cdot 3H_2O$ or with a dimeric species with two bridging chlorides formulated as $[RuCl_2(CO)(PTA)_2]_2 \cdot 8H_2O$. The X-ray structure of complex **32** shows that crystallization with multiple water molecules is not unusual for PTA complexes, and the presence in the ESI-MS spectrum (negative mode) of a main peak at 548.9 m/z, consistent with the anion $[RuCl_3(CO)(PTA)_2]^-$, is in better agreement with the hypothesis of a dinuclear species. Organometallic Ru(II) dimers with bridging chlorides, such as $[RuCl_2(CO)_3]_2$ and $[RuCl_2(\eta^6\text{-}p\text{-cymene})]_2$ (Figure 3.6), are very-well known Ru(II) precursors, whose reactivity is characterized by the facile cleavage of the chloride bridges. Therefore, it is quite likely that **35**, even though dimeric in the solid state, in solution will undergo a similar cleavage and behave as a monomer with a formally vacant position occupied by a labile solvent molecule.

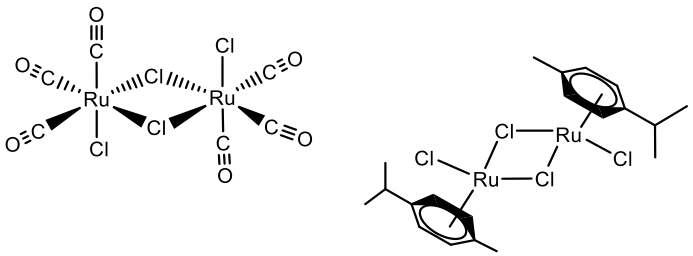

Figure 3.6. Schematic structure of the chloro-bridged dimers $[Ru(CO)_3Cl_2]_2$ (left) and $[RuCl_2(\eta^6\text{-}p\text{-cymene})]_2$.

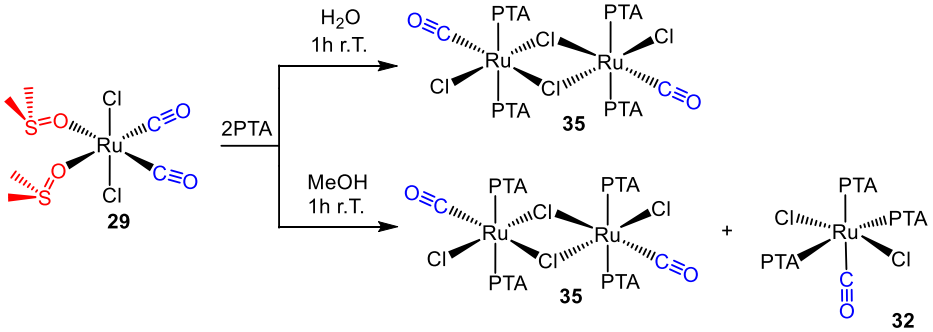

Scheme 3.10. Reactivity of *trans,cis,cis*-$RuCl_2(CO)_2(dmso\text{-}O)_2$ (**29**) with PTA.

In fact, when **35** was treated with a slight excess of pyridine (py, 1.2 eq with respect to Ru) in water at room temperature, the *trans,trans,trans*-$RuCl_2(CO)(py)(PTA)_2$ (**36**) complex was selectively obtained as a yellow precipitate upon evaporation of the solvent (Scheme 3.11). The ^1H NMR spectrum of **36** (Appendix, A3.16) shows three resonances for coordinated py in the aromatic region, plus an AB quartet and a singlet in the PTA region. Integration is consistent with a PTA:py ratio = 2. The ^{31}P NMR spectrum consists of a singlet at –50.0 ppm, in the typical region of mutually *trans* PTAs. The solid state IR spectrum confirmed the presence of CO (carbonyl stretching band at 2010 cm^{-1}) and the ESI-MS (positive mode) presents a peak at 594.0 m/z consistent with $[RuCl_2(CO)(py)(PTAH)(PTA)]^+$.

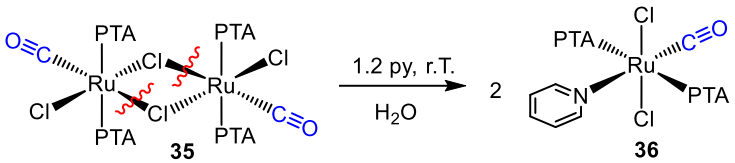

Scheme 3.11. Preparation of *trans,trans,trans*-$RuCl_2(CO)(py)(PTA)_2$ (**36**) upon treatment of $[RuCl_2(CO)(PTA)_2]_2 \cdot 8H_2O$ (**35**) with py in water.

Finally, the reactivity with PTA of the neutral complex with three facial CO ligands and one dmso-O, *fac*-$RuCl_2(CO)_3$(dmso-O) (**30**), was investigated. Only in methanol it was possible to isolate pure products that precipitated spontaneously during the reaction. When **30** was treated with one equivalent of PTA, a white solid (**37**), that is well soluble only in DMSO and water, was collected in good yield (Scheme 3.12). The ^{31}P NMR spectrum of **37** in DMSO-d_6 consists of a singlet at –28.8 ppm, in agreement with PTA *trans* to Cl (Appendix, A3.19), while the ^1H NMR spectrum shows only the resonances of coordinated PTA. The solid state IR spectrum shows two intense bands at 2060 and 1989 cm^{-1} respectively, consistent with the presence of two *cis* CO ligands. The ESI-MS spectrum (positive mode) presents a peak at 409.3 m/z in agreement with the species $[RuCl_2(CO)_2(PTA)Na]^+$, while the negative mode has two peaks at 421.2 and 393.2 m/z, attributable to $[RuCl_3(CO)_2(PTA)]^-$ and $[RuCl_3(CO)(PTA)]^-$, respectively. The elemental analysis is consistent with a

dinuclear species similar to **35**, formulated as $[RuCl_2(CO)_2(PTA)]_2 \cdot H_2O$ (**37**), in which each Ru(II) – besides one terminal and two bridging chlorides – has two *cis* CO ligands, and a single PTA *trans* to Cl. The reaction of **30** with PTA performed in chloroform or dichloromethane led to the same product in a mixture with unreacted precursor.

The formulation of **37** with PTA *trans* to a bridging, rather than to the terminal, chloride is consistent with the presumed reaction mechanism: PTA rapidly replaces the dmso-O of **30**, thus inducing the release of the *trans* CO molecule. The vacant coordination site is then filled through the formation of the chloride bridges, leading to the precipitation of **37** (Scheme 3.12).

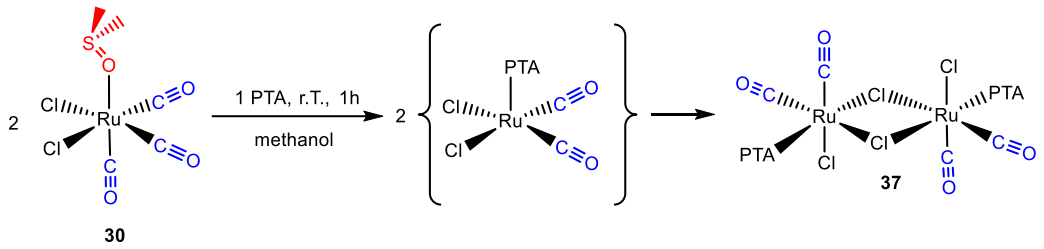

Scheme 3.12. Mechanistic hypothesis for the formation of the dimer $[RuCl_2(CO)_2(PTA)]_2$ (**37**) upon treatment of *fac*-$RuCl_2(CO)_3$(dmso-O) (**30**) with 1 eq of PTA in methanol.

In addition, also the behavior of the complex in water is consistent with PTA being *trans* to a bridging chloride. In fact, the ^{31}P NMR spectrum of **37** recorded in D_2O presents a singlet at –14.6 ppm, attributed to PTA *trans* to H_2O. This could be explained with the rapid cleavage of the chloride bridges and the formation of the neutral species *cis,cis,trans*-$RuCl_2(CO)_2(OH_2)$(PTA). (Scheme 3.13).

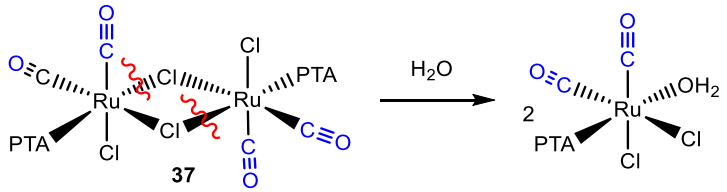

Scheme 3.13. Behavior of the dimer $[RuCl_2(CO)_2(PTA)]_2$ (**37**) in water.

Consistent with this hypothesis, treatment of **37** with a slight excess of py in D_2O afforded crystals of *cis,cis,trans*-$RuCl_2(CO)_2(py)(PTA)$ (**38**). Even though the

crystals were of low quality, the X-ray structure (Appendix, A3.28) unambiguously established the geometry of the complex, with the pyridine *trans* to PTA, i.e. in the place of the bridging chloride (Scheme 3.14).

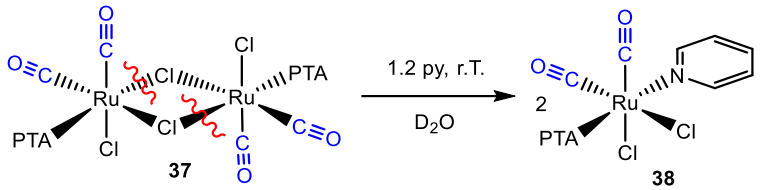

Scheme 3.14. Reactivity of the dimer $[RuCl_2(CO)_2(PTA)]_2 \cdot H_2O$ (**37**) with pyridine in D_2O.

The ^1H NMR spectrum of the crystals in $CDCl_3$ (their solubility was much higher in chloroform than in water) shows three peaks for the coordinated pyridine in the aromatic region. The aliphatic region presents two singlets for PTA. Integration confirms the 1:1 ratio between PTA and py. The ^{31}P NMR spectrum shows a singlet at –28.7 ppm, in the region of a PTA *trans* to an imine (see Chapter 2).
The ESI-MS (positive mode) shows a main peak at 464.9, m/z in agreement with the species $[RuCl_2(CO)_2(py)(PTAH)]^+$. The IR spectrum presents two bands at 2058 and 1994 cm^{-1} in agreement with the presence of two CO ligands in *cis* geometry.

The reaction of **30** with 2 (or more) eq of PTA in methanol at room temperature afforded the mononuclear complex *cis,cis,trans*-$RuCl_2(CO)_2(PTA)_2$ (**39**) as a white powder in good yield (Scheme 3.15). Compound **39** was fully characterized by NMR and IR spectroscopy, mass spectrometry, and its single-crystal X-ray structure was also determined (Figure 3.7). The geometry of **39** is in agreement with the mechanistic hypothesis advanced before for the formation of **37** (Scheme 3.15): in this case, the vacant site *trans* to the first PTA ligand is rapidly occupied by the second PTA molecule.

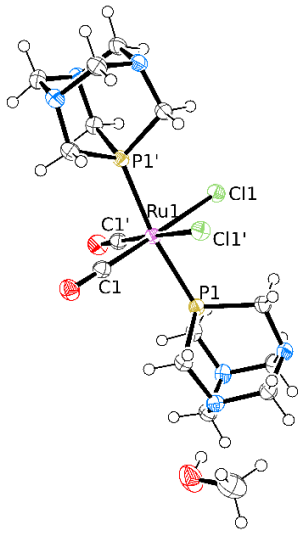

Figure 3.7. X-ray molecular structure (50% probability ellipsoids) of *cis,cis,trans*-$RuCl_2(CO)_2(PTA)_2$ (**39**). Crystals formed spontaneously from a methanol solution. Coordination distances in ångström (Å): Ru1–Cl1 = 2.4370(4), Ru1–C1 = 1.877(2), Ru1–P1 = 2.3397(5).

The solid state IR spectrum shows two intense bands at 2053 and 1988 cm^{-1}, in agreement with the presence of two *cis* CO ligands. Complex **39** is well soluble in water, $CHCl_3$ and DMSO. The ^1H NMR spectrum in $CDCl_3$ consists of two relatively broad singlets in the region of coordinated PTA at 4.58 and 4.42 ppm (Appendix, A3.22). The ^{31}P NMR presents only a singlet at –51.0 ppm, the region of mutually *trans* PTAs. The NMR spectra in D_2O are similar to those in $CDCl_3$ (Appendix, A3.23). The complex slowly and partially releases a Cl. In fact, the ^{31}P NMR spectrum in D_2O after the dissolution presents a singlet at –48.8 ppm, whereas after one day (in the dark) another singlet appears at –45.7, in addition to the first one. The new resonance disappears upon addition of an aliquot of NaCl.

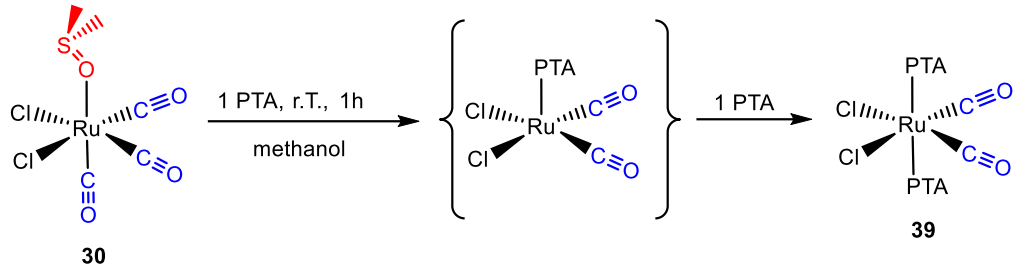

Scheme 3.15. Mechanistic hypothesis for the formation of *cis,cis,trans*-$RuCl_2(CO)_2(PTA)_2$ (**39**) upon treatment of *fac*-$RuCl_2(CO)_3$(dmso-O) (**30**) with two eq of PTA in methanol.

The literature reports that complexes of the type *cis,cis,trans*-$RuX_2(CO)_2L_2$ (where X = Cl or Br and L = PMe_2Ph, $PMePh_2$, $P(CH_2Ph)Ph_2$, $P(OMe)_2Ph$) isomerize to the all-*trans* geometry when irradiated with visible light.[6] In our case, irradiation of a $CDCl_3$ solution of **39** with white light (150 W) induced no changes in the NMR spectra of the complex.

When precursor **30** was reacted with 2 eq of PTA in water (room temperature), rather than in methanol, a mixture of **39** and of the tri-substituted species *cis*,*mer*-$RuCl_2(CO)(PTA)_3$ (**33**) (ca. 2/1 ratio) was obtained upon removal of the solvent (Scheme 3.16). This finding suggests that, unless the dicarbonyl product precipitates from the solution as in methanol, PTA can easily replace also a second CO ligand from **30**. When three equivalents of PTA were used, the relative amount of **33** in the product mixture increased (**39**/**33** = 1/2.75).

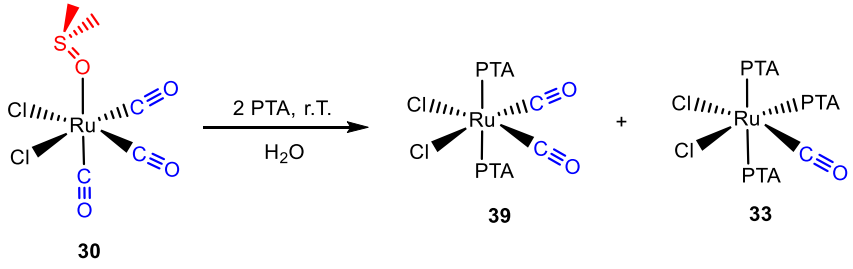

Scheme 3.16. Reactivity of *fac*-$RuCl_2(CO)_3$(dmso-O) (**30**) with PTA in water.

When **30** was treated in water with 1 equivalent of PTA at room temperature, a quite surprising behavior was observed (Scheme 3.17): the addition of the phosphine to a

colorless solution of **30** was immediately accompanied by the development of CO_2 bubbles and the color of the solution turned to yellow. After 20 minutes of stirring, the precipitation of a small amount of an orange powder was observed that, according to the IR spectrum in $CHCl_3$, is mainly composed by the well-known Ru(0) cluster Ru_3CO_{12} (**40**), with minor impurities (Figure 3.8).

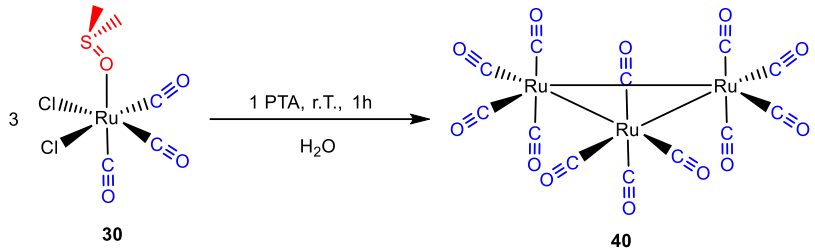

Scheme 3.17. Formation of Ru_3CO_{12} (**40**) upon treatment of *fac*-$RuCl_2(CO)_3$(dmso-O) (**30**) with 1 eq of PTA in water.

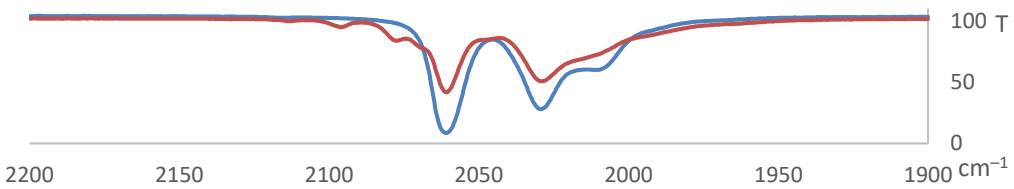

Figure 3.8. IR spectra in $CHCl_3$ of a commercial sample of the Ru_3CO_{12} cluster (blue line) and of the orange powder obtained from the reaction of *fac*-$RuCl_2(CO)_3$(dmso-O) (**30**) with one equivalent of PTA in water (orange line).

From the literature it is known that the Ru(0) cluster **40** can be obtained from the Ru(II) dimer $[Ru(CO)_3Cl_2]_2$ in the presence of KOH and a stream of CO at 75°C in an organic solvent.[14] Briefly, each Ru(II) center in the dimer has three coordinated CO ligands in *fac* geometry that are very electrophilic because of the competition for the π back-donation. One of them undergoes nucleophilic attack by OH^-. This step is followed by decarboxylation of the hydroxycarbonyl adduct $\{Ru(CO)_2Cl_2(COOH)\}^-$ with the formation of a hydride that, after a reductive elimination of HCl and coordination of another CO, leads to the formation of the cluster. We found that the same reaction occurs also using **30** instead of the dimer $[Ru(CO)_3Cl_2]_2$ (indeed, **30** can be considered as an activated monomeric form of

$[Ru(CO)_3Cl_2]_2$).[15] It is surprising that **30** yields the Ru(0) cluster in the absence of added KOH and CO. However, it has to be considered that PTA, besides being a ligand, is also a base ($pK_a = 5.89$)[16] and generates OH^- ions. We argue that when the phosphine is ca. stoichiometric with ruthenium, the nucleophilic attack of OH^- onto one of the CO ligands competes with PTA coordination. Nevertheless, for explaining the formation of the cluster without using a source of CO, the double role of PTA has to be invoked: as seen above, coordination of PTA induces the rapid release of the CO in *trans* position, that can thus bind to another ruthenium fragment leading to the cluster. In fact, when the reaction was performed by addition of a stoichiometric amount of KOH or NEt_3 instead of PTA, uncharacterized red-brown ruthenium-carbonyl precipitates were obtained that – according to their IR spectra – do not contain $Ru_3(CO)_{12}$. In summary, in this reaction also **30**, similarly to PTA, has a double role: part of it undergoes nucleophilic attack on a carbonyl by OH^- and part is the source of CO, thus explaining the very low yield of cluster. When the reaction is performed with two or more equivalents of ligand, PTA binding prevails over the nucleophilic attack of OH^- onto the coordinated carbonyls and formation of the cluster was not observed (Scheme 3.18).

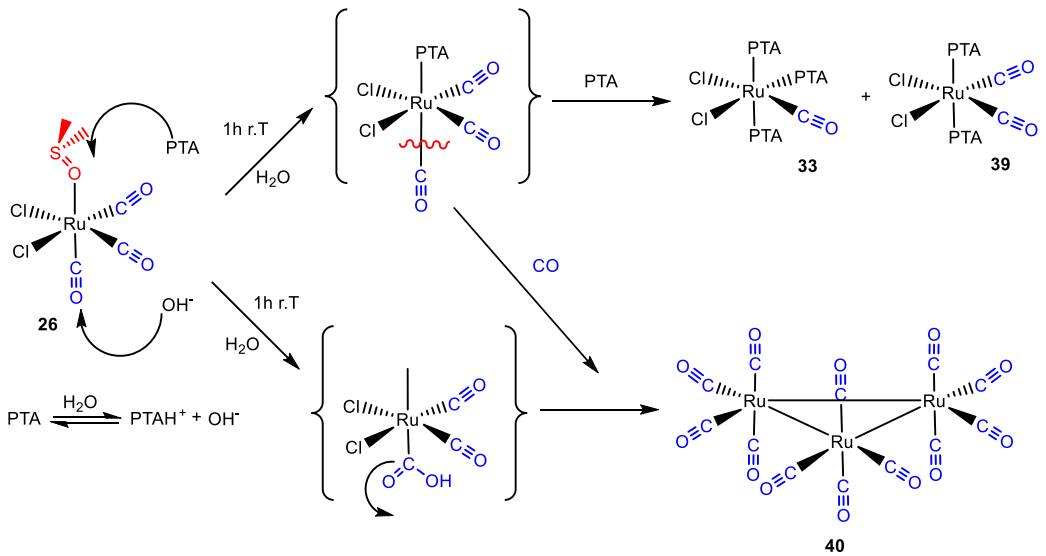

Scheme 3.18. Reactivity of *fac*-$RuCl_2(CO)_3$(dmso-O) (**30**) with PTA in water.

The ^{31}P NMR spectrum of the orange precipitate in DMSO-d_6 does not present any peak for PTA (either free or bound). We observed the slow formation of red-orange crystals after the addition of an excess of PTA to the DMSO solution. Even though the crystals were of low quality, the X-ray structure unambiguously established that they were made of the known cluster $Ru_3(CO)_9(PTA)_3$, that usually is prepared by treating $Ru_3(CO)_{12}$ with a slight excess of PTA in refluxing methanol.[17,18]

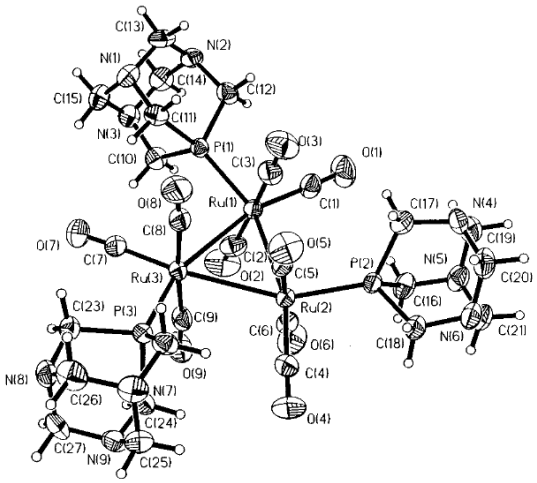

Figure 3.9. X-ray structure (thermal ellipsoids drawn at the 50% probability level) of the cluster $Ru_3(CO)_9(PTA)_3$ reported by Darensbourg's group.[18]

In summary, the reactivity of *fac*-$RuCl_2(CO)_3$(dmso-O) (**30**) towards PTA confirms what seen with the previous Ru-CO-dmso precursors (Scheme 3.19): the phosphorus ligand is able to replace easily one or two CO ligands at room temperature, besides the dmso-O. In methanol we managed to isolate, for the first time, two dicarbonyl complexes, **37** and **39**, that have either one or two PTA ligands, respectively. In fact, only monocarbonyl PTA species were isolated from the reactions of the dicarbonyl precursors with PTA (see above). In water, where **37** and **39** remain in solution, substitution of an additional CO ligand occurs, even when sub-stoichiometric amounts of PTA are used. Moreover, only with **30** the unexpected formation of the cluster Ru_3CO_{12} (**40**) was observed from the reaction with one equivalent of PTA in aqueous solution.

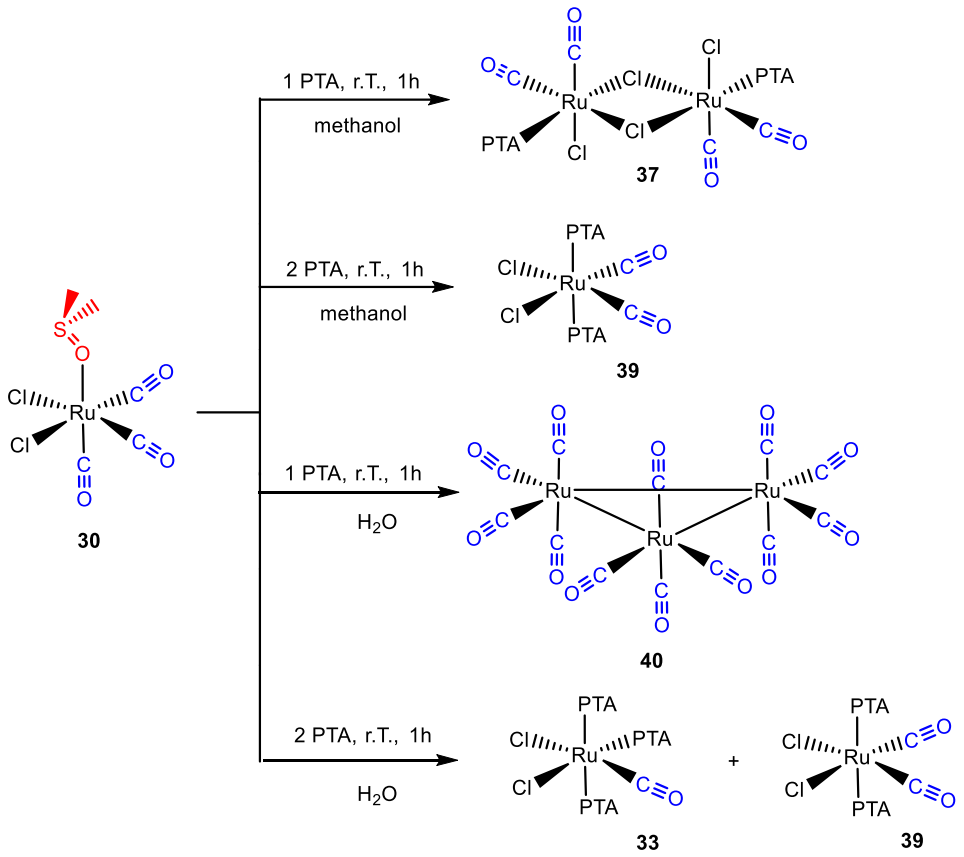

Scheme 3.19. Reactivity of *fac*-$RuCl_2(CO)_3$(dmso-O) (**30**) with PTA.

3.4 Reactions of neutral Ru(II)-PTA complexes with CO

As mentioned already, Darensbourg and coworkers reported that the complex *trans*-$RuCl_2(PTA)_4$ (**1**) reacts with a CO atmosphere in ethanol forming the complex of undefined geometry $RuCl_2(CO)(PTA)_3$ in which CO has replaced one PTA.[1] We decided to study more carefully the reactivity of both isomers *cis*- and *trans*-$RuCl_2(PTA)_4$ towards CO. In our hands, the afore-mentioned preparation could not be reproduced: only unreacted **1** was found after one night treatment with a CO atmosphere. This is not surprising, since **1** is basically insoluble in ethanol (in fact it is prepared from $RuCl_3 \cdot 3H_2O$ and an excess of PTA in refluxing ethanol, from which it precipitates). The reaction was then repeated in $CHCl_3$, where the precursor **1** is

well-soluble. Overnight treatment with CO (1 atm) followed by solvent removal afforded the monocarbonyl complex **32** (Scheme 3.20).

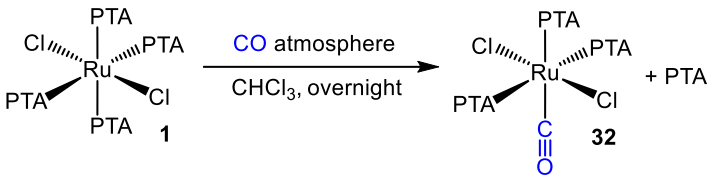

Scheme 3.20. Reactivity of *trans*-$RuCl_2(PTA)_4$ (**1**) with CO.

The monocarbonyl compound **32** was obtained also when **1** was treated with 30 atm of CO in an autoclave for 24h. Upon increasing the reaction temperature to 40 °C two additional singlets were found in the ^{31}P NMR spectrum of the raw product: one corresponding to the dicarbonyl species *cis,cis,trans*-$RuCl_2(CO)_2(PTA)_2$ (**39**) and a new one at –49.3 ppm, region of mutually *trans* PTAs. Slow diffusion of diethyl ether into a chloroform solution of the raw material afforded a small number of yellow crystals that, according to single crystal X-ray analysis, belonged to the new dicarbonyl species *trans,trans,trans*-$RuCl_2(CO)_2(PTA)_2$ (**41**) (Figure 3.10). The Ru–CO bond length in **40** (1.9691(12) Å) is significantly longer than that found in the stereoisomer **39** for the two CO's *trans* to Cl (1.877(2) Å), in agreement with the expected competition between the two mutually *trans* carbonyls. The Ru–P distance in **41** (2.3432(3) Å) is also longer than that distance in **39** (2.3397(5) Å). Unfortunately, the amount of crystals was not sufficient for performing a detailed NMR analysis, and additional crystallization attempts to obtain other batches of pure compound were unsuccessful.

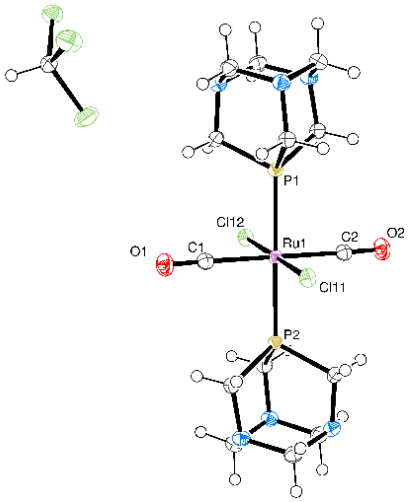

Figure 3.10. X-ray molecular structure (50% probability ellipsoids) of *trans,trans,trans*-$RuCl_2(CO)_2(PTA)_2$ (**41**) with a crystallization molecule of chloroform. Coordination distances in ångström (Å): Ru1–Cl1 = 2.4151(3), Ru1–C1 = 1.9691(12), Ru1–P1 = 2.3432(3).

Compound **32** could be removed from the raw reaction product through a rapid washing with water, as witnessed by the ^{31}P NMR spectrum (in $CDCl_3$) of the remaining solid (Figure 3.11).

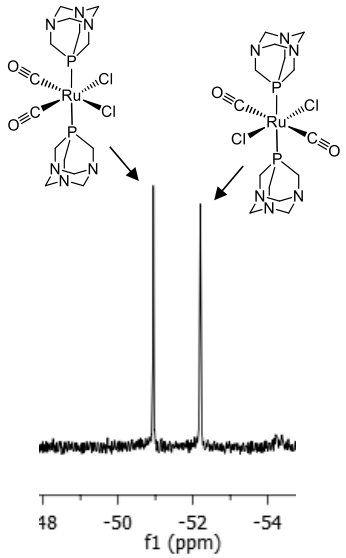

Figure 3.11. ^{31}P NMR spectrum in $CDCl_3$ of a mixture of *trans,trans,trans*-$RuCl_2(CO)_2(PTA)_2$ (**41**) and *cis,cis,trans*-$RuCl_2(CO)_2(PTA)_2$ (**39**).

The IR spectrum of this solution presents three different signals in the CO stretching region: two equally intense bands at 2055 and 1995 cm^{-1} that belong to **39** and an additional one at 2018 cm^{-1} attributed to the antisymmetric carbonyl stretching mode in **41**. Consistent with this hypothesis, the CO stretching band for the structurally similar *trans,trans,trans*-$RuCl_2(CO)_2L_2$ compounds reported in literature (L = PMe_2Ph, $PMePh_2$, PPh_3) falls between 1997 and 2023 cm^{-1} in chloroform.[6] Finally, the ESI-MS spectrum of the same solution shows a main peak at m/z = 479 attributed to a $[Ru(PTA)_2(CO)Cl]^+$ fragment. All these data suggest that the singlet at –49.3 ppm in D_2O ppm (or –52.2 ppm in $CHCl_3$) can be safely attributed to **41**.

Attempts to improve the yield of **41** by increasing the reaction time (from 1 to 4 d), and/or the CO pressure (from 30 to 50 atm) and/or the temperature (from 40 to 60 °C) were unsuccessful and, conversely, led to an increase of the relative amount of **39**, suggesting that the monocarbonyl species **32** is an intermediate in the formation of the two dicarbonyls, and that **41** is a kinetic product (Scheme 3.21).

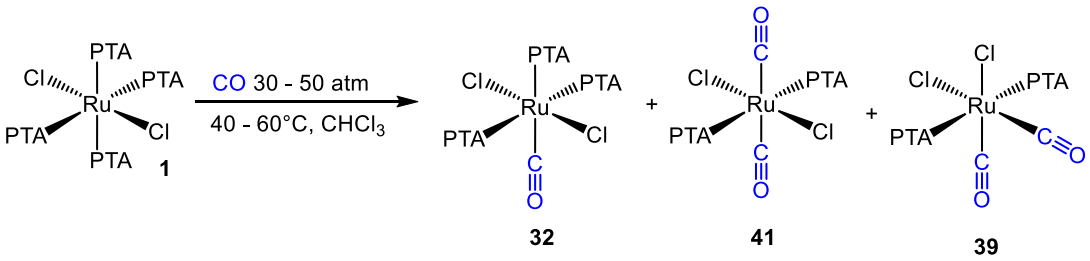

Scheme 3.21. Reactivity of *trans*-$RuCl_2(PTA)_4$ with CO (P = 30 - 50 atm, T = 40 - 60°C) in chloroform.

The use of **32**, rather than **1**, as starting material led to no significant improvement in the attempt to isolate the elusive all *trans* isomer **39**. On the contrary, treatment of **32** with CO under different reaction conditions (T = 50 - 70 °C, P = 30 or 50 atm, t = 13 – 72 h) afforded a raw product containing (according to the ^{31}P NMR spectrum) also different amounts of the *cis* isomer **33**, besides residual **32** and a mixture of **39** and **41**. This finding was not surprising, since complex **32** was found to isomerize to **33** when refluxed in water (see above).

The behavior of the isomer *cis*-$RuCl_2(PTA)_4$ (**2**) towards CO was somehow different. Similarly to the *trans* isomer, **2** did not react with CO in ethanol (where it is insoluble), whereas in chloroform it very slowly afforded *fac*-$RuCl_2(CO)(PTA)_3$ (**34**) in low amount (10%, according to the ^{31}P NMR spectrum, after overnight treatment, Scheme 3.22). An increase of the reaction time to 72h did not improve the yield of **34** significantly (20% of **34**). Full conversion of **2** was not achieved even when the reaction was performed in an autoclave, in different reaction conditions (T: 30 – 50°C, P = 30 – 50 atm, 24 – 48 h).

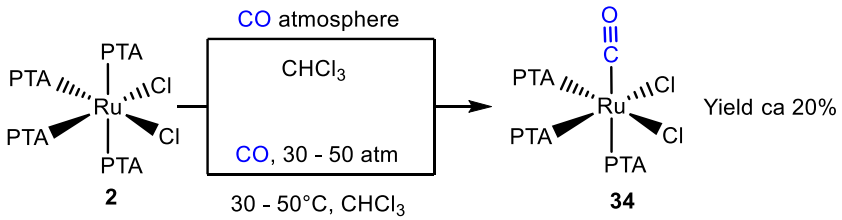

Scheme 3.22. Reactivity of *cis*-$RuCl_2(PTA)_4$ (**2**) with CO in chloroform.

When the reaction between **2** and CO was performed in autoclave for a longer time (110h, r.T., 30 atm), a mixture of products was obtained after evaporation of the solvent. According to the ^{31}P NMR spectrum (performed in D_2O) this mixture contained the signals of unreacted **2** together with **33**, **34** and a new complex (**42**), characterized by an AM_2X system, in 1.5:1:4:7 ratio, respectively. The AM_2X system of **42** consists of two double triplets centered respectively at –31.4 ($^2J_{A\text{-}M}$ = 20.5 Hz, $^2J_{A\text{-}X}$ = 32.8 Hz) and –61.9 ppm ($^2J_{X\text{-}M}$ = 35.8 Hz) (one PTA each) and one double doublet centered at –59.8 ppm (two equivalent PTAs). Washing of the raw solid with chloroform afforded a white residue that, according to the ^{31}P NMR spectrum, is an 8:1 mixture of **42** and **34** (Appendix, A3.26). The ESI-MS spectrum of the solid shows a peak at m/z = 793.1 attributable to the cationic species $[RuCl(CO)(PTA)_4]^+$. Based on these data, the complex was unambiguously formulated as *cis*-$[RuCl(CO)(PTA)_4]Cl$ (**42Cl**), which is the first cationic Ru(II) carbonyl complex with PTA. Single crystals of **42Cl** were obtained upon

recrystallization and X-ray analysis confirmed the nature and geometry of the complex (Figure 3.12). The Ru–P bond length of the PTA *trans* to CO (2.3828(6) Å) is similar to those of the two mutually *trans* PTAs (2.3898(6) and 2.3892(6) Å) and all three are longer than the Ru–P distance *trans* to Cl (2.3107(5) Å). The Ru–CO distance (1.913(2) Å) is similar to that found in **32** (1.928(3) Å), where the CO ligand is also *trans* to PTA. This complex was selectively obtained in good yield, as nitrate salt (**42NO$_3$**), by treatment of **2** with 1 eq of $AgNO_3$ in $CHCl_3$ in atmosphere of CO for 24h (Scheme 3.23).

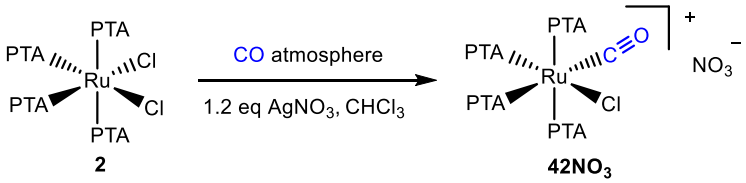

Scheme 3.23. Preparation of *cis*-[RuCl(CO)(PTA)$_4$](NO$_3$) (**42NO$_3$**).

The ^{31}P NMR and ESI-MS spectra of **42NO$_3$**, that is well soluble in water and DMSO, are coincident with those of **42Cl** (Appendix, A3.27). The CO stretching band occurs at 2020 cm^{-1} in the solid state IR spectrum (nujol), i.e. at remarkably higher wavenumbers compared to the neutral mono-carbonyl complexes **31-33**, in agreement with a higher competition for π back-donation and lower electronic density on Ru(II) because of the positive charge of **42**.

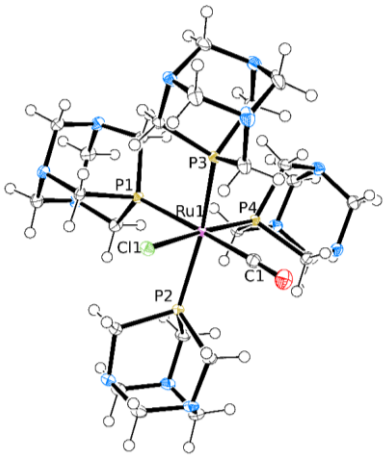

Figure 3.12. X-ray molecular structure (50% probability ellipsoids) of the cationic part of *cis*-[RuCl(CO)(PTA)$_4$](Cl) (**42Cl**). Crystals obtained by recrystallization of the raw product from water/acetone. Coordination distances in ångström (Å): Ru1–Cl1 = 2.4855(5), Ru1–C1 = 1.913(2), Ru1–P1 = 2.3828(6), Ru1–P2 = 2.3898(6), Ru1–P3 = 2.3892(6), Ru1–P4 = 2.3107(5).

Finally, the reactivity of the complex *cis,cis,trans*-RuCl$_2$(dmso-S)$_2$(PTA)$_2$ (**10**) towards CO was also tested. Even if this compound has two relatively labile dmso ligands it reacted with CO only under pressure in autoclave (P = 30 atm, T = 60°C). Under these conditions, a chloroform solution of **10** was completely converted to **39** after 24h. Thus, two CO molecules selective replaced both dmso ligands, with retention of the geometry (Scheme 3.24). At lower temperature **10** did not show any reactivity with CO.

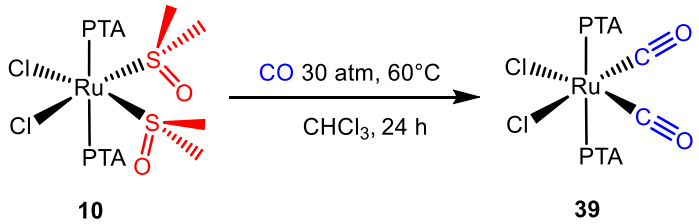

10 **39**

Scheme 3.24. Reactivity of *cis,cis,trans*-RuCl$_2$(dmso-S)$_2$(PTA)$_2$ (**10**) with CO.

Table 3.1. Selected CO stretching bands for compounds **31-33**, **35-37**, **39**, **41** (cm^{-1}).

complex	ν cm^{-1}	CO *trans* to
cis,cis,trans-$RuCl_2(CO)(dmso\text{-}S)(PTA)_2$ (**31**)	1950[a]	Cl
trans,mer-$RuCl_2(CO)(PTA)_3$ (**32**)	1986[a]	PTA
cis,mer-$RuCl_2(CO)(PTA)_3$ (**33**)	1942[a]	Cl
$[RuCl_2(CO)(PTA)_2]_2 \cdot 8H_2O$ (**35**)	1941[a]	Cl
$[RuCl_2(CO)_2(PTA)]_2 \cdot H_2O$ (**37**)	2060, 1989[a]	Cl
cis,cis,trans-$RuCl_2(CO)_2(PTA)_2$ (**39**)	2053, 1988[a]	Cl
trans,trans,trans-$RuCl_2(CO)_2(PTA)_2$ (**41**)	2018[b]	CO

[a] Solid state (Nujol mulls), [b] Chloroform solution.

Table 3.2. Selected coordination bond lengths (Å) in complexes *cis*,*cis*,*trans*-$RuCl_2(CO)(dmso\text{-}S)(PTA)_2$ (**31**), *trans*,*mer*-$RuCl_2(CO)(PTA)_3$ (**32**), *cis*,*mer*-$RuCl_2(CO)(PTA)_3$ (**33**), *cis,cis,trans*-$RuCl_2(CO)_2(PTA)_2$ (**39**), all-*trans*-$RuCl_2(CO)_2(PTA)_2$ (**41**).

	31	**32**	**33**	**39**	**41**
Ru–P (mutually *trans*)	2.385(1), 2.357(1)	2.3399(7), 2.3458(6)	2.3811(5), 2.3488(5)	2.3397(5)	2.3432(3)
Ru–P (*trans* to Cl)			2.2865		
Ru–P (*trans* to CO)		2.3821(7)			
Ru–CO (*trans* to PTA)		1.928(3)			
Ru–CO (*trans* to Cl)	1.80(1)		1.926(3)	1.877(2)	
Ru–CO (*trans* to CO)					1.9691(12)

3.5 Conclusions

In summary, the well-known neutral Ru(II)-CO-dmso complexes *fac*-$RuCl_2(CO)(dmso)_3$ (**26**), *cis*,*cis*,*trans*-$RuCl_2(CO)_2(dmso\text{-}S)_2$ (**27**), *cis*,*cis*,*cis*-$RuCl_2(CO)_2(dmso)_2$ (**28**), *trans*,*cis*,*cis*-$RuCl_2(CO)_2(dmso\text{-}O)_2$ (**29**), and *fac*-$RuCl_2(CO)_3(dmso\text{-}O)$ (**30**) demonstrated to be good precursors for the synthesis of new carbonyl derivatives with PTA. In fact, we could isolate and completely characterize a series of Ru(II)-CO complexes with PTA, which show a good solubility in water and, most often, also in chloroform: *cis,cis,trans*-$RuCl_2(CO)(dmso\text{-}S)(PTA)_2$ (**31**) *trans,mer*-$RuCl_2(CO)(PTA)_3$ (**32**), *cis,mer*-$RuCl_2(CO)(PTA)_3$ (**33**), $[RuCl_2(CO)(PTA)_2]_2 \cdot 8H_2O$ (**35**), $[RuCl_2(CO)_2(PTA)]_2 \cdot H_2O$ (**37**) and *cis,cis,trans*-$RuCl_2(CO)_2(PTA)_2$ (**39**) (Figure 3.13). It was also determined the single X-ray structure of all of them, with the exception of the two dimers.

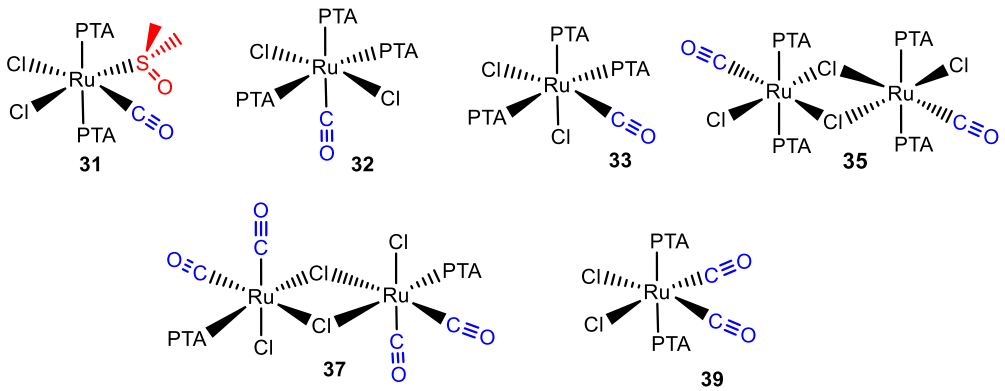

Figure 3.13. Ru(II)-PTA carbonyls complexes synthesized using the well-known neutral Ru(II)-CO-dmso precursors.

The common behavior when a Ru(II)-CO-dmso complex is reacted with PTA is the coordination of two mutually *trans* phosphine ligands even when PTA is in defect, suggesting that this geometry is particularly stable. We were unable to isolate a carbonyl compound with only one bound PTA. Furthermore, in the di- and tri-carbonyl precursors PTA easily replace at least one CO at room temperature, even when there is a residual dmso ligand available in the coordination sphere. As a

consequence, Ru(II)-PTA dicarbonyls could be obtained only from the precursor with 3 CO ligands, and we were unable to isolate Ru(II)-PTA compounds with more than 2 CO ligands. In addition, PTA prefers to avoid binding *trans* to CO. In fact, the only monocarbonyl compound with one PTA *trans* to CO that we managed to isolate *trans*,*mer*-$RuCl_2(CO)(PTA)_3$ (**32**) is a kinetic isomer.

Using the opposite strategy, that is the reaction of Ru(II)-PTA precursors with CO, we found that both *trans*-$RuCl_2(PTA)_4$ (**1**) and *cis*-$RuCl_2(PTA)_4$ (**2**) can replace a single PTA (originally *trans* to another PTA) with CO at ambient pressure, affording respectively *trans,mer*-$RuCl_2(PTA)_3(CO)$ (**32**) and *fac*-$RuCl_2(CO)(PTA)_3$ (**34**, in low yield): i.e. the substitutions do not imply isomerization (Scheme 3.25). In the case of **2**, owing to the *trans*-influence of PTA, it was possible for a CO to replace (partially) one of the two chlorides *trans* to PTA. Assisted removal of the chloride by addition of a soluble silver salt led to the isolation of the unprecedented cationic species *cis*-$[RuCl(CO)(PTA)_4](NO_3)$ (**42NO$_3$**).
Moreover, when treated with CO in more forcing conditions (T = 40 - 60°C, P = 30 - 50 atm) compound **1** could partially replace two PTAs, affording mixtures of **31** together with the two dicarbonyl stereoisomers: *cis,cis,trans*-$RuCl_2(CO)_2(PTA)_2$ (**39**) and all-*trans*-$RuCl_2(CO)_2(PTA)_2$ (**41**). Compound **41**, which is a kinetic intermediate in the transformation of **32** to **39**, was not observed when the Ru(II)-CO-dmso precursors were treated with PTA.

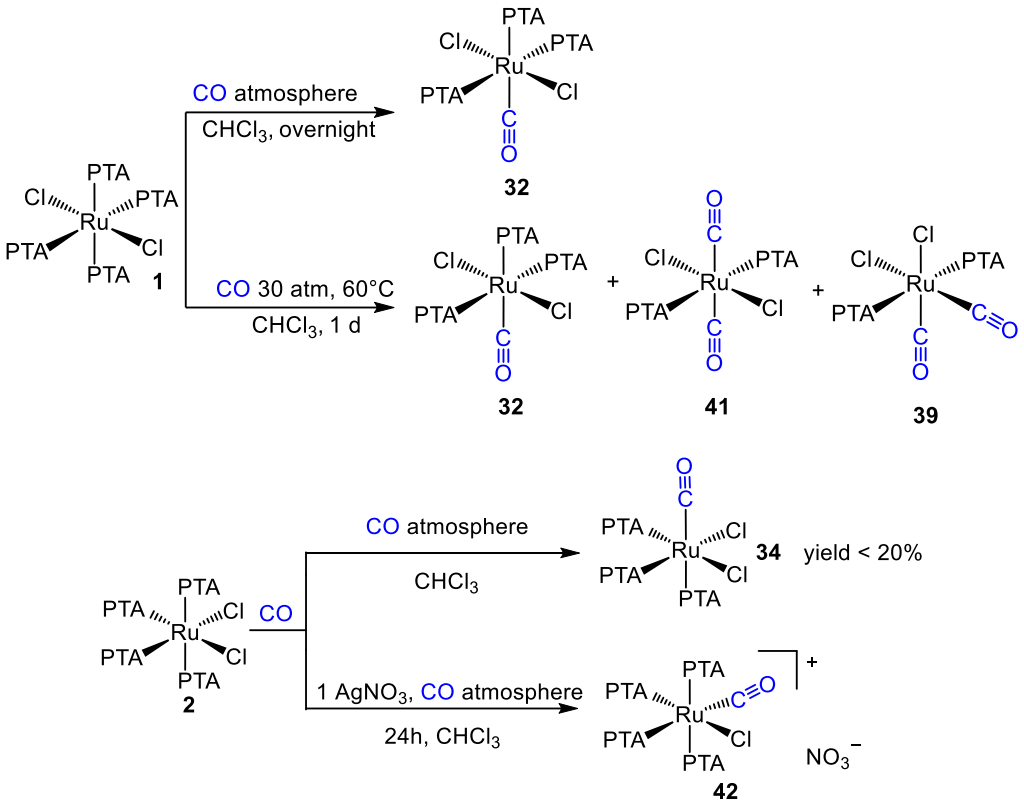

Scheme 3.25. Reactivity of *trans*- (**1**, top) and *cis*-$RuCl_2(PTA)_4$ (**2**, bottom) with CO.

Finally, the compound *cis,cis,trans*-$RuCl_2(dmso\text{-}S)_2(PTA)_2$ (**10**), that was shown to be a good precursor with N-donor ligands (see Chapter 2), reacts with CO only in relatively forcing condition (P = 30 atm, T = 60°C), substituting both dmso ligands and forming *cis,cis,trans*-$RuCl_2(CO)_2(PTA)_2$ (**39**) thus leaving unchanged the geometry of the complex.

To conclude, here is reported the preparation of a series of unprecedented water-soluble Ru(II)-carbonyl complexes with PTA. We found that, as reported in the literature with other phosphines, the Ru(II)-CO-PTA compounds are better prepared by treatment of Ru(II)-carbonyl precursors with PTA rather than the other way around, i.e. treatment of Ru(II)-PTA precursors with CO. However, the two synthetic approaches not necessarily lead to the same products, and compounds **41** and **42** were obtained exclusively by the second route.

3.6 Bibliography

[1] D. J. Darensbourg, F. Joó, M. Kannisto, A. Kathó, J. H. Reibenspies, D. J. Daigle, *Inorg. Chem.,* **1994**, *13*, 200 - 208.

[2] a) M. S. Lupin, B. L. Shaw, *J.Chem.Soc. (A)*, **1968**, 741 - 749; b) T. A. Stephenson, G. Wilkinson, *J. Inorg. Nucl Chem.,* **1966**, 945 - 956.

[3] a) E. Alessio, B. Milani, M. Bolle, G. Mestroni, P. Faleschini, F. Todone, S. Geremia, M. Calligaris, *Inorg. Chem.,* **1995**, *34*, 4722 - 4734; b) E. Alessio, E. Iengo, S. Geremia, M. Calligaris, *Inorg. Chim. Acta*, **2003**, *344*, 183 - 189. c) I. Bratsos, S. Calmo, E. Zangrando, G. Balducci, E. Alessio, *Inorg. Chem*, **2013**, *52*, 12120 - 12130.

[4] J. Chatt, B. L. Shaw and A. E. Field, *J. Chem. Soc.*, **1964**, 3466 - 3475.

[5] D.F. Gill, B. E. Mann, and B. L. Shaw, *J.C.S. Dalton*, **1973**, 311 - 317.

[6] C. F. J. Barnard, J. A. Daniels, J. Jeffery, R. J. Mawby, *Dalton Trans*, **1976**, 953 - 961.

[7] E. Iengo, P. Cavigli, D. Milano, P. Tecilla, *Inorg. Chim. Acta*, **2014**, *17*, 59 - 78.

[8] J. Bravo, S. Bolano, L. Gonsalvi, M. Peruzzini M., *Coord. Chem. Rev.*, **2010**, *254*, 555 - 607.

[9] a) A. Nakao, D. J. Kaczorowski, R. Sugimoto, T. R. Billiar and K. R. McCurry, *J. Clin. Biochem. Nutr.*, **2008**, *42*, 78 - 88; b) R. Motterlini and L. E. Otterbein, *Nat. Rev. Drug Discov.*, **2010**, *9*, 728 - 743; c) M.-L. Wu, Y.-C. Ho and S.-F. Yet, *Antioxid. Redox Signaling*, **2011**, *15*, 1835 - 1846; d) A. Halilovic, K. A. Patil, L. Bellner, G. Marrazzo, K. Castellano, G. Cullaro, M. W. Dunn and M. L. Schwartzman, *J. Cell. Physiol.*, **2011**, *226*, 1732 - 1740; e) A. F. N. Tavares, M. Teixeira, C. C. Romão, J. D. Seixas, L. S. Nobre and L. M. Saraiva, *J. Biol. Chem.*, **2011**, *286*, 26708 - 26717; f) D. Nguyen, T.-K. Nguyen, S. A. Rice and C. Boyer, *Biomacromolecules*, **2015**, *16*, 2776 - 2786.

[10] J. E. Clark, P. Naughton, S. Shurey, C. J. Green, T. R. Johnson, B. E. Mann, R. Foresti, R. Motterlini, *Circ Res.*, **2003**, *93*, 2 - 8.

[11] I. P. Evans, A. Spencer, G. J. Wilkinson, *Chem. Soc., Dalton Trans.*, **1973**, 204 - 209.

[12] F. Battistin, G. Balducci, E. Iengo, N. Demitri, E. Alessio, *Eur. J. Inorg. Chem*, **2016**, *17*, 2850 - 2060.

[13] A. Udvardy, M. Serrano-Ruiz, V. Passarelli, E. Bolyog-Nagy, F. Joó, Á. Kathó, A. Romerosa, *Inorg. Chim. Acta*, **2017**, (doi.org/10.1016/j.ica.2017.04.054).

[14] M. Faurè, C. Saccavono, G. Lavigne, *Inorg Synth*, **2004**, *34*, 110 - 115.

[15] G. Balducci, E. Iengo, N. Demitri, E. Alessio, *Eur. J. Inorg. Chem.*, **2015**, *26*, 4296 - 4311.

[16] J. Kovács, F. Joó, A. Bényei, G. Laurenzy, *Dalton Trans.*, **2004**, 2336 - 2340.

[17] N. Mager, K. Robeyns, S. Hermans, *J. Organomet. Chem.*, **2015**, *794*, 48 - 58.

[18] D.J. Darensbourg, F.A. Beckford, J.H. Reibenspies, *J. Clust. Sci.*, **2000**, *11*, 95 - 107.

CHAPTER 4

Ru(II)-CO-PTA derivatives with 2,2'-bipyridine

4.1 Aim of the Chapter

As mentioned in the Introduction, one of the aims of this investigation is that of obtaining novel water-soluble precursors to be exploited as building blocks in the construction of metal-conjugates and metal-mediated supramolecular assemblies. For this reason, we started a preliminary investigation of the reactivity of the new Ru-CO-PTA complexes described in Chapter 3 towards 2,2'-bipyridine (bpy), used as a model for chelating diimine linkers (e.g. bpyAc and cppH, Figure 4.1). All the reactions were performed in water and the NMR spectra were recorded on the raw products obtained by rotary evaporation of the solvent (except when written differently).

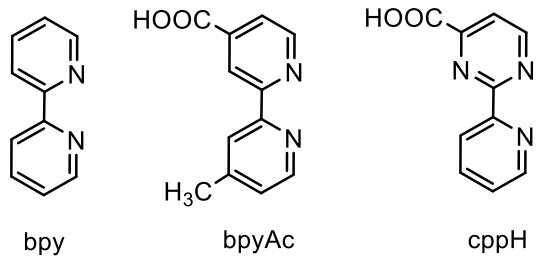

Figure 4.1. 2,2'-bipyridine (bpy) and the chelating diimine linkers bpyAc and cppH.

4.2 Reactions with 2,2′-bipyiridine

The complex *cis*,*cis*,*trans*-$RuCl_2(CO)(dmso\text{-}S)(PTA)_2$ (**31**), with a residual potentially labile ligand (dmso-S), seemed to be a good starting point for this investigation. Complex **31** reacts with bpy in water (either 16h at reflux or 30 min at 150°C in a microwave reactor) by replacing the molecule of dmso and the adjacent chloride yielding *cis*,*trans*-$[Ru(bpy)Cl(CO)(PTA)_2]Cl$ (**43**) (Scheme 4.1).

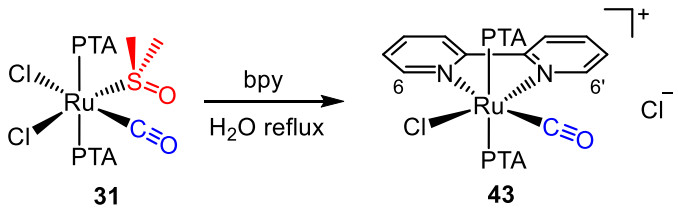

Scheme 4.1. Preparation of *cis,trans*-$[Ru(bpy)Cl(CO)(PTA)_2]Cl$ (**43**) upon treatment of *cis*,*cis*,*trans*-$RuCl_2(CO)(dmso\text{-}S)(PTA)_2$ (**27**) with bpy in water at reflux.

Compound **43** was fully characterized by NMR spectroscopy and mass spectrometry. The ^1H NMR spectrum shows in the aromatic region eight different resonances, one for each proton of bpy, consistent with the asymmetric environment of the diimine ligand (Appendix, A4.1). In agreement with previous findings,[1,2] the most deshielded doublet was assigned to H6, i.e. the proton with a partial positive charge that points towards the adjacent chloride (Scheme 4.1). The PTA region of the spectrum consists of two AB quartets centered respectively at 4.21 and 3.65 ppm; the ^1H-^{13}C HSQC spectrum established that the most downfield one belongs to NCH_2N protons and the other to NCH_2P protons. The ^{31}P NMR spectrum presents a singlet at –50.6 ppm, i.e. in the typical region of mutually *trans* PTAs.

The presence of CO was supported by the IR spectrum in EtOH that shows a band at 1984 cm^{-1} (see also Table 4.1 for a comparison of the carbonyl stretching frequencies of all the derivatives isolated); the stretching frequency is shifted to higher wavenumbers compared to the precursor **31** (1950 cm^{-1}), in agreement with a lower π back-bonding contribution from ruthenium because of the positive charge.

The same product **43** was obtained also by treatment of $[RuCl_2(CO)(PTA)_2]_2 \cdot 8H_2O$ (**35**) with bpy after 2h at reflux (Scheme 4.2). In this case bpy replaces the two bridging chlorides, i.e. the weakest ligands. This reactivity, together with that observed with pyridine and reported earlier, is consistent with the proposed nature of **35**.

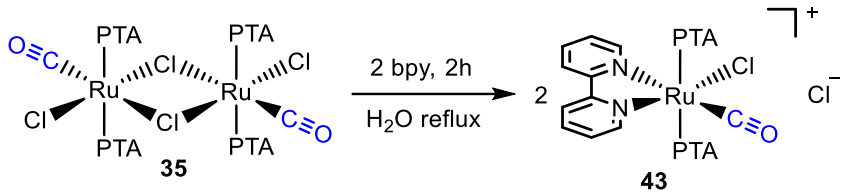

Scheme 4.2. Preparation of *cis,trans*-$[Ru(bpy)Cl(CO)(PTA)_2]Cl$ (**43**) upon treatment of $[RuCl_2(CO)(PTA)_2]_2 \cdot 8H_2O$ **(35)** with bpy in water at reflux.

A very small amount of colorless crystals very slowly grew out of this solution. The single-crystal X-ray structure shows that they are composed by the neutral Ru(II) complex *trans*-$RuCl_2(bpy)(CO)(PTA)$ (**44**) (Figure 4.2).

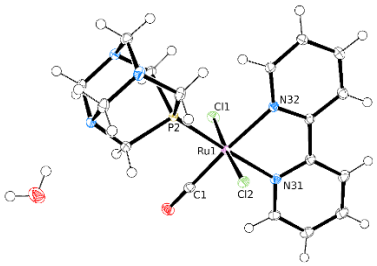

Figure 4.2 X-ray molecular structure (50% probability ellipsoids) of *trans*-$RuCl_2(bpy)(CO)(PTA)$ (**44**) Coordination distances (Å): Ru1–C1 = 1.842(2), Ru1–Cl11 = 2.417(2), Ru1–Cl12 = 2.402(1), Ru1–N31 = 2.134(2), Ru1–N32 = 2.154(1), Ru1–P2 = 2.305(1).

This compound might be a side product of the reaction, formed upon substitution of a bridging chloride and the adjacent PTA of **35** by bpy (Scheme 4.3); as shown in Chapter 2, there are previous examples in which bpy replaced a PTA. As an alternative, **44** might derive from **43**: the driving force of the unprecedented replacement of a PTA by Cl^-, accompanied by isomerization, might be the low solubility of the complex in aqueous solution. A low solubility in water was also observed with the neutral py derivative, *cis,cis,trans*-$RuCl_2(CO)_2(py)(PTA)$ (**38**)

described in Chapter 3, whose crystals spontaneously formed in D_2O, and that was much more soluble in $CDCl_3$.

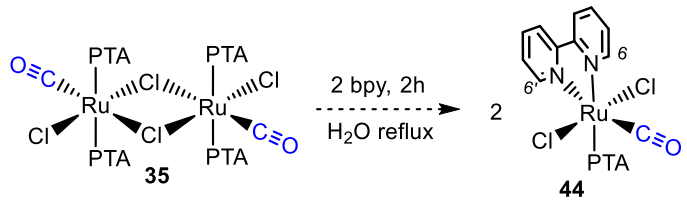

Scheme 4.3. Hypothesis of formation of the side product *trans*-$RuCl_2$(bpy)(CO)(PTA) (**44**).

The crystals of **44** were dissolved in DMSO-d_6. The ^{1}H NMR spectrum presents eight different resonances in the aromatic region, one for each proton of bpy, consistent with the asymmetric environment of the diimine ligand (Appendix, A4.7). The PTA region of the spectrum presents a multiplet and a broad singlet centered at 4.52 ppm and 4.32 ppm, belonging respectively (according to the ^{1}H-^{13}C HSQC spectrum) to the NCH_2N and to the NCH_2P protons. The 1D NOESY spectrum allowed us to assign the aromatic protons: saturation of the multiplet at 9.12 ppm gave an NOE effect with the resonance of the NCH_2P protons of the PTA, thus implying that it belongs to proton H6′, i.e. the one closest to the adjacent PTA. In fact, no NOE effect was observed when the doublet at 9.16 ppm was saturated. The other bpy resonances were then assigned through an ^{1}H-^{1}H COSY spectrum. The ^{31}P NMR spectrum presents a singlet at –38.4 ppm, i.e. in the typical region PTA *trans* to bpy. Thus, all the NMR data are consistent with the structure. Unfortunately the solution was too diluted for recording an IR spectrum.

The reaction of *cis*,*mer*-$RuCl_2(CO)(PTA)_3$ (**33**) with bpy in refluxing water led to the replacement of both chlorides by bpy, affording the dicationic complex *mer*-$[Ru(bpy)(CO)(PTA)_3](Cl)_2$ (**45**) (Scheme 4.4).

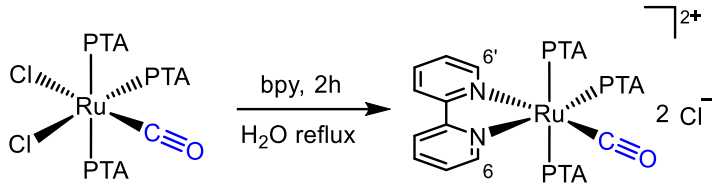

33 **45**

Scheme 4.4. Preparation of *mer*-[Ru(bpy)(CO)(PTA)$_3$](Cl)$_2$ (**45**) upon treatment of *cis*,*mer*-RuCl$_2$(CO)(PTA)$_3$ (**33**) with bpy in water at reflux.

Compound **45**, that is soluble in water, methanol, ethanol and DMSO, was fully characterized by NMR and IR spectroscopy, mass spectrometry, and its single-crystal X-ray structure was also determined (Figure 4.2).

The PTA region of the ^{1}H NMR spectrum consists of two pairs of signals, in a 1:2 ratio. The most intense and upfield shifted multiplets, respectively centered at 4.41 and 3.83 ppm (12H each) were attributed to the two equivalent *trans* PTA ligands, whose protons fall in the shielding cone of the adjacent bpy, while the other two signals, respectively centered at 4.81 ppm (partially overlapped with the water signal) and 4.65 ppm to the PTA *trans* to N. The ^{1}H-^{13}C HSQC spectrum established that, in each set, the deshielded quartet belongs to the N*CH*$_2$N protons and the upfield signal to the N*CH*$_2$P protons. The downfield region of the spectrum shows six resonances in which, according to integration, the unresolved multiplet centered at 8.42 ppm accounts for three protons (indeed, the ^{1}H-^{13}C HSQC spectrum it shows correlations with the resonances of three different carbon atoms of bpy). The 1D NOESY spectrum allowed us to assign the aromatic protons: saturation of the singlet of the NC*H*$_2$P protons of the PTA *trans* to bpy gave an NOE effect with the multiplet at 8.42 ppm (Appendix, A4.13 - 4.14), thus implying that it contains the resonance of proton H6′, i.e. the one closest to the adjacent PTA. The other bpy resonances were then assigned through an ^{1}H-^{1}H COSY spectrum. The ^{31}P NMR spectrum of **45** shows an AX$_2$ system in which the triplet is centered at –49.6 ($^{2}J_{P\text{-}P}$ = 25.2 Hz) ppm and the doublet at –55.6 ppm (Appendix, A4.15). The chemical shift of the triplet, that belongs to the PTA *trans* to bpy is upfield shifted of ca. 10 ppm compared

to the known monocationic Ru(II)-PTA-bpy compounds with PTA *trans* to bpy (i.e. *mer*-[Ru(bpy)Cl(PTA)$_3$](PF$_6$) (**17PF$_6$**) and *fac*-[Ru(bpy)Cl(PTA)$_3$](PF$_6$) (**18**), Chapter 2). The difference might be attributed to the presence of the CO ligand and also to the different net charge of the complexes.

The IR spectrum shows a carbonyl stretching band at 2010 cm^{-1}, i.e. at higher wavenumbers than in the precursor (1942 cm^{-1}), in agreement with the 2+ charge of **45**. For comparison, the CO stretching band in the dicationic monocarbonyl Ru(II) complex *fac*-[Ru(CO)(dmso-O)$_3$(dmso-S)$_2$](PF$_6$)$_2$ falls at 2012 cm^{-1}, suggesting that this parameter is not particularly affected by the nature of the ligands, but rather by the net charge of the complex.[3]

X-ray quality crystals of **45** were obtained upon recrystallization of the raw product from water/acetone (Figure 4.3). The coordination distances are in general agreement with the known *trans* influence of the ligands: thus, the Ru–P bond lengths of the two *trans* PTA ligands (2.3650(5) and 2.3631(4) Å) are slightly longer than the Ru–P distance *trans* to N (2.3391(4) Å). Similarly, the Ru–N bond length *trans* to CO (2.139(1) Å) is longer than that *trans* to P (2.119(1) Å), consistent with the previous finding that CO has a stronger *trans* influence than PTA. Compared with the structure of *trans*-Ru(bpy)Cl$_2$(CO)(PTA) (**44**), the Ru–C bond in **45** is longer (1.8746(14) Å in **45** vs 1.842(2) Å in **44**), consistent with a lower π-back donation from Ru(II) because of the 2+ charge.

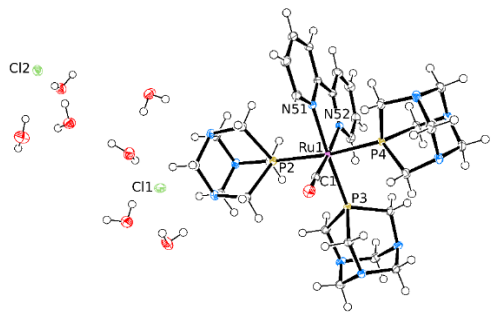

Figure 4.3. X-ray molecular structure (50% probability ellipsoids) of *mer*-[Ru(bpy)(CO)(PTA)$_3$](Cl)$_2$ (**45**) obtained by recrystallization of the raw product from water/acetone. Coordination distances (Å): Ru1–C1 = 1.8746(14), Ru1–N51 = 2.119(1), Ru1–N52 = 2.139(1), Ru1–P2 = 2.3650(4), Ru1–P3 = 2.3391(4), Ru1–P4 = 2.3631(4).

The reaction of *trans*,*mer*-$RuCl_2(CO)(PTA)_3$ (**32**) with bpy led to a mixture of compounds (Scheme 4.5): the ^{31}P NMR spectrum of the raw product shows a singlet at –50.6 ppm for **43** and two AX_2 systems in 1:1.5 ratio, belonging respectively to **45**, and to *mer*-$[Ru(bpy)Cl(PTA)_3]Cl$ (**17**) – already described in Chapter 2 – in which bpy has replaced a chloride and a molecule of CO.

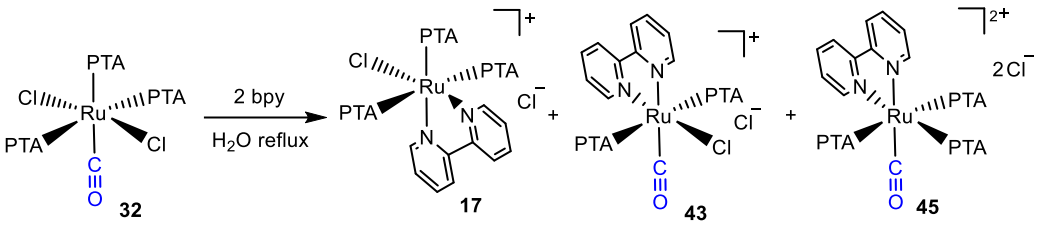

Scheme 4.5. Reactivity of *trans,mer*-$RuCl_2(CO)(PTA)_3$ (**32**) towards bpy in refluxing water.

Treatment of $[RuCl_2(CO)_2(PTA)]_2 \cdot H_2O$ (**37**) with bpy led to the isolation of the new cationic dicarbonyl compound *cis*,*trans*-$[Ru(bpy)(CO)_2Cl(PTA)]Cl$ (**46**) (Scheme 4.6). In fact the ^{31}P NMR spectrum presents a singlet at –25.4 ppm as main signal, i.e. in the typical region of PTA *trans* to Cl. Unlike in the other Ru(II)-PTA complexes in which a PTA is *trans* to Cl (i.e. in the neutral species *cis*-$RuCl_2(PTA)_4$ (**2**), *cis,cis*-$Ru(bpy)Cl_2(PTA)_2$ (**22**), and *cis,mer*-$RuCl_2(CO)(PTA)_3$ (**33**)), in this case the hydrolysis of the chloride was not observed. In fact, no changes were observed in the NMR spectrum after the addition of an excess of NaCl to the D_2O solution. Probably, since **46** is a monocationic dicarbonyl compound, the formation of a dicationic product is unfavorable. This behavior was also observed with the monocataionic monocarbonyl complexes *cis*-$[RuCl(CO)(PTA)_4](NO_3)$ (**42NO$_3$**) described in Chapter 3. The ^1H NMR spectrum shows in the aromatic region four equally intense signals (2H each), in agreement with bpy coordinated in a symmetrical environment (Scheme 4.6). The PTA region of the spectrum presents a broad singlet at 4.09 ppm for the NC*H*$_2$P protons and a multiplet centered at 4.47 ppm for the NC*H*$_2$N protons. The integration ratio of bpy and PTA resonances is consistent with the stoichiometry of the complex. (Appendix, A4.16-A4.18).

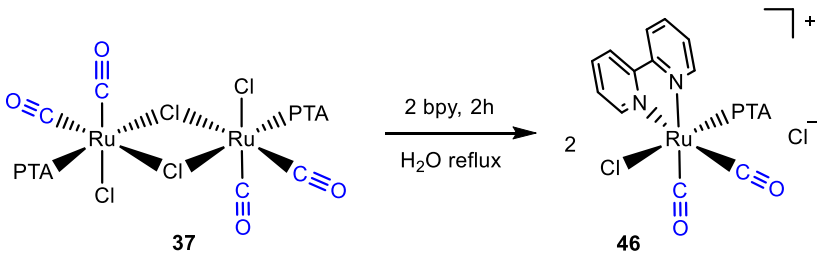

Scheme 4.6. Reactivity of $[RuCl_2(CO)_2(PTA)]_2 \cdot H_2O$ (**37**) towards bpy.

The IR spectrum of **46** in MeOH presents two carbonyl stretching bands at 2085 and 2034 cm^{-1}, in agreement with the presence of two *cis* CO ligands. For comparison, the CO stretching bands in the cationic dicarbonyl Ru(II) complex *cis,fac*-$[Ru(CO)_2Cl(dmso)_3](PF_6)$ fall at 2092 and 2030 cm^{-1}.[3]

The reaction between *cis,cis,trans*-$RuCl_2(CO)_2(PTA)_2$ (**39**) and bpy afforded a mixture of **46** with a new product **47** in ca. 1 / 2 ratio (Scheme 4.7). The PTA region of the ^1H NMR spectrum presents three different signals, two broad singlets and a multiplet, and is scarcely useful for determining the nature of the new species. However, the downfield region of the spectrum shows a new set of four equally intense bpy signals, indicating that also in **47** bpy is coordinated in a symmetrical environment. The ^{31}P spectrum shows a new singlet in the region of mutually *trans* PTAs (–50.9 ppm) attributed to **47**. Based in this spectroscopic evidence, **47** could be formulated as the dicationic species with two mutually *trans* PTAs *cis,trans*-$[Ru(bpy)(CO)_2(PTA)_2](Cl)_2$ (**47**), derived from **39** upon replacement of both chlorides. To be noted that the formation of **46** from **39** involves isomerization: Cl, that was *trans* to CO in the precursor, is *trans* to PTA in **46**.

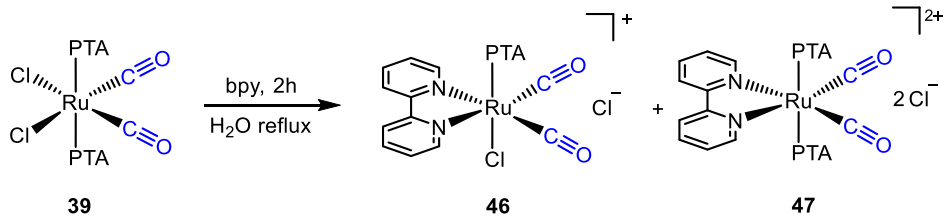

Scheme 4.7. Reactivity of *cis,cis,trans*-$RuCl_2(CO)_2(PTA)_2$ (**39**) towards bpy.

Compound **47** was selectively obtained, as nitrate salt (**47NO3**), when **39** was reacted with bpy in refluxing water after the addition of 2.1 eq of $AgNO_3$ (Scheme 4.8). The ^1H (aromatic region), ^{31}P NMR and ESI-MS spectra of **47NO3**, that is well soluble in water and DMSO, are coincident with those of **47**. The PTA region of the ^1H NMR spectrum (previously not discussed because of the overlaps with the signals of **46**) presents a broad singlet at 3.91 ppm for the NC*H*$_2$P protons and a multiplet centered at 4.30 ppm of NC*H*$_2$N protons. The bpy/PTA integration ratio is in agreement with the proposed stoichiometry (Appendix, A4.19-A4.21). Consistent with the *cis* geometry of the two CO ligands, complex **47** presents two CO stretching bands at 2086 and 2038 cm^{-1}. Compared with the precursor, the IR absorption bands of both **46** and **47** are shifted to higher wavenumbers, in accordance with the positive charge of the two products; it is remarkable that the CO stretching frequencies in **47** are very similar to those found in **46**, despite the higher positive charge. Compound **47** is the first dicationic dicarbonyl Ru(II) compound that we have isolated thus far; the previously prepared dicationic species have a single CO (e.g. *fac*-[Ru(CO)(dmso-O)$_3$(dmso-S)$_2$](PF$_6$)$_2$), and the dicarbonyl compounds were monocationic (e.g. **45**).

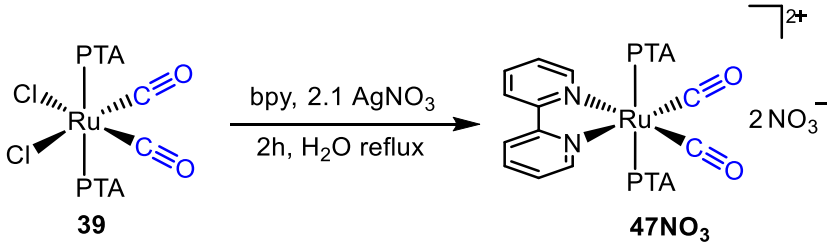

Scheme 4.8. Preparation of *cis,trans*-[Ru(bpy)(CO)$_2$(PTA)$_2$](NO$_3$)$_2$ (**47NO3**).

4.3 Light-induced rearrangements in water-soluble Ru(II)-CO-bpy complexes

Ru(II)-PTA complexes have shown to be photoreactive: *cis*-RuCl$_2$(PTA)$_4$ is prepared from the *trans*- isomer in water upon irradiation with blue light (see Chapter 2). Moreover, as mentioned in Chapter 2, the group of Romerosa has recently

reported a study of the effects of visible light on a series of water-soluble Ru(II) complexes with PTA.[4] They reported the synthesis of *mer*-$[RuCl_3(PTAH)_3](Cl)_2$ (**6**) and its conversion to the *fac*- isomer (**7**) promoted by irradiation with an halogen lamp (Scheme 4.9).

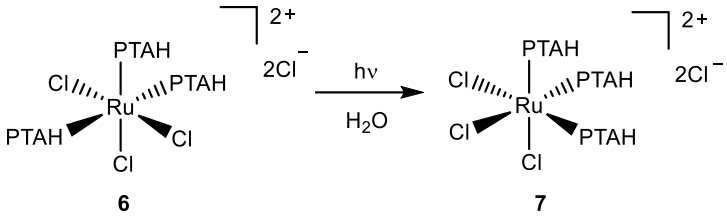

6 **7**

Scheme 4.9. Light-induced interconversion of *mer*-$[RuCl_3(PTAH)_3](Cl)_2$ (**6**) to *fac*-$[RuCl_3(PTAH)_3](Cl)_2$ (**7**).

For this reason we decided to investigate the effect of visible light on the previously described Ru(II)-CO-bpy complexes since all of them are from deep yellow to orange. In general, D_2O solutions of the complexes were directly irradiated in the NMR tube, without isolating the products.

We found that 24 h irradiation with blue light (470 nm) of a D_2O solution of *cis,trans*-$[Ru(bpy)Cl(CO)(PTA)_2]Cl$ (**43**) induces its complete transformation to the unprecedented *cis*- isomer *cis,cis*-$[Ru(bpy)Cl(CO)(PTA)_2]Cl$ (**48**) (Scheme 4.10). In fact, the ^{31}P NMR spectrum of the product presents an AX system of two doublets centered respectively at –25.1 ppm ($^2J_{P\text{-}P}$ = 24.7 Hz) and –42.3 ppm. The first doublet is in the region of PTA *trans* to Cl, while the second in that of PTA *trans* to bpy. The PTA region of the ^1H NMR spectrum shows a broad singlet at 3.93 ppm and three partially overlapped AB systems centered respectively at 4.41, 4.58, and 4.71 ppm. According to the ^1H-^{13}C HSQC spectrum, the singlet and the multiplet at 4.58 ppm belong to NCH_2P protons, while the other two multiplets to NCH_2N protons. The ^1H-^1H COSY shows correlation peaks between the two most upfield signals, attributed to the PTA *trans* to Cl that falls into the shielding cone of the adjacent bpy, as well as between the two most downfield signals (Appendix, A4.22-A4.26). The aromatic region of the spectrum presents eight equally intense signals for bpy

coordinated in an asymmetric environment. The 1D NOESY spectrum allowed us to assign the aromatic resonances: saturation of the singlet of the NCH_2P protons of the PTA *trans* to bpy gave an NOE effect with the multiplet at 9.09 ppm, thus implying that it contains the resonance of proton H6, i.e. the one closest to the adjacent PTA. An IR spectrum of **48** recorded in EtOH solution shows a carbonyl stretching band at 1992 cm^{-1}, i.e. a frequency similar to that of the *trans*-isomer **43** (1984 cm^{-1}).

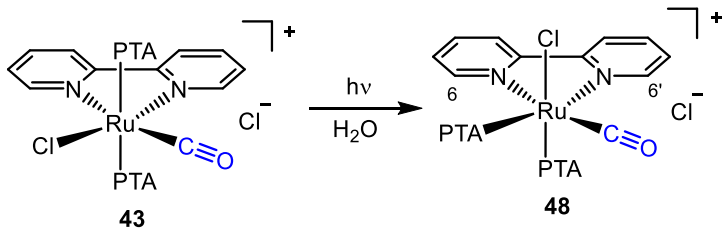

Scheme 4.10. Light-induced isomerization (λ = 470 nm, 24 h) of *cis,trans*-[Ru(bpy)Cl(CO)(PTA)$_2$]Cl (**43**) to *cis,cis*-[Ru(bpy)Cl(CO)(PTA)$_2$]Cl (**48**).

A similar behavior, i.e. a light-induced isomerization, was observed for *cis*,*trans*-[Ru(bpy)(CO)$_2$Cl(PTA)]Cl (**46**) (Scheme 4.11). In this case the process was slower (and less selective) and complete transformation required the irradiation with blue light of an aqueous solution of **46** for 3 days. The ^{31}P NMR spectrum of the product shows a singlet at –39.6 ppm, i.e. in the region of PTA *trans* to bpy together with other less intense signals. The ^{1}H NMR spectrum shows eight major resonances in the aromatic region for asymmetrically bound bpy. The PTA region of the spectrum presents a singlet at 3.21 ppm for the NCH_2P protons and a multiplet centered at 4.23 ppm for the NCH_2N protons. According to the NMR spectra the new compound could be formulated as *cis,cis*-[Ru(bpy)(CO)$_2$Cl(PTA)]Cl (**49**). The IR spectrum in EtOH presents two carbonyl stretching bands at 2006 and 1979 cm^{-1} in agreement with the presence of two CO ligands in *cis* geometry. Compared to the *trans* isomer (2085 and 2034 cm^{-1}), the two bands are shifted to lower wavenumbers, possibly because one CO is *trans* to the good π-donor Cl.

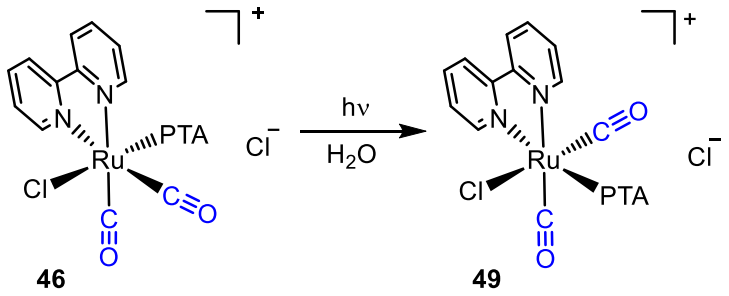

Scheme 4.11. Light-induced isomerization (λ = 470 nm, 72 h) of *cis,trans*-[Ru(bpy)(CO)$_2$Cl(PTA)]Cl (**46**) to *cis,cis*-[Ru(bpy)(CO)$_2$Cl(PTA)]Cl (**49**).

Conversely, compound *cis,trans*-[Ru(bpy)(CO)$_2$(PTA)$_2$](NO$_3$)$_2$ (**47NO$_3$**) was light-stable. The ^{31}P NMR spectrum of a D$_2$O solution of **47NO$_3$** remained unchanged even after one week of irradiation either with blue or visible light.

4.4 Conclusions

In this Chapter the reactivity of the water-soluble Ru(II)-PTA-CO complexes **31**-**33**, **35**, **37**, and **39** with the diimine ligand bpy was investigated. Typically bpy reacts with these compounds by replacing the two weakest ligands (i.e. dmso and/or Cl), affording one main mono- (Scheme 4.12) or dicationic product (Scheme 4.13).

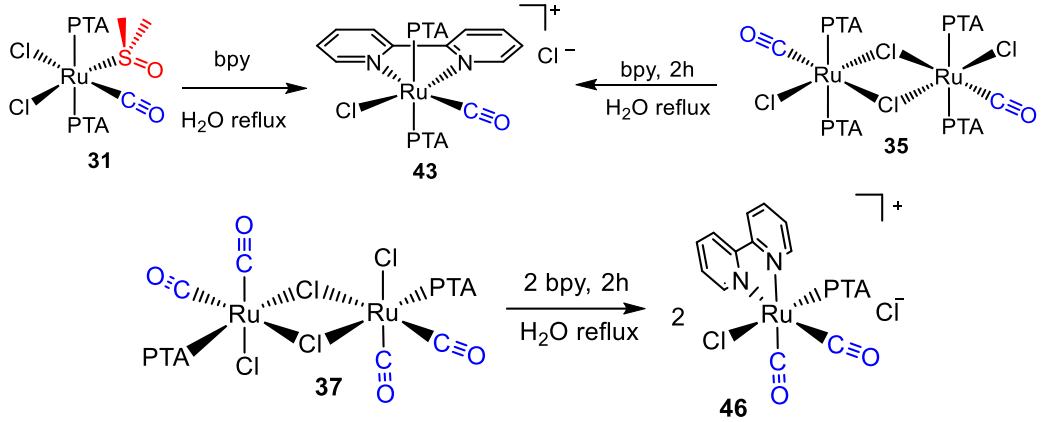

Scheme 4.12. Preparation of the monocationic derivatives **43** and **46**.

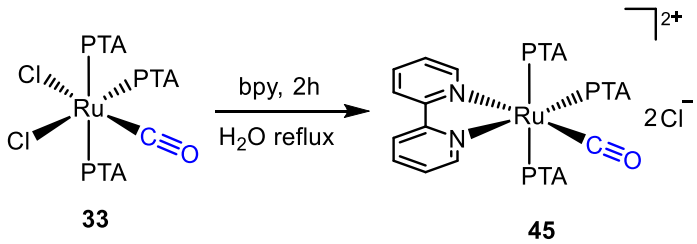

Scheme 4.13. Preparation of the dicationic derivative **45** from **33**.

The reaction of *trans,mer*-$RuCl_2CO(PTA)_3$ (**32**) with bpy led to a mixture of the three species *cis*,*trans*-$[Ru(bpy)Cl(CO)(PTA)_2]Cl$ (**43**), *mer*-$[Ru(bpy)Cl(PTA)_3]Cl$ (**17**), and *mer*-$[Ru(bpy)(CO)(PTA)_3](Cl)_2$ (**45**), obtained respectively by the replacement of a chloride and a PTA (**43**), of a chloride and a CO (**17**), or of the two chlorides (**45**)) (Scheme 4.14).

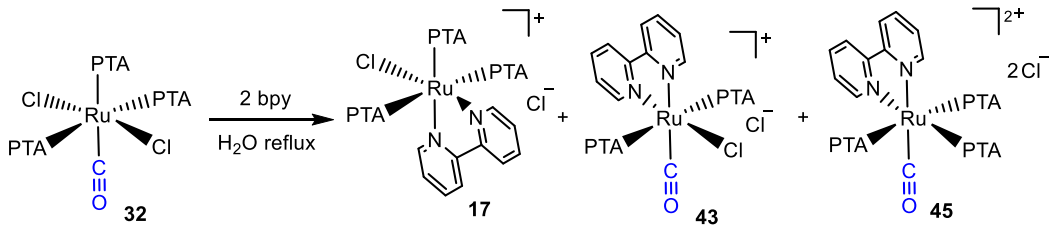

Scheme 4.14. Reactivity of complex *trans,mer*-$RuCl_2(CO)(PTA)_3$ (**32**) with bpy.

Also in *cis,cis,trans*-$RuCl_2(CO)_2(PTA)_2$ (**39**) bpy replaced either both chlorides (forming *cis,trans*-$[Ru(bpy)(CO)_2(PTA)_2](Cl)_2$ (**47**)) or one chloride and one PTA (forming *cis,trans*-$[Ru(bpy)(CO)_2Cl(PTA)]Cl$ (**46**)). In this case, however, the dicationic species **47** could be selectively obtained (as nitrate salt) by removing the chlorides of **39** with $AgNO_3$ (Scheme 4.15).

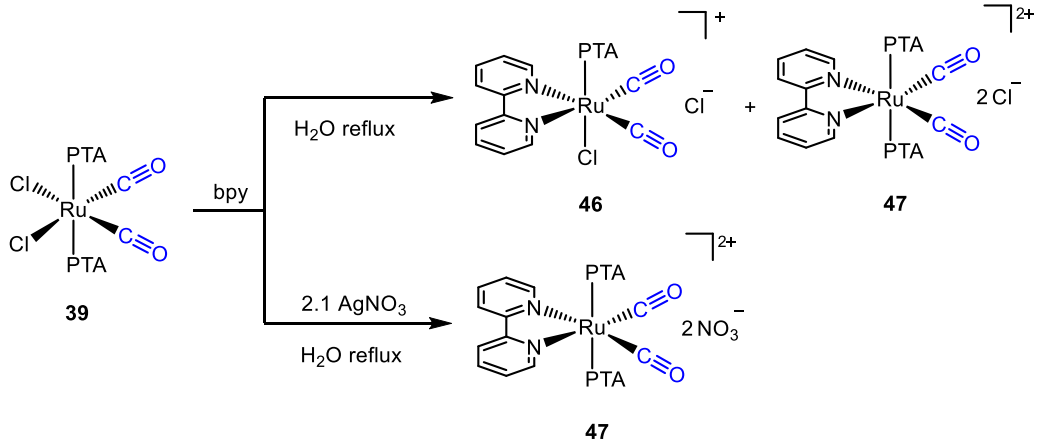

Scheme 4.15. Reactivity of complex *cis,cis,trans*-$RuCl_2(CO)_2(PTA)_2$ (**39**) with bpy.

Finally we found that the unexpected neutral compound *trans*-$Ru(bpy)Cl_2(CO)(PTA)$ (**44**) spontaneously crystallized in small amount out of the aqueous mother liquor of the reaction that transformed $[RuCl_2(CO)(PTA)_2]_2 \cdot 8H_2O$ (**35**) into **43**.

In these reactions the geometry of the PTA ligands remained unchanged, except when one PTA was replaced by bpy (in **43**, **44** and **46**); conversely, in some cases selective isomerization was induced by irradiating the bpy complexes with blue light. Thus, irradiation with blue or visible light transformed *cis*,*trans*-

[Ru(bpy)Cl(CO)(PTA)$_2$]Cl (**43**) into *cis*-[Ru(PTA)$_2$(bpy)Cl(CO)]Cl (**48**), and *cis*,*trans*-[Ru(CO)$_2$Cl(PTA)(bpy)]Cl (**46**) into *cis,cis*-[Ru(CO)$_2$Cl(PTA)(bpy)]Cl (**49**) (Scheme 4.16).

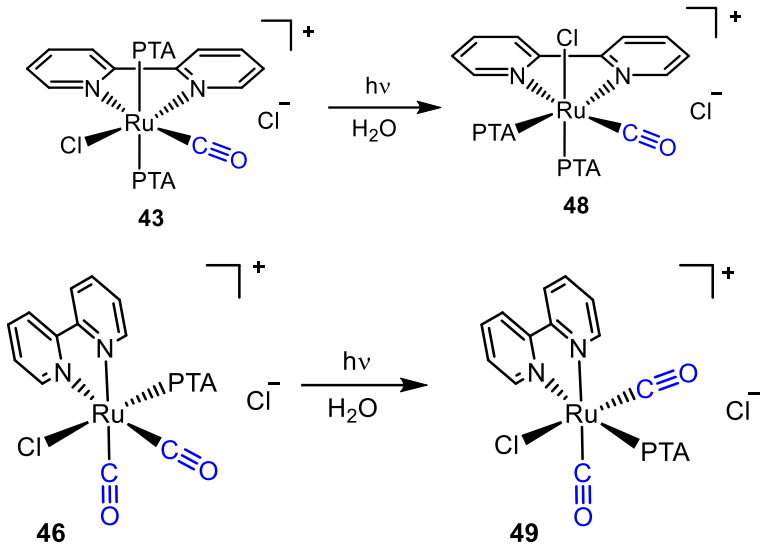

Scheme 4.16. Light-induced isomerization (λ = 470 nm, 72 h) of *cis,trans*-[Ru(bpy)Cl(CO)(PTA)$_2$]Cl (**43**) and *cis*,*trans*-[Ru(bpy)(CO)$_2$Cl(PTA)]Cl (**46**)).

All new compounds were fully characterized through NMR and IR spectroscopy, mass spectrometry and the single-crystal X-ray structures of *trans*-Ru(bpy)Cl$_2$(CO)(PTA) (**44**) and *mer*-[Ru(bpy)(CO)(PTA)$_3$](Cl)$_2$ (**45**) were determined.

Table 4.1 reports the carbonyl stretching bands of complexes **43**, **45**-**49**, that are always higher than in the corresponding neutral precursor, due to the positive charge(s). With the exception of **49**, in all the new compounds the COs (either one or two) are always *trans* to bpy. Only **49**, besides a CO *trans* to bpy, presents a CO *trans* to a chloride. In this case the two carbonyl stretching frequencies are shifted to lower wavenumbers compared to the isomer **46** with the same charge, possibly because the chloride is a good π-donor.

Table 4.1. Carbonyl stretching bands of compounds **43**, **45**-**49** (cm^{-1}).

complex	ν cm^{-1}	CO *trans* to
cis,trans-[Ru(bpy)Cl(CO)$(PTA)_2$]Cl (**43**)	1984[a]	N
mer-[Ru(bpy)(CO)$(PTA)_3$]$(Cl)_2$ (**45**)	2010[b]	N
cis,trans-[Ru(bpy)$(CO)_2$Cl(PTA)]Cl (**46**)	2085, 2034[c]	N
cis,trans-[Ru(bpy)$(CO)_2(PTA)_2$]$(NO_3)_2$ (**47**)	2086, 2038[c]	N
cis,cis-[Ru(bpy)Cl(CO)$(PTA)_2$]Cl (**48**)	1992[a]	N
cis,cis-[Ru(bpy)$(CO)_2$Cl(PTA)]Cl (**49**)	2006, 1979[a]	Cl

[a] EtOH solution, [b] Solid state (Nujol mulls), [c] MeOH solution.

The new Ru(II)-CO-PTA complexes and their derivatives with bpy allowed us to expand the diagnostic Table 2.2 of Chapter 2, that reports the typical ^{31}P NMR chemical shift intervals (Δ) for PTA bound to Ru(II) as a function of the nature of the *trans* ligand. In fact, since the phosphorous chemical shift is strongly influenced by the nature of the ligand in *trans* position, Table 4.2 can be used as a diagnostic tool for establishing the geometry of octahedral Ru–PTA complexes. We observed that when PTA is *trans* to an imine nitrogen (i.e. py, bpy), the ^{31}P NMR chemical shift is affected by the nature of the ligand: when *trans* to py it falls in the range –20 ÷ –23 ppm, whereas when *trans* to bpy or bpyAc it falls in the range –34 ÷ –50 ppm. We argue that this behavior might be due to the different orientation of the aromatic rings containing the imine nitrogen: chelating diimine ligands (i.e. bpy, bpyAc) are in the plane containing PTA, whereas pyridine is typically almost orthogonal to such plane. The different orientation, and consequently different involvement of the π orbitals of these ligands, could explain the different ^{31}P chemical shift intervals for PTA *trans* to pyridine and *trans* to diimine ligands.

Finally, as noted already, there is a rough correlation between the Ru–P bond length and the chemical shift of the ^{31}P NMR resonance: as the Ru–P distance increases,

the phosphorous resonance shifts progressively to lower frequencies; this trend is confirmed also with the two complexes bearing PTA *trans* to CO (*trans,mer*-$RuCl_2(CO)(PTA)_3$ (**32**) and *cis*-$[RuCl(CO)(PTA)_4](NO_3)$ (**42NO$_3$**).

Table 4.2. Typical ^{31}P NMR chemical shift intervals (Δ) and Ru–P distances for PTA bound to octahedral Ru(II) complexes as a function of the nature of the *trans* ligand.

Ligand *trans* to PTA	Δ ^{31}P (ppm)[a]	Δ Ru–P distance (Å)	Ref.
OH_2/OH	–5 ÷ –16	-	Chapter 2, 4, 5
N[b]	–20 ÷ –23	2.1933 ÷ 2.224	Chapter 2
Cl	–14 ÷ –26	2.232 ÷ 2.283	Chapter 2, 4, 6
Br	–24 ÷ –27	2.266 ÷ 2.281	Chapter 2
S[c]	–30 ÷ –45	2.280 ÷ 2.318	1, 7
N[d]	–34 ÷ –50	2.260 ÷ 2.344	Chapter 2, this Chapter, 8, 9, 10, 11, 12, 13, 14, 15,
H	–26.6[e]	2.299 ÷ 2.300	16
P[f]	–45 ÷ –60	2.290 ÷ 2.400	Chapter 2 and 3, this Chapter, 4, 5, 6, 15, 16, 17, 18, 19
CO	–60 ÷ –70	2.3821 ÷ 2.3828	Chapter 3, this Chapter
C[g]	–68.4[e]	2.395(1)	20

[a] For comparison, the singlet of free PTA falls at δ = –98.2 ppm in D_2O and at –102.3 ppm in $CDCl_3$. [b] From pyridine. [c] From [9]aneS3 = 1,4,7-trithiacyclononane. [d] From imine or azole. [e] Single hit. [f] From PTA. [g] From cyclometallated 2-phenylpyridine.

4.5 Bibliography

[1] E. Iengo, N. Demitri, G. Balducci, E. Alessio, *Dalton Trans.*, **2014**, *43*, 12160 - 12163.

[2] F. Battistin, G. Balducci, N Demitri, E. Iengo, B. Milani, E. Alessio, *Dalton Trans.*, **2015**, *44*, 15671 - 15682.

[3] I. Bratsos, S. Calmo, E. Zangrando, G. Balducci, E. Alessio, *Inorg. Chem.*, **2013**, *52*, 12120 - 12130.

[4] A. Udvardy, M. Serrano-Ruiz, V. Passarelli, E. Bolyog-Nagy, F. Joó, Á. Kathó, A. Romerosa, *Inorg. Chim. Acta*, **2017**, (doi.org/10.1016/j.ica.2017.04.054).

[5] J. Kovács, F. Joó, A. Bényei, G. Laurenzy, *Dalton Trans.*, **2004**, 2336 - 2340.

[6] D. J. Darensbourg, F. Joó, M. Kannisto, A. Kathó, J. H. Reibenspies, D. J. Daigle, *Inorg. Chem.*, **1994**, *13*, 200 - 208.

[7] B. Serli, E. Zangrando, T. Gianferrara, C. Scolaro, P. J. Dyson, A. Bergamo, E. Alessio, *Eur. J. Inorg. Chem.*, **2005**, 3423 - 3434.

[8] E. Menéndez-Pedregal, J. Díez, Á. Manteca, J. Sánchez, A. C. Bento, R. García-Navas, F. Mollinedo, M. Pilar Gamasa, E. Lastra, *Dalton Trans.*, **2013**, *42*, 13955 - 13967.

[9] A. Garcia-Fernandez, J. Diez, M. Pilar Gamasa, E. Lastra, *Eur. J. Inorg. Chem.*, **2014**, *5*, 917 - 924.

[10] S. Bolaño, J. Bravo, J. Castro, M. M. Rodriguez-Rocha, M. F. C. G. da Silva, A. J. L. Pombeiro, L. Gonsalvi, M. Peruzzini, *Eur. J. Inorg. Chem.*, **2007**, 5523 - 5532.

[11] A. García-Fernández, J. Díez, A. Manteca, J. Sánchez, M. P. Gamasa, E. Lastra, *Polyhedron*, **2008**, *27*, 1214 - 1228.

[12] S. Bolaño, M. M. Rodriguez-Rocha, J. Bravo, J. Castro, E. Onate, M. Peruzzini, *Organometallics*, **2009**, *28*, 6020 - 6030.

[13] S. Miguel, J. Diez, M. P. Gamasa, M. E. Lastra, *Eur. J. Inorg. Chem.*, **2011**, *951*, 4745 - 4755.

[14] F. Scalambra, M. Serrano-Ruiz, S. Nahim-Granados, A. Romerosa, *Eur. J. Inorg. Chem.*, **2016**, *10*, 1528 - 1540.

[15] A. Wołoszyn, C. Pettinari, R. Pettinari, G. V Badillo Patzmay, A. Kwiecień, G. Lupidi, M. Nabissi, G. Santoni, P. Smoleński, *Dalton Trans.*, **2017**, *46*, 10073 - 10081.

[16] C. A. Mebi, B. J. Frost, *Inorg. Chem.*, **2007**, *46*, 7115 - 7120.

[17] S. Grguric-Sipka, C. R. Kowol, S.-M. Valiahdi, R. Eichinger, M. A. Jakupec, A. Roller, S. Shova, V. B. Arion, B. K. Keppler, *Eur. J. Inorg. Chem.*, **2007**, 2870 - 2878.

[18] D. N. Akbayeva, S. Moneti, M. Peruzzini, L. Gonsalvi, A. Ienco, F. Vizza, *C. R. Chimie*, **2005**, *8*, 1491 - 1496.

[19] A. Udvardy, A. C. Bényei, Á. Kathó, *J. Organomet. Chem.*, **2012**, *717*, 116 - 122.

[20] L. Leyva, C. Sirlin, L. Rubio, C. Franco, R. Le Lagadec, J. Spencer, P. Bischoff, C. Gaiddon, J.-P. Loeffler, M. Pfeffer, *Eur. J. Inorg. Chem.*, **2007**, 3055 - 3066.

CHAPTER 5

The study reported in this Chapter was done in collaboration with the group of Prof. L. Messori, University of Firenze, Italy. This Chapter was published in: F. Battistin, F. Scaletti, G. Balducci, S. Pillozzi, A. Arcangeli, L. Messori, E. Alessio, *Journal of Inorganic Biochemistry*, **2016**, 160, 180-188.

Biological properties of Ru(II)- and Ru(III)-PTA complexes

5.1 State of the Art

As written in the Introduction, since several years the cage-like monodentate phosphine 1,3,5-triaza-7-phosphaadamantane (PTA) has been widely used as a co-ligand in the design of organometallic Ru(II) anticancer compounds. The half-sandwich RAPTA-type compounds $[RuCl_2(\eta^6\text{-arene})(PTA)]$ (RAPTA = Ruthenium-Arene PTA, Figure 5.1) developed by the group of Dyson are the most well-known,[1] but other Ru(II) compounds containing PTA have been investigated for their anticancer[2] or DNA-binding[3] properties.

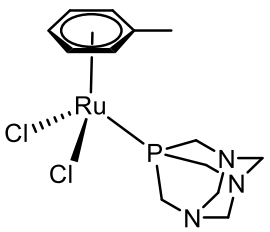

Figure 5.1. A representative example of the RAPTA compounds (RAPTA-T).

Given these premises, we were surprised at realizing that even though PTA has been extensively used as co-ligand in many Ru half-sandwich anticancer compounds, no investigation has been yet performed on the ruthenium-halide complexes of PTA, i.e. on complexes in which PTA is the main ligand. Only very recently the group of Pettinari reported a cytotoxic study of Ru(II) complexes of general formula *cis,trans*-$RuCl_2(PTA)_2(chel)$ and *mer*-$Ru[Cl(PTA)_3(chel)]Cl$ (chel = 2,2'-bipyridine (bpy – **17** described in Chapter 2) or 1,10-phenanthroline (phen)).[4] These compounds were prepared by treatment of $[RuCl_2(COD)]_n$ (COD = 1,5-cyclooctadiene) with

stoichiometric amount of bpy or phen, in EtOH solution at reflux conditions; addition 2 eq of PTA led to *cis,trans*-$RuCl_2(PTA)_2$(chel), while addition of 3 eq of PTA led to *mer*-Ru[$Cl(PTA)_3$(chel)]Cl. All compounds showed to be moderate active in reducing necrotic cell death in multiple myeloma cell lines (IC_{50} values from 65.8 to 197.6 μM).[4]

5.2 Aim of the Chapter

This chapter is focused on a preliminary investigation of the biologic activity of the already described Ru(II)-PTA complexes of general formula *trans*- or *cis*-$Ru(PTA)_4X_2$ (X = Cl (**1**, **2**), Br (**11**, **12**)), and on the Ru(III)-PTA compound *trans*-$[RuCl_4(PTAH)_2]Cl$ (**3**) (Figure 5.2, see also Chapter 2).

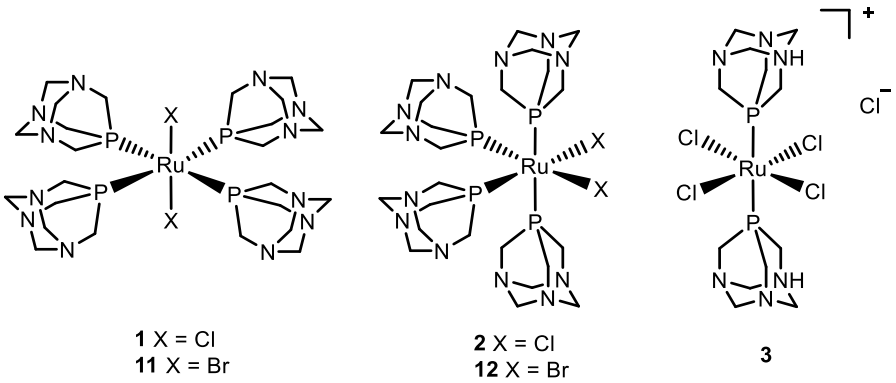

Figure 5.2. Schematic structures of compounds **1** - **3**, **11**, **12**.

In particular we investigated the chemical behavior of the above compounds in water and in physiological buffer, their interactions with two model proteins – cytochrome c (cyt c) and ribonuclease A (RNase A) – as well as with a single strand reference oligonucleotide (5'-CGCGCG-3', ODN4). Their in vitro cytotoxicities against a human colon cancer cell line (HCT-116) and a myeloid leukemia (FLG 29.1) are also reported.

Complex **3** is particularly interesting since it is structurally similar to the two best known Ru(III) anticancer complexes, namely NAMI-A (i.e. [imH]*trans*-$[RuCl_4(dmso\text{-}S)(im)]$, im = imidazole) and NKP1339 (i.e. [Na]*trans*-$[RuCl_4(ind)_2]$, ind = indazole) (Figure 5.3).[5,6]

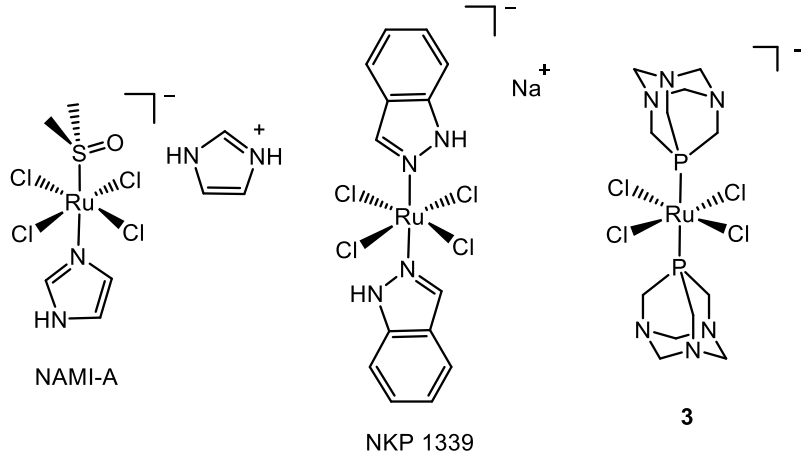

Figure 5.3. Comparison of the structurally related Ru(III) complexes NAMI-A (left), NKP1339 (center) and **3** (represented in its anionic form with unprotonated PTA).

5.3 Spectrophotometric analysis

The studied compounds display a remarkable solubility and a sufficient stability in water (see Chapter 2), thus being well amenable for biological studies. UV-vis absorption spectroscopy was chosen as the election method to monitor the behavior of the five complexes.

The electronic absorption spectra of **1** and **11** in chloroform (Appendix, A5.1) show a single band of low intensity in the visible region (λ_{max} = 452 nm for **1** and 475 nm for **11**), whereas those of the less symmetric *cis* isomers (Appendix, A5.2) are characterized by a broad band, probably the overlap of two bands, at higher frequencies (λ_{max} = 348 nm for **2** and 368 nm for **12**). They are attributed to MLCT transitions from Ru(II) to the π-acceptor PTA, as in the corresponding Ru(II)-CH_3CN[7] and Ru(II)-dmso[8] compounds. Consistent with this assignment, the main absorption band of each Br isomer is red-shifted of ca. 20 nm compared to that of the corresponding Cl species (bromide, being a better π-donor than chloride, leads to an increase in the energy of the filled t_{2g} orbitals).[7] The electronic absorption spectra of **2** and **12** in pure water and after addition of excess NaCl or NaBr are consistent with the NMR findings in D_2O (see Chapter 2): both complexes release the halide *trans* to PTA when dissolved in water, forming the aqua species *cis*-$[RuCl(OH_2)(PTA)_4]^+$ (**2aq**) and *cis*-$[RuBr(OH_2)(PTA)_4]^+$ (**12aq**). (Appendix, A5.3-A5.6; see below the results in phosphate buffer).

The visible region of the absorption spectrum of **3** in water has the typical halide-to-Ru(III) charge-transfer manifold typical of all Ru(III) complexes with a similar structure [7,8,9,10] a main broad band centered 383 nm and a weaker band at 444 nm (Appendix, A5.7). The spectrum shows a very slow decrease of the band intensities (ca. –15 % in 72h at room temperature) without significant shifts in the absorption maxima (Appendix, A5.7). Such spectral changes are not consistent with slow chloride release (in fact, addition of excess NaCl after 72h induces no significant

change in the spectrum),[7,8,9,10] but rather suggest a progressive aggregation (and consequent decrease of the complex concentration), perhaps involving species with different charge derived from the deprotonation equilibria of coordinated $PTAH^+$. Next, the behavior of the five complexes in a reference buffer at physiological pH was monitored over a time period of 24h. Time-dependent spectral profiles for each compound are reported in Figure 5.4 (**1**, **2**, **11**, **12**) and Figure 5.5 (**3**).

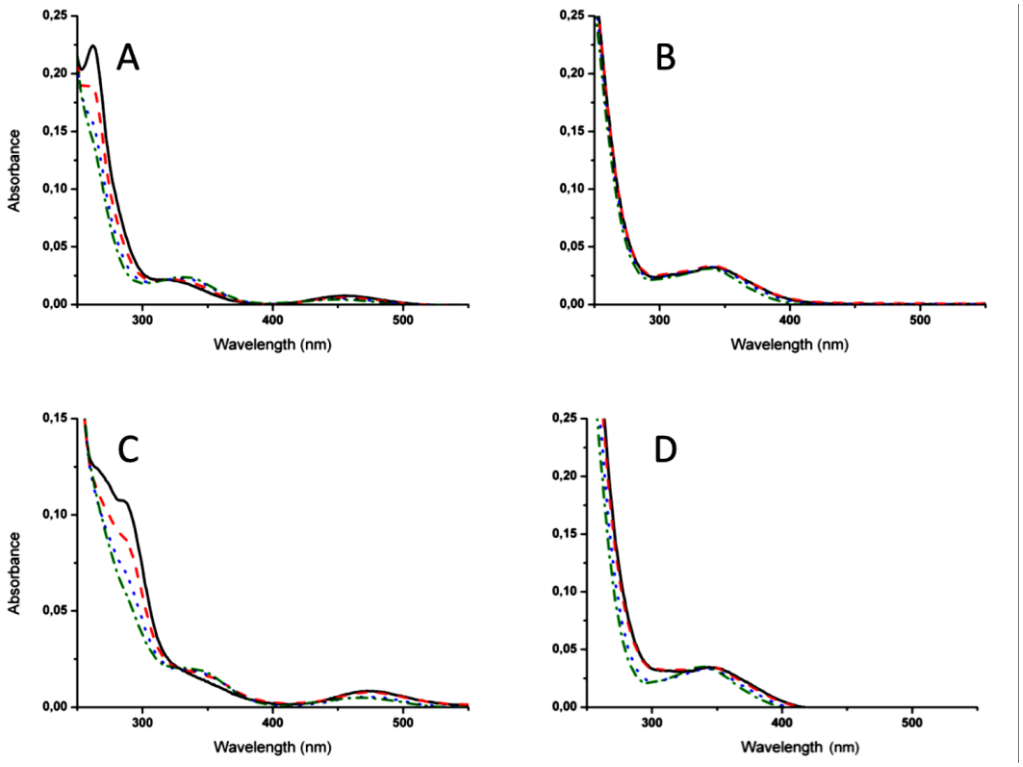

Figure 5.4. Time course UV-vis spectra of compounds **1** (A), **2** (B), **11** (C), and **12** (D) dissolved in 10 mM phosphate buffer, pH 7.4, over 1 hour. Figures show spectra recorded at t = 0 (black solid line), 10 min (red dashed line), 30 min (blue dotted line), and 1h (green dashed-dot line).

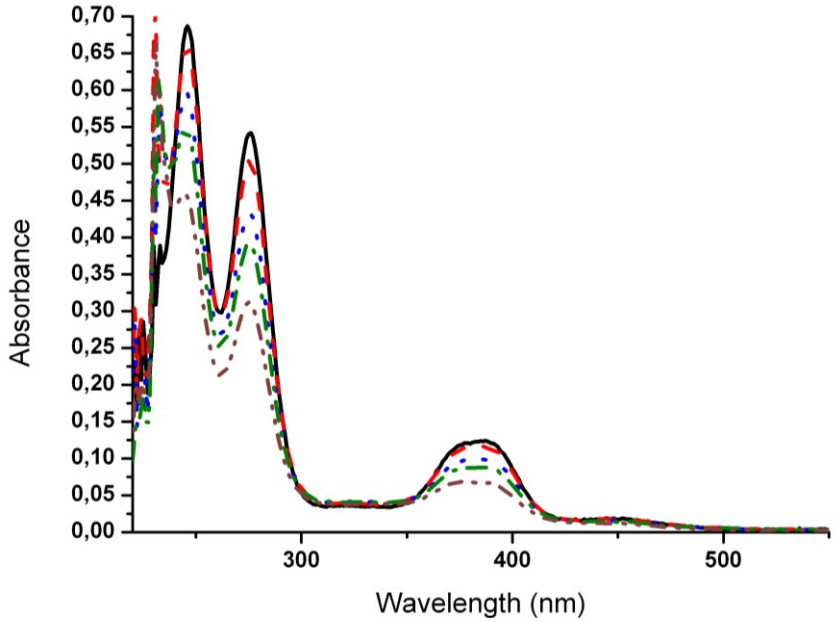

Figure 5.5. Time course UV-vis spectra of compound **3** dissolved in 10 mM phosphate buffer, pH 7.4, over 24 hours. Figures show spectra recorded at t = 0 (black solid line), 1h (red dashed line), 6h (blue dotted line), 12h (green dashed-dot line), and 24h (brown dashed-dot-dot line).

For the *trans* isomers **1** and **11**, contrary to what observed by NMR spectroscopy in D_2O, where they are stable, spectral changes occurred within one hour for each complex (Figure 5.4A and C): the absorption band in the visible region (456 nm for **1** and 475 nm for **11**) progressively disappeared, whereas the band in the near UV region shifted to lower frequencies (325 nm for **1** and 344 nm for **11**). These spectral changes are ascribed to the progressive release of the halide ligands, even though concomitant partial release of PTA cannot be excluded. Conversely, the *cis* isomers **2** and **12** displayed a different behavior, similar to that found in pure water (Figure 5.4B and D): after dissolution of **2** and **12** in the buffer, both complexes showed a similar spectrum, with a band at 340 nm, whereas in chloroform solution compound **12** has a band which is red-shifted of ca. 20 nm compared to that of compound **2** (see above). In addition, the spectra in phosphate buffer showed no significant change with time, consistent with the NMR findings (in D_2O) that evidenced rapid equilibration of the *cis* isomers with the mono- and diaqua species upon release of

the halide ligands. The aquation process, that is expected to be more pronounced at the concentration used in the UV-vis spectra (compared to NMR), apparently leads to the common *cis*-$[Ru(OH_2)_2(PTA)_4]^{2+}$ species.
The spectrum of compound **3** changed with time in a manner similar (but faster) to that observed in pure water (see above) (Figure 5.5).

5.4 Reactions with model proteins

The interactions of compounds **1** - **3**, **11**, **12** with the model proteins RNAse and cyt c were subsequently monitored by ESI-MS analysis. Results are summarized in Figure 5.6 (interaction with cyt c) and in the Appendix (A5.8 - with RNase A). In general, as can be judged from the amount of the metallodrug-protein adducts that are formed, the reactivity is very limited, in particular with compound **3**. Nevertheless, careful analysis of ESI mass spectra allowed us to identify the metallic fragments that are bound to the proteins. In most cases mono-metallated derivatives are formed, in which the metallic fragment consists of the ruthenium center plus a variable number of PTA ligands. In particular, Figure 5.6 shows that in the case of cyt c the main peaks can be assigned to adducts bearing the fragments $[Ru(PTA)]^{2+}$, $[Ru(PTA)_2]^{2+}$ and $[Ru(PTA)_3]^{2+}$, respectively. In some cases fragments containing Cl^- or Br^- were also detected: $[RuCl(PTA)_2]^+$ for compound **1**, $[RuBr(PTA)_4]^+$ for compound **11**, $[RuBr(PTA)_3]^+$ for compound **12**, $[RuCl_3(PTAH)]^+$ and $[RuCl_4(PTAH)_2]^+$ for compound **3**. The interactions with RNase A lead to adducts that are similar to those obtained with cyt c. Moreover, adducts with $[RuCl]^+$ (for compounds **1** and **2**) and $[RuBr]^+$ (for compound **11** and **12**) were also detected.
Overall, the interactions detected between the model proteins and the five ruthenium complexes are rather modest, suggesting that proteins might not be primary and/or relevant targets.

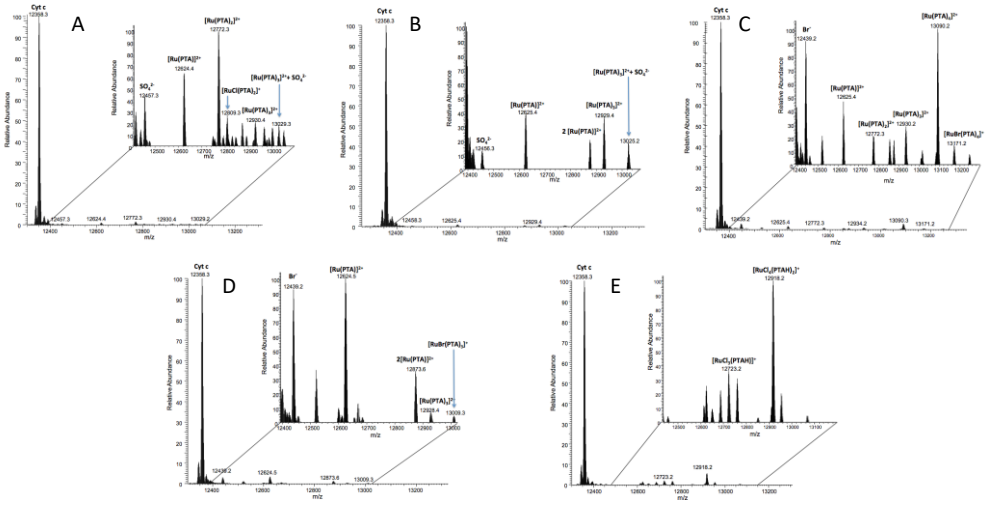

Figure. 5.6. LTQ Orbitrap ESI mass spectra of compound **1** (A), **2** (B), **11** (C), **12** (D) and **3** (E) dissolved in 20 mM ammonium acetate buffer, pH 7.4, in the presence of cyt c after 24h incubation at 37°C. The spectra in the back are the amplification of a region of the front spectra.

5.5 Reactions with a single strand oligonucleotide

The lack of relevant adduct formation with the selected model proteins, together with the evidence in literature that several Pt and Ru-based complexes may exert their biological effects through a direct interaction with DNA,[11] prompted us to study the reactivity of the five ruthenium complexes with a DNA model system.

Investigations were performed on a single strand oligonucleotide, ODN4, (5'-CGCGCG-3'), chosen as reference, and the interactions were monitored through ESI-MS. In this case adduct formation was far more evident than with model proteins, with the exception of compound **3** (Figure 5.7). Adducts between the oligonucleotide and ruthenium fragments containing more than one PTA ligand were identified. Specifically, the main adduct between ODN4 and the *trans* isomers **1** and **11** (Figure 5.7A and C) contains the fragment $[Ru(PTA)_2]^{2+}$, whereas that with the *cis* isomers **2** and **12** (Figure 5.7B and D) bears $[Ru(PTA)_3]^{2+}$. Notably, even though compound **2** was reacted with ODN4 under the same conditions as the other ruthenium complexes, a drastic decay in the intensity of ESI-MS peaks was detected

in this case, which might be tentatively ascribed to the occurrence of aggregation/precipitation processes. Nonetheless, a low intensity spectrum could be obtained (Figure 5.7B) and peak assignment was performed. It is worth mentioning that in this case the peak relative to the free oligonucleotide was not detected after 24h incubation at 37°C, revealing that all the ODN4 has reacted. The only adduct that could be identified was that with the metallic fragment $[Ru(PTA)_3]^{2+}$.

In addition to the main adduct, ESI mass spectra of compounds **1** and **11** show peaks corresponding to derivatives: $2[Ru(PTA)_2]^{2+}$ and $[Ru(PTA)_2]^{2+}$+$[RuCl(PTA)_3]^{+}$ for compound **1**, $[Ru(PTA)_2]^{2+}$+$[RuBr(PTA)_3]^{+}$ and $2[RuBr(PTA)_3]^{+}$ for compound **11**. In the case of compound **12**, other mono- and bis-metallated adducts were also detected (i.e. $[Ru(PTA)_4]^{2+}$ and $2[RuBr(PTA)_3]^{+}$).

The interaction between more inert compound **3** and ODN4 is less evident and only small amounts of adducts could be detected. In fact, Figure 5.7E shows two peaks corresponding to the adducts between ODN4 and the fragments $[Ru(PTA)]^{3+}$ and $[Ru(PTA)_2]^{3+}$, while most of the free compound in solution is in the form $[RuCl_4(PTA)]^{-}$ or $[RuCl_4(PTA)_2]^{-}$ (Appendix, A5.9).

It is evident that, in agreement with the NMR and UV-vis findings reported above, the two *cis* complexes (**2** and **12**) are more reactive than the respective *trans* species (**1** and **11**), and that the adduct formation is more evident with the chloride than with the bromide.

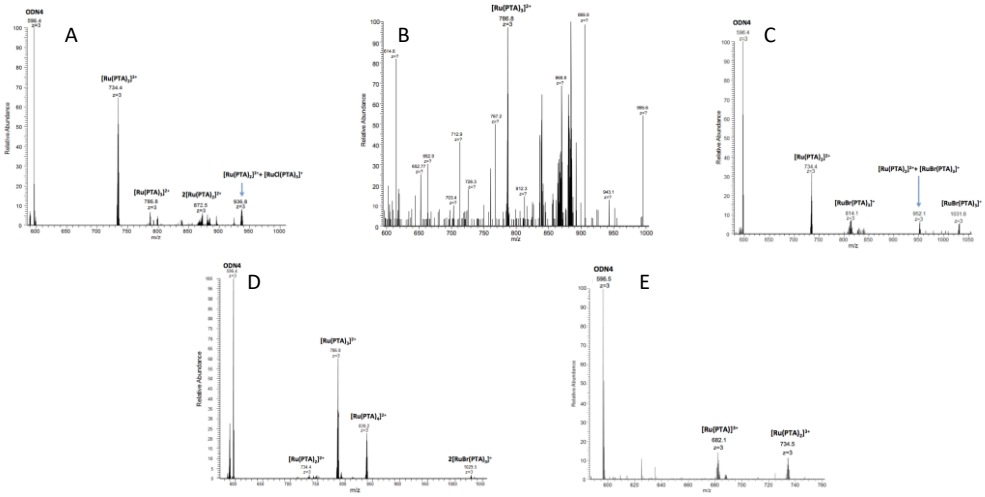

Figure 5.7. LTQ Orbitrap ESI mass spectra of compound **1** (A), **2** (B), **11** (C), **12** (D) and **3** (E) dissolved in milliQ water, in the presence of ODN4 after 24h incubation at 37°C.

5.6 Antiproliferative properties

The antiproliferative properties of compounds **1** - **3**, **11**, **12** were assessed against two cell lines: HCT-116 (human colon cancer) and FLG 29.1 (human acute myeloid leukemia) according to the method described in the experimental section. Both cell lines were treated for 24 hours with increasing concentrations of the drug and IC_{50} values determined (calculated through the Trypan blue exclusion test). The findings are summarized in Table 5.1. In general, the antiproliferative effects are quite moderate, yet the two *cis* isomers **2** and **12** were found to be significantly more effective than the *trans* congeners **1** and **11** in the leukemia cell line, whereas the cytotoxicity of compound **3** is far lower. It is also remarkable that the cytotoxic profile of **1** is virtually identical to that of **11**, and the same similarity was found for the two *cis* isomers **2** and **12**. This finding suggests that – in both cases – similar halide-free species are ultimately responsible for the biological effects. Such species are presumably different for the two stereoisomers because the activity clearly depends on the geometry of the complex. These results, together with the reactivity

profiles toward the oligonucleotide, point out that the biological effects may be related to the direct interaction of these ruthenium compounds with DNA.

Table 5.1. IC_{50} values (μM) for compounds **1** - **3**, **11**, **12** on a solid tumor cell line, HCT 116, and a myeloid leukemia cell lines, FLG 29.1.

Compound	FLG 29.1	HCT 116
trans-$RuCl_2(PTA)_4$ (**1**)	>200	>100
cis-$RuCl_2(PTA)_4$ (**2**)	60.83±0.59	>100
trans-$RuBr_2(PTA)_4$ (**11**)	>200	>100
cis-$RuBr_2(PTA)_4$ (**12**)	59.33±0.41	>100
trans-$[RuCl_4(PTAH)_2]Cl\cdot 2H_2O$ (**3**)	84.91±0.39	>100
Cisplatin	24.33±0.75[12]	7.65 ± 0.63[13]

5.7 Conclusions

In conclusion we found that the chemical behavior of the Ru(II) compounds in aqueous solution depends on their structure and on the pH. In pure water, whereas the *trans* isomers **1** and **3** are very stable (in the dark), the *cis* analogues **2** and **12** readily equilibrate with the aqua species *cis*-$[RuX(OH_2)(PTA)_4]^+$ and *cis*-$[Ru(OH_2)_2(PTA)_4]^{2+}$. However, when dissolved in phosphate buffer at physiological pH, also the *trans* isomers undergo aquation processes that can be mainly ascribed to halide replacement.

In general, compounds **1**, **2**, **11**, **12** showed a pairwise different – structure-related – behavior, clearly indicating that the four isomers do not converge to a common species but rather to two main halide-free stereoisomeric Ru-PTA fragments. Their reactivity towards cyt c and RNase A was found to be quite limited and minimal amounts of protein adducts were formed. Compounds **1**, **2**, **11**, **12** exhibited a far higher reactivity toward the reference oligonucleotide than toward model proteins and substantial amounts of adducts – mainly mono-ruthenated – are indeed formed in which ruthenium fragments are coordinated to DNA nucleobases. The two *cis* isomers (**2** and **12**) turned out to be more reactive than the respective *trans* species (**1** and **11**). Finally, the four Ru(II) compounds manifested rather moderate antiproliferative properties against the two investigated cell lines: HCT-116 (human colon cancer) and FLG 29.1 (human acute myeloid leukemia). Consistent with the results described above, the *cis* isomers **2** and **12** were found to be significantly more effective than the *trans* congeners **1** and **11** in the leukemia cell line FLG 29.1.

The only investigated Ru(III) complex, **3**, deserves a separate comment. It was found to be very inert, both in pure water and in buffer, and basically unreactive towards the investigated biomolecules and devoid of any relevant cytotoxic activity towards the investigated cancer cell lines. Given the structural similarity between **3** and well known anticancer compounds KP1019/NKP1339 and NAMI-A, these findings were particularly disappointing. Nevertheless, they might suggest that for this type of

anionic Ru(III) complexes, cytotoxicity is strictly related to the activation kinetics. Whereas the lack of cytotoxic activity of NAMI-A has been attributed to the fast kinetics that lead to aquated Ru(III) metabolites unable to cross the cell membrane,[14,15] the scarce activity of **3** might be attributed to exceedingly slow kinetics and to the consequential paucity of reactive aqua species. The intermediate activation kinetics (i.e. chloride release) of the cytotoxic KP1019/NKP1339 complexes are apparently in the optimal range for observing *in vitro* activity.

5.8 Bibliography

[1] a) P. J. Dyson, G. Sava, *Dalton Trans.*, **2006**, 1929 - 1933; b) P. J. Dyson, *Chimia*, **2007**, *61,* 698 - 703; c) C. Scolaro, A. Bergamo, L. Brescacin, R. Delfino, M. Cocchietto, G. Laurenczy, T. J. Geldbach, G. Sava, P. J. Dyson, *J. Med. Chem.*, **2005**, *48*, 4161 - 4171; d) A. Bergamo, A. Masi, P. J. Dyson, G. Sava, *Int. J. Oncol.*, **2008**, *33*, 1281 - 1289; e) W. H. Ang, A. Casini, G. Sava, P. J. Dyson, *J. Organomet. Chem.*, **2011**, *696,* 989 - 998; f) C. M. Clavel, E. Paunescu, P. Nowak-Sliwinska, A. W. Griffioen, R. Scopelliti, P. J. Dyson, *J. Med. Chem.*, **2015**, *58*, 3356 - 3365; g) M. V. Babak, S. M. Meier, K. V. M. Huber, J. Reynisson, A. A. Legin, M. A. Jakupec, A. Roller, A. Stukalov, M. Gridling, K. L. Bennett, J. Colinge, W. Berger, P. J. Dyson, G. Superti-Furga, B. K. Keppler, C. G. Hartinger, *Chem. Sci.*, **2015**, *6*, 2449 - 2456.

[2] a) A. García-Fernández, J. Díez, Á. Manteca, J. Sánchez, R. García-Navas, B. G. Sierra, F. Mollinedo, M. Pilar Gamasa, E. Lastra, *Dalton Trans.*, **2010**, *39*, 10186 - 10196; b) E. Menéndez-Pedregal, J. Díez, Á. Manteca, J. Sánchez, A. C. Bento, R. García-Navas, F. Mollinedo, M. Pilar Gamasa, E. Lastra, *Dalton Trans.*, **2013**, *42,* 13955 - 13967; c) S. Seršen, J. Kljun, K. Kryeziu, R. Panchuk, B. Alte, W. Körner, P. Heffeter, W. Berger, I. Turel, *J. Med. Chem.*, **2015**, *58*, 3984 - 3996; d) B. Serli, E. Zangrando, T. Gianferrara, C. Scolaro, P. J. Dyson, A. Bergamo, E. Alessio, *Eur. J. Inorg. Chem.*, **2005**, 3423 - 3434; e) D. N. Akbayeva, L. Gonsalvi, W. Oberhauser, M. Peruzzini, F. Vizza, P. Brueggeller, A. Romerosa, G. Sava, A. Bergamo, *Chem. Commun.*, **2003**, 264 - 265; f) S. Grguric-Sipka, C. R. Kowol, S.-M. Valiahdi, R. Eichinger, M. A. Jakupec, A. Roller, S. Shova, V. B. Arion, B. K. Keppler, *Eur. J. Inorg. Chem.*, **2007**, 2870 - 2878.

[3] a) A. Romerosa, T. Campos-Malpartida, C. Lidrissi, M. Saoud, M. Serrano-Ruiz, M. Peruzzini, J. A. Garrido-Cárdenas, F. García-Maroto, *Inorg. Chem.*, **2006**, *45*, 1289 - 1298; b) A. Romerosa, M. Saoud, T. Campos-Malpartida, C. Lidrissi, M. Serrano-Ruiz, M. Peruzzini, J. A. Garrido, F. García-Maroto, *Eur. J. Inorg. Chem.*, **2007**, 2803 - 2812; c) A. García-Fernández, J. Díez, Á. Manteca, J. Sánchez, M. Pilar Gamasa, E. Lastra, *Polyhedron*, **2008**, *27*, 1214 - 1228.

[4] A. Wołoszyn, C. Pettinari, R. Pettinari, G. V Badillo Patzmay, A. Kwiecień, G. Lupidi, M. Nabissi, G. Santoni¸ P. Smoleński, *Dalton Trans.*, **2011**, *46*, 10073 - 10081.

[5] a) E. Alessio, G. Mestroni, A. Bergamo, G. Sava, *Curr. Topics Med. Chem.*, **2004**, *4*, 1525 - 1535; b) T. Gianferrara, I. Bratsos, E. Alessio, *Dalton Trans.*, **2009**, 7588 - 7598; c) I. Bratsos, T. Gianferrara, E. Alessio, C. G. Hartinger, M. A. Jakupec, B. K. Keppler, *Bioinorganic Medicinal Chemistry* (Ed. E. Alessio), Wiley-VCH, Weinheim, Germany, **2011**, 151 - 174; d) A. Bergamo, C. Gaiddon, J. H. M. Schellens, J. H. Beijnen, G. Sava, *J. Inorg. Biochem.*, **2012**, *106*, 90 - 99.

[6] C. Mari, V. Pierroz, S. Ferrari, G. Gasser, *Chem. Sci.*, **2015**, *6*, 2660 - 2686.

[7] C. M. Duff, G. A. Heath, *J. Chem. Soc. Dalton Trans.*, **1991**, 2401 - 2411.

[8] E. Alessio, *Chem. Rev.*, **2004**, *104*, 4203 - 4242.

[9] E. Alessio, G. Balducci, M. Calligaris, G. Costa, W. M. Attia, G. Mestroni, *Inorg. Chem.*, **1991**, *48*, 609 - 618.

[10] E. Alessio, G. Balducci, A. Lutman, G. Mestroni, M. Calligaris, W. M. Attia, *Inorg. Chim. Acta*, **1993**, *203*, 205 - 217.

[11] a) R. Elizabeth, J. Lippard, S. J. Lippard, *Chem. Rev.,* **1999**, *99,* 2467 - 2498; b) E. Gallori, C. Vettori, E. Alessio, F. G. Vilchez, R. Vilaplana, P. Orioli, A. Casini, L. Messori, *Arch. Biochem. Biophys.*, **2000**, *376*, 156 - 162; c) D. Musumeci, L. Rozza, A. Merlino, L. Paduano, T. Marzo, L. Massai, L. Messori, D. Montesarchio, *Dalton. Trans.*, **2015**, *44,* 13914 - 13925.

[12] T. Marzo, G. Bartoli, C. Gabbiani, G. Pescitelli, M. Severi, S. Pillozzi, E. Michelucci, B. Fiorini, A. Arcangeli, A. G. Quiroga and L. Messori, *Biometals*, **2016**, *29*, 535 - 542.

[13] T. Marzo, S. Pillozzi, O. Hrabina, J. Kasparkova, V. Brabec, A. Arcangeli, G. Bartoli, M. Severi, A. Lunghi, F. Totti, C. Gabbiani, A. G. Quiroga, L. Messori, *Dalton Trans.*, **2015**, *44*, 14896 - 14905.

[14] A. Levina, A. Mitra P. A. Lay, *Metallomics*, **2009**, *1*, 458 - 470.

[15] J. B. Aitken, S. Antony, C. M. Weekley, B. Lai, L. Spiccia, H. H. Harris, *Metallomics*, **2012**, *4*, 1051 - 1056.

CHAPTER 6

This Chapter was published in: F. Battistin, G. Balducci, N. Demitri, E. Iengo, B. Milani, E. Alessio, *Dalton Trans.*, **2015**, 44, 15671 - 15682.

Ru(II) complexes with cppH

6.1 State of the art

As already described in the Introduction, a metal conjugate is a complex molecule in which an organometallic or coordination compound is attached through a linker to an organic macromolecule usually with a high molecular weight. The linker is a molecule that connects the metal compound to the organic macromolecule; in particular, the linker is often a bifunctional chelating agent, that is a molecule with two functional groups – which typically point in opposite directions – that binds both the organic molecule through an organic bond and coordinates the metal fragment, often through a chelating mojety.

A typical example of linker is 4′-methyl-2,2′-bipyridine-4-carboxylic acid (bpyAc, Scheme 6.1), a bidentate diimine that allows for the formation of a covalent bond through the carboxylic group in position 4′, i.e. in the opposite direction compared to the metal chelation.

Most examples of bpyAc involve the attachment of redox and/or luminescent metal fragments (e.g. polypyridyl Ru(II) complexes[1]) to the macromolecular component (e.g. polymers and peptides,[2] PNA sequences,[3] porphyrins,[4,5] biotin pendants[6]).

Even if bpyAc was extensively used as linker, its synthesis is tedious and long. In short, bpyAc is made from direct oxidation of 4,4'-dimethyl-2,2'-bipyridine with SeO_2 followed by treatment of the crude with Ag_2O, that further oxidizes the intermediates with aldehyde groups (Scheme 6.1); finally bpyAc is separated from

the product mixture by Soxhlet extraction. The overall process requires several days.[7]

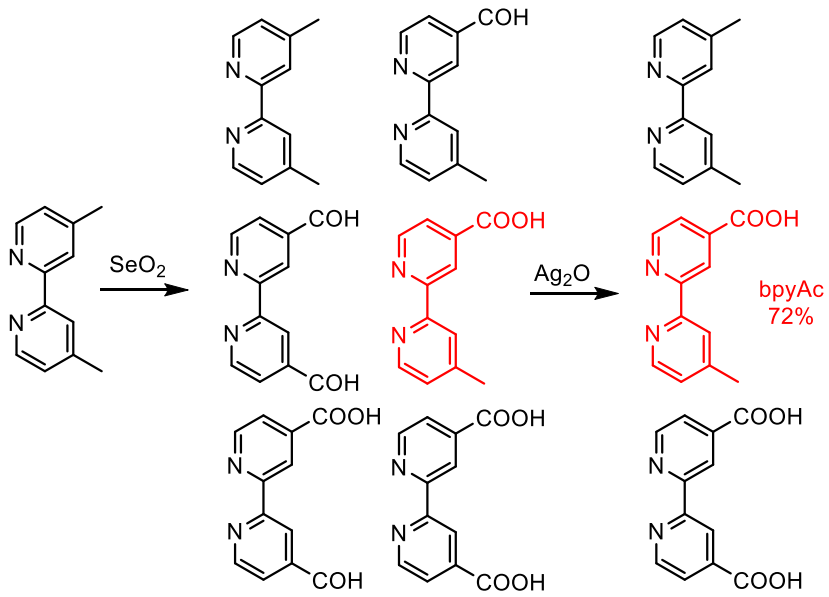

Scheme 6.1. Synthesis of bpyAc, in red.

With the aim of bypassing the difficulties that affect the preparation and purification of bpyAc, in 2009 Spiccia and coworkers introduced an alternative asymmetric diimine ligand bearing a single carboxylate functionality, 2-(2′-pyridyl)pyrimidine-4-carboxylic acid (cppH, Scheme 6.2).[8] The synthesis of cppH is a three steps reaction (Scheme 6.2): in the first step 2-cianopyridine reacts with ammonia to form the intermediate 2-picolinimidamide hydrochloride , that is reacted with acetaldehyde dimethylacetal to give 4-methyl-2-(2′-pyridyl)pyrimidine (mpp). The final product (actually isolated as cppH·HNO_3) is obtained by the oxidation of the methyl to carboxylic group with concentrated nitric acid. This preparation is much faster than that of bpyAc.[8] Moreover, cppH is soluble in a wider range of solvents compared to bpyAc.

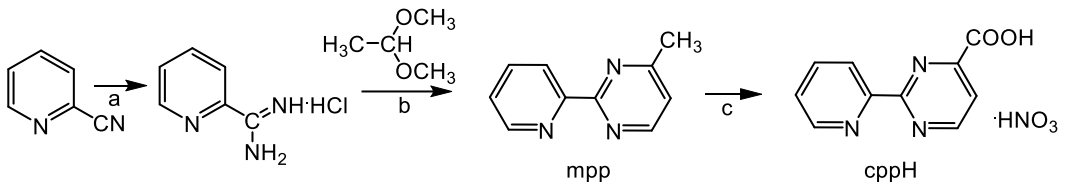

Scheme 6.2. Synthesis of 2-(2′-pyridyl)pyrimidine-4-carboxylic acid (cppH): a) NaOMe, NH_4Cl, MeOH b) NaOEt, reflux c) HNO_3 conc./HCl (1:1 v/v), reflux.

The cppH linker has been used in the preparation of electrochemiluminescent Ru(II)-bioconjugates with PNA and peptides for biosensing and biomedical applications.[9,10] In addition, the coordinatively saturated and substitutionally inert Ru(II) complex $[Ru(dppz)_2(cppH)](PF_6)_2$ (dppz = dipyrido[3,2-a:2′,3′-c]phenazine) was found to be remarkably cytotoxic against different cancer cell lines inducing mitochondria-mediated apoptosis.[10,11] Interestingly, the carboxylic function of cppH was exploited for controlling the cytotoxicity of the complex through a light-triggered mechanism ("photocaging"):[12] conjugation to an appropriate photo-labile protecting group (PLGP) through an esteric bond made the complex inactive. The cytotoxic action was restored in living cells upon light illumination (λ = 350 nm) that photo-cleaved the protecting moiety (Scheme 6.3).

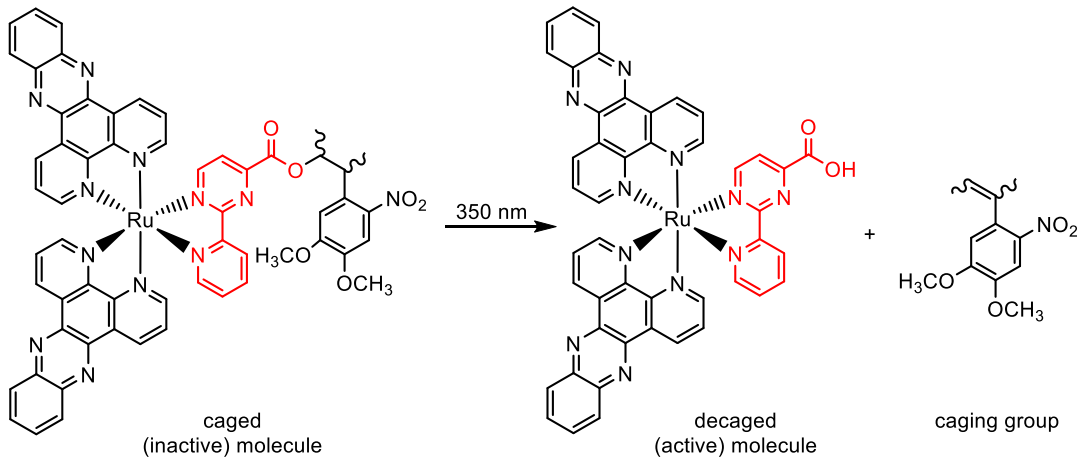

Scheme 6.3. Chemical structure of the photolabile protected (left) and active Ru(II) complex with cppH. The caging group is released upon irradiation at 350 nm.[12]

However, unlike bpyAc, cppH can originate linkage isomers. In fact, its pyrimidine ring can bind to the metal ion either through the nitrogen atom *ortho* (N^o) or *para* (N^p) to the carboxylic group linked to C4. Most of the cppH-Ru(II) conjugates reported so far were prepared following a synthetic route that led selectively to the $\boldsymbol{N^p}$ coordination mode.[8-12] Nevertheless, an example of the $\boldsymbol{N^o}$ coordination mode of cppH on a Ru(II) fragment had been described in the first report on this linker,[8] and the group were I did my Thesis recently demonstrated that the two linkage isomers [Ru([9]aneS$_3$)(cppH-κN^p)(PTA)](Cl)$_2$ and [Ru([9]aneS$_3$)(cppH-κN^o)(PTA)](Cl)$_2$ (**50**$\boldsymbol{N^p}$ and **50**$\boldsymbol{N^o}$, respectively) are formed in comparable amounts when the Ru(II) precursor *fac*-Ru([9]aneS$_3$)Cl$_2$(PTA) ([9]aneS$_3$ = 1,4,7-trithiacyclononane) is treated with cppH in refluxing water (Scheme 6.4).[13] For this reason cppH was defined an "irresolute linker". The two isomers were fully characterized individually, both in the solid state and in solution.

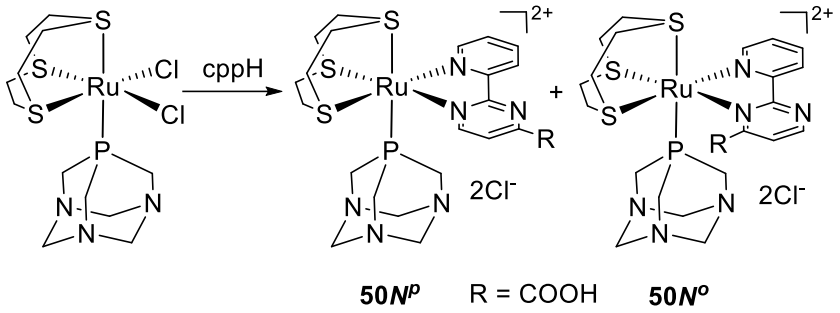

50$\boldsymbol{N^p}$ **50**$\boldsymbol{N^o}$

Scheme 6.4. The formation of the two linkage isomers **50**$\boldsymbol{N^p}$ and **50**$\boldsymbol{N^o}$.

6.2 Aim of the Chapter

Since from the relatively few examples of Ru(II)-cppH complexes reported so far it was unclear if this linker has any preference for one of the two possible coordination modes, we decided to extend our investigation to other Ru(II) precursors and, above all, to establish a spectroscopic fingerprint that might allow us to distinguish the coordination mode of cppH also in the absence of an X-ray structural characterization**.**

In this Chapter we investigated the reactivity of three Ru(II) precursors – *cis*-$RuCl_2(dmso)_4$ (**8**), *trans*-$RuCl_2(dmso\text{-}S)_4$ (**9**) (see Chapter 1), and *trans*,*cis*,*cis*-$RuCl_2(CO)_2(dmso\text{-}O)_2$ (**29**) (see Chapter 2) (Figure 6.1) – towards cppH or, when appropriate, its parent compound and (presumed) model 4-methyl-2-(2′-pyridyl)pyrimidine (mpp) (Figure 6.1) in which a methyl group replaces the carboxylic group on the pyrimidine ring.

The binding mode of cppH and mpp – either through N^o or N^p – was unambiguously established through the $\{^1H,^{15}N\}$- HMBC NMR spectra at natural abundance of ^{15}N isotope (see below).

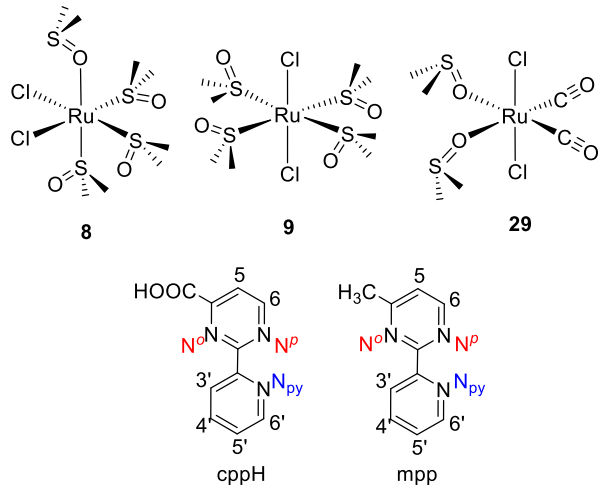

Figure 6.1. The Ru(II) precursors *cis*-$RuCl_2(dmso\text{-}S)_4$ (**8**), *trans*-$RuCl_2(dmso\text{-}S)_4$ (**9**), *trans*,*cis*,*cis*-$RuCl_2(CO)_2(dmso\text{-}O)_2$ (**29**), (top) and diimmine linkers with numbering schemes and labels (bottom) used in this work.

6.3 Reactions with cppH

Compound *trans*,*cis*,*cis*-$RuCl_2(CO)_2$(dmso-O)$_2$ (**29**) reacts with the model diimine bpy, under different reaction conditions, replacing the two dmso-O ligands and affording with high selectivity *trans*,*cis*-$RuCl_2$(bpy)$(CO)_2$.[14] We found that cppH behaves similarly to bpy. Treatment of **29** with cppH in water at room temperature affords a small amount of a crystalline colorless product identified from mass and NMR spectroscopy as *trans*,*cis*-$RuCl_2(CO)_2$(cppH) (**51**) (Scheme 6.5). The single crystal X-ray analysis (Figure 6.2) established that cppH is bound via ***N*^{p}**, i.e. **51** is *trans*,*cis*-$RuCl_2(CO)_2$(cppH-κ*N*^{p}). Similar results were obtained performing the reaction in refluxing water or chloroform (see below). Compound **51** had been previously prepared by Spiccia and coworkers upon treatment of the oligomeric Ru(II)-carbonyl precursor $[Ru(CO)_2(Cl)_2]_n$ with cppH in refluxing methanol.[8] Our X-ray results for compound **51** (space group, unit cell dimensions and atomic coordinates) closely agree with those already published,[8] including the H-bonding scheme of the crystallization water molecule, which is found to interact with the carboxylic hydrogen, the carboxylate oxygen and one chlorido ligand belonging to three distinct neighboring complex moieties. To be noted that, as in the other structurally characterized Ru-(cppH-κ*N*^{p}) complexes,[8,13] the carboxylate group is basically coplanar with the pyrimidine ring.

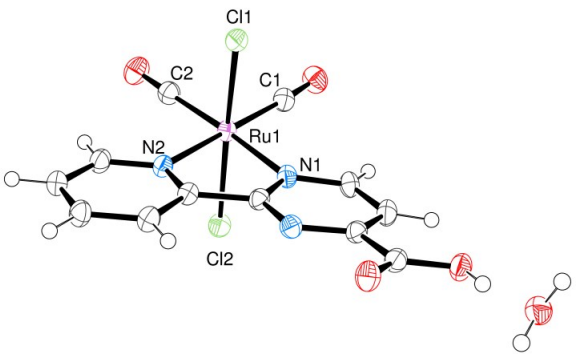

Figure 6.2. X-ray molecular structure (50% probability ellipsoids) of *trans*,*cis*-$RuCl_2(CO)_2$(cppH-κ*N*^{p})·H_2O (**51**). Coordination distances (Å): Ru1–N1 = 2.112(2), Ru1–N2 = 2.103(1), Ru1–Cl1 = 2.3819(7), Ru1–Cl2 = 2.4010(7), Ru1–C1 = 1.891(3), Ru1–C2 = 1.900(3).

Interestingly, when the reaction was performed in methanol (either at room temperature or in refluxing conditions) we found that partial esterification of the carboxylic group occurs and compound **51** co-crystallizes with its methyl ester *trans*,*cis*-$RuCl_2(CO)_2(cppCH_3\text{-}\kappa N^p)$ (**51Me**).[15]

In the X-ray structure (Appendix, A6.21) the asymmetric unit gives an averaged composition of the whole crystal, and it shows the presence of both a methanol molecule (linked through hydrogen bonds to neighboring complexes) and a methyl moiety with reasonable bond lengths. The fraction of complexes with esterified cppH was estimated at 55%, refining the occupancy of the associated methoxy carbon atom (O_{COO}–C_{methyl} bond length 1.460(5) Å) and of the methanol molecule that occupies the same site (O_{COOH}–$O_{methanol}$ bond length 2.44(1) Å). In the ^{1}H NMR spectrum a new set of six aromatic signals, each one falling very close to – when not altogether overlapped with – those of **51**, was observed (ESI). A singlet at δ = 4.02, that integrates for three protons with respect to the aromatic resonances of **51Me**, was attributed to the methoxy group.

In the original preparation by Spiccia and coworkers – performed in methanol – the formation of **51Me** was not observed.[8]

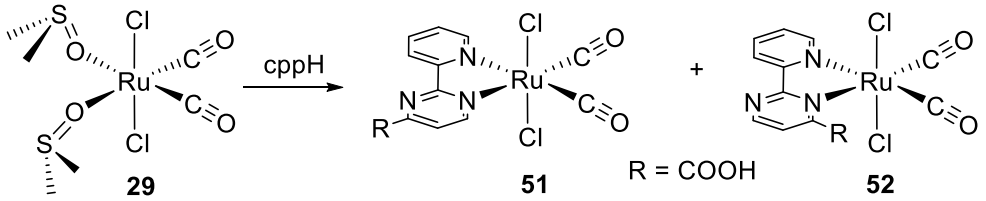

Scheme 6.5. The reaction between **29** and cppH, yielding the two linkage isomers *trans*,*cis*-$RuCl_2(CO)_2(cppH\text{-}\kappa N^p)$ (**51**) and *trans*,*cis*-$RuCl_2(CO)_2(cppH\text{-}\kappa N^o)$ (**52**). The nature of compound **52** was established on the basis of the ^{15}N NMR spectra.

We also found that, regardless of the reaction conditions, a second product (**52**) is always recovered from the mother liquor upon concentration (Scheme 6.5). According to elemental analysis, NMR, IR and mass spectroscopy evidence, this product is an isomer of **51**. The fact that in the ^{1}H NMR spectrum (Figure 6.3) the resonances of the pyridyl protons of **52** are basically coincident with those of **51**,

whereas the two doublets of the pyrimidine protons are shifted upfield ($\Delta\delta$ = –0.36 ppm for H6 and –0.11 ppm for H5) suggested that **52** is the linkage isomer of **51** in which cppH is bound via ***N^o^***, i.e. it is *trans*,*cis*-$RuCl_2(CO)_2$(cppH-κN^o). To be noted that in each compound the ^{1}H NMR assignments of H5 and H6 were fully confirmed by the ^{1}H-^{13}C HSQC spectra, in which H5 and H6 are coupled to carbon resonances that fall at ca. 120 and ca. 160 ppm, respectively (Appendix, A6.5 for **51** and A6.7 for **52**).

Compound **52**, that had not been previously detected, was best obtained in pure form when the reaction was performed in water at room temperature. Under these conditions, the reaction is basically quantitative and the ratio between **51** and **52** is ca. 1:9. A larger amount of **51** was obtained as first precipitate when the reaction was performed at higher temperature, however the second fraction was a mixture of **51** and **52** (refluxing methanol or chloroform), with additional unidentified minor species in the case of refluxing water.

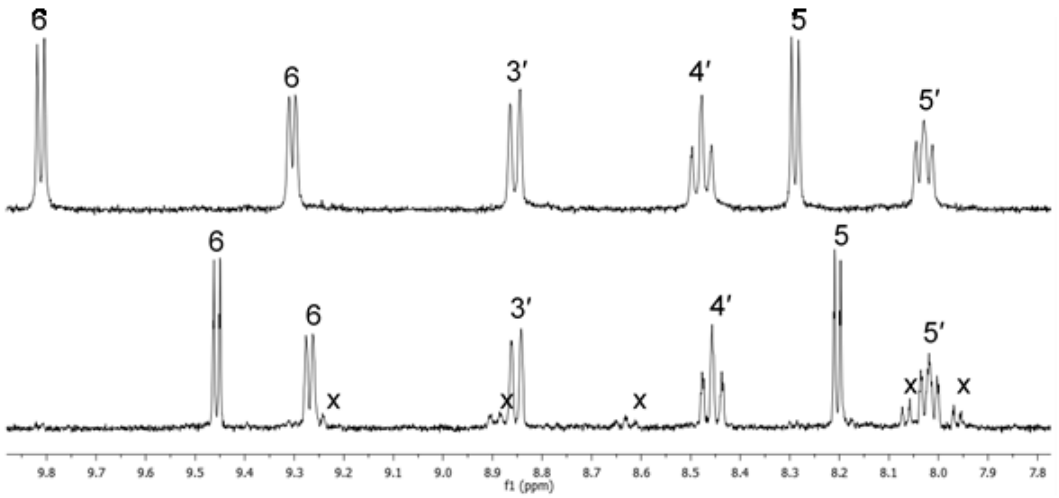

Figure 6.3. The ^{1}H NMR spectra (DMSO-d_6) of *trans*,*cis*-$RuCl_2(CO)_2$(cppH-κN^p) (**51**, top) and *trans*,*cis*-$RuCl_2(CO)_2$(cppH-κN^o) (**52**, bottom), obtained as first and second fraction, respectively, by treatment of **29** with cppH in water at room temperature (details in experimental section). See Figure 6.1 for the labeling scheme of cppH. Some minor unidentified peaks in the spectrum of **52** are labeled with x. To be noted that **52** was recovered from the mother liquor upon complete removal of the aqueous solvent.

Nevertheless, even though quite unlikely according to the known reactivity between **29** and bpy,[14] the spectroscopic data might also be consistent with the hypothesis that **52** is the stereoisomer of **51**, *cis*,*cis*-$RuCl_2(CO)_2$(cppH-κN^p): in fact, in both hypotheses two carbonyl resonances in the ^{13}C NMR spectrum and two CO stretching bands in the IR spectrum would be expected. In the absence of crystals suitable for X-ray investigation, the nature of **52** was eventually determined through ^{15}N NMR spectroscopy (see below).

Our investigation was then extended to the two isomeric Ru(II)-dmso precursors *cis*-$RuCl_2$(dmso-S)$_4$ (**8**) and *trans*-$RuCl_2$(dmso-S)$_4$ (**9**). In recent years, the reactivity of **8** and **9** towards the model diimine bpy was thoroughly investigated by Toyama and coworkers.[16] They found that bpy selectively replaces two dmso ligands and – by a careful choice of the reaction conditions – all the three possible stereoisomeric products, namely *trans,cis*-Ru(bpy)Cl_2(dmso-S)$_2$, *cis,cis*-Ru(bpy)Cl_2(dmso-S)$_2$, and *cis,trans*-Ru(bpy)Cl_2(dmso-S)$_2$ (Figure 6.4), were individually isolated and fully characterized. The all-*cis* complex was found to be the thermodynamically most stable isomer.[17]

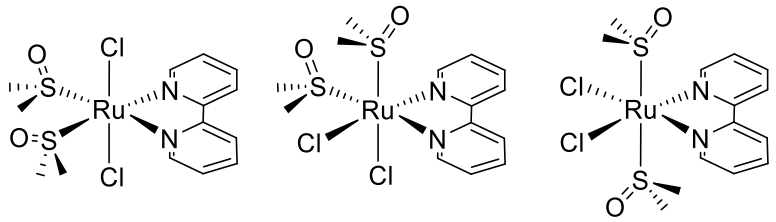

Figure 6.4. The three stereoisomers of Ru(bpy)Cl_2(dmso-S)$_2$.

We found that treatment of both **8** and **9** with cppH under different reaction conditions afforded only small amounts of products, whose NMR spectra had exclusively very broad – almost undetectable – signals. These unexpected findings suggested that cppH reacts with **8** and **9** as a bridging ligand, both through the diimine unit and the carboxylic group, replacing more than two ligands in the precursors and thus leading to oligomeric species (that typically give broad NMR resonances). For this reason, we decided to investigate 4-methyl-2-(2′-

pyridyl)pyrimidine ligand (mpp) instead of cppH. The presence of a methyl in position 4 instead of the –COOH group was anticipated to eliminate the undesired reactivity and – given the similarity between the two diimines – mpp might be considered as a good model for cppH.

6.4 Reactions with mpp

In principle, assuming that mpp reacts with **8** and **9** similarly to bpy,[16] four stereoisomeric products can be expected (being mpp unsymmetrical, two all-*cis* isomers are possible), each of them potentially as a pair of linkage isomers depending on the binding preference of the pyrimidine ring. The dmso resonances in the ^{1}H NMR spectra are anticipated to be essential for determining the geometry of the products.[18,19]

Treatment of *cis*-$RuCl_2$(dmso-S)$_4$ (**8**) with mpp in refluxing ethanol afforded a deep-red solution, from which two types of crystals of the same color, in comparable amounts, were obtained. They were manually separated under the microscope and characterized individually by NMR spectroscopy as the two isomers *cis,trans*-$RuCl_2$(dmso-S)$_2$(mpp) (**53**, Figure 6.5) and *cis,cis*-$RuCl_2$(dmso-S)$_2$(mpp) (**54**, Figure 6.5). Some crystals suitable for X-ray analysis turned out to be of compound **54**. The X-ray analysis established that in both cases (X-ray quality crystals of **53** were obtained by a different route, see below) mpp is bound via N^p, and that in compound **54** the pyridyl ring of mpp is bound trans to dmso-S.

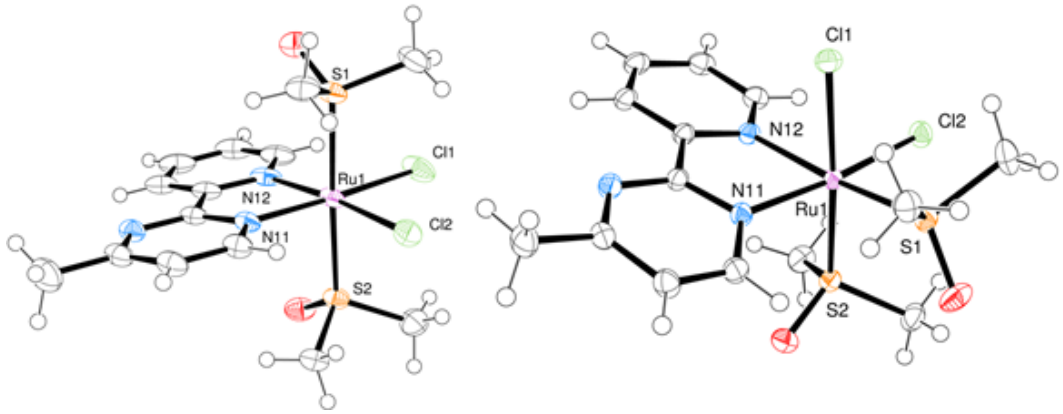

Figure 6.5. The X-ray molecular structures (50% probability ellipsoids) of *cis,trans*-$RuCl_2$(dmso-S)$_2$(mpp-κ*N*^{p}) (**53**, left) and *cis,cis*-$RuCl_2$(dmso-S)$_2$(mpp-κ*N*^{p}) (**54**, right). Coordination distances (Å): **53**: Ru1–N11 = 2.057(2), Ru1–N12 = 2.056(3), Ru1–Cl1 = 2.426(1), Ru1–Cl2 = 2.427(1), Ru1–S1 = 2.1981(9), Ru1–S2 = 2.2977(9). **54**: Ru1–N11 = 2.0525(12), Ru1–N12 = 2.1025(12), Ru1–Cl1 = 2.4396(4), Ru1–Cl2 = 2.4193(4), Ru1–S1 = 2.2742(4), Ru1–S2 = 2.2441(4).

The structure of **53** can be compared with that of the equivalent complex *cis,trans*-$RuCl_2$(dmso-S)$_2$(bpy) (determined at 298K).[16] Replacement of the pyridyl ring of bpy with the 4-methyl-pirimidine ring of mpp leads to no significant difference in the corresponding Ru–N bond length (an overall bond contraction, from 2.083(5) to 2.056(3) Å in **53**, can be fully ascribed to the lower temperature used for data collection in this work). The same is valid for the Ru–S bond lengths. It is worth mentioning that the dmso-S ligands (observed along the S–Ru–S direction) are eclipsed in **53**, whereas they are staggered in the bpy complex, most likely due to a packing effect. Also the single-crystal X-ray structure of **54** is tightly correlated to that of the equivalent bpy complex *cis,cis*-$RuCl_2$(dmso-S)$_2$(bpy) (determined at 296K).[16] Both molecules are chiral and both crystallize as racemic mixtures in centrosymmetric space groups. No significant difference in the coordination sphere was found between the two compounds.

The ^{1}H NMR spectra of both products contain a single set of mpp resonances (Table 6.1). Consistent with the geometries found in the solid state, the spectrum of **53** has two singlets (6H each) in the dmso-S region (the two equivalent dmso ligands have diastereotopic methyls) at δ = 3.18 and 2.98, whereas the spectrum of **54**

has four singlets (3H each) in the same region at δ = 3.53, 3.51, 3.30, and 2.59 (Figure 6.6). The very upfield shifted resonance at δ = 2.59 ppm (correlated in the ^{1}H-^{1}H COSY spectrum to that at 3.30 ppm, Appendix A6.12) is attributed to the methyl group of the dmso-S *trans* to Cl, that sits on top of mpp and feels its shielding cone. A similar effect had been found in the spectrum of the corresponding bpy complex.[16] The singlet of the methyl group of mpp (δ = 2.71) was unambiguously attributed through the ^{1}H-^{13}C HSQC spectrum (Appendix, A6.13), as it correlates with a carbon resonance at ca. 25 ppm, whereas the dmso carbon resonances fall at ca. 45 ppm. The proton NMR spectrum of **54** contained also a minor set, with the same number of resonances, attributable to another isomer with all-*cis* geometry, *cis,cis*-$RuCl_2$(dmso-S)$_2$(mpp) (**55**). This species – that was more abundant in the second batch of precipitate obtained from the concentrated mother liquor of the reaction – might be either the stereoisomer of **54**, in which the pyridyl ring of mpp is bound trans to Cl, or one of the two possible all-*cis* linkage isomers in which mpp is bound via ***N^{o}***. The nature of **55** was established by ^{15}N NMR spectroscopy (see below).

We found that when the reaction between **8** and mpp was repeated under milder conditions (e.g. shorter reaction time and/or lower temperature), the amount of compound **54** in the isolated mixture decreased. For example, operating in refluxing methanol or chloroform, the product is a ca. 4:1 mixture of **54** and **55**, thus allowing us to assign the NMR resonances of **55**. Viceversa, when the reaction was performed for longer reaction times and/or at higher temperature (e.g. refluxing toluene) compound **53** was the prevailing product, suggesting that it is the thermodynamic most stable isomer. This issue, however, was not investigated in detail since it was not the main scope of our work.

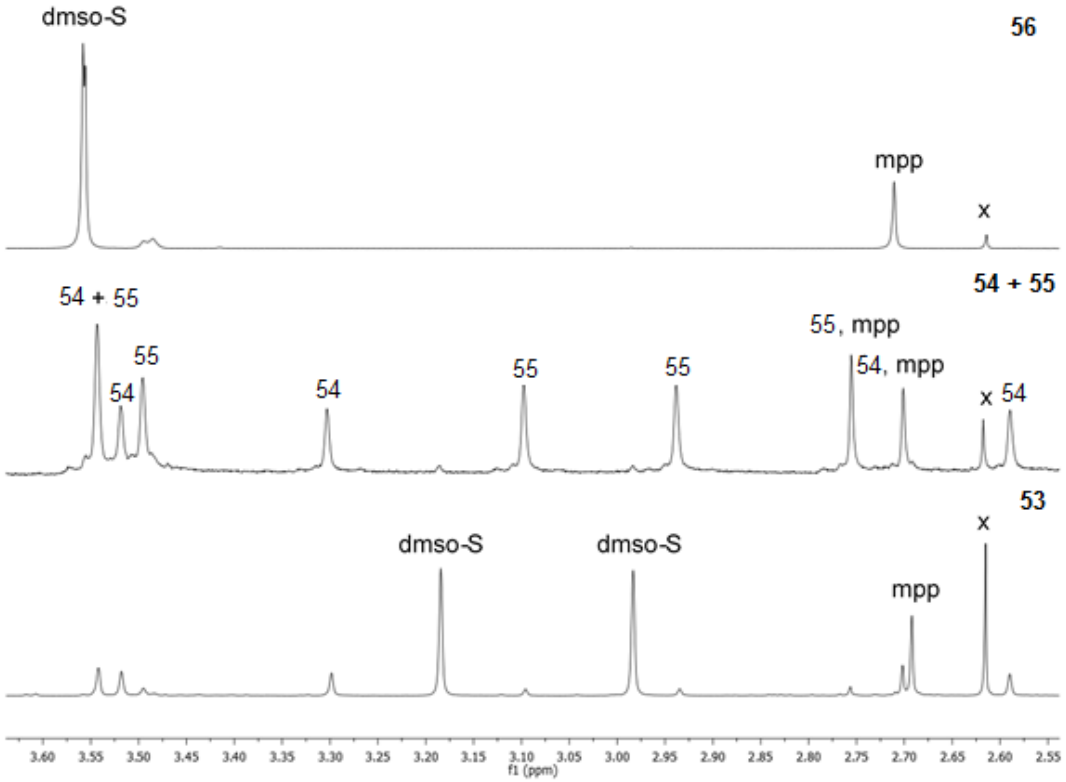

Figure 6.6. The region of the methyl resonances in the ^{1}H NMR spectra ($CDCl_3$) of *cis,trans*-$RuCl_2$(dmso-S)$_2$(mpp-κ*N*^{p}) (**53**, bottom, with minor amounts of **54** and **55**), a mixture of the two *cis,cis*-$RuCl_2$(dmso-S)$_2$(mpp-κ*N*^{p}) isomers (**54** + **55**, middle), and *trans,cis*-$RuCl_2$(dmso-S)$_2$(mpp-κ*N*^{p}) (**56**, top). In the central spectrum, the eight dmso-S resonances are labeled with the number of the corresponding complex. The peak of residual free DMSO is labeled with x.

Consistent with the known reactivity of **9**,[16,19] treatment of this precursor with mpp at room temperature (90 min) afforded, upon concentration, crystals of *trans,cis*-$RuCl_2$(dmso-S)$_2$(mpp) (**56**). The X-ray structure established the geometry of the complex and that, also in this case, mpp is bound via ***N*^{p}** (Figure 6.7). Comparison with the X-ray structure of the analogous bpy derivative *trans,cis*-Ru(bpy)Cl_2(dmso-S)$_2$ shows that the orientation of the two dmso-S ligands is the same in both compounds:[16] one dmso points its O atom towards the *N–N* ligand, whereas the other is oriented such that the ring plane of the diimine bisects its S–CH_3 bonds. As already noted for the bpy derivative, we also find a considerable distortion of the N–N–S–S equatorial plane. These observations add support to the hypothesis, put forward by

Toyama and coworkers,[16] of a high level of steric hindrance on the equatorial plane, with the observed conformation of the dmso ligands being the only one energetically allowed in the solid state. Additional evidence comes from the comparison of the coordination distances. Even though the diffraction measurements were done at 296K for the bpy complex and at 100K in our case, only the Ru–Cl bond distances show a significant contraction (2.416(1), 2.400(1)[16] *vs*. 2.3825(6), 2.3927(6)), whereas the bond distances in the equatorial plane are almost unchanged (Ru–S: 2.273(1), 2.309(1)[16] *vs* 2.2647(6), 2.3002(5); Ru–N: 2.124(3), 2.127(3)[16] *vs*. 2.1258(17),2.1343(17)). The steric encumbrance in the equatorial plane might explain the instability of this species towards isomerization (see below).

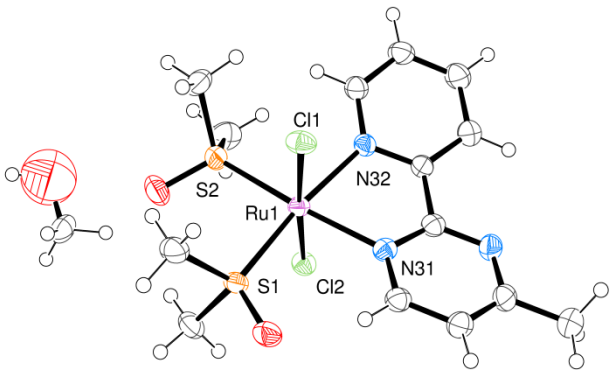

Figure 6.7. The X-ray molecular structure (50% probability ellipsoids) of *trans,cis*-$RuCl_2$(dmso-S)$_2$(mpp-κN^p) (**56**). A disordered CH_3OH crystallization molecule is also shown. Coordination distances (Å): Ru1–N31 = 2.1343(17), Ru1–N32 = 2.1258(17), Ru1–Cl1 = 2.3825(6), Ru1–Cl2 = 2.3927(6), Ru1–S1 = 2.3002(5), Ru1–S2 = 2.2647(6).

In accord with this geometry (the two dmso-S ligands are inequivalent but have equivalent methyls), two partially overlapped and equally intense singlets are found in the dmso-S region of the ^{1}H NMR spectrum (δ = 3.56, Figure 6.6). Compound **56** turned out to be an intermediate in the formation of the three isomers **53**-**55**. In fact, if the rapid precipitation of **56** was not induced and the mother liquor was slowly saturated with diethyl ether over a period of hours, a mixture of **54** (crystals suitable for X-ray analysis) and **55**, with **55** prevailing (ca. 2:3) was obtained. A mixture of **53**-**55** remained in the mother liquor.

Similarly, if the crystals of **56** were not removed from the mother liquor they slowly redissolved (days), eventually affording a mixture of **53**-**55** upon addition of diethyl ether. The NMR spectra of mixtures of **53**-**55** in $CDCl_3$ did not change with time, indicating that these three isomers are not in equilibrium at room temperature. Attempts to obtain crystals of **55** suitable for X-ray analysis were unsuccessful.

The reactivity of the Ru(II)-dmso precursors **8** and **9** towards mpp is summarized in Scheme 6.6, and basically is consistent with the findings by Toyama and coworkers on the corresponding bpy complexes.[16]

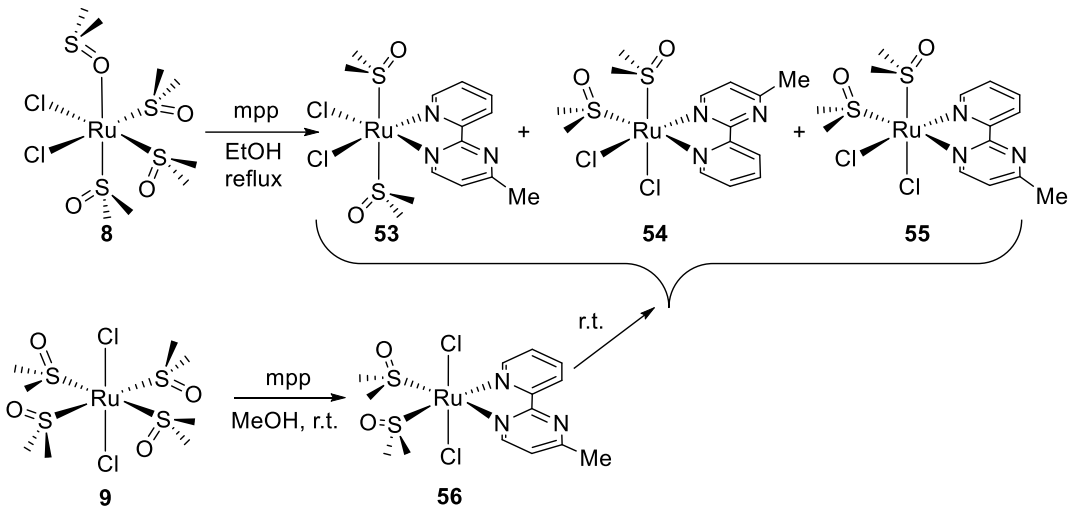

Scheme 6.6. The reactivity of precursors **8** and **9** towards mpp. The nature of compound **55** was established on the basis of the ^{15}N NMR spectra.

Table 6.1 summarizes the ^{1}H NMR resonances of mpp in the four isolated products. It is quite obvious that some resonances (in particular those of H6 and H6') are remarkably affected by the geometry of the complex. Nevertheless, even though the X-ray structures establish that in **53**, **54** and **56** mpp binds to ruthenium via ***N***^{p}, we were unable to find a clear-cut trend in the proton resonances that might be used to determine unambiguously (in the absence of a crystal structure) the nature of compound **55** (in particular with regard to the binding mode of mpp).

Table 6.1. ^{1}H NMR chemical shifts (δ, ppm) of the mpp ligand in compounds **53** – **56**.[a]

	53	**54**	**55**	**56**
H6'	9.58	9.79	9.51	8.96
H6	9.58	9.62	9.79	10.30
H3'	8.54	8.69	8.69	8.78
H4'	7.97	8.08	7.97	8.02
H5'	7.60	7.70	7.54	7.57
H5	7.29	7.32	7.42	7.33
Me	2.69	2.71	2.76	2.71

[a] See Figure 6.1 for labeling scheme.

6.5 {^{1}H,^{15}N}- HMBC NMR experiments

Given the above mentioned limits of ^{1}H NMR spectroscopy, we decided to investigate if the ^{15}N NMR resonances can provide a spectroscopic fingerprint for determining the binding mode of cppH and mpp unambiguously. For this purpose we performed {^{1}H,^{15}N}- HMBC NMR experiments at natural abundance of the ^{15}N isotope to measure the ^{15}N chemical shifts, both in the free ligands and in the complexes. In these experiments, the careful choice of the coupling constants $^{n}J(^{15}N, ^{1}H)$ (n = 2, 3) is of paramount importance. Each ^{15}N resonance was assigned on the basis of the cross peak(s) with the proton(s) closest to the N atom in the molecule, namely H6 for N^{p}, H5 (and $-CH_3$ in mpp) for N^{o} and H6' for N_{py}. A first series of experiments was performed on cppH·HNO_3 and mpp, testing several values of the scalar coupling constants in the range from 1.2 to 12 Hz (with increments ranging from 0.1 to 2 Hz). The value of 11 Hz was established as the most suitable for $^{2}J(^{15}N, ^{1}H)$, i.e. for observing the coupling between H6 and N^{p}, as well as between H6' and the pyridyl N atom N_{py}. A value of 1.8 Hz was instead found to be optimal for

$^3J(^{15}N, ^1H)$, i.e. for observing the coupling between H5 and both N^p and N^o (Appendix, A6.2). Both coupling constants were subsequently used for the experiments on each complex (a value of 1.7 Hz for ^3J, instead of 1.8 Hz, was found to give better results), producing sets of complementary data that allowed us to distinguish between coordinated and unbound nitrogen atoms. In other words, the experiments performed with the smallest coupling constant afforded the chemical shift of N^o, whereas those performed with the larger value of *J* afforded the chemical shifts of N^p and N_{py}. The spectra of **51** and **52** are shown in Figure 6.8. In order to validate the method of analysis on a larger set of compounds, the measurements were performed also on the two cppH linkage isomers [Ru([9]aneS_3)(cppH-κN^p)(PTA)]$(Cl)_2$ and [Ru([9]aneS_3)(cppH-κN^o)(PTA)]$(Cl)_2$ (**50*N*^{p}** and **50*N*^{o}**, respectively, Appendix A6.3) that we had fully characterized previously.[13] The ^{15}N resonances for free ligands and for the complexes, together with the coordination induced shift (CIS) values, are reported in Table 6.2 (cppH) and 6.3 (mpp).

Table 6.2. ^{15}N NMR chemical shifts (δ, ppm vs CH_3NO_2, DMSO-d_6) for cppH·HNO_3 and for the cppH ligand in compounds **50*N*^{p}**, **50*N*^{o}**, **51**, and **52**. Numbers in parentheses are the CIS values calculated as $\delta_{complex} - \delta_{ligand}$.

	cppH·HNO_3	**50*N*^{p}**	**50*N*^{o}**	**51**	**52**
N_{py}	–136.6	–150.4 (–13.8)	–150.6 (–14.0)	–126.5 (10.1)	–126.5 (10.1)
N^p	–84.1	–150.1 (–66.0)	–95.1 (–11.0)	–130.2 (–46.1)	–86.2 (–2.1)
N^o	–95.5	–92.0 (3.5)	–170.6 (–75.1)	–108.9 (13.4)	–143.6 (–48.1)

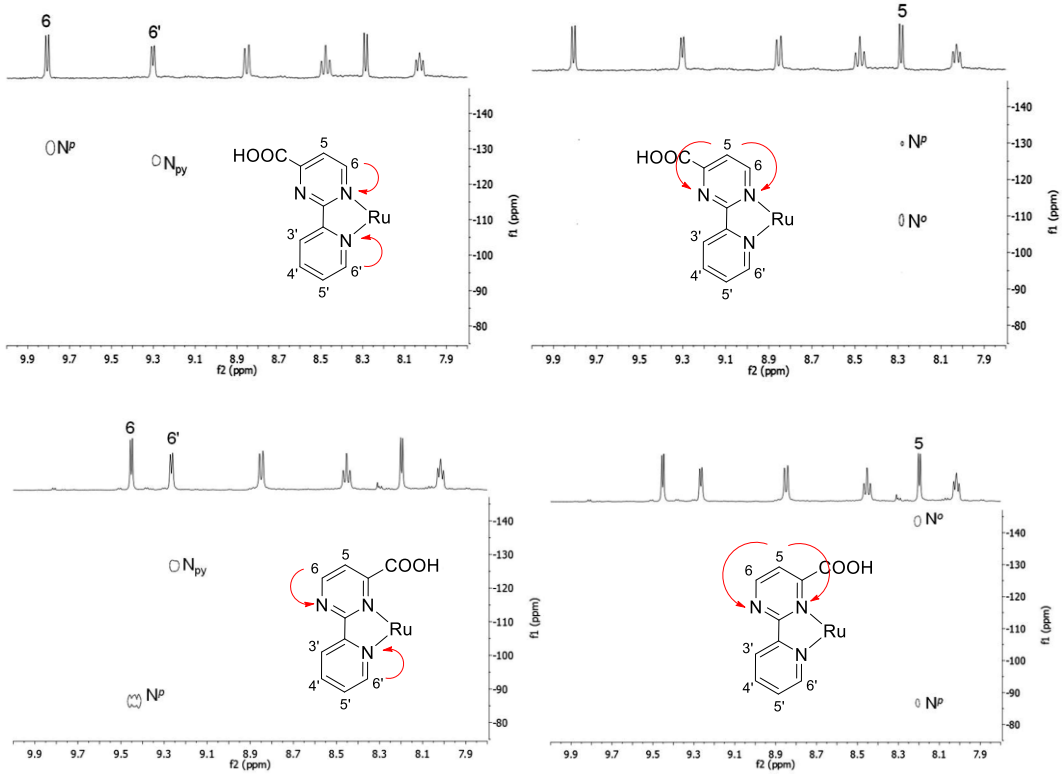

Figure 6.8. {^{1}H,^{15}N}-HMBC spectra of *trans*,*cis*-$RuCl_2(CO)_2$(cppH-κ*N*^{p}) (**51**, top) and *trans*,*cis*-$RuCl_2(CO)_2$(cppH-κ*N*^{o}) (47, bottom) in DMSO-d_6 with J = 11 Hz (left) and J = 1.7 Hz (right).

The ^{15}N resonances of free cppH show that in DMSO the pyridyl nitrogen – i.e. the most basic site of the ligand – is protonated by HNO_3. For this reason its chemical shift is so remarkably upfield shifted compared to those of the N atoms on the pyrimidine ring as well as to the typical values expected for a free nitrogen atom in a pyridyl ring (cfr also the chemical shift of the corresponding unprotonated N atom in free mpp, Table 6.3).[20,21] The results obtained with **50*N*^{p}**, **50*N*^{o}** and **51** clearly showed that coordination to Ru(II) induces a remarkable upfield shift for the ^{15}N resonance (except for that of N_{py}, see above), with CIS values ranging from ca. –45 to –75 ppm, whereas the unbound N atom resonates at a frequency similar to that of the free ligand (CIS values from –11.0 to +13.4 ppm). Our results are consistent with the literature data indicating that the binding of imine nitrogen atoms to Ru(II) involves significant

^{15}N shielding effects, thus resulting in negative CIS values.[20] The differences in the chemical shifts of the bound N^{p} atoms observed between **51** and **50** are attributable to the different ligand environment and charge of the species. Finally, the ^{15}N chemical shifts measured for **52** clearly indicate that in this complex cppH is indeed bound via ***N^{o}***, and **52** is therefore the linkage isomer of **51**, i.e. *trans*,*cis*-$RuCl_2(CO)_2$(cppH-κ*N^{o}*) (Figure 6.8).

Similar experiments were performed on mpp and on its four complexes. The results are reported in Table 6.3 (see also Appendix, A6.8 for the {^{1}H,^{15}N}-HMBC spectrum of mpp, A6.14-A6.16 for {^{1}H,^{15}N}-HMBC spectra of **53-55** and A6.19, A6.20 for the {^{1}H,^{15}N}-HMBC spectrum of **56**). From the values of ^{15}N chemical shifts of the pyrimidine N atoms it can be concluded that also in **55** mpp is bound via ***N^{p}*** and therefore this complex is the missing all-*cis* stereoisomer rather than the linkage isomer of **54**.

Table 6.3. ^{15}N NMR chemical shifts (δ, ppm vs CH_3NO_2, $CDCl_3$) for the mpp ligand free and in compounds **53-56**. Numbers in parentheses are the CIS values calculated as $\delta_{complex}-\delta_{ligand}$.

	mpp	**53**	**54**	**55**	**56**
N_{py}	–71.2	–145.0 (–73.8)	–130.7 (–59.5)	–135.9 (–64.7)	–124.6 (–53.4)
N^{p}	–101.2	–160.4 (–59.2)	–153.4 (–52.2)	–147.6 (–46.4)	–143.3 (–42.1)
N^{o}	–92.5	–90.2 (2.3)	–87.7 (4.8)	–88.7 (3.8)	–89.5 (3.0)

6.6 Conclusions

First of all, we demonstrated that the ^{15}N NMR chemical shifts of the diimine linker 2-(2′-pyridyl)pyrimidine-4-carboxylic acid (cppH), obtained through {^{1}H,^{15}N}-HMBC NMR spectra at natural abundance of the ^{15}N isotope, unambiguously establish the coordination mode of the pyrimidine ring (either via N^o or N^p). In fact, coordination of cppH to Ru(II) induces a marked upfield shift for the resonance of the N atoms directly bound to the metal, with coordination induced shifts (CIS) ranging from ca. –45 to –75 ppm, depending on the complex, whereas the unbound N atom resonates at a frequency similar to that of the free ligand. Similar results were found for the complexes of the parent diimmine ligand 4-methyl-2-(2′-pyridyl)pyrimidine (mpp). This ligand, having a methyl instead of the –COOH group in position 4 of the pyrimidine ring, cannot be exploited as a linker but, given the strict similarity with cppH, was considered as a good model thereof. When the ^{15}N chemical shifts of the pyrimidine N atoms in the free ligands are compared (Table 6.2 and 6.3), it is clear that N^p is affected much more than N^o by the nature of the substituent on position 4. The replacement of the electron-donor group $–CH_3$ (mpp) with the electron-withdrawing group –COOH (cppH) induces a remarkable shift to higher frequency of the N^p resonance (–101.2 vs –84.1 ppm).

Our method was first validated on a number of Ru(II) complexes with either cppH or mpp in which the coordination mode of the diimine was known from X-ray structure determinations, and then it was used to determine the ligand binding mode in two complexes, namely **52** and **55**, for which the X-ray structure was not available. More specifically, we investigated the reactivity of the Ru(II) carbonyl complex *trans*,*cis*,*cis*-$RuCl_2(CO)_2$(dmso-O)$_2$ (**29**) towards cppH. Compound **29** proved once more to be an excellent precursor for the selective preparation of *trans*,*cis*-$RuCl_2(CO)_2$(*N*-*N*) complexes when treated with diimines (*N*-*N*), including cppH. Most importantly, cppH confirmed to be an “irresolute linker”,

as we had previously found in its reaction with the Ru(II) precursor *fac*-Ru([9]aneS$_3$)Cl$_2$(PTA) that afforded comparable amounts of the two linkage isomers [Ru([9]aneS$_3$)(cppH-κ*N*^{p})(PTA)](Cl)$_2$ and [Ru([9]aneS$_3$)(cppH-κ*N*^{o})(PTA)](Cl)$_2$ (**50*N*^{p}** and **50*N*^{o}**, respectively).[13] In fact, we found that treatment of **29** with cppH affords both linkage isomers *trans*,*cis*-RuCl$_2$(CO)$_2$(cppH-κ*N*^{p}) (**51**) and *trans*,*cis*-RuCl$_2$(CO)$_2$(cppH-κ*N*^{o}) (**52**), with **52** largely prevailing when the reaction is performed in water at room temperature. The binding mode of cppH in compound **52** was established through the ^{15}N NMR experiments. Typically, in all solvents investigated (i.e. water, chloroform, methanol) **51** precipitates spontaneously whereas **52**, more soluble, is found only when the mother liquor is analyzed. Most likely for this reason compound **51** had been already prepared – even though from a different Ru(II)-carbonyl precursor – and fully characterized, whereas its linkage isomer **52** had escaped detection. It is quite remarkable that in this case, unlike in that of **50*N*^{p}** and **50*N*^{o}**, each linkage isomer can be easily obtained in pure form by exploiting their different solubility properties. Thus, using compounds **51** and **52** as precursors, the preparation of isomeric Ru-conjugates that differ only in the orientation of the organic macromolecule (e.g. a peptide or a porphyrin) and the assessment of their individual properties might eventually become possible.

We also found that when the reaction between **29** and cppH is performed in methanol, partial esterification of the carboxylic group occurs and a mixture of **51** and of *trans*,*cis*-RuCl$_2$(CO)$_2$(cppMe-κ*N*^{p}) (**51Me**) cocrystallizes. The single crystal X-ray structures of both pure **51** and of this mixture were determined.

The Ru(II)-dmso precursors *cis*-RuCl$_2$(dmso-S)$_4$ (**8**) and *trans*-RuCl$_2$(dmso-S)$_4$ (**9**) turned out to be unsuitable for the preparation of cppH complexes, since they originate oligomers. Conversely, their reactivity with mpp is similar to that observed with bpy.[24] All the four possible stereoisomers – namely *cis,trans*-RuCl$_2$(dmso-S)$_2$(mpp-κ*N*^{p}) (**53**), the two *cis,cis*-RuCl$_2$(dmso-S)$_2$(mpp-κ*N*^{p}) isomers (**54** + **55**), and

trans,cis-$RuCl_2$(dmso-S)$_2$(mpp-κN^p) (**56**) – were obtained and individually characterized through NMR spectroscopy. The X-ray structures of three of them, **53**, **54**, and **56**, were also determined. According to ^{15}N NMR spectroscopy, and in agreement with the X-ray structures, in all cases mpp is always bound via $\boldsymbol{N^p}$. No trace of $\boldsymbol{N^o}$ linkage isomers was found for the mpp complexes. When this behavior is compared with that of cppH, it can be concluded that mpp is not such a good model for cppH. As suggested by the comparison of the ^{15}N chemical shift values of $\boldsymbol{N^p}$ in the free ligands the methyl group in position 4 makes the trans N atom a better nucleophile compared to cppH and the $\boldsymbol{N^p}$ coordination mode becomes largely preferred over the alternative $\boldsymbol{N^o}$.

6.7 Bibliography

[1] N. Nickita, M. J. Belousoff, A. I. Bhatt, A. M. Bond, G. B. Deacon, G. Gasser, L. Spiccia, *Inorg. Chem.*, **2007**, *46*, 8638 - 8651.

[2] (a) M. H. V. Huynh, D. M. Dattelbaum, T. J. Meyer, *Coord. Chem. Rev.*, **2005**, *249*, 457 - 483; (b) C. N. Fleming, M. K. Brennaman, J. M. Papanikolas, T. J. Meyer, *Dalton Trans.*, **2009**, 3903 - 3910; (c) M. K. Brennaman, C. N. Fleming, C. A. Slate, S. A. Serron, S. E. Bettis, B. W. Erickson, J. M. Papanikolas, T. J. Meyer, *Phys. Chem. B*, **2013**, *117*, 6352 - 6363.

[3] (a) A. Hess, N. Metzler-Nolte, *Chem. Commun.*, **1999**, 885 - 886; (b) J. C. Verheijen, G. A. Van der Marel, J. H. Van Boom, N. Metzler-Nolte, *Bioconjugate Chem.*, **2000**, *11*, 741 - 743; (c) N. Nickita, G. Gasser, A. M. Bond, L. Spiccia, *Eur. J. Inorg. Chem.*, **2009**, 2179 - 2186.

[4] (a) T. Gianferrara, I. Bratsos, E. Iengo, B. Milani, A. Oštrić, C. Spagnul, E. Zangrando and E. Alessio, *Dalton Trans.*, **2009**, 10742 - 10756; (b) T. Gianferrara, A. Bergamo, I. Bratsos, B. Milani, C. Spagnul, G. Sava, E. Alessio, *J. Med. Chem.*, **2010**, *53*, 4678 - 4690; (c) C. Spagnul, R. Alberto, G. Gasser, S. Ferrari, V. Pierroz, A. Bergamo, T. Gianferrara and E. Alessio, *J. Inorg. Biochem.*, **2013**, *122*, 57 – 65; (d) T. Gianferrara, C. Spagnul, R. Alberto, G. Gasser, S. Ferrari, V. Pierroz, A. Bergamo, E. Alessio, *ChemMedChem*, **2014**, *9*, 1231 - 1237.

[5] (a) J. Schneider, K. Q. Vuong, J. A. Calladine, X.-Z. Sun, A. C. Whitwood, M. W. George and R. N. Perutz, *Inorg. Chem.*, **2011**, *50*, 11877 - 11889; (b) C. D. Windle, M. V. Câmpian, A.-K. Duhme-Klair, E. A. Gibson, R. N. Perutz and J. Schneider, *Chem. Commun.*, **2012**, *48*, 8189 - 81910.

[6] (a) K. Y. Zhang, K. K.-W. Lo, *Inorg. Chem.*, **2009**, *48*, 6011 - 6025; (b) K. K.-W. Lo, S. P.-Y. Li, K. Y. Zhang, *New J. Chem.*, **2011**, *35*, 265 - 287.

[7] D. G. McCafferty, B. M. Bishop, C. G. Wall, S. G. Hughes, S. L. Mecklenberg, T. J. Meyer, B. W. Erickson, *Tetrahedron*, **1995**, *51*, 1093 - 1106.

[8] N. Nickita, G. Gasser, P. Pearson, M. J. Belousoff, L. Y. Goh, A. M. Bond, G. B. Deacon, L. Spiccia, *Inorg. Chem.*, **2009**, *48*, 68 - 81.

[9] (a) T. Joshi, G. J. Barbante, P. S. Francis, C. F. Hogan, A. M. Bond, G. Gasser, L. Spiccia, *Inorg. Chem.*, **2012**, *51*, 3302 - 3315; (b) T. Joshi, G. Gasser, L. L. Martin, L. Spiccia, *RSC Adv.,* **2012**, *2*, 4703 - 4712; (c) T. Joshi. M. Patra, L. Spiccia, G. Gasser, *Artificial DNA: PNA & XNA*, **2013**, *4*, 11 - 18; (d) C. Bischof, T. Joshi, A. Dimri, L. Spiccia, Schatzschneider, U. *Inorg. Chem.*, **2013**, *52*, 9297 - 9308.

[10] T. Joshi, V. Pierroz, S. Ferrari, G. Gasser, *ChemMedChem*, **2014**, *9*, 1231 - 1237.

[11] V. Pierroz, T. Joshi, A. Leonidova, C. Mari, J. Schur, I. Ott, L. Spiccia, S. Ferrari, G. Gasser, *J. Am. Chem. Soc.*, **2012**, *134*, 20376 - 20387.

[12] T. Joshi, V. Pierroz, C. Mari, L. Gemperle, S. Ferrari, G. Gasser, *Angew. Chem. Int. Ed.*, **2014**, *53*, 2960 - 2963.

[13] E. Iengo, N. Demitri, G. Balducci, E. Alessio, *Dalton Trans.*, **2014**, *43*, 12160 - 12163.

[14] G. Balducci, E. Iengo, N. Demitri, E. Alessio, *Eur. J. Inorg. Chem.*, **2015**, *26*, 4296 - 4311.

[15] The esterification process is presumably catalyzed by the crystallization molecule of HNO_3 that accompanies cppH.

[16] M. Toyama, K. Inoue, S. Iwamatsu, N. Nagao, *Bull. Chem. Soc. Jpn.*, **2006**, *79*, 1525 - 1234.

[17] To be noted that in 2008 Natarajan and coworkers published, without any experimental evidence, that treatment of **3** with bpy in refluxing chloroform affords *trans,cis*-Ru(bpy)Cl_2(dmso-S)$_2$ (V. Mahalingam, N. Chitrapriya, F. R. Fronczek, K. Natarajan, *Polyhedron*, **2008**, *27*, 1917-1924.). Based on the results reported in ref. 16 and in this manuscript, such conclusion is to be considered wrong.

[18] Contrary to what stated in ref 16, the number of dmso resonances depends exclusively on the symmetry of the complex and not on the presence of dynamic processes such as rotation about the Ru–S bond.

[19] E. Alessio, *Chem. Rev*., **2004**, *104*, 4203 - 4242.

[20] L. Pazderski, T. Pawlak, G. Sitkowski, L. Kozerski, E. Szlyk, *Magn. Reson. Chem*, **2010**, *48*, 450 - 457.

[21] L. Pazderski, T. Pawlak, G. Sitkowski, L. Kozerski, E. Szlyk, *Magn. Reson. Chem*, **2011**, *49*, 237 - 241.

CHAPTER 7

Novel Ru(II) bioconjugates with neurotensin

7.1 State of the art

As mentioned in the Introduction, the synthesis and biological evaluation of metal-bioconjugates is an active field of the bioinorganic field, with applications in radiolabeling, biosensing, as well as anticancer and antimicrobial drug development.[1]

Among the investigated biomolecules, particularly interesting are the receptor-binding peptides, such as neurotensin (NT) and ocreotide, an analogue of somatostatin. Such peptides have a high affinity for receptors that are overexpressed in several tumors so they can be used to selectively internalize the bound metal into target cancer cells in the so-called "trojan horse approach".[2,3]

Neurotensin (NT) is a tridecapeptide hormone with primary structure pGlu-Leu-Tyr-Glu-Asn-Lys-Pro-Arg-Arg-Pro-Tyr-Ile-Leu that is recognized by three NT receptors (NTR1–3). All three receptors recognize the C-terminal hexapeptide sequence NT(8–13), which is thus sufficient for recognition and binding (Figure 7.1).

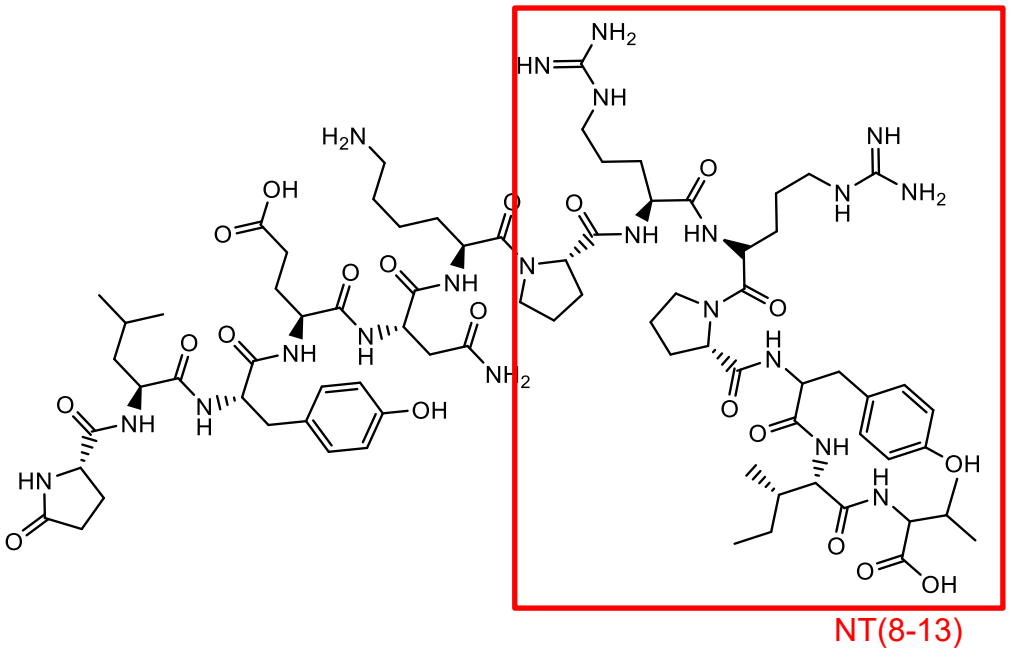

Figure 7.1. Schematic representation of Neurotensin; the red box indicates the fragment 8-13.

Since both NTR1 and NTR3 are upregulated in several human cancers such as colon, pancreatic, prostate, and lung cancer,[4] bioconjugates with this peptide, in particular the fragment NT(8-13), are interesting candidates for antiproliferative applications. In the literature there are some examples of bioconjugates with the NT, in which the peptide is bound – through a peptidic bond – either to a functionalized arene of a ferrocene or ruthenocene derivative,[5] or to a platinum(IV) moiety through its succinate axial ligands (Figure 7.2).[6]

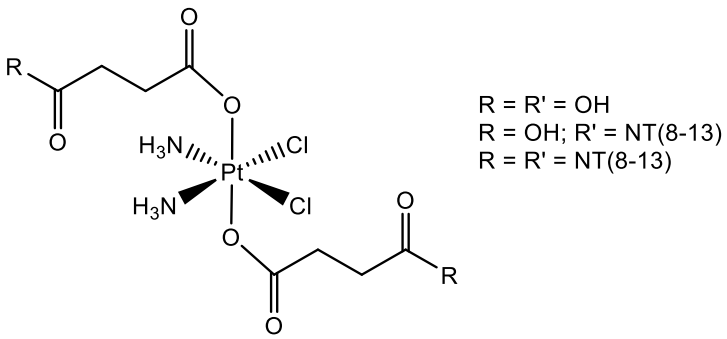

Figure 7.2. Schematic representation of Platinum(IV) precursor (R = R′ = OH) and two derivatives with neurotensin: the mono-conjugate (R = OH, R′ = NT(8-13)) and the bis-conjugate (R = R′ = NT(8-13).

7.2 Aim of the Chapter

This Chapter describes the synthesis and characterization of novel Ru(II) bioconjugates with potential antitumor activity. The bioconjugates were prepared during a six-month stage in the group of Prof. Nils Metzler-Nolte at the University of Bochum (Germany), who has a consolidate experience in the preparation, characterisation and utilisation of novel metal-bioconjugates with peptides and other biomolecules.

In Chapter 6 we described the synthesis of two Ru(II) complexes with the diimine linker cppH that are linkage isomers: *trans*,*cis*-$RuCl_2(CO)_2$(cppH-κN^p) (**51**) and *trans*,*cis*-$RuCl_2(CO)_2$(cppH-κN^o) (**52**) (Figure 7.3). Previously, cppH has been used in the preparation of Ru(II)-bioconjugates with PNA and peptides for biosensing and biomedical applications; in all the reported examples the ligand was always bonded through the *para* nitrogen atom of the pyrimidine ring.[7,8]

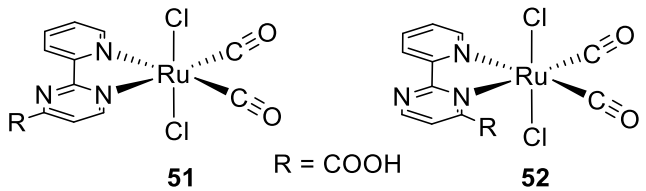

Figure 7.3. Schematic representation of the precursors *trans*,*cis*-$RuCl_2(CO)_2$(cppH-κN^p) (**51**) and *trans*,*cis*-$RuCl_2(CO)_2$(cppH-κN^o) (**52**).

We argued that the two linkage isomers **51** and **52** might offer – in principle – the unique opportunity to prepare unprecedented stereoisomeric Ru-bioconjugates that differ only in the orientation of the organic macromolecule with respect to the metal fragment, and to investigate if they behave differently in terms of activity/selectivity in biological experiments. Thus, the cppH carboxylic group of both isomers was exploited for linking the C-terminal hexapeptide sequence of neurotensin, NT(8–13) (Arg-Arg-Pro-Tyr-Ile-Leu or RRPYIL), which is sufficient for recognition and binding. Cytotoxicity assays against three different cell lines: colon adenocarcinoma

(HT-29), breast cancer (MCF-7) and pancreatic cancer (PT-45), were selected as biological tests to be performed both on the precursors and bioconjugates.

7.3 Synthesis of bioconjugates

NT(8-13) was synthesized by Solid Phase Peptide Synthesis (SPPS, see the Experimental Part for details), then the same procedure was used for preparing the desired bioconjugates by forming a peptide bond between the terminal arginine of the peptide and the carboxylic group of cppH in both linkage isomer **51** and **52**.

For the complex **52** (N^o isomer) it was possible to isolate the bioconjugate **57** adapting a previously established peptide coupling procedure.[10] After purification of the reaction product with preparative HPLC (in general, every bioconjugate was purified using preparative HPLC), analytical HPLC showed a single peak (performed with a linear gradient of A (H_2O/CH_3CN/TFA 95:5:0.1, v/v/v) and B (CH_3CN/H_2O/TFA 95:5:0.1, v/v/v) (TFA = Trifluoroacetic Acid), retention time (Rt) 18.2 min), suggesting that the product **57** was in pure form. In the ESI MS spectrum the molecular peak $[M+H]^+$ at 1227.3 m/z was consistent with the expected product (1226.6 m/z) (Scheme 7.1). At this stage, however, it was impossible to establish the binding mode of the cppH linker in **57**. In addition, given that the HPLC elution time of the conjugate is mainly dictated by the peptide fragment (**51**, **52**, NT(8-13) and cppH-NT have Rt of 12.2, 10.5, 15.9 and 16.4 min respectively), it cannot be excluded that compound **57** is actually a mixture of the two possible linkage isomers, provided that they have undistinguishable retention times.

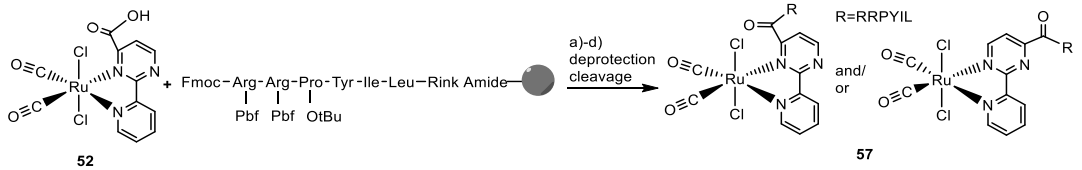

Scheme 7.1. The last step of the synthesis of **57** using SPPS. (a) Fmoc deprotection, (b) washing the resin with 4×DMF and 3×DCM, (c) coupling for 1h (coupling mixture: PyBOP/DIPEA 5/10), (d) washing the resin with 4×DMF and 3×DCM. (PyBOP = benzotriazol-1-yl-oxytripyrrolidinophosphonium hexafluorophosphate, DIPEA = *N*,*N*-Diisopropylethylamine). R is the peptide sequence: Arg-Arg-Pro-Tyr-Ile-Leu.

The behavior of the N^p isomer **51** was different: it was not possible to isolate a bioconjugate, because none of the mixtures of coupling agents tried for different

reaction times (from 1 to 7 days), either at room temperature or using a microwave (60°C or 80°C), led to a product in acceptable yield.

Given these results, a different synthetic strategy for obtaining the bioconjugates was explored. NT(8-13) was first linked to cppH through a peptidic bond between the carboxylic group of cppH and the amino group of the terminal arginine using SPPS. The cppH-NT moiety was deprotected and cleaved from the resin, and then it was reacted with the Ru(II) precursor *trans,cis,cis*-$RuCl_2(CO)_2(dmso\text{-}O)_2$ (**29**) in aqueous solution at room temperature, i.e. under the conditions that, with cppH, lead to a mixture of the two linkage isomers **51** and **52** (see Chapter 6).

Treatment of **29** with cppH-NT at room temperature for 60h, during which time the solution color changed from pale yellow to orange, afforded a bioconjugate whose ESI MS and analytical HPLC signatures were equal to those of the bioconjugate **57** described above. Thus, the two synthetic pathways described in Schemes 7.1 and 7.2 led to the same product **57**, within the above mentioned limits. NMR characterization was planned to define the coordination mode of cppH to the ruthenium center (see below).

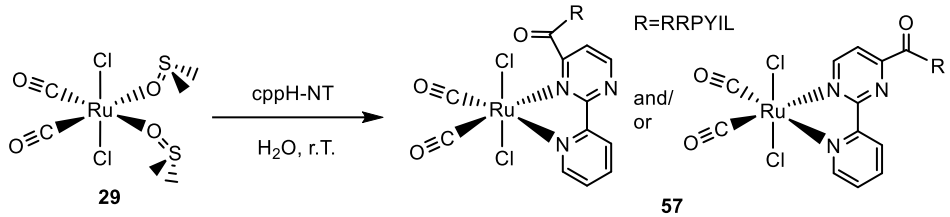

Scheme 7.2. The alternative synthesis of **57**. R is the peptide sequence: Arg-Arg-Pro-Tyr-Ile-Leu.

Given its good reactivity, the peptide-functionalized cppH was reacted also with two additional Ru(II) precursors, Ru([9]aneS_3)Cl_2(dmso) (**58**), and Ru([9]aneS_3)Cl_2(PTA) (**59**) (PTA = 1,3,5-triaza-7-phosphaadamantane). These complexes, whose reactivity towards chelating diimines is known, were chosen because the face-capping tridentate ligand [9]aneS_3 gives a geometrical restrain that reduces the number of possible stereoisomers with asymmetric ligands such as cppH.

It is known from the literature that treatment of **58** with a chelating diimine such as 2,2′-bipyridine (bpy) in refluxing ethanol for 1 hour leads selectively to [Ru([9]aneS$_3$)Cl(bpy)]Cl.[9]

Similarly, we found that [Ru([9]aneS$_3$)Cl(cppH)]Cl (**60**) precipitates spontaneously when **58** is reacted with unmodified cppH in refluxing water. X-ray quality crystals of **60** were obtained upon slow evaporation of the mother liquor after removal of the precipitate (Scheme 7.3). Ethanol was avoided as solvent in order to prevent the esterification of the carboxylic group, as observed in Chapter 6. The model compound **60** was fully characterized by NMR spectroscopy, mass spectrometry, and its single-crystal X-ray structure was also determined (Figure 7.4).

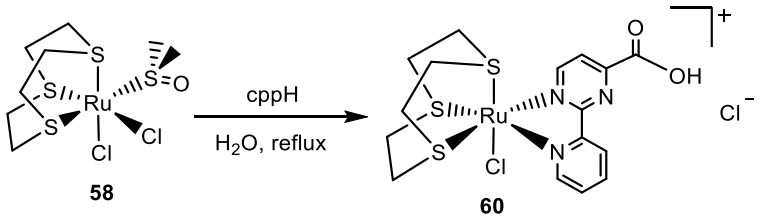

Scheme 7.3. Synthesis of [Ru([9]aneS$_3$)Cl(cppH)]Cl (**60**).

The single crystal X-ray analysis established that cppH is bound via ***N^p***, i.e. **60** is [Ru([9]aneS$_3$)Cl(cppH-κ*N^p*)]Cl. The ^{1}H NMR spectrum in D$_2$O shows two pairs of six resonances for cppH, due to the chloride hydrolysis equilibrium of compound **60** with the corresponding aqua species **60aq**. In **60aq** the aromatic resonances are slightly downfield shifted (ca 0.1 ppm) compared to those of the parent complex, and their relative intensity decreases upon adding an excess of NaCl (Appendix, A7.1).

Compound **60** was obtained also when the reaction between **58** and cppH was performed at room temperature, i.e. in the conditions that in the case of **29** led to the isolation of the *N^o* isomer **52**. In this case, the formation of the *N^o* isomer of **60** was not observed.

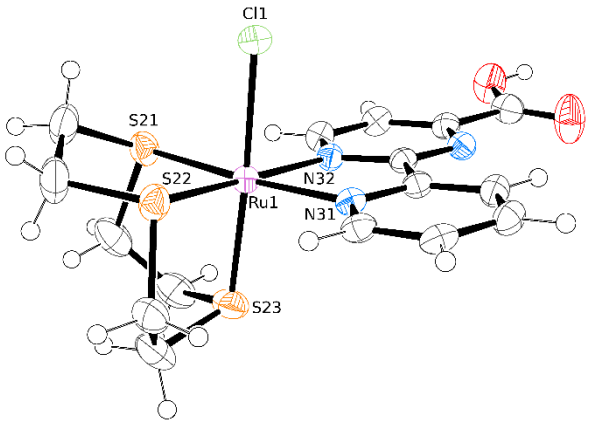

Figure 7.4. X-ray molecular structures (50% probability ellipsoids) of [Ru([9]aneS$_3$)Cl(cppH-κ*N*^{p})]Cl (**60**). The chloride is omitted for clarity. Coordination distances in ångström (Å): **60**: Ru1–Cl1 = 2.4319(7), Ru1–N31 = 2.094(3), Ru1–N32 = 1.092(3), Ru1–S21 = 2.304(1), Ru1–S22 = 2.2936(9), Ru1–S23 = 2.2785(9).

The conjugate **61** was obtained in pure form, according to the analytical HPLC, from the reaction between **58** and cppH-NT in water at 80°C for 5h (Scheme 7.4); in this case the color of the solution changed from yellow to deep red during the reaction. The molecular peak found in the ESI MS spectrum (1394.4 m/z) is in agreement with that expected for the cationic species [Ru([9]aneS$_3$)Cl(cppH-NT)]$^+$ (1394.2 m/z).

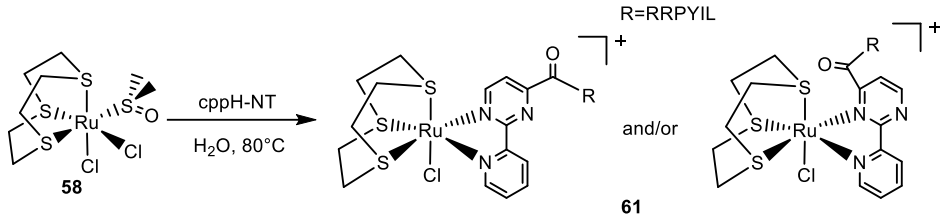

Scheme 7.4. Synthesis of bioconjugate **61**. R is the peptide sequence: Arg-Arg-Pro-Tyr-Ile-Leu.

As already stated in Chapter 6, the complex Ru([9]aneS$_3$)Cl$_2$(PTA) (**59**) reacts in refluxing water with cppH forming both linkage isomers [Ru([9]aneS$_3$)(cppH-κ*N*^{p})(PTA)](Cl)$_2$ and [Ru([9]aneS$_3$)(cppH-κ*N*^{o})(PTA)](Cl)$_2$ in ca 3/2 ratio (they could be separated after recrystallization by manual separation of the different types of crystals).[10]

The reaction between **59** and cppH-NT was performed at 80°C in water for 8h and afforded the bioconjugate **62** (Scheme 7.5). The reaction was accompanied by a color

change from yellow to red. According to the analytical HPLC, the bioconjugate was pure and the value of the molecular peak in the ESI MS spectrum (1438.6 m/z) was consistent with the expected product ($[M–H]^+$ 1438.4 m/z).

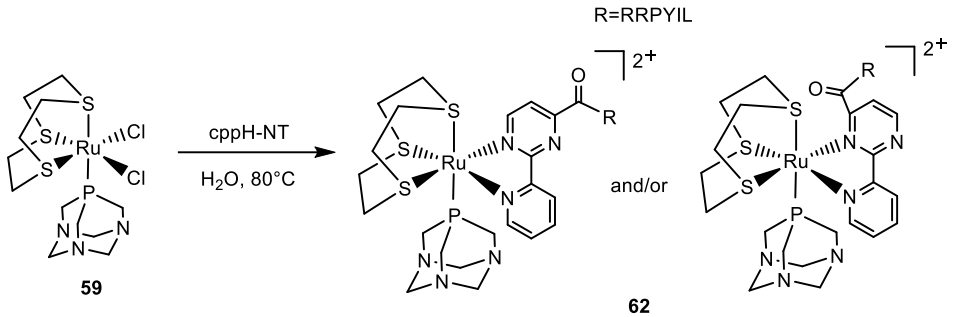

Scheme 7.5. Synthesis of bioconjugate **62**. R is the peptide sequence: Arg-Arg-Pro-Tyr-Ile-Leu.

As before with **57**, also with **61** and **62** it was not possible, at this stage, to assess the binding mode of cppH or even if each product was actually pure or a mixture of the two possible linkage isomers (assuming that they have equal retention times at HPLC analysis).

7.4 NMR characterization

All the prepared bioconjugates were characterized by NMR spectroscopy for determining the coordination mode of the cppH-NT unit to the ruthenium center. Resonances were assigned through conventional ^{1}H-^{1}H COSY and ^{1}H-^{13}C HSQC NMR spectra.

The ^{1}H NMR spectrum in DMSO-d_6 of bioconjugate **57** obtained using SPPS from *trans*,*cis*-$RuCl_2(CO)_2$(cppH-κN^o) and NT(8-13) presents six well resolved signals for coordinated cppH in the aromatic region. The comparison with the NMR spectra of the two linkage isomers *trans*,*cis*-$RuCl_2(CO)_2$(cppH-κN^p) (**51**) and *trans*,*cis*-$RuCl_2(CO)_2$(cppH-κN^o) (**52**) suggests that in this bioconjugate the cppH-NT is bonded through the N^p (Figure 7.5, see also Table 7.1). In fact, all the signals of **57** have chemical shifts very similar to those of **51** except for H3′ on the pyridyl ring,

probably due to some interaction with the peptide. Accordingly, **57** was formulated as *trans,cis*-$RuCl_2(CO)_2$(cppH-NT-κN^p). This finding was rather surprising, considering that in the starting complex **52** cppH was bound through N^o, and suggested that, during the SPPS synthesis, the cppH isomerized to the N^p isomer.

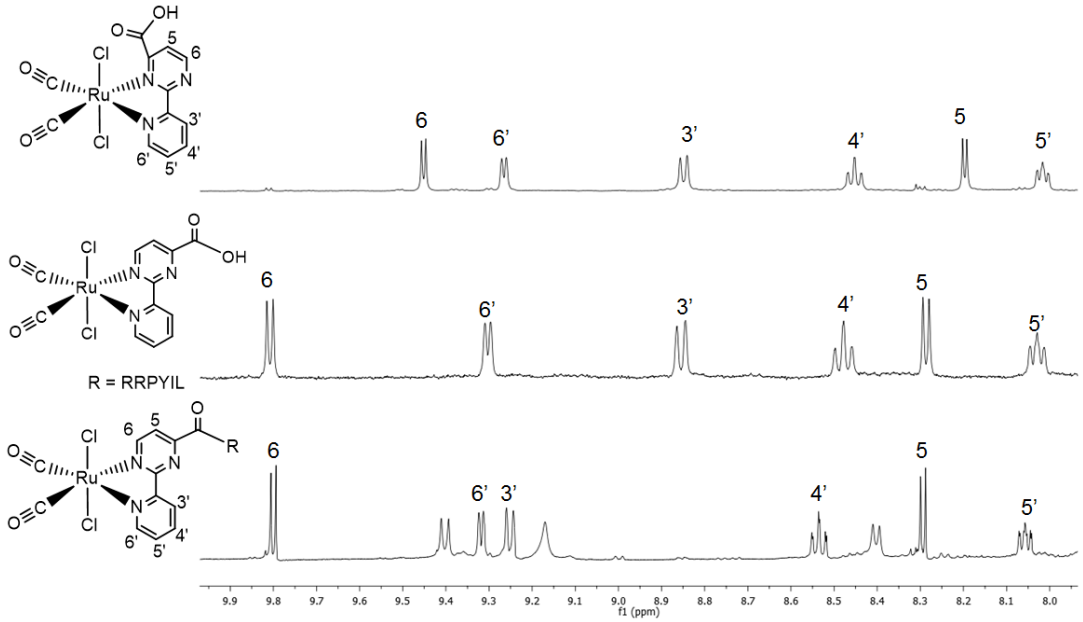

Figure 7.5. ^{1}H NMR spectra in DMSO-d_6 in the aromatic region of *trans*,*cis*-$RuCl_2(CO)_2$(cppH-κN^o) (**52**) (top), *trans*,*cis*-$RuCl_2(CO)_2$(cppH-κN^p) (**51**) (middle) and *trans*,*cis*-$RuCl_2(CO)_2$(cppH-NT) (**57**) (bottom). R is the peptide sequence: Arg-Arg-Pro-Tyr-Ile-Leu.

The aromatic region shows also four resonances for the amidic protons of the peptide. In fact, in the ^{1}H-^{13}C HSQC spectrum these peaks have no correlation crosspeaks with carbon resonances (Appendix, A7.3) and in the ^{1}H-^{1}H COSY spectrum they correlate with the protons on the respective Cα, whose resonances fall between 4.0 and 4.6 ppm (Figure 7.6). Moreover, the resonance at ca. 9.17 ppm, that has no correlation peak in the ^{1}H-^{1}H COSY and ^{1}H-^{13}C HSQC spectra, was assigned to the proton of the hydroxyl group of the Tyrosine. Finally, at ca. 7 ppm it is possible to distinguish two doublets, correlated in the ^{1}H-^{1}H COSY spectrum, for the *ortho* and *meta* protons of the phenyl ring of the Tyrosine, and two broad singlets for the two guanidinium NH protons of the two Arginines. All the remaining signals belong to the peptide chain and were not analyzed in detail (Appendix, A7.4)

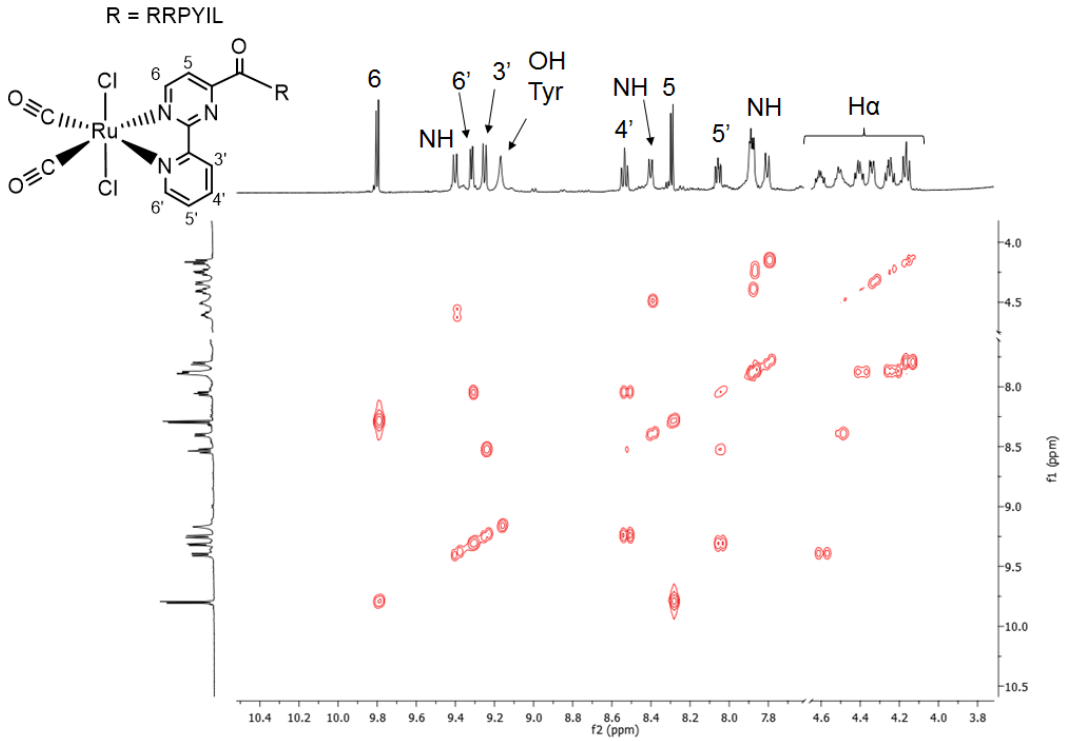

Figure 7.6. ^{1}H-^{1}H COSY in DMSO-d_6 of the selected regions of **57**. R is the peptide sequence: Arg-Arg-Pro-Tyr-Ile-Leu. NH indicates the amidic protons of the peptide.

The ^{1}H NMR spectrum of the same compound dissolved in D_2O presents twice the number of cppH-NT resonances in the aromatic region (Figure 7.7). The two sets of four resonances for the protons on the pyridine ring of cppH-NT are well resolved (the attributions of 3′ and 6′ are consistent with the ^{13}C NMR chemical shifts, obtained through an ^{1}H-^{13}C HSQC spectrum), while the signals for protons 5 and 6 of the pyrimidine ring are partially or completely overlapped. Each of them integrates as the sum of the two resonances of each proton of the pyridine ring. Thus, there are two species in ca. 3/2 ratio (blue/red) that presumably have the pyrimidine rings in very similar environments (overlapping resonances) and the pyridine rings in relatively different environments. It is worth nothing that typically the opposite occurs in case of linkage isomers of cppH, i.e. the resonances of the pyrimidine protons are affected much more than those of the pyridine protons by the different binding mode. The region of the peptide resonances is obviously more complicated.

However, it is possible to distinguish two sets of resonances (two doublets each) for the aromatic protons of Tyr that are basically in the same 3/2 intensity ratio as the cppH protons (Figure 7.8). They are pairwise connected in the ^{1}H-^{1}H COSY spectrum according to their relative intensity. The upfield part of the spectrum, with the other peptide resonances, is shown in the Appendix (A7.4).

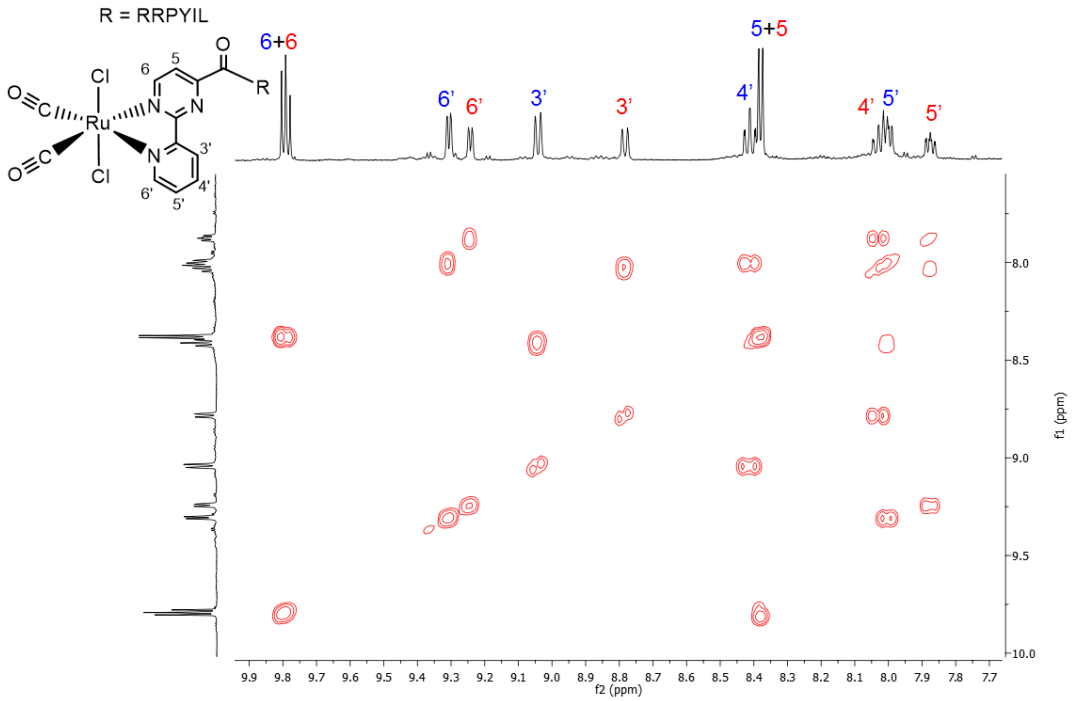

Figure 7.7. ^{1}H-^{1}H COSY in D_2O of the aromatic region of **57**. R is the peptide sequence: Arg-Arg-Pro-Tyr-Ile-Leu.

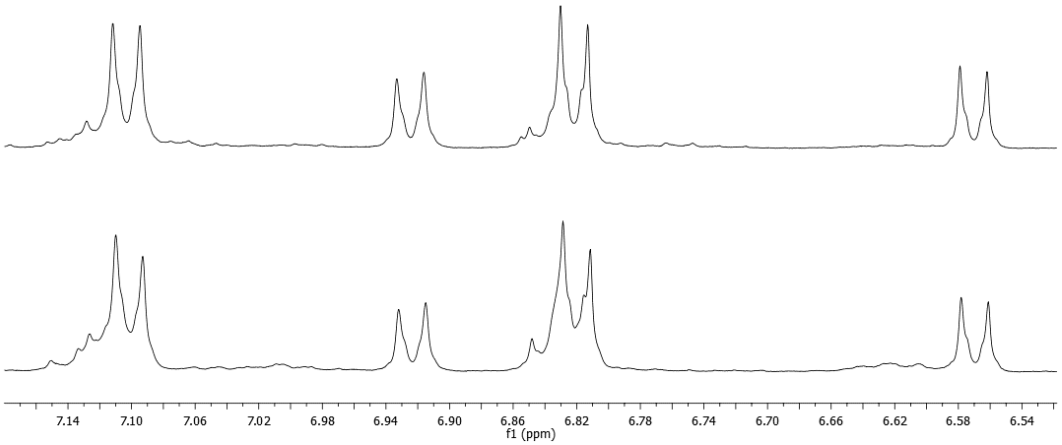

Figure 7.8. ^{1}H NMR spectra in D_2O (region of the aromatic protons of Tyr) of bioconjugate **57** obtained from the reaction (using SPPS) between *trans*,*cis*-$RuCl_2(CO)_2$(cppH-κN^o) and NT(8-13) (top), and from the reaction in solution between *trans,cis,cis*-$RuCl_2(CO)_2(dmso\text{-}O)_2$ and cppH-NT (bottom).

An increase in the temperature (up to 65°C) induced no significant change in the aromatic region of the ^{1}H NMR spectrum, thus suggesting that the two species are not in a conformational equilibrium.

Then the effect of pH on the NMR spectrum was investigated. The pD of the original D_2O solution (ca. 3.5) was gradually increased to 8 by stepwise addition of small volumes of a NaOD solution, and spectra were recorded after each step. Also in this case no significant change was observed in the aromatic region of the spectrum. Similarly unchanged was the spectrum of the final pD 8 solution when recorded at higher temperature (up to 65°C).

The bioconjugate **57** obtained through the other synthetic procedure, i.e. by treating *trans*,*cis*,*cis*-$RuCl_2(CO)_2(dmso\text{-}O)_2$ with cppH-NT in aqueous solution at room temperature, has the same NMR spectral features (Figure 7.8 and 7.9). The ^{1}H resonances are the same, also in terms of relative intensities; the only difference between the two NMR spectra is the presence of different amounts of minor impurities.

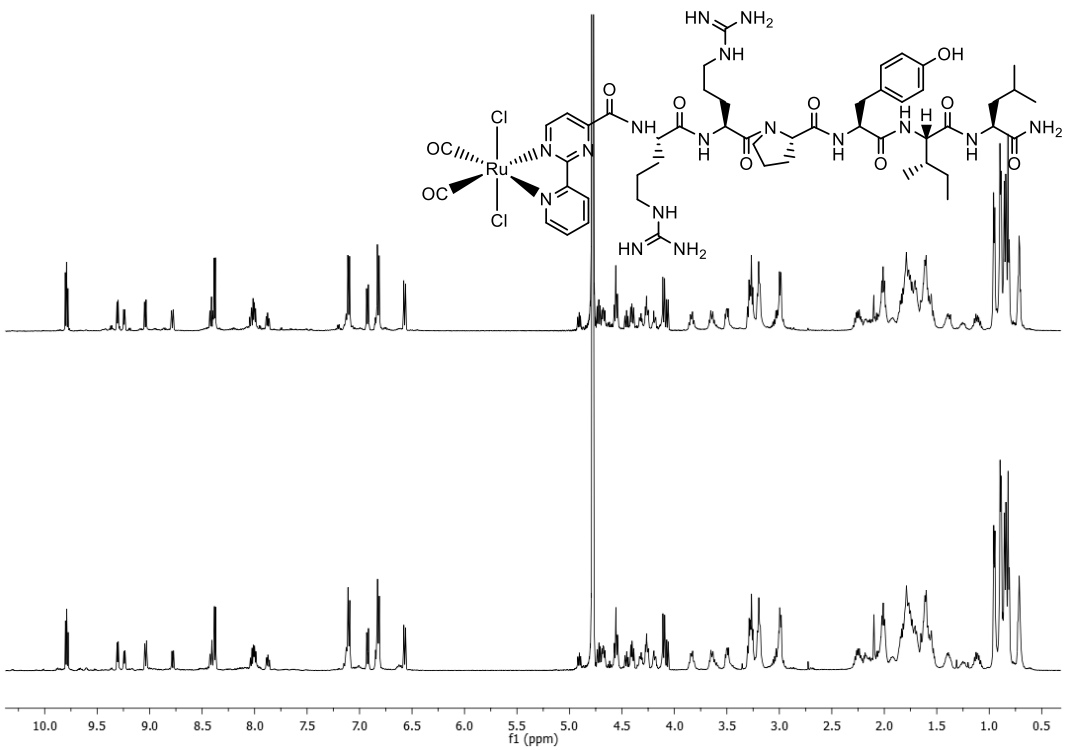

Figure 7.9. ^{1}H NMR spectra in D_2O of the bioconjugate **57** obtained from the reaction (using SPPS) between *trans*,*cis*-$RuCl_2(CO)_2$(cppH-κN^o) and NT(8-13) (top), and from the reaction in solution between *trans,cis,cis*-$RuCl_2(CO)_2(dmso)_2$ and cppH-NT (bottom).

In conclusion, the NMR spectra in DMSO-d_6 show that both synthetic procedures afford the same bioconjugate *trans*,*cis*-$RuCl_2(CO)_2$(cppH-NT) (**57**) in pure form and that the cppH-NT is bonded through the N^p.

On the contrary, the NMR spectra in D_2O show that in this solvent **57** originates two very similar bioconjugates. The spectra were not affected by an increase in temperature and by changing the pH of the solution. For the moment we have no clear explanation for this finding. Typically, in *trans*-{$RuCl_2$} fragments chloride hydrolysis is unlikely to occur, and was not observed in the corresponding cppH complexes. Since the NMR spectra of the two species differ mainly in the resonances of the pyridine ring of cppH-NT, we argue that they might derive from some intra- or inter-molecular interaction between the peptide and the pyridine ring of cppH. This hypothesis is also in agreement with the results of **61** and **62** shown below.

In fact, the ^{1}H NMR spectrum in DMSO-d_6 of [Ru([9]aneS$_3$)Cl(cppH-NT)]$^{+}$ (**61**) is similar to that of **57**. The downfield region presents six signals for the bonded cppH and other four signals for the amidic protons, partially overlapped with the cppH resonances, that in the ^{1}H-^{1}H COSY spectrum have crosspeaks with protons in the peptide zone (Appendix, A7.6).

The comparison with the resonances of the corresponding complex with unmodified cppH **60** suggests that in **61** the cppH-NT is bonded through N^{p} (see also Table 7.1). Accordingly, **60** was formulated as [Ru([9]aneS$_3$)Cl(cppH-NT-κN^{p}). Only the resonance of proton 3′ on the pyridine ring of **61** is downfield shifted compared to **60**, so that it falls at higher frequency than that of 6′. The two resonances are easily distinguished in the ^{1}H-^{13}C HSQC spectrum since 3′ has a correlation peak with a carbon at ca 127 ppm, while 6′ with a carbon at 155 ppm (Appendix, A7.7). Typically in Ru(II)-cppH complexes the resonances of protons 6 and 6′, that are adjacent to the bonded nitrogen atoms, are the most downfield signals. In this case some interaction between the peptide and the pyridine ring might be invoked to explain the variation of chemical shift for the signal of proton 3′.

The ^{1}H spectrum of **61** in D_2O, however, presents more resonances compared to that in DMSO-d_6, as in case of **57**. The spectrum is additionally complicated by the partial hydrolysis of the chloride. In fact, the addition of excess NaCl simplifies the spectrum since it reverts the aquation equilibrium, leaving only the resonances of non-hydrolyzed species (Figure 7.10). The behavior is similar to that found for the model complex **60** with unmodified cppH (Appendix, A7.1).

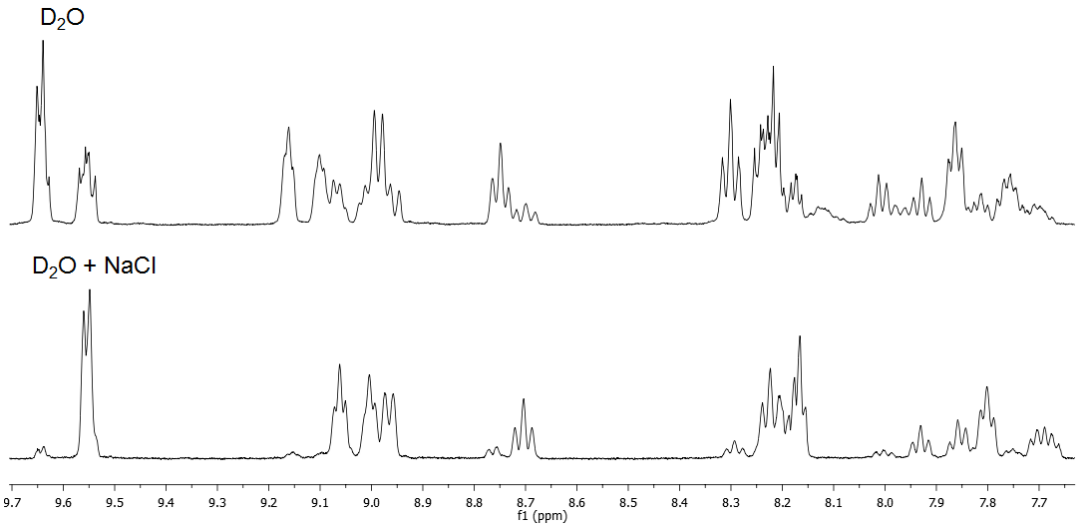

Figure 7.10. Downfield region of ^{1}H NMR spectrum of [Ru([9]aneS$_3$)Cl(cppH-NT)]$^{+}$ after dissolution in D_2O (top) and after addition of an excess of NaCl (bottom).

Figure 7.11 shows the ^{1}H-^{1}H COSY spectrum of the cppH-NT region in **61**: it is possible to distinguish at least three different sets of signals for three different major species in ca. 1/1/3 ratio (red/green/blue). The three species have very similar (overlapping) resonances for the pyrimidine protons 5 and 6 (thus suggesting that they are not linkage isomers), whereas several resonances of the pyridine protons are well resolved. In more detail, the two minor species (red and green) have very similar resonances for the pyridine protons, which are rather different from those of the main species (blue). In particular, the resonances of the pyridyl protons 3′ and 4′ of the minor species are upfield shifted compared to those of the main species. The region of the tyrosine resonances is rather complex (see below) but it is consistent with the presence of at least three species. Integration established that in each species the peptide chain is still attached to cppH.

The upfield part of the spectrum, with the other peptide resonances, is shown in the Appendix (A7.9).

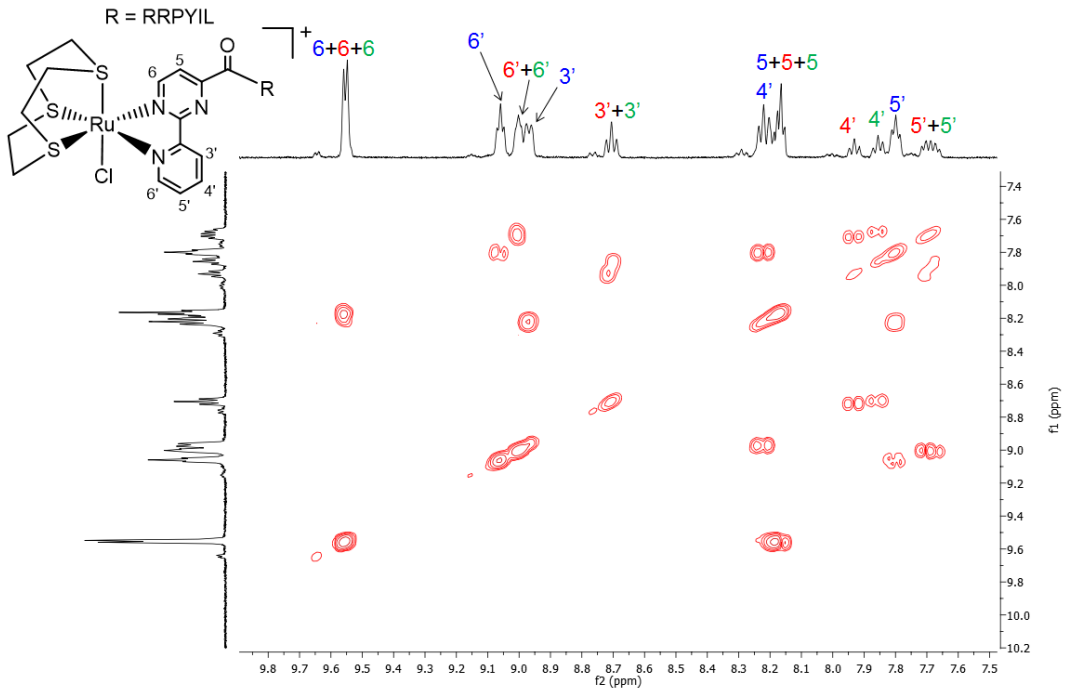

Figure 7.11. Downfield region of the ^{1}H-^{1}H COSY in D_2O + NaCl of [Ru([9]aneS$_3$)Cl(cppH-NT)]$^{+}$ (**61**). R is the peptide sequence: Arg-Arg-Pro-Tyr-Ile-Leu.

Thus, according to NMR data, when dissolved in D_2O compound **61** consists of at least three different species; all of them have the bonded cppH-NT moiety and differ mainly for the chemical shifts of the pyridine ring protons. As above for **57**, the NMR data are not consistent with the presence of linkage isomers or conformers. Conversely, the spectrum of the same compound **61** recorded in DMSO-d_6 presents peaks for only one species, in agreement with HPLC and ESI MS data.

Also in case of [Ru([9]aneS$_3$)(cppH-NT)(PTA)]$^{2+}$ (**62**), the ^{1}H NMR spectrum in DMSO-d_6 presents six signals for cppH-NT, partially overlapped with those of amide protons of the peptide. The comparison of the resonances with the two linkage isomers of the corresponding complex with unmodified cppH, **50*N*^{p}** and **50*N*^{o}**, suggests that in the bioconjugate **62** the cppH-NT in bonded through N^{p}, (see also Table 7.1). Also in this case, as for **61**, the resonance of the pyridine ring proton 3′ is downfield shifted compared to **50*N*^{p}** and falls at higher frequency than 6′ (Appendix, A7.10 and A7.11). The ^{31}P NMR spectrum of **62** shows a broad singlet

centered at –39.1 ppm that is similar to that for the corresponding model complex **50** with unmodified cppH (–34.9 for the N^p isomer and –35.0 for the N^o isomer, recorded in D_2O instead of DMSO-d_6).

The ^{1}H NMR spectrum of **62** in D_2O is similar to those of the other bioconjugates (Figure 7.12). As above for compound **61**, it is possible to distinguish at least three different sets in ca 1/1.5/2.5 ratio (green/red/blue) that differ mainly in the resonances of the pyridine ring protons. Two sets (red and green) are almost completely overlapped: only the resonances of proton 4′ are resolved. Moreover, each signal of the blue set also seems to be the sum of two very similar, almost completely overlapped resonances (e.g. see the signal of H6′ in Figure 7.12). The region of tyrosine resonances (Figure 7.13) is consistent with the presence of four species. In conclusion, compound **62** in aqueous solution is most likely a mixture of four very similar species. When the integration of the cppH protons is compared with those of PTA and aromatic protons of Tyr, it established that in each species PTA is still bonded to the ruthenium center and the peptide chain is connected to cppH. The upfield part of the spectrum, with the other peptide resonances, is shown in Appendix (A7.13).

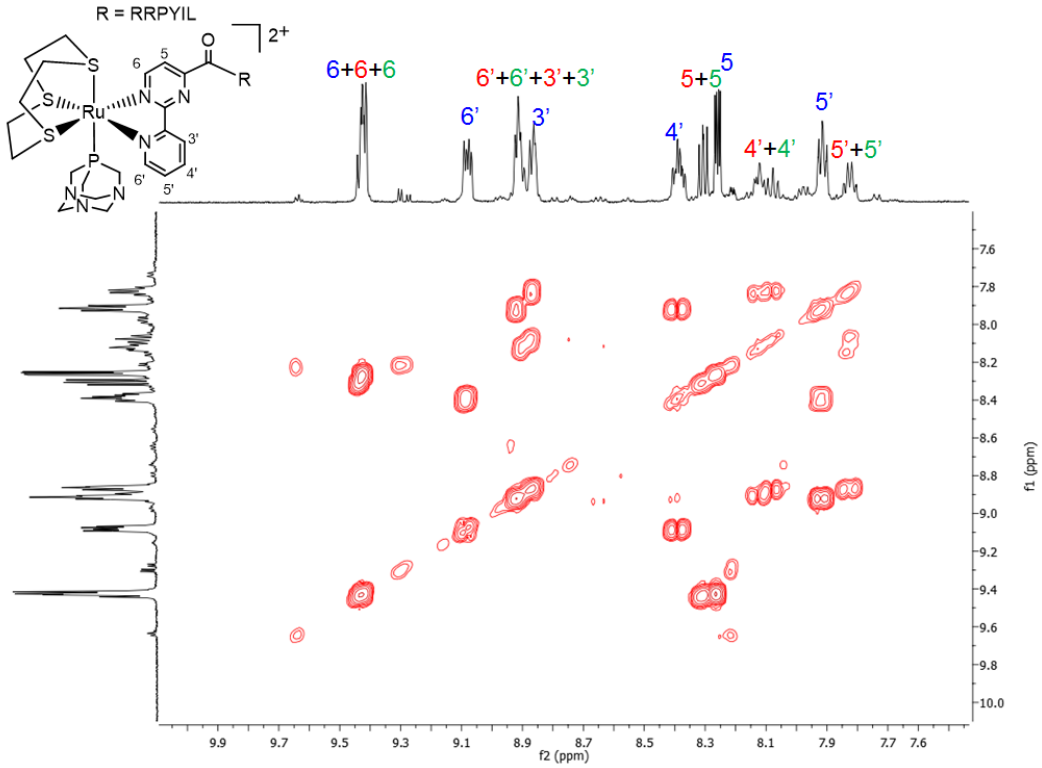

Figure 7.12. Downfield region of the ^{1}H-^{1}H COSY in D_2O of [Ru([9]aneS_3)(cppH-NT)(PTA)]$^{++}$ (**62**). R is the peptide sequence: Arg-Arg-Pro-Tyr-Ile-Leu.

Also in this case an increase in temperature (up to 65°C) and an increase in pD (from ca. 3 to ca. 8) left the ^{1}H NMR spectrum substantially unchanged.

As above mentioned, in the ^{1}H NMR spectra in D_2O the complexity of the cppH region is mirrored in that of the aromatic protons of Tyr (Figure 7.13): this region in the spectrum of **57** (top) is much simpler than those of the bioconjugates with [9]aneS_3, **61** (middle) and **62** (bottom). The spectra of **61** and **62** are consistent with the presence of three or more species, as indicated by the cppH region.

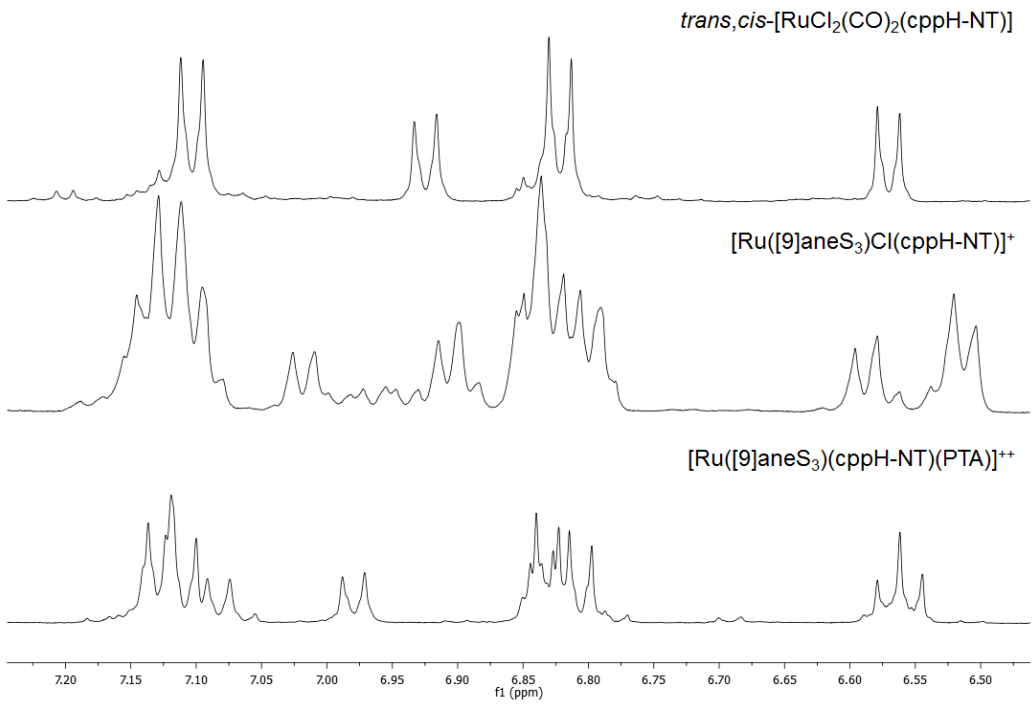

Figure 7.13. ^{1}H NMR spectra in D_2O (region of the aromatic Tyr protons) of *trans*,*cis*-$RuCl_2(CO)_2$(cppH-NT) (top), $[Ru([9]aneS_3)Cl(cppH\text{-}NT)^+$ (middle – D_2O + NaCl) and $[Ru([9]aneS_3)(cppH\text{-}NT)(PTA)]^{2+}$ (bottom).

7.5 Antiproliferative properties

The antiproliferative properties of compounds **29**, **51**, **52**, **57** - **59**, **61**, **62** were assessed against three different cell lines: colon adenocarcinoma (HT-29), breast cancer (MCF-7) and pancreatic cancer (PT-45) according to the method described in the Experimental Section. All the cell lines were treated for 48 hours with increasing concentrations of each comopund. None of the precursors and bioconjugates showed antiproliferative activity, even at the concentration of 200 μM.

7.6 Conclusions

In this Chapter we described the preparation of three novel Ru(II)–NT(8-13) bioconjugates with two different approaches and their characterization (Figure 7.14). The original aim of the work was that of preparing two stereoisomeric bioconjugates starting from the two linkage isomers *trans*,*cis*-$RuCl_2(CO)_2$(cppH-κN^p) (**51**) and *trans*,*cis*-$RuCl_2(CO)_2$(cppH-κN^o) (**52**). The SPPS approach applied to complex **52** and NT(8-13) afforded the bioconjugate *trans,cis*-$RuCl_2(CO)_2$(cppH-NT-κN^p) **(57**), whereas it was ineffective with the N^p isomer **51**. The second synthetic approach, i. e. the preparation of cppH-NT using SPPS followed by its reaction with the precursor of **51** and **52**, *trans,cis,cis*-$RuCl_2(CO)_2$(dmso-O)$_2$ (**29**), afforded again **57**. Two additional bioconjugates, [Ru([9]aneS_3)Cl(cppH-NT)]Cl (**61**) and [Ru([9]aneS_3)(cppH-NT)(PTA)]$^{2+}$ (**62**), were prepared by reaction of cppH-NT with the appropriate Ru(II) precursors.

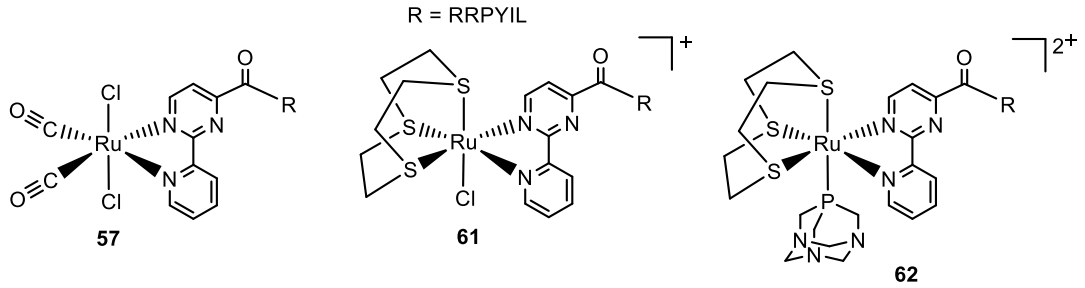

Figure 7.14. Schematic representation of the bioconjugates synthesized: *trans,cis*-$RuCl_2(CO)_2$(cppH-NT) (**57**), [Ru([9]aneS_3)Cl(cppH-NT)]$^+$ (**61**) and [Ru([9]aneS_3)(cppH-NT)(PTA)]$^{2+}$ (**62**). R is the peptide sequence: Arg-Arg-Pro-Tyr-Ile-Leu.

The NMR characterization in DMSO-d_6 revealed that, in accordance with HPLC and ESI-MS data, each bioconjugate is a single compound and of quite good purity. The cppH chemical shifts are in accordance with the presence of a single stereoisomer, in which the linker is bound to Ru(II) through N^p: Table 7.1 shows the ΔδH between the diagnostic chemical shits of the pyrimidine protons in the model complexes with cppH (both isomers when possible) and their corresponding bioconjugates, in D_2O (where in all species these resonances are overlapped). It results that the ΔδH

between *trans*,*cis*-$RuCl_2(CO)_2$(cppH-NT) (**57**) and **51** (N^p isomer) is 0.15 whereas it is 0.64 with respect to **52** (N^o isomer). This finding implies that, during the SPPS between **52** and NT, the cppH isomerizes from N^o to N^p. The behavior is similar also for the bionconjugate $[Ru([9]aneS_3)(cppH\text{-}NT)(PTA)]^{2+}$ (**62**) In the case of the model complex $[Ru([9]aneS_3)Cl(cppH\text{-}\kappa N^p)]^+$ (**60**), where only the N^p isomer was isolated, the ΔδH with respect to **61** is 0.04, suggesting also in this bioconjugate cppH is bonded through the *para* nitrogen atom.

Table 7.1. ^{1}H NMR chemical shifts of pyrimidine ring protons in D_2O for model complexes with cppH (both N^p and N^o linkage isomers when possible) and their corresponding bioconjugates with cppH-NT. In green there are the values of $\Delta\delta H(\delta_{bioconjugate} - \delta_{complex})$.

Complexes	H6	H5
trans,*cis*-$RuCl_2(CO)_2(cppH\text{-}\kappa N^p)$ (**51**)	9.64	8.22
trans,*cis*-$RuCl_2(CO)_2$(cppH-NT) (**57**)	9.79	8.38
	0.15	0.15
trans,*cis*-$RuCl_2(CO)_2(cppH\text{-}\kappa N^o)$ (**52**)	9.17	7.72
trans,*cis*-$RuCl_2(CO)_2$(cppH-NT) (**57**)	9.79	8.38
	0.62	0.66
$[Ru([9]aneS_3)Cl(cppH\text{-}\kappa N^p)]^+$ (**60**)	9.52	8.11
$[Ru([9]aneS_3)Cl(cppH\text{-}NT)]^+$ (**61**)	9.55	8.16
	0.03	0.05
$[Ru([9]aneS_3)(cppH\text{-}\kappa N^p)(PTA)]^{2+}$ (**50*N*^{p}**)	9.28	8.16
$[Ru([9]aneS_3)(cppH\text{-}NT)(PTA)]^{2+}$ (**62**)	9.42	8.26
	0.14	0.10
$[Ru([9]aneS_3)(cppH\text{-}\kappa N^o)(PTA)]^{2+}$ (**50*N*^{o}**)	9.13	7.64
$[Ru([9]aneS_3)(cppH\text{-}NT)(PTA)]^{2+}$ (**62**)	9.42	8.26
	0.29	0.62

However, when dissolved in D_2O each bioconjugate generates a mixture of two (**57**) or even three or four species (**61** and **62**), each one containing the cppH-NT fragment (and the PTA ligand in **62**). This finding is in contrast with the single peak observed in analytical HPLC. Each species is characterized by a set of very similar proton resonances in the cppH region, always consistent with cppH bound through N^p, thus

they are not linkage isomers. The NMR spectra were unaffected by an increase of the temperature up to 65°C, thus suggesting that the species are not in dynamic equilibrium, as well as by increasing the pD from ca. 3 to ca. 8. The presence of many species is observed only when the bioconjugates are dissolved in D_2O; this could be tentatively explained with some kind of strong intra- or inter-molecular interaction involving the Ru center and the peptide chain. Since mainly the resonances of the pyridine protons of cppH are affected, it is reasonable to hypothesize that this ring is involved in the above mentioned interactions. We notice that, contrary to **57**, in **61** and **62** Ru is a stereogenic center, thus – given the presence of chiral atoms on the peptide chain – diastereoisomeric derivatives may form. However, this observation does not explain the difference observed between DMSO-d_6 and D_2O, and why two species are observed in D_2O also for **57**. Unfortunately, the metal-bioconjugates are not typically characterized through NMR spectroscopy, and thus our data can be hardly compared with the literature.

Unluckily, none of the tested compounds – both precursors bioconjugates – showed any antiproliferative properties. Thus, the presence of the NT peptide proved to be ineffective for promoting cytotoxicity. Due to the lack of activity, no experiments for evaluating the ruthenium uptake by the cells were performed.

7.7 Bibliography

[1] a) A. F. A. Peacock, P. J. Sadler, *Chem. Asian J.*, **2008**, *3*, 1890 - 1899; b) C. Hartinger, P. J. Dyson, *Chem. Soc. Rev.*, **2009**, *38*, 391 - 401; c) T. R. John-son, B. E. Mann, J. E. Clark, R. Foresti, C. J. Green, R. Motterlini, *Angew. Chem. Int. Ed.*, **2003**, *42*, 3722 - 3729; d) C. S. Allardyce, A. Dorcier, C. Scolaro, P. J. Dyson, *Appl. Organomet. Chem.*, **2005**, *19*, 1 - 10; e) E. Meggers, *Curr. Opin. Chem. Biol.*, **2007**, *11*, 287 –-292; f) D. R. van Staveren, N. Metzler-Nolte, *Chem. Rev.*, **2004**, *104*, 5931 - 5986; g) M. Wenzel, A. I. Chiriac, A. Otto, D. Zweytick, C. May, C. Schumacher, R. Gust, H. B. Albada, M. Penkova, U. Kramer, R. Erd-mann, N. Metzler-Nolte, S. K. Straus, E. Bremer, D. Becher, H. Brçtz-Oes-terhelt, H.-G. Sahl, J. E. Bandow, *Proc. Natl. Acad. Sci. USA*, **2014**, *111*, 1409 - 1418; h) A. Gross, D. Habig, N. Metzler-Nolte, *ChemBioChem*, **2013**, *14*, 2472 - 2479; Metzler-Nolte, P. J. Dyson, *Organometallics*, **2012**, *31*, 5677 - 5685; i) G. Gasser, N. Metzler-Nolte, *Curr. Opin. Chem. Biol.*, **2012**, *16*, 84 - 91; j) G. Gasser, I. Ott, N. Metzler-Nolte, *J. Med. Chem.*, **2011**, *54*, 3 - 25.

[2] M. De Jong, W.A Breeman,W. H. Bakker, P. P. Kooij, B. F. Bernard, L. J. Hofland, T. J. Visser, A. Srinivasan, M. A.Schmidt, J. L. Erion, J. E. Bugaj, H. R. Mäcke, E. P. Krenning, *Cancer Res.*, **1998**, *58*, 437 - 441.

[3] a) J. C. Reubi, B. Waser, H. Friess, M. Buchler, J. Laissue, *Gut*, **1998**, *42*, 546 - 550; b) R. A. Ehlers, S. Kim, Y. Zhang, R. T. Ethridge, C. Murrilo, M. R. Hellmich, D. B. Evans, C. M. Townsend Jr., B. Mark Evers, *Ann. Surg.*, **2000**, *231*, 838 - 848.

[4] (a) B. M. Evers, M. Izukura, D. H. Chung, D. Parekh, K. Yoshinaga, G. H. Greeley, Jr., T. Uchida, C. M. Townsend, Jr., J. C. Thompson, *Gastroenterology*, **1992**, *103*, 86 - 91; (b) J. Elek, W. Pinzon, K. H. Park and R. Narayanan, *Anticancer Res.*, **2000**, *20*, 53 - 58; (c) S. Somai, A. Gompel, W. Rostene and P. Forgez, *Biochem. Biophys. Res. Commun.*, **2002**, *295*, 482 - 488; (d) L. Seethalakshmi, S. P. Mitra, P. R. Dobner, M. Menon and R. E. Carraway, *Prostate*, **1997**, *31*, 183 - 192; (e) I. Sehgal, S. Powers, B. Huntley, G. Powis, M. Pittelkow and N. J. Maihle, *Proc. Natl. Acad. Sci. U. S. A.*, **1994**, *91*, 4673 - 4677; (f) B. M. Evers, Z. Zhou, V. Dohlen, S. Rajaraman, J. C. Thompson and C. M. Townsend Jr., *Ann. Surg.*, **1996**, *223*, 461 - 470.

[5] M. Maschke, J. Grohmann, C. Nierhaus, M. Lieb, N. Metzler-Nolte, *ChemBioChem*, **2015**, *16*, 1333 - 1342.

[6] L. Gaviglio, A. Gross, N. Metzler-Nolte, Mauro Ravera, *Metallomics*, **2012**, *4*, 260 - 266.

[7] (*a*) T. Joshi, G. J. Barbante, P. S. Francis, C. F. Hogan, A. M. Bond, G. Gasser, L. Spiccia, *Inorg. Chem.*, **2012**, *51*, 3302 - 3315; (*b*) T. Joshi, G. Gasser, L. L. Martin, L. Spiccia, *RSC Adv.*, **2012**, *2*, 4703 - 4712; (*c*) T. Joshi. M. Patra, L. Spiccia, G. Gasser, *Artificial DNA: PNA & XNA*, **2013**, *4*, 11 - 18; (*d*) C. Bischof, T. Joshi, A. Dimri, L. Spiccia, U. Schatzschneider, *Inorg. Chem.*, **2013**, *52*, 9297 - 9308.

[8] T. Joshi, V. Pierroz, S. Ferrari, G. Gasser, *ChemMedChem,* **2014**, *9*, 1231 - 1237.

[9] a) B. J. Goodfellow, V. Félix, S. M. D. Pacheco, J. P. de Jesus, M. G. B. Drew, *Polyhedron*, **1997**, *16*, 393 - 401; b) J. Madureira, T. M. Santos, B. J. Goodfellow, M. Lucena, J. Pedrosa de Jesus, M. G. Santana-Marques, M. G. B. Drew, V. Felix, *Dalton Trans.*, **2000**, 4422 - 4431.

[10] E. Iengo, N. Demitri, G. Balducci, E. Alessio, *Dalton Trans.*, **2014**, *43*, 12160 - 12163.

CHAPTER 8

Photolabile complexes for light-triggered drug release

8.1 State of the art

In therapy, light-triggered treatments are appealing since – in principle – they can generate a drug with high spatial and temporal selectivity, resulting in a greater specificity of action. Such treatments require light-activated prodrugs that – ideally – are inactive and non-toxic in the dark, whereas they are locally activated in vivo upon irradiation with visible light. In this context, photodynamic therapy (PDT), a clinically approved treatment for some skin diseases, age-related macular degeneration and some cancers, is the most well-known application. PDT uses a photosensitizer (PS) at non-toxic concentrations that, in the most common type II mechanism, upon light-excitation catalytically generates singlet oxygen ($^1O_2$) or other highly cytotoxic ROS such as superoxide radical anions.[1] Another phototherapy approach is the so-called photoactivated chemotherapy (PACT) in which a kinetically inert and biologically non-active prodrug is irreversibly activated by irradiation with visible light that induces the cleavage of a photolabile protecting group.[2] The photoactivation process is also called photo-uncaging. Compared to PDT, PACT is a stoichiometric rather than catalytic process, but has the advantage of not depending on the presence of molecular oxygen. Thus, in principle, PACT agents are active also in hypoxic tumor tissues. In general, ideal PDT or PACT agents are water-soluble and resistant to photobleaching. In addition, they should be

activated within the phototherapeutic window (λ > 600 nm), where light is more penetrating into the tissues and less harmful.

By virtue of their peculiar light absorption properties and rich photoreactivity, d-block metal compounds are attracting rapidly increasing interest as potential PDT and PACT agents.[3,4,5,6,7] Among them, Ru(II) compounds are extensively investigated due to their superior photophysical and photochemical properties.[8,9,10] For example, even though most PDT photosensitizers used in clinic are based on porphyrin derivatives,[11] a Ru(II)-polypyridyl complex (TLD-1433) is undergoing a phase I clinical trial in Canada as PDT agent in patients with bladder cancer.[12,13]

A typical reaction that can occur in inorganic PACT agents is the photo-induced release of ligands from coordinatively-saturated and inert prodrugs. The most extensively investigated class of ruthenium PACT agents is that of polypyridyl complexes of the $[Ru(bpy)_3]^{2+}$ family that contain (at least) one sterically hindering diimine such as 6,6′-dimethyl-2,2′-bipyridine (dmbpy).[14] The strain induced by such a ligand in the coordination sphere promotes the light-induced population of low-lying dissociative metal-centered triplet excited states (^{3}MC) and consequently its release. Coordination and organometallic Ru(II) compounds in which visible light triggers the release of a single monodentate ligand have also been investigated.[15,16]

A careful design of the metal prodrug can lead to metal complexes with dual activity, i.e. photo-triggered ligand release (PACT) and singlet oxygen production (PDT).[17] The activation of coordinatively-saturated cytotoxic Ru complexes through the photo-deprotection of a ligand has been also been reported.[18]

In photo-labile metal complexes the focus can be on the activated metal fragment, that may bind to biomolecules such as DNA through its newly generated coordination sites,[14,19] or on the released ligand if itself a pharmacologically-active molecule,[20] or on the combined action of both.[21] In polypyridyl Ru(II) complexes the increased cytotoxicity is generally attributed to the intracellular formation of the bis-aqua complex *cis*-$[Ru(bpy)_2(OH_2)_2]^{2+}$ species. However, a very recent paper by

Bonnet and coworkers demonstrated that in the case of $[Ru(bpy)_2(dmbpy)]^{2+}$ the photo-released dmbpy ligand, rather than the ruthenium bis-aqua fragment, is responsible for the observed phototoxicity.[22]

In the recent past, the group where I did my Thesis reported that dicationic Ru(II) complexes, such as $[Ru([9]aneS_3)(bpy)(py)](PF_6)_2$ ([9]aneS$_3$ = 1,4,7-trithiacyclononane, bpy = 2,2′-bipyridine), are inert in the dark but rapidly and quantitatively release the pyridine ligand in aqueous solution when illuminated with blue light (λ = 420 nm).[23,24] Since the photo-generated aqua species $[Ru([9]aneS_3)(bpy)(OH_2)]^{2+}$ showed a substantial lack of cytotoxicity (against the MDA-MB-231 human mammary carcinoma cell line) we suggested that Ru(II) compounds of this type might be suitable PACT agents for the light-triggered release of coordinated drugs (*photo-uncaging*).[25]

8.2 Aim of the Chapter

This Chapter reports the work on the model complexes of the type $[Ru([9]aneS_3)(chel)(py)](Cl)_2$, where chel is a chelating diimine. The aim was that of establishing if complexes of this series, bearing a pharmacologically active molecule in the place of pyridine, can be realistically used within the photo-uncaging strategy. First, it was investigated if the absorption maxima in the visible spectrum and the photoinduced release of pyridine can be tuned by changing the nature of the diimine ligand. For this purpose, the model complexes with chel = 1,10-phenanthroline (phen), 4,7-diphenil-1,10-phenanthroline (4,7-Ph_2phen), dipyrido-[3,2-*a*:2′,3′-*c*]phenazine (dppz), 2,2′-biquinoline (bq) were prepared, fully characterized and investigated. The photo-induced release of py was qualitatively investigated by ^{1}H NMR and UV-vis spectroscopy. A particularly detailed experimental and theoretical investigation was performed on the bq derivative, for explaining its peculiar spectral features and photochemical behavior.

8.3 Diimine Ligands

The series of chelating diimines used in this Chapter, with different size and aromaticity, are shown in Figure 8.1. The 2,2′-biquinoline ligand, owing to its steric demand, is known to induce deformation in the pseudo-octahedral coordination sphere of Ru(II) complexes that can improve the photo-induced dissociation of ligands.[14b,15] In addition, its low-lying acceptor orbitals are expected to red-shift the ^{1}MLCT absorption maximum typical of diimine-Ru(II) complexes closer to the PDT window.[26,27]

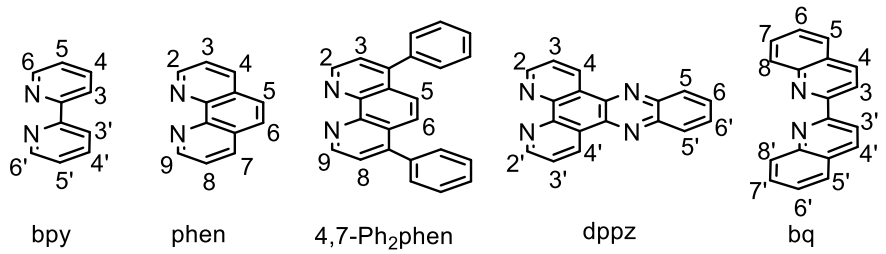

Figure 8.1. The diimine ligands used in this Chapter with proton labelling scheme for NMR purposes: 2,2′-bipyridine (bpy), 1,10-phenanthroline (phen), 4,7-diphenil-1,10-phenanthroline (4,7-Ph_2phen), dipyrido-[3,2-*a*:2′,3′-*c*]phenazine (dppz), 2,2′-biquinoline (bq).

8.4 Synthesis of the complexes

The Ru(II) compounds were prepared as chloride salts, rather than as PF_6 salts, for improving aqueous solubility. A two-step procedure was followed (Scheme 8.1).

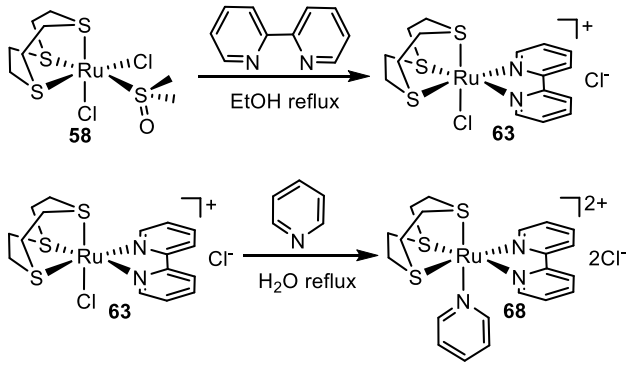

Scheme 8.1. Synthetic procedure for the [Ru([9]aneS_3)(chel)(py)]$(Cl)_2$ compounds **68** – **72**, exemplified in the case of chel = bpy.

In the first step, modified from the literature,[28] treatment of the [Ru([9]aneS$_3$)(dmso-S)Cl$_2$] precursor with a two-fold excess of chel in refluxing ethanol (3h) afforded the known mono-cationic intermediates of formula [Ru([9]aneS$_3$)(chel)Cl]Cl(chel = bpy (**63**), phen (**64**), 4,7-Ph$_2$phen (**65**), dppz (**66**)) in good isolated yields (65 – 85%). The insertion of bq was more difficult, possibly due also to the low solubility of the ligand in ethanol. A microwave assisted reaction in ethanol (140°C, 90 min) was preferred to prolonged reflux for obtaining [Ru([9]aneS$_3$)(bq)Cl]Cl (**67**) in good yield. All complexes, already reported in the literature either as Cl or PF_6 salts,[28,29] were characterized by NMR and UV-vis spectroscopy (Appendix, A8.8), and mass spectrometry. They are well soluble in ethanol, chloroform, DMSO, and – with the exception of **65** and **66** – also in water.

As clearly shown by ^{1}H NMR spectroscopy (Appendix, A8.1), in D$_2$O compounds **63** – **67** are in equilibrium – to different extents – with the corresponding aqua species [Ru([9]aneS$_3$)(chel)(OH$_2$)]$^{2+}$ (**63aq** – **67aq**). In **63aq** – **66aq** the aromatic resonances are slightly downfield shifted (ca. 0.1 pm or less) compared to those of the parent complex, and their relative intensity increases upon diluting the solution and decreases (or disappears altogether) upon adding an excess of NaCl. In the case of **67** a single set of resonances is observed in D$_2$O, suggesting that no significant equilibration with the aqua species **67aq** occurs at typical NMR concentrations. The resonances of **67aq** appear upon dilution, and in this case some of them are shifted upfield compared to those of **67** (e.g. the doublet of H8,8′ falls at 9.26 ppm in **67** and at 9.09 ppm in **67aq**). The resonances of [Ru([9]aneS$_3$)(dppz)Cl]$^+$ (**66**), that are sharp in CDCl$_3$, are rather broad and have concentration-dependent shifts in D$_2$O, most likely due to stacking interactions occurring in solution. Consistent with this hypothesis, they (and those of **66aq** as well) become sharper upon diluting the solution.

Treatment of intermediates **63** – **67** with a slight excess of pyridine in refluxing water afforded the corresponding dicationic complexes [Ru([9]aneS$_3$)(chel)(py)](Cl)$_2$

(chel = bpy (**68**), phen (**69**), 4,7-Ph_2phen (**70**), dppz (**71**), bq (**72**)) that, with the exception of **68** previously reported by us as PF_6 salt,[23] are described here for the first time. They were fully characterized as **63** – **67** above, and the single-crystal X-ray structures of **69** (Appendix, A8.10) and **72** (Figure 8.2) were also determined. In **72**, as in its precursor **67** and other bq octahedral complexes,[14b,15,28,29,30] the distortion in the geometry induced by the sterically demanding diimine is evident. In particular, the average plane of bq is remarkably tilted relative to the equatorial coordination plane (37.43 (4)°, with the "front" of the ligand pointing towards the axial py), whereas the twist about the C–C bond between the two quinolines (3.9(2)°) is negligible. The geometrical features of coordinated bq are similar also in the *trans*-$RuCl_2$(bq)$(CO)_2$ (**73**) complex (Figure 8.2), in which the other ligands are sterically undemanding and that we expressly prepared for the sake of comparison. Another major structural difference in **72** concerns the rotation of the py ligand about the Ru–N bond: in **72** py is ca. orthogonal compared to the other similar complexes (e.g. ca. 76° with respect to complex **68**), most likely for avoiding steric clashes between the *o*H atoms of py and H8,8′ of bq.

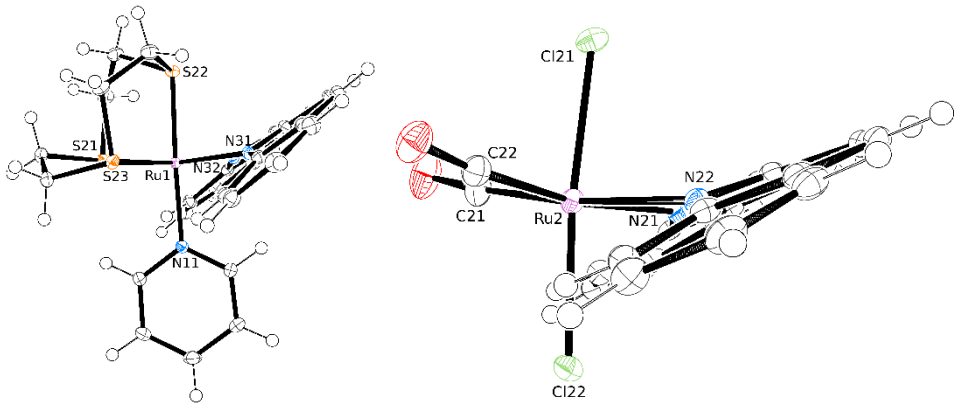

Figure 8.2. X-ray molecular structures (50% probability ellipsoids) of [Ru([9]aneS_3)(bq)(py)]$(Cl)_2$ (**72**) (left) and of *trans*-$RuCl_2$(bq)$(CO)_2$ (**73**) (right). The two chlorides and an ethanol crystallization molecule in **72** omitted for clarity. Only one of the two independent molecules of **73** present in the unit cell is shown. Coordination distances in ångström (Å): **72**: Ru1–N11 = 2.121(1), Ru1–N31 = 2.116(1), Ru1–N32 = 2.107(1), Ru1–S21 = 2.3221(3), Ru1–S22 = 2.3113(3), Ru1–S23 = 2.3178(5); **73**: Ru2–C21 = 1.899(2), Ru2–C22 = 1.897(2), Ru2–Cl21 = 2.3858(5), Ru2–Cl22 = 2.4179(5), Ru2–N21 = 2.139(2), Ru2–N22 = 2.136(2).

All dicationic complexes are fairly soluble in water. The ^{1}H NMR spectra of compounds **68** – **71** (Appendix, A8.2-A8.5) are unexceptional and, as for the corresponding precursors, consistent with the C_S symmetry of each complex cation. The most downfield resonance is that of the protons adjacent to the N atoms of the diimine ligand. The ^{1}H NMR spectrum of the bq compound **72** is treated in more detail below.

The electronic absorption spectra of **68** – **71** in the visible region are characterized by two bands of roughly comparable intensities (ε in the range 3000 - 6000 M^{-1} cm^{-1}), partially or completely overlapped, at 350 - 430 nm. The spectrum of **72**, instead, shows two rather sharp and more intense bands at 359 and 378 nm, whereas the lowest energy MLCT band – in good agreement with the expectations – is red-shifted, with an absorption maximum at nearly 500 nm (Figure 8.3).

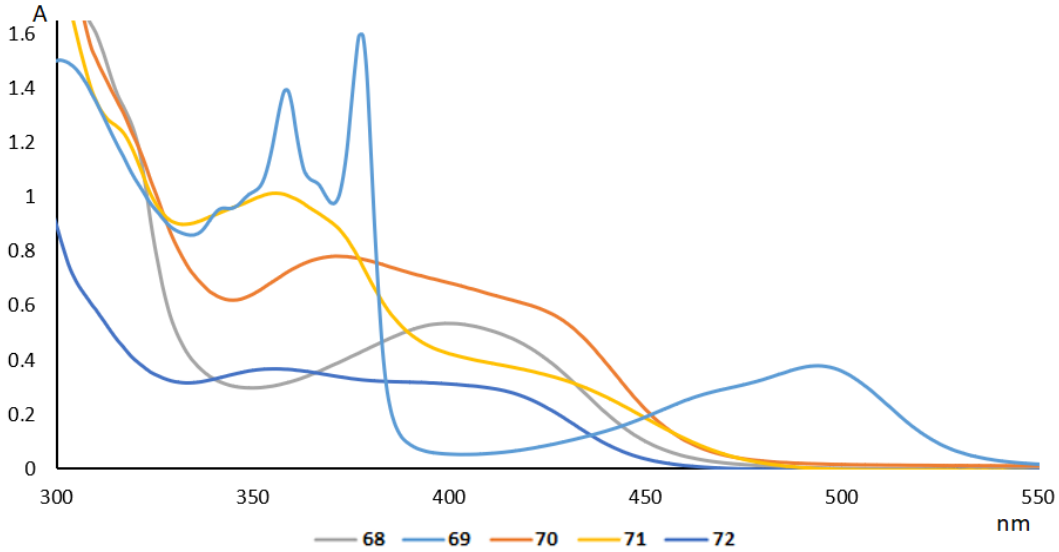

Figure 8.3. UV-vis spectra of compounds **68** – **72** (ca. in 0.1 mM H_2O) in the visible region.

8.4.1 The 2,2′-biquinoline complexes

In the ^{1}H NMR spectrum of 2,2′-biquinoline the most downfield resonance is that of H3,3′, followed by that of H4,4′. The *anti* conformation assumed by the two quinolines in the free ligand brings N′ close to H3 (and N to H3′), and the deshielding

of H3,3′ was attributed mainly to the electrostatic effect of the lone pairs (Figure 8.4).[31] When symmetrically bound to diamagnetic octahedral metal centers, such as in $Re(CO)_3(bq)Br$,[32] the proton NMR spectrum of bq undergoes remarkable changes: the doublet of H8,8′ becomes the most downfield signal ($\Delta\delta$ = 0.71 ppm), whereas that of H3,3′ is shifted to lower frequencies ($\Delta\delta$ = –0.50 ppm). Such variations are attributable to the conformational change of the ligand (from *anti* to *syn*) and to its coordination. Regretfully, in the other symmetrical Ru-bq compounds such as $[Ru(phen)_2(bq)](PF_6)_2$,[14b] $[Ru(\eta^6\text{-p-cymene})(bq)Cl](PF_6)$,[33] and $[Ru(bq)_3][(PF_6)_2$,[34] the proton NMR spectra were not assigned.

We found that, whereas the ^{1}H NMR spectrum of **67** is consistent with such features, the spectrum of **72** is quite different and more similar to that of the free ligand: the resonance of H8,8′ falls to lower frequencies than those of H3,3′ and H4,4′ (Figure 8.4).

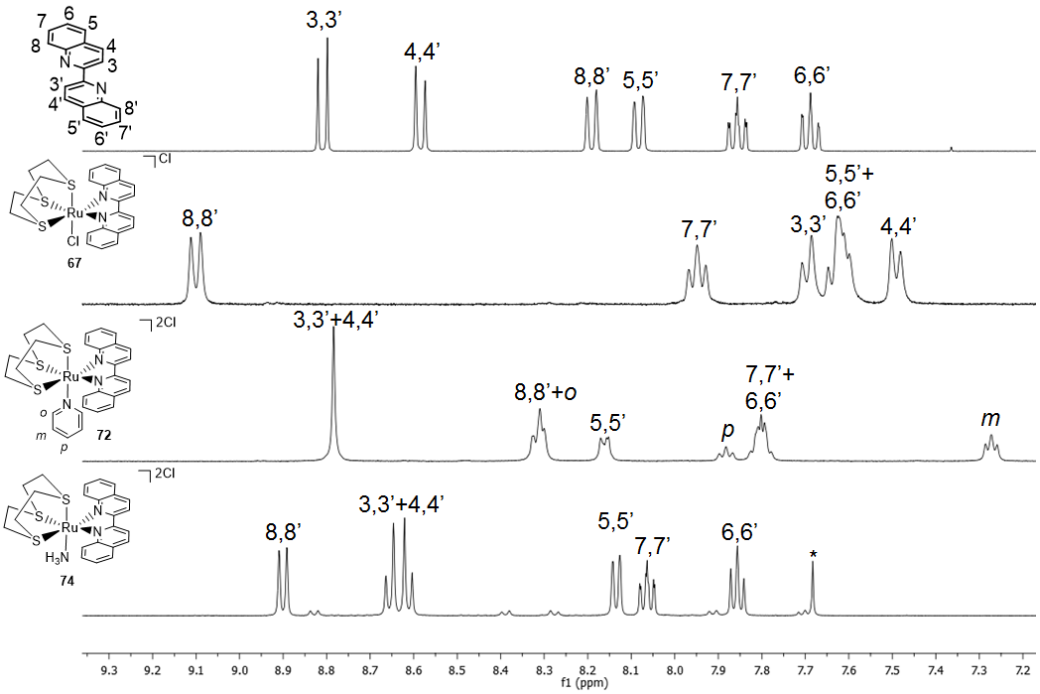

Figure 8.4. ^{1}H NMR spectrum (aromatic region) of, from top to bottom: 2,2′-biquinoline, $[Ru([9]aneS_3)(bq)Cl]Cl$ (**67**), $[Ru([9]aneS_3)(bq)(py)](Cl)_2$ (**72**), and $[Ru([9]aneS_3)(bq)(NH_3)](Cl)_2$ (**74**). The spectrum of bq is in DMSO-d_6, the others in D_2O. In the spectrum of **74** the asterisk indicates residual chloroform.

Since these changes in the chemical shifts of the bq protons between **67** and **72** could not be attributed to different conformational strains in the bq frame (see above), we came to the conclusion that the H8,8′ doublet in **72** is shifted upfield by the shielding cone of the adjacent axial pyridine. In order to confirm this hypothesis, that is consistent also with the orientation of py evidenced by the X-ray structure shown in Figure 8.2, we prepared the complex with NH_3 in the place of pyridine, i.e. $[Ru([9]aneS_3)(bq)(NH_3)](Cl)_2$ (**74**). Indeed, even though the structural features in **74** (Figure 8.5) are again similar to those of **67** and **72** (e.g. the tilt angle of bq is 38.89(3)°), the NMR spectral pattern of coordinated bq follows the "normal" order, and the H8,8′ doublet is again the most downfield resonance.[35]

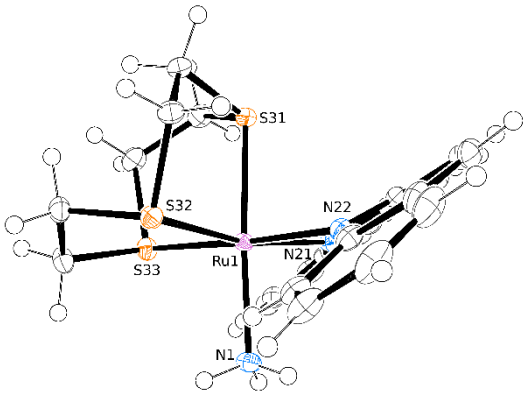

Figure 8.5. X-ray molecular structure (50% probability ellipsoids) of $[Ru([9]aneS_3)(bq)(NH_3)](Cl)_2$ (**74**). The two chlorides and a methanol crystallization molecule omitted for clarity. Coordination distances in ångström (Å): Ru1–N1 = 2.164(1), Ru1–N21 = 2.135(1), Ru1–N22 = 2.100(1), Ru1–S31 = 2.3121(4), Ru1–S32 = 2.3341(4), Ru1–S33 = 2.3277(3).

8.5 Photo-induced release of ligands

In the dark, compounds **68** – **72** are stable in D_2O (3 mM solutions) for at least 24h at ambient temperature, no changes in the NMR spectra were observed.

The group where I did my Thesis recently demonstrated that, when irradiated with blue light at 420 nm, $[Ru([9]aneS_3)(bpy)(py)](PF_6)_2$ rapidly and quantitatively releases the coordinated pyridine.[23]

Compounds **68** – **71** have a similar behavior: when irradiated with blue light (LED, λ = 470 nm, 40 mW) they release the coordinated pyridine at comparable rates and extents, generating selectively the corresponding aqua species (**63aq** – **66aq**) in equilibrium with the chlorido species (**63** – **66**) (Scheme 8.2). No other reaction occurs.

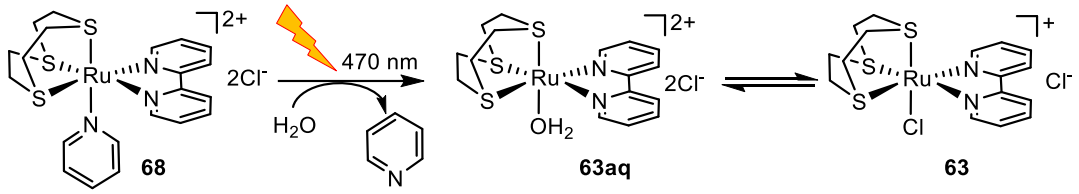

Scheme 8.2. Photo-dissociation of pyridine from compounds **68** – **71**, exemplified in the case of chel = bpy.

The photo-reactions were performed in D_2O and quantitatively monitored by ^1H NMR spectroscopy. An example is reported in Figure 8.6. In the case of the dppz complex **71**, the resonances of the photo-generated aqua and chlorido species – as mentioned above – are rather broad; the sharp pyridine signals allowed reliable integration to be performed. Table 8.1 reports the percentage amount of photo-released pyridine as a function of the irradiation time.

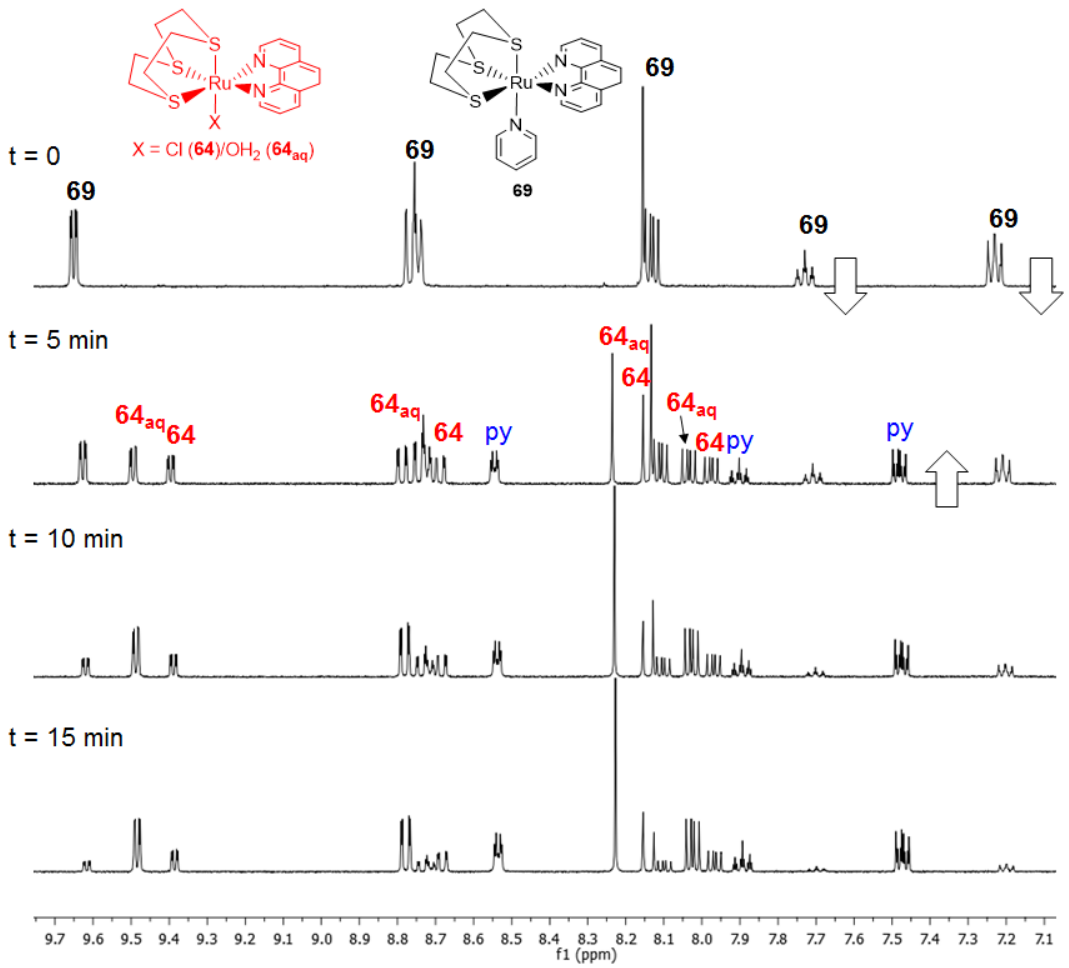

Figure 8.6. Photo-induced dissociation of pyridine from [Ru([9]aneS$_3$)(phen)(py)](Cl)$_2$ (**69**) monitored as a function of the irradiation time (λ = 470 nm, 40 mW) by ^{1}H NMR spectroscopy in D_2O. The positive charges of the complexes are omitted.

Table 8.1. Extent of photo-released pyridine as a function of the irradiation time (LED, λ = 470 nm, 40 mW).

complex	diimine ligand	5 min	10 min	15 min	30 min
68	bpy	80,0%	92,8%	93,3%	98,8%
69	phen	60,0%	78,2%	87,8%	96,6%
70	4,7- Ph$_2$phen	75,0%	78,8%	81,4%	95,4%
71	dppz	50,0%	75,0%	85,0%	97,7%

In summary, the photo-dissociation of py is almost complete after 30 min of illumination and the bpy complex **68** is the fastest one, even though it has the smallest

absorption coefficient at 470 nm. We found that the dppz complex **71**, that has a very weak absorption at ca. 540 nm (Appendix, A8.9), is still photoactive when irradiated with green light at 530 nm, even though the photo-release of pyridine is slower: 33% after 15 min (λ = 530 nm, 30 mW) compared to 78% when irradiation was performed at 470 nm with the same power.

The behavior of the bq complex **72** upon illumination is quite different and photo-dissociation of both py and bq in ca. equal amounts occurs. In general, contrary to the expectations, the complex is more photo-stable compared to **68** – **71**: after 2h of illumination at 470 nm (40 mW) in D_2O ca. 25% of **72** is still present in solution. The interpretation of the NMR spectra (Figure 8.7) was made more difficult by the following facts: *i*) 2,2′-biquinoline is insoluble in water, thus the resonances of photo-released bq cannot be seen; *ii*) the chemical shifts of the bq resonances in both **67** and **67aq**, i.e. the Ru complexes obtained upon photo-release of py, as well as the ratio between the two species, are concentration-dependent; *iii*) (most of) the released py binds to the $\{Ru([9]aneS_3)(py)\}^{2+}$ fragment (thus the resonances of free py are not clearly seen), affording the $[Ru([9]aneS_3)(py)_2(OH_2)]^{2+}$ complex cation that, in addition, is in equilibrium with $[Ru([9]aneS_3)(py)_2Cl]^{+}$. The resonances of these latter species were unambiguously identified: for this purpose we made [Ru([9]aneS3)(py)$_2$Cl]Cl (**75**), that in aqueous solution equilibrates with $[Ru([9]aneS_3)(py)_2(OH_2)]^{2+}$ (**75aq**). When a D_2O solution of **72** was irradiated with green light (30 mW) at 530 nm a similar behavior was observed, but the photo-release of both bq and py is slower. A similar photochemistry was observed when the irradiation of **72** was performed in DMSO-d_6 where the resonances of free bq (that is soluble) could be observed: in this medium the photo-induced dissociation of bq prevails over that of py (Appendix, A8.7).

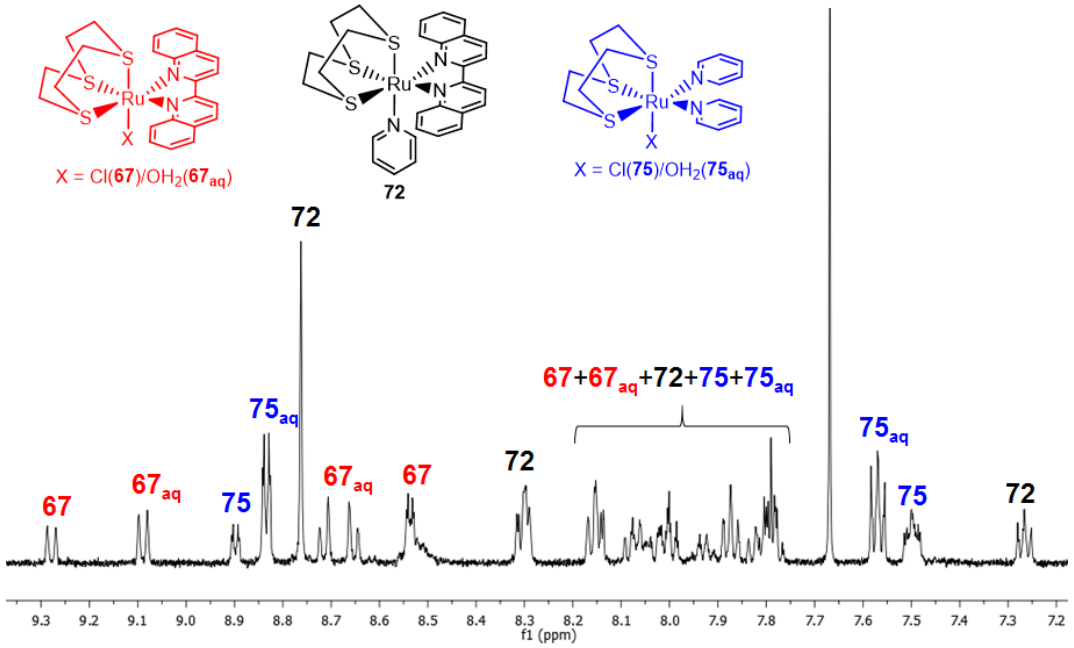

Figure 8.7. ^{1}H NMR spectrum of the reaction mixture obtained upon irradiation (λ = 470 nm, 40 mW, 180 min) of a D_2O solution of [Ru([9]aneS_3)(bq)(py)]$(Cl)_2$ (**72**). The positive charges of the complexes are omitted.

Although parallel photo-release of two different ligands has not been often described, it has been observed recently in the complex [Ru(bpy)(dmbpy)(L-proline)]PF_6, in which substitution of both dmbpy and L-proline occurred upon illumination.[36]

8.6 Theoretical calculations[c]

Intrigued by the remarkably different photochemical behavior of the biquinoline complex **72**, we performed a series of theoretical calculations on it and on the corresponding bpy complex **68**, taken as model for the other diimine compounds **69**–**71**. Structure-wise, complex **10** has two main geometrical differences compared to the canonical features of **68**, that are likely to be related to its different photochemistry: the tilted geometry of bq and the orientation of py (see above).

[c] Calculations were done by Dr. Gabriele Balducci.

First of all, our computational protocol (DFT with plane wave basis set, pseudopotentials and periodic boundary conditions) was tested on compound **68** that had been previously investigated using a different computational approach (DFT with localized basis functions).[23] The results obtained in terms of optimized geometry, calculated MOs, and electronic transitions were in excellent agreement with those reported in the literature, thus confirming the reliability of our protocol. Next, the calculations were extended to **72**.

Figure 8.8 shows the density of states and its projection onto selected atomic orbitals of the Ru, py and bq or bpy ligands for complexes **72** and **68** in the ground state configuration.

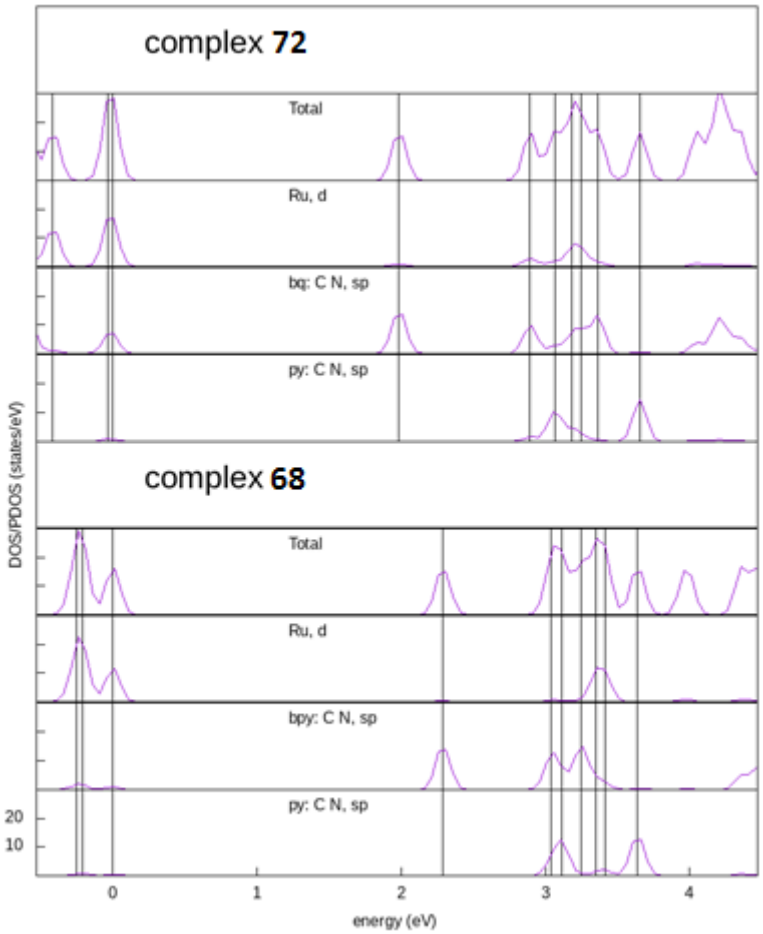

Figure 8.8. Density of states (DOS) and its projection onto selected atomic orbitals for complexes **72** (top) and **68** (bottom). Vertical lines indicate the energy of the molecular orbitals in the range from

HOMO–2 to LUMO+6. Plots have been aligned so that the energy of the HOMO's for the two complexes is 0.0 eV.

Consistent with the red-shifted absorption band in the UV-vis spectrum, and with the general features expected for bq complexes (i.e. stabilized bq π* orbitals relative to those of bpy),[14b,15] the HOMO−LUMO energy gap in **72** is smaller than in **68** (2.01 vs 2.32 eV). TDDFT calculations well reproduced the experimental absorption spectrum of both complexes (Figure 8.9 and Appendix, A8.11) and allowed us to assign also the character of each band (Appendix, Table A8.1),[37] thus confirming that the lowest energy transition has a ca. 85 – 90% HOMO → LUMO component.[23] In both complexes the LUMO is almost coincident with a π* MO of the diimine ligand (Appendix, A8.12). However, we notice that whereas in the bpy complex the three frontier occupied orbitals – HOMO, HOMO−1 and HOMO−2 (Appendix, A8.12) – have an almost exclusive metal-centered character, i.e. are coincident with the filled d orbitals of Ru(II), in **10** the HOMO and HOMO−1 get an appreciable contribution from the atomic orbitals of C and N atoms of the biquinoline ligand (see also Figure 8.8). We argue that the tilted orientation of bq in **10** is responsible for the mixing of diimine π orbitals with the filled d orbitals of Ru(II). Therefore, the lowest energy electronic transition can be safely labeled as a pure MLCT in **68**, whereas it has a π − π*component in **72**.

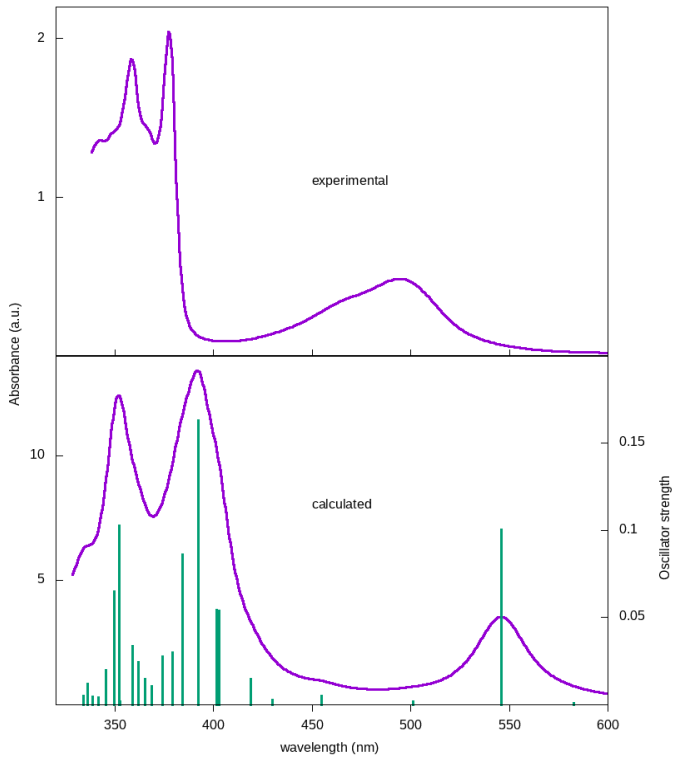

Figure 8.9. Experimental (top) and calculated (with the "turbo_lanczos" program, bottom) absorption spectra for complex **72**. The vertical bars in the simulated spectrum are the calculated transitions (with the "turbo_davidson" code), with height equal to the oscillator strength.

Consistent with what previously observed, in **68** the LUMO+4 and LUMO+5 MOs have a strong metal d-antibonding component; in addition, they have a significant σ-antibonding character towards the bpy and – above all – the pyridine ligands (Figure 8.10). Thus, the light-induced population of such orbitals is presumably responsible for the photo-dissociation of py. Conversely, in **72** the orbitals with the most relevant d* component are the LUMO+3 and LUMO+4, and they have a relevant bq – rather than py – contribution (Figure 8.10). This finding is consistent with what established for Ru(II)-polypyridyl complexes that contain bq, in which distortion is known to lower the energy of a dissociative metal-centred state.[14b,15] In addition, whereas LUMO+4 has a significant σ-antibonding character towards bq, in both the LUMO+3 and LUMO+4 the antibonding character towards py is mainly of π symmetry (i.e. involving p atomic orbitals normal to the py plane). This finding, i.e.

the increase of π back-bonding from the filled metal orbital to the π* orbitals of py, is most likely attributable to the different orientation of py in the bq complex and might account for the less-pronounced light-induced dissociation of pyridine in **72**.

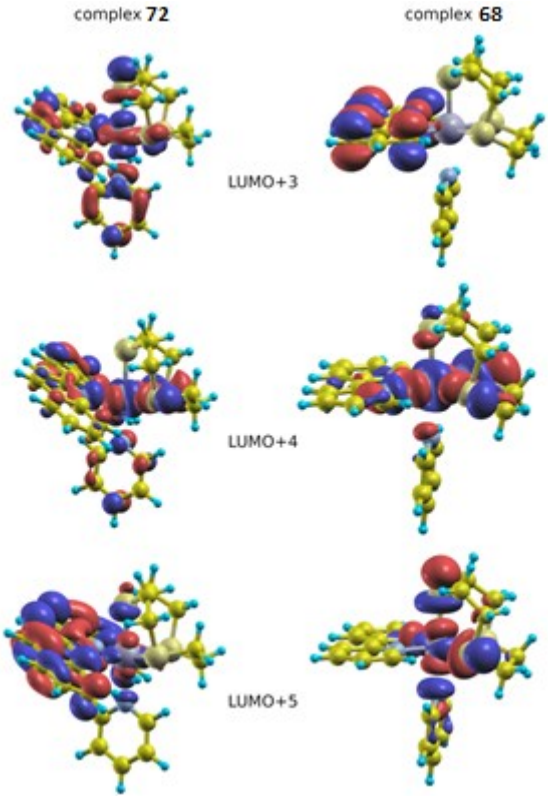

Figure 8.10. Selected virtual molecular orbitals for **68** (right) and **72** (left) in the singlet ground state.

The other significant photochemical difference between the two complexes concerns the photo-induced dissociation of the chelating diimine, that occurs in **72** (bq) but not in **68** (bpy). We observe that the binding of bq is arguably weaker compared to that of bpy because of its tilted coordination geometry that leads to a smaller overlap in the bonding orbitals.

In conclusion, contrary to what has been found by Turro and coworkers for *mer*-$[Ru(tpy)(chel)(py)]^{2+}$ species (chel = bpy or bq), where the distortions induced by the bulky bq led to an increased photo-induced release of py compared to bpy,[15] in this case – mainly because of the *facial*, rather than *meridional*, geometry of the

complex – the distortions led to the preferential photo-dissociation of biquinoline itself.[38]

Although triplet states are generally thought to be responsible for the photochemistry of ruthenium complexes via facile intersystem crossing, we are confident that our analysis based on singlet ground and excited states captures the essential features of complex **72**. In fact, the already reported study on complex **68** has shown that triplet excited states trace the character and ground state orbital composition of the singlet counterparts.[23]

8.7 Conclusions

The photo-triggered release of pyridine from the series of water-soluble model complexes [Ru([9]aneS$_3$)(chel)(py)](Cl)$_2$ was thoroughly investigated as a function of the nature of thechelating diimine (chel = 2,2′-bipyridine (bpy, **68**) 1,10-phenanthroline (phen, **69**), 4,7-diphenil-1,10-phenanthroline (Ph$_2$phen, **70**), dipyrido-[3,2-*a*:2′,3′-*c*]phenazine (dppz, **71**), 2,2′-biquinoline (bq, **72**)) (Figure 8.11). In **68** – **72**, owing to the face-capping 1,4,7-trithiacyclononane ligand ([9]aneS$_3$), the leaving ligand (py) and the diimine have a facial arrangement. Our aim is that of establishing if this type of complexes in the future might be realistically used in photoactivated chemotherapy (PACT).

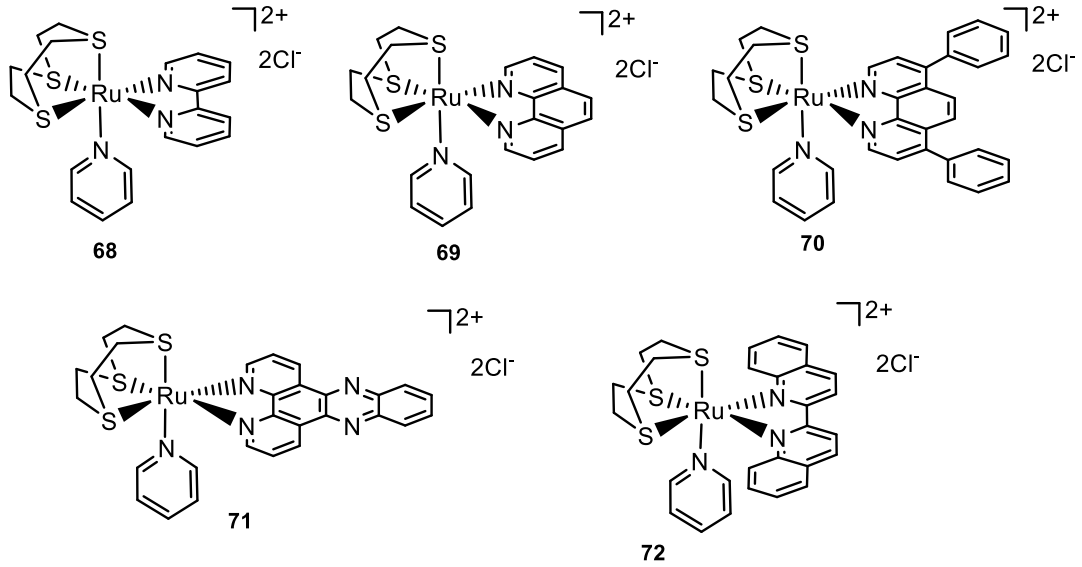

Figure 8.11. Schematic representation of complexes studied for the photo-triggered release of pyridine.

We found that compounds **68** – **71** behave quite homogeneously and their photochemical behavior is not particularly affected by the nature of the diimine: when irradiated with light at 470 nm, they rapidly and quantitatively release the coordinated pyridine, generating selectively the corresponding aqua species [Ru([9]aneS$_3$)(chel)(OH$_2$)]$^{2+}$ (**63aq** – **66aq**). Even though **68** was found to be non-

phototoxic against the MDA-MB-231 human mammary carcinoma cells,[25] in the future we plan to investigate the phototoxicity also of **69** – **71**, as well as the $^1O_2$ production on selected compounds. The more lipophilic compounds in the series might be expected to have better accumulation in cancer cells and potentially show higher phototoxicity. We also argue that upon illumination the extended aromatic dppz ligand could generate singlet oxygen, thus giving to complex **71** two mechanisms of phototoxicity.

In addition, we plan to bind the anticancer drug CHS-828 (Figure 8.12) in the place of pyridine on the {Ru([9]aneS$_3$)(chel)} scaffold,[39] and investigate its photo-triggered release also in terms of in vitro phototoxicity against cancer cell lines. The photo-uncaging of anticancer drugs is a PACT strategy that does not require the concomitant formation of a cytotoxic metal fragment.

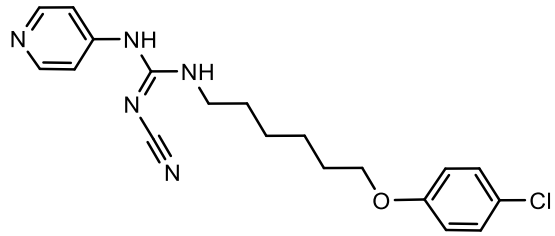

Figure 8.12. Schematic structure of the anticancer drug CHS-828.

Complex **72** turned out to behave quite differently from to the others in the series. As expected, the low-lying acceptor orbitals of bq induce a red-shift in the MLCT absorption maximum of the complex from ca. 430 to ca. 500 nm. However, contrary to the expectations, complex **10** turned out to be more photo-stable compared to **68** – **71** and – upon prolonged illumination with blue light – photo-dissociation of both py and bq, in ca. equal amounts, occurs. The single crystal X-ray structure of **72** showed that in this complex, besides the expected distortion of coordinated bq due to its steric demand (a >35° tilt relative to the equatorial coordination plane), the orientation of py is ca. orthogonal compared to that found in **68** and **69**. A detailed theoretical investigation performed on **72** (and on **68** for comparison), showed that

the biquinoline-induced geometrical distortions lead to differences in the nature of the excited states that might account for the different photochemical behavior of this complex.

In view of the potential investigation of these complexes as PACT agents, we observe that – unlike the rest of the series – upon irradiation with visible light complex **72** could generate *in vivo* a Ru(II)-aqua species with two or even three coordination sites that is expected to be more reactive, and thus more cytotoxic, compared to the mono-aqua species generated from **68** – **71** (e.g. it might be capable of cross linking DNA). Consistent with this hypothesis, we found that the $[Ru([9]aneS_3)(py)(OH_2)_2]^{2+}$ species binds rapidly the small amount of photo-released pyridine.

Finally, in the future it would be interesting to make the 6,6′-dimethyl-2,2′-bipyridine (dmbpy) analogue of these complexes. It might be expected to behave similarly to the bq complex and the photo-released dmbpy could induce cell death according to what shown by Bonnet and coworkers.[22]

8.8 Bibliography

[1] a) D. E. J. G. J. Dolmans, D. Fukumura, R. K. Jain, *Nat. Rev. Cancer*, **2003**, *3*, 380 - 387; b) A. Juzeniene, Q. Peng, J. Moan, *Photochem. Photobiol. Sci.*, **2007**, *6*, 1234 - 1245; c) T. Debele, S. Peng, H.-C. Tsai, *Int. J. Mol. Sci.*, **2015**, *16*, 22094 - 22136.

[2] G. Mayer, A. Heckel, *Angew. Chem. Int. Ed.*, **2006**, *45*, 4900 - 4921.

[3] K. Szaciłowski, W. Macyk, A. Drzewiecka-Matuszek, M. Brindell, G. Stochel, *Chem. Rev.*, **2005**, *105*, 2647 - 2694.

[4] a) N. J. Farrer, L. Salassa, P. J. Sadler, *Dalton Trans.*, **2009**, 10690 - 10701; b) N. A. Smith, P. J. Sadler, *Phil. Trans. R. Soc. A*, **2013**, *371*, 20120519.

[5] U. Schatzschneider, *Eur. J. Inorg. Chem.*, **2010**, 1451 - 1467.

[6] E. Ruggiero, S. Alonso-de Castro, A. Habtemariam, L. Salassa, *Struct. Bond.*, **2015**, *165*, 69 - 108.

[7] J. D. Knoll, C. Turro, *Coord. Chem. Rev.*, **2015**, *282-283*, 110 - 126.

[8] H. Yin, M. Stephenson, J. Gibson, E. Sampson, G. Shi, T. Sainuddin, S. Monro, S. A. McFarland, *Inorg. Chem.*, **2014**, *53*, 4548 - 4559.

[9] C. Mari, V. Pierroz, S. Ferrari, G. Gasser, *Chem. Sci.*, **2015**, *6*, 2660 - 2686.

[10] V. H. S. van Rixel, B. Siewert, S. L. Hopkins, S. H. C. Askes, A. Busemann, M. A. Sieglerb, S. Bonnet, *Chem. Sci.*, **2016**, *7*, 4922 - 4929.

[11] a) M. Ethirajan, Y. Chen, P. Joshi, R. K. Pandey, *Chem. Soc. Rev.*, **2011**, *40*, 340 - 362; b) A. B. Ormond, H. S. Freeman, *Materials*, **2013**, *6*, 817 - 840.

[12] http://theralase.com/pressrelease/health-canada-approves-clinical-trial-application-anti-cancer-drug/. http://theralase.com/pressrelease/theralase-research-published-international-peer-reviewed-journal/.

[13] a) G. Shi, S. Monro, R. Hennigar, J. Colpitts, J. Fong, K. Kasimova, H. Yin, R. DeCoste, C. Spencer, L. Chamberlain, A. Mandel, L. Lilge and S. A. McFarland, *Coord. Chem. Rev.*, **2015**, *282 - 283*, 127 - 138; b) J. Fong, K. Kasimova, Y. Arenas, P. Kaspler, S. Lazic, A. Mandel, L. Lilge, *Photochem. Photobiol. Sci.*, **2015**, *14*,

2014 - 2023; c) P. Kaspler, S. Lazic, S. Forward, Y. Arenas, A. Mandela, L. Lilge, *Photochem. Photobiol. Sci.*, **2016**, *15*, 481 - 495.

[14] a) B. S. Howerton, D. K. Heidary, E. C. Glazer, *J. Am. Chem. Soc.*, **2012**, *134*, 8324 - 8327; b) E. Wachter, D. K. Heidary, B. S. Howerton, S. Parkin, E. C. Glazer, *Chem. Commun.*, **2012**, *48*, 9649 - 9651; c) D. Havrylyuk, D. K. Heidary, L. Nease, S. Parkin, E. C. Glazer, *Eur. J. Inorg. Chem.*, **2017**, 1687 - 1694.

[15] J. D. Knoll, B. A. Albani, C. B. Durr, C. Turro, *J. Phys. Chem. A*, **2014**, *118*, 10603 - 10610.

[16] a) S. Betanzos-Lara, L. Salassa, A. Habtemariam, P. J. Sadler, *Chem. Commun.*, **2009**, 6622 - 6624; b) S. Betanzos-Lara, L. Salassa, A. Habtemariam, O. Novakova, A. M. Pizarro, G. J. Clarkson, B. Liskova, V. Brabec, P. J. Sadler, *Organometallics*, **2012**, *31*, 3466 - 3479.

[17] a) M. A. Sgambellone, A. David, R. N. Garner, K. R. Dunbar, C. Turro, *J. Am. Chem. Soc.*, **2013**, *135*, 11274 - 11282; b) Y. Chen, W. Lei, G. Jiang, Y. Hou, C. Li, B. Zhang, Q. Zhou, X. Wang, *Dalton Trans.*, **2014**, *43*, 15375 - 15384; c) J. D. Knoll, B. A. Albani, C. Turro, *Acc. Chem. Res*., **2015**, *48*, 2280 - 2287; d) T. Sainuddin, M. Pinto, H. Yin, M. Hetu, J. Colpitts, S. A. McFarland, *J. Inorg. Biochem.*, **2016**, *158*, 45 - 54.

[18] T. Joshi, V. Pierroz, C. Mari, L. Gemperle, S. Ferrari, G. Gasser, *Angew. Chem. Int. Ed.*, **2014**, *53*, 2960 - 2963; b) C. Mari, V. Pierroz, A. Leonidova, S. Ferrari, G. Gasser, *Eur. J. Inorg. Chem.*, **2015**, 3879 - 3891.

[19] a) A. N. Hidayatullah, E. Wachter, D. K. Heidary, S. Parkin, E. C. Glazer, *Inorg. Chem.*, **2014**, *53*, 10030 - 10032; b) K. T. Hufziger, F. S. Thowfeik, D. J. Charboneau, I. Nieto, W. G. Dougherty, W. S. Kassel, T. J. Dudley, E. J. Merino, E. T. Papish, J. J. Paul, *J. Inorg. Biochem.*, **2014**, *130*, 103 - 111.

[20] a) T. Respondek, R. N. Garner, M. K. Herroon, I. Podgorski, C. Turro, J. J. Kodanko, *J. Am. Chem. Soc.*, **2011**, *133*, 17164 - 17167; b) R. Sharma, J. D. Knoll, P. D. Martin, I. Podgorski, C. Turro, J. J. Kodanko, *Inorg. Chem*., **2014**, *53*, 3272 - 3274; c) N. Karaoun, A. K. Renfrew, *Chem. Commun.*, **2015**, *51*, 14038 - 14041; H. Chan, J. B. Ghrayche, J. Wei, A. Renfrew, *Eur. J. Inorg. Chem.*, **2017**, 1679 - 1686.

[21] A. Zamora, C. A. Denning, D. K. Heidary, E. Wachter, L. A. Nease, J. Ruiz, E. C. Glazer, *Dalton Trans.*, **2017**, *46*, 2165 - 2173.

[22] J. A. Cuello-Garibo, M. S. Meijer, S. Bonnet, *Chem. Commun.*, **2017**, *53*, 6768 - 6771.

[23] G. Ragazzon, I. Bratsos, E. Alessio, L. Salassa, A. Habtemariam, R. J. McQuitty, G. J. Clarkson, P. J. Sadler, *Inorg. Chim. Acta*, **2012**, *393*, 230 - 238.

[24] The photo-triggered ligand release is more efficient compared to the corresponding photoactivable organometallic compounds of the type [Ru(η^6-arene)(N-N)(py)]$(PF_6)_2$ previously developed by Sadler and co-workers (ref 16).

[25] I. Finazzi, I. Bratsos, T. Gianferrara, A. Bergamo, N. Demitri, G. Balducci, E. Alessio, *Eur. J. Inorg. Chem.*, **2013**, 4743 - 4753.

[26] F. Barigelletti, A. Juris, V. Balzani, P. Belser, A. von Zelewsky, *Inorg. Chem.*, **1983**, *22*, 3335 - 3339.

[27] E. Baranoff, J.-P. Collin, J. Furusho, Y. Furusho, A.-C. Laemmel, J.-P. Sauvage, *Inorg. Chem.*, **2002**, *41*, 1215 - 1222.

[28] B. J. Goodfellow, V. Félix, S. M. D. Pacheco, J. P. de Jesus, M. G. B. Drew, *Polyhedron*, **1997**, *16*, 393 - 401.

[29] J. Madureira, T. M. Santos, B. J. Goodfellow, M. Lucena, J. P. de Jesus, M. G. Santana-Marques, M. G. B. Drew, V. Félix, *J. Chem. Soc., Dalton Trans.*, **2000**, 4422 - 4431.

[30] B. Machura, R. Kruszynski, *Polyhedron* **2007**, *26*, 3336 - 3342.

[31] a) J. A. G. Drake, D. W. Jones, *Org. Magn. Res.*, **1982**, *18*, 42 - 44; b) A. G. Osborne, R. Green, I. H. Sadler, D. Reed, *Magn. Res. Chem.*, **1989**, *27*, 4 - 12.

[32] S. A. Moya, J. Guerrero, R. Pastene, R. Schmidt, R. Sariego, R. Sartori, J. Sanz-Aparicio, I. Fonseca, M. Martinez-Ripoll, *Inorg. Chem.*, **1994**, *33*, 2341 - 2346.

[33] R. Lalrempuia, M. R. Kollipara, *Polyhedron,* **2003**, *22*, 3155 - 3160.

[34] P. Belser, A. von Zelewsky, *Helv. Chim. Acta*, **1980**, *63*, 1675 - 1702.

[35] We found that in the ^{1}H NMR spectra of complexes **67**, **72**, and **74**, the chemical shifts of the bq protons are remarkably affected by the nature of the solvent (e.g. DMSO-d_6 vs D_2O), even though the sequence order is maintained (Appendix, A8.6).

[36] J. A. Cuello-Garibo, E. Perez-Gallent, L. van der Boon, M. A. Siegler, S. Bonnet, *Inorg. Chem.*, **2017**, *56*, 4818 - 4828.

[37] The calculated UV-vis spectra of complexes **67** and **72** reproduce quite well the general spectral features, even though the absorption bands are red-shifted of ca. 60 nm compared to experimental spectra. Calculations were performed in the vacuo and this might be one of the reasons for this general shift. To be noted that in ref. 23 the singlet excited state transitions for complex **67**, calculated with a different approach, had a numerically similar shift – but in the opposite direction – with respect to the experimental transitions.

[38] The photo-release of bq from **72** is not attributable to the longer irradiation times: it occurs (in low amounts) also for short irradiation times and increases with the irradiation time, i.e. it is not a photo-bleaching of the complex.

[39] P. Hovstadius, R. Larsson, E. Jonsson, T. Skov, A.-M. Kissmeyer, K. Krasilnikoff, J. Bergh, M. O. Karlsson, A. Lönnebo, J. Ahlgren, *Clin. Cancer Res.*, **2002**, *8*, 2843 - 2850.

CHAPTER 9

Experimental Section

9.1 Materials

All chemicals were purchased from Sigma-Aldrich and used as received. Solvents were of reagent grade. The precursors *trans*-$RuCl_2(PTA)_4$ (**1**)[1] *cis*-$RuCl_2(dmso)_4$ (**8**)[2] *trans*-$RuCl_2(dmso\text{-}S)_4$ (**9**),[2] *cis,fac*-$[RuCl(dmso\text{-}O)_2(dmso\text{-}S)_3](PF_6)$ (**20**),[3] *fac*-$[Ru(dmso\text{-}O)_3(dmso\text{-}S)_3](CF_3SO_3)_2$ (**21**),[4] *cis,cis,cis*-$RuCl_2(CO)_2(dmso\text{-}O)_2$ (**28**),[5] *trans,cis,cis*-$RuCl_2(CO)_2(dmso\text{-}O)_2$ (**29**),[5] $Ru([9]aneS_3)Cl_2(dmso)$ (**58**),[6] $[Ru([9]aneS_3)Cl(PTA)]Cl$ (**59**),[7] $[(dmso)_2H]$*trans*-$[RuCl_4(dmso\text{-}S)_2]$[8] and the ligands bpyAc,[9] mpp[10] and cppH[10] were synthesized as described in the literature.

9.2 Instrumental methods

Mono- (^1H (400 or 500 MHz), ^{13}C (125.7 MHz), ^{31}P (161 or 202 MHz)) and bi-dimensional (^1H-^1H COSY, ^1H-^{13}C HSQC, ^{31}P-^{31}P COSY and ^1H-^{31}P HMBC, ^1H-^1H NOESY) NMR spectra were recorded at room temperature on a JEOL Eclipse 400FT, on a Varian 400 or on a Varian 500 spectrometer. ^1H and ^{13}C chemical shifts were referenced to the peak of residual non-deuterated solvent (δ = 7.26 and 77.16 for $CDCl_3$, 2.50 and for 39.52 DMSO-d_6) or were measured relative to the internal standard DSS (δ = 0.00) for D_2O. ^{31}P chemical shifts were measured relative to external 85% H_3PO_4 at 0.00 ppm. ^1H-^{31}P HMBC were recorded using the standard sequence HMBCAD on the Varian 500 spectrometer with a coupling constant (^2J) of 5-10 Hz.

The ^{15}N NMR spectra (50.65 MHx) were recorded using the standard ^1H-^{15}N gHMBC sequence of the 500 MHz Varian spectrometer. Multiple bond-correlation experiments were optimized with the following coupling constants: $^3J(^{15}N, ^1H) = 1.8$

Hz and $^{2}J(^{15}N, ^{1}H)$ = 11 Hz. A relaxation delay of 1s was used in all experiments on the free ligands and in the experiments with $^{2}J(^{15}N, ^{1}H)$ = 11 Hz on the complexes, whereas a delay of 2s was used in the long range coupling experiments performed on the complexes. The number of transients per increment was either 32 or 64 with a total acquisition time ranging from 3 to 11 h.

ESI mass spectra were collected in the positive mode (when not specified) and negative mode on a Perkin-Elmer APII spectrometer at 5600 eV.

UV-vis spectra were obtained on an Agilent Cary 60 spectrophotometer, using 1.0 cm path-length quartz cuvettes (3.0 mL).

Solid state infrared spectra were obtained as Nujol mulls between NaCl plates and recorded on a Perkin-Elmer Fourier transform infrared/Raman 2000 instrument in the transmission mode. Solution spectra ($CHCl_3$, MeOH and EtOH) in the CO stretching region were recorded between CaF_2 plates (0.5 mm spacer).

A pressurized vessel (autoclave) connected to a thermostat was used for the reaction with CO at different pressure (30, 40 or 50 atm).

A CEM Discover microwave reactor was used for the microwave assisted reactions using a 10 mL vessel.

Elemental analyses were performed in the Department of Chemistry of the University of Bologna (Italy).

Elemental analyses were performed in the Department of Chemistry of the University of Bologna (Italy).

A home-made LED apparatus was used for performing the photochemical reactions. Briefly, it consists of a plastic-coated cylindric well capable of hosting an NMR tube or a test-tube (Ø = 20 mm, h = 110 mm). The inside of the apparatus is lined with four pairs of LED stripes, each containing five LEDs of the same color that emit in a narrow spectral range (ca. 10 nm). LED stripes of the same color are located opposite to each other. One or more colors can be activated at the same time, and the

LED emission power can be regulated from 1 to 40 mW. The blue (λ = 470 nm) and green (λ= 530 nm) LEDs were used in this case.

HPLC analysis and purification: Analytical HPLC was performed on a Smartline instrument (Knauer, Berlin, Germany) with a Reprosil-Pur C-18 reversed-phase column at a flow rate of 1.0 mL/min. Preparative HPLC was performed on a Varian Prostar with a HIBAR Lichrospher 100 RP-18e reversed-phase column at a flow rate of 20 mL/min. Analytical and preparative runs were performed with a linear gradient of 5% buffer B per min starting at 5 min of buffer A (buffer A = H_2O/MeCN/TFA 95:5:0.1, v/v/v, buffer B = MeCN/H_2O/TFA 95:5:0.1, v/v/v) was used.

Lyophilization was performed on an ALPHA 1-4 LDplus lyophilizator (Martin Christ, Osterode am Harz, Germany).

9.3 X-ray diffraction measurements

Data collections were performed by Dr. Gabriele Balducci (University of Trieste) at the X-ray diffraction beamline (XRD1) of the Elettra Synchrotron of Trieste (Italy) equipped with a Pilatus 2M image plate detector.

Collection temperature was 100K (nitrogen stream supplied through an Oxford Cryostream 700); the wavelength of the monochromatic X-ray beam was 0.700°A and the diffractograms were obtained with the rotating crystal method. The crystals were dipped in N-paratone and mounted on the goniometer head with a nylon loop. The diffraction data were indexed, integrated and scaled using the XDS code.[11] The structures were solved by the dual space algorithm implemented in the SHELXT code.[12] Fourier analysis and refinement were performed by the full-matrix least-squares methods based on F2 implemented in SHELXL.[13] The Coot program was used for modeling.[14] Anisotropic thermal motion was allowed for all non-hydrogen atoms. Hydrogen atoms were placed at calculated positions with isotropic factors U = 1.2×Ueq, Ueq being the equivalent isotropic thermal factor of the bonded non hydrogen atom.

9.4 Spectrophotometric studies

To assess the stability of the compounds in physiological like conditions, spectrophotometric studies were performed by a Varian Cary 50 Bio UV–vis spectrophotometer. Freshly prepared concentrated solutions (10^{-2} M for compounds **1**, **2**, **11** and **12**, 10^{-4} M for compound **3**) of each compound dissolved in milliQ water were diluted in phosphate buffer (PB, 10 mM phosphate, pH 7.4). The concentration of each compound in the final sample was 3×10^{-5} M. The resulting solutions were monitored by collection of the electronic spectra for 24 h at room temperature.

9.5 Interactions with biomolecules

Ruthenium complex–protein/oligonucleotide adducts were prepared starting from a solution of each model protein at a concentration of 10^{-4} M in 20 mM ammonium acetate buffer, pH 7.4, or from a 10^{-4} M solution of ODN4 in milliQ water. Then, the ruthenium complex was added (3:1 metal-to-protein/oligonucleotide ratio) to the solution and the mixture was incubated at 37 °C for 24 h, using Thermoblock (Falc, TD15093). Protein samples were analyzed after a 20-fold dilution with milliQ water (the final concentration of the protein was 5 μM), while ODN4 samples were diluted with a mixture of 50% milliQ water and 50% MeOH to a final concentration of 10 μM. ESI-MS spectra were recorded by direct introduction of the sample at a flow rate of 5 μL/min into an Orbitrap high-resolution mass spectrometer (Thermo Scientific, San Jose, CA, USA) equipped with a conventional ESI source. The working conditions for ruthenium complex-protein adducts were as follows: spray voltage 3.1 kV, capillary voltage 45 V and capillary temperature 220 °C. The sheath and the auxiliary gasses were set at 17 (arbitrary units) and 1 (arbitrary unit), respectively. For acquisition, Xcalibur 2.0 (Thermo Scientific) was used and monoisotopic and average deconvoluted masses were obtained by using the integrated Xtract tool. For spectrum acquisition, a nominal resolution (at m/z 400)

of 100,000 was used. ESI-MS spectra of the ruthenium complex-ODN adducts were recorded in negative ion mode. The working conditions were as follows: spray voltage 4.5 kV, capillary voltage –10 V and capillary temperature 270 °C. The sheath gas was set at 10 (arbitrary units) whereas auxiliary gas was kept at 5 (arbitrary units).

9.6 Cellular studies

Cell cultures. HCT-116 (human colon cancer) and FLG 29.1 (human myeloid leukemia) cell lines were maintained in RPMI 1640 medium supplemented with 2 mM L-glutamine, 10% bovine calf serum (HyClone) and maintained at 37°C in a humidified atmosphere in 5% CO_2 in air.

Pharmacology experiments. Cells were seeded in a 96-well flat-bottomed plate (Corning-Costar, Corning, NY, USA) at a cell density of 10^4 cells per well in RPMI complete medium. Each ruthenium compound (**1**, **2**, **3**, **11** and **12**) was added at final concentrations of 200 μM, 100 μM, 50 μM, 10 μM, and 2 μM. After 24 h, viable cells (determined by Trypan blue exclusion) were counted in triplicate using a haemocytometer. Each experimental point represents the mean of four samples carried out in three separate experiments.

Trypan blue assay. Cells viability was assessed by the Trypan blue exclusion assay. In brief, 10 μl of 0.4% trypan blue solution was added to 10 μl cell suspension in culture medium. The suspension was gently mixed and transferred to a haemocytometer. Viable and dead cells were identified and counted under a light microscope. Blue cells failing to exclude dyes were considered nonviable, and transparent cells were considered viable. The percentage of viable cells was calculated on the basis of the total number of cells (viable plus nonviable). The IC_{50} value (i.e. the dose that caused apoptosis of 50% of cells) was calculated by fitting the data points (after 24 h of incubation) with a sigmoidal curve using Calcusyn software (Biosoft).

MTT assay. Dulbecco's Modified Eagle's Medium (DMEM), containing 10% fetal calf serum, 1% penicillin and streptomycin, was used as growth medium. MCF-7, HT-29 and PT-45 cells were detached from the wells with trypsin and EDTA, harvested by centrifugation and resuspended again in cell culture medium. The assays have been carried out on 96 well plates with 6000 cells per well for all the cell lines. After 24 h of incubation at 37° C and 10% CO_2, the cells were treated with the compounds **29**, **51**, **52**, **57 - 59**, **61**, **62** at 1, 10, 20, 40, 80, 100, 200 µM concentration (with DMSO concentrations of 0.5%) with a final volume of 200 µL per well. For a negative control, one series of cells was left untreated. The cells were incubated for 48 h followed by adding 50 µL MTT (2.5 mg/mL). After an incubation time of 2 h, the medium was removed and 200 µL DMSO were added. The formazan crystals were dissolved and the absorption was measured at 550 nm, using a reference wavelength of 620 nm.

9.7 Computational methods

Calculations were done by Dr. Gabriele Balducci. It was performed periodic first principle calculations in the frame of density functional theory (DFT) with the Kohn–Sham orbitals expanded in a basis of plane waves and the effects of atomic core regions accounted for by pseudopotentials. The QUANTUM ESPRESSO suite of codes was used for all the computations.[15] To model an isolated molecule using a periodic code like QUANTUM ESPRESSO, a "molecule in the box" approach can be used: a single molecule is simulated in a unit cell large enough to minimize any interaction between the molecule itself and any of its periodic images. A cubic unit cell with edge length of 19.0 Å for complex **68** and 20.0 Å for complex **72** was found to give a minimum separation of 10 Å between nearest atoms of any two contiguous images. Both total energy and scf potential were corrected for the effect of the fictitious periodicity with the Martyna-Tuckerman method.[16] Ultrasoft pseudopotentials were used throughout the calculations.[17] The exchange–correlation

part of the energy functional was modeled with the (spin-unpolarized) generalized gradient approximation (GGA), in the PBE parameterization.[18] The plane wave expansion of the crystalline orbitals was truncated at a cutoff energy of 340 eV and a corresponding tenfold cutoff was used for the expansion of the augmentation charge needed by the ultrasoft pseudopotential method. Integrals over the first Brillouin zone in reciprocal space were approximated by evaluations of the integrand functions at the gamma point. Convergence thresholds for geometry optimization were 1.4×10^{-4} eV for total energy and 2.6×10^{-2} eV/Å for the maximum force component acting on atoms; a threshold of 1.4×10^{-8} eV was imposed for self-consistency. Excited state calculations and UV–vis spectra simulation were performed with time dependent DFT (TDDFT). The QUANTUM ESPRESSO suite offers two codes for this purpose. The "turbo_davidson" code implements an improved Davidson-like algorithm for the computation of individual excitations clustered around a target energy value, which, differently from the "conventional" Davidson algorithm, can be located anywhere in the spectrum. The "turbo_lanczos" program uses a so-called "pseudo-Hermitian" variant of the recursive Lanczos scheme to evaluate the whole absorption spectrum in a given energy range using only the occupied states obtained in a previous self-consistent field calculation. Both codes rely upon the formulation of the TDDFT problem in terms of the linearized quantum Liouville equation and the details about the algorithms can be found in the original papers.[19,20] 60 trial vectors, a maximum of 200 basis vectors in the Davidson subspace and a convergence threshold of 1.0×10^{-4} for the squared modulus of the residue were used for the "turbo_davidson" runs; 5000 Lanczos iterations for each of the three directions of the full dynamical polarizability tensor were used in the UV–vis spectrum simulation with the "turbo_lanczos" code.

9.8 Synthesis of the complexes

***cis*-$RuCl_2(PTA)_4$ (2).**

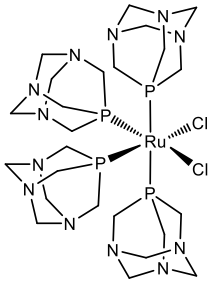

A procedure similar to that reported by Romerosa and co-workers,[21] i.e. photo-isomerization of **1** in aqueous solution, was followed. *trans*-$RuCl_2(PTA)_4$ (**1**, 50.0 mg, 0.062 mmol) was dissolved in 5 mL of water and irradiated with blue light (λ = 470 nm, 40 mW) for 1 h, during which time the orange solution turned to yellow. Complete removal of the solvent by rotary evaporation afforded pure **1**, according to ^{1}H and ^{31}P NMR spectra, as a yellow solid (Yield: 48.0 mg, 96%). Elemental analysis calcd for [$C_{24}H_{48}N_{12}Cl_2P_4Ru$] ($M_W$: 800.57): C 36.01; H 6.04; N 20.99. Found: C 36.12; H 6.19; N 21.12. ^{1}H NMR (D_2O + NaCl), δ (ppm): 4.65 (m, 24H, NCH_2N), 4.47 (br s, 12H, NCH_2P, mutually *trans* PTAs), 4.14 (br s, 12H, NCH_2P, PTA *trans* to Cl). ^{31}P NMR (D_2O+ NaCl), δ (ppm): –21.6 (t, 2P, $^{2}J_{P\text{-}P}$ = 28.5 Hz, PTA *trans* to Cl), –57.6 (t, 2P, mutually *trans* PTAs).^{1}H NMR ($CDCl_3$), δ (ppm): 4.48 (m, 24H, NCH_2N), 4.47 (br s, 12H, NCH_2P, mutually *trans* PTAs), 4.04 (br s, 12H, NCH_2P, PTA *trans* to Cl). ^{13}C NMR from the HSQC spectrum ($CDCl_3$), δ (ppm): 73.1 (N*C*H_2P), 58.7 (N*C*H_2N mutually *trans* PTAs), 54.8 (N*C*H_2P PTAs *trans* to Cl) ^{31}P NMR ($CDCl_3$), δ (ppm): –24.1 (t, 2P, $^{2}J_{P\text{-}P}$ = 28.6 Hz, PTAs *trans* to Cl), –59.4 (t, 2P, mutually *trans* PTAs). ESI mass spectrum: 765.1 *m*/*z* (calcd 765.1) $(M - Cl)^+$, 608.2 *m/z* (calcd 608.0) $(M - Cl - PTA)^+$. UV-vis ($CHCl_3$): λ_{max} (ε, L mol^{-1} cm^{-1}) = 344 (1022) nm.

***cis*-[RuCl(OH$_2$)(PTA)$_4$](PF$_6$)·CH$_3$OH (2$_{aq}$).**

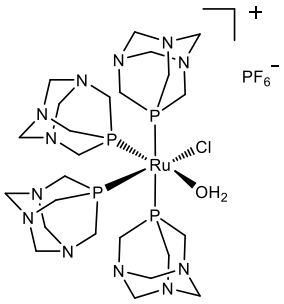

[RuCl(dmso)$_5$](PF$_6$) (38.3 mg, 0.057 mmol) was dissolved in 10 mL of methanol. Five eq. of PTA (44.8 mg, 0.29 mmol) were added and the solution was left standing overnight in the dark. Yellow crystals formed slowly from the concentrated solution (5 mL). Some crystals were fished out for X-ray diffraction, the others were filtered, washed with diethyl ether and dried *in vacuo* (Yield: 22.8 mg, 42%). [$C_{24}H_{50}N_{12}ClP_5F_6ORu{\cdot}CH_3OH$] ($M_W$: 960.15): C 31.27; H 5.67; N 17.51. Found: C 31.47; H 5.83; N 17.70. ^{1}H-NMR (D$_2$O), δ (ppm): 4.59 (m, 24H, NC*H*$_2$N), 4.26 (d, 12H, NC*H*$_2$P), 4.11 (s, 6H, NC*H*$_2$P), 3.97 (s, 6H, NC*H*$_2$P), 3.34 ppm (s, 3H, MeOH free). ^{31}P-NMR (D$_2$O), δ (ppm): –12.7 (dt, 1P, $^2J_{AM}$ = 30.3 Hz, $^2J_{AX}$ = 34.8 Hz, PTA *trans* to OH$_2$), –22.7 (dt, 1P, $^2J_{XM}$ = 26.1 Hz, $^2J_{XA}$ = 34.8Hz, PTA *trans* to Cl), –52.6 (dd, 2P, $^2J_{MX}$ = 26.1 Hz, $^2J_{MA}$ = 30.3 Hz, mutually *trans* PTAs), –143.2 (septet, 1P, PF$_6$). ESI mass spectrum: 765.1 m/z (calcd 765.1) $(M - H_2O)^+$.

***trans*-[RuCl$_4$(PTAH)$_2$]Cl (3).**

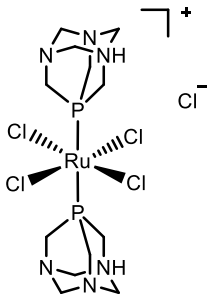

[(dmso)$_2$H]*trans*-[RuCl$_4$(dmso-S)$_2$] (150.0 mg, 0.27 mmol) was dissolved in 15 mL of methanol, obtaining an orange solution. 0.500 µL of 37% aqueous HCl and two equivalents of PTA (84.8 mg, 0.54 mmol) were added; a brown solid began to

precipitate immediately. The mixture was stirred for 1 h and then the solid was collected by filtration, washed with methanol and diethyl ether and dried *in vacuo*. The solid was dissolved in 4.5 mL of water at reflux. Abundant small crystals of **3**, suitable for X-ray diffraction, were obtained upon allowing the solution to cool down to room temperature. The crystals were filtered, washed with a small amount of water and dried *in vacuo* (yield: 115.8 mg, 72%). Elemental analysis calcd for [$C_{12}H_{26}N_6Cl_5P_2Ru{\cdot}2H_2O$] ($M_W$: 630.67): C 22.85; H 4.79; N 13.33. Found: C 23.36; H 4.51; N 13.05. ^{1}H NMR (D_2O), δ (ppm): 0.37 (br s, 12H), –1.17 (br s, 12H). ESI mass spectrum: 400.7 *m*/*z* $(M - PTA)^-$, calcd 400.0.

***cis,cis,trans*-RuCl$_2$(dmso-S)$_2$(PTA)$_2$ (10).**

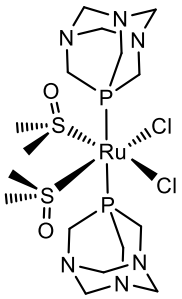

A different procedure compared to that reported by Kathó and coworkers was followed.[22] *cis*-RuCl$_2$(dmso-S)$_4$ (**8**) (340 mg, 0.70 mml) was partially dissolved in 5 mL of methanol. A solution of PTA (220 mg, 1.4 mmol, 10 ml of methanol) was added dropwise in 15 minutes. A pale yellow solid began to form after few minutes. The product was filtered after standing overnight, washed with methanol and diethyl ether and dried in vacuo (Yield: 357 mg, 80%). According to the ^{1}H and ^{31}P NMR spectra the product was pure **10**. X-ray quality crystals of **10** were obtained by slow diffusion of diethyl ether into a methanol solution of the complex. Elemental analysis calcd for [$C_{16}H_{36}N_6Cl_2P_2S_2O_sRu$] (MW: 642.55): C 29.91; H 5.65; N 13.08. Found: C 29.99; H 5.60; N 13.15. ^{1}H NMR (D_2O), δ (ppm): 4.51 (br s, 12H, NC*H*$_2$N), 4.32 (br s, 12H, NC*H*$_2$P), 3.38 (s, 12H, dmso-S). ^{31}P NMR (D_2O), δ (ppm): –57.9 (s). ^{1}H NMR ($CDCl_3$), δ (ppm): 4.52, 4.47 (ABq, 12H, J_{AB} = 13.0 Hz, NC*H*$_2$N), 4.41 (br s,

12H, NCH_2P), 3.32 (s, 12H, dmso-S). ^{13}C NMR ($CDCl_3$), δ (ppm): 73.1 (NCH_2N), 51.3 (NCH_2P), 51.1 (dmso-S). ^{31}P NMR ($CDCl_3$), δ (ppm): –63.5 (s). ESI mass spectrum: 643.0 m/z (calcd 643.3) (M^+).

***trans*-RuBr$_2$(PTA)$_4$ (11).**

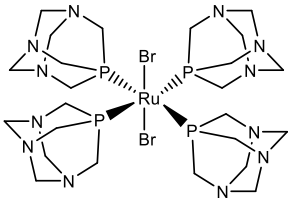

$RuBr_3 \cdot 3H_2O$ (60.0 mg, 0.15 mmol) was partially dissolved in 7 mL of ethanol. A slight excess of PTA (96.55 mg, 0.615 mmol) was added and the mixture was refluxed for 3 h. A clear solution was obtained within 1 h from which a dark red solid began to form. It was eventually removed by filtration and washed with ethanol. The solid was treated on the filter with chloroform (*ca*. 10 mL) to obtain an orange solution. A small amount of grey solid that remained undissolved on the filter was discarded. The solvent was completely removed by rotary evaporation, affording pure **11**, according to ^{1}H and ^{31}P NMR spectra (Yield: 93.9 mg, 68%). X-ray quality crystals of **11** were obtained by slow diffusion of diethyl ether into a chloroform solution of the complex. Elemental analysis for the raw material: calcd for [$C_{24}H_{48}N_{12}Br_2P_4Ru \cdot 5H_2O$] ($M_W$: 979.48): C, 29.43; H, 5.97; N, 17.16. Found: C, 29.57; H, 6.10; N, 17.09. ^{1}H NMR (D_2O), δ (ppm): 4.61 (br s, 24H, NCH_2N), 4.40 (br s, 24H, NCH_2P). ^{13}C NMR from the HSQC spectrum (D_2O), δ (ppm): 70.5 (N*C*H$_2$N), 51.9 (N*C*H$_2$P). ^{31}P-NMR (D_2O), δ (ppm): –54.5 (s). ^{1}H NMR ($CDCl_3$), δ (ppm): 4.60, 4.55 (ABq 24H, NCH_2N, J_{AB} 13.2 Hz), 4.46 (br s, 24H, NCH_2P). ^{13}C NMR from the HSQC spectrum ($CDCl_3$), δ (ppm): 73.5 (N*C*H$_2$N), 54.0 (N*C*H$_2$P). ^{31}P NMR ($CDCl_3$), δ (ppm): –56.5 (s). ESI mass spectrum (*m*/*z*): 811.12 $(M - Br)^+$, calcd 811.59; 733.97 $(M - PTA + H^+)^+$, calcd 733.32.

***cis*-RuBr$_2$(PTA)$_4$ (12).**

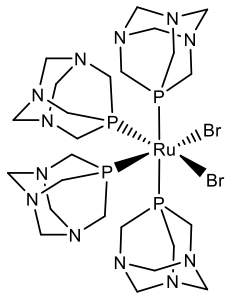

trans-RuBr$_2$(PTA)$_4$ (**11**) (50.0 mg, 0.056 mmol) was dissolved in 5 mL of water and irradiated with blue light (λ = 470 nm, 40 mW) for 2.30 h. The orange solution turned to yellow within 1 h. Complete removal of the solvent by rotary evaporation afforded pure **12**, according to ^{1}H and ^{31}P NMR spectra, as a yellow solid (Yield: 48.0 mg, 96%). X-ray quality crystals of **12** were obtained by slow diffusion of acetone into a water solution of the complex. Elemental analysis calcd for [$C_{24}H_{48}N_{12}Br_2P_4Ru\cdot5H_2O$] ($M_W$: 979.48): C, 29.43; H, 5.97; N, 17.16. Found: C, 29.55; H, 6.109; N, 17.07.^{1}H NMR (D_2O + exc. NaBr, see Chapter 1), δ (ppm): 4.70 (m, 24H, NC*H*$_2$N), 4.56 (br s, 12H, NC*H*$_2$P), 4.23 (br s, 12H, NC*H*$_2$P). ^{31}P NMR (D_2O + exc. NaBr, see Chapter 1), δ (ppm): –24.1 (t, 2P, $^{2}J_{P\text{-}P}$ = 28.2 Hz, PTA *trans* to Br), –64.7 (t, 2P, $^{2}J_{P\text{-}P}$ = 28.2 Hz, mutually *trans* PTAs). ^{1}H NMR ($CDCl_3$), δ (ppm): 4.54 (br s, 12H, NC*H*$_2$P), 4.50 (m, 24H, NC*H*$_2$N), 4.12 (br s, 12H, NC*H*$_2$P). ^{13}C NMR from the HSQC spectrum ($CDCl_3$), δ (ppm): 73.0 (N*C*H$_2$N), 59.2 (N*C*H$_2$P), 55.4 (N*C*H$_2$P). ^{31}P NMR ($CDCl_3$), δ (ppm): –27.0 (t, 2P, $^{2}J_{P\text{-}P}$ = 27.4 Hz , PTA *trans* to Br), –67.3 (t, 2P, $^{2}J_{P\text{-}P}$ = 27.4 Hz, mutually *trans* PTAs). ESI mass spectrum (*m*/*z*): 811.12 (M – Br)$^{+}$, calcd 811.59.

***cis,mer*-$RuCl_2$(dmso-S)$(PTA)_3$ (13).**

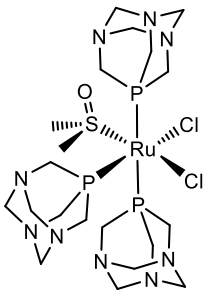

trans-$RuCl_2(PTA)_4$ (**1**) (30.0 mg, 0.038 mmol) was partially dissolved in 1 mL of DMSO and the mixture was warmed to 70°C under stirring. After 2h of reaction, the residual unreacted **1** was filtered off. Dropwise addition of acetone to the mother liquor induced the formation of a pale yellow precipitate within 24h. It was removed by filtration, washed with diethyl ether and dried *in vacuo*. According to the ^{1}H and ^{31}P NMR spectra it was a mixture of **13** and **2** in ca. 40:60 ratio (Yield: 9 mg, 33%). ^{1}H NMR ($CDCl_3$), δ (ppm) (in the PTA region, the resonances of **2** and **13** overlap to such an extent that those of **13** could not be distinguished): 3.20 (s, 6H, dmso-S). ^{31}P NMR ($CDCl_3$), δ (ppm): –25.6 (t, 1P, $^2J_{P\text{-}P}$ = 27.9 Hz, PTA *trans* to Cl), –61.0 (d, 2P, mutually *trans* PTAs).

***trans,mer*-$RuCl_2(CH_3CN)(PTA)_3$ (14) and *cis,mer*-$RuCl_2(CH_3CN)(PTA)_3$ (15).**

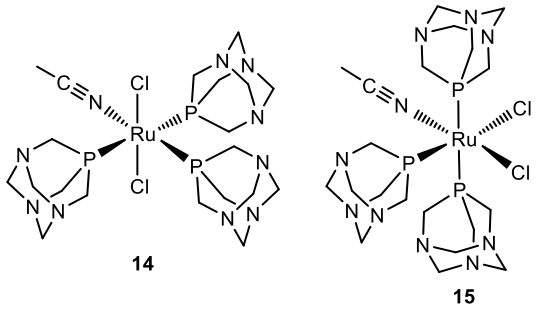

14 **15**

trans-$RuCl_2(PTA)_4$ (**1**) (60.0 mg, 0.075 mmol) was partially dissolved in 8 mL of acetonitrile and refluxed for 2 h. Upon heating complex **1** dissolved completely. The originally yellow solution became progressively paler and a pale yellow solid began to form after ca. 1 h. After cooling to room temperature, the product was filtered,

washed with acetonitrile and diethyl ether and dried *in vacuo*. According to ^{1}H and ^{31}P NMR spectra it was a mixture of **14**, **15** and **1** in ca. 68:17:15 % ratio (Yield: 15 mg, 29%). ^{1}H NMR ($CDCl_3$), δ (ppm) of **14** and **15**: 4.45 (m, NC*H*$_2$N), 4.04 (br s, NC*H*$_2$P) (it was not possible to distinguish the PTA resonances of **14** and **15**), 2.46 (s, 3H, C*H*$_3$CN of **15**), 2.30 (s, 3H, C*H*$_3$CN of **14**). ^{31}P NMR ($CDCl_3$), δ (ppm) of **7**: –16.1 (t, 1P, $^{2}J_{P\text{-}P}$ = 28.5 Hz, PTA *trans* to CH_3CN), –53.3 (d, 2P, mutually *trans* PTAs). ^{31}P NMR ($CDCl_3$), δ (ppm) of **15**: –24.0 (t, 1P, $^{2}J_{P\text{-}P}$ = 37.2 Hz, PTA *trans* to Cl), –54.3 (d, 2P, mutually *trans* PTAs).

***mer*-[Ru(bpy)Cl(PTA)$_3$]Cl (17).**

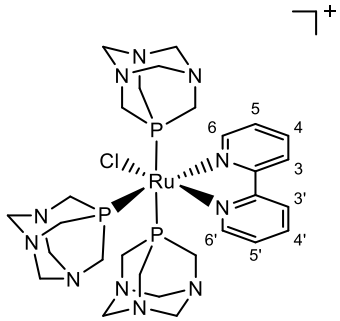

trans-$RuCl_2(PTA)_4$ (**1**) (40.0 mg, 0.050 mmol) was dissolved in 5 mL of water. One eq. of 2,2'-bipyridine (8.2 mg, 0.050 mmol) was added and the light-protected mixture was refluxed for 1 h. The yellow solution turned rapidly orange. The solvent was rotary evaporated affording a yellow solid that, according to the ^{1}H and ^{31}P NMR spectra, was a ca. equimolar mixture of free PTA and **17** with PTAO as impurity (less than 5% of PTA). X-ray quality crystals of **17** were obtained by slow diffusion of acetone into a water solution of the complex. Elemental analysis calcd for [$C_{28}H_{44}N_{11}Cl_2P_3Ru{\cdot}6H_2O$] ($M_W$: 907.70): C 37.05; H 6.22; N 16.97. Found: C 36.87; H 6.03; N 16.87. Larger amounts of pure complex for the NMR characterization were obtained as PF_6 salt (**17PF$_6$**): the raw material (48.1 mg) was dissolved in 1 mL of water and 1 mL of a solution of $NaPF_6$ (12.5 mg, 0.075 mmol) was added. The yellow crystals that formed in few hours were removed by filtration and dried *in vacuo* (Yield: 28.1 mg, 62%). The product was pure **17PF$_6$** according to the ^{1}H and

^{31}P NMR spectra. ^{1}H NMR (D_2O) δ (ppm): 9.45 (d, 1H, H6), 8.65 (d, 1H, H3), 8.55 (d, 1H, H3'), 8.41 (m, 2H, H4 + H6'), 8.18 (t, 1H, H4'), 7.94 (t, 1H, H5), 7.58 (t, 1H, H5'), 4.93, 4.85 (ABq, 6H, NC*H*$_2$N, J_{AB} = 13.1 Hz, PTA *trans* to N), 4.52 (br s, 6H, NC*H*$_2$P, PTA *trans* to N), 4.54, 4.45 (ABq, 12H, J_{AB} = 13.9 Hz, NC*H*$_2$N, mutually *trans* PTAs), 3.72 (br s, 12H, NC*H*$_2$P, mutually *trans* PTAs). ^{13}C NMR (partial) from the HSQC spectrum (D_2O), δ (ppm): 156.2 (C6'), 150.7 (C6), 146.8 (C4), 138.9 (C4'), 128.2 (C5'), 127.3 (C5), 125.6 (C3'), 124.9 (C3), 70.7 (N*C*H$_2$N, PTA *trans* to N), 70.5 (N*C*H$_2$N, mutually *trans* PTAs), 52.2 (N*C*H$_2$P, PTA *trans* to N), 46.6 (N*C*H$_2$P, mutually *trans* PTAs). ^{31}P NMR (D_2O), δ (ppm) –30.2 (t, 1P, $^{2}J_{P\text{-}P}$ = 32.8 Hz, PTA *trans* to N), –47.6 (d, 2P, mutually *trans* PTAs). –144.4 (septet, PF_6). ESI mass spectrum: 764.2 *m/z* (calcd 764.2) (M^+), 607.2 *m/z* (calcd. 607.1) $(M - PTA)^+$. UV-vis (H_2O): λ_{max} (ε, L mol^{-1} cm^{-1}) = 390 (1310) nm.

***fac*-[Ru(bpy)Cl(PTA)$_3$]Cl (18).**

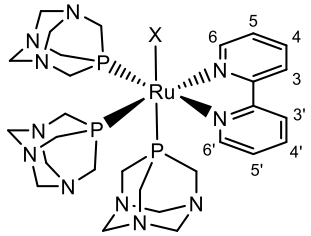

X = Cl/OH$_2$

cis-$RuCl_2(PTA)_4$ (**2**) (45.0 mg, 0.056 mmol) was dissolved in 8 mL of water. Five eq. of 2,2'-bipyridine (43.9 mg, 0.280 mmol) and one eq. of $AgNO_3$ (9.6 mg, 0.056 mmol) were added and the light-protected mixture was refluxed for 1 h. The yellow solution turned rapidly orange and a grey precipitate of AgCl formed. The mixture was filtered over a pad of Celite and the clear solution was rotary evaporated to dryness affording a yellow solid that, according to the ^{1}H and ^{31}P NMR spectra, was a mixture of **17** and **18** in 1/7 ratio. No residual **2** was present. The pure *facial* isomer for full characterization was obtained as PF_6 salt (**18PF$_6$**): the raw mixture (87.3 mg) was dissolved in 1 mL of water and 1 mL of a solution of $NaPF_6$ (18.6 mg, 0.11 mmol) was added. The yellow microcrystalline solid that formed within few hours

at room temperature was removed by filtration, washed with cold water and dried *in vacuo* (Yield: 14.1 mg, 31%). The product was pure **18PF$_6$** according to the ^{1}H and ^{31}P NMR spectra. Low quality single crystals of fully protonated **18**, as *fac*-[Ru(bpy)Cl(PTAH)$_3$][0.5Cl][3.5ClO$_4$], used for X-ray diffraction analysis, were obtained by adding a 0.5 M solution of HClO$_4$ into a water solution of the complex. Elemental analysis calcd for **18PF$_6$** [$C_{28}H_{44}N_{11}ClP_4F_6Ru$] ($M_W$: 909.13): C 36.99; H 4.88; N 16.95. Found: C 37.18; H 4.90; N 17.03. ^{1}H NMR (D_2O + NaCl) δ (ppm): 8.99 (br s, 2H, H6,6'), 8.54 (d, 2H, H3,3'), 8.29 (t, 2H, H4,4'), 7.80 (t, 2H, H5,5'), 4.65 (m, partially overlapped by the water signal, 12H, NC*H*$_2$N, PTA *trans* to N), 4.49 (m, partially overlapped by the singlet at 4.44, 6H, NC*H*$_2$N, PTA *trans* to Cl), 4.44 (s, 12H, NC*H*$_2$P, PTA *trans* to N), 3.88 (s, 6H, NC*H*$_2$P, PTA *trans* to Cl). ^{13}C NMR (partial) from the HSQC spectrum (D_2O), δ (ppm): 154.5 (C6,6'), 140.3 (C4,4'), 126.5 (C5,5'), 124.7 (C3,3'), 70.7 (N*C*H$_2$N, PTA *trans* to Cl), 70.5 (N*C*H$_2$N, PTA *trans* to N), 52.2 (N*C*H$_2$P, PTA *trans* to Cl), 46.6 (N*C*H$_2$P, PTA *trans* to N). ^{31}P NMR (D_2O), δ (ppm): –24.3 (t, 1P, $^2J_{P\text{-}P}$ = 29.2 Hz, PTA *trans* to Cl), –43.1 (d, 2P, PTA *trans* to N). –144.4 (septet, 1P, PF_6). ^{1}H NMR (D_2O) δ (ppm) of **18$_{aq}$**: 8.95 (br s, 2H, H6,6'), 8.58 (d, 2H, H3,3'), 8.33 (t, 2H, H4,4'), 7.83 (t, 2H, H5,5'), 4.65 (m, 12H, NC*H*$_2$N,), 4.46 (s, 12H, NC*H*$_2$P,) (it was not possible to distinguish the PTA resonances of **18** and **18$_{aq}$**), 4.43 (m, 6H, NC*H*$_2$N, PTA *trans* to OH_2), 3.84 (s, 6H, NC*H*$_2$P, PTA *trans* to OH_2). ^{31}P NMR (D_2O), δ (ppm) of **18$_{aq}$**: –17.7 (t, 1P, $^2J_{P\text{-}P}$ = 30.2 Hz, PTA *trans* to OH_2), –43.5 (d, 2P, PTA *trans* to N). –144.4 (septet, 1P, PF_6). ESI mass spectrum: 764.2 *m/z* (calcd 764.2) (M^+), 607.2 *m/z* (calcd. 607.1) (M – PTA)$^+$. UV-vis (H_2O): λ_{max} (ε, L mol^{-1} cm^{-1}) = 385 (2385) nm.

***cis,cis*-Ru(bpy)Cl$_2$(PTA)$_2$ (22).**

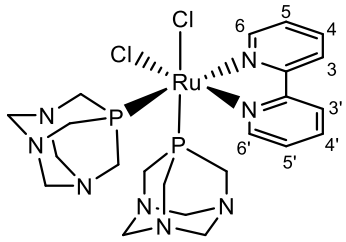

cis,cis,trans-RuCl$_2$(dmso-S)$_2$(PTA)$_2$ (**10**) (70.0 mg, 0.109 mmol) was partially dissolved in 10 mL of ethanol. Two eq. of 2,2'-bipyridine (34.0 mg, 0.218 mmol) were added and the mixture was refluxed for 6h. The clear solution obtained upon warming gradually become ruby-red and a precipitate of the same color began to form after 4 h. The mixture was concentrated to ca. 3 mL and the precipitate was filtered after overnight standing at room temperature, washed with diethyl ether and dried *in vacuo* (Yield: 42.0 mg, 54%). According to the ^{1}H and ^{31}P NMR spectra the product was pure **22**. X-ray quality crystals of **22** were obtained by slow diffusion of diethyl ether into a methanol solution of the complex. Elemental analysis calcd for [$C_{22}H_{32}N_8Cl_2P_2Ru$] (M_W: 642.46): C 41.13; H 5.02; N 17.44. Found: C 41.16; H 5.00; N 17.45. ^{1}H NMR ($CDCl_3$) δ (ppm): 9.88 (d, 1H, H6 bpy), 8.55 (d, 1H, H6' bpy), 8.10 (d, 1H, H3 bpy), 8.04 (d, 1H, H3' bpy), 7.95 (t, 1H, H4 bpy), 7.78 (t, 1H, H4' bpy), 7.58 (t, 1H, H5 bpy), 7.20 (t, 1H, H5' bpy), 4.64 (s, 6H, NC*H*$_2$N, PTA *trans* to N), 4.60, 4.53 (ABq, 6H, J_{AB} = 15.0 Hz, NC*H*$_2$P, PTA *trans* to N), 4.39, 4.19 (ABq, 6H, J_{AB} = 13.0 Hz, NC*H*$_2$N, PTA *trans* to Cl), 3.70, 3.59 (ABq, 6H, J_{AB} = 15.1 Hz, NC*H*$_2$P, PTA *trans* to Cl). ^{13}C NMR (partial) from the HSQC spectrum ($CDCl_3$) δ (ppm): 156.7 (C6'), 151.1 (C6), 136.9 (C4), 135.2 (C4'), 125.8 (C5), 125.2 (C5'), 122.9 (C3'), 121.7 (C3), 73.31 (N*C*H$_2$N, PTA *trans* to N), 72.0 (N*C*H$_2$N, PTA *trans* to Cl), 54.0 (N*C*H$_2$P, PTA *trans* to N), 53.2 (N*C*H$_2$P, PTA *trans* to Cl). ^{31}P NMR ($CDCl_3$) (ppm): δ –21.6 (d, 1P, $^{2}J_{P\text{-}P}$ = 34.4 Hz, PTA *trans* to Cl), –36.2 (d, 1P, *trans* to N). ^{1}H NMR of **22$_{aq}$** (D_2O) δ (ppm): 9.51 (d, 1H, H6 bpy), 8.53 (d, 1H, H6' bpy), 8.49 (d, 1H, H3 bpy), 8.42 (d, 1H, H3' bpy), 8.27 (t, 1H, H4 bpy), 8.09 (t, 1H,

H4' bpy), 7.80 (t, 1H, H5 bpy), 7.50 (t, 1H, H5' bpy), 4.66 (s, 6H, NC*H*$_2$N, PTA *trans* to N), 4.45 (s, 6H, NC*H*$_2$P, PTA *trans* to N), 4.38, 4.27 (ABq, 6H, J_{AB} = 13.3 Hz, NC*H*$_2$N, PTA *trans* to OH_2), 3.66 (m, 6H, NC*H*$_2$P, PTA *trans* to OH_2). ^{31}P NMR (D_2O) δ (ppm): –7.0 (d, $^2J_{P\text{-}P}$ = 37.7 Hz, PTA *trans* to OH_2), –31.9 (d, PTA *trans* to N). ^{1}H NMR of **22** (D_2O + NaCl) δ (ppm): 9.45 (d, 1H, H6 bpy), 8.55 (m, 1H, H6' bpy), 8.44 (d, 2H, H3 e H3'), 8.22 (t, 1H, H4 bpy), 8.02 (t, 1H, H4' bpy), 7.75 (t, 1H, H5 bpy), 7.45 (t, 1H, H5' bpy), 4.38 (m, 12H, NC*H*$_2$N), 3.65 (m, 12H, NC*H*$_2$P) (it was not possible to distinguish the PTA resonances of **22** and **22$_{aq}$**). ^{31}P NMR (D_2O + NaCl) δ (ppm): –12.7 (d, $^2J_{P\text{-}P}$ = 37.1 Hz, PTA *trans* to Cl), –33.8 (d, PTA *trans* to N). ESI mass spectrum: 607.0 *m/z* (calcd. 607.1) $(M - Cl)^+$. UV-vis (H_2O): λ_{max} (ε, L mol^{-1} cm^{-1}) = 412 (2839) nm.

***cis,cis*-Ru(bpyAc)Cl$_2$(PTA)$_2$ (23).**

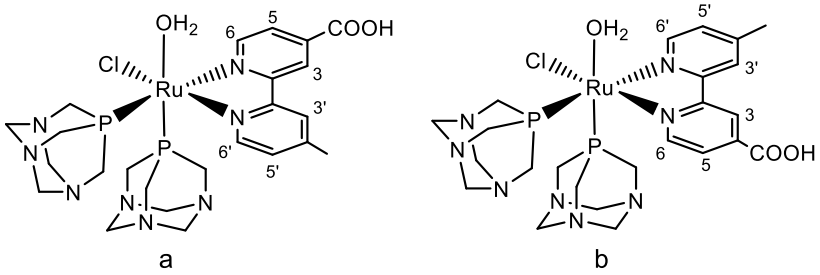

cis,cis,trans-$RuCl_2$(dmso-S)$_2$(PTA)$_2$ (**10**) (50.0 mg, 0.078 mmol) was partially dissolved in 15 mL of ethanol. Two eq. of 4′-methyl-2,2′-bipyridine-4-carboxylic acid (bpyAc, 33.4 mg, 0.156 mmol) were added and the mixture was refluxed for 6h. The clear solution obtained upon warming became gradually deep red. Upon cooling to room temperature, a red powder precipitated and was filtered, washed with ethanol and diethyl ether and dried *in vacuo*. (Yield: 20.0 mg, 37%). According to the ^{1}H and ^{31}P NMR spectra the product was pure **23**, as a nearly equimolar mixture of the two stereoisomers **23a** and **23b** Elemental analysis calcd for [$C_{24}H_{34}N_8Cl_2P_2O_2Ru$] ($M_W$: 700.5): C 41.15; H 4.39; N 16.00. Found: C 41.05; H 4.33; N 15.95. ^{1}H NMR (D_2O) of **23$_{aq}$** δ (ppm): 9.58 (d, 1H, H6 **23a$_{aq}$**), 9.31 (d, 1H, H6' **23b$_{aq}$**), 8.74 (s, 1H, H3 **23a$_{aq}$**), 8.67 (s, 1H, H3 **23b$_{aq}$**), 8.57 (d, 1H, H6 **23b$_{aq}$**), 8.42 (s, 1H, H3' **23b$_{aq}$**), 8.36

(s, 1H, H3' **23a$_{aq}$**), 8.32 (d, 1H, H6' **23a$_{aq}$**), 8.06 (d, 1H, H5 **23a$_{aq}$**), 7.76 (d, 1H, H5 **23b$_{aq}$**), 7.68 (d, 1H, H5' **23b$_{aq}$**), 7.39 (d, 1H, H5' **23a$_{aq}$**), (the PTA resonances of **23a$_{aq}$** and **23b$_{aq}$** overlapped and could not be distinguished) 4.84 (br s, 12H, NC*H*$_2$N, PTA *trans* to N), 4.54 (br s, 12H, NC*H*$_2$P, PTA *trans* to N), 4.43 (m, 12H, NC*H*$_2$N, PTA *trans* to OH_2), 3.77, 3.72 (ABq, 12H, NC*H*$_2$P, J_{AB} = 14.7 Hz, PTA *trans* to OH_2), 2.64 (s, 3H, CH_3 **23b$_{aq}$**), 2.56 (s, 3H, CH_3 **23a$_{aq}$**). ^{13}C NMR of **23$_{aq}$** (partial) from the HSQC spectrum (D_2O), δ (ppm): 157.7 (C6 **23b$_{aq}$**), 156.4 (C6' **23a$_{aq}$**), 150.7 (C6 **23a$_{aq}$**), 149.2 (C6' **23b$_{aq}$**), 128.3 (C5' **23a$_{aq}$**), 127.8 (C5' **23b$_{aq}$**), 125.5 (C5 **23b$_{aq}$**), 125.1 (C5 **23a$_{aq}$**), 124.7 (C3' **23b$_{aq}$**), 123.1 (C3 **23b$_{aq}$**), 122.5 (C3 **23a$_{aq}$**), 125.7 (C3' **23a$_{aq}$**), (the PTA resonances of **23a$_{aq}$** and **23b$_{aq}$** overlapped and could not be distinguished) 70.5 (N*C*H$_2$N, PTA *trans* to N), 70.5 (N*C*H$_2$N PTA *trans* to OH_2), 49.9 (N*C*H$_2$P, PTA *trans* to OH_2), 49.5 (N*C*H$_2$P, PTA *trans* to N), 21.0 (CH_3 **23b$_{aq}$**), 20.0 (CH_3 **23a$_{aq}$**). ^{31}P NMR of **23$_{aq}$** (D_2O) δ (ppm): –4.0 (m, 4P, PTA *trans* to OH_2), –26.0 (m, 4P, PTA *trans* to N). ^{31}P NMR of **23** (D_2O + NaCl) δ (ppm): –9.5 (m, 4P, PTA *trans* to Cl), –25.4 (m, 4P, PTA trans to N). ESI mass spectrum: 665.2 *m*/*z* (calcd. 665.1) $(M - Cl)^+$. UV-vis (H_2O): λ_{max} (ε, L mol^{-1} cm^{-1}) = 412 (1615) nm.

***trans,cis,cis*-RuCl$_2$(PTA)$_2$(py)$_2$ (24).**

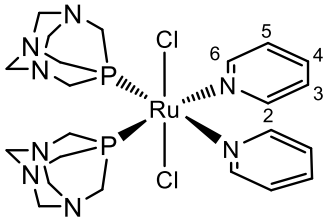

cis,cis,trans-RuCl$_2$(dmso-S)$_2$(PTA)$_2$ (20 mg, 0.031 mmol) was partially dissolved in 2 mL of EtOH. Four equivalents of pyridine (10 µL, 0.124 mmol) were added and the mixture was refluxed for 6h. The clear solution obtained upon warming became gradually orange. Upon cooling to room temperature, an orange powder precipitated and was filtered, washed with ethanol and diethyl ether and dried *in vacuo*. (Yield: 10.9 mg, 55%). According to the ^{1}H and ^{31}P NMR spectra the product was pure **24**. Elemental analysis calcd for [$C_{22}H_{34}Cl_2N_8P_2Ru$] (M_W: 644.1): C 41.00; H 5.32; N

11.00. Found: C 40.95; H 5.23; N 11.05. ^{1}H NMR (D_2O) δ (ppm): 9.08 (d, 4H, H2,6), 8.11 (t, 2H, H4), 7.66 (t, 4H, H3,5), 4.49, 4.44 (ABq, 12H, NC*H*$_2$N), 4.02 (br s, 12H, NC*H*$_2$P). ^{13}C NMR from the HSQC spectrum (D_2O), δ (ppm): 151.0 (C2,6), 139.6 (C4), 125.9 (C3,5), 70.4 (N*C*H$_2$N), 47.0 (N*C*H$_2$P). ^{31}P NMR (D_2O) δ (ppm): –50.0 (s, 2P).

***trans,mer*-RuCl$_2$(py)(PTA)$_3$ (25).**

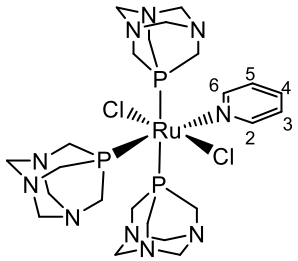

cis,cis,trans-RuCl$_2$(dmso-S)$_2$(PTA)$_2$ (20 mg, 0.031 mmol) was partially dissolved in 2 mL of $CHCl_3$ or in a 4/5 mixture of $CHCl_3$/EtOH. Four equivalents of pyridine (10 μL, 0.124 mmol) were added and the mixture was refluxed for 6h. The clear solution obtained upon warming became gradually orange. After cooling down the solution, the addition of few drops of diethyl ether led the formation of X-ray quality crystals that were filtered, washed with EtOH and diethyl ether and dried *in vacuo* (Yield: 7.8 mg, 35%). According to the ^{1}H and ^{31}P NMR spectra the product was pure **24**. Elemental analysis calcd for [$C_{23}H_{41}Cl_2N_{10}P_3Ru$] ($M_W$: 722.1): C 38.23; H 5.72; N 19.39. Found: C 38.15; H 5.73; N 19.35. ^{1}H NMR ($CDCl_3$) δ (ppm): 9.49 (d, 2H, H2,6), 7.86 (t, 1H, H4), 7.43 (t, 2H, H3,5), 4.62, 4.56 (ABq, 6H, NC*H*$_2$N, PTA *trans* to py), 4.47, 4.36 (ABq, 12H, NC*H*$_2$N, mutually *trans* PTAs), 4.27 (br s, 6H, NC*H*$_2$P, PTA *trans* py), 3.92 (br s, 12H, NC*H*$_2$P, mutually *trans* PTAs). ^{13}C NMR from the HSQC spectrum ($CDCl_3$), δ (ppm): 152.2 (C2,6), 137.7 (C4), 124.7 (C3,5), 73.3 (N*C*H$_2$N, PTA *trans* to py), 73.1 (N*C*H$_2$N, mutually *trans* PTAs), 55.6 (N*C*H$_2$P, PTA *trans* to py), 53.4 (N*C*H$_2$P, mutually *trans* PTAs). ^{31}P NMR ($CDCl_3$) δ (ppm): –22.5 (t, 1P, $^{2}J_{P\text{-}P}$ = 34.5 Hz, PTA *trans* to py), –54.2 (d, 2P, mutually *trans* PTAs).

***fac*-RuCl$_2$(CO)(dmso)$_3$ (26).**

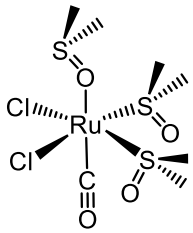

1 g amount of *cis*-RuCl$_2$(dmso)$_4$ (**8**) (2 mmol) was partially dissolved in 60 mL of methanol in a flask closed with a stopcock. The flask was first connected to a vacuum line and then to a reservoir of CO. Within 1.5 h the starting material dissolved completely and a clear pale yellow solution was obtained. After an additional hour of reaction, the solution was concentrated to 5 mL. Yellow crystals of the product formed in a few hours from the solution. They were filtered off, washed with cold methanol and diethyl ether, and vacuum dried. (Yield: 0.54 g, 60%). Selected IR absorption (cm^{-1}): 1995 (ν_{CO}), ^{1}H-NMR ($CDCl_3$) δ (ppm): 3.43 (s, 6H, dmso-S), 3.26 (s, 6H, dmso-S), 2.85 ppm (s, 6H, DMSO-O).

***cis*,*cis*,*trans*-RuCl$_2$(CO)$_2$(dmso-S)$_2$ (27).**

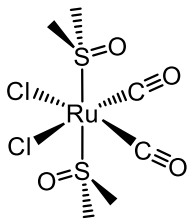

A 0.5 g amount of *cis*-RuCl$_2$(DMSO)$_4$ (**8**) (1 mmol) was heated to reflux in 100 mL of toluene under a stream of CO for 3 h. The resulting colorless solution was concentrated to 90mL and stored at room temperature. Needle-shaped crystals of the product formed within 1 days and were then filtered, washed with diethyl ether, and vacuum dried. Other fractions were collected from the mother liquor upon concentration to 70 mL. (Yield: 0.100 g, 25%). Selected IR absorption (cm^{-1}): 2089 (ν_{CO}), 2035 (ν_{CO}). ^{1}H NMR spectrum ($CDCl_3$) δ (ppm): 3.44 ppm (s, 12H, dmso-S).

***fac*-$RuCl_2(CO)_3$(dmso-O) (30).**

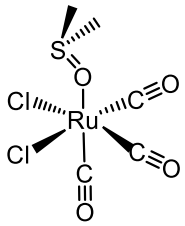

A 0.5 g amount of *cis*-$RuCl_2(DMSO)_4$ (**8**) (2 mmol) was partially dissolved in 40 mL of absolute ethanol and put in autoclave with 30 atm of CO at 80°C for 4 h. The resulting pale yellow solution was rotary evaporated to an oil that was threated with diethyl ether (10 mL x 3 times). The resulting pale yellow precipitate was filtered, washed with cold ethanol and diethyl ether, and vacuum dried. Sometimes it could be necessary put again the precipitate in autoclave for other 4 h with 30 atm of CO at 80°C. (Yield: 0.23 g, 70%). Selected IR absorption (cm^{-1}): 2129 (ν_{CO}), 2060 (ν_{CO}). ^{1}H NMR spectrum ($CDCl_3$) δ (ppm): 2.83 ppm (s, 6H, dmso-O).

***cis,cis,trans*-$RuCl_2CO$(dmso-S)$(PTA)_2$ (31).**

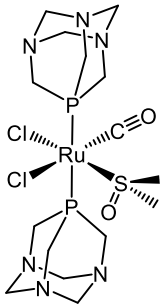

We found two different ways to prepare **31** using different precursors: *fac*-$RuCl_2(CO)(dmso)_3$ (**26**, 60 mg, 0.14 mmol) was partially dissolved in 3 mL of methanol. Two equivalent of PTA (44 mg, 0.28 mmol) were added and the mixture was stirred in the dark for one day. During the time the mixture became a yellow solution and after 8h a white precipitate became to form. The precipitate was filtered and washed with MeOH and diethyl ether and dried *in vacuo* (Yield: 60.9 mg, 73%). The solid was pure **31**, according to ^{1}H and ^{31}P NMR.

X-ray quality crystals of **31** were obtained by slow diffusion of diethyl ether into a chloroform solution of the complex. Elemental analysis calcd for [$C_{15}H_{30}Cl_2N_6O_2P_2SRu$] ($M_W$: 592.0): C 30.41; H 5.10; N 11.97. Found: C 30.45; H 5.19; N 11.88. ^{1}H-NMR (D_2O) δ (ppm): 4.55 (br. s, 12H, NC*H*$_2$N), 4.40 (br s, 12H, NC*H*$_2$P), 3.34 (s, 6H, dmso). ^{13}C NMR from the HSQC spectrum (D_2O), δ (ppm): 70.2 (N*C*H$_2$N), 50.42 (dmso), 48.6 (N*C*H$_2$P). ^{31}P NMR (D_2O), δ (ppm): –52.8 (s, 2P). ^{1}H-NMR ($CDCl_3$) δ (ppm): 4.53 (br. S, 12H, NC*H*$_2$N), 4.48,4.39 (ABq, 12H, NC*H*$_2$P), 3.26 (s, 6H, dmso). ^{13}C NMR from the HSQC spectrum ($CDCl_3$), δ (ppm): 73.6 (N*C*H$_2$N), 50.9 (N*C*H$_2$P), 50.9 (N*C*H$_2$P). ^{31}P NMR ($CDCl_3$), δ (ppm): –54.8 (s, 2P). Selected IR absorption (cm^{-1}): 1950 (ν_{CO}). ESI mass spectrum: 593.0 *m/z* (calcd 593.0) $(M+H)^+$.

Compound **31** was obtained also in the same conditions (MeOH and two equivalents of PTA) using *cis,cis,trans*-$RuCl_2(CO)_2(dmso)_2$ (**27**, 50 mg, filtered after 1h – Yield: 58.6 mg, 63%), *cis,cis,cis*-$RuCl_2(CO)_2(dmso)_2$ (**28**, 50 mg, filtered after 3.5h, Yield: 53.9 mg, 70%) and a mixture of **27** and **28** (filtered after 1.5h – Yield: 50%).

***trans*,*mer*-$RuCl_2CO(PTA)_3$ (32).**

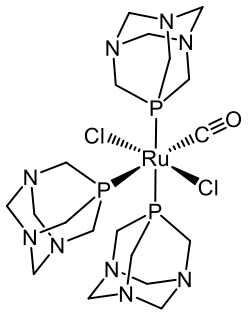

Microwave: *fac*-$RuCl_2(CO)(dmso)_3$ (**26**, 60 mg, 0.14 mmol) was partially dissolved in 2 mL of ethanol. Six equivalent of PTA (131.9 mg, 0.84 mmol) were added and the mixture was put in the microwave at 130°C for 30'. After the reaction a yellow precipitated was formed that was filtered and washed with ethanol and diethyl ether and dried *in vacuo* (Yield: 78.9 mg, 84%). The solid was pure **32**, according to ^{1}H and ^{31}P NMR.

Refluxing ethanol: *fac*-$RuCl_2(CO)(dmso)_3$ (**26**, 60 mg, 0.14 mmol) was partially dissolved in 7 mL of ethanol. Six equivalent of PTA (131.9 mg, 0.84 mmol) were added and the mixture was refluxed for 15h within the formation of a yellow precipitate. After the reaction, the solid was filtered and washed with ethanol and diethyl ether and dried *in vacuo* (Yield: 80.7 mg, 86%). The solid was pure **32**, according to ^{1}H and ^{31}P NMR.

X-ray quality crystals of **32** were obtained by slow diffusion of diethyl ether into a chloroform solution of the complex. Elemental analysis calcd for $[C_{19}H_{36}Cl_2N_5OP_3Ru]$ (M_W: 671.07): C 33.99; H 5.40; N 18.77. Found: C 33.95; H 5.49; N 18.84. ^{1}H-NMR ($CDCl_3$) δ (ppm): 4.58 (m, 18H, NCH_2N), 4.37 (br s, 12H, NCH_2P, mutually *trans* PTAs), 4.32 (br s, 6H, NCH_2P, PTA *trans* CO). ^{13}C NMR from the HSQC spectrum ($CDCl_3$), δ (ppm): 73.2 (N*C*H_2N), 52.4 (N*C*H_2P, mutually *trans* PTAs), 52.2 (N*C*H_2P, PTA *trans* CO). ^{31}P NMR ($CDCl_3$), δ (ppm): –56.0 (d, J = 40.4 Hz, 2P, mutually *trans* PTAs), –63.6 (t, 1P, PTA *trans* CO). ^{1}H-NMR (D_2O) δ (ppm): 4.60 (m, 18H, NCH_2N), 4.37 (br s, 12H, NCH_2P, mutually *trans* PTAs), 4.32 (br s, 6H, NCH_2P, PTA *trans* CO). ^{13}C NMR from the HSQC spectrum (D_2O), δ (ppm): 70.6 (N*C*H_2N), 49.7 (N*C*H_2P, mutually *trans* PTAs), 49.6 (N*C*H_2P, PTA *trans* CO). ^{31}P NMR ($CDCl_3$), δ (ppm): –54.3 (d, J = 39.6 Hz, 2P, mutually *trans* PTAs), –60.7 (t, 1P, PTA *trans* CO). Selected IR absorption (cm^{-1}): 1986 (ν_{CO}). ESI mass spectrum: 672.1 *m/z* (calcd 672.1) $(M+H)^+$, 636.1 *m/z* (calcd 636.1) $(M–Cl)^+$, 608.1 *m/z* (calcd 608.1) $(M–Cl–CO)^+$, 479.1 *m/z* (calcd 479.0) $(M–Cl–PTA)^+$.

***cis,mer*-$RuCl_2CO(PTA)_3$ (33).**

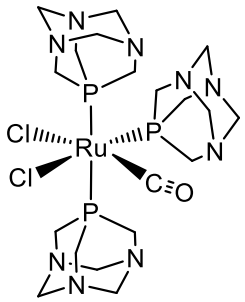

fac-$RuCl_2(CO)(dmso)_3$ (**26**, 60 mg, 0.14 mmol) was dissolved in 4 mL of water. Three equivalents of PTA (0.065 mg, 0.41 mmol) were added and the solution was refluxed for 4h. During the time the color of the solution changed from pale yellow to yellow. After the reaction, the solvent was removed by rotary evaporation obtaining a yellow oil from which X-ray quality crystals formed after 10 days. Crystals were filtered and washed with acetone and diethyl ether and dried *in vacuo* (Yield: 75.1 mg, 80%). The solid was pure **33**, according to ^{1}H and ^{31}P NMR. Elemental analysis calcd for $[C_{19}H_{36}Cl_2N_5OP_3Ru]$ (M_W: 671.07): C 33.99; H 5.40; N 18.77. Found: C 33.90; H 5.35; N 18.74. ^{1}H-NMR (D_2O + NaCl) δ (ppm): 4.49 (m, 18H, NC*H*$_2$N), 4.33 (br s, 12H, NC*H*$_2$P, mutually *trans* PTAs), 4.12 (br s, 6H, NC*H*$_2$P, PTA *trans* Cl). ^{13}C NMR from the HSQC spectrum (D_2O + NaCl), δ (ppm): 70.9 (N*C*H$_2$N), 70.5 (N*C*H$_2$N), 52.2 (N*C*H$_2$P), 46.6 (N*C*H$_2$P). ^{31}P NMR (D_2O + NaCl), δ (ppm): –20.7 (t, J = 25.5 Hz, 1P, PTA *trans* Cl), –51.9 (d, 2P, mutually *trans* PTAs). Selected IR absorption (cm^{-1}): 1942 (ν_{CO}). ESI mass spectrum: 636.1 *m/z* (calcd 636.1) $(M–Cl)^+$.

[RuCl$_2$(CO)(PTA)$_2$]$_2$·8H$_2$O (35).

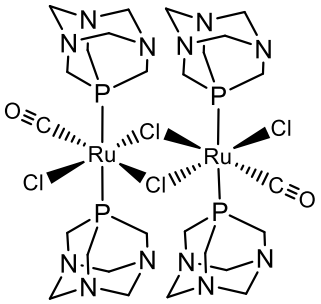

trans,*cis,cis*-RuCl$_2$(CO)$_2$(dmso-O)$_2$ (**29**, 100 mg, 0.26 mmol) was dissolved in 3 mL of water obtaining a yellow solution. Two equivalents of PTA (81.8 mg, 0.52 mmol) were added obtaining a yellow solution. After the reaction, the water was removed by rotary evaporation obtaining a yellow oil. Treatment of the oil with acetone (5 mL, 4 times) afforded to a yellow precipitate that was filtered, washed with acetone and diethyl ether and dried *in vacuo.* (Yield: 136.6 mg, 98%). The solid was pure **35**, according to ^{1}H and ^{31}P NMR. Elemental analysis calcd for [$C_{26}H_{64}Cl_4N_{12}O_{10}P_4Ru_2$] ($M_W$: 1172.07): C 26.63; H 5.50; N 14.33. Found: C 26.84; H 5.50; N 14.50. ^{1}H-NMR (D$_2$O) δ (ppm): 4.57 (br s, 24H, NC*H*$_2$N), 4.27 (br s, 24H, NC*H*$_2$P). ^{13}C NMR from the HSQC spectrum (D$_2$O), δ (ppm): 70.6 (N*C*H$_2$N), 46.9 (N*C*H$_2$P). ^{31}P NMR (D$_2$O), δ (ppm): –47.2 (2P, mutually *trans* PTAs). ^{1}H-NMR (DMSO-*d*$_6$) δ (ppm): 4.45 (br s, 24H, NC*H*$_2$N), 4.12 (br s, 24H, NC*H*$_2$P). ^{13}C NMR from the HSQC spectrum (DMSO-*d*$_6$), δ (ppm): 72.6 (N*C*H$_2$N), 49.7 (N*C*H$_2$P). ^{31}P NMR (DMSO-*d*$_6$), δ (ppm): –51.2 (2P, mutually *trans* PTAs). Selected IR absorption (cm^{-1}): 1941 (ν_{CO}). ESI mass spectrum (positive mode): 479.1 *m/z* (calcd 479.1) ([RuCl(CO)(PTA)$_2$]$^+$). ESI mass spectrum (negative mode): 548.1 *m/z* (calcd 548.1) ([RuCl$_3$(CO)(PTA)$_2$]$^-$).

***trans,trans,trans*-$RuCl_2(CO)(py)(PTA)_2$ (36).**

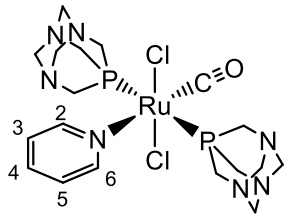

$[RuCl_2(CO)(PTA)_2]_2 \cdot 8H_2O$ (**35**, 30 mg, 0.026 mmol) was dissolved in 3 mL of water obtaining a yellow solution; 1.2 equivalents of pyridine (5.6 µL, 0.030 mmol) were added and the solution was stirred at room temperature for three days. After the reaction, the water was removed by rotary evaporation and the precipitate was treated with acetone and filtered, washed with acetone and diethyl ether obtaining a yellow powder that was dried *in vacuo*. (Yield: 9.2 mg, 60%). The solid was pure **36** according to ^1H and ^{31}P NMR. Elemental analysis calcd for $[C_{18}H_{29}Cl_2N_7OP_2Ru]$ (M_W: 593.03): C 36.43; H 4.93; N 16.52. Found: C 36.48; H 4.89; N 16.54. ^1H-NMR (D_2O) δ (ppm): 9.08 (d, 2H, H2,6), 8.11 (t, 1H, H4), 7.66 (t, 2H, H3,5), 4.35 (m, 12H, NC*H*$_2$N), 3.90 (br s, 12H, NC*H*$_2$P). ^{13}C NMR from the HSQC spectrum (D_2O), δ (ppm): 151.0 (C2,6), 139.6 (C4), 125.9 (C3,5), 70.6 (N*C*H_2N), 47.0 (N*C*H_2P). ^{31}P NMR (D_2O), δ (ppm): –50.0 (2P, mutually *trans* PTAs). Selected IR absorption (cm^{-1}): 2010 (ν_{CO}). ESI mass spectrum: 594.0 *m/z* (594.3 calcd) $(M+H)^+$.

$[RuCl_2(CO)_2(PTA)]_2 \cdot H_2O$ (37).

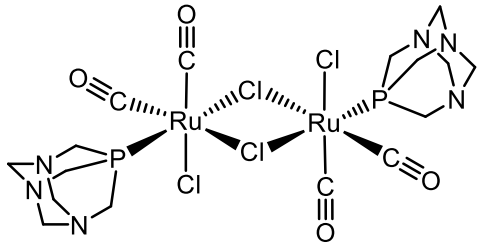

cis,fac-$RuCl_2(CO)_3$(dmso-O) (**30**, 60 mg, 0.14 mmol) was dissolved in 3 mL of methanol. After the addition of one equivalent of PTA (44 mg, 0.28 mmol), a white solid starts to precipitate. The mixture was filtered and washed with MeOH and diethyl ether and dried *in vacuo* (Yield: 80.5 mg, 73%). The solid was pure **37**,

according to ^{1}H and ^{31}P NMR. Elemental analysis calcd for [$C_{16}H_{26}Cl_4N_6O_5P_2Ru_2$] ($M_W$: 787.83): C 24.38; H 3.32; N 10.66. Found: C 24.28; H 3.43; N 10.66. (M_W: 787.8). ^{1}H-NMR (DMSO-d_6) δ (ppm): 4.43 (m, 24H, NCH_2N + NCH_2P). ^{31}P NMR (DMSO-d_6), δ (ppm): –28.8 (2P, PTA *trans* to Cl). Selected IR absorption (cm^{-1}): 2060 (ν_{CO}), 1989 (ν_{CO}). ESI mass spectrum (positive mode): 409.3 *m/z* (calcd 409.1) ([$RuCl_2(CO)_2(PTA)Na]^+$). ESI mass spectrum (negative mode): 421.2 *m/z* (calcd 421.3) ([$RuCl_3(CO)_2(PTA)]^-$), 393.2 *m/z* (calcd 393.3) ([$RuCl_3(CO)(PTA)]^-$).

***cis,cis,trans*-$RuCl_2(CO)_2(py)(PTA)$ (38).**

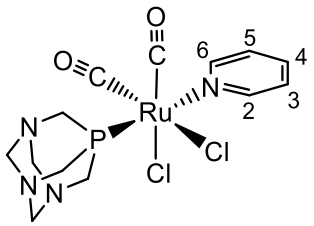

[$RuCl_2(CO)_2(PTA)]_2 \cdot H_2O$ (**37**, 30 mg, 0.038 mmol) was partially dissolved in 3 mL of water obtaining a colorless solution; 1.2 equivalents of pyridine (8.0 μL, 0.046 mmol) were added and the solution was stirred at room temperature for three days. After the reaction, the water was removed by rotary evaporation and the precipitate was extracted with chloroform and rotary evaporated to dryness (Yield: 7.3 mg, 55%). The solid was pure **38** according to ^{1}H and ^{31}P NMR. Elemental analysis calcd for [$C_{13}H_{17}Cl_2N_4O_2PRu$] ($M_W$: 463.95): C 32.63; H 3.69; N 15.27. Found: C 32.58; H 2.59; N 12.04. ^{1}H-NMR ($CDCl_3$) δ (ppm): 8.91 (d, 2H, H2,6), 7.87 (t, 1H, H4), 7.45 (t, 2H, H3,5), 4.60 (br s, 6H, NCH_2N), 4.53 (br s, 6H, NCH_2P). ^{31}P NMR ($CDCl_3$), δ (ppm): –28.8 (1P, PTA *trans* to py). Selected IR absorption (cm^{-1}): 2058 (ν_{CO}), 1994 (ν_{CO}). ESI mass spectrum: 464.9 *m/z* (464.5 calcd) $(M+H)^+$.

***cis,cis,trans*-$RuCl_2(CO)_2(PTA)_2$ (39).**

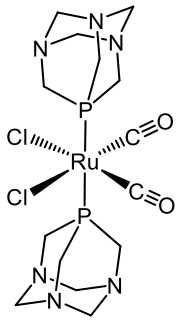

cis,fac-$RuCl_2(CO)_3$(dmso-O) (**30**, 60 mg, 0.14 mmol) was dissolved in 3 mL of methanol. After the addition of two equivalents of PTA (44 mg, 0.28 mmol), a white solid starts to precipitate. The mixture was filtered and washed with MeOH and diethyl ether and dried *in vacuo* (Yield: 60.9 mg, 73%). The solid was pure **39**, according to ^{1}H and ^{31}P NMR. X-ray quality crystals were obtained upon slowly evaporation of the solvent in a MeOH solution of **3**. Elemental analysis calcd for [$C_{14}H_{24}Cl_2N_6O_2P_2Ru$] ($M_W$: 541.99): C 31.01; H 4.46; N 15.50. Found: C 31.08; H 4.49; N 15.54. ^{1}H-NMR (D_2O) δ (ppm): 4.61 (br s, 12H, NC*H*$_2$N), 4.44 (br s, 12H, NC*H*$_2$P). ^{13}C NMR from the HSQC spectrum (D_2O), δ (ppm): 70.6 (N*C*H_2N), 48.2 (N*C*H_2P). ^{31}P NMR (D_2O), δ (ppm): –48.6 (2P, mutually *trans* PTAs). ^{1}H-NMR (DMSO-*d*$_6$) δ (ppm): 4.47 (m, 12H, NC*H*$_2$N), 4.31 (br s, 12H, NC*H*$_2$P). ^{13}C NMR from the HSQC spectrum (DMSO-*d*$_6$), δ (ppm): 72.1 (N*C*H_2N), 50.0 (N*C*H_2P). ^{31}P NMR (DMSO-*d*$_6$), δ (ppm): –50.3 (2P, mutually *trans* PTAs). ^{1}H-NMR ($CDCl_3$) δ (ppm): 4.58 (br s, 12H, NC*H*$_2$N), 4.41 (br s, 12H, NC*H*$_2$P). ^{31}P NMR ($CDCl_3$), δ (ppm): –51.0 (2P, mutually *trans* PTAs). Selected IR absorption (cm^{-1}): 2053 (ν_{CO}), 1988 (ν_{CO}). ESI mass spectrum: 479.9 *m/z* (479.5 calcd) $(M–Cl–CO)^+$.

Compound **30** was obtained also using *cis,cis,trans*-$RuCl_2(dmso)_2(PTA)_2$ (**10**, 10 mg, 0.016 mmol) dissolved in 5 mL of $CHCl_3$, put in autoclave with CO (30 atm) and heated at 60°C for 24h. The resulting colorless solution was rotary evaporated to a white powder that is pure **30** according ^{1}H and ^{31}P NMR spectra. (Yield: 8.2 mg, 93%).

***cis*-[RuCl(CO)(PTA)$_4$](NO$_3$) (42NO$_3$).**

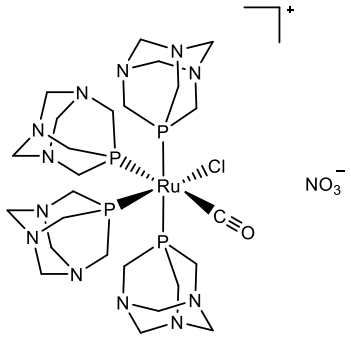

cis-RuCl$_2$(PTA)$_4$ (**2**, 50 mg, 0.062 mmol) was partially dissolved in 9 mL of CHCl$_3$; 1.2 equivalents of AgNO$_3$ (12.8 mg, 0.075 mmol) were added and the flask was first connected to a vacuum line and then to a reservoir of CO. After few minutes it was observed the formation of a white precipitate. After 1 day of reaction, the solid was filtered and extracted with water and then rotary evaporated to dryness. The solid was pure **42NO$_3$**, according to ^{1}H and ^{31}P NMR. (Yield 30.0 mg, 57%). Elemental analysis calcd for [C$_{25}$H$_{48}$ClN$_{12}$O$_4$P$_4$Ru] (M$_W$: 855.16): C 35.11; H 5.66; N 21.29. Found: C 35.18; H 5.69; N 21.24. ^{1}H-NMR (D$_2$O) δ (ppm): 4.65 (m, 32H, NC*H*$_2$N + NC*H*$_2$P), 4.32 (br s, 6H, NC*H*$_2$P). 4.19 (br s, 6H, NC*H*$_2$P). ^{13}C NMR from the HSQC spectrum (D$_2$O), δ (ppm): 70.52 (N*C*H$_2$N), 55.5 (N*C*H$_2$P), 52.1. ^{31}P NMR (D$_2$O), δ (ppm): –31.4 (1P, $^2J_{A\text{-}M}$ = 20.5 Hz, $^2J_{A\text{-}X}$ = 32.8 Hz, PTA *trans* to Cl), –59.8 ppm (2P, mutually *trans* PTAs), –61.9 ppm (1P, $^2J_{X\text{-}M}$ = 35.8 Hz, PTA *trans* to CO). Selected IR absorption (cm^{-1}): 2020 (ν_{CO}). ESI mass spectrum: 793.1 *m/z* (793.5 calcd) (M$^+$).

***cis,trans*-[Ru(bpy)Cl(CO)(PTA)$_2$]Cl (43).**

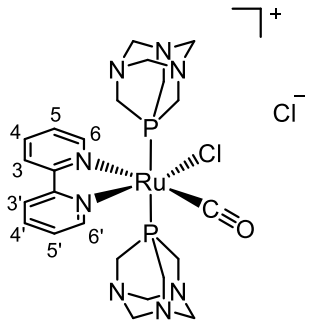

cis,cis,trans-RuCl$_2$CO(dmso-S)(PTA)$_2$ (**31**) (40.0 mg, 0.067 mmol) was dissolved in 5 mL of water. One eq. of 2,2'-bipyridine (10.5 mg, 0.067 mmol) was added and the light-protected mixture was refluxed for 16 h or put in a microwave reactor at 150°C for 30'. The yellow solution turned rapidly orange. The solvent was rotary evaporated affording a yellow solid that was washed with acetone, filtered and dried *in vacuo*. The solid was pure **43**, according to ^{1}H and ^{31}P NMR. (Yield 30.0 mg, 57%). **43** was also obtained also by treatment of [RuCl$_2$(CO)(PTA)$_2$]$_2$·8H$_2$O (**35**, 20 mg, 0.034 mmol) with bpy (5.3 mg, 0.034 mmol) after 2h at reflux. Elemental analysis calcd for [C$_{23}$H$_{32}$Cl$_2$N$_8$OP$_2$Ru] (M$_W$: 670.06): C 41.20; H 4.81; N 16.71. Found: C 41.27; H 4.83; N 16.77. ^{1}H-NMR (D$_2$O) δ (ppm): 9.27 (d, 1H, H6), 8.93 (d, 1H, H6'), 8.66 (d, 1H, H3), 8.55 (d, 1H, H3'), 8.42 (t, 1H, H4), 8.23 (t, 1H, H4'), 7.96 (t, 1H, H5), 7.60 (d, 1H, H5'), 4.41, 4.31 (ABq, 12H, NC*H*$_2$N), 3.82, 3.76 (ABq, 12H, NC*H*$_2$P). ^{13}C NMR from the HSQC spectrum (D$_2$O), δ (ppm): 155.7 (C6'), 149.0 (C6), 141.0 (C4), 139.4 (C4'), 128.1 (C5'), 127.9 (C5), 125.0 (C3'), 124.8 (C3), 70.3 (N*C*H$_2$N), 46.3 (N*C*H$_2$P). ^{31}P NMR (D$_2$O), δ (ppm): –50.6 (2P, mutually *trans* PTAs). Selected IR absorption (cm^{-1}): 1984 (ν$_{CO}$). ESI mass spectrum: 635.6 *m/z* (635.9 calcd) (M$^+$).

***mer*-[Ru(bpy)(CO)(PTA)$_3$](Cl)$_2$ (45).**

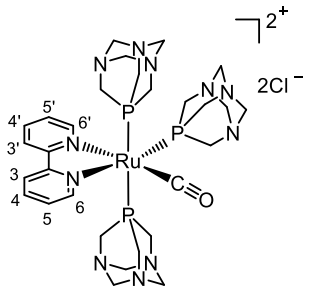

cis,mer-$RuCl_2CO(PTA)_3$ (**33**) (40.0 mg, 0.060 mmol) was dissolved in 5 mL of water. One eq. of 2,2'-bipyridine (9.4 mg, 0.060 mmol) was added and the light-protected mixture was refluxed for 1 h. The yellow solution turned rapidly to orange. The solvent was rotary evaporated affording a yellow solid that was washed with acetone, filtered and dried *in vacuo.* The solid was pure **44**, according to ^{1}H and ^{31}P NMR. (Yield 30.0 mg, 60%). X-ray quality crystals of **33** were obtained by slow diffusion of acetone into a water solution of the complex. Elemental analysis calcd for $[C_{30}H_{47}Cl_2N_{11}OP_3Ru]$ (M_W: 842.67): C 42.76; H 5.62; N 18.28. Found: C 42.70; H 5.69; N 18.24. ^{1}H-NMR (D_2O) δ (ppm): 9.07 (d, 1H, H6), 8.92 (m, 2H, H3 + H3'), 8.53 (m, 3H, H6' + H4 + H4'), 7.99 (m, 2H, H5 + H5'), 4.85, 4.73 (ABq, 6H, NC*H*$_2$N PTA *trans* to N), 4.66 (br s, 6H, NC*H*$_2$P, PTA *trans* to N) 4.40 (m, 12H, NC*H*$_2$N mutually *trans* PTAs), 3.86, 3.80 (ABq, 12H, NC*H*$_2$P). ^{13}C NMR from the HSQC spectrum (D_2O), δ (ppm): 154.9 (C6), 153.8 (C6'), 142.4 (C4 + C4'), 129.9 (C5 + C5'), 126.9 (C3 + C3'). ^{31}P NMR (D_2O), δ (ppm): –49.6 (1P, $^{2}J_{P\text{-}P}$ = 25.2 Hz, PTA *trans* to N), –55.4 (2P, mutually *trans* PTAs). Selected IR absorption (cm^{-1}): 2010 (ν_{CO}). ESI mass spectrum: 631.6 *m/z* (631.7 calcd) $(M–PTA+OH)^+$.

***cis,trans*-[Ru(bpy)(CO)$_2$Cl(PTA)]Cl (46).**

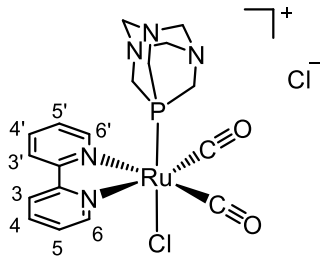

$[RuCl_2(CO)_2(PTA)]_2 \cdot H_2O$ (**37**, 30 mg, 0.038 mmol) was dissolved in 5 mL of water. One eq. of 2,2'-bipyridine (5.9 mg, 0.038 mmol) was added and the light-protected mixture was refluxed for 1 h. The colorless solution turned rapidly to orange-red. The solvent was rotary evaporated affording an orange solid that was washed with acetone, filtered and dried *in vacuo.* The solid was pure **46**, according to ^{1}H and ^{31}P NMR. (Yield 13.4 mg, 65%). Elemental analysis calcd for $[C_{18}H_{20}Cl_2N_5O_2PRu]$ (M_W: 541.34): C 39.94; H 3.72; N 12.94. Found: C 39.94; H 3.72; N 12.94. ^{1}H-NMR (D_2O) δ (ppm): 9.08 (d, 2H, H6,6'), 8.67 (d, 2H, H3,3') 8.44 (t, 2H, H4,4'), 7.91 (t, 2H, H5,5'), 4.46 (m, 6H, NC*H*$_2$N), 4.09 (br s, 6H, NC*H*$_2$P). ^{13}C NMR from the HSQC spectrum (D_2O), δ (ppm): 153.5 (C6,6'), 142.0 (C4,4'), 129.0 (C5,5'), 125.5 (C3,3'), 70.3 (N*C*H$_2$N), 50.6 (N*C*H$_2$P). ^{31}P NMR (D_2O), δ (ppm): –25.5 (1P, PTA *trans* to N). Selected IR absorption (cm^{-1}): 2085 (ν_{CO}), 2034 (ν_{CO}).

***cis,trans*-[Ru(bpy)(CO)$_2$(PTA)$_2$](NO$_3$)$_2$ (47).**

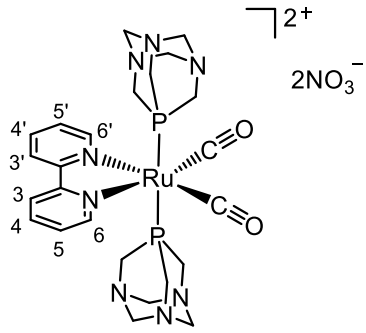

cis,cis,trans-$RuCl_2CO_2(PTA)_2$ (**39**) (40.0 mg, 0.074 mmol) was dissolved in 8 mL of water. 2.1 eq of $AgNO_3$ (26.4 mg, 0.155mmol) were added to the solution; one eq. of 2,2'-bipyridine (11.6 mg, 0.074 mmol) was added and the light-protected

mixture was refluxed for 1 h. After few minutes it was observed the formation of a grey precipitate; the colorless solution turned rapidly to orange-red. At the end of reaction, the grey precipitate was filtered. The solvent was rotary evaporated affording a red solid that was washed with acetone, filtered and dried *in vacuo.* The solid was pure **47**, according to ^{1}H and ^{31}P NMR. (Yield 30.0 mg, 57%). Elemental analysis calcd for [$C_{24}H_{32}N_{10}O_8P_2Ru$] ($M_W$: 751.60): C 38.35; H 4.29; N 17.03. Found: C 38.30; H 4.22; N 17.09. ^{1}H-NMR (D_2O), δ (ppm): 9.02 (d, 2H, H6,6'), 8.82 (d, 2H, H3,3') 8.57 (t, 2H, H4,4'), 8.02 (t, 2H, H5,5'), 4.47, 4.43 (ABq, 12H, NC*H*$_2$N), 4.04 (br s, 6H, NC*H*$_2$P). ^{13}C NMR from the HSQC spectrum (D_2O), δ (ppm): 153.9 (C6,6'), 142.7 (C4,4'), 129.1 (C5,5'), 126.7 (C3,3'), 70.4 (N*C*H$_2$N), 47.8 (N*C*H$_2$P). ^{31}P NMR (D_2O), δ (ppm): –50.9 (1P, mutually *trans* PTAs). Selected IR absorption (cm^{-1}): 2086 (ν_{CO}), 2038 (ν_{CO}).

***cis,cis*-[Ru(bpy)Cl(CO)(PTA)$_2$]Cl (48).**

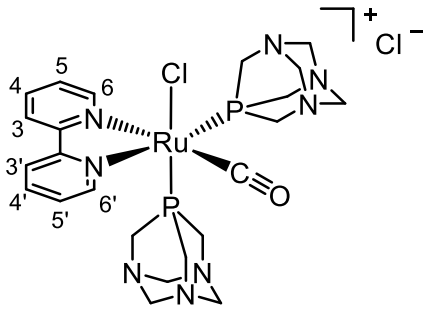

cis,trans-[Ru(bpy)Cl(CO)(PTA)$_2$]Cl (**43**, 10.0 mg, 0.015 mmol) was dissolved in 2 mL of water and irradiated with blue light (λ = 470 nm, 40 mW) for 24 h. Complete removal of the solvent by rotary evaporation afforded pure **48**, according to ^{1}H and ^{31}P NMR spectra, as a yellow solid (Yield: 9.5 mg, 95%). Elemental analysis calcd for [$C_{23}H_{32}Cl_2N_8OP_2Ru$] ($M_W$: 670.06): C 41.20; H 4.81; N 16.71. Found: C 41.15; H 4.89; N 16.74. ^{1}H-NMR (D_2O) δ (ppm): 9.09 (d, 1H, H6), 8.75 (d, 1H, H6'), 8.65 (d, 1H, H3), 8.58 (d, 1H, H3'), 8.41 (t, 1H, H4), 8.32 (t, 1H, H4'), 7.87 (t, 1H, H5), 7.81 (d, 1H, H5'), 4.61 (m, 6H, NC*H*$_2$N), 4.45 (m, 6H NC*H*$_2$P) 4.31, 4.16 (ABq, 6H, NC*H*$_2$N), 3.80 (br s, 12H, NC*H*$_2$P). ^{13}C NMR from the HSQC spectrum (D_2O), δ

(ppm): 153.4 (C6), 153.3 (C6'), 141.5 (C4), 140.7 (C4'), 128.4 (C5), 128.1 (C5'), 125.5 (C3), 125.0 (C3), 70.6 (N*C*H$_2$N), 70.3 (NC*H*$_2$N), 80.8 (NC*H*$_2$P), 49.0 (N*C*H$_2$P). ^{31}P NMR (D$_2$O), δ (ppm): –25.0 (1P, $^2J_{P\text{-}P}$ = 24.8 Hz, PTA *trans* to Cl), –42.4 (1P, PTA *trans* to N). Selected IR absorption (cm^{-1}): 1992 (ν_{CO}). ESI mass spectrum: 635.4 *m/z* (635.9 calcd) (M$^+$).

***trans*,*cis*-RuCl$_2$(CO)$_2$(cppH-κ*N*^{p}) (51) and *trans*,*cis*-RuCl$_2$(CO)$_2$(cppH-κ*N*^{o}) (52).**

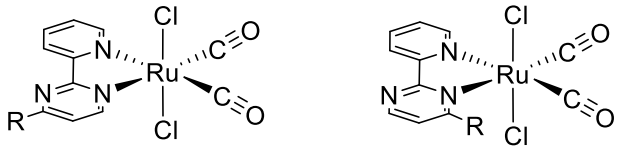

51 **52**

A 30.0 mg amount of *trans,cis,cis*-RuCl$_2$(CO)$_2$(dmso-O)$_2$ (**29**, 0.078 mmol) was partially dissolved in 1.5 mL of water. One eq. of cppH·HNO$_3$ (20.0 mg, 0.078 mmol) was added and the mixture was refluxed for 1 h in the dark. A clear solution was rapidly obtained upon warming, from which a very pale yellow precipitate began to form after ca. 15 min of reflux. It was eventually removed by filtration, rapidly washed with water and dried *in vacuo* (Yield 15.0 mg, 45%). The product was pure **51** according to the ^{1}H NMR spectrum. *trans*,*cis*-RuCl$_2$(CO)$_2$(cppH-κ*N*^{p}) (**51**): Elemental analysis calcd for [C$_{12}$H$_7$N$_3$Cl$_2$O$_4$Ru·H$_2$O] (M$_W$: 447.19): C 32.23; H 2.03; N 9.39. Found: C 32.50; H 1.96; N 9.28. ^{1}H NMR (DMSO-*d*$_6$) δ (ppm): 9.82 (d, *J* = 5.7 Hz, 1H, H6), 9.31 (d, *J* = 5.2 Hz, 1H, H6'), 8.86 (d, *J* = 7.9, 1.3 Hz, 1H, H3'), 8.48 (t, *J* = 7.9, 1.5 Hz, 1H, H4'), 8.29 (d, *J* = 5.7 Hz, 1H, H5), 8.03 (t, *J* = 5.2 Hz 1H, H5'). ^{13}C NMR (DMSO-*d*$_6$), δ (ppm): 195.66 (CO), 195.42 (CO), 162.72 (C6), 153.79 (C6'), 141.35 (C4'), 130.29 (C5'), 126.57 (C3'), 122.69 (C5); unassigned resonances of the four quaternary carbon atoms: 163.41, 162.46, 158.06, 151.79.^{15}N NMR (DMSO-*d*$_6$), δ (ppm): –108.9 (*N*^{o}), –126.5 (N$_{py}$), –130.2 (*N*^{p}). Selected IR absorption (cm^{-1}): 2069 (ν_{CO}, s) 2013 (ν_{CO}, s). ESI mass spectrum: *m*/*z* 428.0 (M – H$^+$).

When the reaction was performed at room temperature in the absence of stirring (30.0 mg of **29**, 20.0 mg of cppH·HNO_3, 2 mL of water) a small amount of almost colorless crystals of **51** grew spontaneously from the pale-orange solution within 4 h. The crystals, that were removed by filtration, washed with a minimum amount of water and dried *in vacuo*, were used for the X-ray structural analysis (Yield: 2.5 mg, 7.5%). The mother liquor was rotary-evaporated to an oil, that was treated with diethyl ether to give a pale yellow solid. It was filtered, washed with diethyl ether and dried *in vacuo* (Yield 22.2 mg, 66%). The product was almost pure **52** according to the ^{1}H NMR spectrum. *trans*,*cis*-$RuCl_2(CO)_2$(cppH-κN^o) (**52**): Elemental analysis calcd for [$C_{12}H_7N_3Cl_2O_4Ru$] (M_W: 429.18): C 33.58; H 1.64; N 9.79. Found: C 33.39; H 1.54; N 9.61. ^{1}H NMR (DMSO-d_6) δ (ppm): 9.46 (d, J = 4.9 Hz, 1H, H6), 9.27 (d, J = 5.4 Hz, 1H, H6'), 8.85 (d, J = 8.1 Hz, 1H, H3'), 8.46 (t, J = 7.9, 1H, H4'), 8.20 (d, J = 4.9 Hz, 1H, H5), 8.02 (t, J = 5.4 Hz, 1H, H5'). ^{13}C NMR (DMSO-d_6) δ (ppm): 196.31 (CO), 194.17 (CO), 162.72 (C6), 153.34 (C6'), 141.17 (C4'), 130.09 (C5'), 127.10 (C3'), 120.83 (C5); unassigned resonances of the four quaternary carbon atoms: 165.21, 161.82, 161.09, 152.39. ^{15}N NMR (DMSO-d_6) δ (ppm): –86.2 (N^o), –126.5 (N_{py}), –143.6 (N^p). Selected IR absorption (cm^{-1}): 2059 (ν_{CO}), 2013 (ν_{CO}). ESI mass spectrum: m/z 428.0 ($M - H^+$).

Mixtures of *cis,trans*-$RuCl_2$(dmso-S)$_2$(mpp-κN^p) (53), *cis,cis*-$RuCl_2$(dmso-S)$_2$(mpp-κN^p) (54), and *cis,cis*-$RuCl_2$(dmso-S)$_2$(mpp-κN^p) (55).

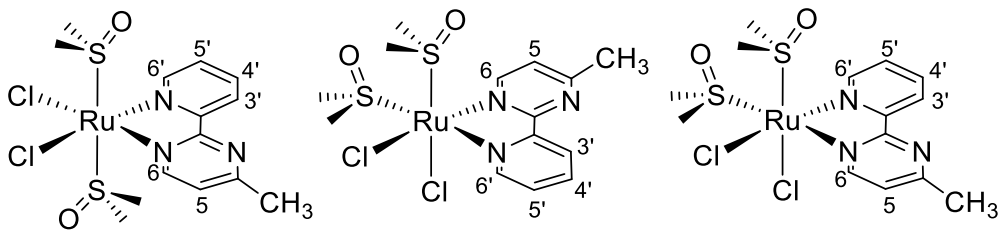

53 **54** **55**

Refluxing toluene: A 50.0 mg amount of *cis*-$RuCl_2$(dmso-S)$_4$ (**8**, 0.10 mmol) was dissolved in 10 mL of toluene. A slight excess of mpp (21.0 mg, 0.12 mmol) was added and the mixture was refluxed for 1.5 h. The yellow solution turned rapidly

dark brown upon warming, and a precipitate began to form after ca. 1 h of reflux. It was eventually removed by filtration, washed with diethyl ether and dried *in vacuo* (Yield 32.0 mg, 64%). According to the ^{1}H NMR spectrum, the product was a ca. 1:2:1 mixture of **53**-**55**. Elemental analysis calcd for [$C_{14}H_{21}N_3Cl_2O_2RuS_2$] ($M_W$: 499.45): C 33.67; H 4.24; N 8.41. Found: C 33.52; H 4.32; N 8.50. A second fraction of solid was obtained from the mother liquor: after complete rotary evaporation of the solvent, the oil obtained was treated with diethyl ether to obtain a solid that was filtered, washed with diethyl ether and dried *in vacuo* (Yield 15.0 mg, 30%). According to the ^{1}H NMR spectrum this fraction was a ca. 1:1:1 mixture of **53**-**55**.

Refluxing ethanol: A 50.0 mg amount of *cis*-$RuCl_2(dmso)_4$ (**8**, 0.10 mmol) was dissolved in 10 mL of ethanol. A slight excess of mpp (21.0 mg, 0.12 mmol) was added and the mixture was refluxed for 2h. After cooling, the solution was rotary-evaporated to ca. 3 mL and diethyl ether was added dropwise to the point of cloudiness. Red-orange crystals formed within 4h and a few of them were fished out the solution: According to the ^{1}H NMR spectrum, they were a ca. 3:1 mixture of **53** and **54** with a small amount of **5**. Some crystals were selected for X-ray analysis and turned out to be of compound **53**. A second fraction of precipitate, obtained from the mother liquor upon further concentration and addition of diethyl ether, was a ca. equimolar mixture of **53**-**55**.

Methanol at ambient temperature: A 50.0 amount of *trans*-$RuCl_2(dmso\text{-}S)_4$ (**9**, 0.10 mmol) was dissolved in 10 mL of methanol and a slight excess of mpp (21.0 mg, 0.12 mmol) was added. The yellow solution turned rapidly deep red. After 90 min it was rotary evaporated to ca. 5 mL and diethyl ether was slowly added dropwise. Red crystals formed within 24h and were removed by filtration, washed with diethyl ether and dried *in vacuo* (Yield: 18 mg, 36%). According to the ^{1}H NMR spectrum the crystalline product was a ca. 2:3 mixture of **54** and **55**. Some crystals were selected for X-ray analysis and turned out to be of compound **54**. To be noted that when the

solution was concentrated to a smaller volume, precipitation of the kinetic intermediate **56** occurred (see below).

cis,trans-$RuCl_2$(dmso-S)$_2$(mpp-κN^p) (**53**): ^{1}H NMR ($CDCl_3$) δ (ppm): 9.58 (m, 2H, H6' overlapped with H6), 8.54 (d, J = 7.9 Hz, 1H, H3'), 7.97 (m, 1H, H4' overlapped with H4' of **55**), 7.60 (t, J = 6.7 Hz, 1H, H5'), 7.29 (d, 1H, H5), 3.18 (s, 6H), 2.98 (s, 6H), 2.68 (s, 3H). Selected ^{13}C NMR from the HSQC spectrum ($CDCl_3$) δ (ppm): 159.4 (C6), 153.7 (C6'), 136.4 (C4'), 127.4 (C5'), 125.3 (C3'), 121.0 (C5), 41.5 and 41.3 (dmso-S), 24.1 (CH_3 mpp). ^{15}N NMR ($CDCl_3$) δ (ppm): –90.2 (N^o), –145.0 (N_{py}), –160.4 (N^p).

cis,cis-$RuCl_2$(dmso-S)$_2$(mpp-κN^p) (**54**, py of mpp *trans* to dmso-S): ^{1}H NMR ($CDCl_3$) δ (ppm): 9.79 (m, 1H, H6' overlapped with H6 of **55**), 9.62 (d, J = 6.2 Hz, 1H, H6), 8.69 (m, 1H, H3' overlapped with H3' of **55**), 8.08 (t, J = 7.6 Hz, 1H, H4'), 7.70 (t, J = 6.6 Hz, 1H, H5'), 7.32 (d, 1H, H5), 3.53 (s, 3H), 3.51 (s, 3H) 3.30 (s, 3H), 2.71 (s, 3H), 2.59 (s, 3H). Selected ^{13}C NMR from the HSQC spectrum ($CDCl_3$), δ (ppm): 161.6 (C6), 152.3 (C6'), 138.2 (C4'), 127.3 (C5'), 125.9 (C3'), 120.8 (C5), 46.6 and 46.4 (dmso-S trans to N), 45.5 and 44.0 (dmso-S trans to Cl), 23.9 (CH_3 mpp). ^{15}N NMR ($CDCl_3$), δ (ppm): –87.7 (N^o), –130.7 (N_{py}), –153.4 (N^p).

cis,cis-$RuCl_2$(dmso-S)$_2$(mpp-κN^p) (**55**, py of mpp *trans* to Cl): ^{1}H NMR ($CDCl_3$), δ (ppm): 9.79 (m, 1H, H6 overlapped with H6' **54**), 9.51 (d, J = 6.2 Hz, 1H, H6'), 8.69 (m, 1H, H3' overlapped with H3' of **54**), 7.97 (m, 1H, H4' overlapped with H4' of **54**), 7.54 (t, J = 6.6 Hz, 1H, H5'), 7.42 (d, 1H, H5), 3.49 (m, J = 9.5 Hz, 6H), 3.09 (s, 3H), 2.93 (s, 3H), 2.76 (s, 3H). Selected ^{13}C NMR from the HSQC spectrum ($CDCl_3$), δ (ppm): 158.5 (C6), 155.7 (C6'), 136.8 (C4'), 127.5 (C5'), 125.9 (C3'), 121.2 (C5), 46.6 and 46.5 (dmso-S trans to N), 45.0 and 44.5 (dmso-S trans to Cl), 24.2 (CH_3 mpp).^{15}N NMR ($CDCl_3$), δ (ppm): –88.7 (N^o), –135.9 (N_{py}), –147.6 (N^p).

***trans,cis*-RuCl$_2$(dmso-S)$_2$(mpp-κ*N^p*) (56).**

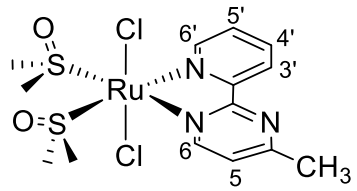

A 50.0 amount of *trans*-RuCl$_2$(dmso-S)$_4$ (**9**, 0.10 mmol) was dissolved in 10 mL of methanol and a slight excess of mpp (21.0 mg, 0.12 mmol) was added. The initial yellow solution turned rapidly deep red. After 90 min it was rotary evaporated to ca. 2 mL, rapidly affording red crystals of **56** suitable for X-ray diffraction (Yield 14 mg, 28%). Similar results were obtained when the reaction was performed in chloroform at room temperature. In this case, after 90 min the solution was rotary evaporated to an oil that, treated with diethyl ether, afforded a red-orange solid that was filtered, washed with diethyl ether and dried *in vacuo*. (Yield: 80.1 mg, 76%). The product was (almost) pure **56** according to ^{1}H NMR spectrum. Elemental analysis calcd for [$C_{14}H_{21}N_3Cl_2O_2RuS_2$] ($M_W$: 499.45): C 33.67; H 4.24; N 8.41. Found: C 33.76; H 4.16; N 8.38. ^{1}H NMR ($CDCl_3$), δ (ppm): 10.30 (br s, 1H, H6), 8.96 (br s, 1H, H6'), 8.78 (d, J = 7.9 Hz, 1H, H3'), 8.02 (t, J = 7.7 Hz, 1H, H4'), 7.57 (t, J = 6.6 Hz, 1H, H5'), 7.33 (d, J = 6.0 Hz, 1H, H5), 3.56 (d, J = 1.2 Hz, 12H), 2.71 (s, 3H). Selected ^{13}C NMR from the HSQC spectrum ($CDCl_3$), δ (ppm): 160.7 (C6), 152.6 (C6'), 138.3 (C4'), 126.7 (C5'), 126.3 (C3'), 120.8 (C5), 45.4 (dmso-S), 23.8 (CH_3 mpp). ^{15}N NMR ($CDCl_3$), δ (ppm): –89.5 (*N^o*), –124.6 (N_{py}), –143.3 (*N^p*).

Solid-phase peptide synthesis. Peptides were synthesized manually at room temperature by using a Fmoc-protecting strategy and a Rink amide resin. Reactions were carried out in polypropylene syringes on a mechanical shaker. The resin was swollen in DMF before use.

Fmoc-deprotection: 20% piperidine in DMF was added to the resin for 2 x 10 min.

Washing: After each coupling and deprotection step, the resin was thoroughly washed with DMF, DCM and DMF.

Coupling: Fmoc-protected amino acids (4 eq.) were preactivated with TBTU (4 eq.), HOBT (4 eq.) and DIPEA (8 eq.) in DMF for 1 min, mixed with the resin and shaken for 1 hour.

Final cleavage: Final cleavage from the resin and side chain deprotection of the peptides was accomplished by using a mixture of 90% TFA, 5% TIS and 5% H_2O for 4 hours at room

temperature. Cleaved peptides were precipitated with ice-cold dietyl ether, centrifuged and washed two times with dietyl ether. The peptides were lyophilized and purified by preparative HPLC.

NT-cppH.

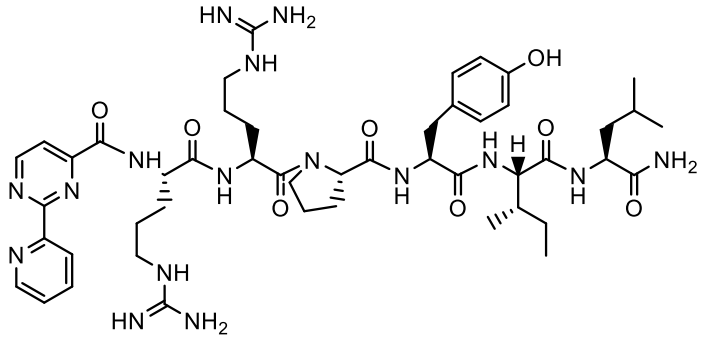

The peptide was synthesized by solid phase peptide synthesis as described in the general experimental procedure. The coupling with cppH·HNO_3 was performed with TBTU/HOBT/DIPEA 4/4/5 for two hours.

calcd for $C_{48}H_{69}N_{15}O_9$: 999.54; MS (ESI, +ve mode): m/z 999.68 $[M+H]^+$, t_R=16.4 min.

***trans*,*cis*-RuCl$_2$(CO)$_2$(cppH-NT-κ*N*^{o}) (57).**

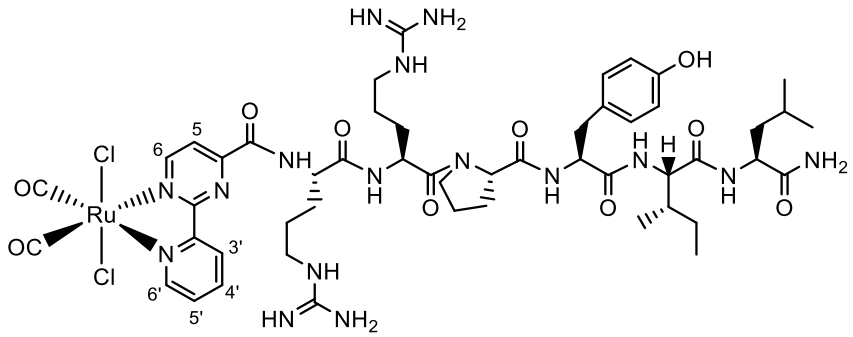

This bioconjugate was prepared using two different approaches: SPPS between *trans*,*cis*-RuCl$_2$(CO)$_2$(cppH-κ*N*^{o}) (**52**) and NT(8-13) and the reaction in solution between *trans*,*cis*,*cis*-RuCl$_2$(CO)$_2$(dmso)$_2$ (**29**) and cppH-NT (see Chapter 7 for details).

SPPS: The peptide NT(8-13) was synthesized by solid phase peptide synthesis as described in the general experimental procedure. The coupling between NT(8-13) and *trans*,*cis*-RuCl$_2$(CO)$_2$(cppH-κ*N*^{o}) (**52**) was performed using PyBOP/DIPEA/Ru(II) 5/10/5 for two days, light protected; the cleavage and deprotection were done using TFA/phenol/TIS in 85/10/5 ratio for 2 h. The solution was lyophilized and purified using semi preparative HPLC. Purified: 10.9 mg (0.02 mmol, 62%).

Solution: A 15 mg amount of *trans*,*cis*,*cis*-RuCl$_2$(CO)$_2$(dmso)$_2$ (**29**) (0.039 mmol) was partially dissolved in 2.5 mL of water. One equivalent of cppH-NT (39 mg, 0.039 mmol) was added and the mixture was stirred for two days at room temperature, light protected. A clear yellow solution was obtained in one hour. After 24h hours the solution turned in orange. The solution was lyophilized and purified using semi preparative HPLC. Purified: 28.8 mg (0.023 mmol, 6%). $C_{50}H_{69}Cl_2N_{15}O_{11}Ru$: 1227.37; MS (ESI, +ve mode): m/z 1227.25 $[M+H]^+$, t_R=18.2 min. Selected ^{1}H NMR resonances (DMSO-d_6), δ (ppm): 9.81 (d, 1H, H6), 9.40 (d, 1H, NH), 9.31 (d, 1H, H6'), 9.15 (d, 1H, H3'), 9.17 (br s, 1H, OH Tyr), 8.53 (t, 1H, H4'), 8.40 (d, 1H, NH), 8.29 (d, 1H, H5), 8.06 (t, 1H, H5'), 7.88-7.82 (m, 4H, NH),

6.99, 6.62 (d, 4H, H2,6 and 5,3 Tyr) 4.65-4.10 (m, 6H, Hα peptide). Selected ^{13}C NMR from the HSQC spectrum (DMSO-d_6), δ (ppm): 163.3 (C6), 154.2 (C6'), 141.4 (C4'), 130.9 (C5'), 130.2 (C Tyr), 127.6 (C3'), 121.0 (C5), 115.5 (C Tyr), 59.5-50.6 (Cα peptide).

[Ru([9]aneS$_3$)Cl(cppH-κ*N*^{p})]Cl (60).

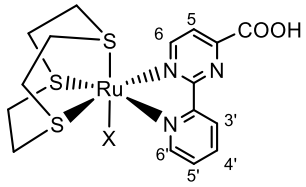

A 30 mg amount of Ru([9]aneS$_3$)Cl$_2$(dmso) (**58**) (0.068 mmol) was dissolved in 2 mL of water. One equivalent of cppH (18.6 mg, 0.068 mmol) was added and the mixture was refluxed for 5 h. A clear orange solution was obtained within few minutes that turned rapidly in red. After the reaction the solvent was concentrated and X-ray quality crystals became to form after 2 days. The crystals were filtered, washed with cold water and acetone and dried *in vacuo*. (Yield: 30.1 mg, 80%). Elemental analysis calcd for [$C_{16}H_{19}N_2Cl_2O_2S_3Ru$] ($M_W$: 552.91): C 34.72; H 3.46; N 7.59. Found: C 34.76; H 3.40; N 7.52. ^1H NMR (D_2O + NaCl), δ (ppm): 9.47 (d, 1H, H6), 9.04 (d, 1H, H6'), 8.89 (d, 1H, H3'), 8.22 (t, 1H, H4'), 8.13 (d, 1H, H5), 7.78 (t, 1H, H5'), 2.85 (m, 12H, [9]aneS$_3$). ^{13}C NMR (D_2O + NaCl), δ (ppm): δ = 162.0 (C6), 152.9 (C6'), 138.8 (C4'), 129.03 (C5'), 126.4 (C3'), 121.4 (C5), 31.2 ([9]aneS$_3$).

[Ru([9]aneS$_3$)Cl(cppH-NT)]Cl (61).

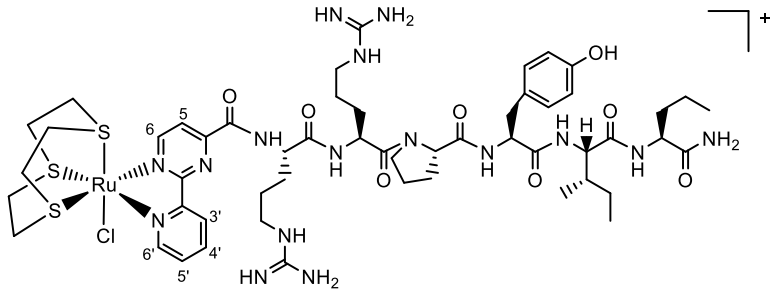

A 15 mg amount of Ru([9]aneS$_3$)Cl$_2$(dmso) (**58**) (0.034 mmol) was dissolved in 1 mL of water. One equivalent of cppH-NT (17 mg, 0.034 mmol) was added and the mixture was heated at 80°C for 5 h. A clear yellow solution was obtained within few minutes that turned rapidly in red. The solution was lyophilized and purified using semi preparative HPLC. Purified: 30.8 mg (0.02 mmol, 65%). $C_{56}H_{87}ClN_{15}O_{10}S_4Ru$: 1394.43; MS (ESI, +ve mode): m/z 1394.81 $[M+H]^+$, t_R=17.5 min. Selected ^{1}H NMR resonances (DMSO-d_6), δ (ppm): 9.51 (d, 1H, H6), 9.29 (m, 1H, NH), 9.18 (br s, 1H, OH Tyr), 9.11 (d, 1H, H3'), 9.04 (d, 1H, H6'), 8.65 (d, 1H, NH), 8.38 (m, 1H, NH), 8.31 (t, 1H, H4'), 8.11 (d, 1H, H5), 7.89 (m, 1H, NH), 7.82 (m, 2H, H5' + NH), 6.99, 6.60 (d, 4H, H2,6 and 5,3 Tyr), 4.70-4.10 (m, 6H, Hα peptide). Selected ^{13}C NMR from the HSQC spectrum (DMSO-d_6), δ (ppm): 163.2 (C6), 153.8 (C6'), 138.6 (C4'), 130.5 (C Tyr), 129.6 (C5'), 126. 9 (C3'), 120.0 (C5), 115.2 (C Tyr), 59.5-50.7 (Cα peptide).

[Ru([9]aneS$_3$)(cppH-NT)(PTA)]Cl$_2$ (62).

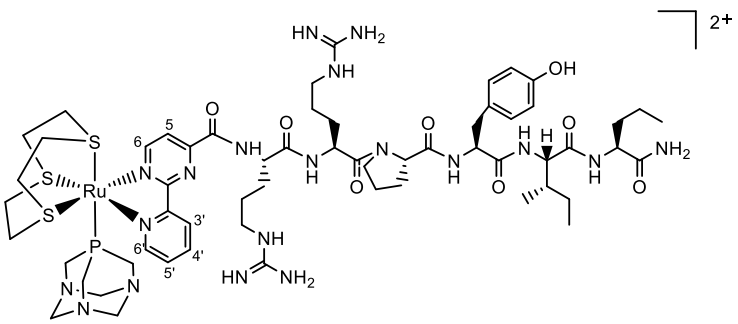

A 25 mg amount of [Ru([9]aneS$_3$)Cl(PTA)]Cl (**59**) (0.050 mmol) was dissolved in 1 mL of water. One equivalent of cppH-NT (50 mg, 0.050 mmol) was added and the mixture was heated at 80°C for 8 h. A clear yellow solution was obtained within few minutes that turned slowly in orange. The solution was lyophilized and purified using semi preparative HPLC. Purified: 43.2 mg (0.03 mmol, 60%). $C_{60}H_{95}N_{19}O_8PS_3Ru$: 1438.56; MS (ESI, +ve mode): m/z 1438.93 $[M+H]^+$, t_R=16.6 min. Selected ^{1}H NMR resonances (DMSO-d_6), δ (ppm): 9.27 (m, 4H, H6 + H3' + NH + OH Tyr), 8.82 (d, 1H, H6'), 8.43 (m, 2H, H4' + NH), 8.12 (d, 1H, H5), 7.89 (m, 2H, H5' + NH), 7.83, 7.74 (d, 2H, NH), 7.01, 6.62 (d, 4H, H2,6 and 5,3 Tyr) 4.70-4.10 (m, 6H, Hα peptide). Selected ^{13}C NMR from the HSQC spectrum (DMSO-d_6), δ (ppm): 163.4 (C6), 154.8 (C6'), 140.0 (C4'), 130.9 (C5'), 130.5 (C Tyr), 127. 9 (C3'), 121.4 (C5), 115.2 (C Tyr), 59.5-51.1 (Cα peptide). ^{31}P NMR resonance (DMSO-d_6), δ (ppm): –39.1 (br s, 1P, PTA *trans* to S).

[Ru([9]aneS$_3$)(chel)Cl]Cl (chel = bpy (63), phen (64), 4,7-Ph$_2$phen (65), dppz (66)).

These complexes were prepared according to a modified literature procedure.[23] A 100 mg amount of Ru([9]aneS$_3$)Cl$_2$(dmso-S) (**58**) (0.23 mmol) was partially dissolved in 15 mL of EtOH. Two equivalents (0.46 mmol) of chel (72 mg of bpy (**63**), 83.5 mg of phen (**64**), 153.2 mg of 4,7-Ph$_2$phen (**65**), 129.1 of dppz (**66**)) were added and the mixture was refluxed for 3 h. After 10 minutes of refluxing the solution changed from yellow to orange (for **63** and **64**) or orange-brown (for **65**) or red (for

66). Precipitation of the product in pure form (according to ^{1}H NMR spectra) from the concentrated solution (ca. 8 mL) occurred upon standing at r.t.. It was removed by filtration, washed with few mL of EtOH and diethyl ether and dried *in vacuo*. Yields from 65 to 85%.

[Ru([9]aneS$_3$)(bpy)Cl]Cl (63).

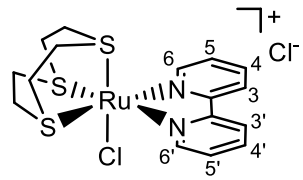

Elemental analysis calcd for [$C_{16}H_{20}N_2Cl_2RuS_3$] (M_W = 509,2): C 37.79; H 3.96; N 5.51. Found: C 37.68; H 4.05; N 5.60. ^{1}H NMR (D_2O), δ (ppm): 9.05 (d, 2H, H6,6′), 8.47 (d, 2H, H3,3′), 8.13 (t, 2H, H4,4′), 7.62 (t, 2H, H5,5′), 2.77 (m, 12H, [9]aneS$_3$, partially overlapped with the corresponding resonances of **63$_{aq}$**). ESI mass spectrum: 473.0 *m/z* (calcd 473.1) $[M]^+$. UV-vis (H_2O): λ_{max} (ε, L mol^{-1} cm^{-1}) = 361 (2359), 417 (4296) nm.

[Ru([9]aneS$_3$)(phen)Cl]Cl (64).

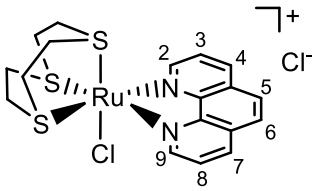

Elemental analysis calcd for [$C_{18}H_{20}N_2Cl_2RuS_3$] (M_W = 533.3): C 40.60; H 3.79; N 5.26. Found: C 40.52; H 3.68; N 5.18. ^{1}H NMR (D_2O), δ (ppm): 9.48 (d, 2H, H2,9), 8.78 (t, 2H, H4,7), 8. 22 (s, 2H, H5,6), 8.02 (d, 2H, H3,8), 2.73 (m, 12H, [9]aneS$_3$, partially overlapped with the corresponding resonances of **64$_{aq}$**). ^{1}H NMR ($CDCl_3$), δ (ppm): 9.36 (d, 2H, H2,9), 8.49 (d, 2H, H4,7), 8.05 (s, 2H, H5,6), 7.87 (d, 2H, H3,8), 2.97 (m, 12H, [9]aneS$_3$).^{13}C NMR from HSQC ($CDCl_3$), δ: 152.2 (C2,9), 136.3 (C4,7), 127.8 (C5,6), 126.0 (C3,8), 34.1 ([9]aneS$_3$). ESI mass spectrum: 497.0 *m/z* (calcd 497.1) $[M]^+$. UV-vis (H_2O): λ_{max} (ε, L mol^{-1} cm^{-1}) = 369 (4711), 415 (4423) nm.

[Ru([9]aneS$_3$)(4,7-Ph$_2$phen)Cl]Cl (65).

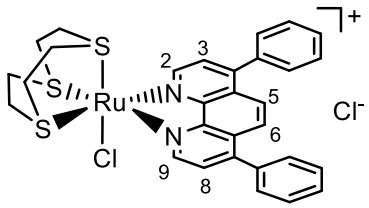

Elemental analysis calcd for [$C_{30}H_{28}N_2Cl_2RuS_3$] (M_W = 685.4): C 52.62; H 4.12; N 4.09. Found: C 52.73; H 4.20; N 4.17. ^{1}H NMR (D_2O), δ (ppm): 9.52 (d, 2H, H2,9), 8.15 (s, 2H, H5,6), 7.98 (d, 2H, H3,8), 7.69 (br s, 10H, Ph), 2.92 (m, 12H, [9]aneS$_3$, partially overlapped with the corresponding resonances of **65$_{aq}$**). ^{1}H NMR ($CDCl_3$), δ (ppm): 9.40 (d, 2H, H2,9), 8,07 (s, 2H, H5,6), 7.78 (d, 2H, H3,8), 7.57 (m, 10H, Ph), 3.03 (m, 12H, [9]aneS$_3$). ^{13}C NMR from HSQC ($CDCl_3$), δ (ppm): 151.9 (C2,9), 129.2 (Ph), 124.0 (C5,6), 122.4 (C3,8), 35.0 ([9]aneS$_3$). ESI mass spectrum: 649.1 *m*/*z* (calcd 649.3) $[M]^+$. UV-vis (H_2O): λ_{max} (ε, L mol^{-1} cm^{-1}) = 370 (6598), 408 (5786) nm.

[Ru([9]aneS$_3$)(dppz)Cl]Cl (66).

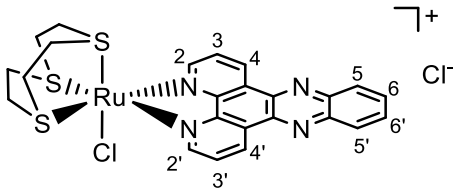

Elemental analysis calcd for [$C_{24}H_{22}N_4Cl_2RuS_3$] (M_W = 635.5): C 45.42; H 3.49; N 8.83. Found: C 45.50; H 3.58; N 8.91. ^{1}H NMR ($CDCl_3$), δ (ppm): 9.77 (d, 2H, H2,2′), 9.42 (d, 2H, H4,4′), 8.46 (d, 2H, H5,5′), 8.08 (d, 2H, H6,6′), 8.00 (t, 2H, H3,3′), 3.01 (m, 12H, [9]aneS$_3$). ^{13}C NMR from HSQC ($CDCl_3$), δ (ppm): 153.6 (C4,4′), 134.3 (C2,2′), 131.3 (C6,6′), 130.6 (C5,5′), 126.3 (C3,3′), 33.2 ([9]aneS$_3$). ESI mass spectrum: 599.0 *m*/*z* (calcd 599.1) $[M]^+$. UV-vis (H_2O): λ_{max} (ε, L mol^{-1} cm^{-1}) = 357 (6875), 423 (4750) nm.

[Ru([9]aneS$_3$)(bq)Cl]Cl (67).

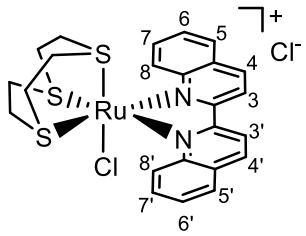

A 50 mg amount of Ru([9]aneS$_3$)Cl$_2$(dmso-S) (**58**) (0.12 mmol) was partially dissolved in 2 mL of EtOH and two equivalents (0.24 mmol) of 2,2′-biquinoline (60 mg) were added. The mixture was microwave-heated at 140°C for 90 min. The white powder (unreacted bq) was removed by filtration. Evaporation of the solvent afforded a purple solid that was dissolved in water and filtered to remove the remaining traces of unreacted bq. The solution was rotary evaporated to dryness and the solid (pure **67**, according to the ^{1}H NMR spectrum) was dried *in vacuo.* (Yield 51.1 mg, 66%). Elemental analysis calcd for [$C_{24}H_{24}N_2Cl_2RuS_3$] (M_W = 607.9): C 47.36; H 3.97; N 4.60. Found: C 47.28; H 3.88; N 4.51. ^{1}H NMR (D_2O), δ (ppm): 9.10 (d, 2H, H8,8′), 7.95 (t, 2H, H7,7′), 7,65 (d, 2H, H4,4′), 7,73 (m, 4H, H5,5′ + H6,6′), 7.49 (d, 2H, H3,3′), 2.43 (m, 12H, [9]aneS$_3$). ^{13}C NMR from HSQC (D_2O), δ (ppm): 139.0 (C4,4′), 132.8 (C7,7′), 129.6 (C5,5′), 129.1 (C3,3′), 128.6 (C8,8′), 119.4 (C6,6′), 33.1 ([9]aneS$_3$). ESI mass spectrum: 573.1 *m*/*z* (calcd 573.2) $[M]^+$. UV-vis (H_2O): λ_{max} (ε, L mol^{-1} cm^{-1}) = 356 (20106), 373 (19574), 515 (4787) nm.

[Ru([9]aneS$_3$)(chel)(py)](Cl)$_2$ (chel = bpy (68), phen (69), 4,7-Ph$_2$phen (70), dppz (71), bq (72)).

The preparations were performed in light-protected glassware. The precursor complex (0.13 mmol, i.e. 60 mg of **63**, 69 mg of **64**, 89 mg of **65**, 82 mg of **66**, 83 mg of **67**) was dissolved in 5 mL of H_2O and a 50 μL amount of pyridine (0.6 mmol) was added. The solution was refluxed for 3h, then the solution was rotary evaporated to dryness. The obtained solid was sonicated with 2 mL of acetone, then removed by filtration, washed with acetone and diethyl ether, and dried *in vacuo*. According to

the ^{1}H NMR spectra, in each case the product (i.e. **68**, **69**, **70**, **71** and **72**, respectively) was obtained in pure form. Yields from 65 to 85%. X-ray quality crystals of **69** and **72** were obtained by slow diffusion of diethyl ether into an EtOH solution of the complex.

[Ru([9]aneS$_3$)(bpy)(py)](Cl)$_2$ (68).

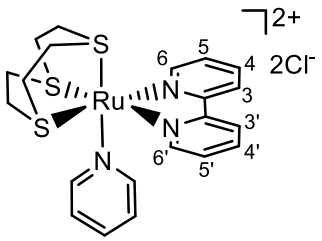

Elemental analysis calcd for [$C_{21}H_{25}N_3Cl_2RuS_3$] (M_W = 588.2): C 42.93; H 4.29; N 7.15. Found: C 42.65; H 4.25; N 7.08. ^{1}H NMR (D_2O), δ (ppm): 9.23 (d, 2H, H6,6′), 8.66 (d, 2H, *o*-py), 8.38 (d, 2H, H3,3′), 8.16 (t, 2H, H4,4′), 7.77 (d, 3H, *p*-py + H5,5′), 7.26 (t, 2H, *m*-py), 2,90 (m, 12H, [9]aneS$_3$). ESI mass spectrum: 473.0 *m*/*z* (calcd 473.1) [M – py + Cl]$^+$. UV-vis (H_2O): λ_{max} (ε, L mol^{-1} cm^{-1}) = 401 (4666) nm.

[Ru([9]aneS$_3$)(phen)(py)](Cl)$_2$ (69).

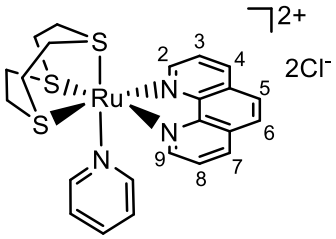

Elemental analysis calcd for [$C_{23}H_{25}N_3Cl_2RuS_3$] (M_W = 612.4): C 45.17; H 4.12; N 6.87. Found: C 45.25; H 4.20; N 6.98. ^{1}H NMR (D_2O), δ (ppm): 9.63 (d, 2H, H2,9), 8.76 (d, 2H, *o*-py), 8.72 (m, 2H, H4,7), 8.15 (s, 2H, H5,6), 8.11 (t, 2H, H3,8), 7.71 (d, 1H, *p*-py), 7.20 (t, 2H, *m*-py), 3.01 (m, 12H, [9]aneS$_3$). ^{13}C NMR from HSQC (D_2O), δ (ppm): 153.3 (C2,9), 152.9 (*o*-py), 138.2 (C4,7), 138.5 (C3,8 + C5,6), 129.0 (*p*-py), 126.8 (*m*-py), 32.2 ([9]aneS$_3$). ESI mass spectrum: 497.0 *m*/*z* (calcd 497.1) [M – py + Cl]$^+$. UV-vis (H_2O): λ_{max} (ε, L mol^{-1} cm^{-1}) =353 (5153), 405 (4384) nm.

[Ru([9]aneS$_3$)(4,7-Ph$_2$phen)(py)](Cl)$_2$ (70).

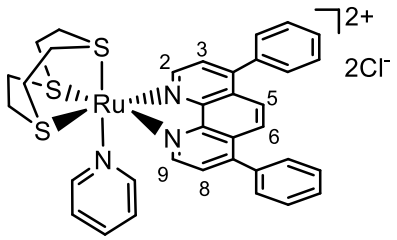

Elemental analysis calcd for [$C_{35}H_{33}N_3Cl_2RuS_3$] (M_W = 764.2): C 55.04; H 4.35; N 5.50. Found: C 55.11; H 4.44; N 5.61. ^{1}H NMR (D_2O), δ (ppm): 9.73 (d, 2H, H2,9), 8.87 (d, 2H, *o*-py), 8.09 (d, 2H, H3,8), 7.81 (m, 3H, H5,6 + *p*-py), 7.60 (m, 10H, Ph), 7.34 (t, 2H, *m*-py), 3.11 (m, 12H, [9]aneS$_3$). ^{13}C NMR from HSQC (D_2O), δ (ppm): 152.9 (C2,9), 151.9 (*o*-py), 125.1 (C5,6) 130.5 (C3,8 + *p*-py), 126.9 (Ph), 126.7 (*m*-py), 33.4 ([9]aneS$_3$). ESI mass spectrum: 649.1 *m*/*z* (calcd 649.3) [M – py + Cl]$^+$. UV-vis (H_2O): λ_{max} (ε, L mol^{-1} cm^{-1}) = 467 (7800), 413 (6600) nm.

[Ru([9]aneS$_3$)(dppz)(py)](Cl)$_2$ (71).

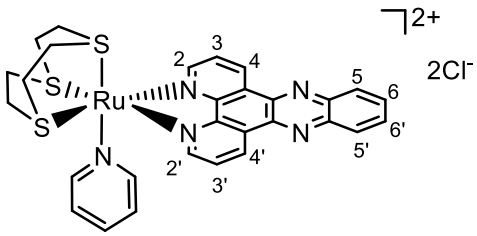

Elemental analysis calcd for [$C_{29}H_{27}N_5Cl_2RuS_3$] (M_W = 714.1): C 48.80; H 3.81; N 9.81. Found: C 48.72; H 3.71; N 9.73. ^{1}H NMR (D_2O), δ (ppm): 9.76 (d, 2H, H2,2′), 9.03 (d, 2H, *o*-py), 8.85 (s, 2H, H4,4′), 8.11 (t, 2H, H3,3′), 8.00 (t, 2H, *p*-py), 7.59 (m, 6H, H5,5′ + H6,6′ + *m*-py), 3.05 (m, 12H, [9]aneS$_3$). ^{13}C NMR from HSQC (D_2O), δ (ppm): 155.3 (C2,2′), 152.2 (*o*-py), 139.6 (C4), 133.3 (C3,3′), 133.2 (*p*-py), 128.1 (C5,5′ + (C6,6′), 126.8 (*m*-py), 31.8 ([9]aneS$_3$). ESI mass spectrum: 599.0 *m*/*z* (calcd 599.1) [M – py + Cl]$^+$. UV-vis (H_2O): λ_{max} (ε, L mol^{-1} cm^{-1}) = 355 (11882), 423 (4117) nm.

[Ru([9]aneS$_3$)(bq)(py)](Cl)$_2$ (72).

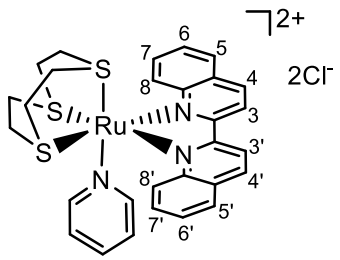

Elemental analysis calcd for [$C_{29}H_{27}N_3Cl_2RuS_3$] (M_W = 688.87): C 50.65; H 4.25; N 6.11 Found: C 50.73; H 4.32; N 6.21. ^{1}H NMR (D_2O), δ (ppm): 8.79 (s, 4H, H3,3′ + H4,4′), 8.32 (m, 4H, H8,8′ + *o*-py), 8.17 (m, 2H, H5,5′), 7.88 (m, 1H, *p*-py), 7.80 (m, 4H, H7,7′ + H6,6′), 7.28 (t, 2H, *m*-py), 2.52 (m, 12H, [9]aneS$_3$). ^{13}C NMR from HSQC (D_2O), δ (ppm): 154.9 (*o*-py), 141.0 (C3,3′), 139.5 (*p*-py), 133.3 (C4,4′), 129.7 (C7,7′), 128.8 (C5,5′), 127.0 (*m*-py), 126.9 (C8,8′), 120.3 (C6,6′), 35.8 ([9]aneS$_3$). ESI mass spectrum: 573.1 *m*/*z* (calcd 573.2) [M – py + Cl]$^+$. UV-vis (H_2O): λ_{max} (ε, L mol^{-1} cm^{-1}) = 359 (14161), 378 (16207), 466 (2854), 493 (3771) nm.

***trans,cis*-Ru(bq)Cl$_2$(CO)$_2$ (73).**

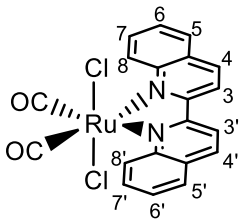

To a 60 mg amount of *trans,cis,cis*-RuCl$_2$(CO)$_2$(dmso-O)$_2$ (**29**) (0.16 mmol) dissolved in 3 mL of $CHCl_3$, 1 eq of 2,2′-biquinoline (43.2 mg) was added and the mixture was sonicated for a few minutes until complete dissolution of the ligand (yellow solution). After 4h small red crystals began to form. Crystals were filtered after one day and washed with $CHCl_3$ and diethyl ether and dried *in vacuo* (Yield 57.1 mg, 75%).

Elemental analysis calcd for [$C_{20}H_{12}N_2$ Cl_2O_2Ru] (M_W = 484.83): C 49.60; H 2.50; N 5.78 Found: C 49.72; H 2.61; N 5.89. ^{1}H NMR ($CDCl_3$), δ (ppm): 9.25 (d, 1H,

H8,8′), 8.56 (d, 1H, H3,3′), 8.35 (d, 1H, H4,4′), 8.04 (t, 1H, H7,7′), 7.98 (d, 1H, H5,5′), 7.79 (t, 1H, H6,6′). ^{13}C NMR ($CDCl_3$) δ (ppm): 195.61 (CO), 141.24 (C3,3′), 133.29 (C7,7′), 129.65 (C8,8′), 129.51 (C6,6′), 129.35 (C5,5′), 119.37 (C4,4′). ESI mass spectrum: 448.6 *m*/*z* (calcd 448.8) $[M - Cl]^+$**.** Selected IR absorption (cm^{-1}): Nujol, 2051 (ν_{CO}, s), 1981 (ν_{CO}, s).

[Ru([9]aneS$_3$)(bq)(NH$_3$)](Cl)$_2$ (74).

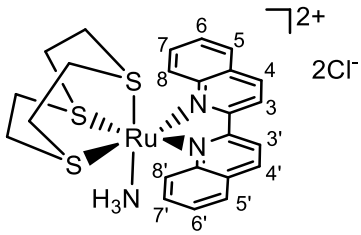

A 20 mg amount of [Ru([9]aneS$_3$)(bq)Cl][Cl] (**67**) (0.033 mmol) was dissolved in 1 mL of H_2O; a 45 µL volume of a 25% ammonia solution in water (0.42 mmol) was added and the mixture was heated in the microwave at 110°C for 150 min. Then the solvent was rotary evaporated completely and the resulting oil was crushed with $CHCl_3$ obtaining a dark red solid that was filtered, washed with $CHCl_3$ and diethyl ether and dried *in vacuo*. According to the ^{1}H NMR spectrum the product was pure **74**. X-ray quality crystals of **74** were obtained by slow diffusion of diethyl ether into a methanol solution of the complex. (Yield 14.4 mg, 70%). Elemental analysis calcd for [$C_{24}H_{27}N_3Cl_2RuS_3$] (M_W = 624.48): C 46.07; H 4.35; N 6.72 Found: C 45.99; H 4.28; N 6.63. ^{1}H NMR (D_2O), δ (ppm): 8.91 (d, 2H, H8,8′), 8.65 (m, 4H, H3,3′+H4,4′), 8.14 (s, 2H, H5,5′), 8.06 (t, 2H, H7,7′), 7.86 (t, 2H, H6,6′), 3.53 (br s, 3H, NH_3), 2.63 (m, 12H, [9]aneS$_3$). ^{13}C NMR from HSQC (D_2O), δ (ppm): 134.6 (C3,3′), 131.2 (C7,7′), 129.3 (C5,5′), 129.2 (C6,6′), 126.8 (C8,8′), 120.11 (C4,4′), 33.2 ([9]aneS$_3$). ESI mass spectrum: 573.0 *m*/*z* (calcd 573.2) $[M - NH_3 + Cl]^+$.

[Ru([9]aneS$_3$)(py)$_2$Cl]Cl (75).

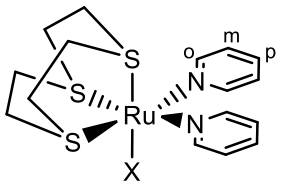

A 50 mg amount of Ru([9]aneS$_3$)Cl$_2$(dmso-S) (**58**) (0.13 mmol) was partially dissolved in 10 mL of EtOH; a 36 μL volume of pyridine (0.52 mmol) was added and the mixture was refluxed for 5 h. During the heating a clear yellow-orange solution was obtained, from which a yellow precipitate started to form. After cooling the mixture to r.t., the product was removed by filtration, washed with EtOH and diethyl ether and dried *in vacuo*. (Yield 49.7 mg, 75%). The product was pure **75** according to the ^{1}H NMR spectrum. Elemental analysis calcd for [$C_{16}H_{22}N_2Cl_2RuS_3$] (M_W = 509.94): C 37.64; H 4.34; N 5.49 Found: C 37.78; H 4.44; N 5.58. ^{1}H NMR (D_2O), δ (ppm): 8.70 (d, 4H, *o*-py), 7.87 (t, 2H, *p*-py), 7.43 (t, 4H, *m*-py), 2.41 (m, 12H, [9]aneS$_3$ partially overlapped with the corresponding resonances of **75$_{aq}$**). ESI mass spectrum: 475.0 *m*/*z* (calcd 475.1) $[M]^+$.

9.9 Bibliography

[1] a) D. J. Darensbourg, F. Joó, M. Kannisto, A. Katho, J. H. Reibenspies, *Organometallics,* **1992**, *11*, 1990 - 1993; b) D. J. Darensbourg, F. Joó, M. Kannisto, A. Kathó, J. H. Reibenspies, D. J. Daigle, *Inorg. Chem.*, **1994**, *33*, 200 - 208.

[2] I. Bratsos, E. Alessio, *Inorg. Synth.*, **2010**, *35*, 148 - 152.

[3] I. Bratsos, C. Simonin, E. Zangrando, T. Gianferrara, A. Bergamo, E. Alessio, *Dalton Trans.*, **2011**, *40*, 9533 - 9543.

[4] E. Iengo, E. Zangrando, E. Baiutti, F. Munini, E. Alessio, *Eur. J. Inorg. Chem.*, **2005**, 1019 - 1031.

[5] E. Alessio, B. Milani, M. Bolle, G. Mestroni, P. Faleschini, F. Todone, S. Geremia, M. Calligaris, *Inorg. Chem.*, **1995**, *34*, 4722 - 4734.

[6] B. J. Goodfellow, V. Félix, S. M. D. Pacheco, J. P. de Jesus, M. G. B. Drew, *Polyhedron* **1997**, *16*, 393 - 401.

[7] a) B. Serli, E. Zangrando, T. Gianferrara, C. Scolaro, P. J. Dyson, A. Bergamo, E. Alessio, *Eur. J. Inorg. Chem.*, **2005**, 3423 - 3434. b) E. Iengo, N. Demitri, G. Balducci, E. Alessio, *Dalton Trans.*, **2014**, *43*, 12160 - 12163.

[8] E. Alessio, G. Balducci, M. Calligaris, G. Costa, W. M. Attia, G. Mestroni, *Inorg. Chem.*, **1991**, *48,* 609 - 618.

[9] D. G. McCafferty, B. M. Bishop, C. G. Wall, S. G. Hughes, S. L. Mecklenberg, T. J. Meyer, B. W. Erickson, *Tetrahedron*, **1995**, *51*, 1093 - 1106.

[10] N. Nickita, G. Gasser, P. Pearson, M. J. Belousoff, L. Y. Goh, A. M. Bond, G. B. Deacon, L. Spiccia, *Inorg. Chem.*, **2009**, *48*, 68 - 81.

[11] W. Kabsch, *Acta Cryst. D*, **2010**, *66*, 125 - 132.

[12] G. M. Sheldrick, *Acta Cryst. A*, **2015**, *72*, 3 - 8.

[13] G. M. Sheldrick, *Acta Cryst.*, **2008**, *64*, 112 - 122.

[14] P. Emsley, K. Cowtan, *Acta Cryst. D*, **2004**, *60*, 2126 - 2132.

[15] P. Giannozzi, S. Baroni, N. Bonini, M. Calandra, R. Car, C. Cavazzoni, D. Ceresoli, G. L. Chiarotti, M. Cococcioni, I. Dabo, A. Dal Corso, S. Fabris, G. Fratesi, S. de Gironcoli, R. Gebauer, U. Gerstmann, C. Gougoussis, A. Kokalj, M. Lazzeri, L. Martin-Samos, N. Marzari, F. Mauri, R. Mazzarello, S. Paolini, A. Pasquarello, L. Paulatto, C. Sbraccia, S. Scandolo, G. Sclauzero, A. P. Seitsonen, A. Smogunov, P. Umari, R. M. Wentzcovitch, *J.Phys.:Condens.Matter*, **2009**, *21*, 395502; http://arxiv.org/abs/0906.2569.

[16] G. J. Martyna, M. E. Tuckerman, *J. Chem. Phys.*, **1999**, *110*, 2810 - 2821.

[17] D. Vanderbilt, *Phys. Rev. B*, **1990**, *41*, 7892 - 7895.

[18] J. P. Perdew, K. Burke, M. Ernzerhof, *Phys. Rev. Lett.*, **1996**, *77*, 3865 - 3868.

[19] O. B. Malcioglu, R. Gebauer, D. Rocca, S. Baroni, *Comput. Phys. Commun.*, **2011**, *182*, 1744 - 1754.

[20] X. Ge, S. J. Binnie, D. Rocca, R. Gebauer, S. Baroni, *Comput. Phys. Commun.*, **2014**, *185*, 2080 - 2089.

[21] R. Girotti, A. Romerosa, S. Mañas, M. Serrano-Ruiz, R. N. Perutz, *Inorg. Chem.*, **2009**, *48*, 3692 - 3698.

[22] A. Udvardy, A. C. Bényei, Á. Kathó, *J. Organomet. Chem.*, **2012**, *717*, 116 - 122.

[23] G. Ragazzon, I. Bratsos, E. Alessio, L. Salassa, A. Habtemariam, R. J. McQuitty, G. J. Clarkson, P. J. Sadler, *Inorg. Chim. Acta*, **2012**, *393*, 230 - 238.

Appendix of Chapter 2

Figures A2.1-A2.3. NMR characterization in $CDCl_3$ and D_2O of *trans*-$RuCl_2(PTA)_4$ (**1**).

Figures A2.4-A2.6. NMR characterization in $CDCl_3$ and D_2O of *cis*-$RuCl_2(PTA)_4$ (**2**).

Figures A2.7-A2.8. NMR characterization in $CDCl_3$ of *trans*-$RuCl_2(PTA)_4$ (**11**).

Figures A2.9-A2.10. NMR characterization in $CDCl_3$ and D_2O of *cis*-$RuCl_2(PTA)_4$ (**12**).

Figure A2.11. ^{31}P NMR spectrum in $CDCl_3$ of *cis*,*mer*-$RuCl_2$(dmso-S)$(PTA)_3$ (**13**).

Figures A2.12-A2.13. ^{31}P NMR spectra in $CDCl_3$ of *trans*,*mer*-$RuCl_2(CH_3CN)(PTA)_3$ (**14**) and *cis*,*mer*-$RuCl_2(CH_3CN)(PTA)_3$ (**15**).

Figure A2.14. Inversion recovery ^1H NMR spectrum in D_2O of *trans*-$[RuCl_4(PTAH)_2]Cl$ (**3**).

Figures A2.15-A2.19. NMR characterization in D_2O of *mer*-$[Ru(bpy)Cl(PTA)_3](PF_6)$ (**17**).

Figures A2.20-A2.22. NMR characterization in D_2O of *fac*-$[Ru(bpy)Cl(PTA)_3](PF_6)$ (**18**).

Figure A2.23. ^1H and ^{31}P NMR spectra in D_2O of *mer*-$[RuCl(cppH)(PTA)_3]Cl$ (**19**).

Figures A2.24-A2.26. NMR characterization in $CHCl_3$ and D_2O of *cis,cis,trans*-$RuCl(dmso\text{-}S)_2(PTA)_2$ (**10**).

Figures A2.27-A2.32. NMR characterization in $CHCl_3$ and D_2O of *cis,cis*-$Ru(bpy)Cl_2(PTA)_2$ (**22**).

Figures A2.33-A2.37. NMR characterization in D_2O of *cis,cis*-$Ru(bpyAc)Cl_2(PTA)_2$ (**23**).

Figures A2.38-A2.40. NMR characterization in $CDCl_3$ of *trans,mer*-$[RuCl_2(PTA)_3(py)]$ (**25**).

Figure A2.41. ^1H NMR spectrum in $CDCl_3$ of of the reaction between *cis,cis,trans*-$RuCl_2(dmso\text{-}S)_2(PTA)_2$ (**10**) and 4'MPyP.

Figures A2.42-A2.46. UV spectra of *cis*-$RuCl_2(PTA)_4$ (**2**), *mer*-$[Ru(bpy)Cl(PTA)_3](PF_6)$ (**17**), *fac*-$[Ru(bpy)Cl(PTA)_3](PF_6)$ (**18**), *cis*,*cis*-$Ru(bpy)Cl_2(PTA)_2$ (**22**), *cis*,*cis*-$[Ru(bpy)Cl(OH_2)(PTA)_2]^+$ (**22$_{aq}$**) and *cis*,*cis*-$[Ru(bpyAc)Cl(OH_2)(PTA)_2]^+$ (**23$_{aq}$**).

Figure A2.47. ^{31}P NMR pH titration of complex *cis,cis,trans*-$RuCl_2(dmso\text{-}S)_2(PTA)_2$ (**10**) in D_2O.

Figure A2.48. Molecular structure (50% probability ellipsoids) of *fac*-$[Ru(bpy)Cl(PTAH)_{2.5}(PTA)_{0.5}](ClO_4)_{3.5}\cdot 2.5H_2O$ (**18**).

Figure A2.49. Molecular structure (50% probability ellipsoids) of the two crystallographically independent molecules of *cis*-$[RuCl(OH_2)(PTA)_4](PF_6)\cdot CH_3OH$ (**2$_{aq}$**).

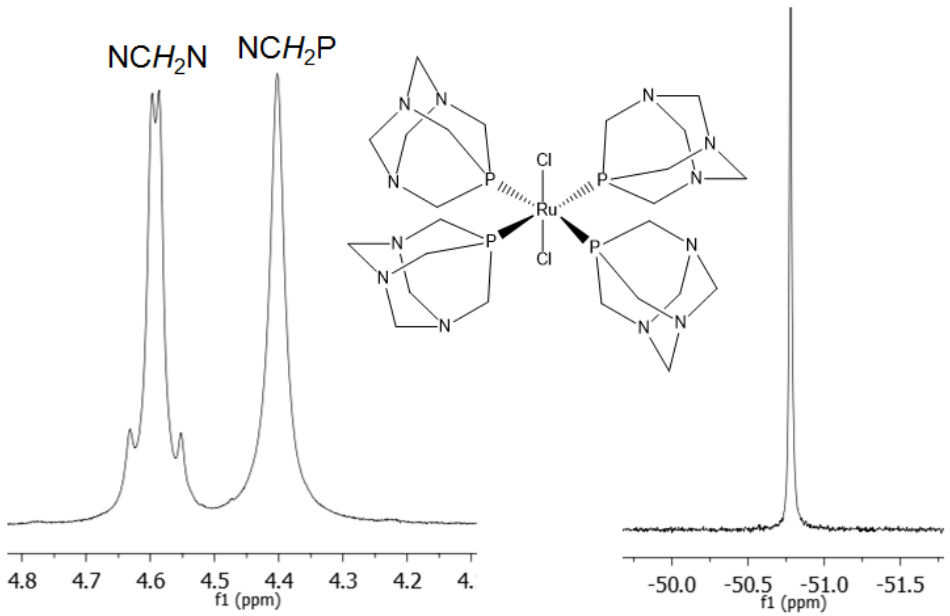

Figure A2.1. ^{1}H (left) and ^{31}P (right) NMR spectra in $CDCl_3$ of *trans*-$RuCl_2(PTA)_4$ (**1**).

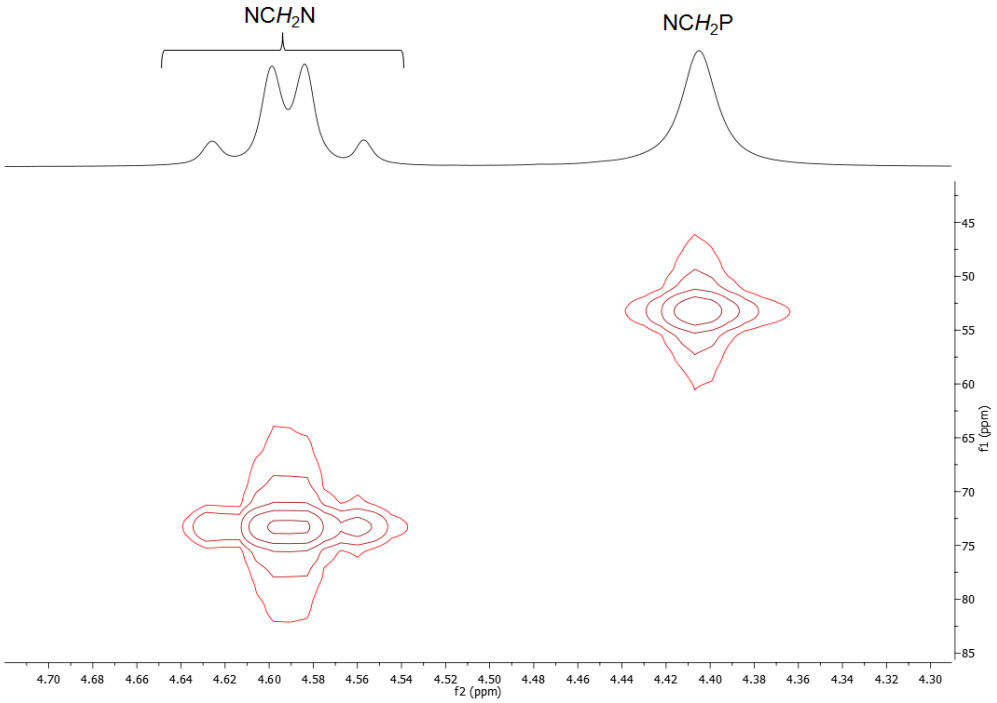

Figure A2.2. ^{1}H-^{13}C HSQC NMR spectrum in $CDCl_3$ of *trans*-$RuCl_2(PTA)_4$ (**1**).

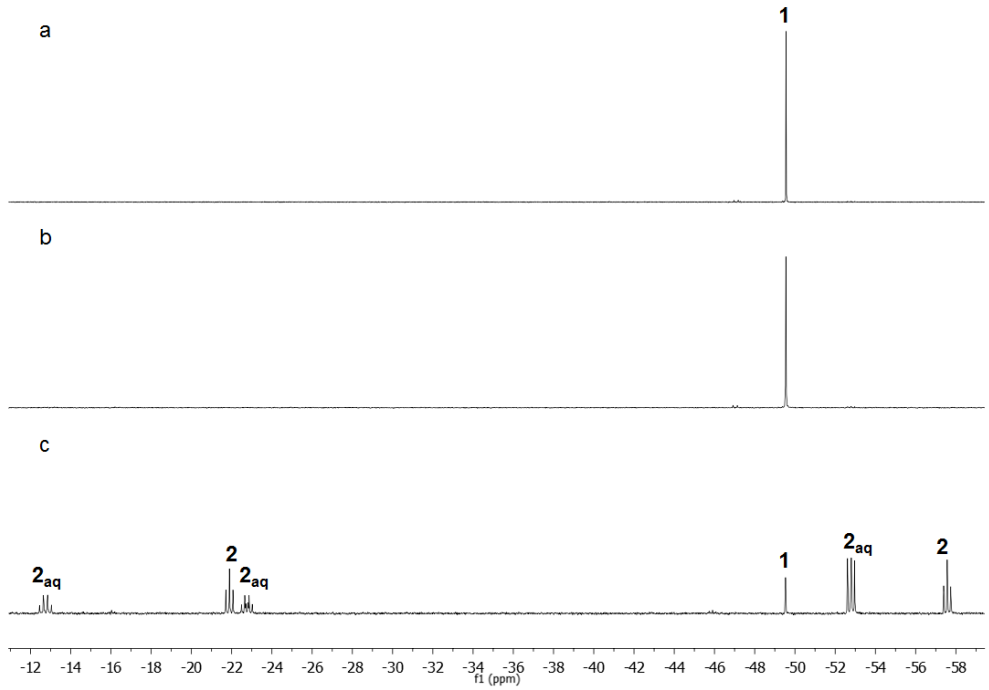

Figure A2.3. ^{31}P NMR spectra of *trans*-$RuCl_2(PTA)_4$ (**1**) in D_2O registered: immediately after dissolution (a), after 8 days in the dark (b), after exposure to diffused indoor light for 8 days (c).

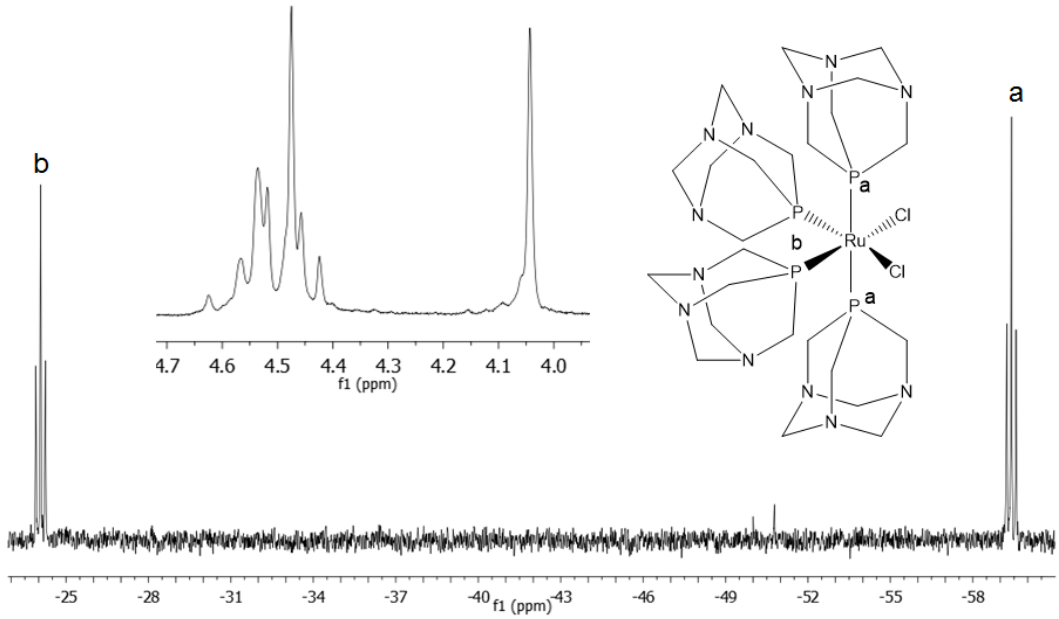

Figure A2.4. ^{1}H (insert) and ^{31}P NMR spectra in $CDCl_3$ of *cis*-$RuCl_2(PTA)_4$ (**2**).

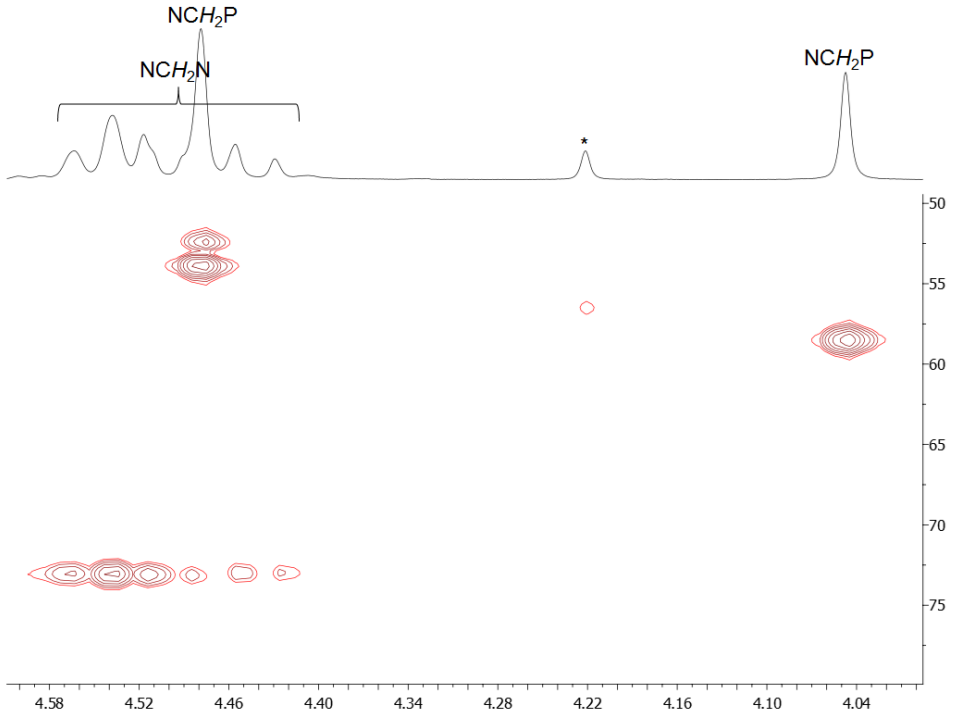

Figure A2.5. ^{1}H-^{13}C HSQC NMR spectrum in $CDCl_3$ of *cis*-$RuCl_2(PTA)_4$ (**2**). The peak marked with an asterisk belongs to a minor unidentified impurity.

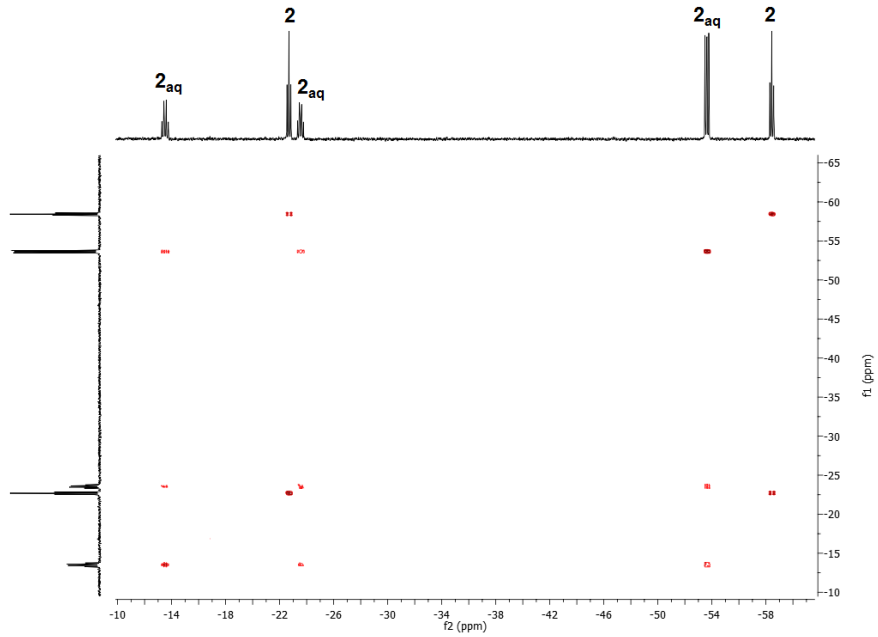

Figure A2.6. ^{31}P-^{31}P COSY NMR spectrum of *cis*-$RuCl_2(PTA)_4$ (**2**) in D_2O.

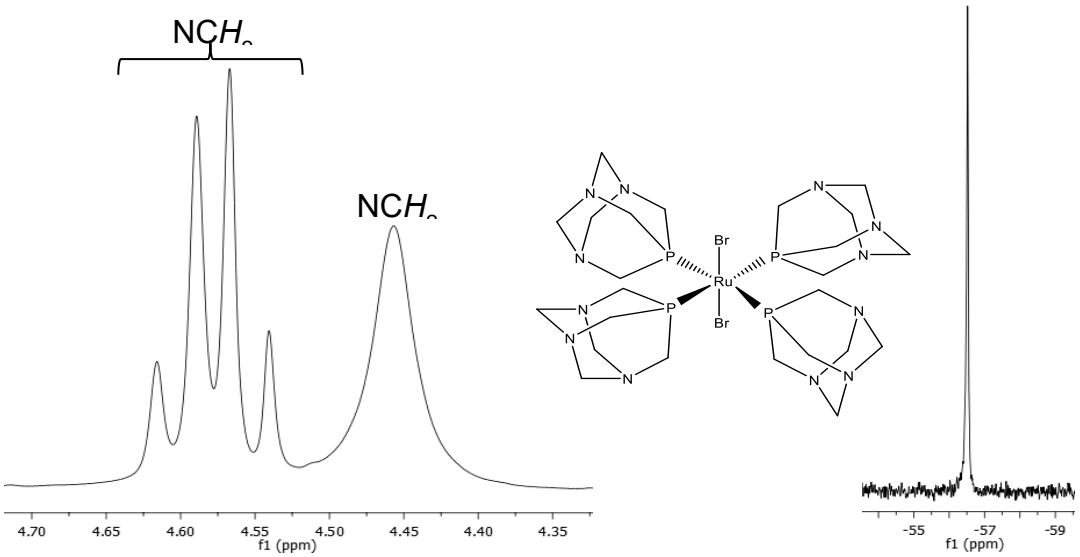

Figure A2.7. ^{1}H (left) and ^{31}P (right) NMR spectra in $CDCl_3$ of *trans*-[$RuBr_2(PTA)_4$] (**11**).

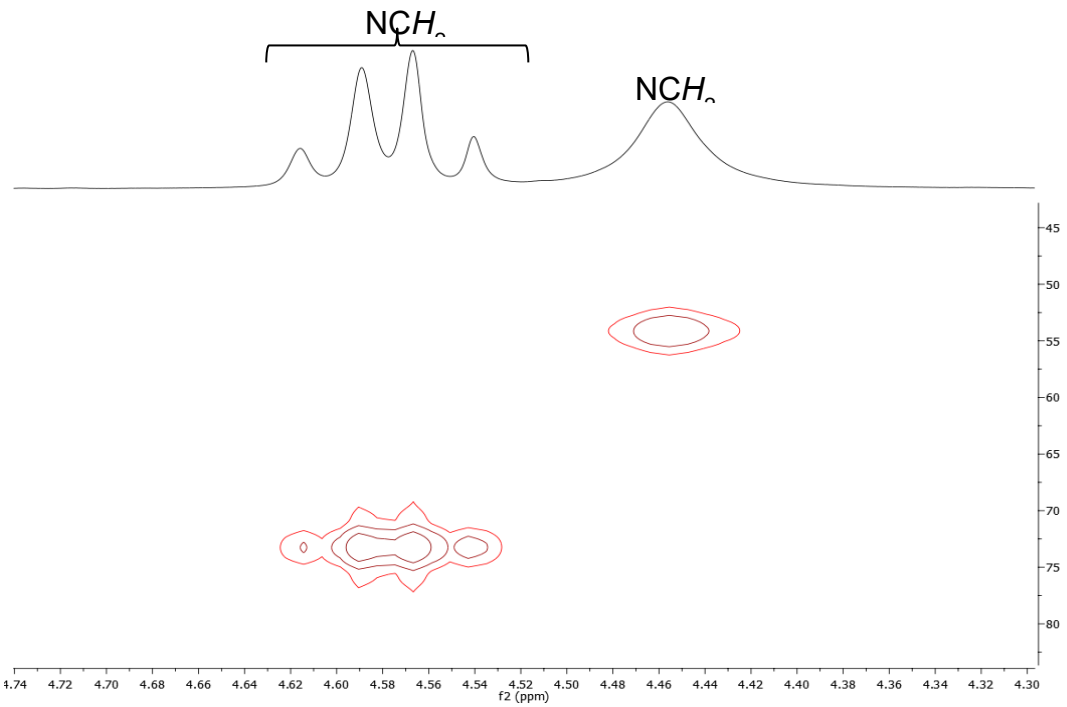

Figure A2.8. ^{1}H-^{13}C HSQC NMR spectrum in $CDCl_3$ of *trans*-[$RuBr_2(PTA)_4$] (**11**).

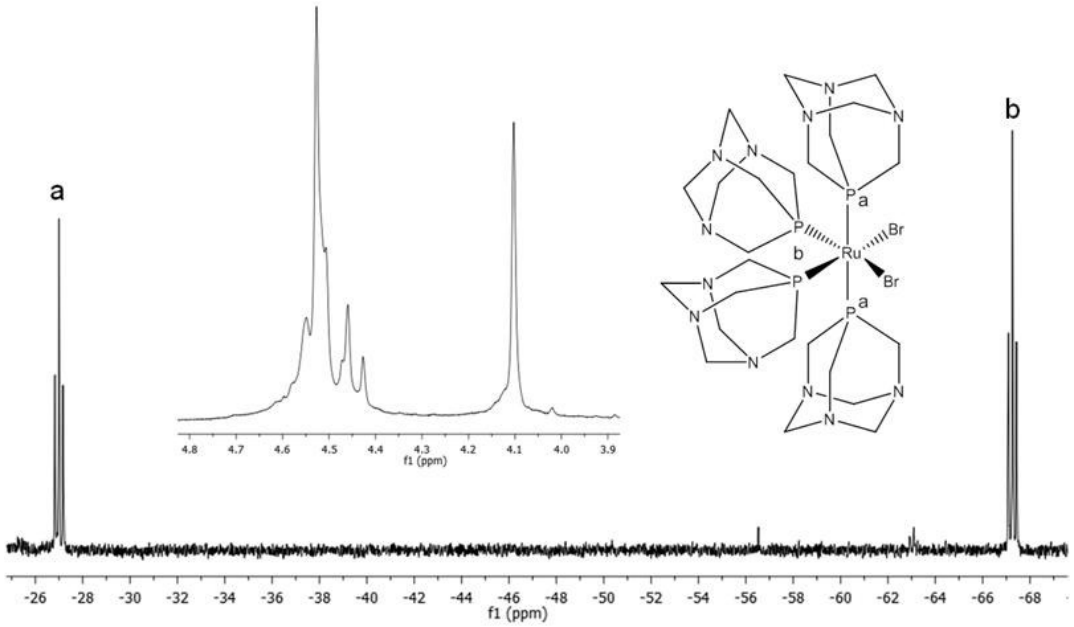

Figure A2.9. ^{1}H (insert) and ^{31}P NMR spectra in $CDCl_3$ of *cis*-[$RuBr_2(PTA)_4$] (**12**).

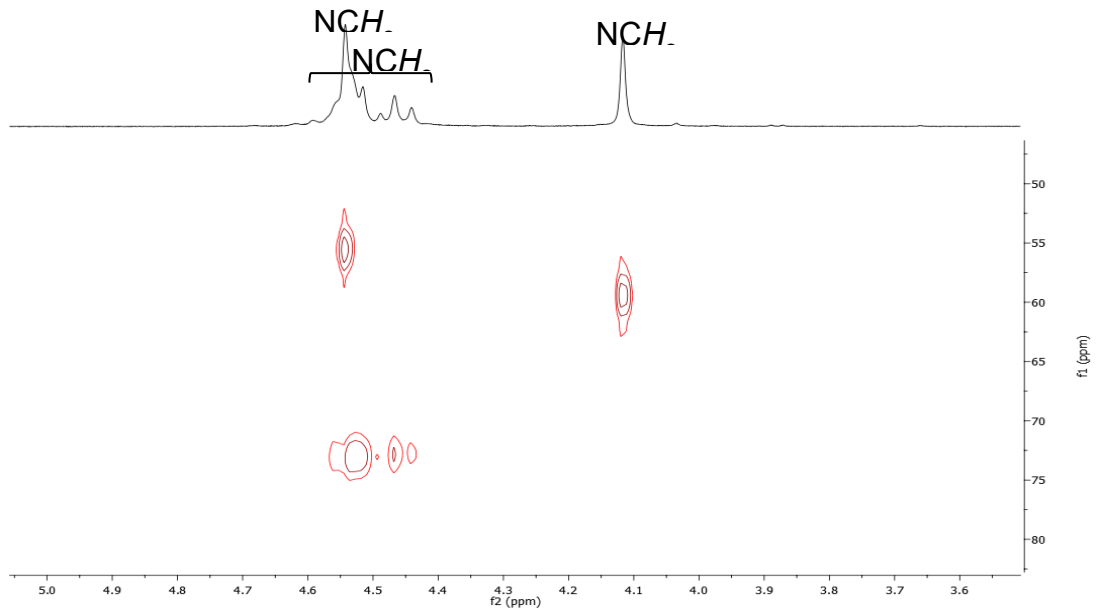

Figure A2.10. ^{1}H-^{13}C HSQC NMR spectrum in $CDCl_3$ of *cis*-[$RuBr_2(PTA)_4$] (**12**).

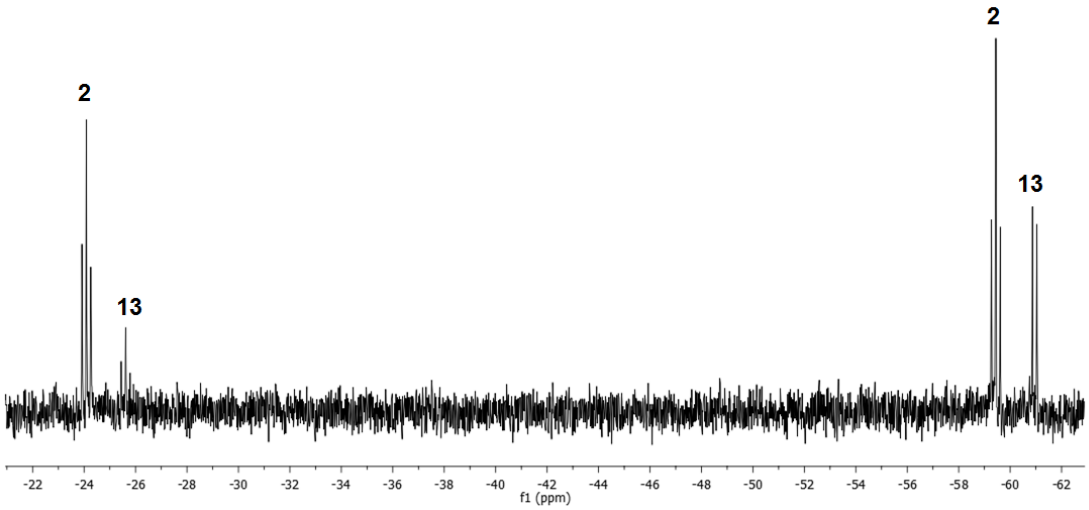

Figure A2.11. ^{31}P NMR spectrum in $CDCl_3$ of the precipitate obtained by heating *trans*-[$RuCl_2(PTA)_4$] (**1**) in DMSO at 70°C. **13** is *cis,mer*-$RuCl_2$(dmso-S)$(PTA)_3$.

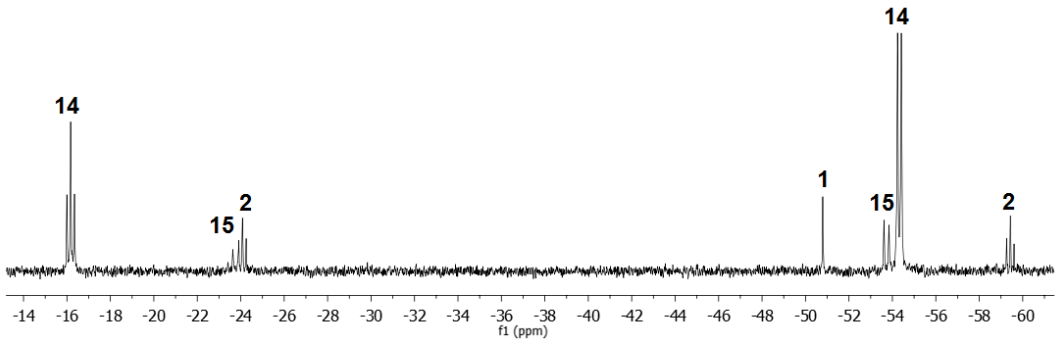

Figure A2.12. ^{31}P NMR spectrum in $CDCl_3$ of the precipitate obtained by refluxing *trans*-$RuCl_2(PTA)_4$ (**1**) in CH_3CN for 3.5h. **14** is *trans,mer*-$RuCl_2(CH_3CN)(PTA)_3$ and **15** is *cis,mer*-$RuCl_2(CH_3CN)(PTA)_3$.

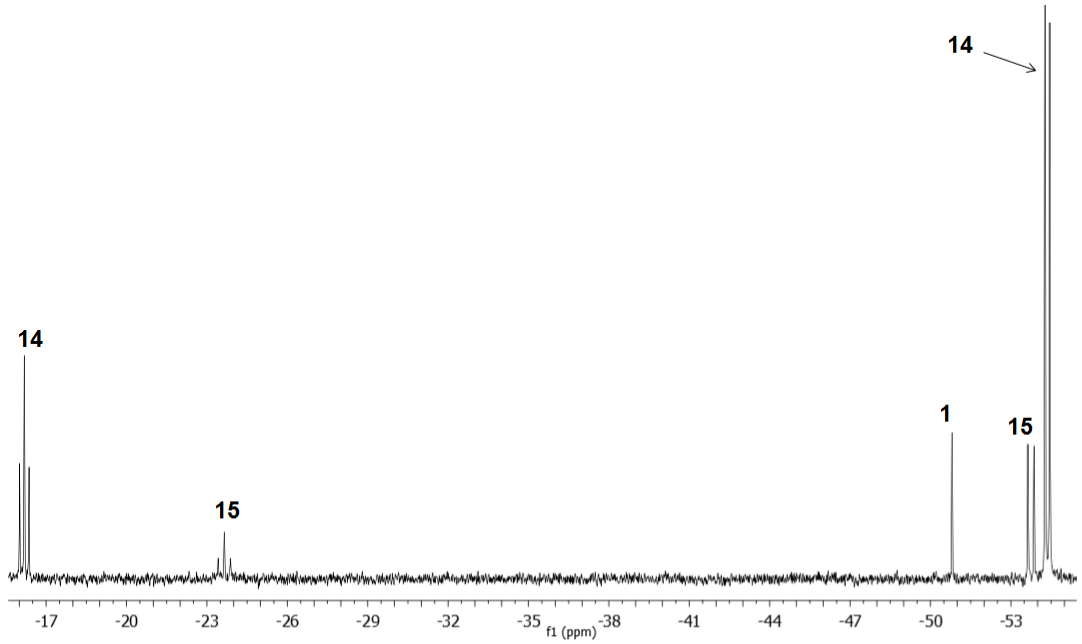

Figure A2.13. ^{31}P NMR spectrum in $CDCl_3$ of the precipitate obtained by refluxing *trans*-$RuCl_2(PTA)_4$ (**1**) in CH_3CN for 2h.

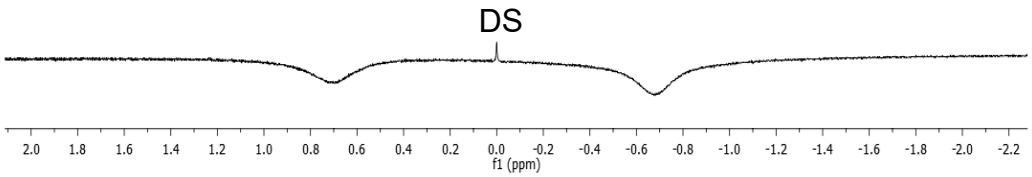

Figure A2.14. Inversion recovery ^1H NMR spectrum in D_2O of *trans*-$[RuCl_4(PTAH)_2]Cl$ (**3**). Upward: diamagnetic signal of DSS (internal standard for D_2O); downward: paramagnetic signals of PTA.

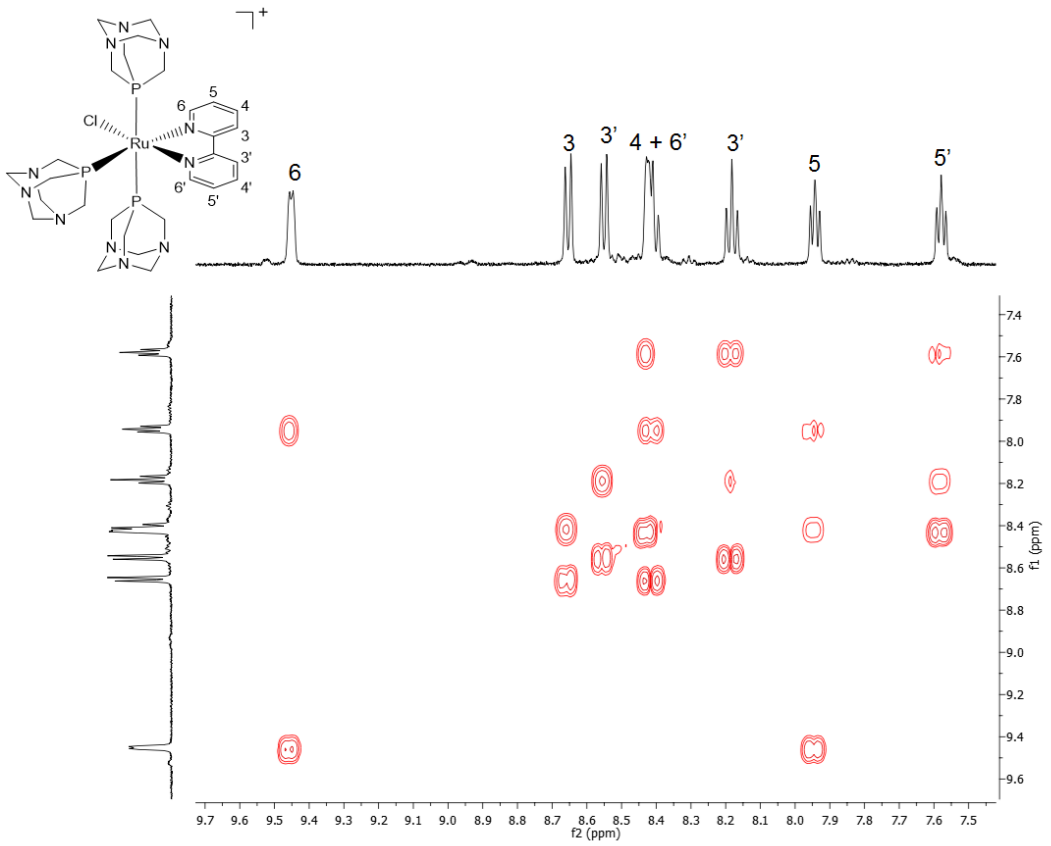

Figure A2.15. ^{1}H-^{1}H COSY NMR spectrum (bpy region) in D_2O of *mer*-[Ru(bpy)Cl(PTA)$_3$](PF$_6$) (**17PF$_6$**).

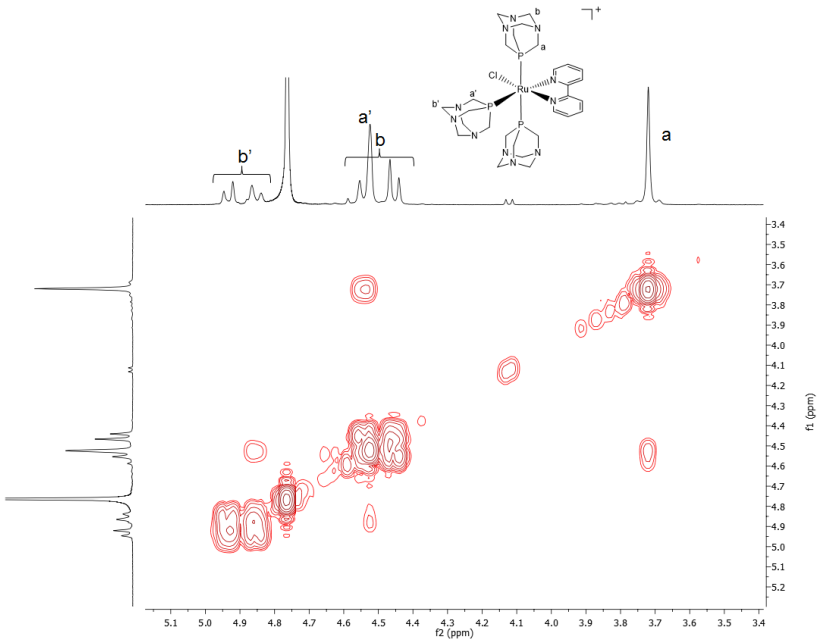

Figure A2.16. ^{1}H-^{1}H COSY NMR spectrum (PTA region) in D_2O of *mer*-[Ru(bpy)Cl(PTA)$_3$](PF$_6$) (**17PF$_6$**).

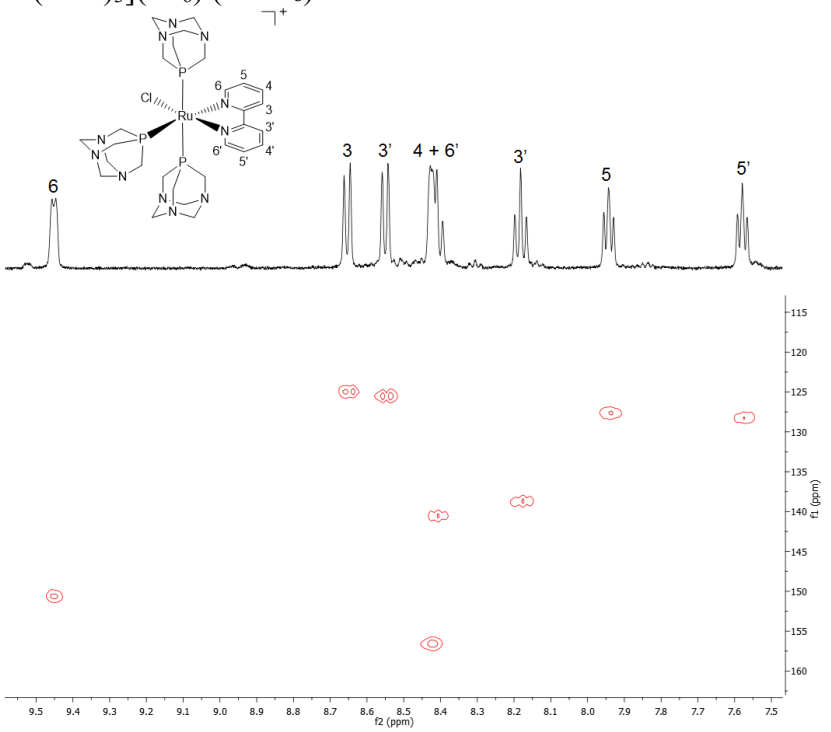

Figure A2.17. ^{1}H-^{13}C HSQC NMR spectrum (bpy region) in D_2O of *mer*-[Ru(bpy)Cl(PTA)$_3$](PF$_6$) (**17PF$_6$**).

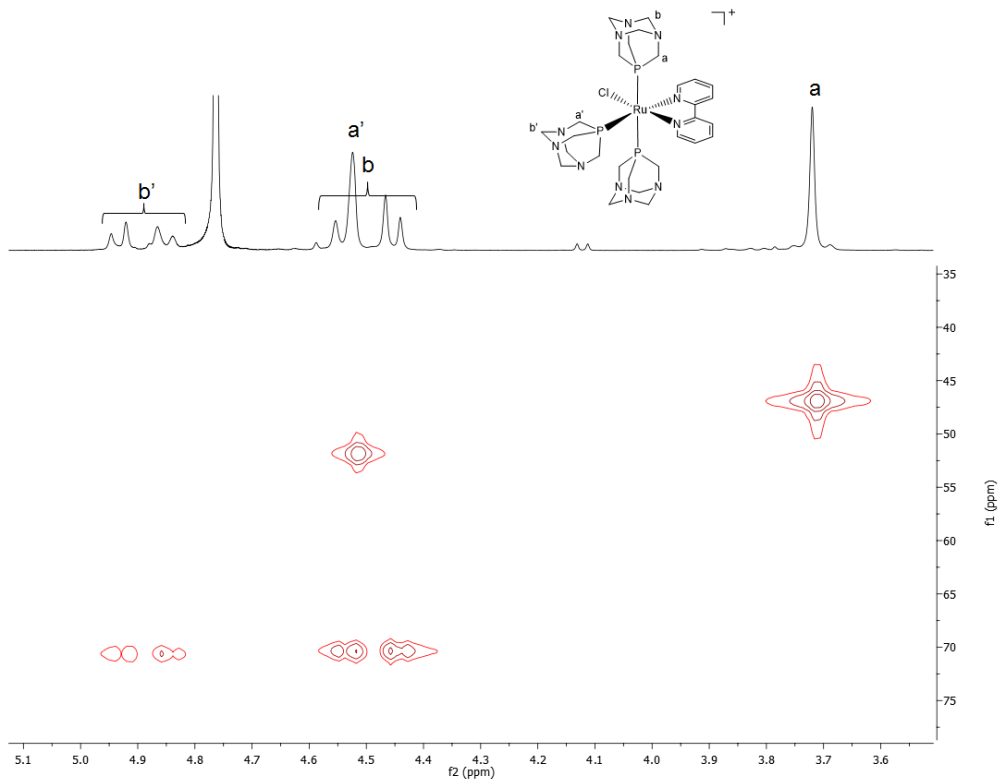

Figure A2.18. ^{1}H-^{13}C HSQC NMR spectrum (PTA region) in D_2O of *mer*-[Ru(bpy)Cl(PTA)$_3$](PF$_6$) (**17PF$_6$**).

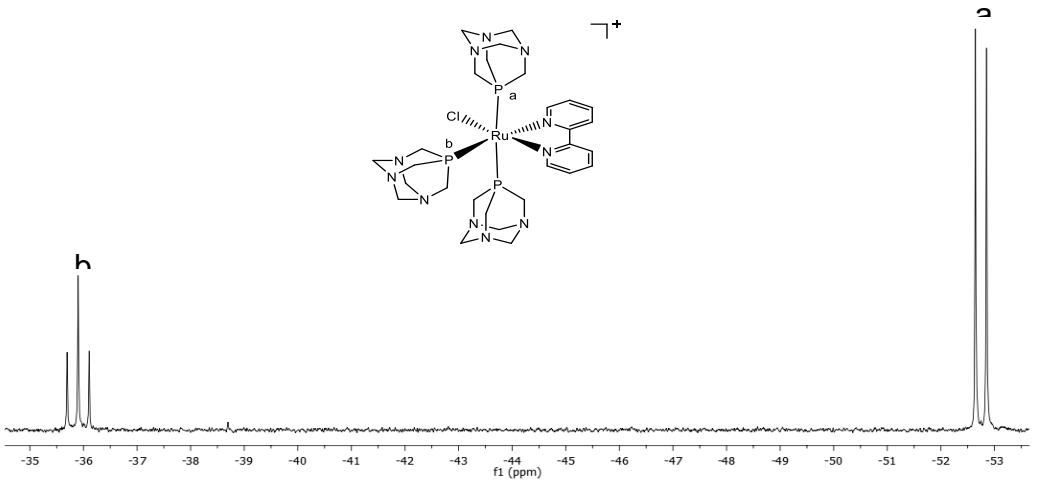

Figure A2.19. ^{31}P NMR spectrum in D_2O of *mer*-[Ru(bpy)Cl(PTA)$_3$](PF$_6$) (**17PF$_6$**).

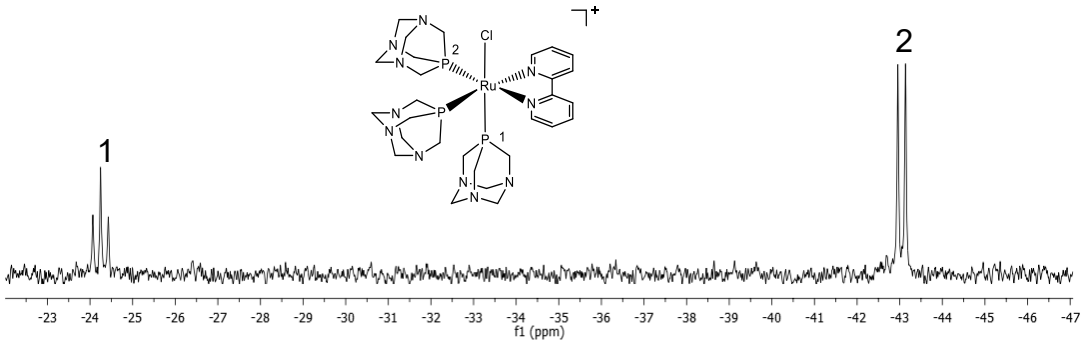

Figure A2.20. ^{31}P NMR spectrum of *fac*-[Ru(bpy)Cl(PTA)$_3$](PF$_6$) (**18PF$_6$**) in D$_2$O after addition of an aliquot of NaCl.

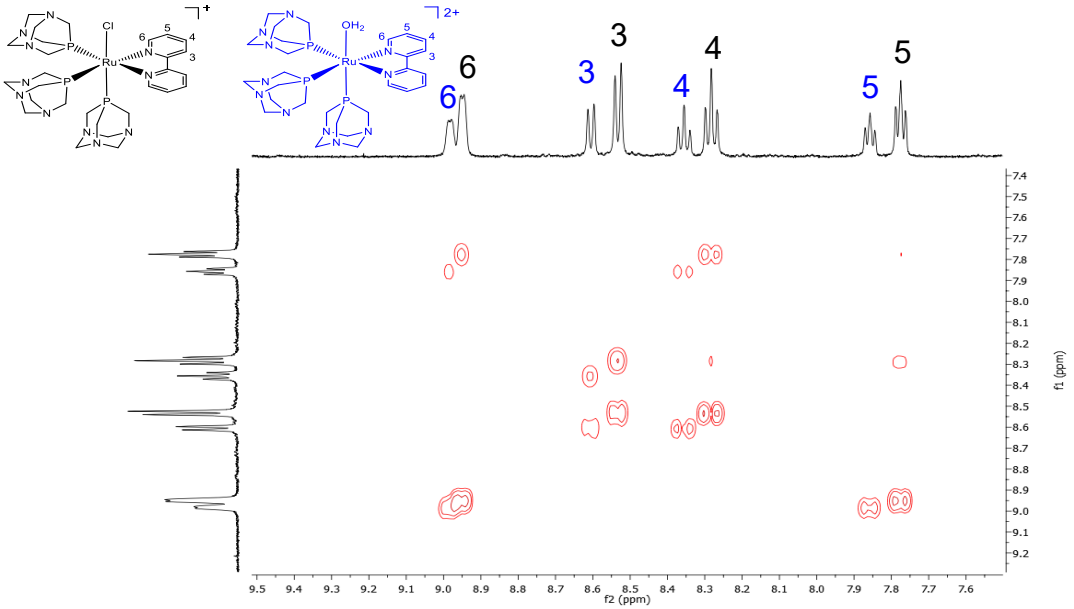

Figure A2.21. ^{1}H-^{1}H COSY NMR spectrum (bpy region) in D$_2$O of *fac*-[Ru(bpy)Cl(PTA)$_3$](PF$_6$) (**18PF$_6$**, black labels) that equilibrates with *fac*-[Ru(bpy)(OH$_2$)(PTA)$_3$]Cl(PF$_6$) (**18$_{aq}$**, blue labels).

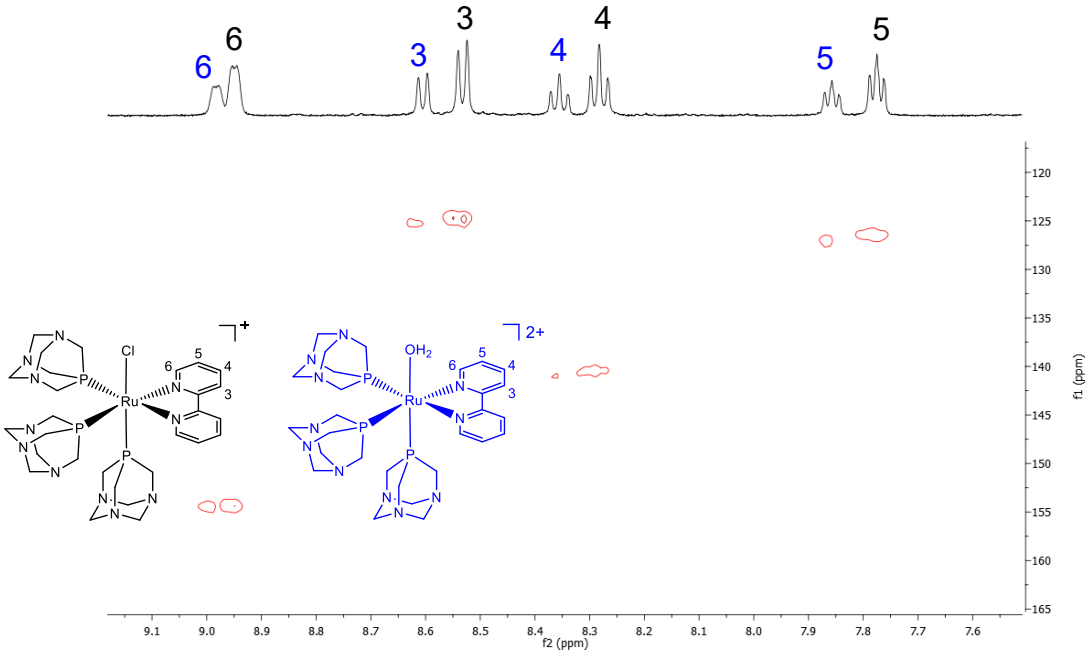

Figure A2.22. ^{1}H-^{13}C HSQC NMR spectrum (bpy region) in D_2O of *fac*-[Ru(bpy)Cl(PTA)$_3$](PF$_6$) (**18PF$_6$**, black labels) that equilibrates with *fac*-[Ru(bpy)(OH$_2$)(PTA)$_3$]Cl(PF$_6$) (**18$_{aq}$**, blue labels).

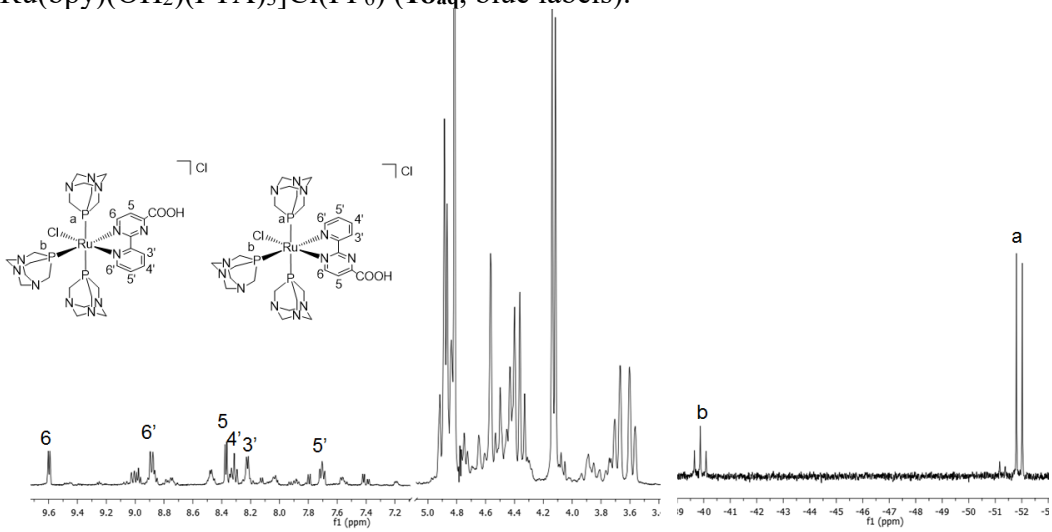

Figure A2.23. ^{1}H (left) and ^{31}P (right) NMR spectra in D_2O of *mer*-[RuCl(cppH)(PTA)$_3$]Cl (**19**).

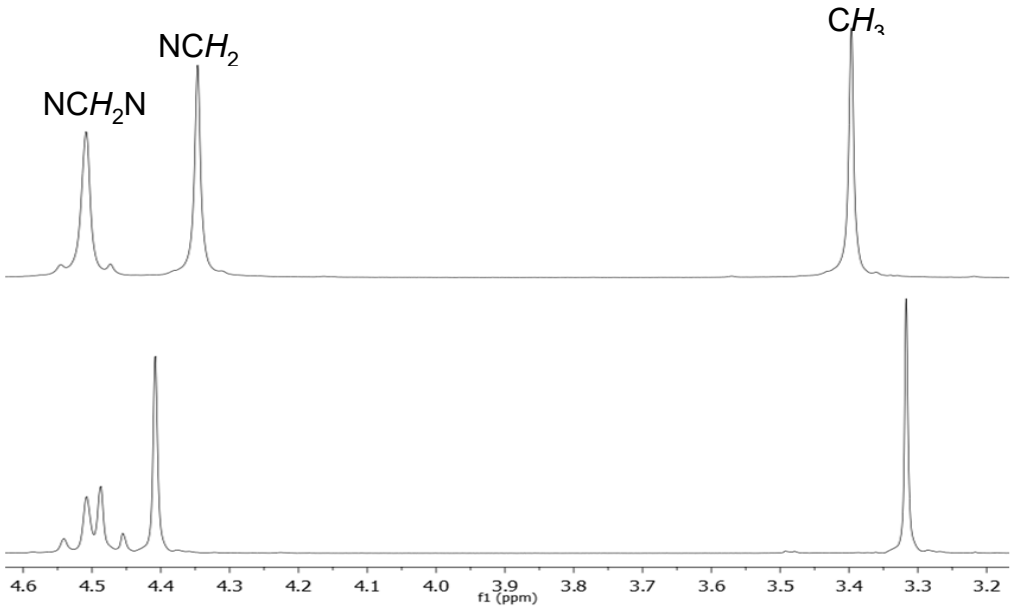

Figure A2.24. ^{1}H NMR spectra of *cis,cis,trans*-$RuCl_2(dmso\text{-}S)_2(PTA)_2$ (**10**) in D_2O (top) and in $CDCl_3$ (bottom).

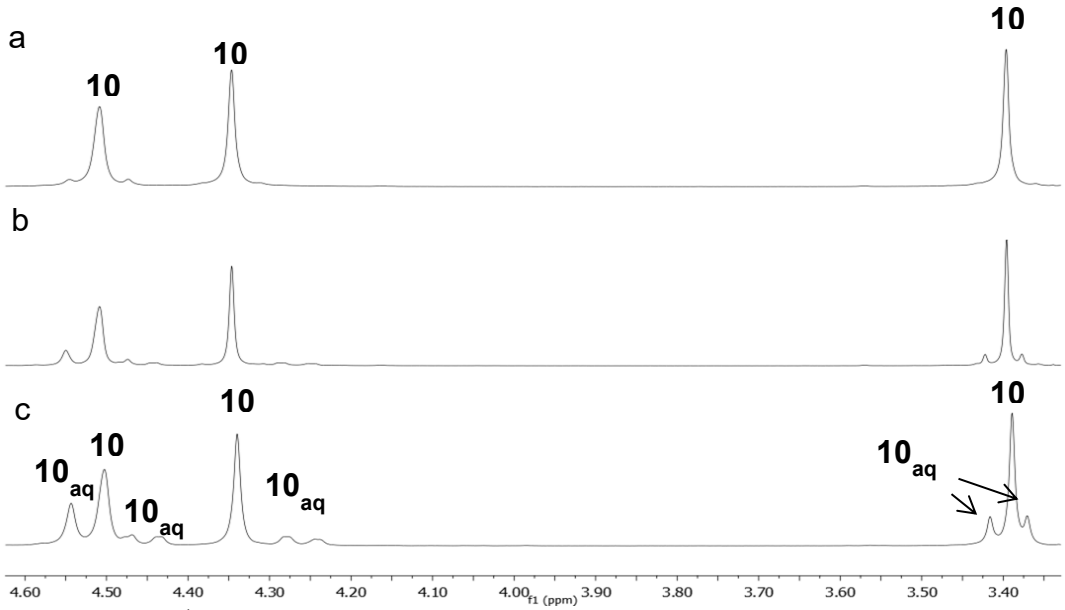

Figure A2.25. ^{1}H NMR spectra of *cis,cis,trans*-$RuCl_2(dmso\text{-}S)_2(PTA)_2$ (**10**) in D_2O registered immediately after dissolution (a); after 20 hours in the dark (b); after 120 hours in the dark (c).

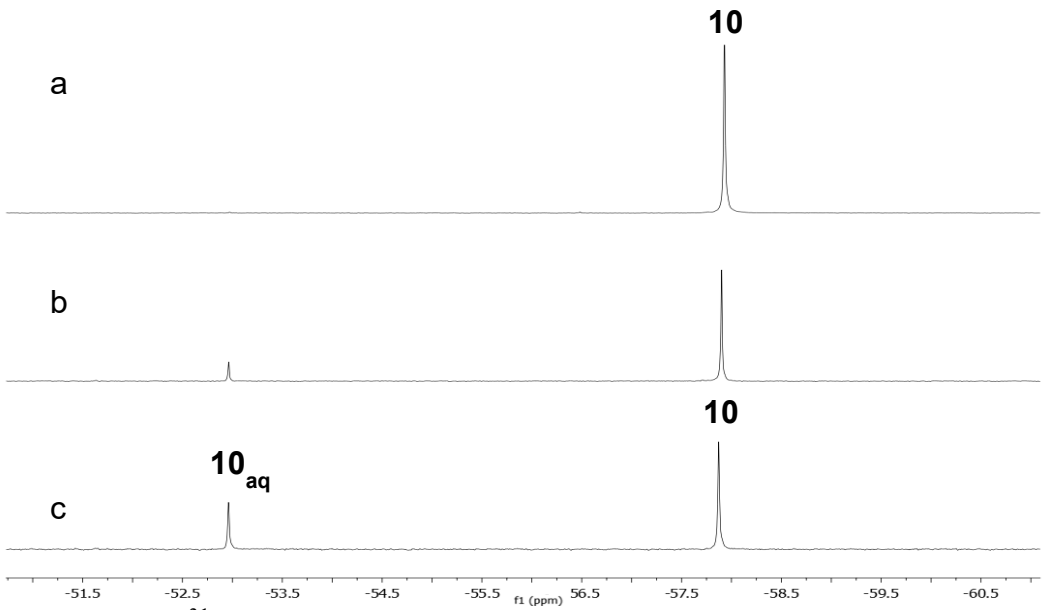

Figure A2.26. ^{31}P NMR spectra of *cis,cis,trans*-$RuCl_2(dmso\text{-}S)_2(PTA)_2$ (**10**) in D_2O registered immediately after dissolution (a); after 20 hours in the dark (b); after 120 hours in the dark (c).

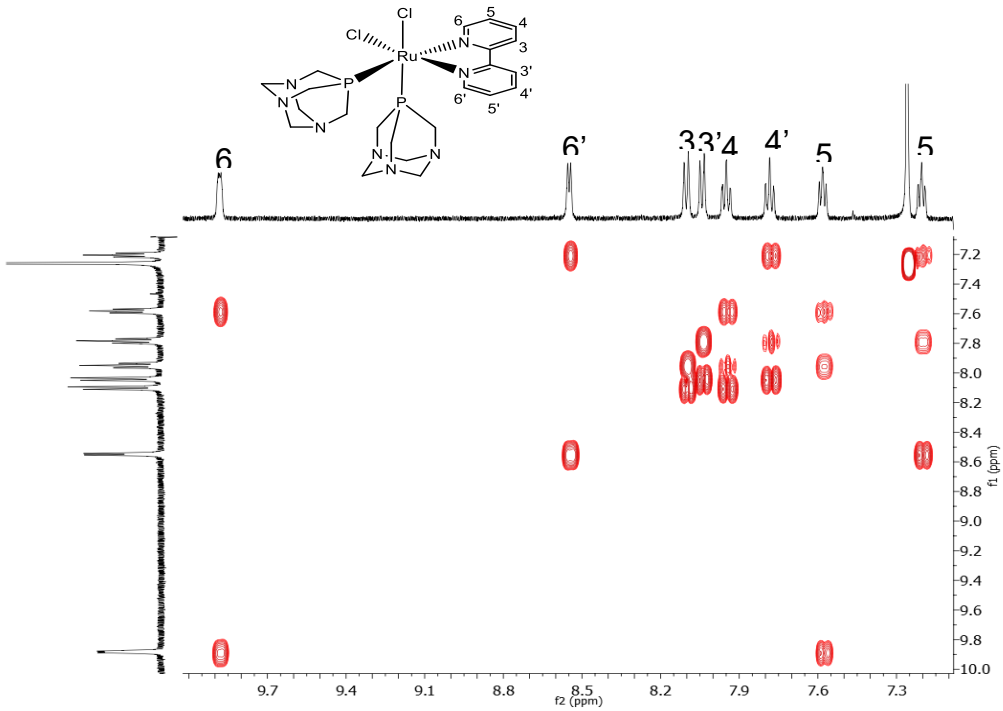

Figure A2.27. ^1H-^1H COSY NMR spectrum (bpy region) in $CDCl_3$ of *cis,cis*-$Ru(bpy)Cl_2(PTA)_2$ (**22**).

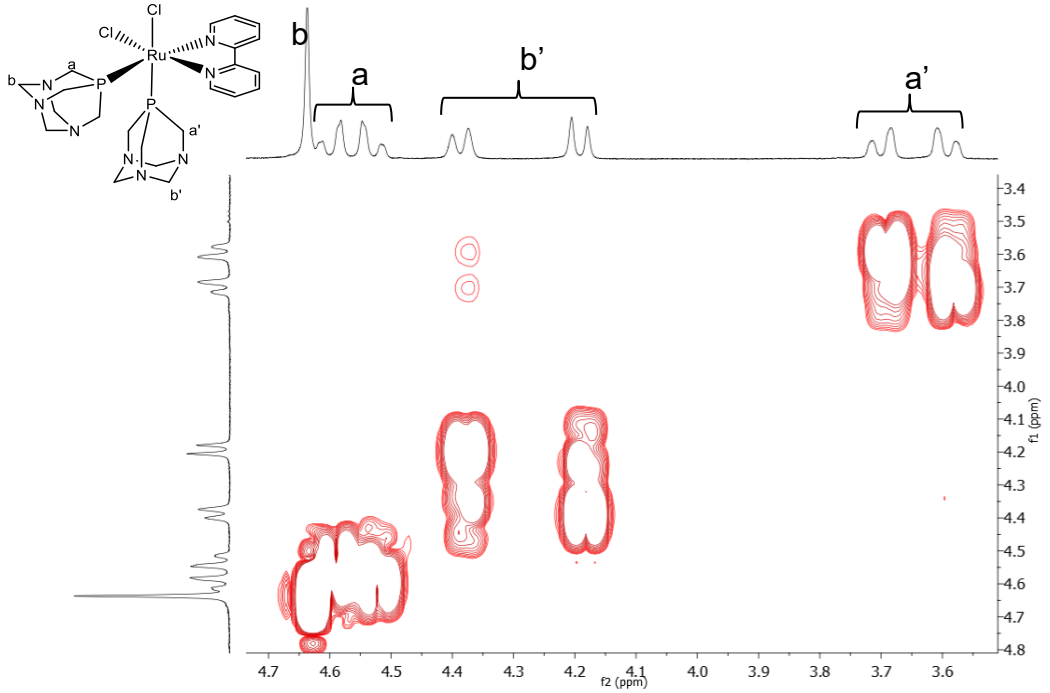

Figure A2.28. ^{1}H-^{1}H COSY NMR spectrum (PTA region) in $CDCl_3$ of *cis,cis*-Ru(bpy)Cl_2(PTA)$_2$ (**22**).

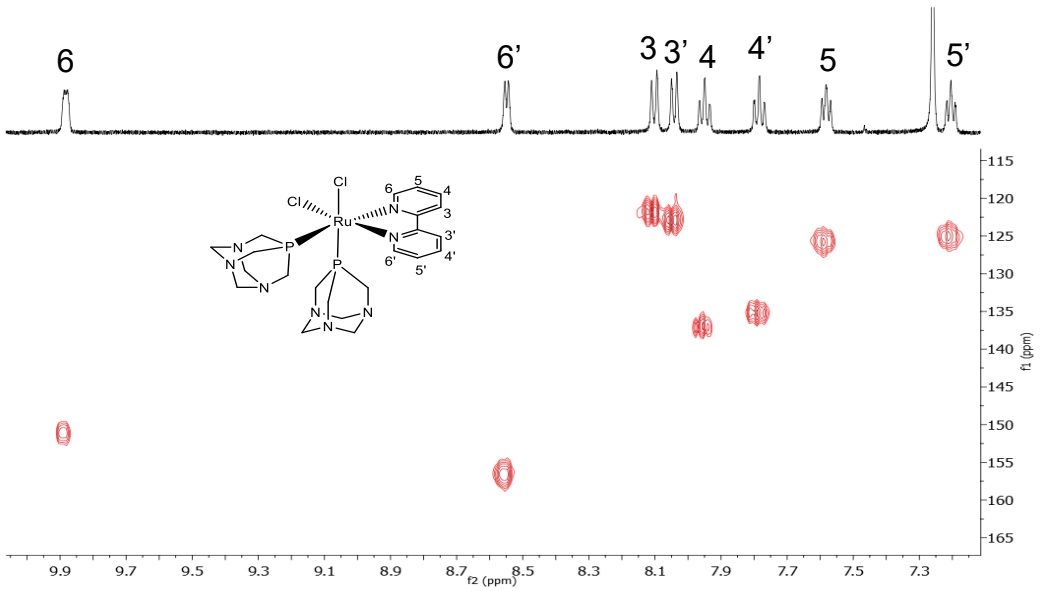

Figure A2.29. ^{1}H-^{13}C HSQC NMR spectrum (bpy region) in $CDCl_3$ of *cis,cis*-Ru(bpy)Cl_2(PTA)$_2$ (**22**).

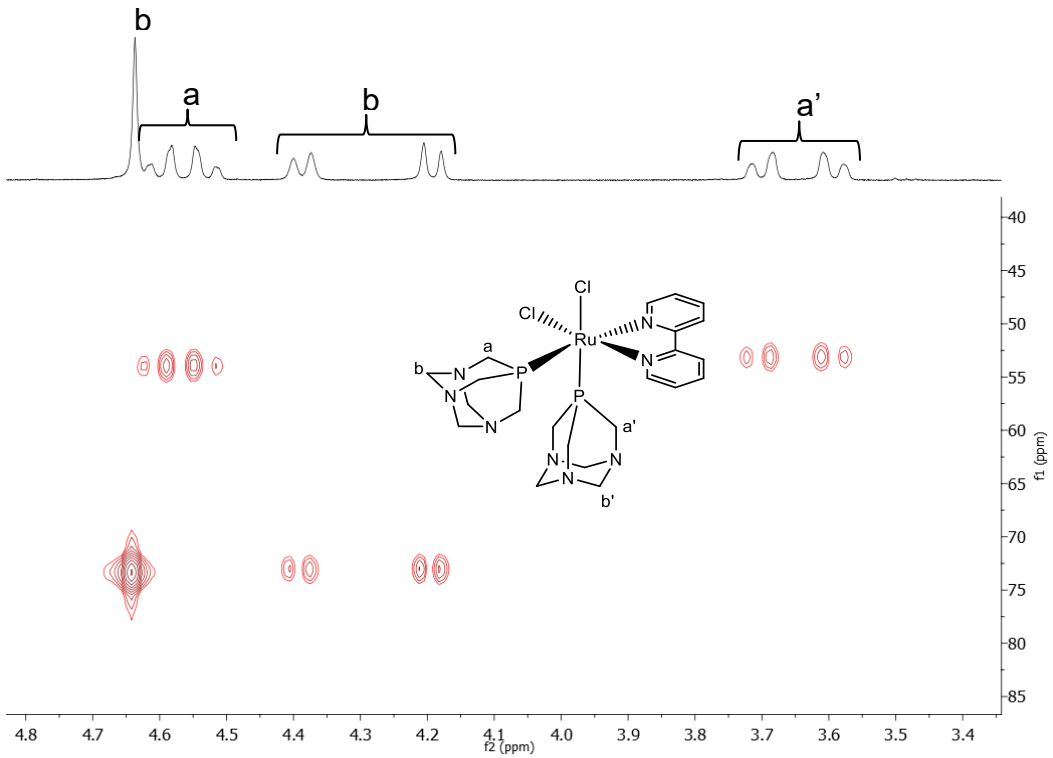

Figure A2.30. ^{1}H-^{13}C HSQC NMR spectrum (PTA region) in $CDCl_3$ of *cis,cis*-$Ru(bpy)Cl_2(PTA)_2$ (**22**).

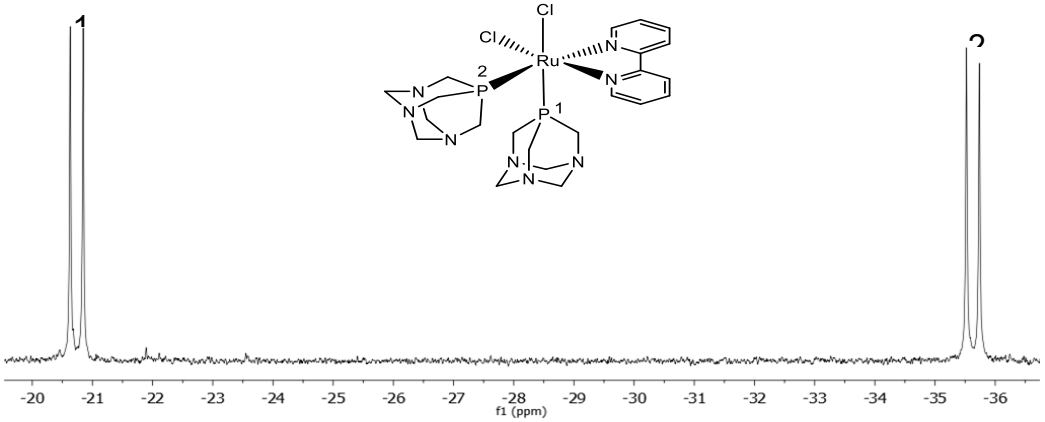

Figure A2.31. ^{31}P NMR spectrum in $CDCl_3$ of *cis,cis*-$Ru(bpy)Cl_2(PTA)_2$ (**22**).

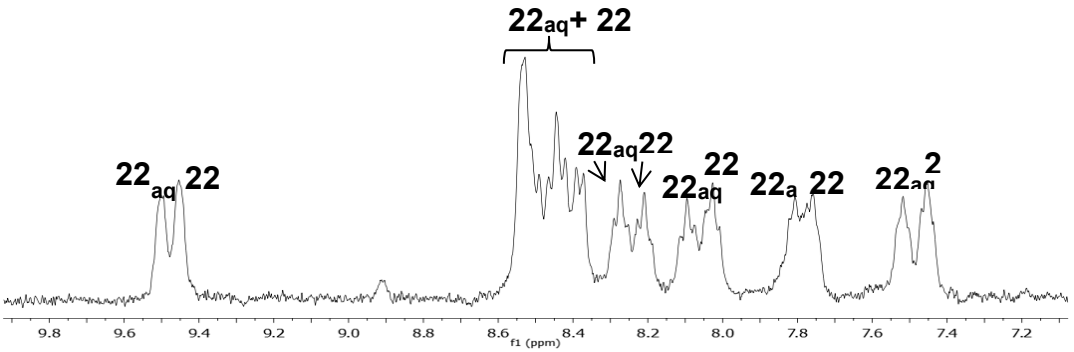

Figure A2.32. ^{1}H NMR spectrum (bpy region) in D_2O of *cis,cis*-[Ru(bpy)Cl(OH_2)($PTA)_2]^+$ (**22$_{aq}$**) after addition of an aliquot of NaCl.

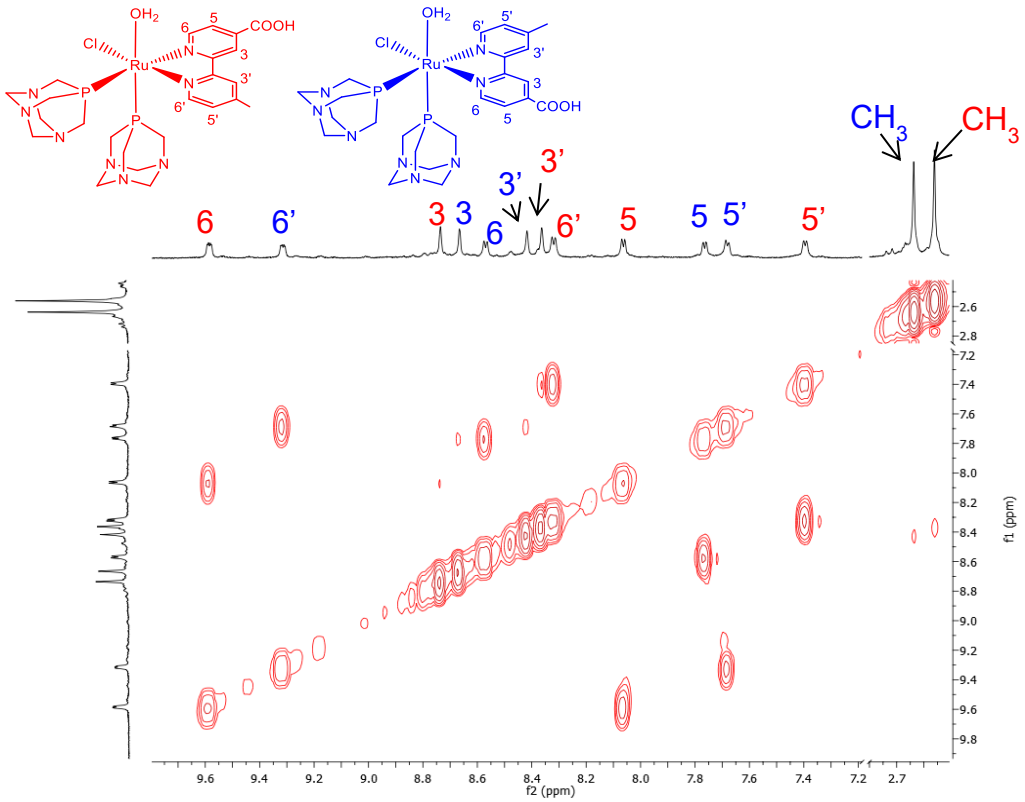

Figure A2.33. ^{1}H-^{1}H COSY NMR spectrum (bpyAc region) in D_2O of the mixture of the two isomers of *cis,cis*-Ru(bpyAc)Cl(OH_2)($PTA)_2$: **23a$_{aq}$** (red) and **23b$_{aq}$** (blue).

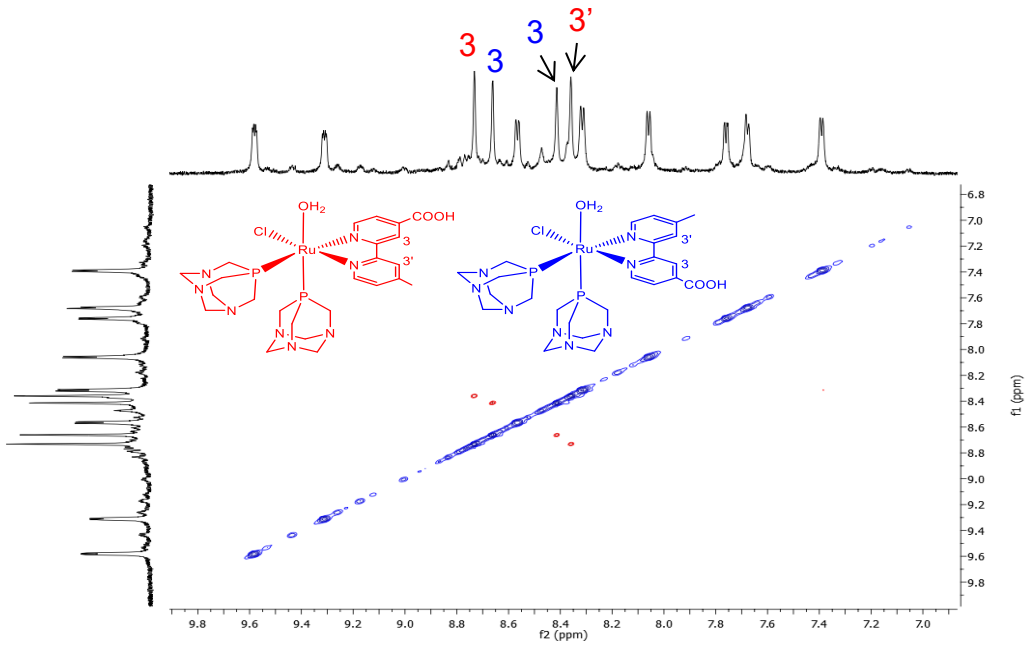

Figure A2.34. ^{1}H-^{1}H NOESY NMR spectrum (aromatic region) in D_2O of the mixture of the two isomers of *cis,cis*-Ru(bpyAc)Cl(OH_2)$(PTA)_2$: **23a$_{aq}$** (red) and **23b$_{aq}$** (blue).

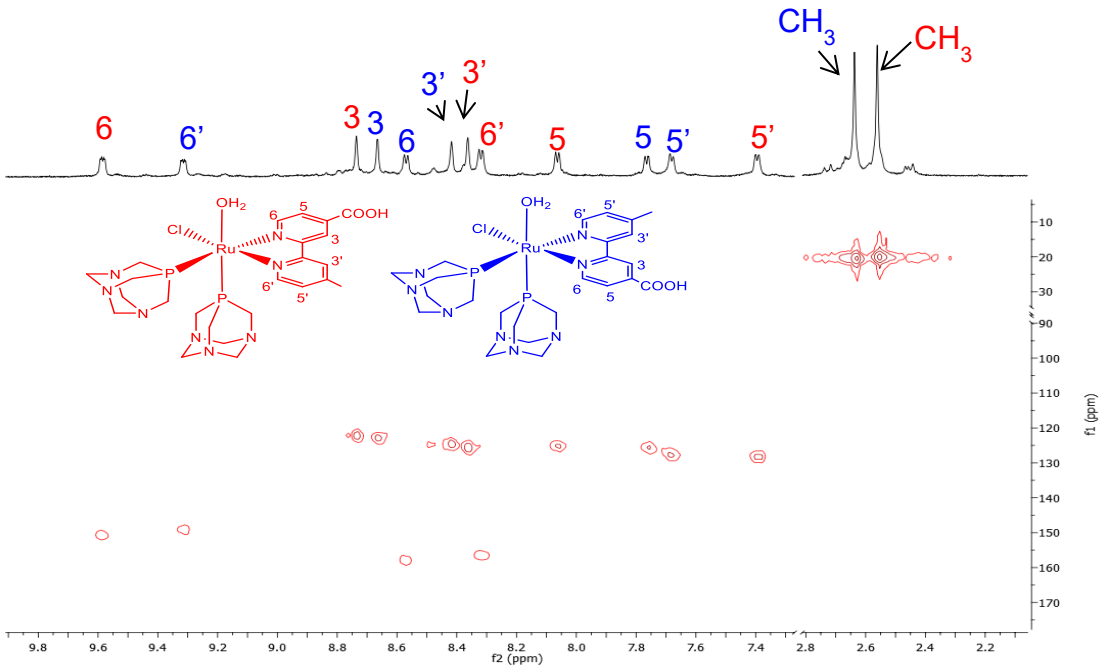

Figure A2.35. ^{1}H-^{13}C HSQC NMR spectrum (bpyAc region) in D_2O of the mixture of the two isomers of *cis,cis*-Ru(bpyAc)Cl(OH_2)$(PTA)_2$: **23a$_{aq}$** (red) and **23b$_{aq}$** (blue).

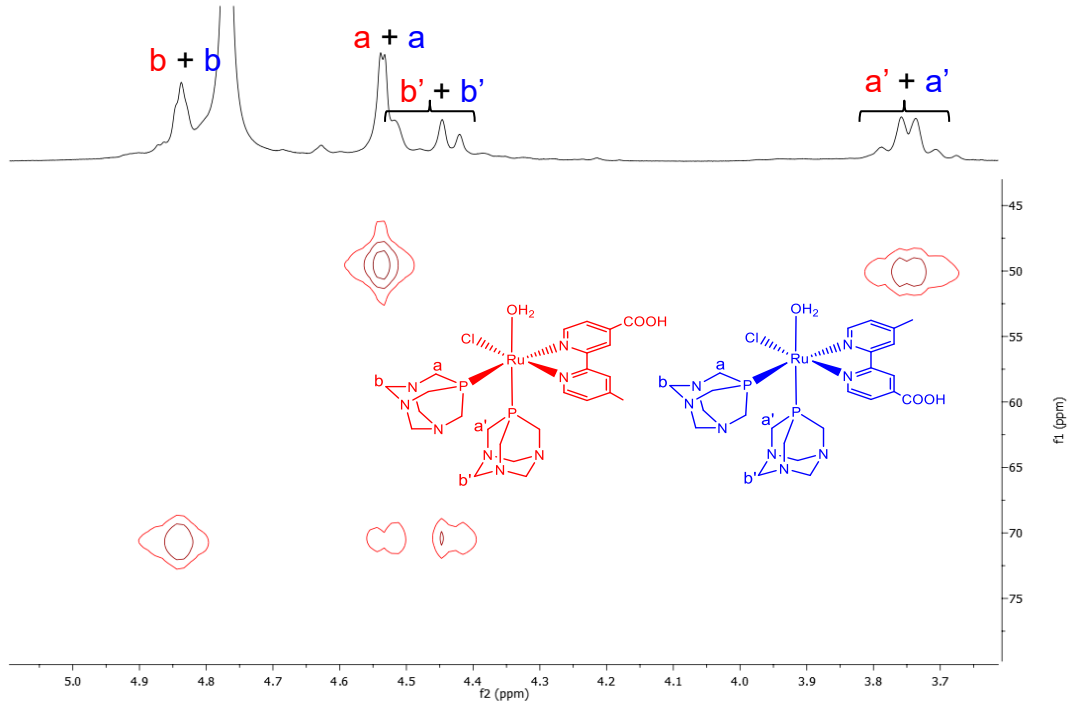

Figure A2.36. ^{1}H-^{13}C HSQC NMR spectrum (PTA region) in D_2O of the mixture of the two isomers of *cis,cis*-Ru(bpyAc)Cl(OH_2)$(PTA)_2$: **23a$_{aq}$** (red) and **23b$_{aq}$** (blue).

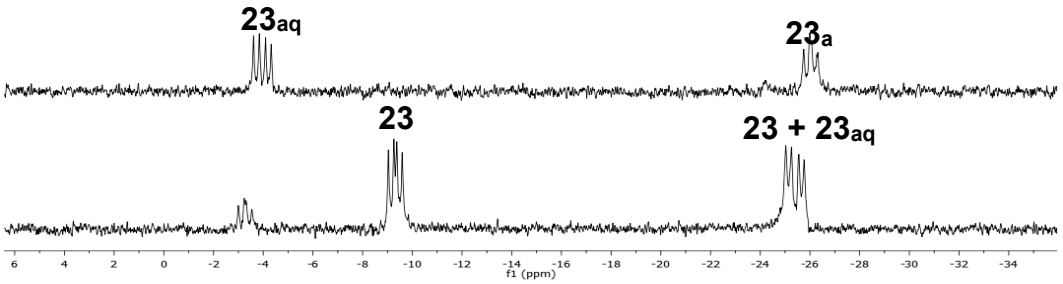

Figure A2.37. ^{31}P NMR spectra in D_2O of the mixture of the two isomers of *cis,cis*-Ru(bpyAc)Cl(OH_2)$(PTA)_2$ (**23$_{aq}$**) (top) and after addition of an aliquot of NaCl, affording a mixture of **23** and **23$_{aq}$** (bottom).

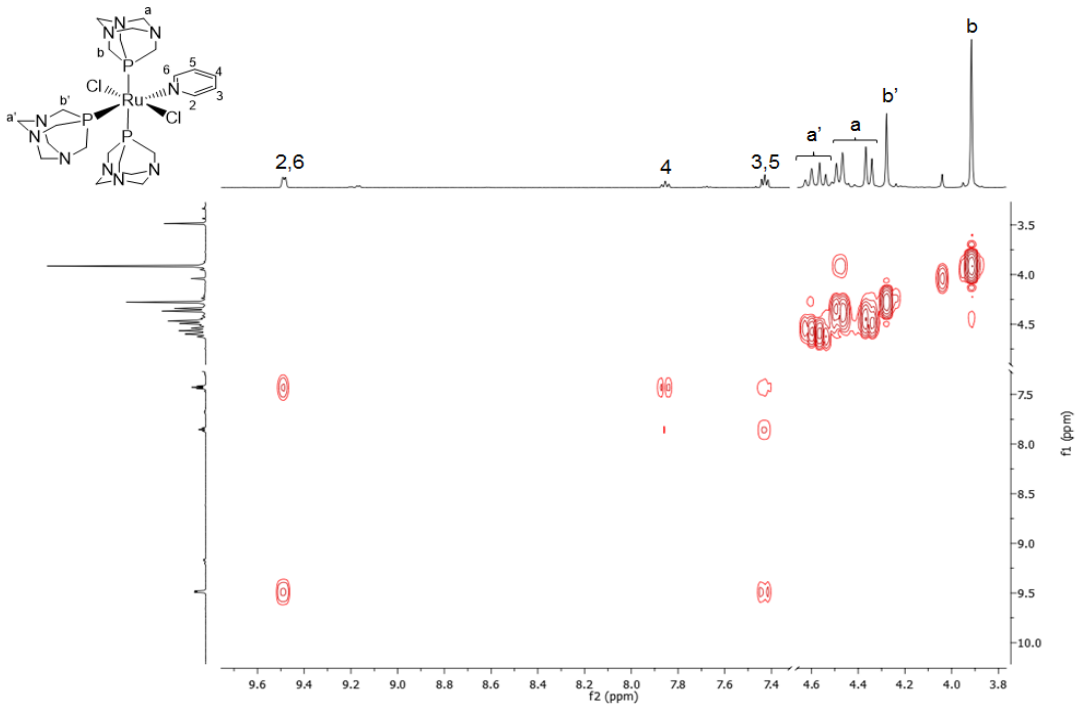

Figure A2.38. ^{1}H-^{1}H COSY spectrum in $CDCl_3$ of *trans,mer*-[$RuCl_2(PTA)_3(py)$] (**25**). See the inset drawing for the peak labels.

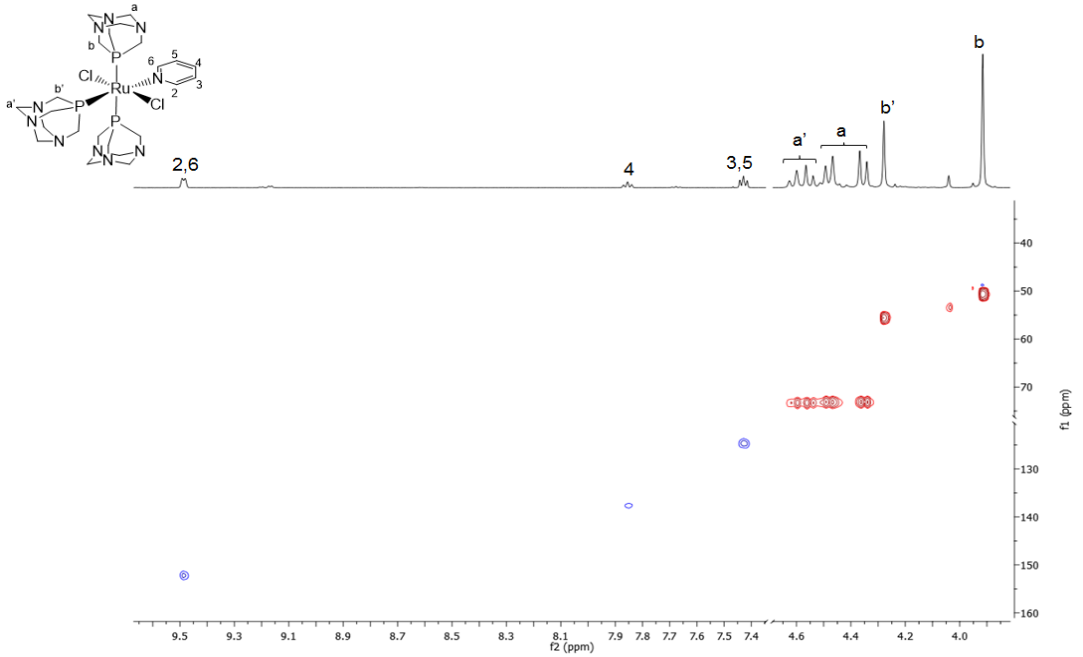

Figure A2.39. ^{1}H-^{13}C HSQC spectrum in $CDCl_3$ of *trans,mer*-[$RuCl_2(PTA)_3(py)$] (**25**). See the inset drawing for the peak labels.

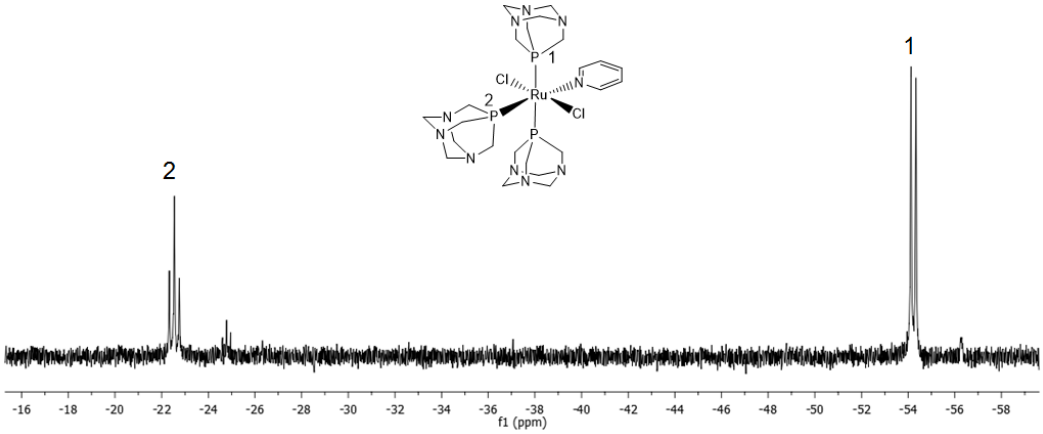

Figure A2.40. ^{31}P NMR spectrum in $CDCl_3$ of *trans,mer*-$[RuCl_2(PTA)_3(py)]$ (**25**).

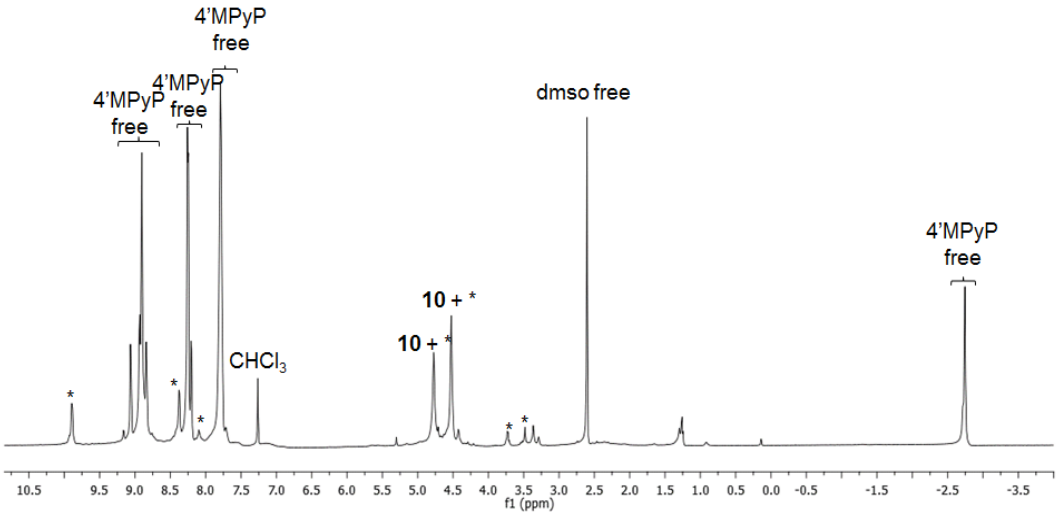

Figure A.41. ^{1}H NMR spectrum in $CDCl_3$ of the reaction between *cis,cis,trans*-$RuCl_2(dmso\text{-}S)_2(PTA)_2$ (**10**) and 4'MPyP. With the * are indicated the signals of the products.

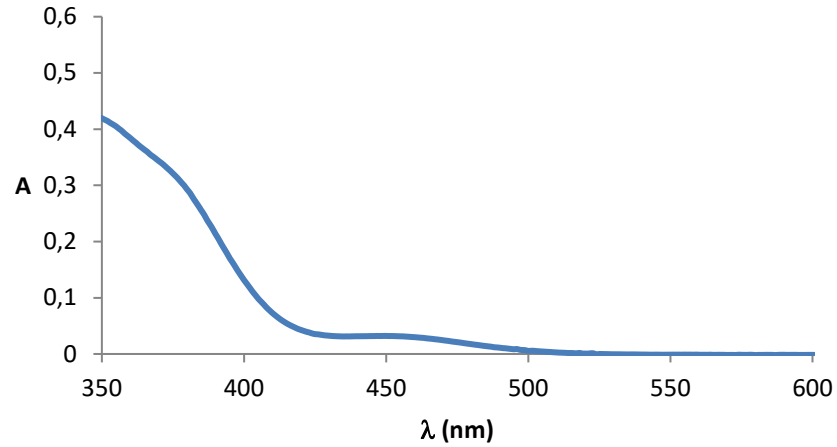

Figure A2.42. UV spectrum of *cis*-$RuCl_2(PTA)_4$ (**2**) in $CDCl_3$.

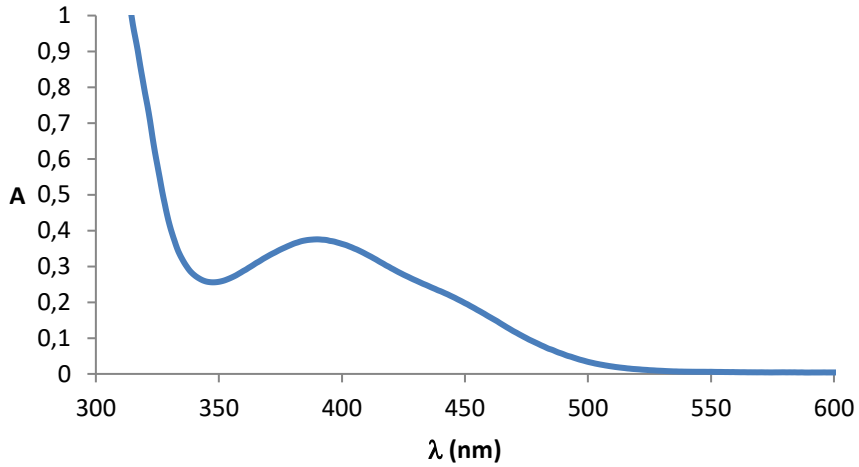

Figure A2.43. UV spectrum of *mer*-$[Ru(bpy)Cl(PTA)_3](PF_6)$ (**17PF$_6$**) in H_2O.

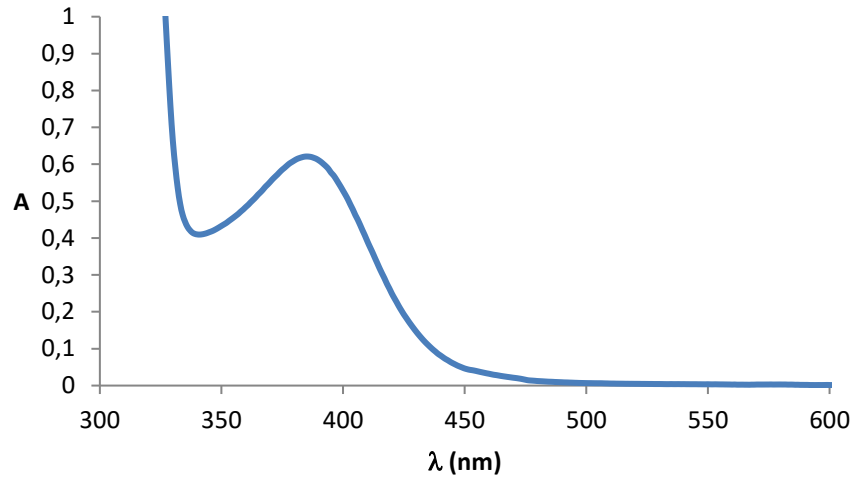

Figure A2.44. UV spectrum of *fac*-[Ru(bpy)Cl(PTA)$_3$](PF$_6$) (**18PF$_6$**) in H_2O.

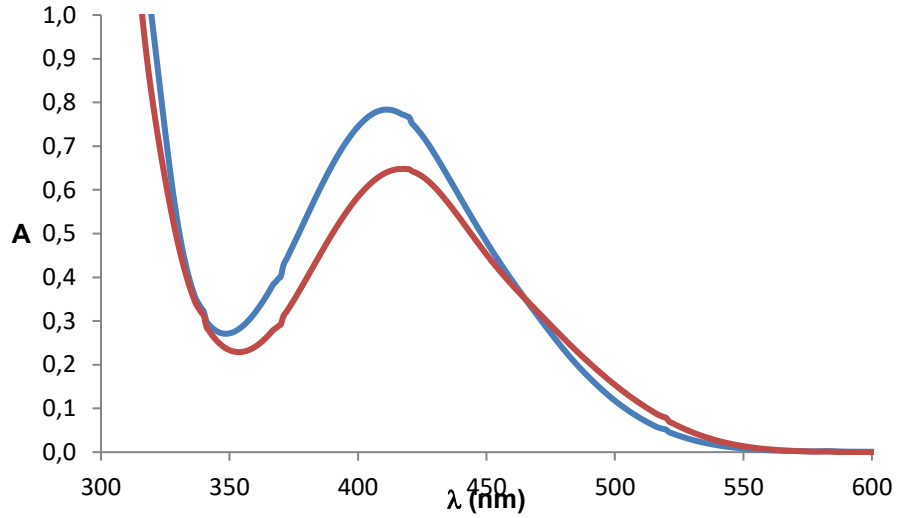

Figure A2.45. UV spectrum of *cis,cis*-[Ru(bpy)Cl(OH$_2$)(PTA)$_2$]$^+$ (**22$_{aq}$**) (blue) in H_2O and after addition of aliquots of NaCl (**22**, red).

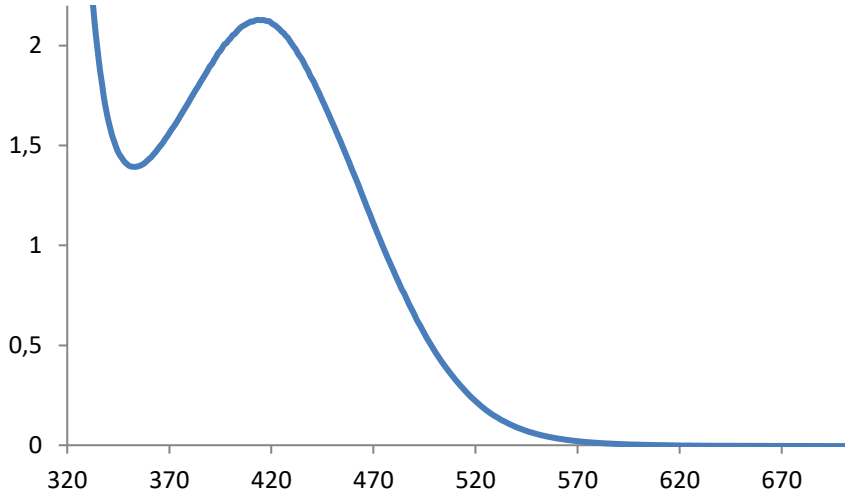

Figure A2.46. UV spectrum of *cis,cis*-[Ru(bpyAc)Cl(OH_2)($PTA)_2$]$^+$ (**23$_{aq}$**) in H_2O.

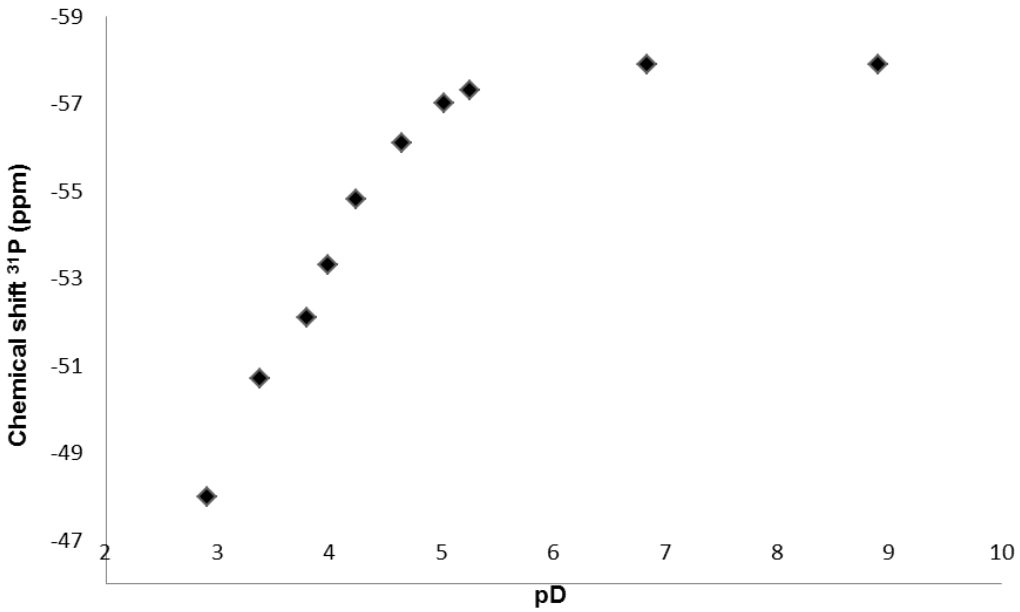

Figure A2.47. ^{31}P NMR pH titration of complex *cis,cis,trans*-$RuCl_2(dmso)_2(PTA)_2$ (**10**) in D_2O.

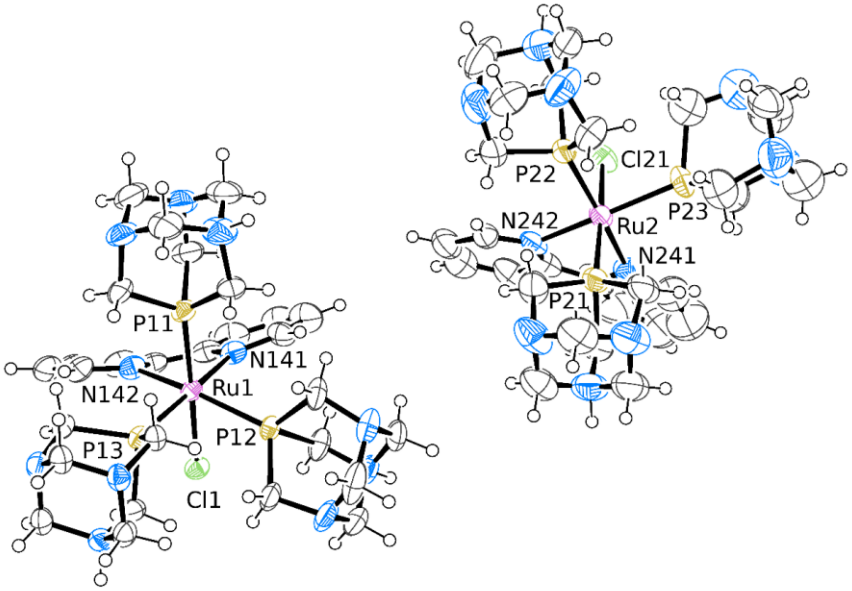

Figure A2.48. Molecular structure (50% probability ellipsoids) of *fac*-$[Ru(bpy)Cl(PTAH)_{2.5}(PTA)_{0.5}](ClO_4)_{3.5}\cdot 2.5H_2O$ (**18**). All three PTA ligands are protonated in molecule Ru1, whereas only two PTA ligands are protonated in molecule Ru2. Disordered ClO_4^- anions and water molecules have been omitted for clarity.

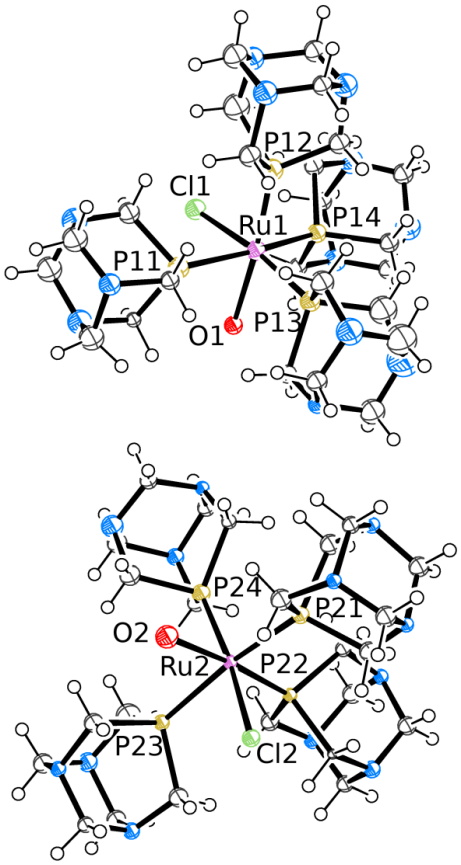

Figure A2.49. Molecular structure (50% probability ellipsoids) of the two crystallographically independent molecules of *cis*-$[RuCl(OH_2)(PTA)_4](PF_6)\cdot CH_3OH$ (**2**$_{aq}$), after structure solution and one least squares (isotropic) refinement cycle with hydrogen atoms added at calculated positions (but not for the coordinated water molecule). Two PF_6^- anions and two methanol solvent molecules have been omitted for clarity.

Appendix of Chapter 3

Figures A3.1-A3.5. NMR characterization in $CDCl_3$ and D_2O of *cis*,*cis*,*trans*-$[RuCl_2(CO)(dmso\text{-}S)(PTA)_2]$ (**31**).

Figures A3.6-A3.9. NMR characterization in $CDCl_3$ and D_2O of *trans,mer*-$[RuCl_2(CO)(PTA)_3]$ (**32**).

Figures A3.10-A3.12. NMR characterization in D_2O of *cis,mer*-$[RuCl_2(CO)(PTA)_3]$ (**33**).

Figures A3.13-A3.15. NMR characterization in D_2O of the dimer $[RuCl_2(CO)(PTA)_2]_2 \cdot 8H_2O$ (**35**).

Figures A3.16-A.18. NMR characterization in D_2O of *trans,trans,trans*-$RuCl_2(CO)(py)(PTA)_2$ (**36**).

Figure A3.19. ^{31}P NMR spectrum in DMSO-d_6 of dimer $[RuCl_2(CO)_2(PTA)]_2 \cdot H_2O$ (**37**).

Figures A3.20-A.21. NMR characterization in $CDCl_3$ of *cis,cis,trans*-$RuCl_2(CO)_2(py)(PTA)$ (**38**).

Figures A3.22-A3.25. NMR characterization in $CDCl_3$ and D_2O of *cis,cis,trans*-$[RuCl_2(CO)_2(PTA)_2]$ (**39**).

Figure A3.26. ^{31}P NMR spectrum of the mixture f*ac*-$[RuCl_2(CO)(PTA)_3]$ (**34**) and *cis*-$[RuCl(CO)(PTA)_4](Cl)$ (**42Cl**) in D_2O.

Figures A3.27. ^{1}H and ^{31}P NMR spectrum of *cis*-$[RuCl(CO)(PTA)_4]NO_3$ (**42NO3**).

Figure A3.28. X-ray molecular structure of *cis,cis,trans*-$RuCl_2(CO)_2(py)(PTA)$ (**38**).

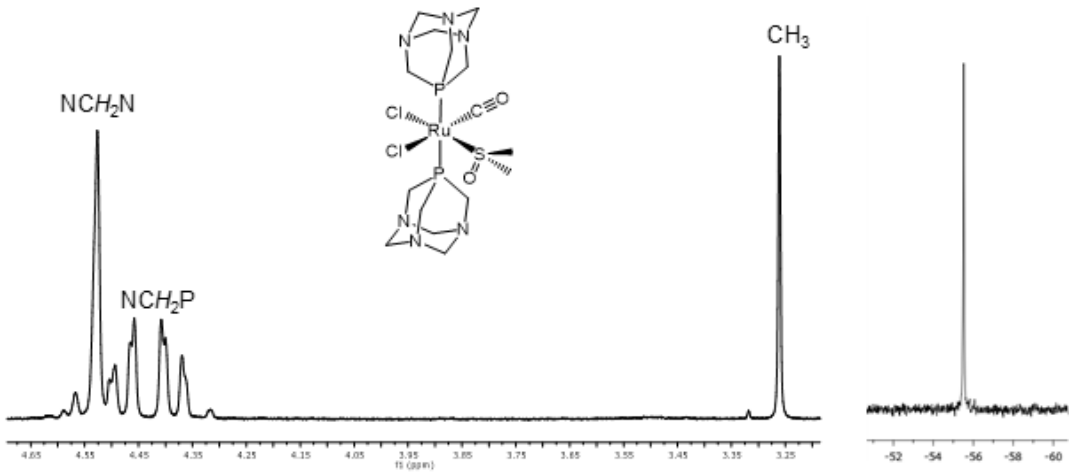

Figure A3.1. ^{1}H (left) and ^{31}P (right) NMR spectra of *cis*,*cis*,*trans*-[$RuCl_2(CO)(dmso\text{-}S)(PTA)_2$] (**31**) in $CDCl_3$.

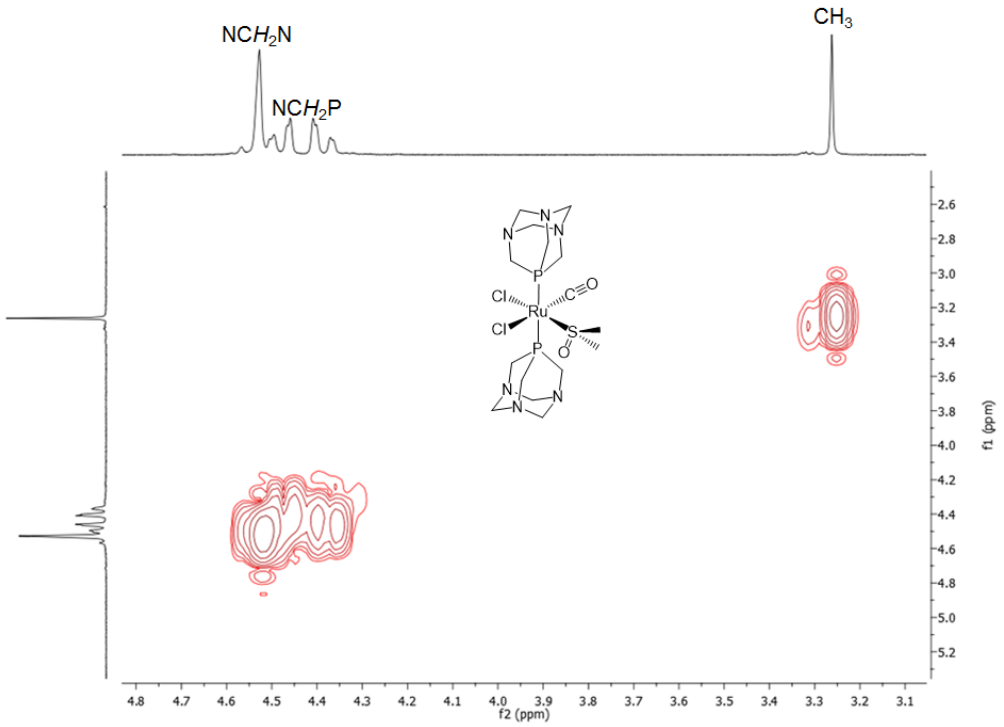

Figure A3.2. ^{1}H-^{1}H COSY NMR spectrum of *cis*,*cis*,*trans*-[$RuCl_2(CO)(dmso\text{-}S)(PTA)_2$] (**31**) in $CDCl_3$.

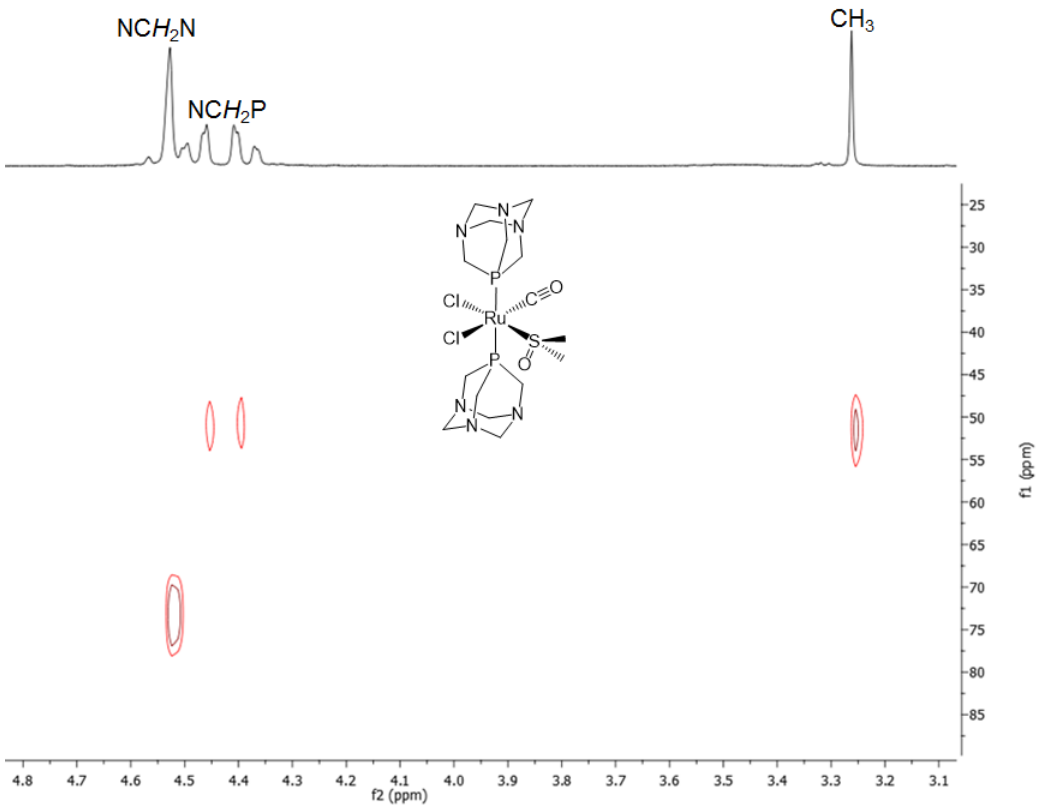

Figure A3.3. ^{1}H-^{13}C HSQC NMR spectrum of *cis*,*cis*,*trans*-[$RuCl_2(CO)$(dmso-S)$(PTA)_2$] (**31**) in $CDCl_3$.

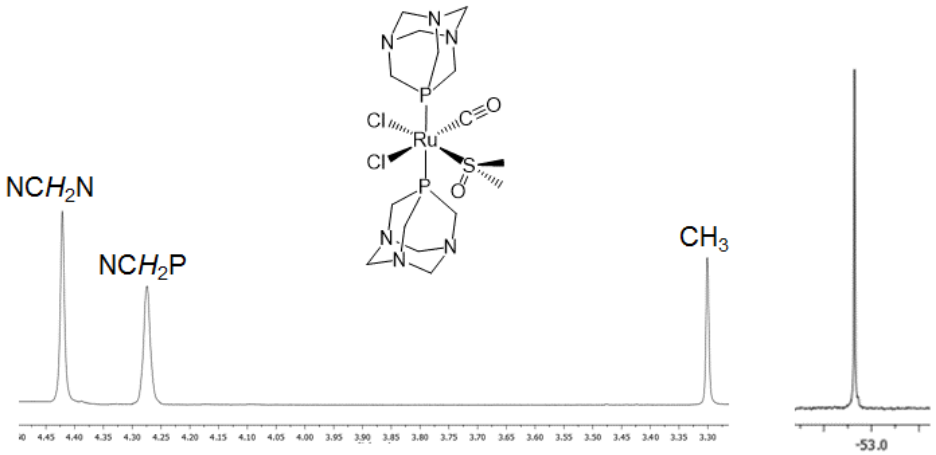

Figure A3.4. ^{1}H (left) and ^{31}P (right) NMR spectra of *cis*,*cis*,*trans*-[$RuCl_2(CO)(dmso\text{-}S)(PTA)_2$] (**31**) in D_2O.

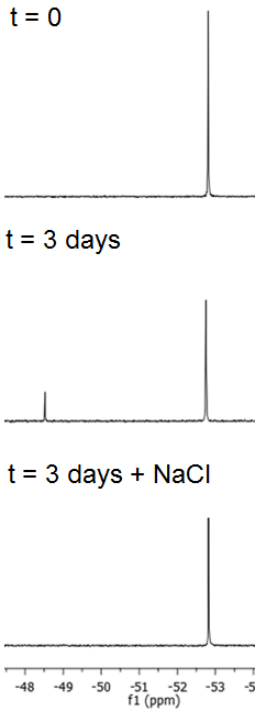

Figure A3.5. ^{1}H NMR spectra of *cis*,*cis*,*trans*-[$RuCl_2(CO)(dmso\text{-}S)(PTA)_2$] (**31**) in D_2O immediately after dissolution (top), after 3 days (middle) and after an excess of NaCl.

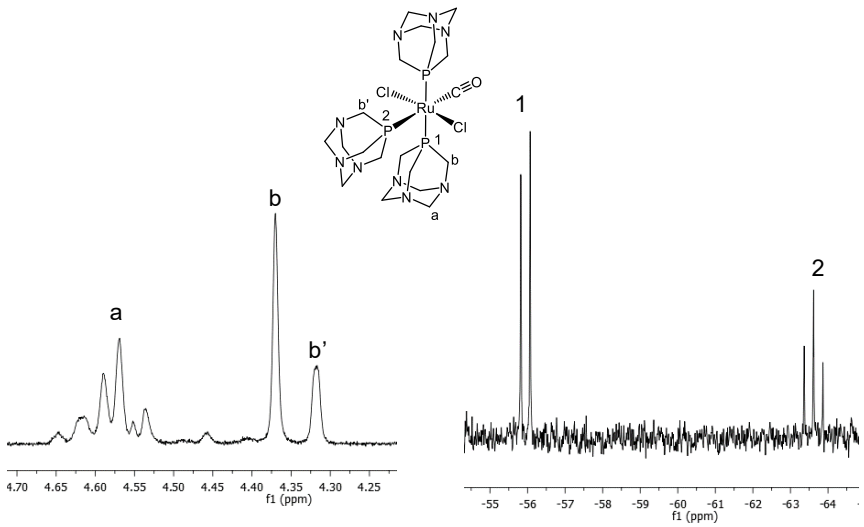

Figure A3.6. ^{1}H (left) and ^{31}P (right) NMR spectra of *trans,mer*-$[RuCl_2(CO)(PTA)_3]$ (**32**) in $CDCl_3$.

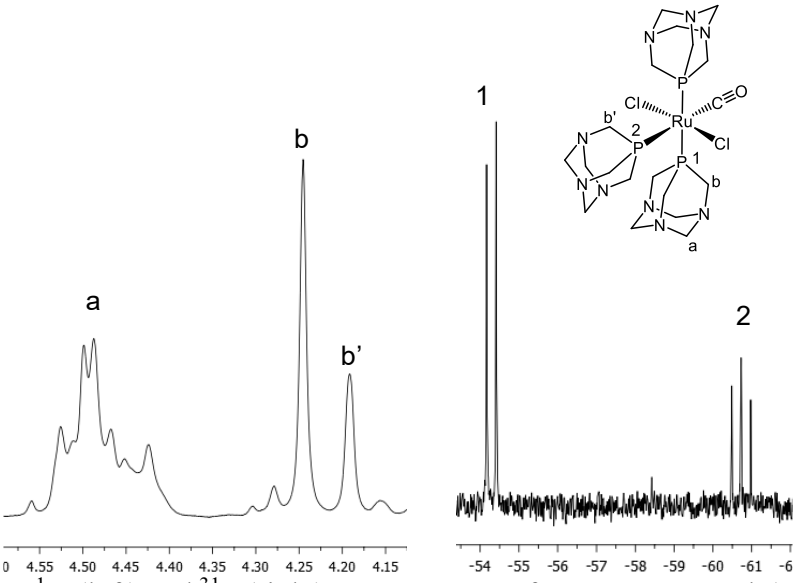

Figure A3.7. ^{1}H (left) and ^{31}P (right) NMR spectra of *trans,mer*-$[RuCl_2(CO)(PTA)_3]$ (**32**) in D_2O.

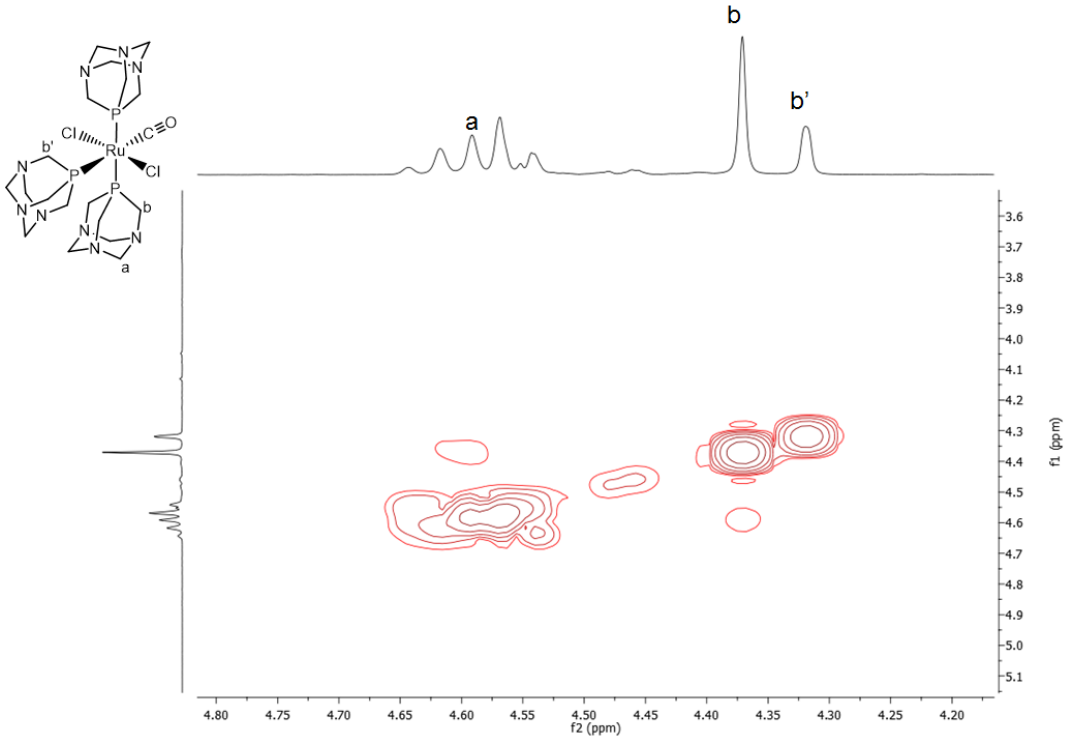

Figure A3.8. ^{1}H-^{1}H COSY NMR spectrum of *trans,mer*-[$RuCl_2(CO)(PTA)_3$] (**32**) in $CDCl_3$.

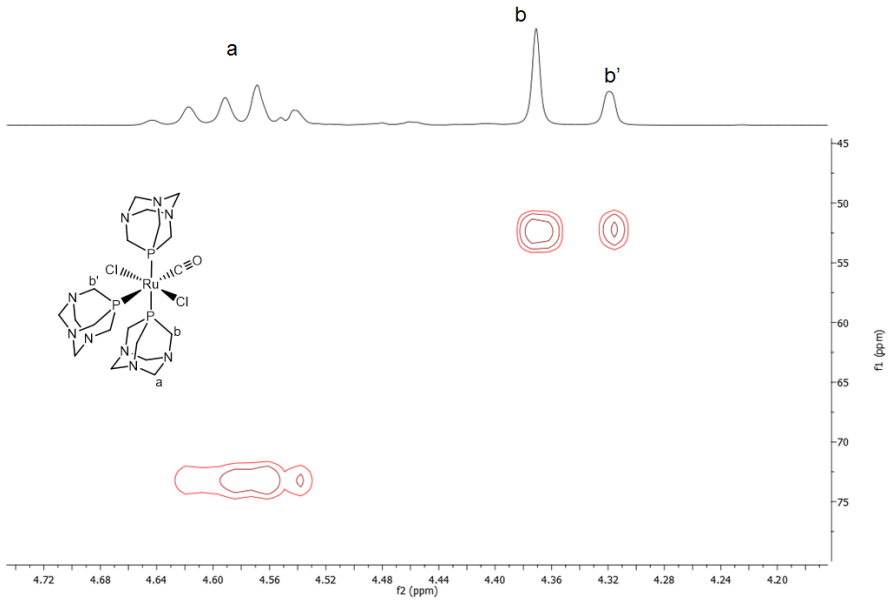

Figure A3.9. ^{1}H-^{13}C HSQC NMR spectrum of *trans,mer*-[$RuCl_2(CO)(PTA)_3$] (**32**) in $CDCl_3$.

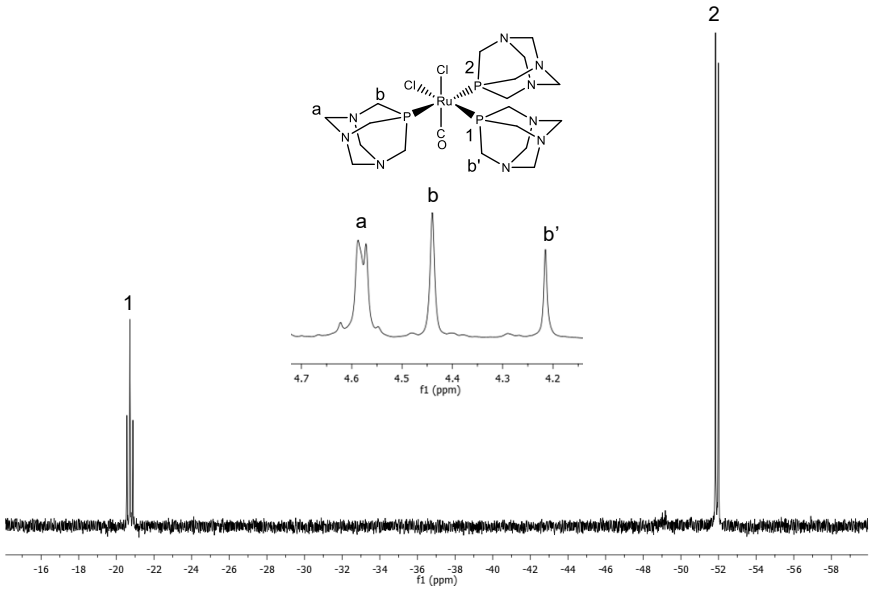

Figure A3.10. ^{1}H (insert) and ^{31}P NMR spectra of *cis*,*mer*-[$RuCl_2(CO)(PTA)_3$] (**33**) in D_2O + NaCl.

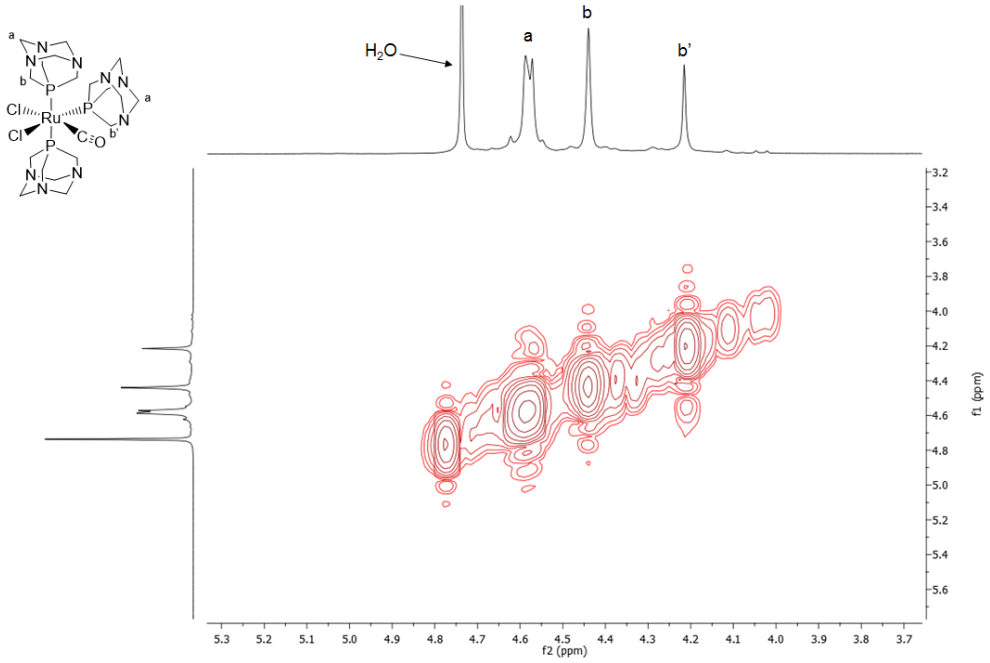

Figure A3.11. ^{1}H-^{1}H COSY NMR spectrum of *cis*,*mer*-[$RuCl_2(CO)(PTA)_3$] (**33**) in D_2O + NaCl.

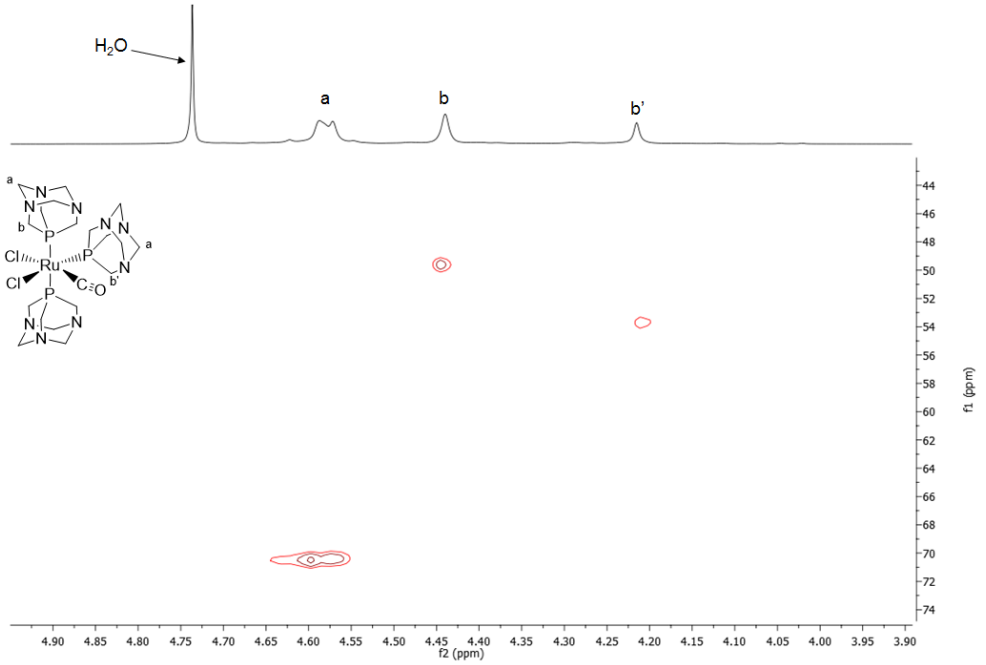

Figure A3.12. ^{1}H-^{13}C HSQC NMR spectrum of *cis*,*mer*-[$RuCl_2(CO)(PTA)_3$] (**33**) in D_2O + NaCl.

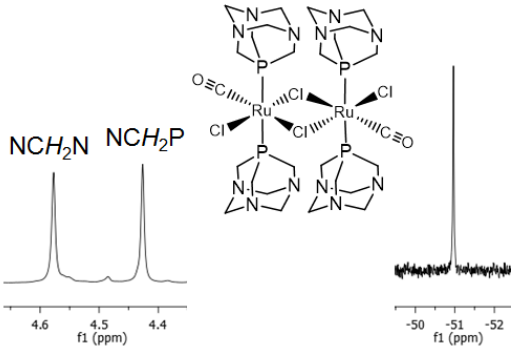

Figure 3.13. ^{1}H (left) and ^{31}P NMR (right) spectra of [$RuCl_2(CO)(PTA)_2]_2 \cdot 8H_2O$ (**35**) in D_2O.

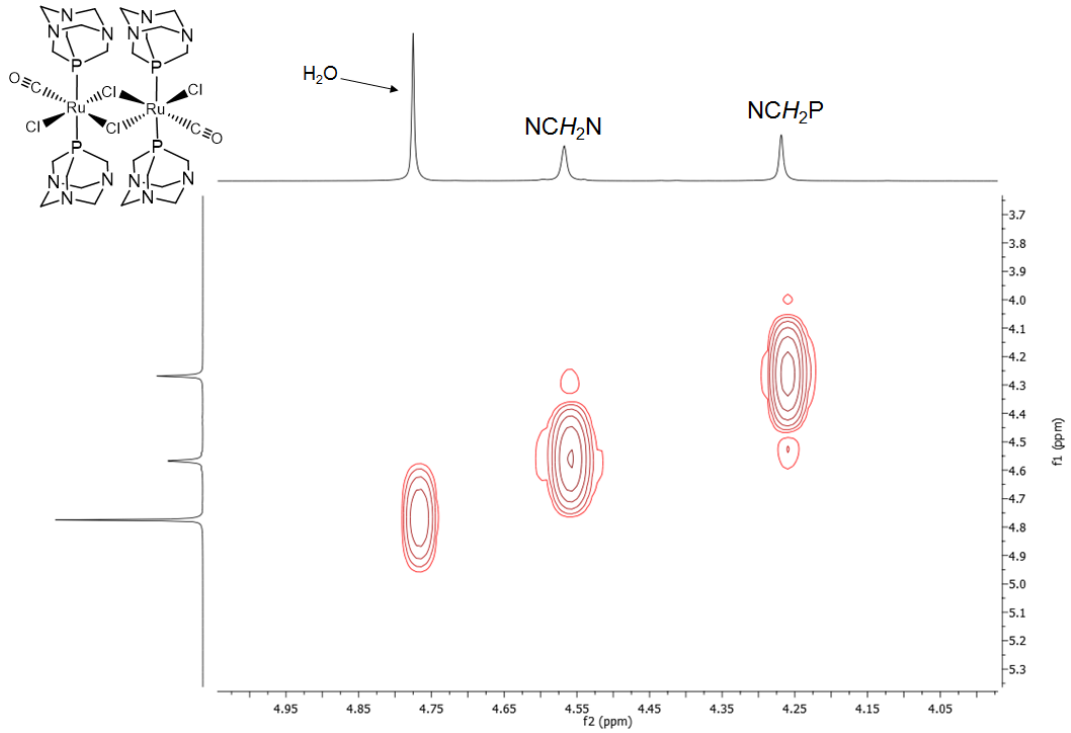

Figure 3.14. ^{1}H-^{1}H COSY NMR spectrum of $[RuCl_2(CO)(PTA)_2]_2 \cdot 8H_2O$ (**35**) in D_2O.

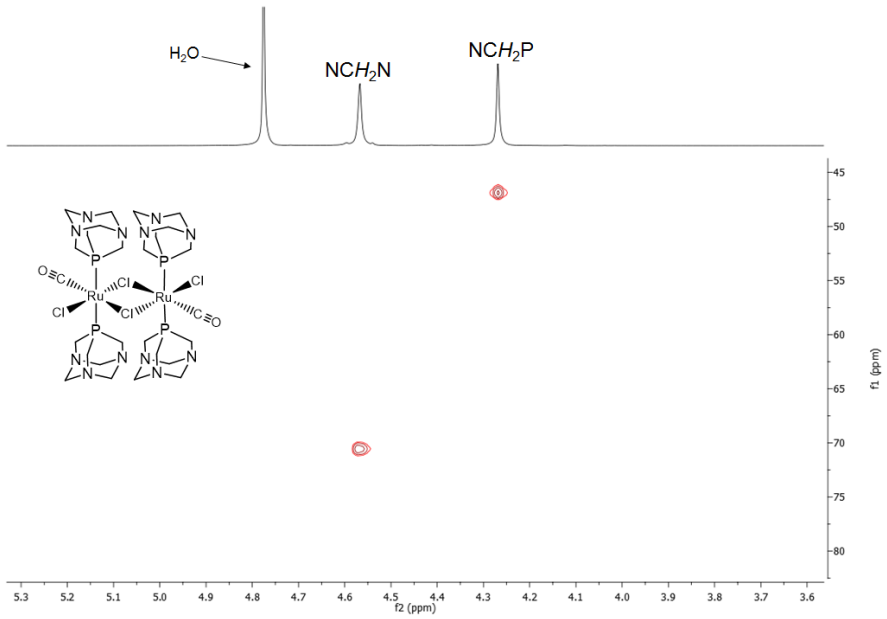

Figure 3.15. ^{1}H-^{13}C HSQC NMR spectrum of $[RuCl_2(CO)(PTA)_2]_2 \cdot 8H_2O$ (**35**) in D_2O.

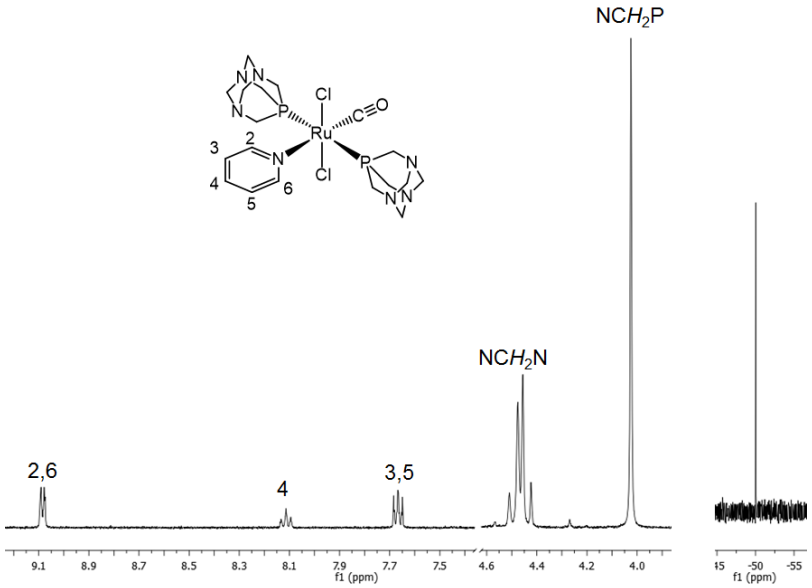

Figure A3.16. ^{1}H (left) and ^{31}P (right) NMR spectra of *trans,trans,trans*-$[RuCl_2(CO)(py)(PTA)_2]$ (**36**) in D_2O.

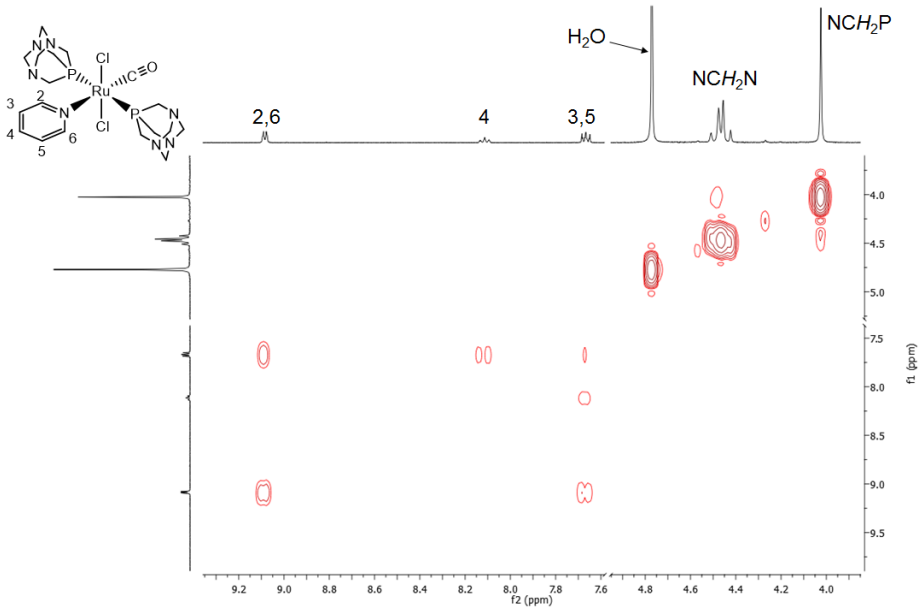

Figure 3.17. ^{1}H-^{1}H COSY NMR spectrum of *trans,trans,trans*-$RuCl_2(CO)(py)(PTA)_2$ (**36**) in D_2O.

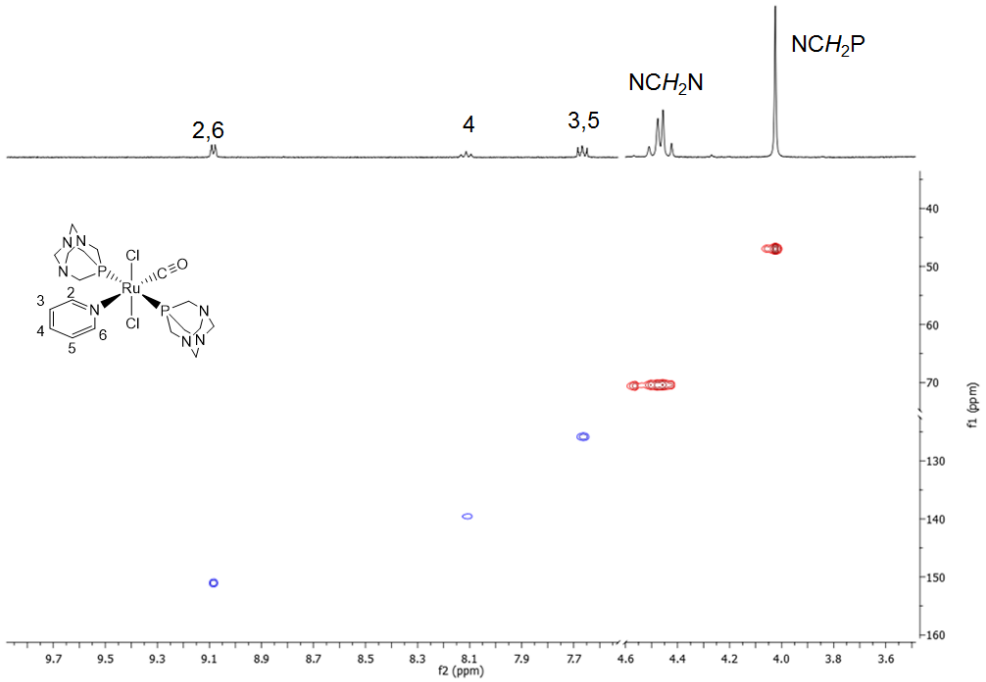

Figure 3.18. ^{1}H-^{13}C HSQC NMR spectrum of *trans,trans,trans*-$RuCl_2(CO)(py)(PTA)_2$ (**36**) in D_2O.

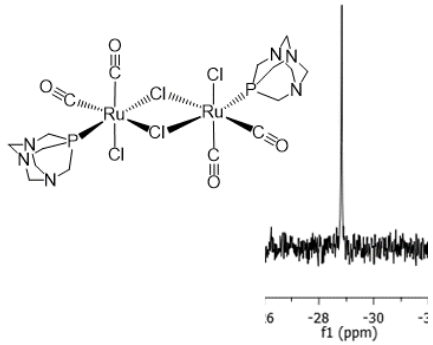

Figure A3.19. ^{31}P NMR spectra of the dimer $[RuCl_2(CO)_2(PTA)]_2 \cdot H_2O$ (**37**) in DMSO-d_6.

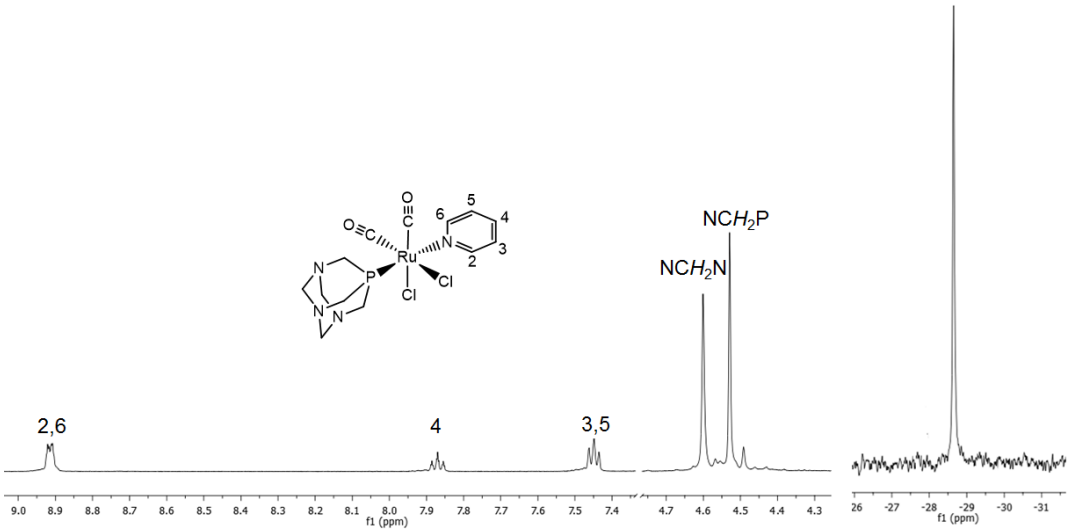

Figure A3.20. ^{1}H (left) and ^{31}P (right) NMR spectra of *cis,cis,trans*-$RuCl_2(CO)_2(py)(PTA)$ (**38**) in $CDCl_3$.

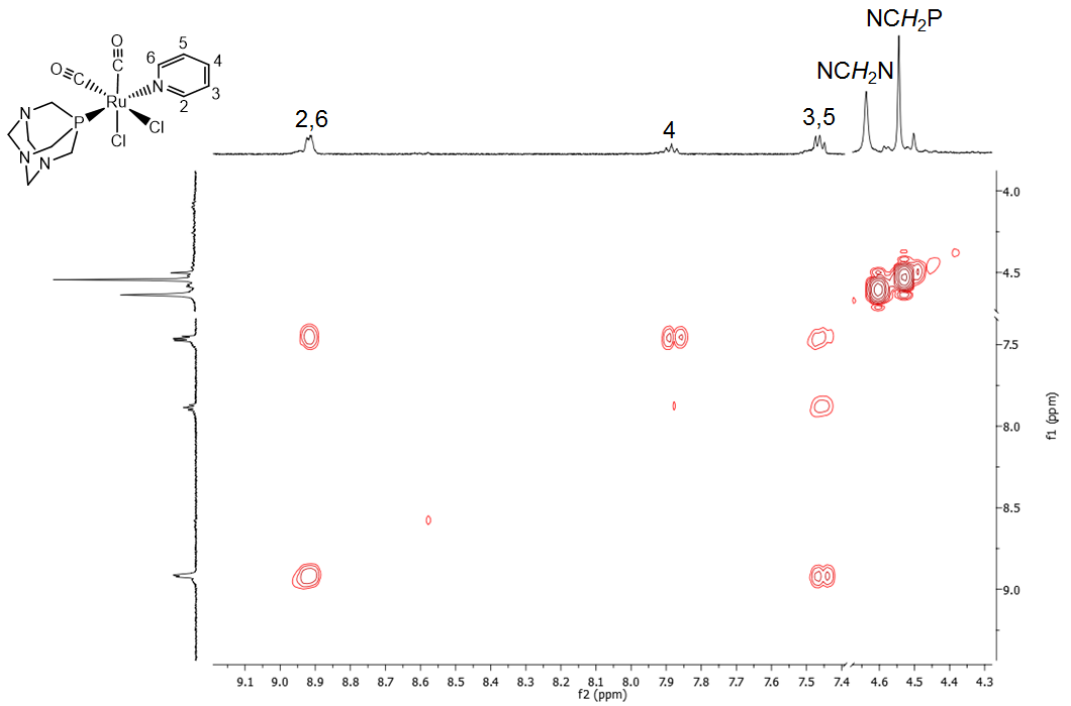

Figure A3.21. ^{1}H-^{1}H COSY NMR spectrum of *cis,cis,trans*-$RuCl_2(CO)_2(py)(PTA)$ (**38**) in $CDCl_3$.

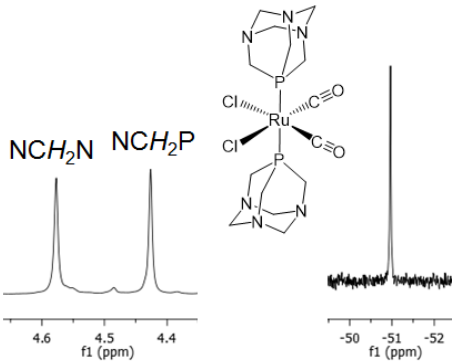

Figure A3.22 ^{1}H (left) and ^{31}P (right) NMR spectra of *cis,cis,trans*-$[RuCl_2(CO)_2(PTA)_2]$ (**39**) in $CDCl_3$.

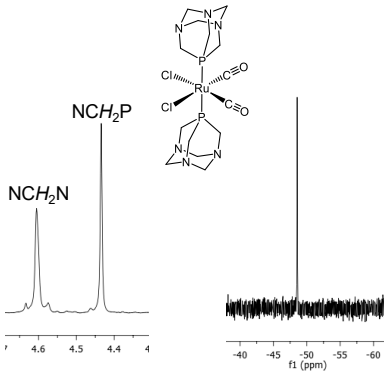

Figure A3.23. ^{1}H (left) and ^{31}P (right) NMR spectra of *cis,cis,trans*-$[RuCl_2(CO)_2(PTA)_2]$ (**39**) in D_2O.

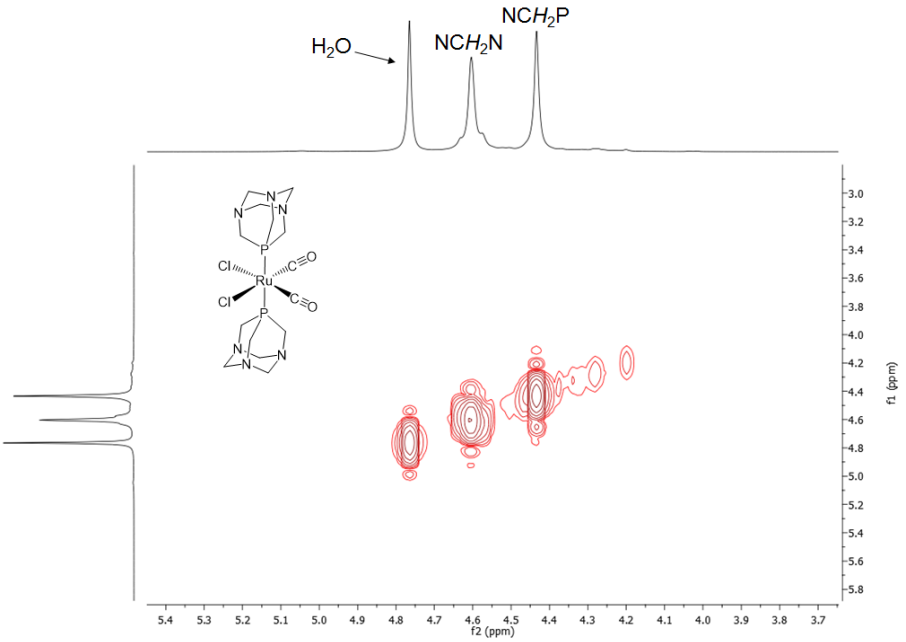

Figure A3.24. ^{1}H-^{1}H COSY NMR spectrum of *cis,cis,trans*-[$RuCl_2(CO)_2(PTA)_2$] (**39**) in D_2O.

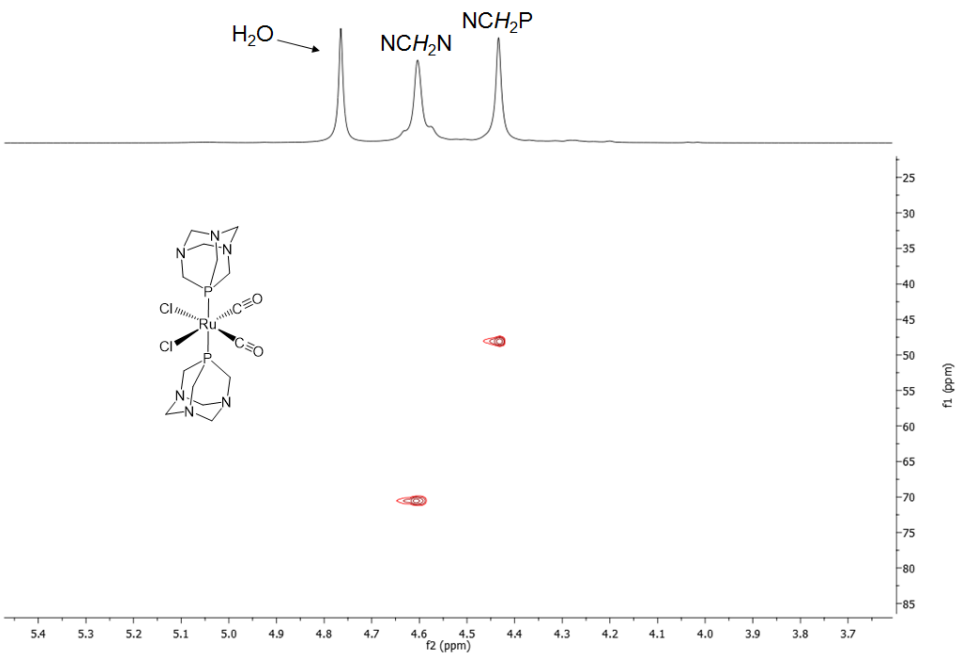

Figure A3.25. ^{1}H-^{1}C HSCQ NMR spectrum of *cis,cis,trans*-[$RuCl_2(CO)_2(PTA)_2$] (**39**) in D_2O.

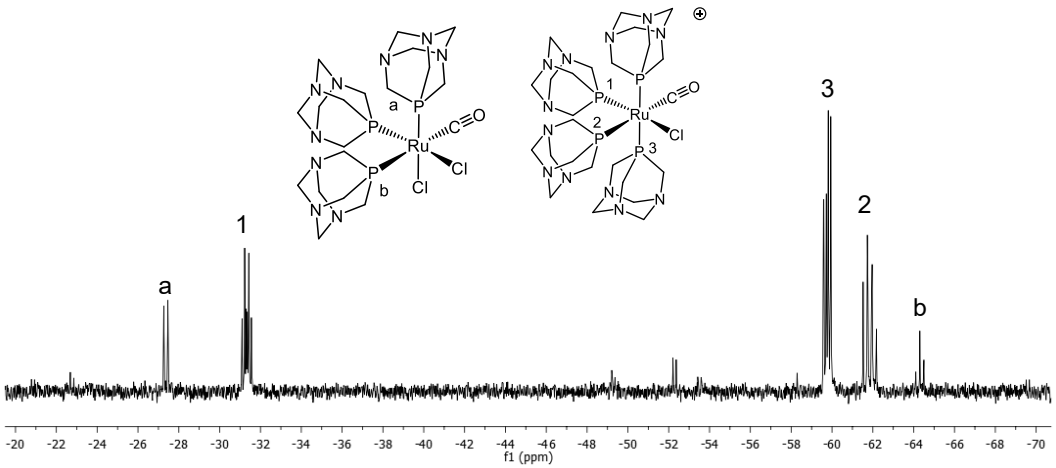

Figure A3.26. ^{31}P NMR spectrum of the mixture f*ac*-[$RuCl_2(CO)(PTA)_3$] (**34**) and *cis*-[$RuCl(CO)(PTA)_4$](Cl) (**42Cl**) in D_2O.

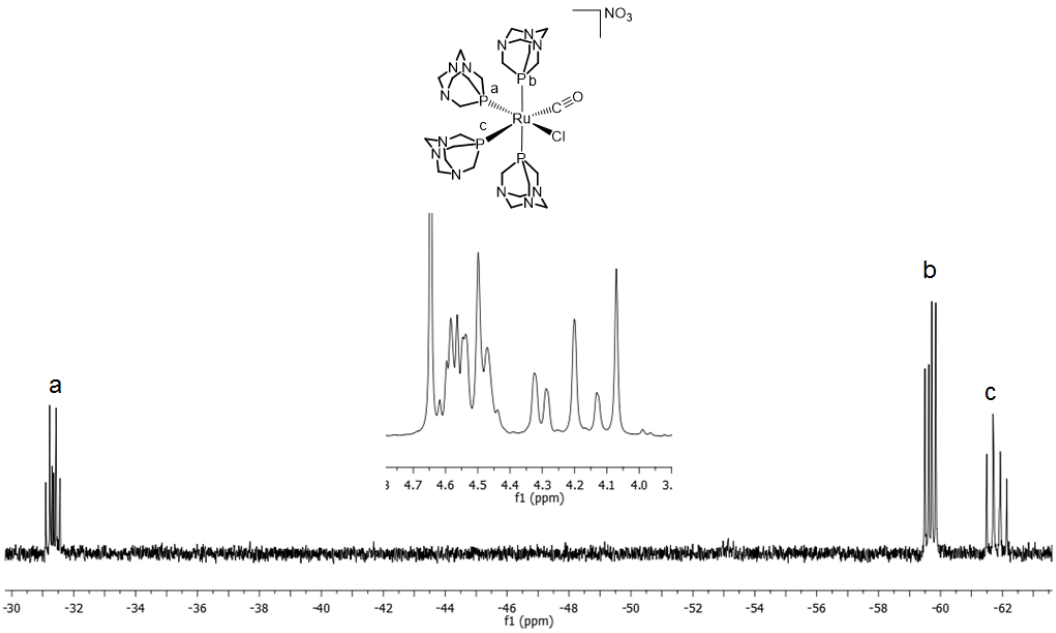

Figure A3.27. ^{1}H (insert) and ^{31}P NMR spectra of *cis*-[$RuCl(CO)(PTA)_4$]NO_3 (**42NO3**) in D_2O.

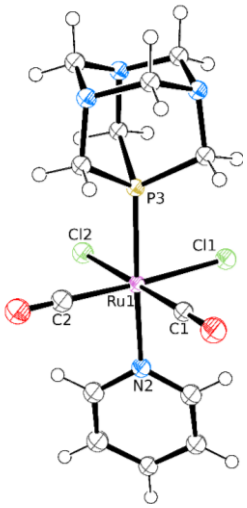

Figure A3.28. X-ray molecular structure (50% probability ellipsoids) of *cis,cis,trans*-$RuCl_2(CO)_2(py)(PTA)$ (**38**). The crystals spontaneously form in D_2O after one week.

Appendix of Chapter 4

Figures A4.1-A4.5. NMR characterization in D_2O of *cis,trans*-[Ru(bpy)Cl(CO)(PTA)$_2$]Cl (**43**).

Figures A4.6-A4.8. NMR characterization in DMSO-d_6 of *trans,cis*-Ru(bpy)Cl$_2$(CO)PTA (**44**).

Figures A4.9-A4.15. NMR characterization in D_2O of *mer*-[Ru(bpy)(CO)(PTA)$_3$]Cl$_2$ (**45**).

Figures A4.16-A4.18. NMR characterization in D_2O of *cis,trans*-[Ru(bpy)(CO)$_2$Cl(PTA)]Cl (**46**).

Figures A4.19-A4.21. NMR characterization in D_2O of *cis,trans*-[Ru(bpy)(CO)$_2$(PTA)$_2$](NO$_3$)$_2$ (**47**).

Figures A4.22-A4.26. ^{31}P NMR spectrum in DMSO-d_6 of *cis,cis*-[Ru(bpy)Cl(CO)(PTA)$_2$]Cl (**48**).

Figures A4.20-A4.21. NMR characterization in $CDCl_3$ of *cis,cis,trans*-RuCl$_2$(CO)$_2$(py)(PTA) (**38**).

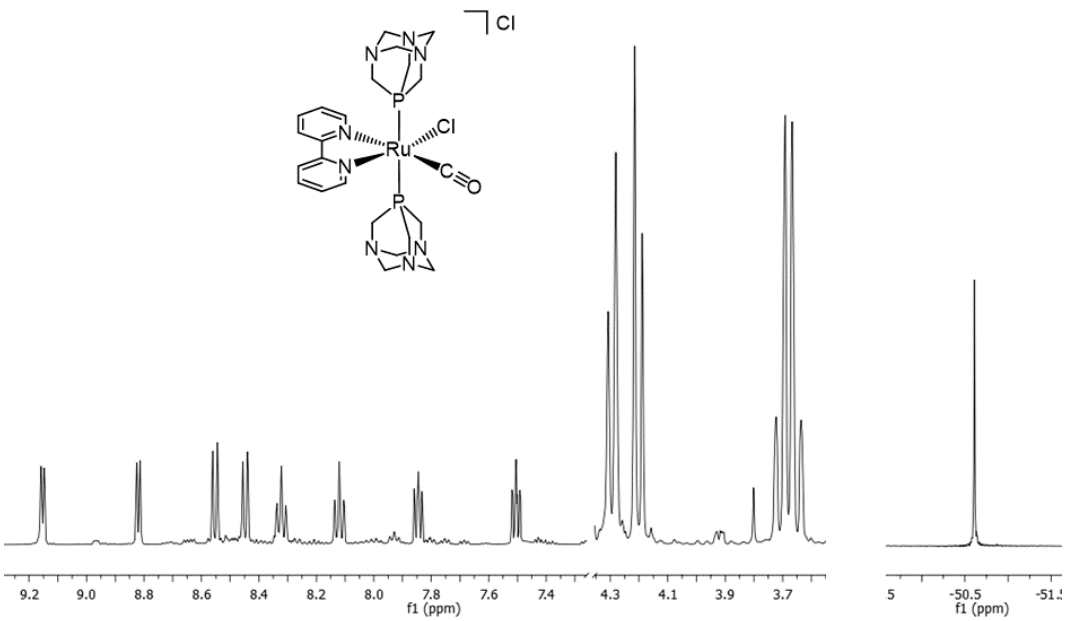

Figure A4.1. ^{1}H (left) and ^{31}P (right) NMR spectra of *cis,trans*-[Ru(bpy)Cl(CO)(PTA)$_2$]Cl (**43**) in D_2O.

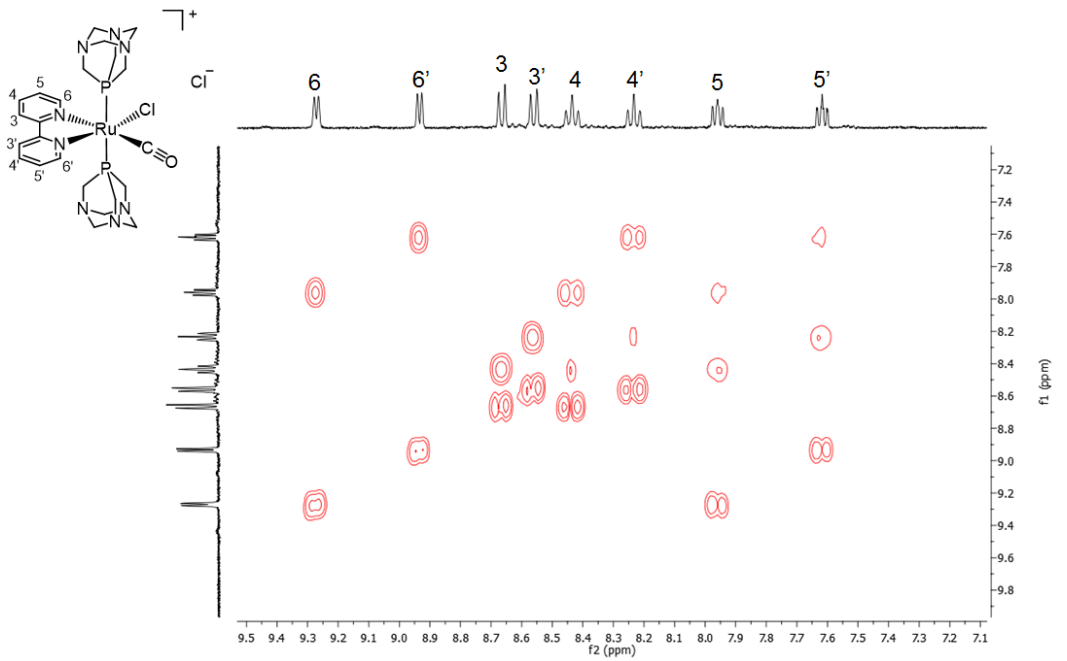

Figure A4.2. ^{1}H-^{1}H COSY NMR spectrum (bpy region) of *cis,trans*-[Ru(bpy)Cl(CO)(PTA)$_2$]Cl (**43**) in D_2O.

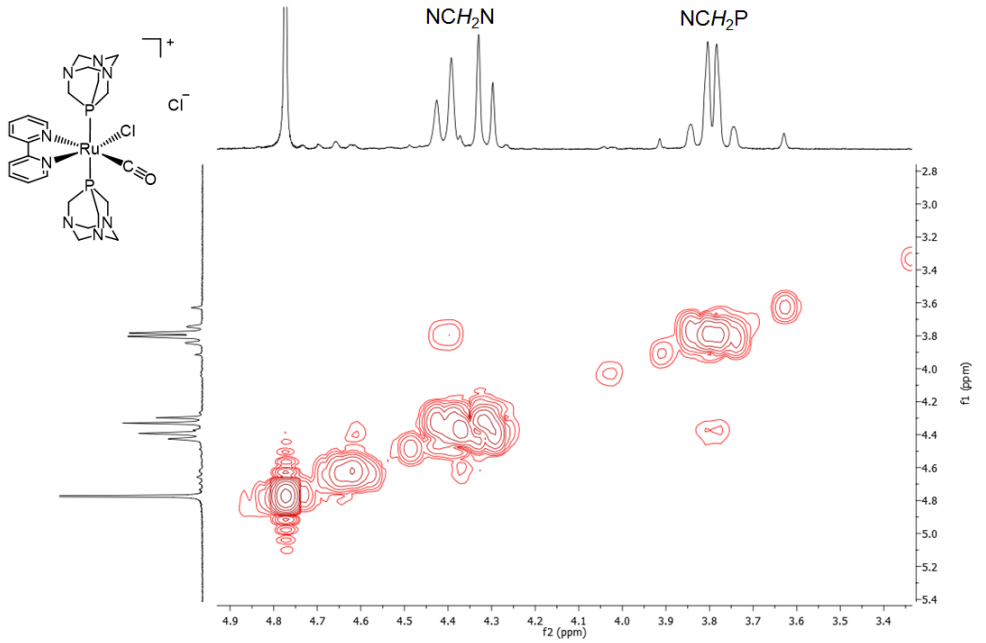

Figure A4.3. ^{1}H-^{1}H COSY NMR spectrum (PTA region) of *cis,trans*-[Ru(bpy)Cl(CO)(PTA)$_2$]Cl (**43**) in D_2O.

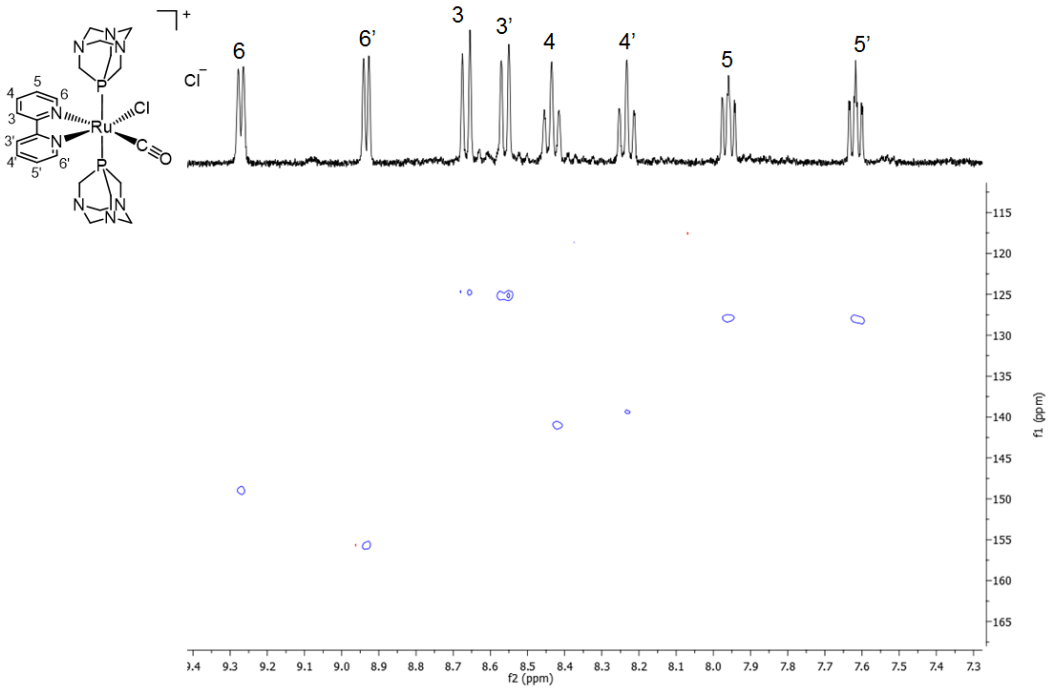

Figure A4.4. ^{1}H-^{13}C HSQC NMR spectrum (bpy region) of *cis,trans*-[Ru(bpy)Cl(CO)(PTA)$_2$]Cl (**43**) in D_2O.

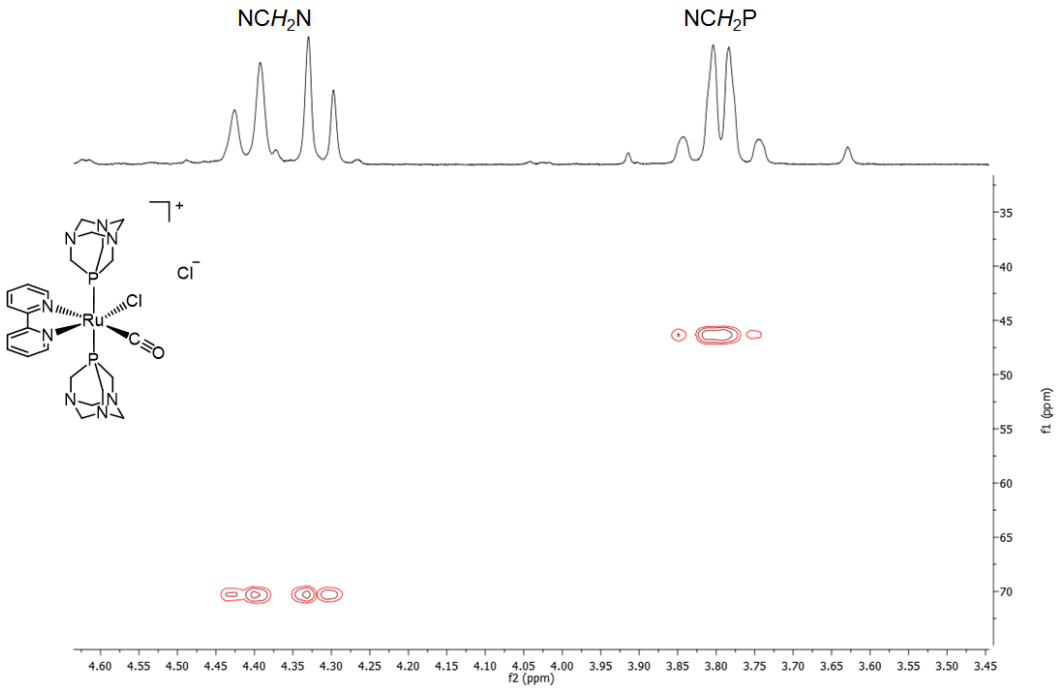

Figure A4.5. ^{1}H-^{13}C HSQC NMR spectrum (PTA region) of *cis,trans*-[Ru(bpy)Cl(CO)(PTA)$_2$]Cl (**43**) in D_2O.

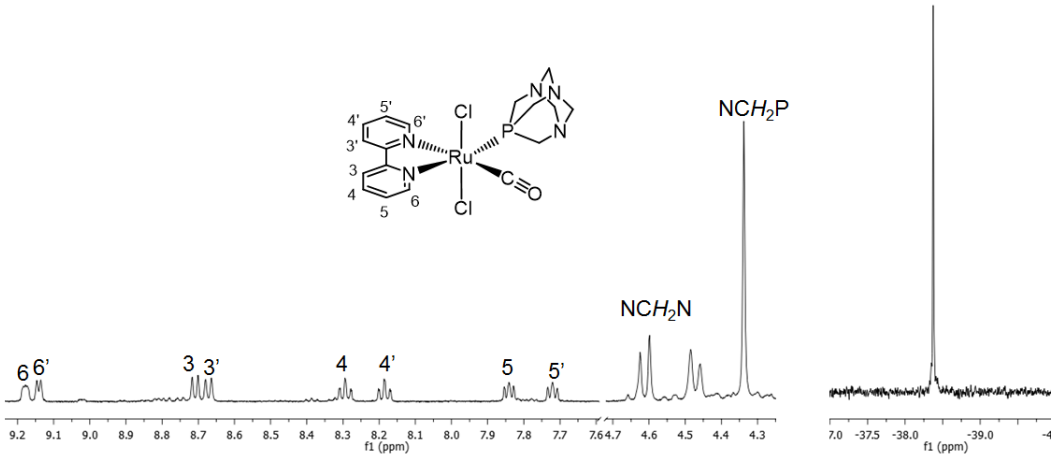

Figure A4.6. ^{1}H (left) and ^{31}P (right) NMR spectra of *trans,cis*-Ru(bpy)Cl$_2$(CO)PTA (**44**) in DMSO-d_6.

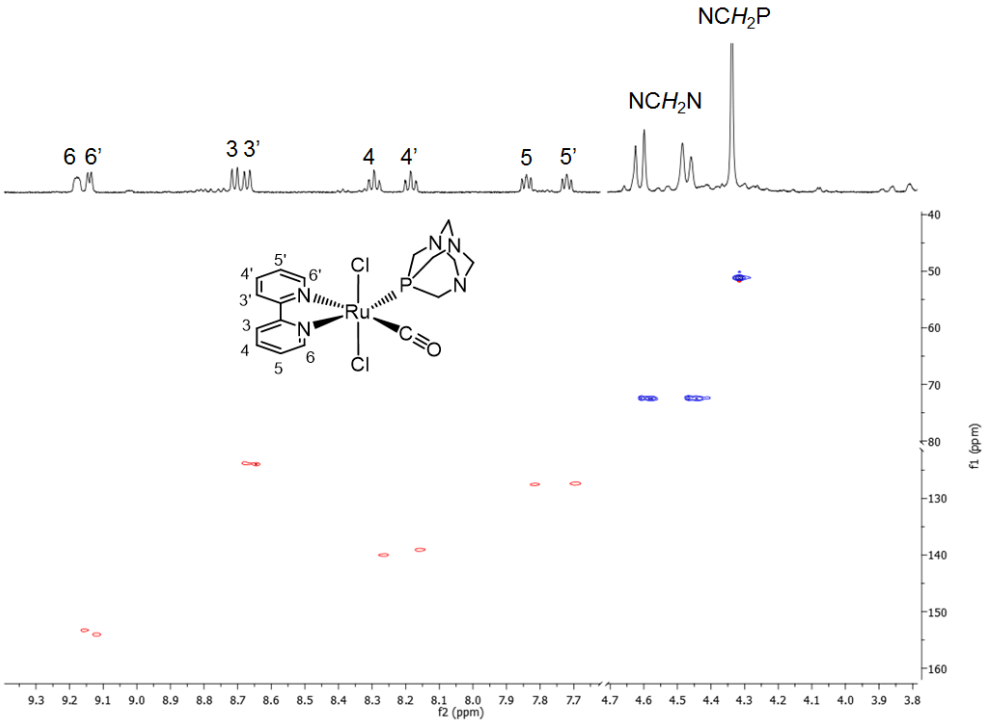

Figure A4.8. ^{1}H-^{13}C HSQC NMR spectrum of *trans,cis*-Ru(bpy)Cl$_2$(CO)PTA (**44**) in DMSO-*d*$_6$.

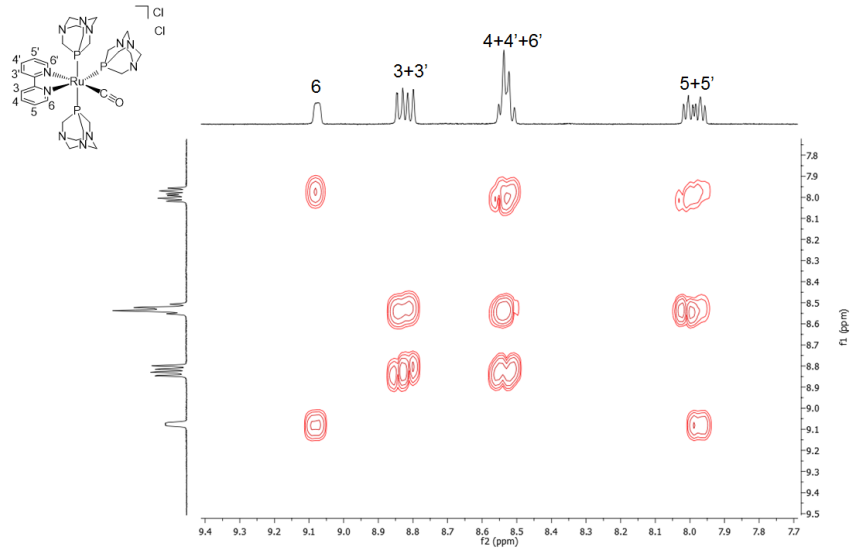

Figure A4.9 ^{1}H-^{1}H COSY NMR spectrum (bpy region) of *mer*-[Ru(bpy)(CO)(PTA)$_3$]Cl$_2$ (**45**) in D$_2$O.

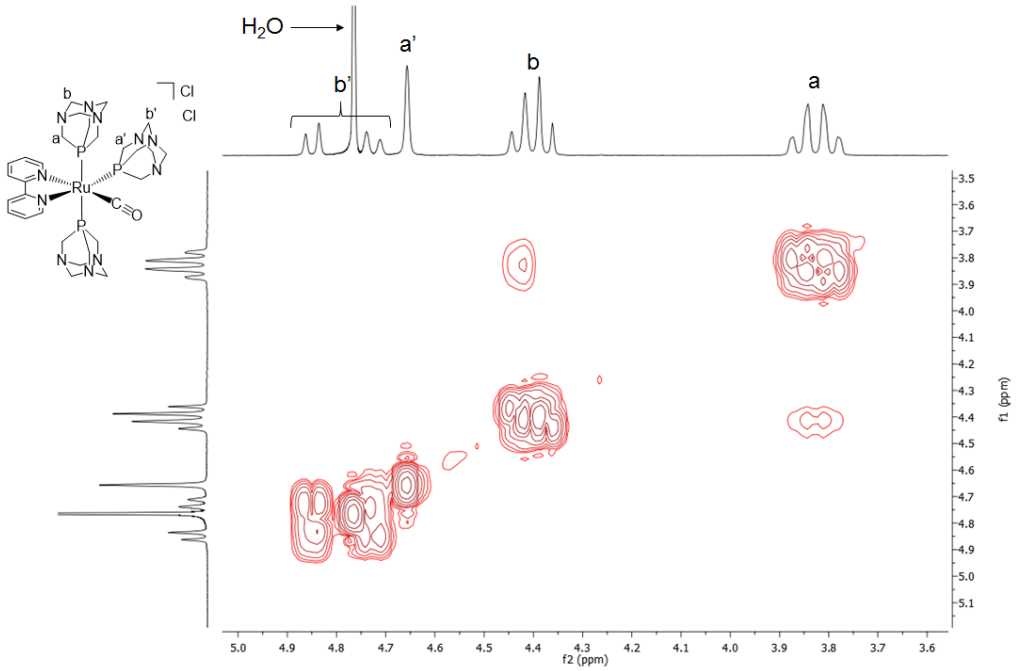

Figure A4.10 ^{1}H-^{1}H COSY NMR spectrum (PTA region) of *mer*-[Ru(bpy)(CO)(PTA)$_3$]Cl$_2$ (**45**) in D$_2$O.

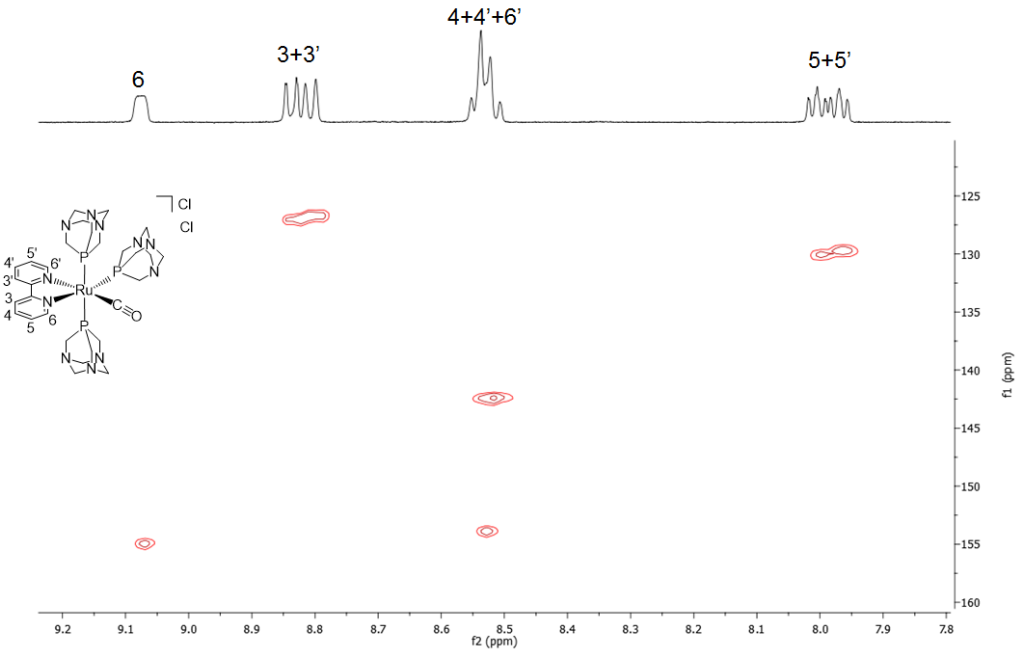

Figure A4.11 ^{1}H-^{13}C HSQC NMR spectrum (bpy region) of *mer*-[Ru(bpy)(CO)(PTA)$_3$]Cl$_2$ (**45**) in D$_2$O.

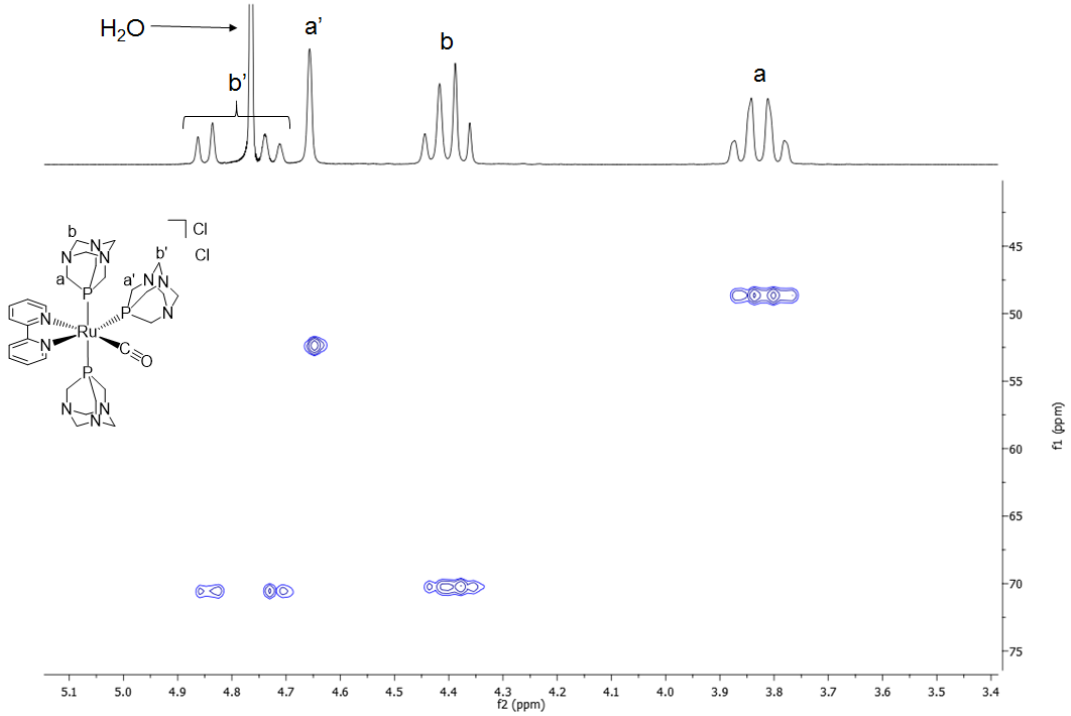

Figure A4.12 ^{1}H-^{13}C HSQC NMR spectrum (PTA region) of *mer*-[Ru(bpy)(CO)(PTA)$_3$]Cl$_2$ (**45**) in D_2O.

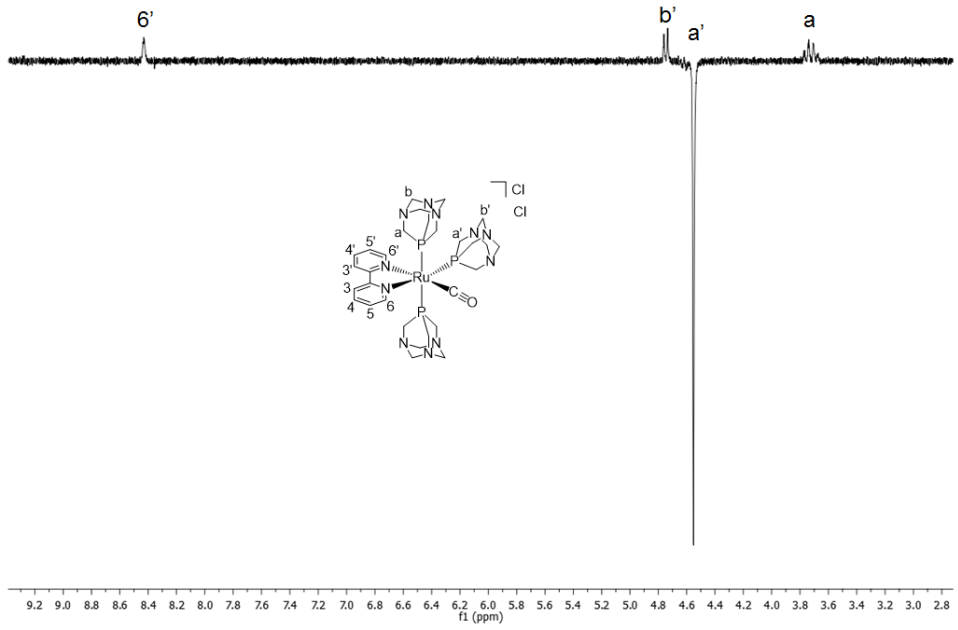

Figure A4.13 1D NOESY NMR spectrum of *mer*-[Ru(bpy)(CO)(PTA)$_3$]Cl$_2$ (**45**) in D_2O.

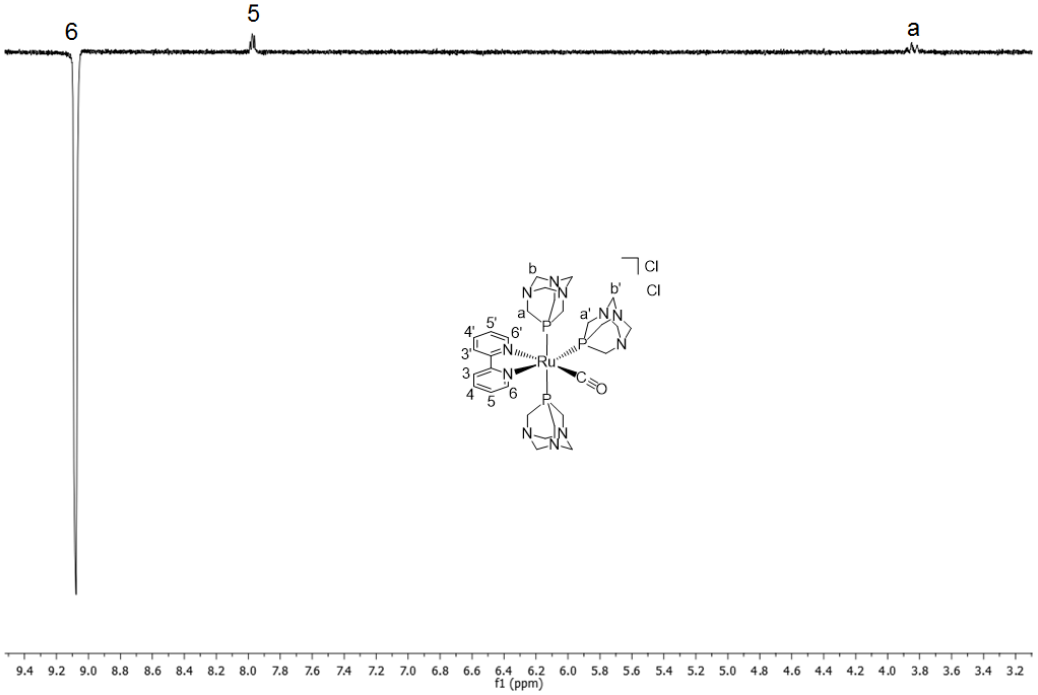

Figure A4.14 1D NOESY NMR spectrum of *mer*-[Ru(bpy)(CO)(PTA)$_3$]Cl$_2$ (**45**) in D_2O.

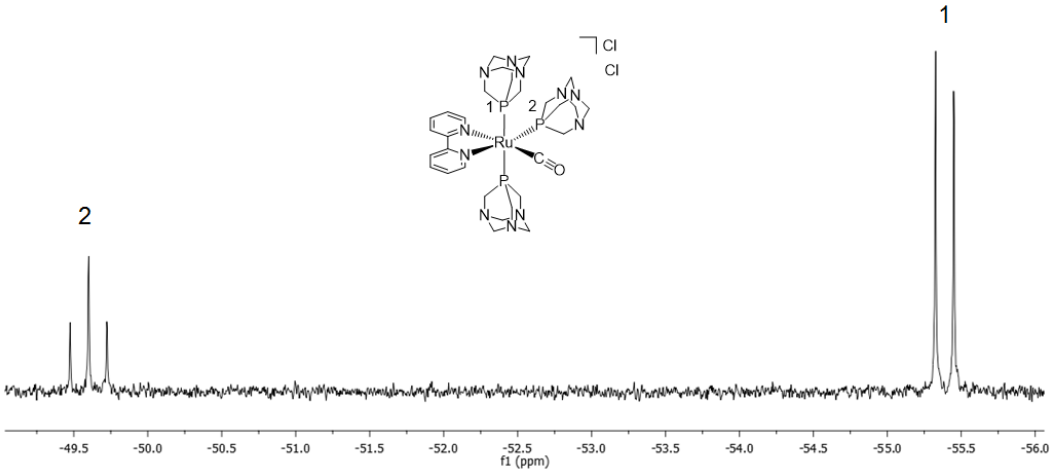

Figure A4.15 ^{31}P NMR spectrum of *mer*-[Ru(bpy)(CO)(PTA)$_3$]Cl$_2$ (**45**) in D_2O.

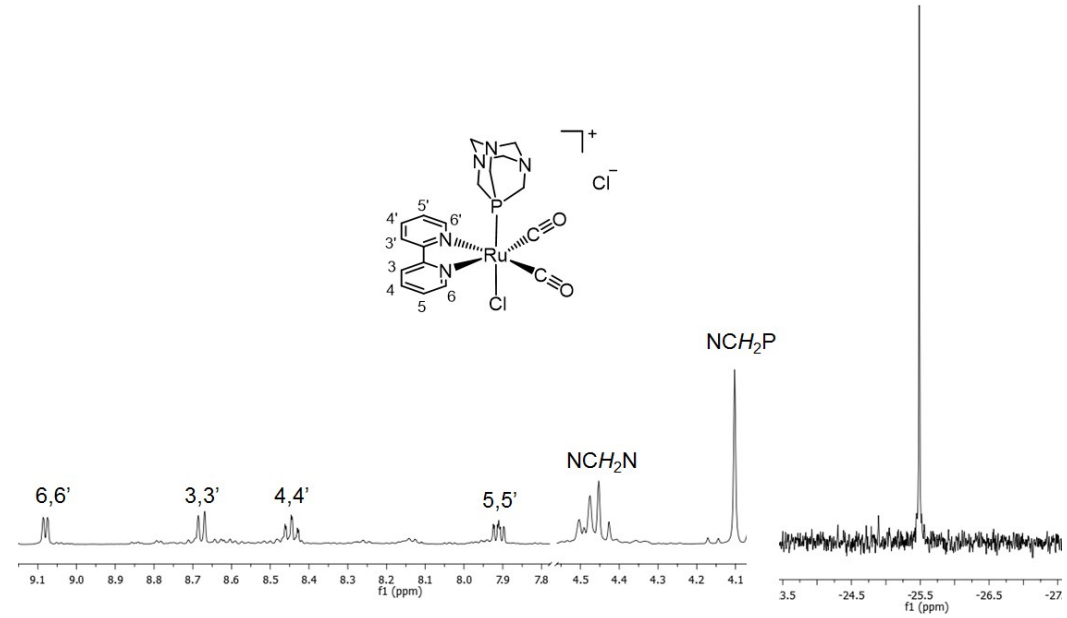

Figure 4.16. ^{1}H (left) and ^{31}P (right) NMR spectra of *cis,trans*-[Ru(bpy)(CO)$_2$Cl(PTA)]Cl (**46**) in D_2O.

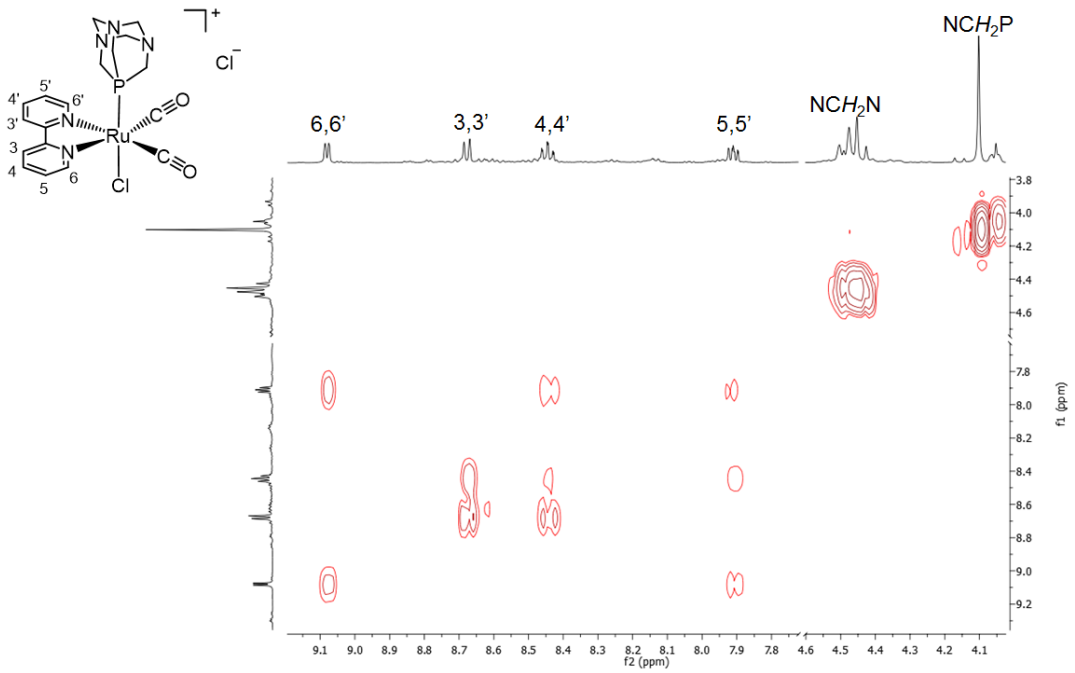

Figure A4.17. ^{1}H-^{1}H COSY NMR spectrum of *cis,trans*-[Ru(bpy)(CO)$_2$Cl(PTA)]Cl (**46**) in D_2O.

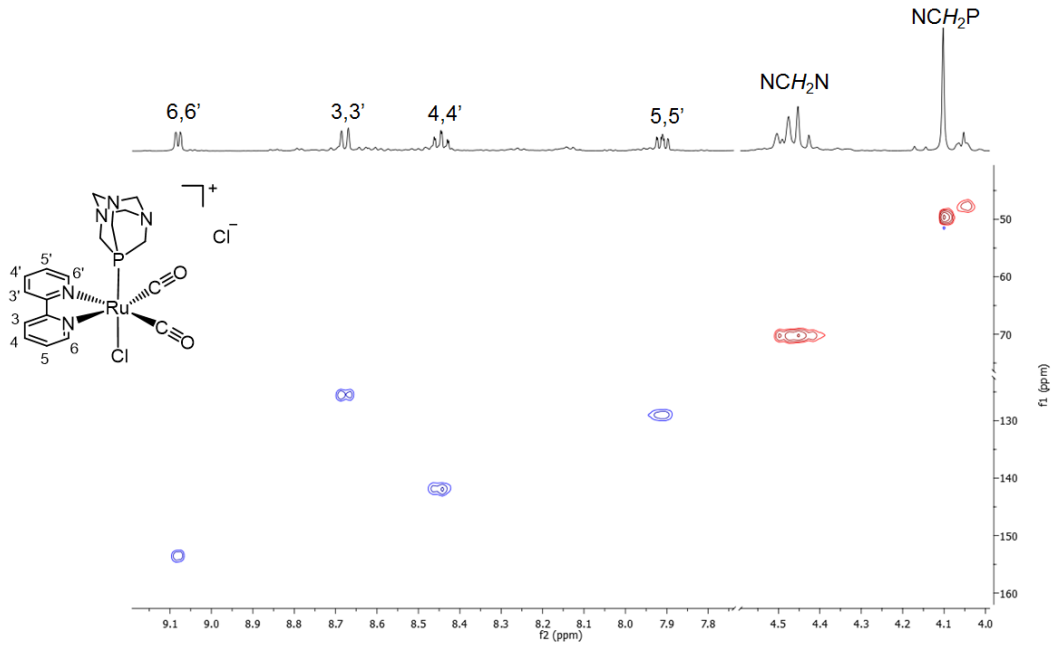

Figure A4.18. ^{1}H-^{13}C HSQC NMR spectrum of *cis,trans*-[Ru(bpy)(CO)$_2$Cl(PTA)]Cl (**46**) in D_2O.

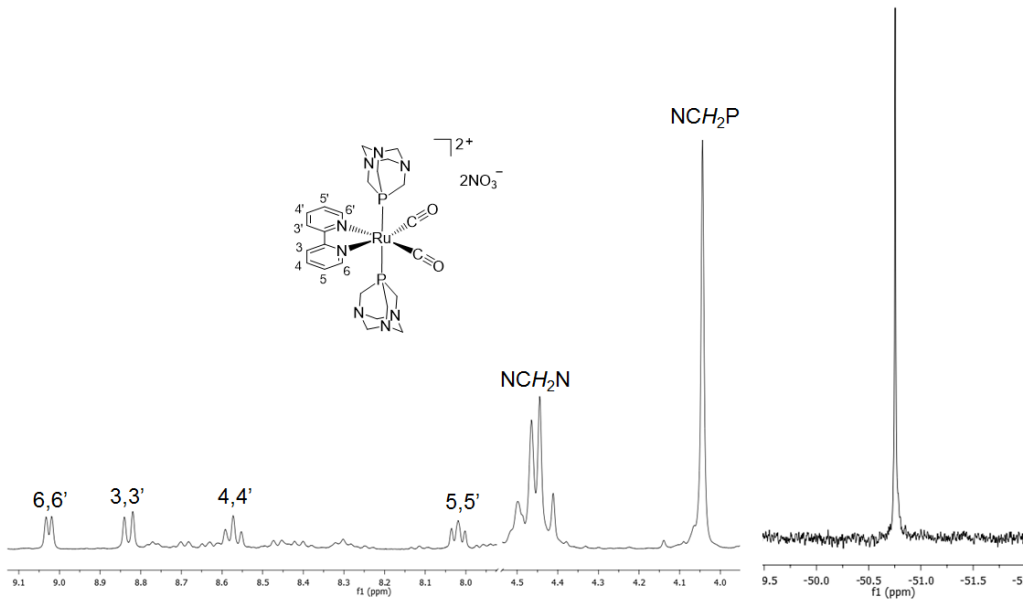

Figure 4.19. ^{1}H (left) and ^{31}P (right) NMR spectra of *cis,trans*-[Ru(bpy)(CO)$_2$(PTA)$_2$](NO$_3$)$_2$ (**47**) in D_2O.

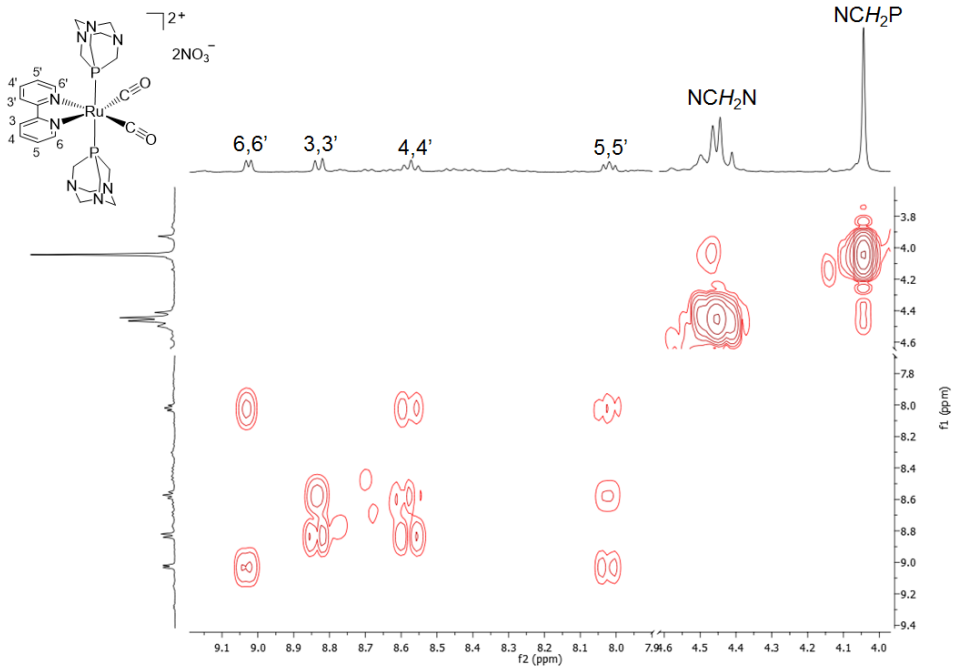

Figure A4.20. ^{1}H-^{1}H HSQC NMR spectrum of *cis,trans*-[Ru(bpy)(CO)$_2$(PTA)$_2$](NO$_3$)$_2$ (**47**) in D$_2$O.

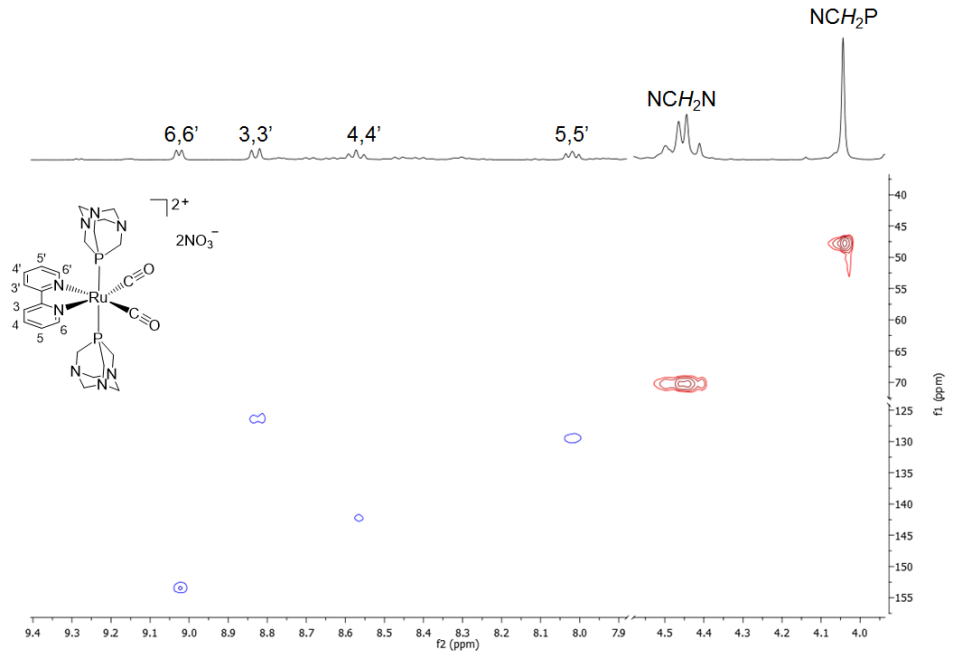

Figure A4.21. ^{1}H-^{13}C HSQC NMR spectrum of *cis,trans*-[Ru(bpy)(CO)$_2$(PTA)$_2$](NO$_3$)$_2$ (**47**) in D$_2$O.

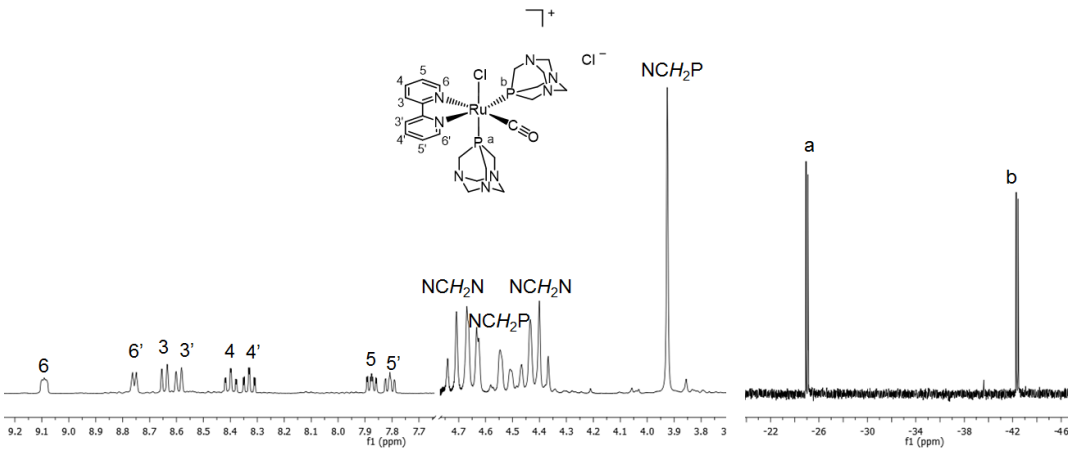

Figure A4.22. ^{1}H (left) and ^{31}P (right) NMR spectra of *cis,cis*-[Ru(bpy)Cl(CO)(PTA)$_2$]Cl (**48**) in D_2O.

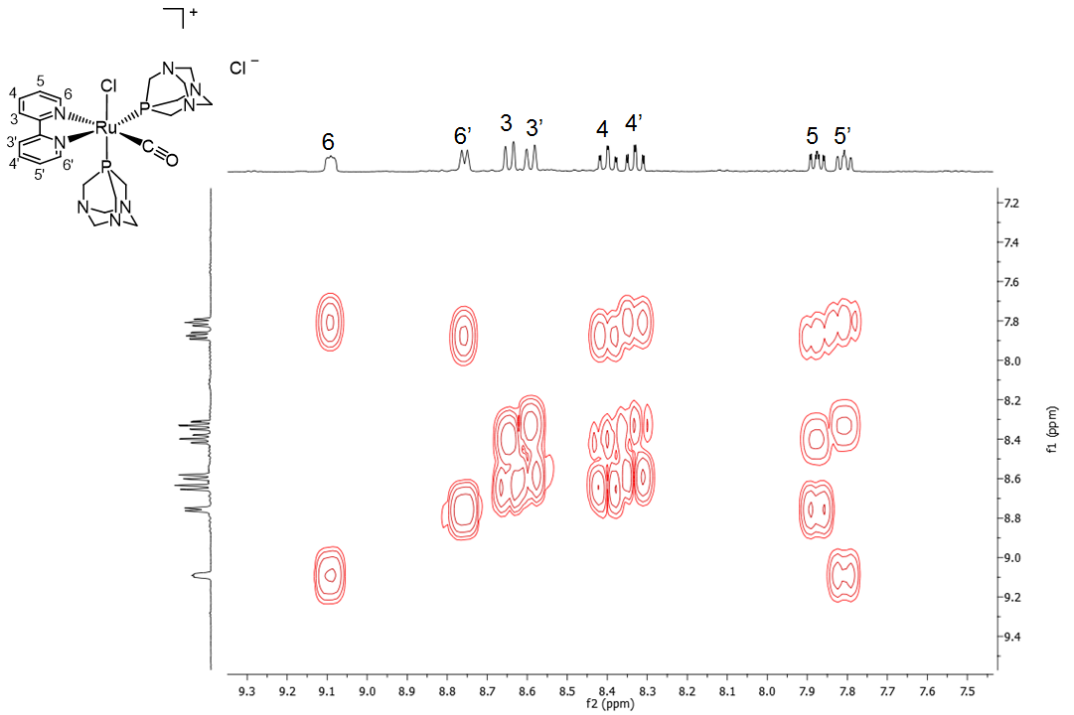

Figure A4.23. ^{1}H-^{1}H COSY NMR spectrum (bpy region) of *cis,cis*-[Ru(bpy)Cl(CO)(PTA)$_2$]Cl (**48**) in D_2O.

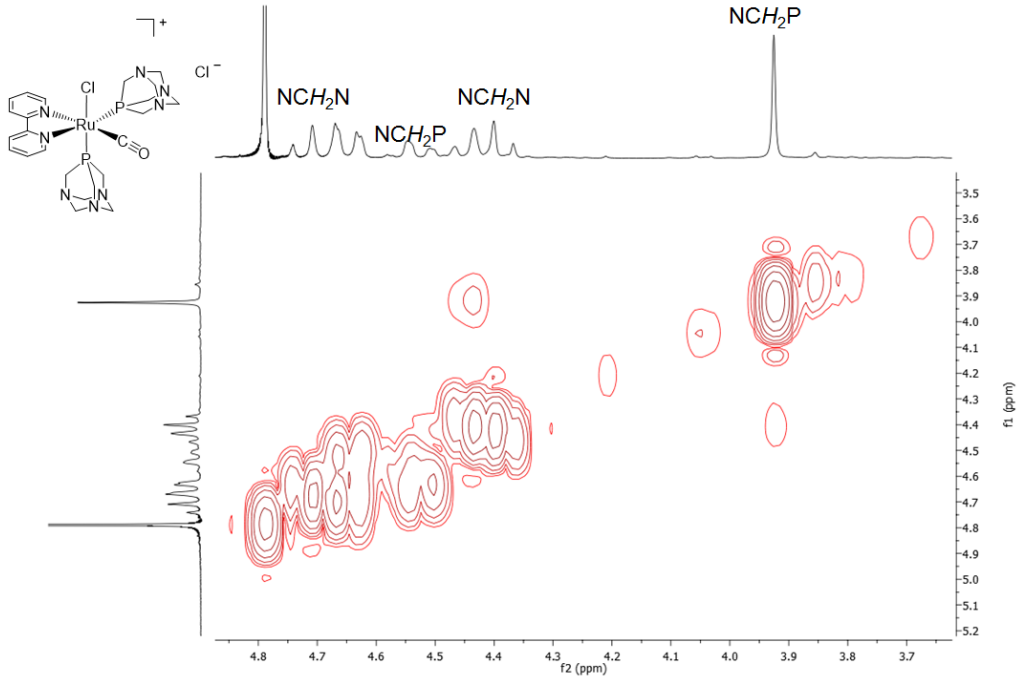

Figure A4.24. ^{1}H-^{1}H COSY NMR spectrum (PTA region) of *cis,cis*-[Ru(bpy)Cl(CO)(PTA)$_2$]Cl (**48**) in D_2O.

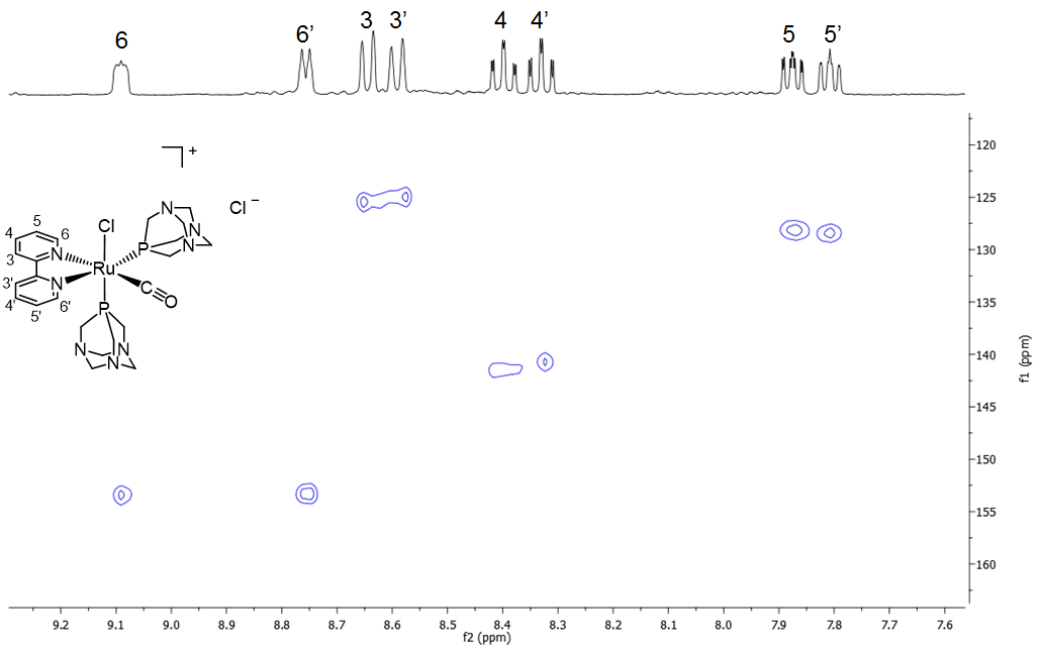

Figure A4.25. ^{1}H-^{13}C HSQC NMR spectrum (bpy region) of *cis,cis*-[Ru(bpy)Cl(CO)(PTA)$_2$]Cl (**48**) in D_2O.

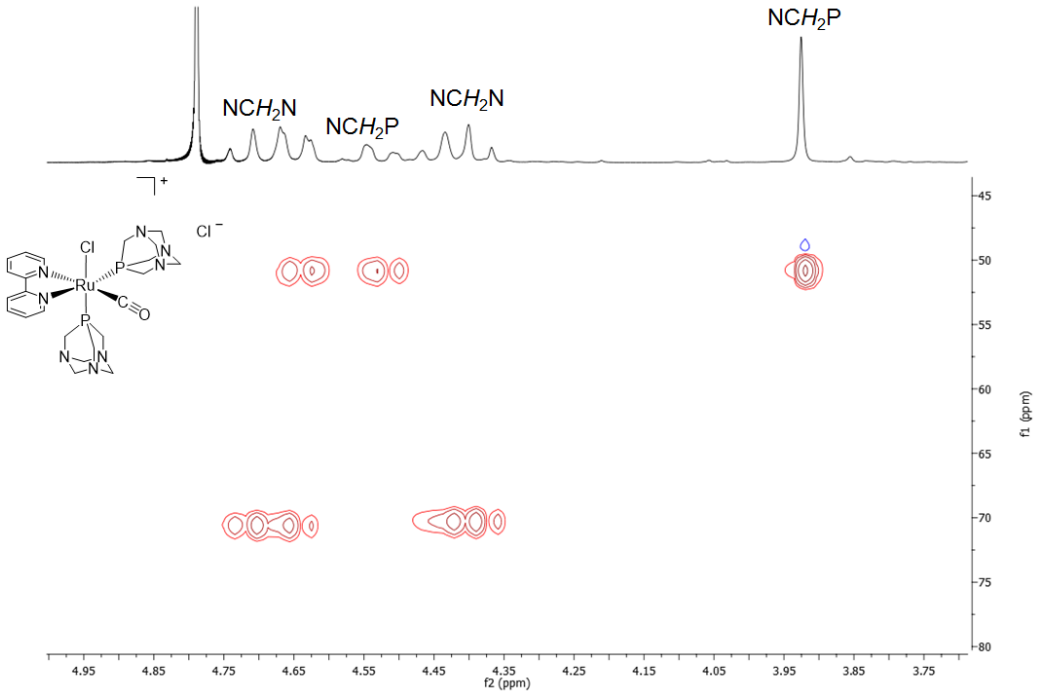

Figure A4.26. ^{1}H-^{13}C HSQC NMR spectrum (PTA region) of *cis,cis*-[Ru(bpy)Cl(CO)(PTA)$_2$]Cl (**48**) in D_2O.

Appendix of Chapter 5

Figures A5.1-A5.2. UV-vis spectra of 1.5 mM solutions of *trans*-$RuCl_2(PTA)_4$ (**1**), *cis*-$RuCl_2(PTA)_4$ (**2**), *trans*-$RuBr_2(PTA)_4$ (**8**) and *cis*-$RuBr_2(PTA)_4$ (**9**) in $CHCl_3$.

Figures A5.3-5.7. UV-vis spectra of *trans*-$RuCl_2(PTA)_4$ (**1**), *cis*-$RuCl_2(PTA)_4$ (**2**), *trans*-$RuBr_2(PTA)_4$ (**8**), *cis*-$RuBr_2(PTA)_4$ (**9**) and *trans*-$[RuCl_4(PTAH)_2]Cl$ (**3**) in H_2O.

Figure A5.8. LTQ Orbitrap ESI mass spectra of of *trans*-$RuCl_2(PTA)_4$ (**1**), *cis*-$RuCl_2(PTA)_4$ (**2**), *trans*-$RuBr_2(PTA)_4$ (**8**), *cis*-$RuBr_2(PTA)_4$ (**9**) and *trans*-$[RuCl_4(PTAH)_2]Cl$ (**3**) dissolved in 20 mM ammonium acetate buffer, pH 7.4, in the presence of RNase A.

Figure A5.9. LTQ Orbitrap ESI mass spectrum of *trans*-$[RuCl_4(PTAH)_2]Cl$ (**3** dissolved in milliQ water, in the presence of ODN4.

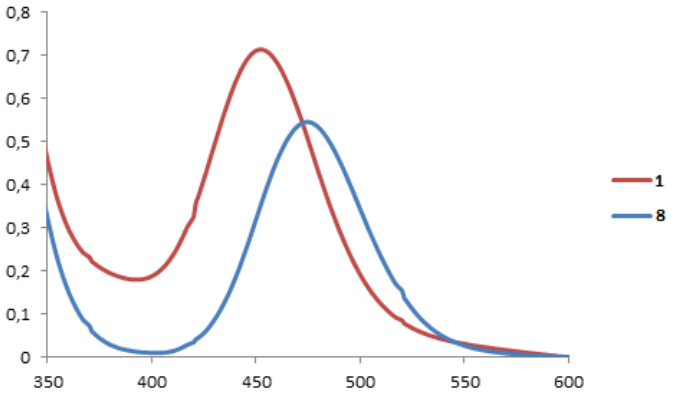

Figure A5.1. UV-vis spectra of 1.5 mM solutions of *trans*-[$RuCl_2(PTA)_4$] (**1**) and *trans*-[$RuBr_2(PTA)_4$] (**8**) in $CHCl_3$.

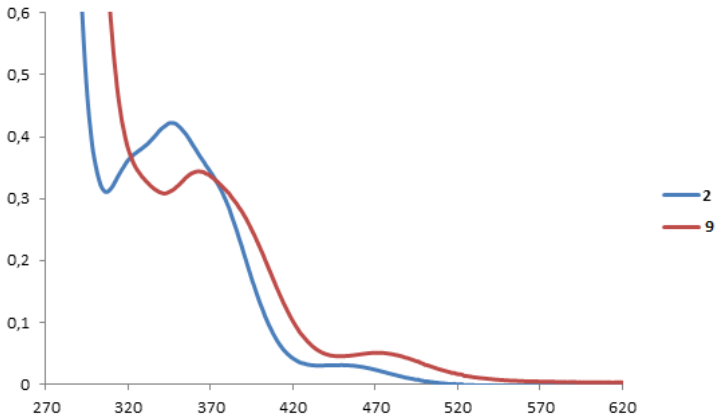

Figure A5.2. UV-vis spectra of saturated solutions of *cis*-[$RuCl_2(PTA)_4$] (**2**, blue line) and *cis*-[$RuBr_2(PTA)_4$] (**9**, red line) in $CHCl_3$.

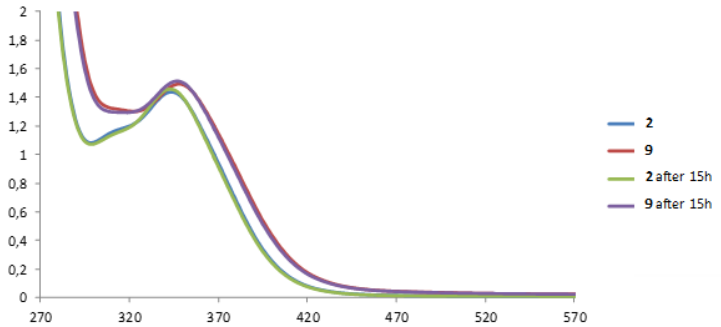

Figure A5.3. UV-vis spectra of *cis*-[$RuCl_2(PTA)_4$] (**2**) 1.0 mM solution in H_2O and of *cis*-[$RuBr_2(PTA)_4$] (**9**) 1.1 mM solution in H_2O, immediately after dissolution (**2** blue, **9** red) and after 15 hours at room temperature (**2** green, **9** purple).

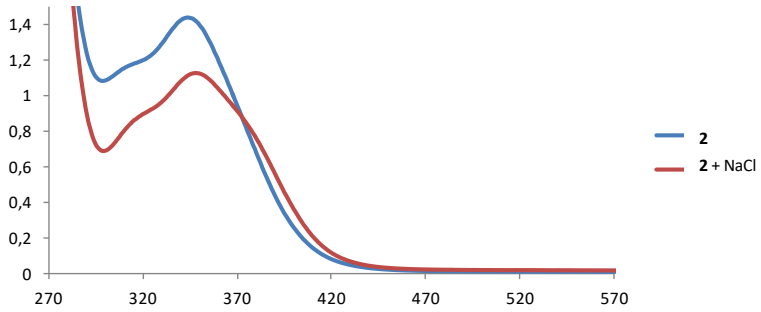

Figure A5.4. UV-vis spectra of a 1.0 mM solution of *cis*-[$RuCl_2(PTA)_4$] (**2**) in H_2O immediately after dissolution (blue line) and after addition of an excess of NaCl (red).

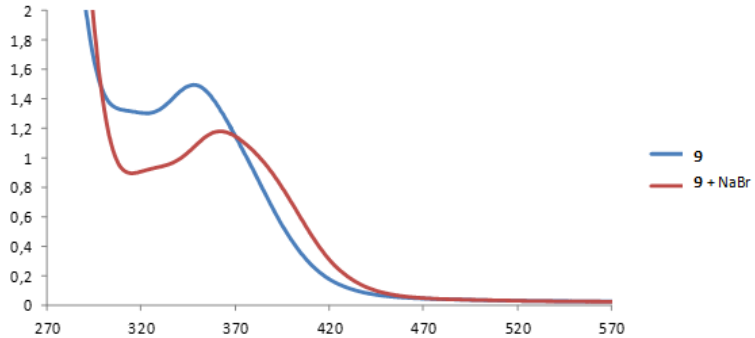

Figure A5.5. UV-vis spectra of a 1.1 mM solution of *cis*-[$RuBr_2(PTA)_4$] (**9**) in H_2O immediately after dissolution (blue line) and after addition of an excess of NaBr (red).

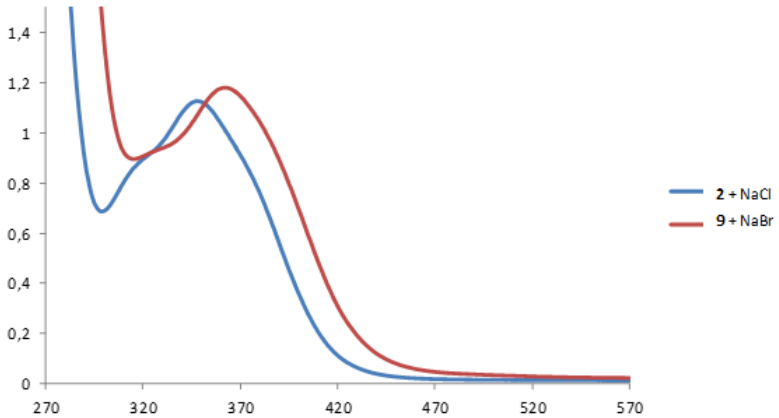

Figure A5.6. UV-vis spectra of ca. equimolar aqueous solutions of *cis*-[$RuCl_2(PTA)_4$] (**2**) after addition of an excess of NaCl (blue) and of *cis*-[$RuBr_2(PTA)_4$] (**9**) after addition of an excess of NaBr (red).

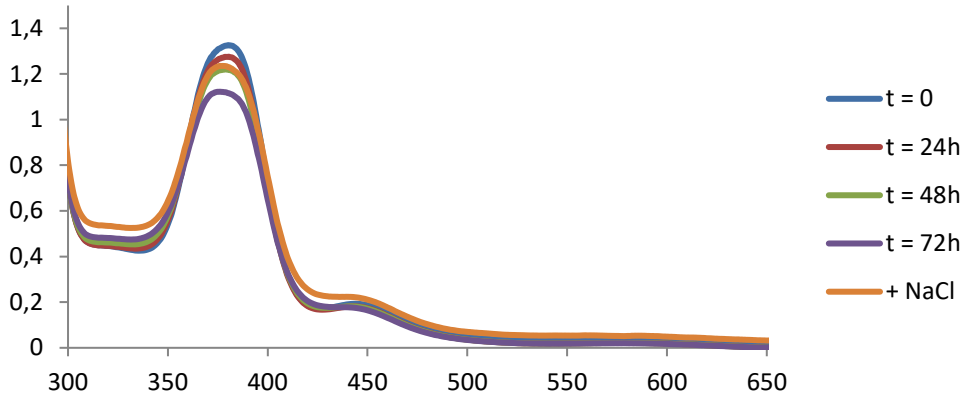

Figure A5.7. UV-vis spectra of a 0.4 mM solution of *trans*-[$RuCl_4(PTAH)_2$]Cl (**3**) in H_2O during time: immediately after dissolution (blue), 24 h (red), 48 h (green), 72 h (purple) and after addition of an excess of NaCl (orange).

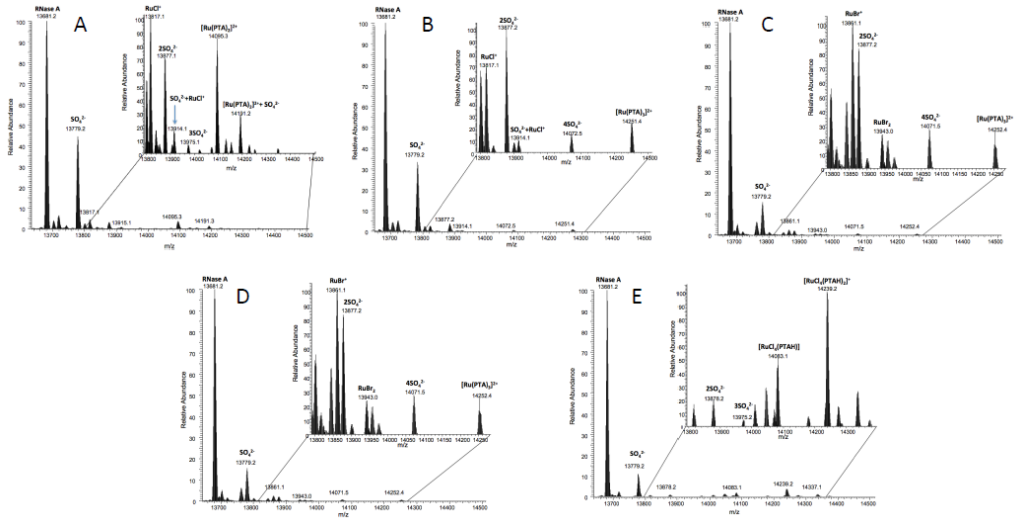

Figure A5.8. LTQ Orbitrap ESI mass spectra of compounds **1** (A), **2** (B), **8** (C), **9** (D), and **3** (E) dissolved in 20 mM ammonium acetate buffer, pH 7.4, in the presence of RNase A after 24h incubation at 37°C.

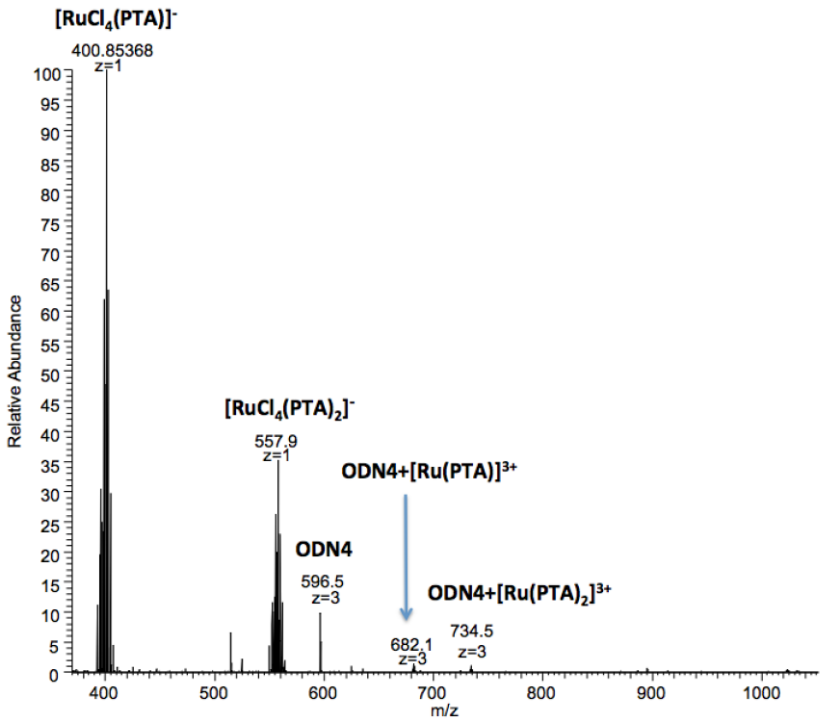

Figure A5.9. LTQ Orbitrap ESI mass spectrum of compound **3** dissolved in milliQ water, in the presence of ODN4 after 24h incubation at 37°C.

Appendix of Chapter 6

Figure A6.1. ^{1}H NMR spectrum of a mixture of *trans,cis*-$RuCl_2(CO)_2$(cppH) (**51**) and *trans,cis*-$RuCl_2(CO)_2$(cppMe) (**51Me**) in DMSO-d_6.

Figure A6.2. {^{1}H,^{15}N}- HMBC spectra of cppH·HNO_3 in DMSO-d_6.

Figures A6.3 {^{1}H,^{15}N}- HMBC spectra (cppH region) of a mixture of [Ru([9]aneS_3)(cppH-κN^p)(PTA)]$(Cl)_2$ and [Ru([9]aneS_3)(cppH-κN^o)(PTA)]$(Cl)_2$ (**50*N*^{p}** and **50*N*^{o}**) in DMSO-d_6

Figures A6.4-A6.5. NMR characterization of *trans*,*cis*-$RuCl_2(CO)_2$(cppH-κN^p) (**51**) in DMSO-d_6.

Figures A6.6-A6.7. NMR characterization of *trans*,*cis*-$RuCl_2(CO)_2$(cppH-κN^o) (**52**) in DMSO-d_6.

Figures A6.8. {^{1}H,^{15}N}- HMBC spectrum of mpp in $CDCl_3$.

Figures A6.9-A6.13 NMR characterization of *cis,trans*-$RuCl_2$(dmso-S)$_2$(mpp-κN^p) (**53**, with minor amounts of **54** and **55**) in $CDCl_3$.

Figures A6.14-A6.16. NMR characterization of a mixture of the two *cis,cis*-$RuCl_2$(dmso-S)$_2$(mpp-κN^p) isomers (**54** + **55**) in $CDCl_3$.

Figures A6.17-A6.20. NMR characterization of *trans,cis*-$RuCl_2$(dmso-S)$_2$(mpp-κN^p) (**56**) in $CDCl_3$.

Figure A6.21. Molecular structure (50% probability ellipsoids) of *trans,cis*-$RuCl_2(CO)_2$(cppH-κN^p) (**51**), *trans,cis*-$RuCl_2(CO)_2$(cppCH_3-κN^p) (**51Me**), and of the 55/45 mixture **51**/**51Me**.

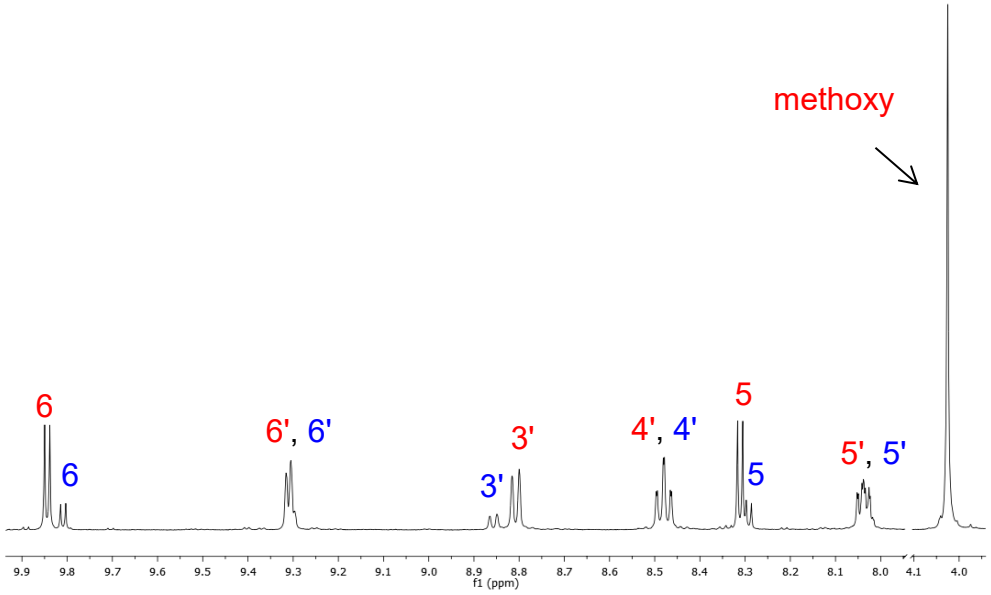

Figure A6.1. ^{1}H NMR spectrum of a mixture of *trans,cis*-$RuCl_2(CO)_2$(cppH) (**51**, blue labels) and *trans,cis*-$RuCl_2(CO)_2$(cppMe) (**51Me**, red labels) in DMSO-d_6.

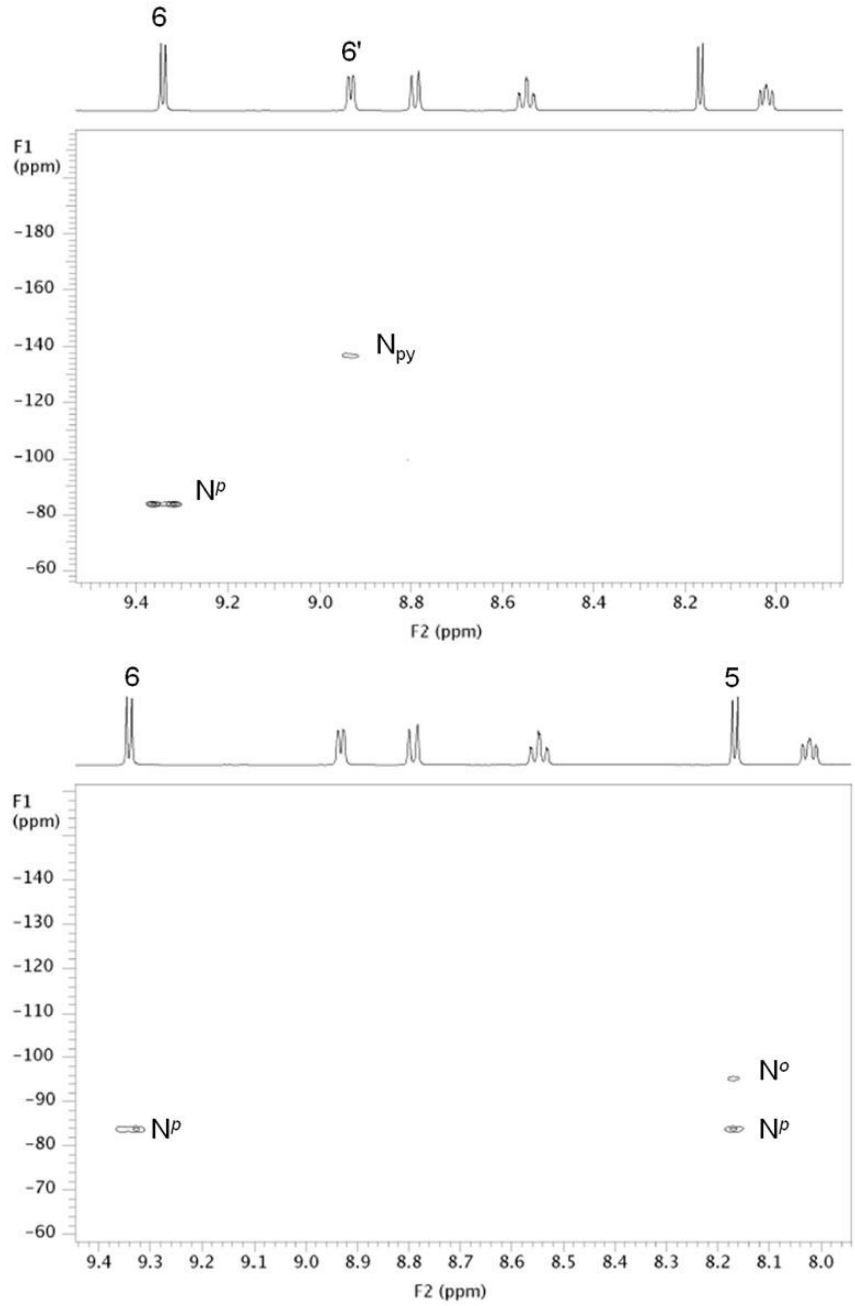

Figure A6.2. $\{^1H,^{15}N\}$- HMBC spectra of cppH·HNO_3 in DMSO-d_6 with J = 11 Hz (top) and with J = 1.8 Hz (bottom).

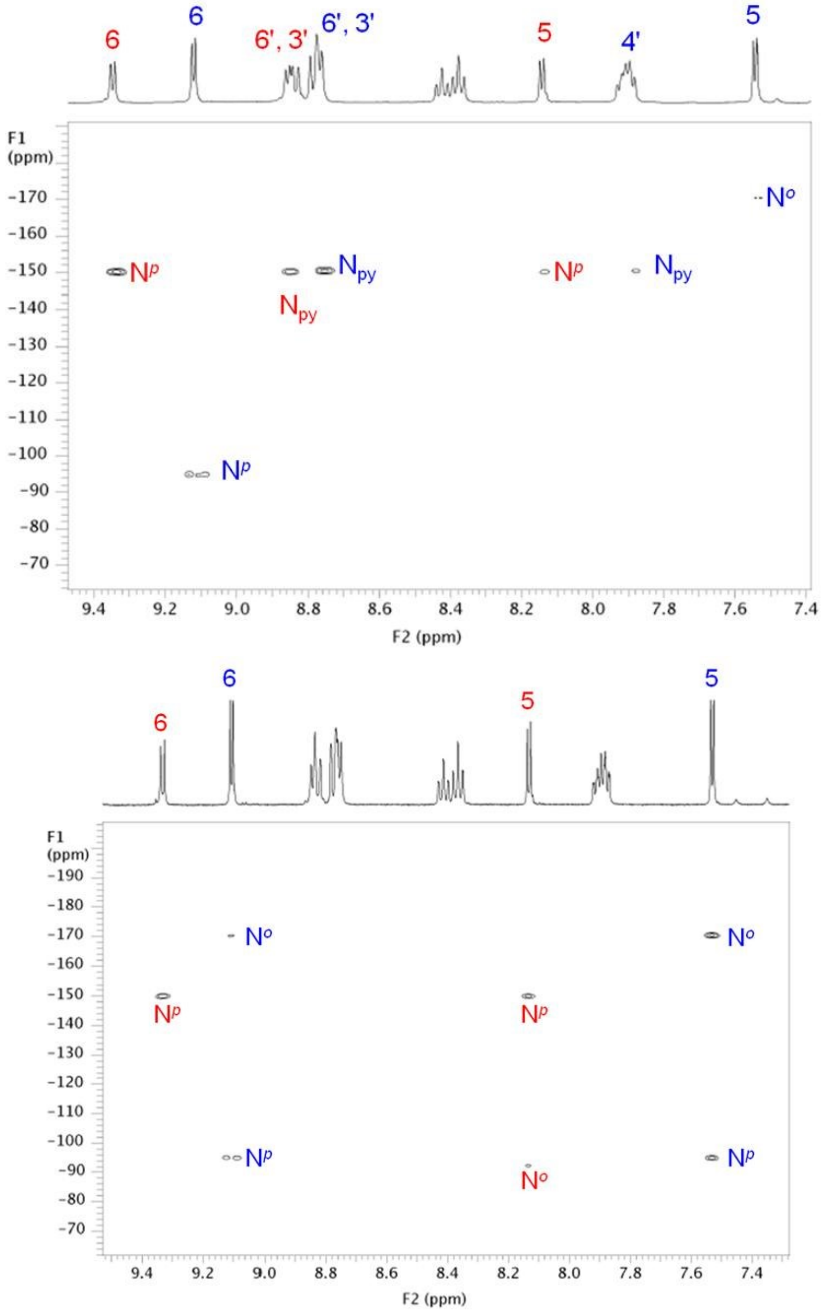

Figure A6.3. {^{1}H,^{15}N}- HMBC spectra (cppH region) of a mixture of [Ru([9]aneS$_3$)(cppH-κN^p)(PTA)][Cl$_2$] and [Ru([9]aneS$_3$)(cppH-κN^o)(PTA)][Cl$_2$] (**50*N*^{p}** and **50*N*^{o}**) in DMSO-d_6 with J = 11 Hz (top) and J = 1.8 Hz (bottom).

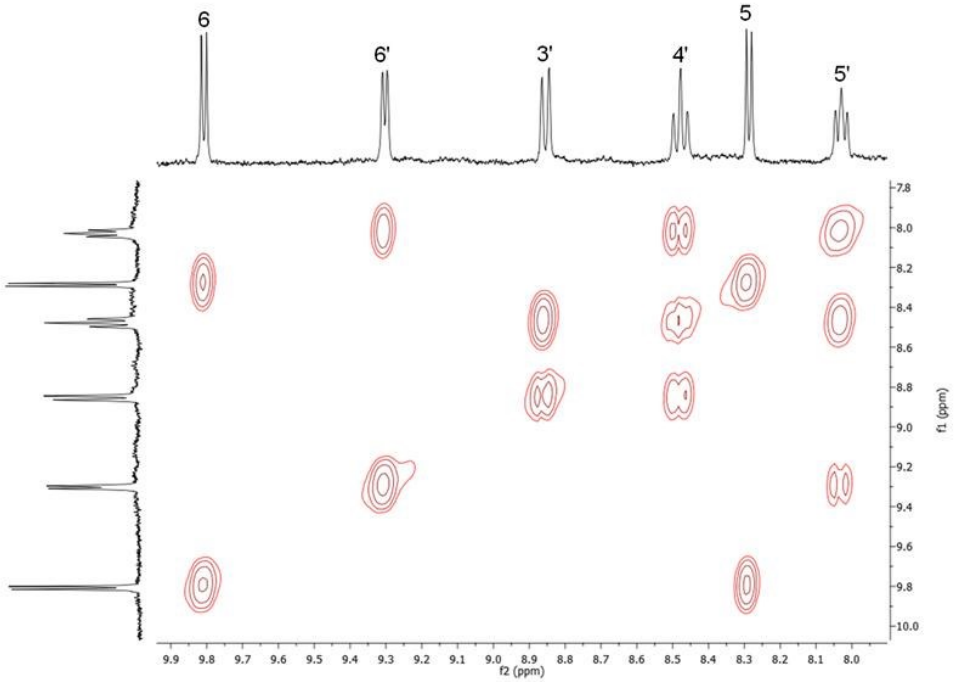

Figure A6.4. ^{1}H-^{1}H COSY NMR spectrum of *trans*,*cis*-$RuCl_2(CO)_2$(cppH-κN^p) (**51**) in DMSO-d_6.

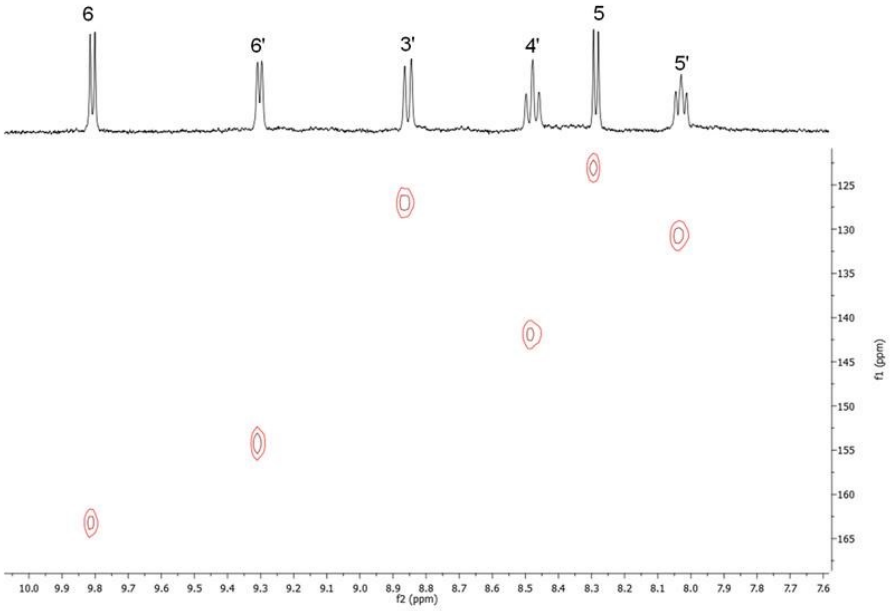

Figure A6.5. ^{1}H-^{13}C HSQC NMR spectrum of *trans*,*cis*-$RuCl_2(CO)_2$(cppH-κN^p) (**51**) in DMSO-d_6.

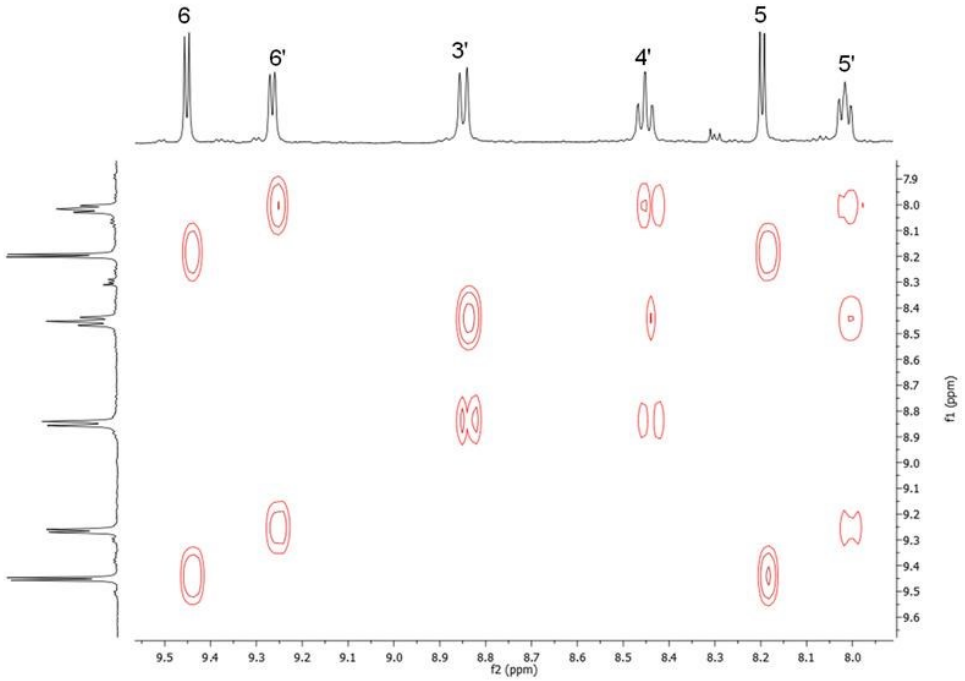

Figure A6.6. ^{1}H-^{1}H COSY NMR spectrum of *trans*,*cis*-$RuCl_2(CO)_2$(cppH-κN^o) (**52**) in DMSO-d_6.

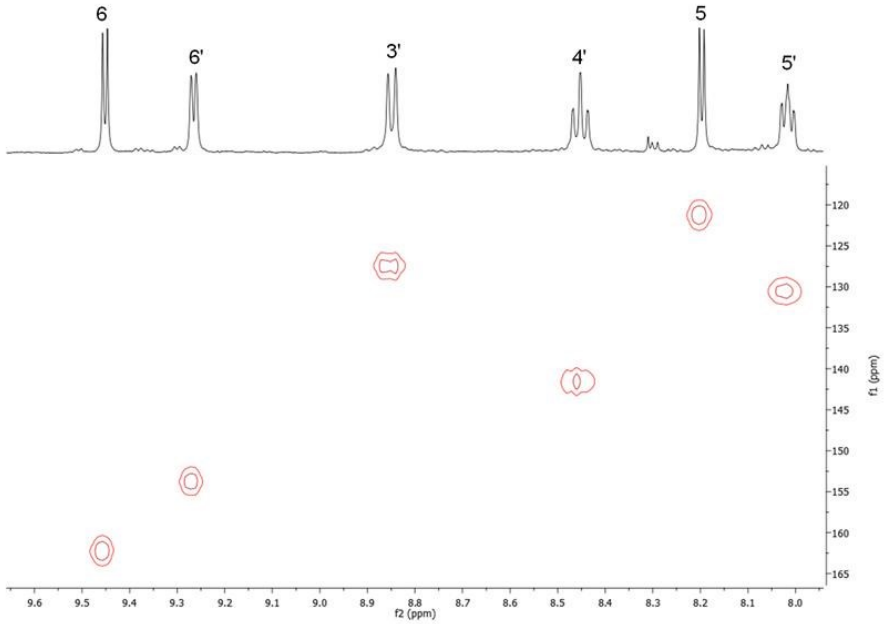

Figure A6.7. ^{1}H-^{13}C HSQC NMR spectrum of *trans*,*cis*-$RuCl_2(CO)_2$(cppH-κN^o) (**52**) in DMSO-d_6.

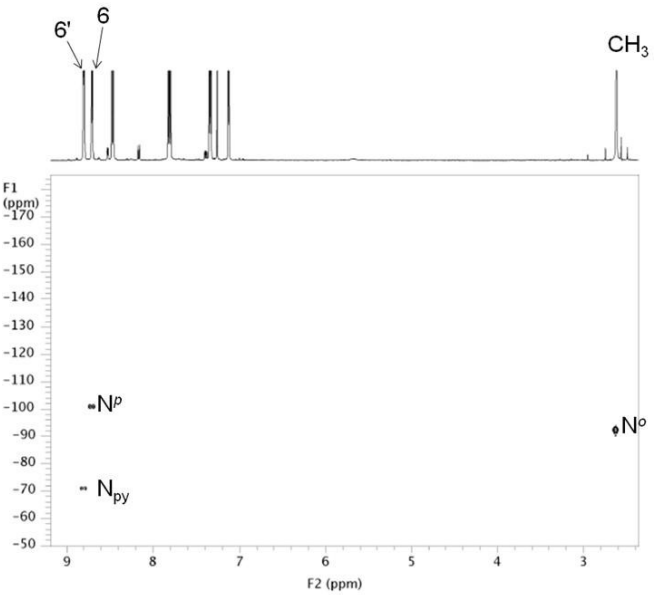

Figure A6.8. {^{1}H,^{15}N}- HMBC spectrum of mpp with J = 11 Hz in $CDCl_3$.

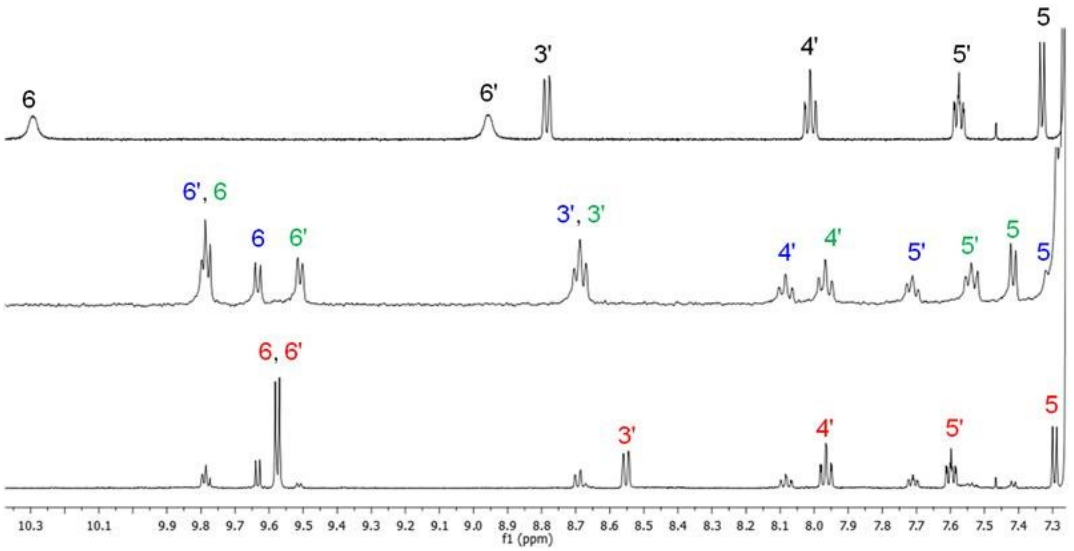

Figure A6.9. ^{1}H NMR spectra (aromatic region) of *cis,trans*-$RuCl_2$(dmso-S)$_2$(mpp-κN^p) (**53**, bottom, with minor amounts of **54** and **55**), a mixture of the two *cis,cis*-$RuCl_2$(dmso-S)$_2$(mpp-κN^p) isomers (**54** + **55**, middle), and *trans,cis*-$RuCl_2$(dmso-S)$_2$(mpp-κN^p) (**56**, top) in $CDCl_3$.

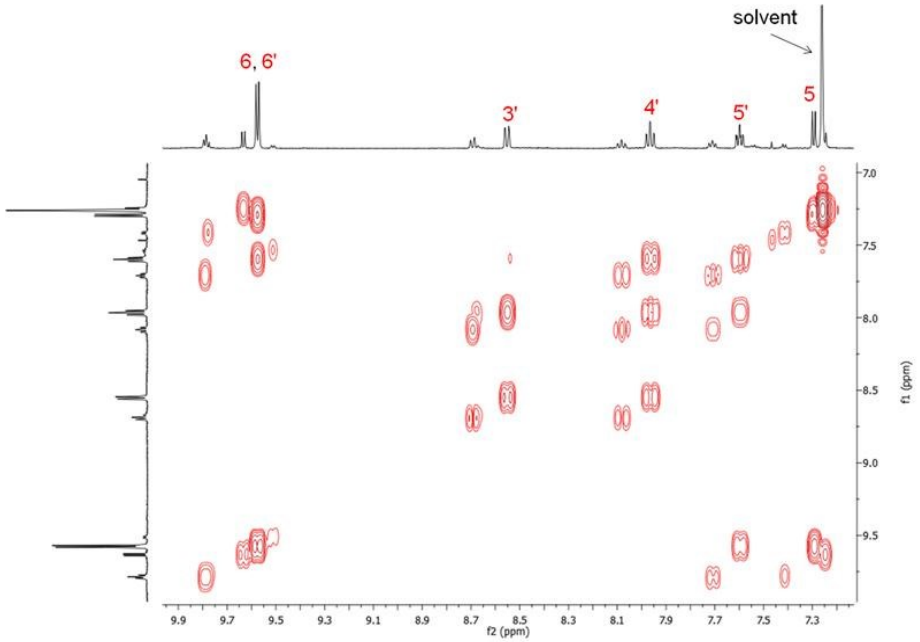

Figure A6.10. ^{1}H-^{1}H COSY NMR spectrum (aromatic region) of *cis,trans*-$RuCl_2$(dmso-S)$_2$(mpp-κ*N*^{p}) (**53**, with minor amounts of **54** and **55**) in $CDCl_3$.

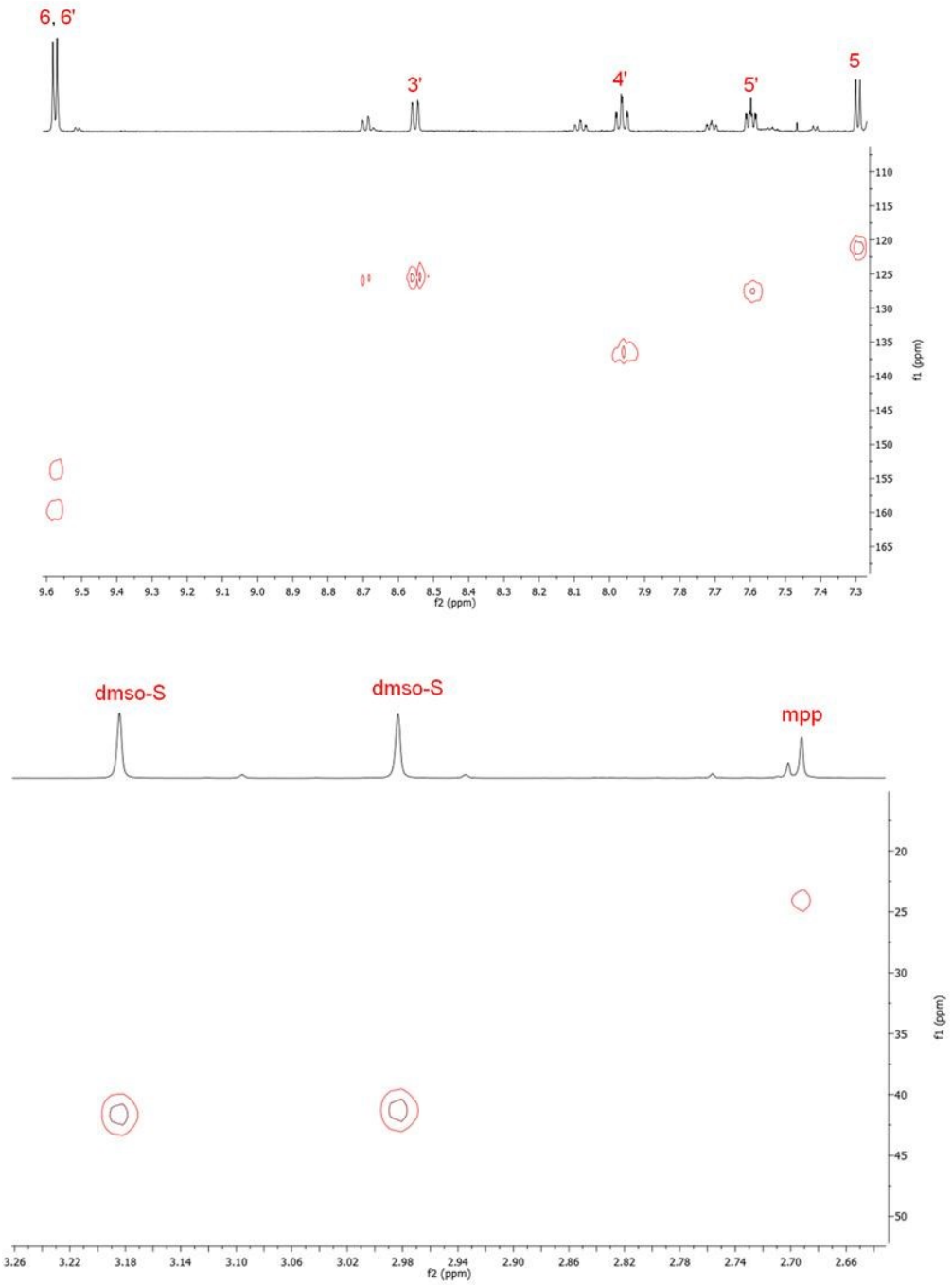

Figure A6.11. ^{1}H-^{13}C HSQC NMR spectrum of *cis,trans*-$RuCl_2(dmso\text{-}S)_2(mpp\text{-}\kappa N^p)$ (**53**, with minor amounts of **54** and **55**) in $CDCl_3$: aromatic region (top) and methyl region (bottom).

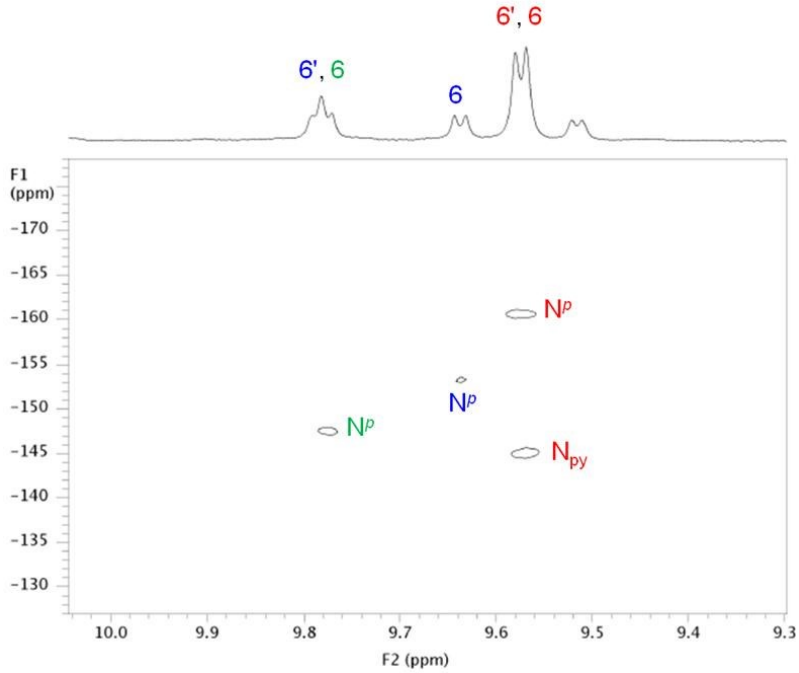

Figure A6.12. {^{1}H,^{15}N}- HMBC spectrum (aromatic resonances of mpp) of a mixture of *cis,trans*-$RuCl_2$(dmso-S)$_2$(mpp-κ*N*^{p}) (**53**), and the two *cis,cis*-$RuCl_2$(dmso-S)$_2$(mpp-κ*N*^{p}) isomers (**54** + **55**), with J = 11 Hz in $CDCl_3$.

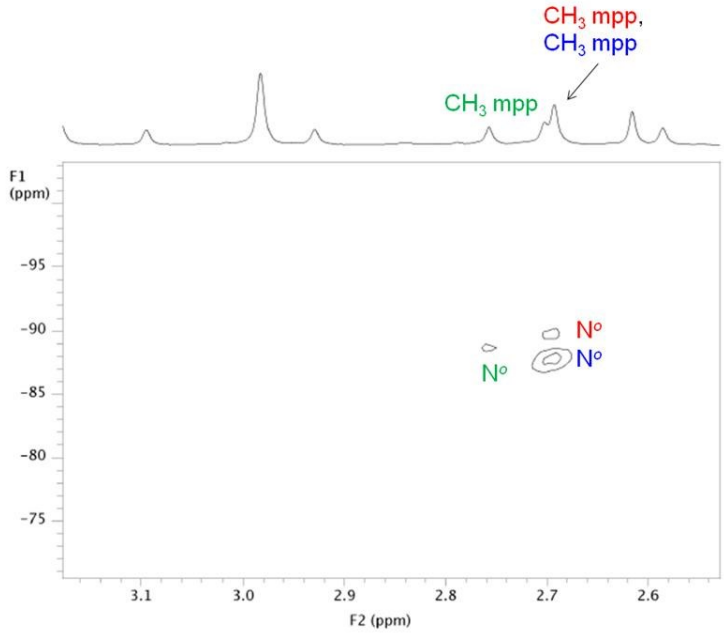

Figure A6.13. {^{1}H,^{15}N}- HMBC spectrum (region of methyl resonances) of a mixture of *cis,trans*-$RuCl_2$(dmso-S)$_2$(mpp-κ*N*^{p}) (**53**), and the two *cis,cis*-[$RuCl_2$(dmso-S)$_2$(mpp-κ*N*^{p})] isomers (**54**+ **55**), with J = 1.8 Hz in $CDCl_3$.

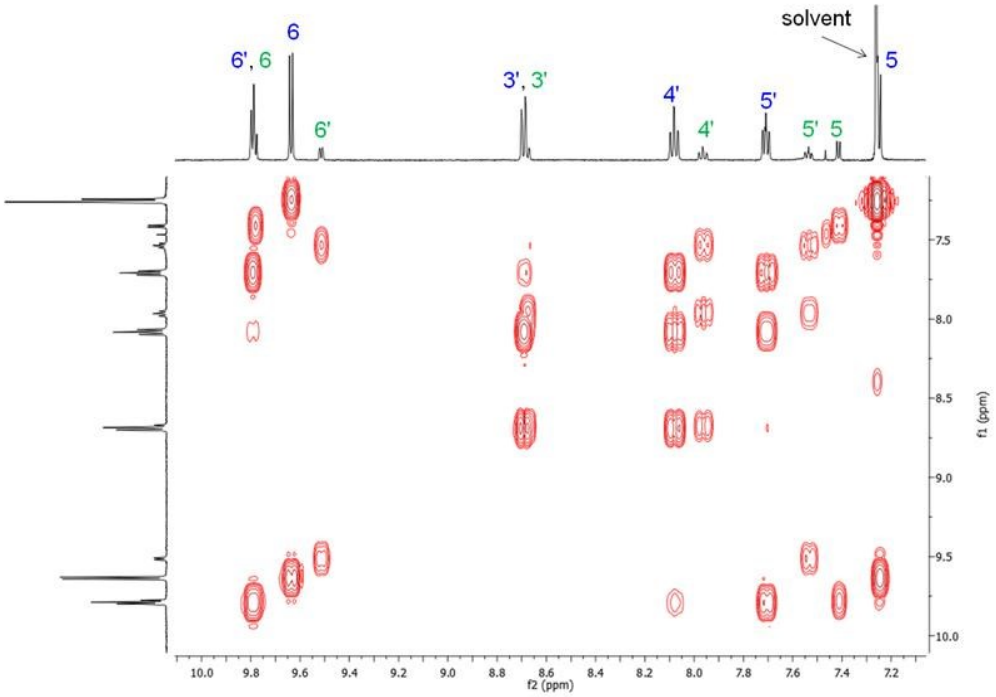

Figure A6.14. ^{1}H-^{1}H COSY NMR spectrum (aromatic region) of a mixture of the two *cis,cis*-$RuCl_2(dmso\text{-}S)_2(mpp\text{-}\kappa N^p)$ isomers (**54** + **55**) in $CDCl_3$.

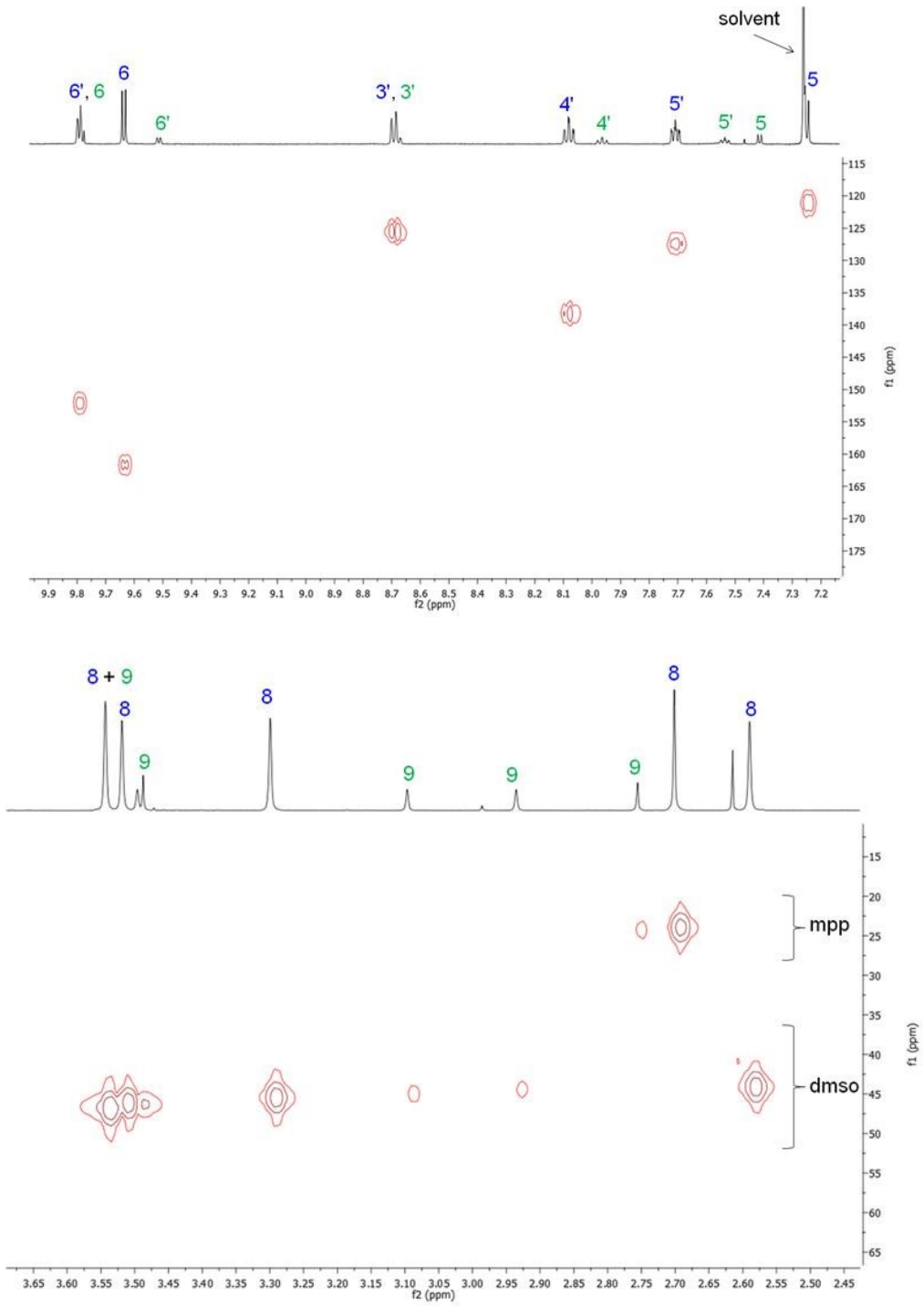

Figure A6.15. ^{1}H-^{13}C HSQC NMR spectrum of a mixture of the two *cis,cis*-$RuCl_2$(dmso-S)$_2$(mpp-κ*N*^{p}) isomers (**54** + **55**) in $CDCl_3$: aromatic region (top) and methyl region (bottom).

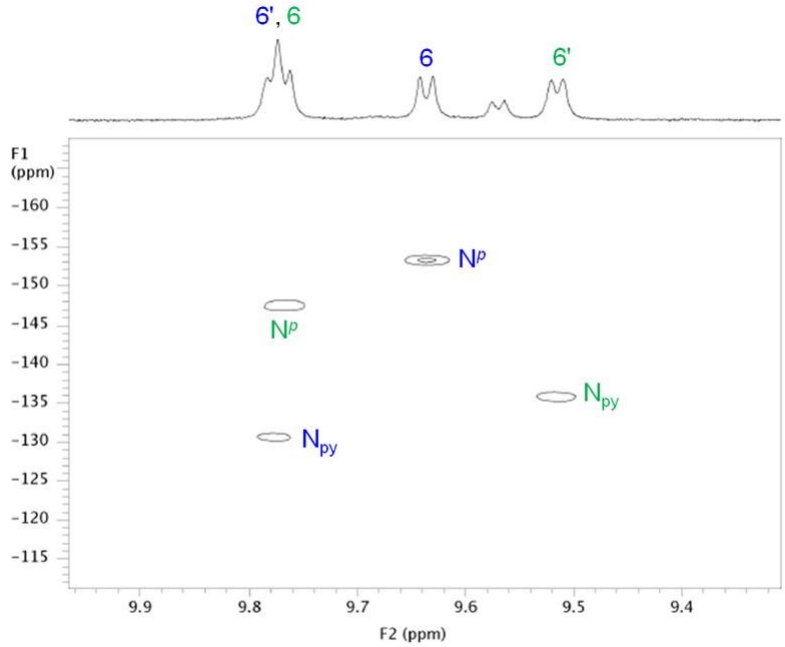

Figure A6.16. {^{1}H,^{15}N}- HMBC spectrum (aromatic resonances of mpp) of a mixture of the two *cis,cis*-$RuCl_2$(dmso-S)$_2$(mpp-κ*N*^{p}) isomers (**54** + **55**) with J = 11 Hz in $CDCl_3$.

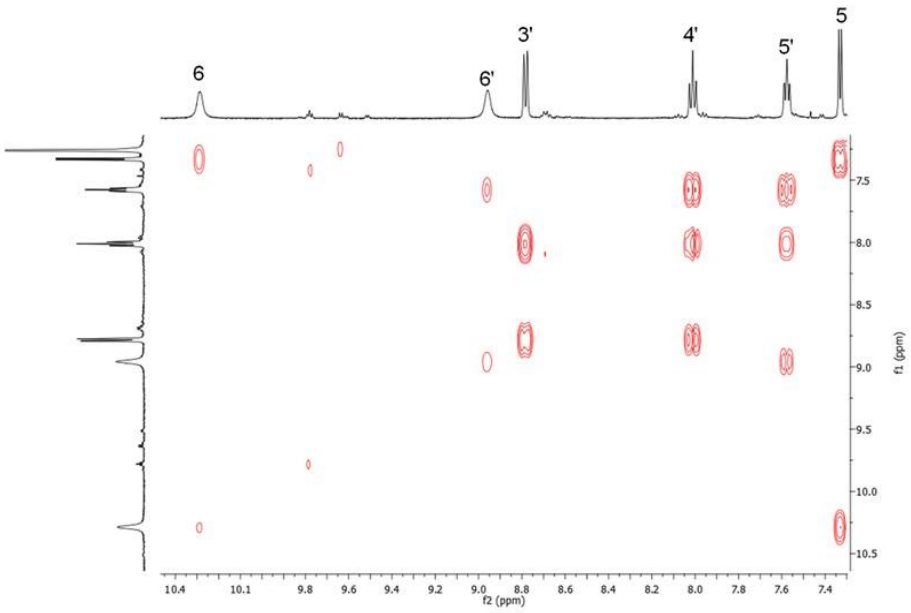

Figure A6.17. ^{1}H-^{1}H COSY NMR spectrum (aromatic region) of *trans,cis*-$RuCl_2$(dmso-S)$_2$(mpp-κ*N*^{p}) (**56**) in $CDCl_3$.

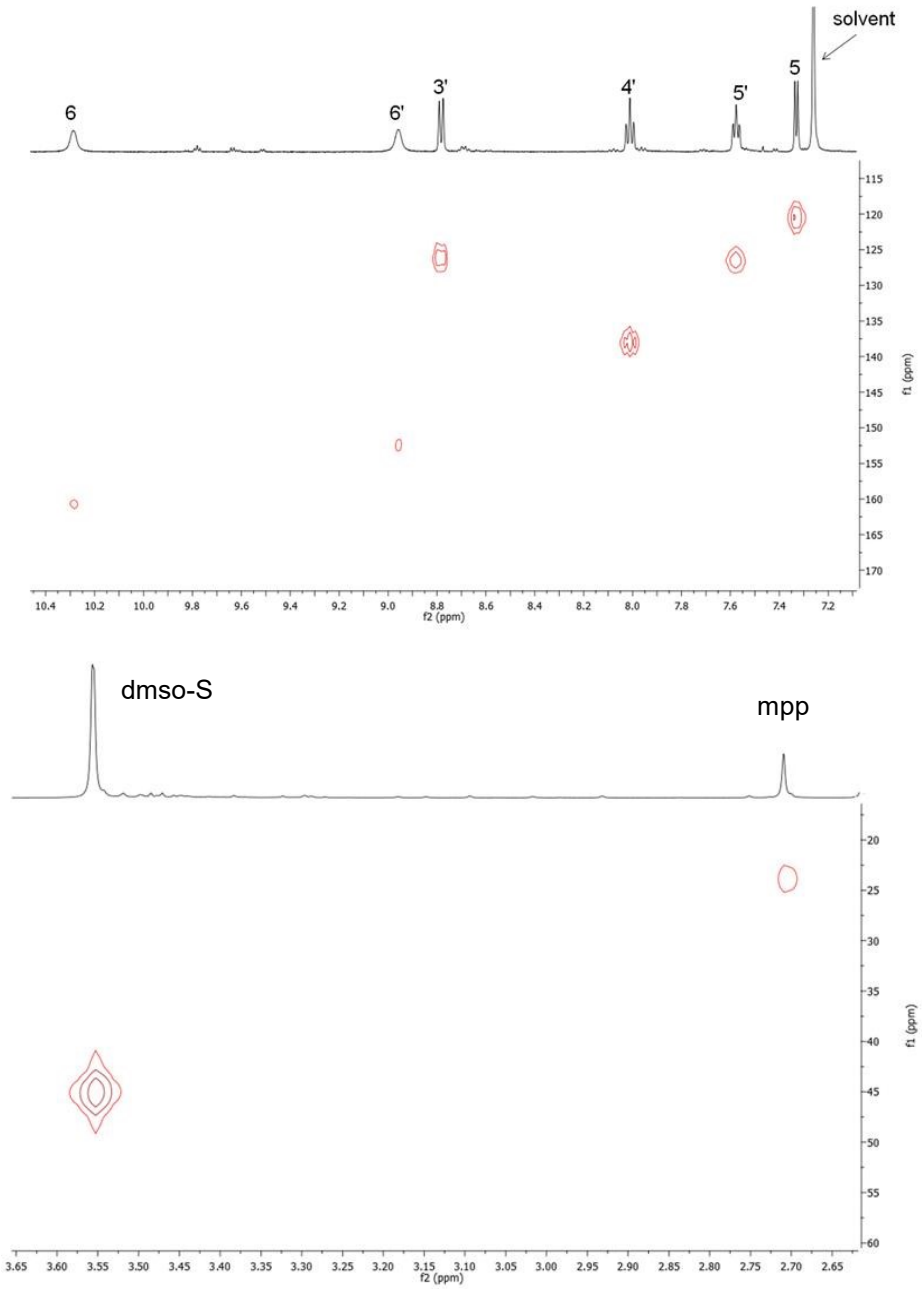

Figure A6.18. ^{1}H-^{13}C HSQC NMR spectrum of *trans,cis*-$RuCl_2$(dmso-S)$_2$(mpp-κ*N*^{p}) (**56**) in $CDCl_3$: aromatic region (top) and methyl region (bottom).

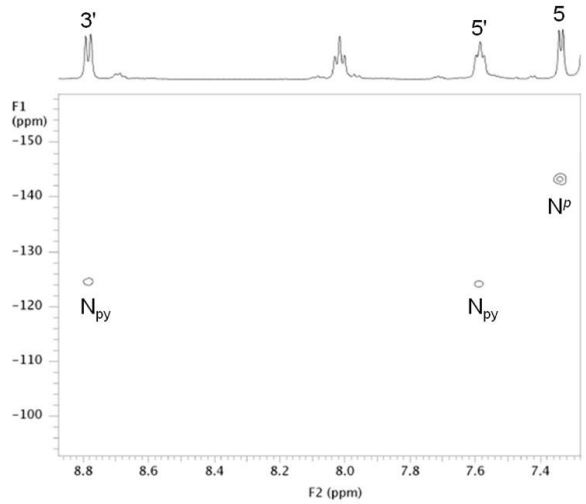

Figure A6.19. {^{1}H,^{15}N}- HMBC spectrum (aromatic resonances of mpp) of *trans,cis*-$RuCl_2$(dmso-S)$_2$(mpp-κ*N*^{p}) (**56**) with J = 11 Hz in $CDCl_3$.

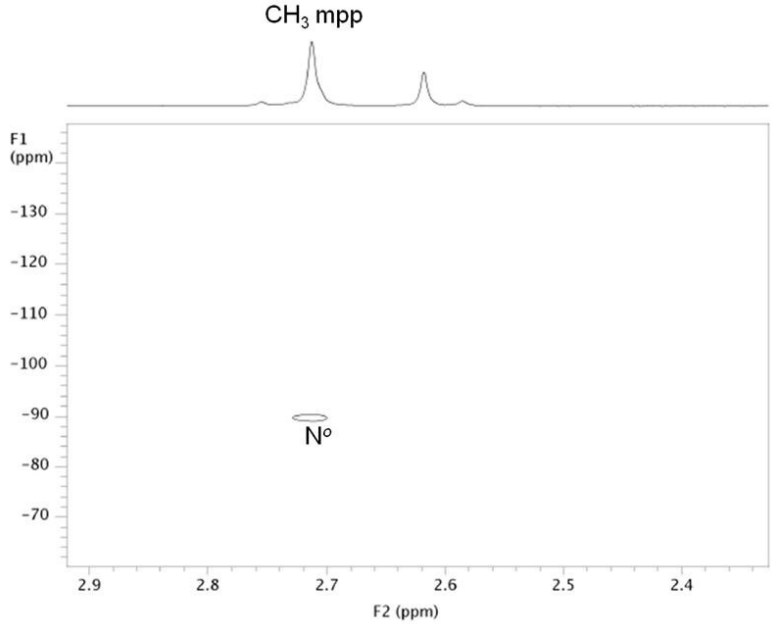

Figure A6.20. {^{1}H,^{15}N}- HMBC spectrum (region of methyl resonance) of *trans,cis*-$RuCl_2$(dmso-S)$_2$(mpp-κ*N*^{p}) (**56**) with J = 11Hz in $CDCl_3$.

X-ray structure of 51/51Me

As said in the text, when the preparation of **51** was performed in methanol part of the carboxylate groups of coordinated cppH are methylated and a mixture of *trans,cis*-$RuCl_2(CO)_2$(cppH-κN^p) (**51**) and *trans,cis*-$RuCl_2(CO)_2$(cppCH_3-κN^p) (**51Me**) cocrystallyzes. The fraction of molecules with esterified cppH has been estimated at 45%. The X-ray structures of **51**, **51Me**, and of the mixture **51**/**51Me** after refinement are shown in Figure A6.21.

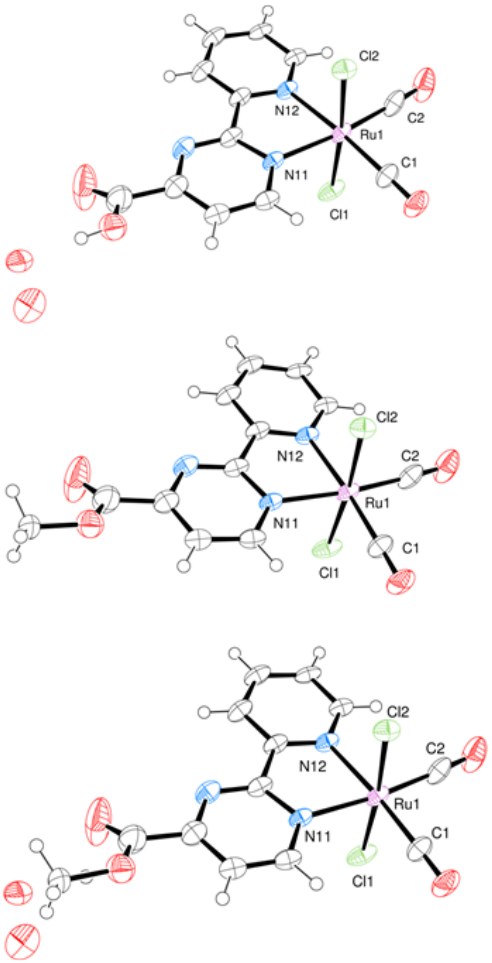

Figure A6.21. X-ray structures (50% probability ellipsoids) of *trans,cis*-$RuCl_2(CO)_2$(cppH-κN^p) (**51**, top), *trans,cis*-$RuCl_2(CO)_2$(cppCH_3-κN^p) (**51Me**, middle), and of the 55/45 mixture **51**/**51Me** (bottom). Coordination distances (Å): Ru1–N11 = 2.122(3), Ru1–N12 = 2.114(3), Ru1–Cl1 = 2.388(1), Ru1–Cl2 = 2.396(1), Ru1–C1 = 1.879(6), Ru1–C2 = 1.874(5).

Appendix of Chapter 7

Figures A7.1-A7.2. NMR characterization of [Ru([9]aneS$_3$)Cl(cppH)]$^+$ (**60**) in D_2O.

Figures A7.3-A7.5. NMR characterization of *trans,cis*-$RuCl_2(CO)_2$(cppH-NT) (**57**) in DMSO-d_6 and D_2O.

Figures A7.6-A7.9. NMR characterization of [Ru([9]aneS$_3$)Cl(cppH-NT)]$^+$ (**61**) in DMSO-d_6 and D_2O.

Figures A7.10-A7.13. NMR characterization of [Ru([9]aneS$_3$)(cppH-NT)(PTA)]$^{2+}$ (**62**) in DMSO-d_6 and D_2O.

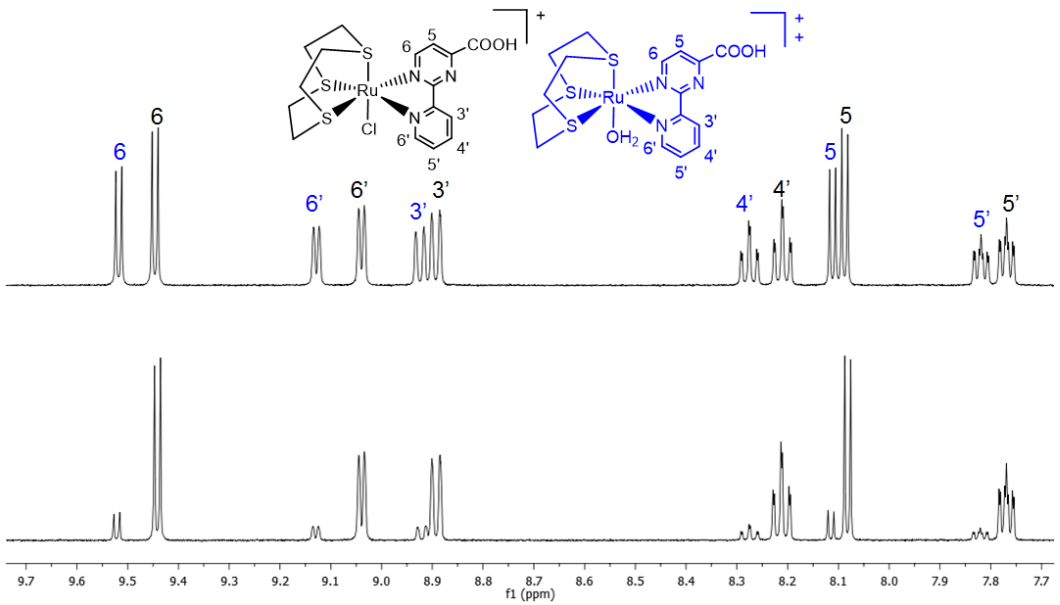

Figure A7.1. ^{1}H NMR spectra in D_2O of $[Ru([9]aneS_3)Cl(cppH)]^{+}$ (**60**) after dissolution in D_2O (top) and after addition of an excess of NaCl (bottom).

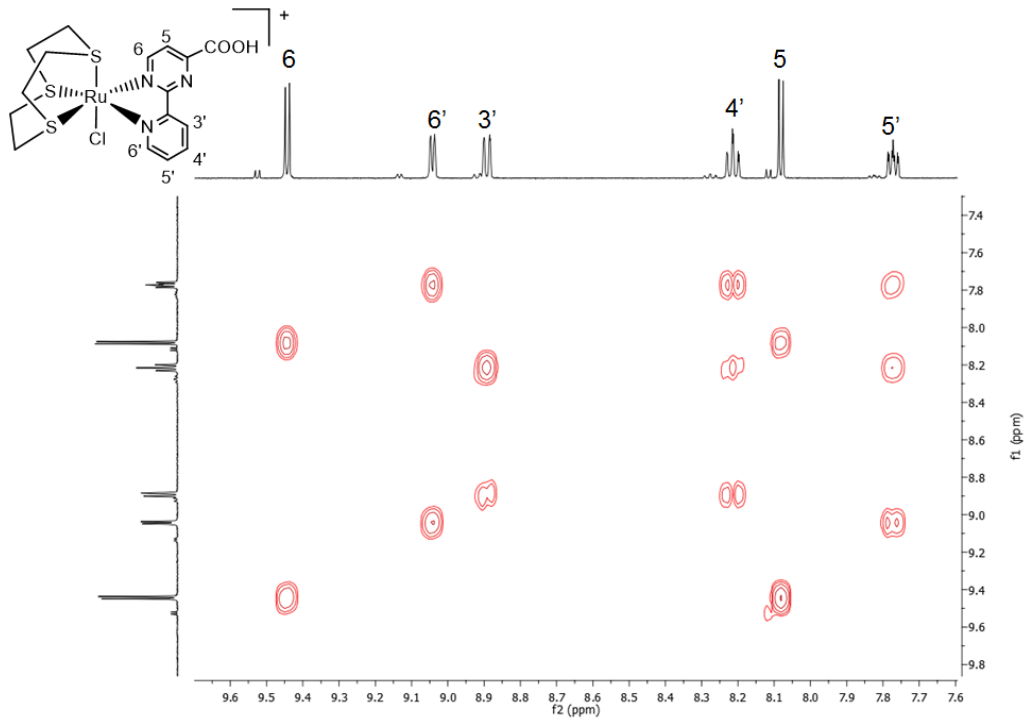

Figure A7.2. ^{1}H-^{1}H COSY NMR spectrum in D_2O of $[Ru([9]aneS_3)Cl(cppH)]^{+}$ (**60**).

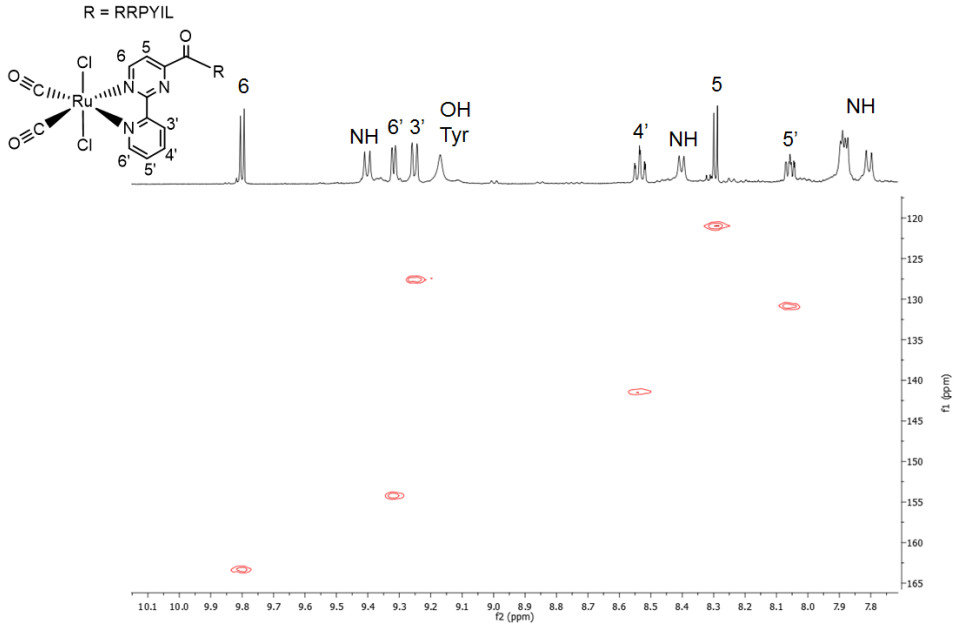

Figure A7.3. ^{1}H-^{13}C HSQC NMR spectrum in DMSO-d_6 of the aromatic region of *trans,cis*-$RuCl_2(CO)_2$(cppH-NT) (**57**). R is the peptide sequence: Arg-Arg-Pro-Tyr-Ile-Leu. NH indicates the amidic protons of the peptide.

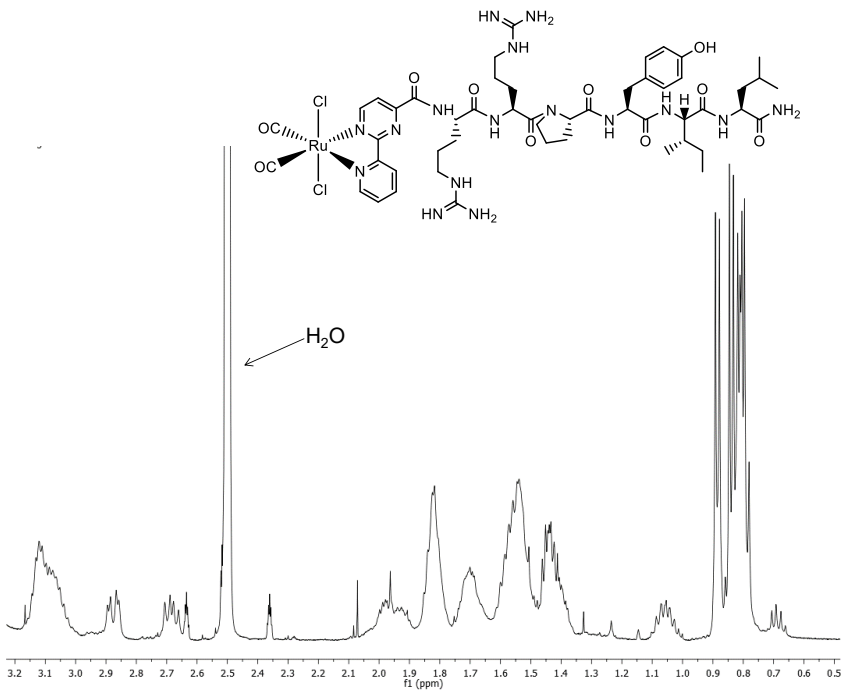

Figure A7.4. Upfield region of ^{1}H NMR spectrum in DMSO-d_6 of *trans,cis*-$RuCl_2(CO)_2$(cppH-NT) (**57**).

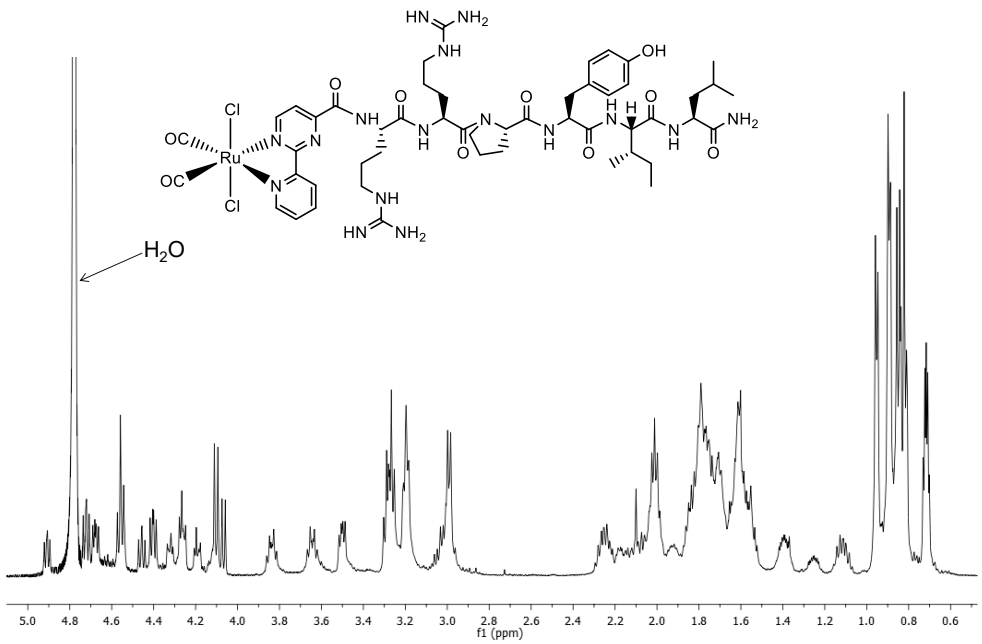

Figure A7.5. Upfield region of ^{1}H NMR spectrum in D_2O of *trans,cis*-$RuCl_2(CO)_2$(cppH-NT) (**57**).

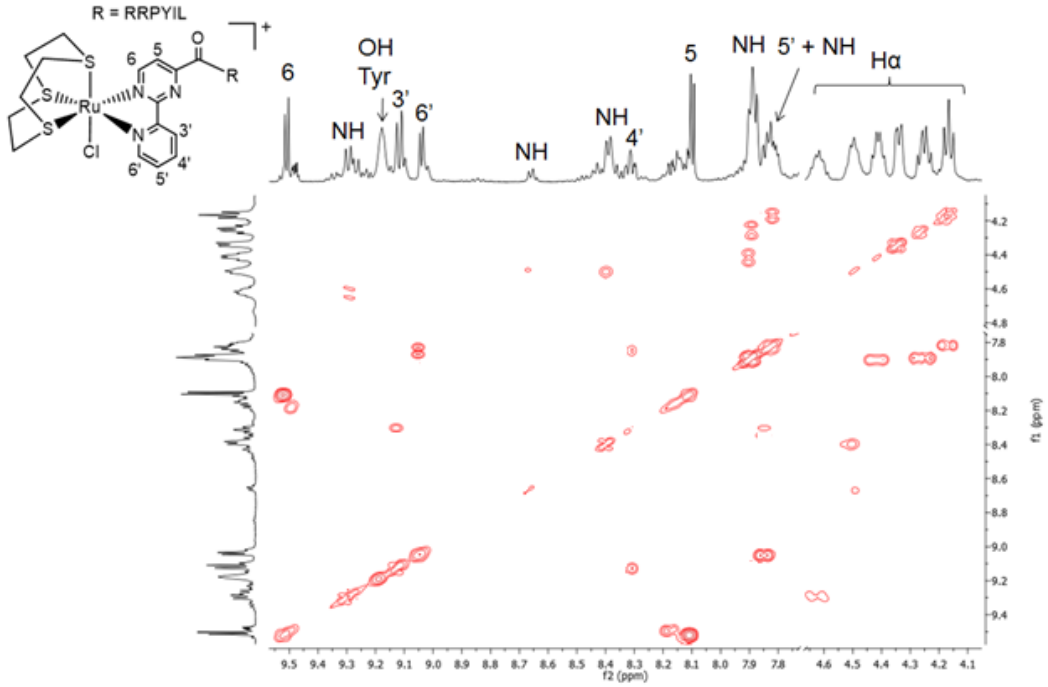

Figure A7.6. ^{1}H-^{1}H COSY NMR spectrum in DMSO-d_6 of the aromatic region of $[Ru([9]aneS_3)Cl(cppH\text{-}NT)]^{+}$ (**61**). R is the peptide sequence: Arg-Arg-Pro-Tyr-Ile-Leu. NH indicates the amidic protons of the peptide.

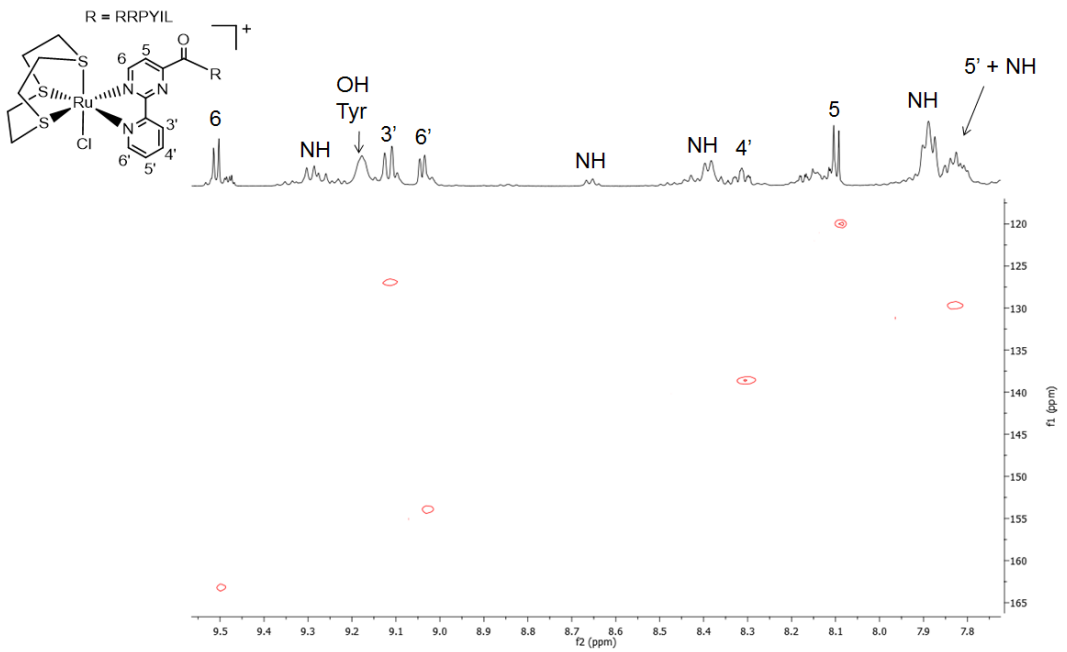

Figure A7.7. ^{1}H-^{13}C HSQC NMR spectrum in DMSO-d_6 of the aromatic region of [Ru([9]aneS$_3$)Cl(cppH-NT)]$^+$ (**61**). R is the peptide sequence: Arg-Arg-Pro-Tyr-Ile-Leu. NH indicates the amidic protons of the peptide.

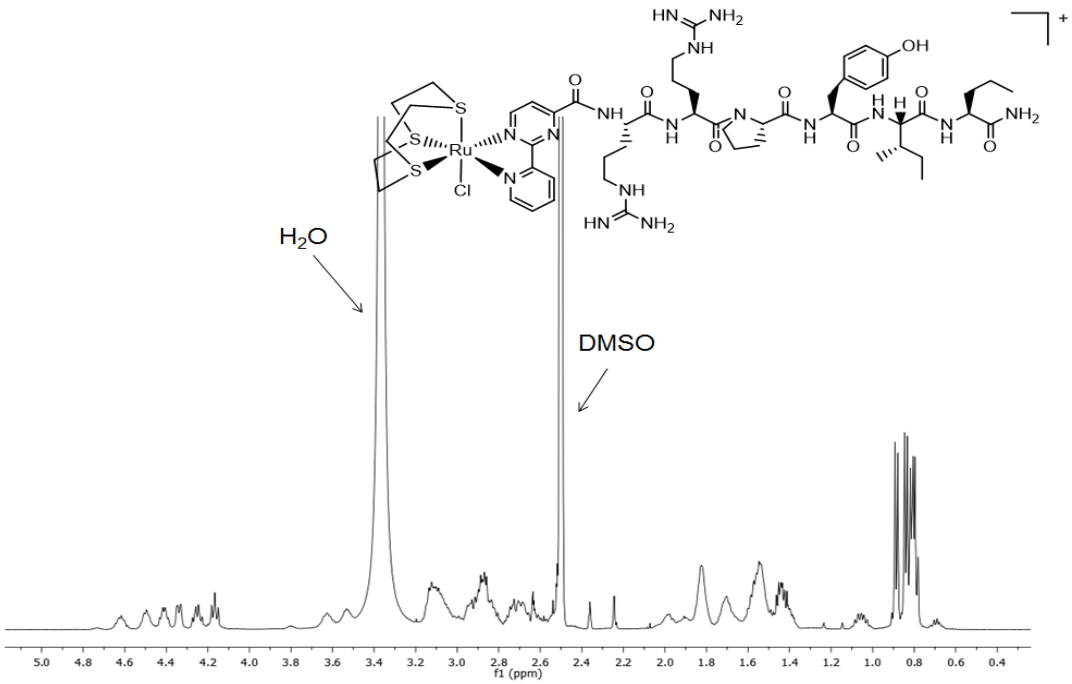

Figure A7.8. Upfield region of ^{1}H NMR spectrum in DMSO-d_6 of [Ru([9]aneS$_3$)Cl(cppH-NT)]$^+$ (**61**).

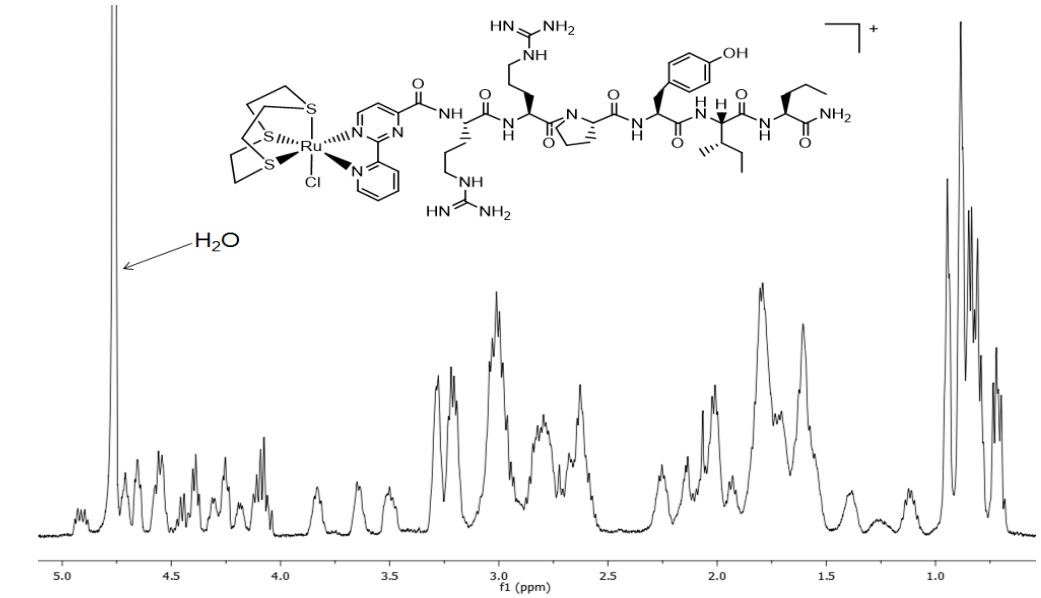

Figure A7.9. Upfield region of ^{1}H NMR spectrum in D_2O of [Ru([9]aneS$_3$)Cl(cppH-NT)]$^{+}$ (**61**).

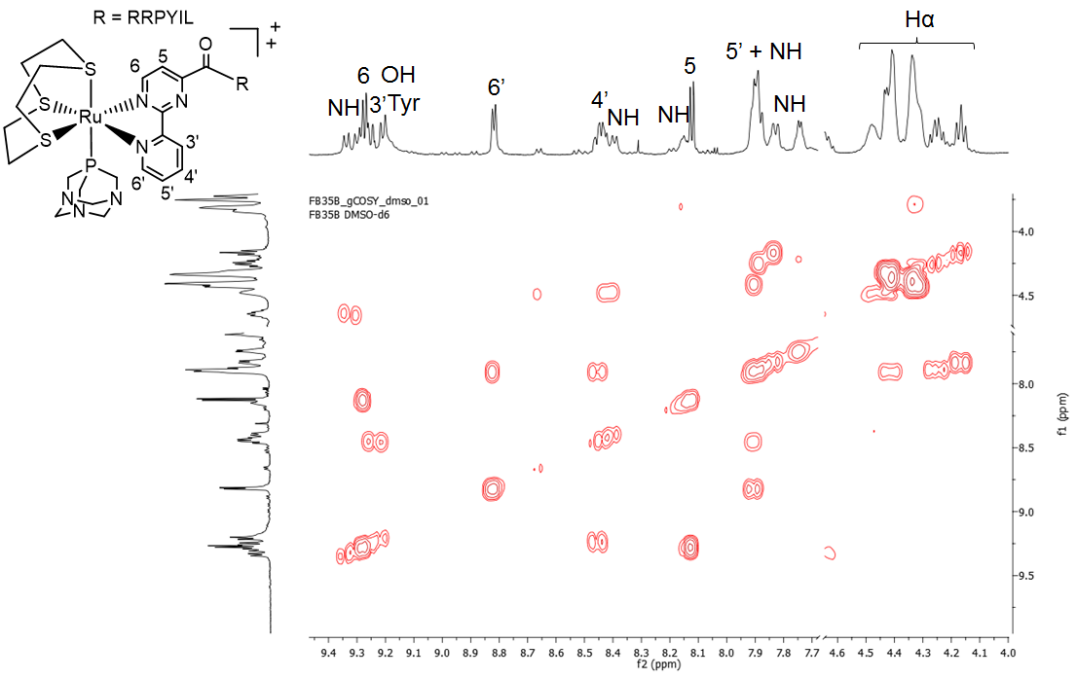

Figure A7.10. ^{1}H-^{1}H COSY NMR spectrum in DMSO-*d*$_6$ of the aromatic region of [Ru([9]aneS$_3$)(cppH-NT)(PTA)]$^{2+}$ (**62**). R is the peptide sequence: Arg-Arg-Pro-Tyr-Ile-Leu. NH indicates the amidic protons of the peptide.

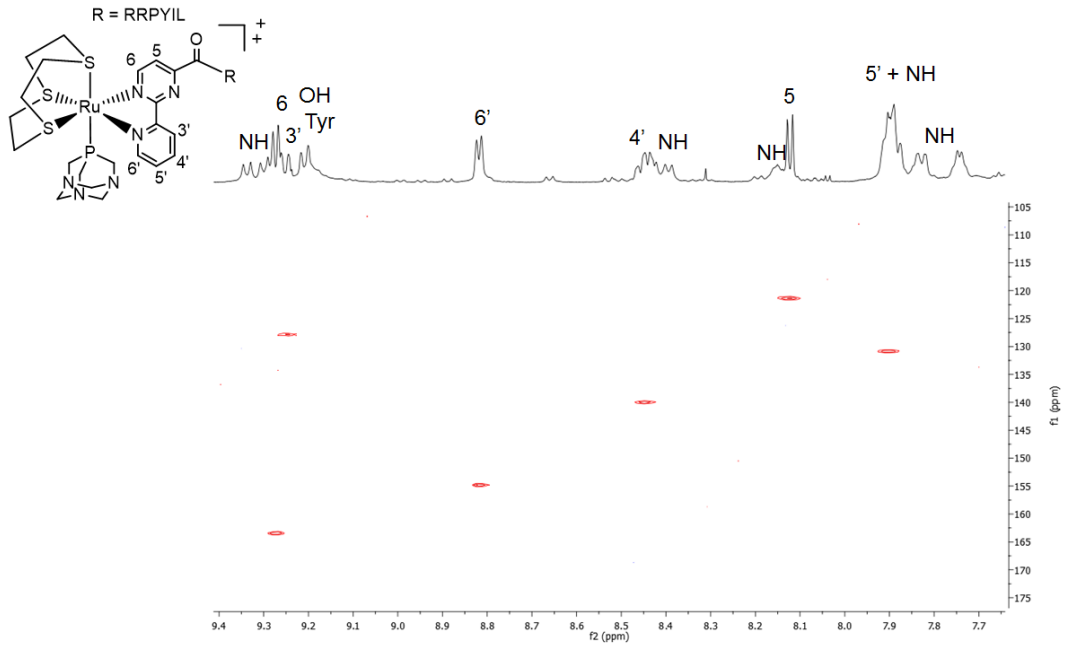

Figure A7.11. ^{1}H-^{13}C HSQC NMR spectrum in DMSO-d_6 of the aromatic region of $[Ru([9]aneS_3)(cppH\text{-}NT)(PTA)]^{2+}$ (**62**). R is the peptide sequence: Arg-Arg-Pro-Tyr-Ile-Leu. NH indicates the amidic protons of the peptide.

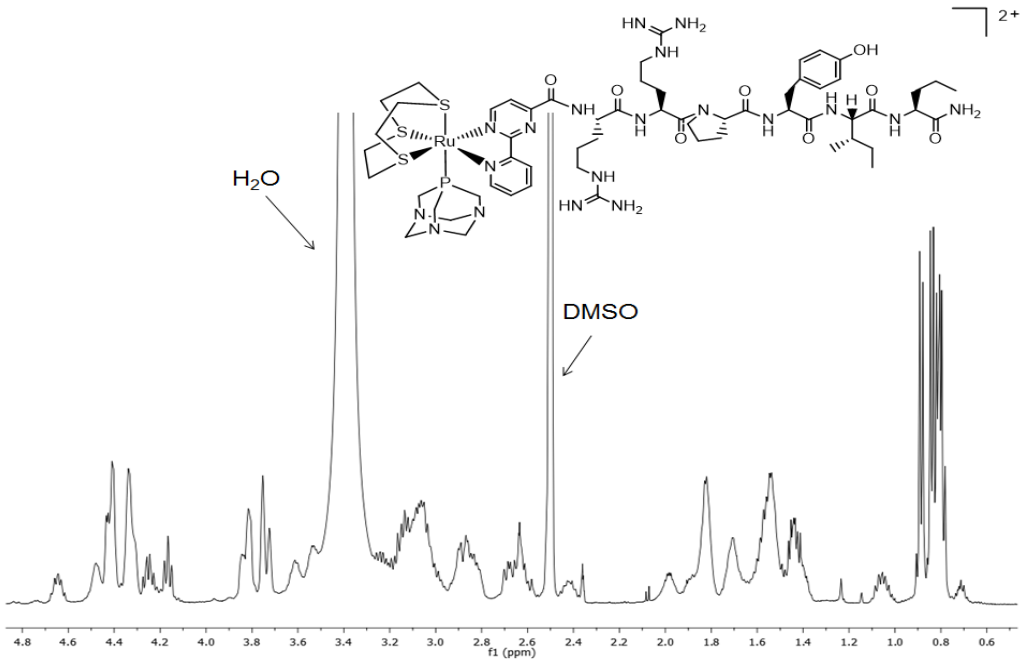

Figure A7.12. Upfield region of ^{1}H NMR spectrum in DMSO-d_6 of $[Ru([9]aneS_3)(cppH\text{-}NT)(PTA)]^{2+}$ (**62**).

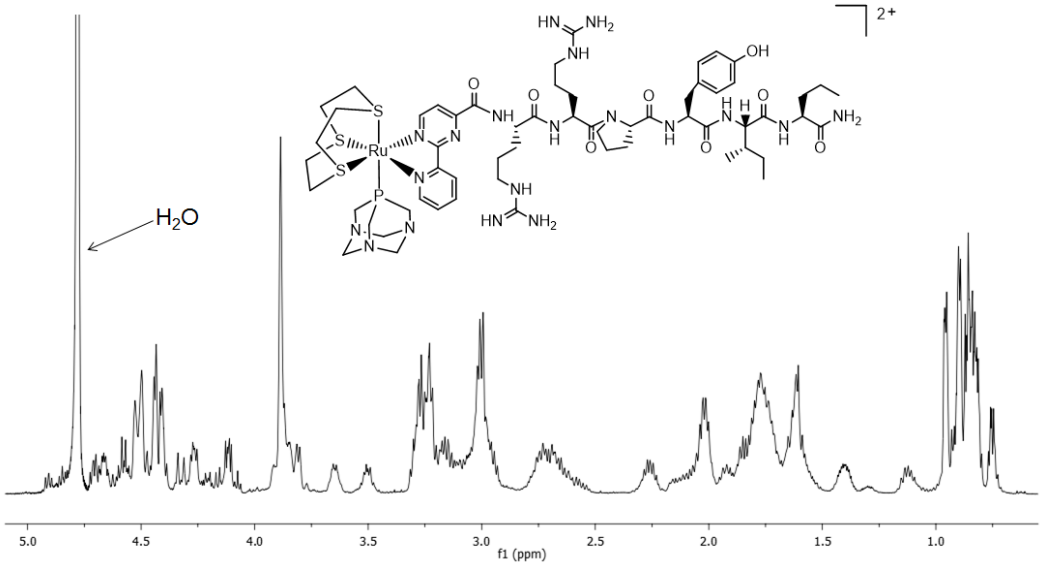

Figure A7.13. Upfield region of ^{1}H NMR spectrum in D_2O of $[Ru([9]aneS_3)(cppH\text{-}NT)(PTA)]^{2+}$ (**62**).

Appendix of Chapter 8

Figure A8.1. ^{1}H NMR spectrum (aromatic region) in D_2O of [Ru([9]aneS$_3$)(bpy)Cl]Cl (**63**), and [Ru([9]aneS$_3$)(bpy)(OH$_2$)](Cl)$_2$ (**63$_{aq}$**).

Figures A8.2-A8.5. ^{1}H NMR spectra in D_2O of [Ru([9]aneS$_3$)(bpy)(py)](Cl)$_2$ (**68**), [Ru([9]aneS$_3$)(phen)(py)](Cl)$_2$ (**69**), [Ru([9]aneS$_3$)(4,7-Ph$_2$phen)(py)](Cl)$_2$ (**70**), [Ru([9]aneS$_3$)(dppz)(py)](Cl)$_2$ (**71**).

Figure A8.6. ^{1}H NMR spectrum in DMSO-*d*$_6$ of [Ru([9]aneS$_3$)(bq)(py)](Cl)$_2$ (**72**) after 240 min of irradiation (λ = 470 nm, 40 mW).

Figure A8.7. ^{1}H NMR spectrum in D_2O of [Ru([9]aneS$_3$)(bq)(py)](Cl)$_2$ (**72**) at different irradiation times (λ = 470 nm, 40 mW).

Figure A8.8. UV-vis spectra of compounds [Ru([9]aneS$_3$)(bpy)Cl]Cl (**63**), [Ru([9]aneS$_3$)(phen)Cl]Cl (**64**), [Ru([9]aneS$_3$)(4,7-Ph$_2$phen)Cl]Cl (**65**), [Ru([9]aneS$_3$)(dppz)Cl]Cl (**66**), [Ru([9]aneS$_3$)(bq)Cl]Cl (**67**) (ca. in 0.1 mM H_2O) in the visible region.

Figure A8.9. UV-vis spectra of [Ru([9]aneS$_3$)(dppz)](Cl)$_2$ (**66**) (ca. in 0.1 mM H_2O) in between 450 and 600 nm.

Figure A8.10. Molecular structure (50% probability ellipsoids) of [Ru([9]aneS$_3$)(phen)(py)](Cl)$_2$·EtOH (**69**).

Figure A8.11. Experimental and calculated (with the "turbo_lanczos" program) absorption spectra for [Ru([9]aneS$_3$)(bpy)(py)](Cl)$_2$ (**68**). The vertical bars in the simulated spectrum are the calculated transitions (with the "turbo_davidson" code), with height equal to the oscillator strength.

Figure A8.12. Selected molecular orbitals for [Ru([9]aneS$_3$)(bpy)(py)](Cl)$_2$ (**68**) and [Ru([9]aneS$_3$)(bq)(py)](Cl)$_2$ (**72**) in the singlet ground state.

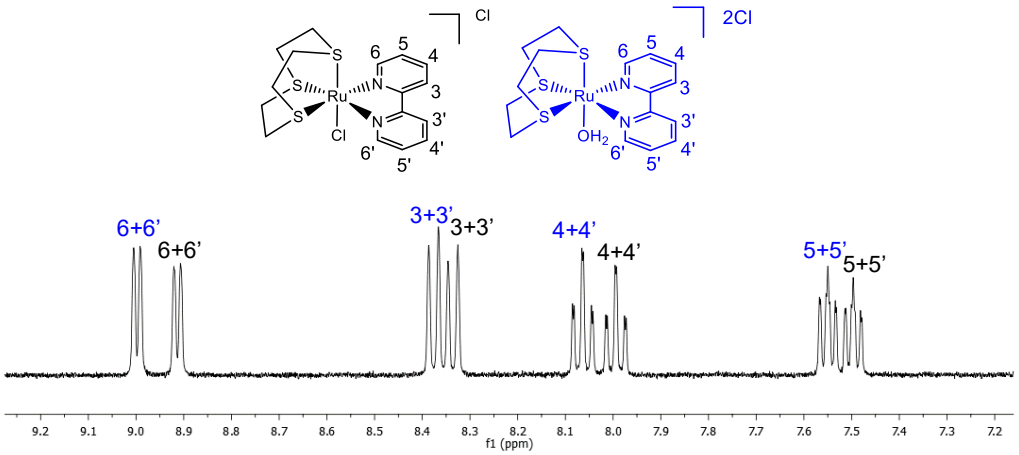

Figure A8.1. ^{1}H NMR spectrum (aromatic region) in D_2O of [Ru([9]aneS$_3$)(bpy)Cl]Cl (**63**), and [Ru([9]aneS$_3$)(bpy)(OH$_2$)](Cl)$_2$ (**63$_{aq}$**).

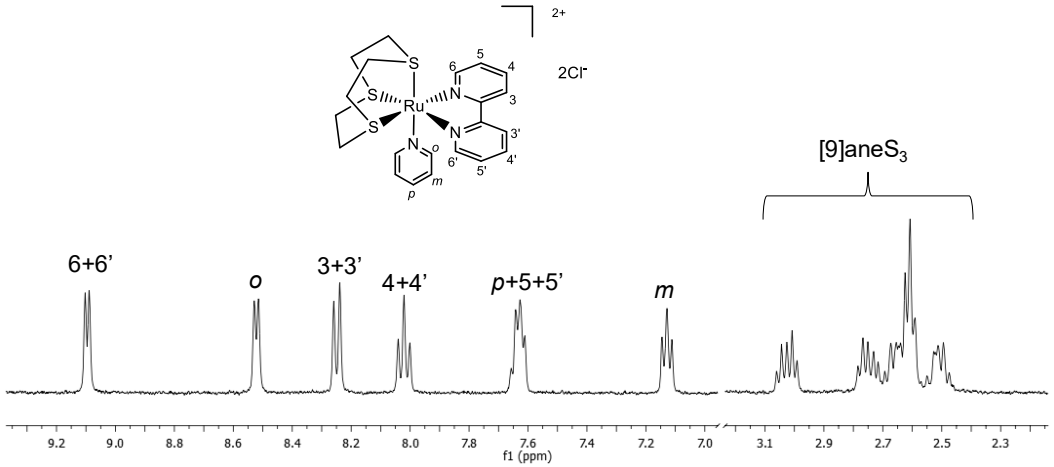

Figure 8.2. ^{1}H NMR spectrum in D_2O of [Ru([9]aneS$_3$)(bpy)(py)](Cl)$_2$ (**68**).

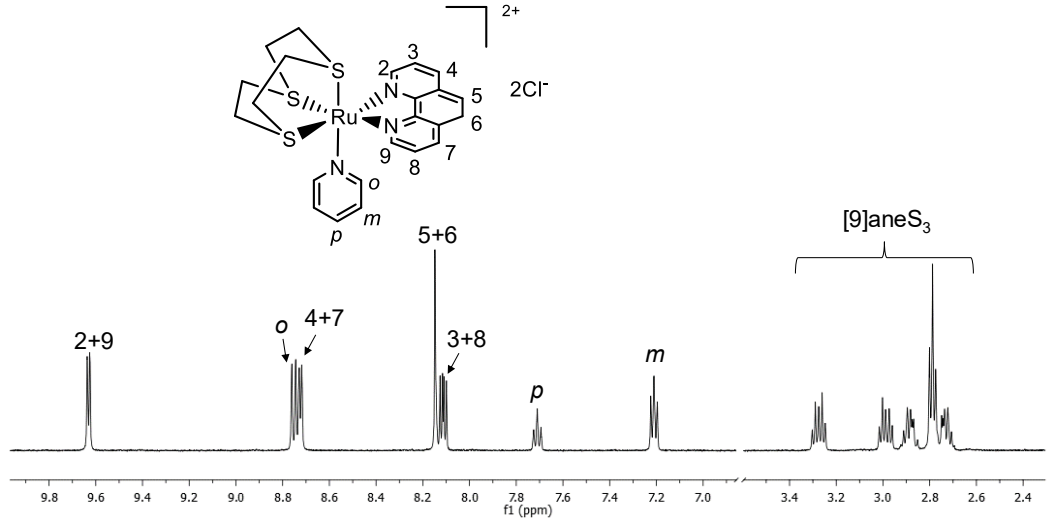

Figure A8.3. ^{1}H NMR spectrum in D_2O of [Ru([9]aneS_3)(phen)(py)]$(Cl)_2$ (**69**).

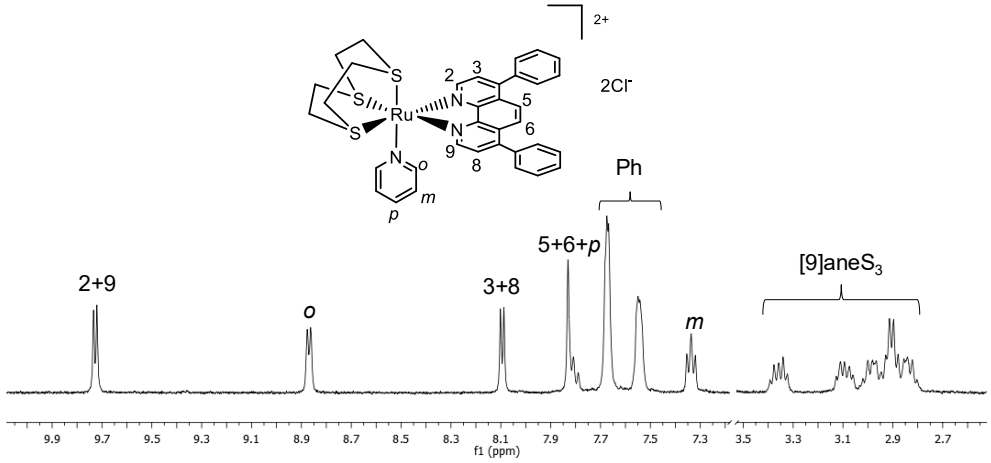

Figure A8.4. ^{1}H NMR spectrum in D_2O of [Ru([9]aneS_3)(4,7-Ph_2phen)(py)]$(Cl)_2$ (**70**).

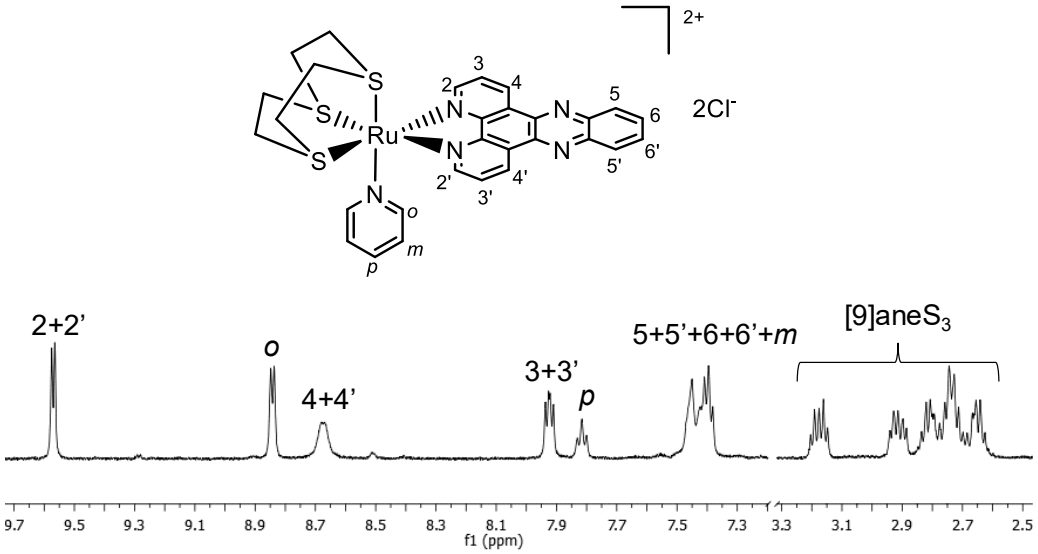

Figure A8.5. ^{1}H NMR spectrum in D_2O of [Ru([9]aneS_3)(dppz)(py)]$(Cl)_2$ (**71**).

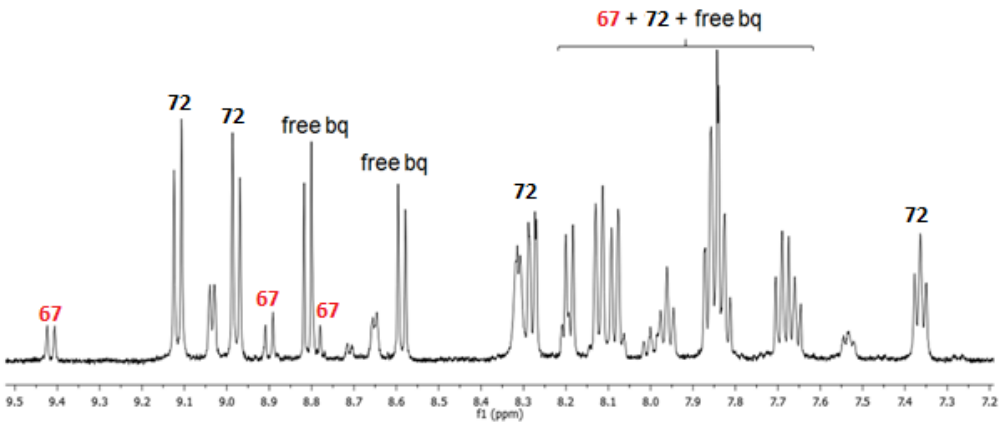

Figure A8.6. ^{1}H NMR spectrum in DMSO-d_6 of [Ru([9]aneS_3)(bq)(py)]$(Cl)_2$ (**72**) after 240 min of irradiation (λ = 470 nm, 40 mW).

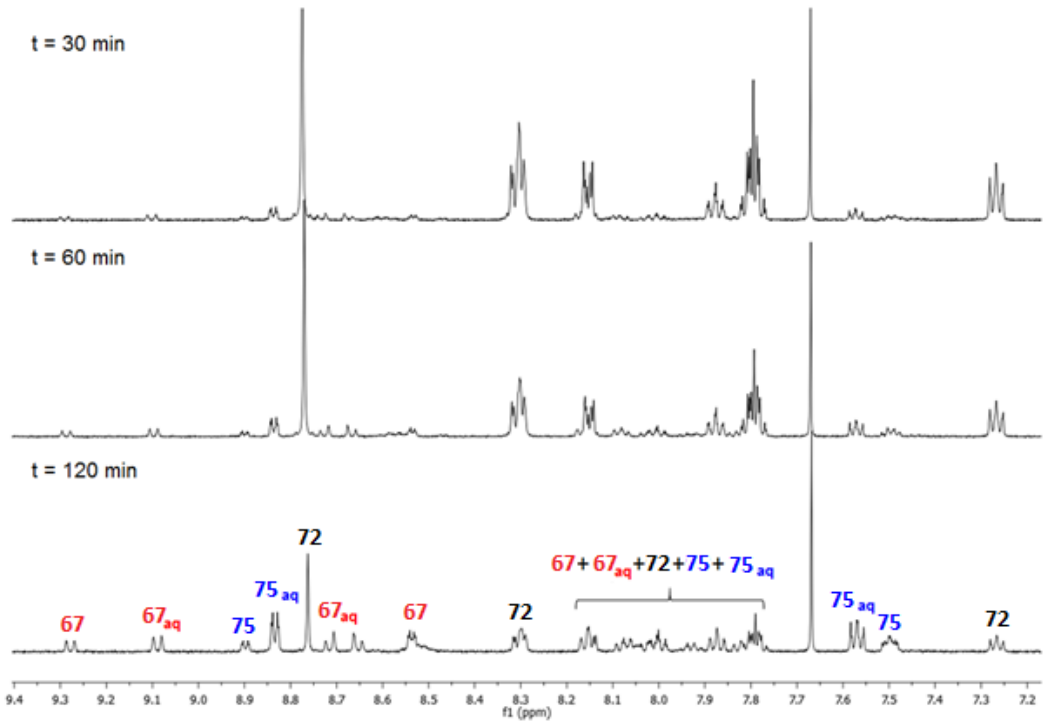

Figure A8.7. ^{1}H NMR spectrum in D_2O of [Ru([9]aneS$_3$)(bq)(py)](Cl)$_2$ (**72**) after 30 min (top), 60 min (middle) and 120 min (bottom) of irradiation (λ = 470 nm, 40 mW).

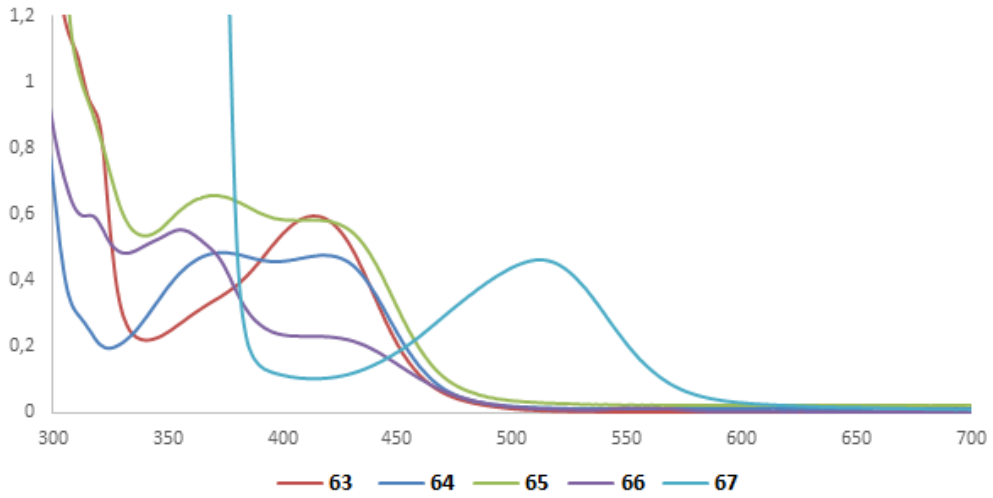

Figure A8.8. UV-vis spectra of [Ru([9]aneS$_3$)(bpy)Cl]Cl (**63**), [Ru([9]aneS$_3$)(phen)Cl]Cl (**64**), [Ru([9]aneS$_3$)(4,7-Ph$_2$phen)Cl]Cl (**65**), [Ru([9]aneS$_3$)(dppz)Cl]Cl (**66**), [Ru([9]aneS$_3$)(bq)Cl]Cl (**67**) (ca. in 0.1 mM H_2O) in the visible region.

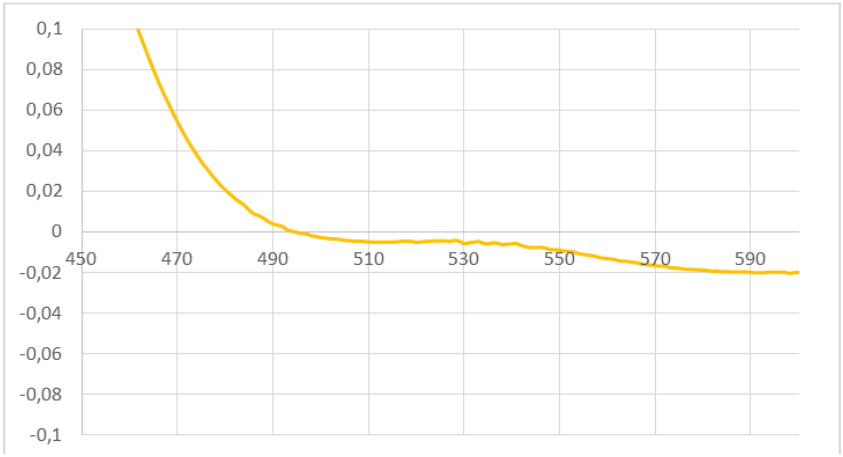

Figure A8.9. UV-vis spectrum of [Ru([9]aneS$_3$)(dppz)(py)](Cl)$_2$ (**71**) (ca. in 0.1 mM H_2O) between 450 and 600 nm.

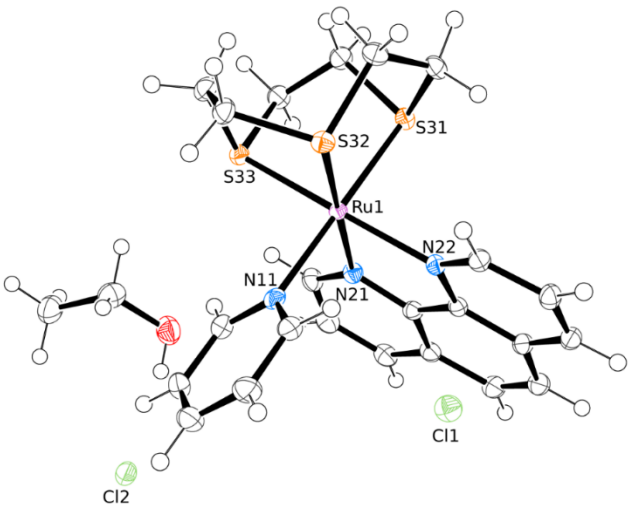

Figure A8.10. Molecular structure (50% probability ellipsoids) of [Ru([9]aneS$_3$)(phen)(py)](Cl)$_2$·EtOH (**69**).

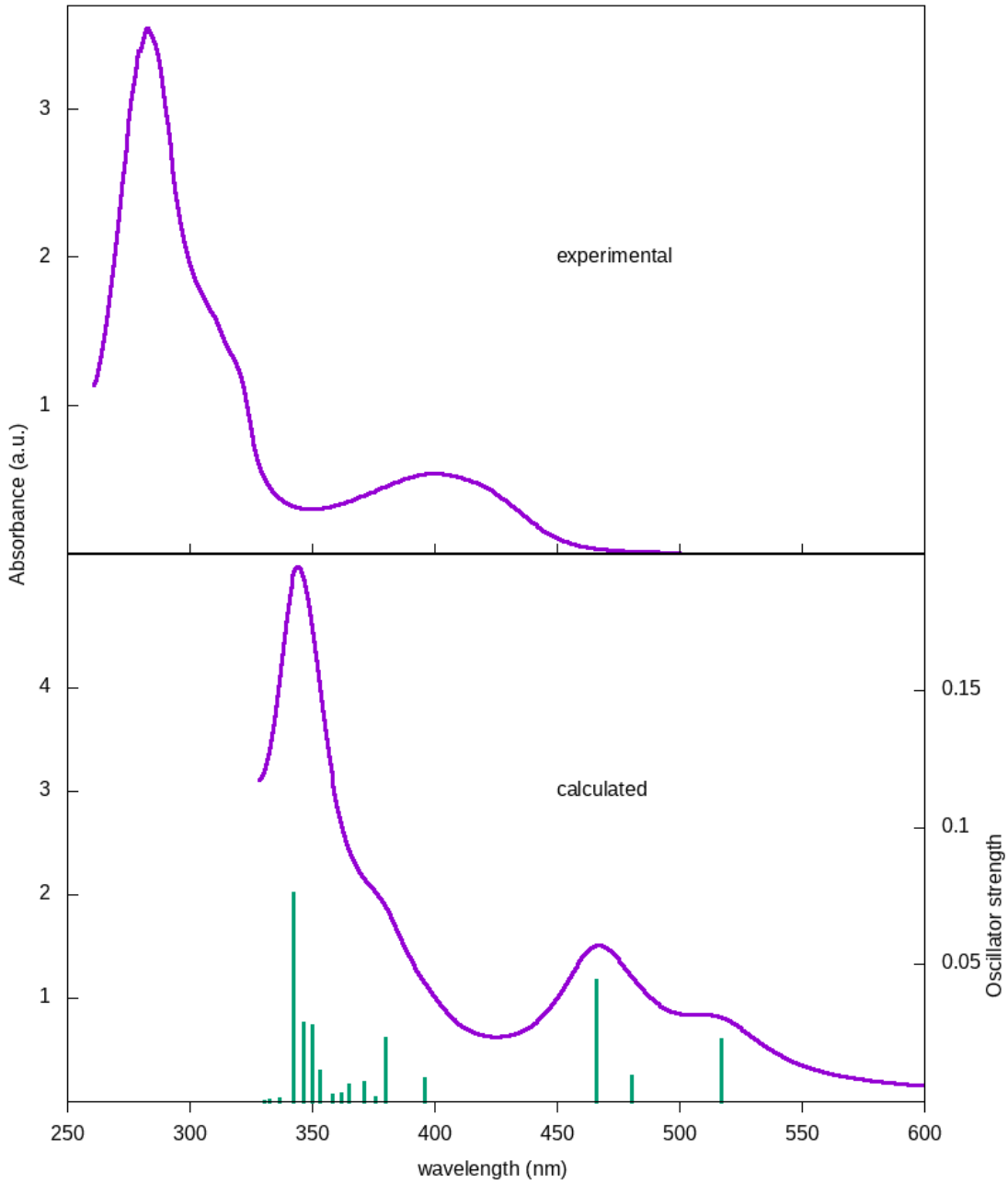

Figure A8.11. Experimental (top) and calculated (with the "turbo_lanczos" program, bottom) absorption spectra for complex [Ru([9]aneS$_3$)(bpy)(py)](Cl)$_2$ (**68**). The vertical bars in the simulated spectrum are the calculated transitions (with the "turbo_davidson" code), with height equal to the oscillator strength.

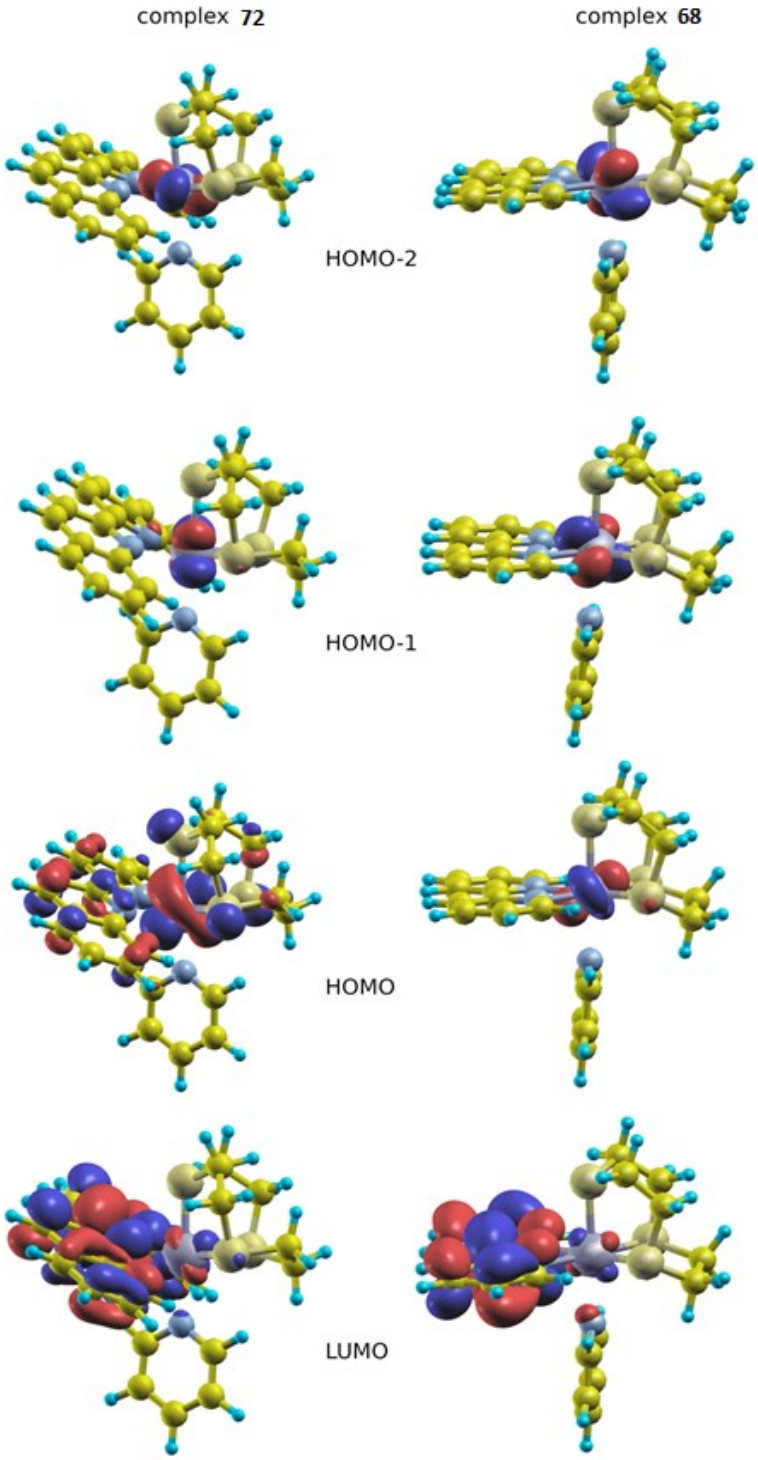

Figure A8.12. Selected molecular orbitals for [Ru([9]aneS$_3$)(bpy)(py)](Cl)$_2$ (**68**) (right) and [Ru([9]aneS$_3$)(b7)(py)](Cl)$_2$ (**72**) (left) in the singlet ground state.

Table A8.1. Selected TDDFT singlet transitions for [Ru([9]aneS$_3$)(b7)(py)](Cl)$_2$ (**72**). Only contributions ≥ 2% are reported.

Energy (eV)	Wavelength (nm)	Oscillator strength	Major contributions
2.2707	546	0.1006	HOMO→LUMO 84% HOMO–1→LUMO 12% HOMO–1→LUMO+1 2%
2.7264	455	0.0052	HOMO–3→LUMO 88% HOMO–4→LUMO 5% HOMO–1→LUMO 2%
2.9608	419	0.0147	HOMO→LUMO+1 63% HOMO–4→LUMO 17% HOMO–5→LUMO 7% HOMO–1→LUMO+1 5% HOMO–3→LUMO 3%
3.0767	403	0.0537	HOMO→LUMO+2 41% HOMO–1→LUMO+1 25% HOMO→LUMO+1 12% HOMO–4→LUMO 11% HOMO–1→LUMO+2 7%
3.0881	401	0.0542	HOMO–1→LUMO+1 59% HOMO→LUMO+2 15% HOMO–1→LUMO+2 7%

			HOMO→LUMO+3 6% HOMO–5→LUMO 4% HOMO–4→LUMO 2%
3.1606	392	0.1629	HOMO→LUMO+2 35% HOMO–4→LUMO 20% HOMO→LUMO+1 17% HOMO–1→LUMO+5 7% HOMO–5→LUMO 6% HOMO–1→LUMO+3 5% HOMO–1→LUMO+2 3%
3.2265	384	0.0863	HOMO–1→LUMO+2 66% HOMO→LUMO+4 9% HOMO→LUMO+3 8% HOMO–4→LUMO 5% HOMO–1→LUMO+3 3% HOMO→LUMO+2 2% HOMO→LUMO+1 2%
3.2706	379	0.0298	HOMO→LUMO+3 73% HOMO→LUMO+4 9% HOMO–1→LUMO+3 3% HOMO–5→LUMO 2%

			HOMO–1→LUMO+5 2% HOMO–1→LUMO+4 2% HOMO–1→LUMO+1 2% HOMO→LUMO+2 2%
3.3145	374	0.0278	HOMO–1→LUMO+3 61% HOMO→LUMO+4 16% HOMO–1→LUMO+2 6% HOMO–2→LUMO+1 5% HOMO–3→LUMO+1 3% HOMO→LUMO+2 2%
3.3646	368	0.0106	HOMO–2→LUMO+1 63% HOMO→LUMO+4 24% HOMO–1→LUMO+5 6% HOMO→LUMO+3 2%
3.3961	365	0.0147	HOMO–1→LUMO+4 42% HOMO–2→LUMO+1 15% HOMO–3→LUMO+1 13% HOMO→LUMO+4 13% HOMO→LUMO+3 4% HOMO–1→LUMO+3 3% HOMO–1→LUMO+2 2%

			HOMO→LUMO+5 2%
3.4274	362	0.0245	HOMO→LUMO+5 36% HOMO–1→LUMO+4 16% HOMO→LUMO+4 14% HOMO–2→LUMO+1 10% HOMO–1→LUMO+3 10% HOMO–5→LUMO+1 3%
3.4543	359	0.0336	HOMO→LUMO+5 52% HOMO–1→LUMO+4 17% HOMO–1→LUMO+3 7% HOMO→LUMO+4 5% HOMO–4→LUMO+1 4% HOMO–1→LUMO+5 3% HOMO–2→LUMO+2 2%
3.5194	352	0.1029	HOMO–1→LUMO+5 39% HOMO–2→LUMO+2 38% HOMO–2→LUMO+3 5% HOMO–4→LUMO 4% HOMO→LUMO+4 3% HOMO–3→LUMO+5 2%
3.5475	349	0.0652	HOMO–2→LUMO+2 41%

			HOMO–1→LUMO+5 27% HOMO–2→LUMO+3 8% HOMO–3→LUMO+2 6% HOMO–3→LUMO+1 4% HOMO–4→LUMO 2% HOMO–3→LUMO+3 2%